

The Molecular Mechanism of Major Histocompatibility Complex Class I Peptide Binding and Exchange

by
Ankur Saikia

A thesis submitted in partial fulfilment
of the requirements for the degree of

**Doctor of Philosophy
in Biochemistry**

Approved: Dissertation Committee

Prof. Dr. Sebastian Springer

Jacobs University Bremen gGmbH

Prof. Dr. Christian Hammann

Jacobs University Bremen gGmbH

Prof. Dr. Christian Freund

Freie Universität Berlin

Date of Defence: 21 February 2022

Department of Life Sciences and Chemistry

Statutory Declaration

Family Name, Given/First Name	Saikia, Ankur
Matriculationnumber	20331912
What kind of thesis are you submitting: Bachelor-, Master- or PhD-Thesis	PhD-Thesis

English: Declaration of Authorship

I hereby declare that the thesis submitted was created and written solely by myself without any external support. Any sources, direct or indirect, are marked as such. I am aware of the fact that the contents of the thesis in digital form may be revised with regard to usage of unauthorized aid as well as whether the whole or parts of it may be identified as plagiarism. I do agree my work to be entered into a database for it to be compared with existing sources, where it will remain in order to enable further comparisons with future theses. This does not grant any rights of reproduction and usage, however.

The Thesis has been written independently and has not been submitted at any other university for the conferral of a PhD degree; neither has the thesis been previously published in full.

German: Erklärung der Autorenschaft (Urheberschaft)

Ich erkläre hiermit, dass die vorliegende Arbeit ohne fremde Hilfe ausschließlich von mir erstellt und geschrieben worden ist. Jedwede verwendeten Quellen, direkter oder indirekter Art, sind als solche kenntlich gemacht worden. Mir ist die Tatsache bewusst, dass der Inhalt der Thesis in digitaler Form geprüft werden kann im Hinblick darauf, ob es sich ganz oder in Teilen um ein Plagiat handelt. Ich bin damit einverstanden, dass meine Arbeit in einer Datenbank eingegeben werden kann, um mit bereits bestehenden Quellen verglichen zu werden und dort auch verbleibt, um mit zukünftigen Arbeiten verglichen werden zu können. Dies berechtigt jedoch nicht zur Verwendung oder Vervielfältigung.

Diese Arbeit wurde in der vorliegenden Form weder einer anderen Prüfungsbehörde vorgelegt noch wurde das Gesamtdokument bisher veröffentlicht.

24.01.2022

Ankur, Saikia

.....
Date, Signature

Acknowledgements

It was a very excited and cheerful journey on the way to completing my research studies. As I pause and reflect, it was a wonderful experience with many generous, supportive, talented and cheerful people around me, all of whom I may not be able to mention here.

I can only begin to express my deepest gratitude and appreciation to my supervisor Prof. Dr. Sebastian Springer providing me the opportunity to work on this exciting project and for his unwavering support throughout the journey. You helped me in every step, be it your scientific vision, brainstorming for hours during discussions or helping me with reviewing and shaping my manuscripts and thesis. I would not have been able to complete it without your help. Working under his direction was a tremendous honor and privilege. THANK YOU! Sebastian, I appreciate everything you have done for me.

I am deeply indebted to my committee members: Prof. Dr. Christian Freund and Prof. Dr. Christian Hammann, for investing their time in evaluating my thesis, providing valuable scientific suggestions, and encouraging me to remain focused during my project work.

I must also thank Prof. Martin Zacharias, Prof. Sunil Kumar Saini, Prof. Sine Reker Hadrup, Dr. Christian Kleusch, Dr. Quentin Canelle, Dr. Maria Garcia, Prof. Charlotte Uetrecht, Janine-Denise Kopicki, Dr. Dominik Maurer, and Dr. Andreas Moritz. It was a pleasure to collaborate with you; I couldn't have completed my dissertation without your aid and advice.

I am very grateful to all members of the Springer group: Swapnil, Raghavendra, Sujit, Zeynep Hein, Cindy, Venkat, Natalia, Nauria, Antonia, Fernando, and Franzi for creating a friendly atmosphere and for all those productive discussions. Special thanks to Uschi for running our lab and ordering lab reagents for my experiments on time. I would also like to thank graduate students Andries, Pegi, Andreea, Pranathi, Chantal, and Ana for their help with this project. I would also like to thank Brix lab and Hamman lab members for their help throughout this journey.

I want to express my gratitude to Jacobs University's campus life team members and technical and non-technical staff for their support. I'm also grateful for the funding provided by the Deutsche Forschungsgemeinschaft (DFG).

My thank also to the Indian community in Bremen. My time during this research would not have been livelier and more relaxing.

I want to pay infinite love and regards to my companion Rini and daughter Davina. Rini, my better half, words fall short of expressing my thanks to you. But still, thank you for

everything, understanding me, encouraging me during stress, and your unconditional support. Thank you, my angel Davina for being my stress buster.

Last but not least, I would like to thank my father, Dr. Abani Kumar Saikia and my mother, Mrs. Monimala Borah Saikia, for their guidance, care and nurturing me to be what I am today. I must also thank my beloved sisters, Dr. Mousumee Saikia and Dr. Moitrayee Saikia, who had constantly encouraged me. Many thanks to my in-laws and entire family for believing in me. I hope I have made you proud.

Shoot for the moon. Even if you miss, you'll land among the stars.

-Les Brown

Abstract

Major histocompatibility class I (MHC-I) molecules are key to our body's immune defence against pathogens and tumors by presenting the cytosolic peptidome to cytotoxic T lymphocytes (CTLs). MHC-I/peptide (pMHC) complexes are presented on the cell surface, and recognition by CTLs results in a kill signal and the destruction of aberrant cells. The crucial criterion in the selection of peptides to be presented at the cell surface is the peptide editing process that leads to the stable binding of the octa- to nonameric peptides to MHC-I molecules.

In this thesis, I have described the use of small molecule-assisted refolding of MHC-I proteins for generating their empty, peptide-receptive forms. I have also developed alternative methods for peptide exchange and novel thermostability and peptide affinity measurements, which can contribute significantly to the understanding of MHC-I selection mechanism and developing reagents for clinical applications.

The refolding of classical human MHC-I molecules *in vitro* has always required full-length peptides, whereas empty, stable forms have been nearly impossible to obtain. The Springer group has previously demonstrated that both wild type and Y84C/A139C-modified disulfide bond-stabilized MHC-I molecules can be folded in the presence of an excess of a dipeptide, but importantly, allotype-specific dipeptide sequences are needed. To discover them, I have developed a competitive enzyme-linked immunosorbent assay (cELISA) and used it to screen dipeptides and tripeptides that modulate MHC-I refolding. The folded dsMHC-I molecules can subsequently be stripped of dipeptides in a washing process to generate the empty forms. These empty dsMHC-I proteins are significantly thermostable in solution, withstand freeze-thaw, and demonstrate rapid peptide binding kinetics. Such empty dsMHC-I molecules can be used in rapid multimer generation, as they can be loaded with the peptide of interest just in a few minutes. In our publication, the crystal structure of disulfide-stabilized HLA-A*02:01 (dsA2) with a TCR shows that the peptide binding specificity and the T cell receptor fingerprint are of the dsA2 are nearly identical to those of the wild type A2.

Empty MHC-I molecules have a wide range of potential applications that were never possible previously. One might use these molecules to fish out peptides from tumor tissues or infected cells before characterizing them using mass spectrometry. One might use them for priming T cells with low-affinity epitopes and for rapid monitoring of T cell response in immunotherapy. We can also compare the peptide affinities from *in-vitro* assays by monitoring direct binding of the peptide to empty dsMHC-I molecules. We have successfully developed a new assay based on microscale thermophoresis, which can be developed into a high-throughput peptide affinity screening platform with potential practical applications in research and even treatment.

Taken together, in the future, we will be able to accelerate the process of neoepitope discovery and provide efficient, and robust solutions to accelerate immunotherapeutic treatments.

Table of contents

Statutory declaration.....	i
Acknowledgements.....	ii
Abstract	iv
Table of contents.....	vi
List of figures.....	x
List of tables.....	xiii
List of abbreviations.....	xiv
Chapter 1. Introduction	1
1.1. Antigen presentation by MHC class I molecules	1
1.2. Structure of MHC-I molecules.....	2
1.3. How peptides bind to MHC-I molecules.....	3
1.4. MHC-I molecule polymorphism and allotype distribution.....	4
1.5. Cancer Immunotherapy	6
1.6. The role of MHC-I molecules in immunotherapy.....	8
1.7. Generation of pMHC multimers by peptide exchange	12
1.8. MHC-I disulfide mutants as empty peptide-receptive molecules	15
1.9. Aim and scope of the thesis work	17
1.10. Overview of the chapters of this thesis.....	18
1.11. References.....	22
Chapter 2. Materials and Methods.....	31
2.1. Background.....	31
2.2. Protein expression and inclusion body preparation.....	31
2.3. Protein refolding	39
2.4. Protein Purification	55

2.5. Thermal Stability Measurement.....	75
2.6. Peptide binding and peptide exchange	85
2.7. Competitive ELISA.....	103
Chapter 3. Screening for dipeptides/tripeptides that stabilize and promote MHC-I refolding in a competitive ELISA assay.....	123
3.1. Background.....	123
3.2. Assay principle	125
3.3. The species- and conformation-specific mAbs, W6/32 (HLA-I) and 30-5-7 (L ^d).....	125
3.4. cELISA assay development.....	126
3.5. Screening results:	131
3.6. Discussion.....	135
Reference.....	136
Chapter 4. Methods to monitor MHC-I peptide exchange and binding	139
4.1. Introduction	139
4.2. Kinetic parameters of receptor-ligand binding	140
4.3. Fluorescence anisotropy	143
4.4. Microscale thermophoresis.....	147
4.5. Discussion.....	152
4.6. Reference	153
Chapter 5. Peptide MHC-I complex stability measured by nanoscale differential scanning fluorimetry reveals the molecular mechanism of thermal denaturation	157
5.1. Abstract	158
5.2. Introduction	159
5.3. Results	160
5.4. References	172
5.5. Supplementary Materials.....	176

Chapter 6. Empty MHC class I molecules for improved detection of antigen-specific T cells.....	183
6.1. Abstract.....	184
6.2. Introduction.....	185
6.3. Results	186
6.4. Discussion.....	196
6.5. Materials and Methods	198
6.6. Acknowledgments.....	205
6.7. Author contributions.....	206
6.8. Competing interests.....	206
6.9. Data and materials availability.....	206
6.10. References.....	207
6.11. Supplementary information	209
Chapter 7. Use of empty disulfide-stabilized A2 molecule for the high-throughput screening of TCR ligands.	219
7.1. Abstract.....	220
7.2. Introduction.....	221
7.3. Results	222
7.4. Discussion.....	233
7.5. Materials and method	234
7.6. Acknowledgments.....	239
7.7. Authors contributions.....	239
7.8. Data and materials availability.....	239
7.9. References	240
7.10. Supplementary information	242
Chapter 8. Mapping the peptide binding groove of MHC class I.....	261
8.1. Abstract.....	262
8.2. Teaser	262

8.3. Introduction	263
8.4. Results	264
8.5. Discussion.....	277
8.6. Materials and Methods	281
8.7. Acknowledgments.....	283
8.8. Funding:.....	283
8.9. References	284
8.10. Supplementary Information	288
Chapter 9. Molecular Mechanisms of chaperone-independent peptide exchange reveal allotype specific long-range peptide-MHC-I interactions	303
9.1. Abstract	304
9.2. Introduction	305
9.3. Results	305
9.4. Discussion.....	312
9.5. Methods	315
9.6. References	317
9.7. Supplementary Information.....	319
Chapter 10. Discussion (Outlook).....	325
10.1. How might a universal peptide exchange method revolutionize the field?	325
10.2. Screening dipeptides for refolding different human allotypes for quick peptide exchange.....	326
10.3. Development of a robust peptide screening platform using nanoDSF and MST.....	327
10.4. Understanding peptide binding in practical application	327
10.5. Future perspectives.....	328
10.6. References	330

List of figures

Figure 1-1. Schematics of MHC-I antigen presentation.....	1
Figure 1-2. Peptide binding to the ER-luminal domain of MHC-I complex as depicted in the crystal structure (PDB ID: 1KPV).....	2
Figure 1-3. Peptide-MHC-I interaction.	3
Figure 1-4. Schematics of tumor neoantigen screening process.	9
Figure 1-5. Hypothetical mechanistic model of dipeptide-catalyzed peptide exchange on MHC-I.	14
Figure 3-1. Steps involved in the cELISA.....	126
Figure 3-2. Assay parameter optimization (see text for details).....	129
Figure 4-1. Occupancy at equilibrium.....	142
Figure 4-2. Schematic of binding equilibrium shown by exponential kinetics.	142
Figure 4-3. Principle of fluorescence anisotropy assay to measure peptide-MHC-I interaction.	143
Figure 4-4. Representative dipeptide-mediated peptide exchange assay.	145
Figure 4-5. Thermophoresis assay.	147
Figure 4-6. Representative graph for typical MHC-I peptide binding measured by MST assay	149
Figure 5-1: Measuring protein unfolding with nanoDSF.	161
Figure 5-2. Comparing nanoDSF with other methods.	162
Figure 5-3. Biophysical parameters influencing rpMHC thermal denaturation.	163
Figure 5-4. NanoDSF studies for the quality control of rpMHCs.....	164
Figure 5-5. Isothermal analysis of folding energies.....	165
Figure 5-6. Affinity screening of mutant peptides and sequence-specific influence of free peptide concentration on rpMHC thermostability.....	166
Figure 6-1: dsA2 molecules are peptide-receptive and form stable complexes with associated peptides.	187
Figure 6-2. Improved and efficient antigen-specific T cell detection using dsA2 molecules.....	190

Figure 6-3. dsA2 molecules used in combinatorial color-encoding effectively detects virus-and melanoma-associated antigen-specific T cells.....	192
Figure 6-4. Empty-loadable MHC-I multimers for efficient detection of antigen-specific T cells.	194
Figure 6-5. Detection of neoantigen specific T cell recognition in cancer.....	196
Figure 7-1. Overview of disulfide-stabilized HLA-A*02:01 production and usage for affinity measurements.	223
Figure 7-2. Association and dissociation behavior of 1G4 TCR with different pMHC complexes.	224
Figure 7-3. Crystal structure of ESO 9V dsA*02:01 and ESO9V wtA*02:01 in complex with 1G4.	225
Figure 7-4. Affinities of the SV9 specific bs-868Z11-CD3 bsTCR with different MHC monomers and peptide ligands.....	227
Figure 7-5. Binding motif of bs-868Z11-CD3 generated using dsA*02:01 generated positional scanning library as soluble analyte and immobilized bsTCR.	229
Figure 7-6. Result of coincubation assays with peptide-loaded target cells, Jurkat effector cells, and bs-868Z11-CD3 at six different concentrations.....	231
Figure 8-1. Disulfide-stabilized HLA-A*02:01.....	266
Figure 8-2. Overall area under the curve (AUC) for the detected dsA2 mass species in presence of YF9, NV9, and GV9 at different acceleration voltages.	267
Figure 8-3. Ion-source decay causes linear dependence of the ligand-bound dsA2 fraction on cone voltage.	268
Figure 8-4. Relation of thermal stability and affinity for dsA2/peptide complexes.....	270
Figure 8-5. Charge-reduced NV9 variants analyzed at 10 V.....	272
Figure 8-6. Truncated NV9 variants analyzed at 10 V.....	274
Figure 8-7. Detected dsA2 mass species in presence of two corresponding truncated NV9 variants.	276
Figure 8-8. Favored amino acid positions within the HLA-A*02:01 peptide binding pocket.	278
Figure 9-1. Dipeptides and acidification promote peptide exchange on wtA2 and wtA24.	307

Figure 9-2. Acidification affects peptide association and dissociation on dsA2, but not peptide-dsMHC-I complex stability.....	309
Figure 9-3. NaCl attenuates peptide exchange, equilibrium binding affinity and association on dsA2, but not dsA24.....	310
Figure 9-4. Acidification, dipeptides and disulfide stabilisation synergize in accelerating peptide exchange.....	311

List of tables

Table 1-1. Coverage of most frequent MHC-I allotypes globally and in Europe.....	5
Table 1-2. Selected list of FDA-approved immunotherapeutic drugs.....	7
Table 3-1. Different plate types used in cELISA assay	127
Table 3-2. Short peptide screening in cELISA for different HLA allotypes.....	132
Table 4-1: Assays developed so far to monitor peptide-MHC-I interactions.....	139
Table 4-2. Dipeptides modulating peptide exchange	146
Table 4-3. MST Screening Data	150
Table 5-1. Features of the prominent methods for pMHC thermal stability measurements	160

List of abbreviations

A2	HLA-A*02:01 (the most common human MHC class I allotype)
A2-Y84C	HLA-A*02:01(Y84C/A134C)
ADCs	Antibody-drug conjugates
ADCC	Antibody-dependent cell-mediated cytotoxicity
APC	Antigen-presenting cell
aAPCs	Artificial APCs
ATC	Adoptive cell therapy
AUC	Area under the curve
BCG	Bacillus Calmette-Guérin
B _{max}	Maximal binding capacity
β ₂ m	Beta-2 microglobulin (the light chain of MHC class I)
BSA	Bovine serum albumin
CAR T cell	Chimeric antigen receptor T cell
CD8	Cluster of differentiation 8 (a TCR coreceptor)
CD33	Cluster of differentiation 33
CID	Collision-induced dissociation
CTL	Cytotoxic T lymphocyte (killer T cell)
CTLA-4	CTL-associated antigen 4
Dig	Digoxigenin (a detergent)
Dnp	Dinitrophenol
DSF	Differential scanning fluorimetry (to measure protein denaturation)
dsA2	Disulfide-stabilized HLA-A*02:01 [=HLA-A*02:01(Y84C/A134C)]
dsMHC-I	Disulfide-stabilized MHC-I
DTT	Dithiothreitol
EBV	Epstein-Barr virus

EC ₅₀	Half-effective concentration
EDTA	Ethylenediaminetetraacetic acid
ELISA	Enzyme-linked immunosorbent assay
ELISpot	Enzyme-linked immune absorbent spot
EMBL	European molecular biology laboratory
ER	Endoplasmic reticulum
ERAP1	ER aminopeptidase associated with antigen processing 1
ERp57	Endoplasmic reticulum-resident protein of 57 kDa
ESI	Electrospray ionization
FA	Fluorescence anisotropy
FACS	Fluorescence-activated cell sorting
FDA	US food and drug administration
FITC	Fluorescein isothiocyanate
FP	Fluorescence polarization
GCha	Glycyl-cyclohexylalanine (a dipeptide)
CCit	Glycyl-citrulline (a dipeptide)
GHle	Glycyl-homoleucine (a dipeptide)
GF	Glycyl-phenylalanine (a dipeptide)
GL	Glycyl-leucine (a dipeptide)
GM	Glycyl-methionine (a dipeptide)
GuHCl	Guanidine hydrochloride
H-2K ^b	Histocompatibility-2 K ^b (a murine MHC class I molecule)
hβ ₂ m	Human β ₂ m
HC	Heavy chain
HLA	Human leukocyte antigen (the human MHC)
HLA-A2	HLA-A*02:01
HIV	Human immunodeficiency virus

IC ₅₀	Half Inhibitory concentration
ICIs	Immune checkpoint inhibitors
iDSF	Isothermal analysis of nanoscale differential scanning fluorimetry
IFN- α_2	Interferon-alpha 2
IPTG	Isopropyl β -D-1-thiogalactopyranoside
IV9	Peptide ILKEPVHGV (single-letter amino acid notation)
K _d	Equilibrium constant (of dissociation)
K _{d,low} & K _{d,high}	Dissociation constant determined by native MS
K _{d,th}	Dissociation constant predicted by NetMHC
k _{on}	Association rate constant
k _{off}	Dissociation rate constant
LC-MS/MS	Liquid chromatography with tandem mass spectrometry
MD	Molecular dynamics
MES	2-(N-morpholino) ethanesulfonic acid
MHC	Major histocompatibility complex (a gene region)
MHC-I	MHC class I molecules
MHC-II	MHC class II molecules
MS	Mass spectrometry
MST	Microscale thermophoresis
MW	Molecular weight
NaOH	Sodium hydroxide
NanoDSF	Nanoscale differential scanning fluorimetry
NMR	Nuclear magnetic resonance
NV9	Peptide NLVPMVATV (single-letter amino acid notation)
NV9-FITC	Peptide NLVPK _{FITC} VATV, i.e., labeled with FITC on the lysine side chain
PBS	Phosphate buffered saline
PDB	Protein data bank

PD1	Programmed cell death 1
PD-L1	PD-ligand 1
PLC	Peptide loading complex
pMHC	Peptide-MHC class I complex
PMSF	Phenyl methyl sulfonyl fluoride
QC	Quality control
SEC	Size exclusion chromatography
SOP	Standard operating procedure
SDS-PAGE	Sodium dodecyl sulphate polyacrylamide gel electrophoresis
TAP	Transporter associated with antigen processing
TAPBPR	Transporter associated with antigen processing binding protein-related
TCR	T cell receptor
TDTF	Thermal denaturation measured using tryptophan fluorescence
T _m	Midpoint of thermal denaturation transition (melting temperature)
UV	Ultraviolet
WES	Whole-exome sequencing
wtA2	Wild type HLA-A*02:01

Chapter 1. Introduction

1.1. Antigen presentation by MHC class I molecules

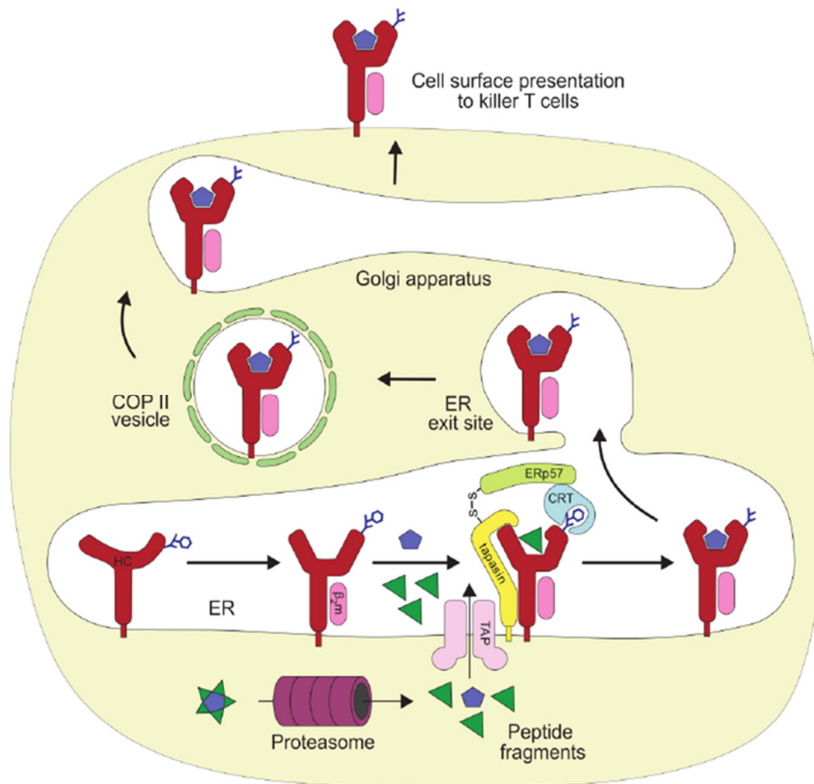


Figure 1-1. Schematics of MHC-I antigen presentation.

Following an infection or during cancer, non-self proteins are expressed in the cytoplasm. The cellular proteasomes (purple) eventually degrade non-self and the self proteins into smaller peptide fragments that are further transported into the lumen of ER by hetero-dimeric TAP transporters (light pink). MHC-I heavy chain (red) folds with β_2m (pink) and is then loaded with specific peptides (blue pentagons and green triangles) in the context of the peptide loading complex (PLC). The PLC consists of seven subunits, including tapasin (yellow), ERp57 (green), and calreticulin (CRT, blue) together with TAP and pMHC-I. Following peptide loading, the pMHC-I complexes travel to the cell surface to present the peptides to killer T cells (not shown) for immune surveillance. Figure reused from [1] with permission.

In vertebrates, all nucleated cells express major histocompatibility complex class I (MHC-I) molecules (proteins) on their cell surface [2,3]. They are key proteins of the adaptive immune response against viruses and cancer cells [4,5]. MHC-I molecules are synthesized and assembled in the endoplasmic reticulum (ER) [6]. To prevent them from denaturing, the empty molecules are stabilized by the lectin chaperone calreticulin, the protein disulfide isomerase ERp57, and the dedicated chaperone protein tapasin together called the peptide loading complex or PLC (**Figure 1-1**) [1,7]. They then bind to foreign or self-peptides that were degraded by the proteasome [8] and

transported into the ER lumen by the transporter associated with antigen processing (TAP) [9–11]. When a high-affinity peptide binds to the MHC-I molecule, the chaperones are released, and the peptide/MHC-I (pMHC) complex leaves the ER to be presented to CD8⁺ T cells (cytotoxic T cells, CTL) on the cell surface [3,12]. This process, called antigen presentation, allows the CTL to identify and eliminate virally infected cells or cancers [13]. So-called professional antigen-presenting cells (APCs), mainly dendritic cells, can also present peptides derived from exogenous proteins on their class I molecules (cross-presentation) [14–16].

1.2. Structure of MHC-I molecules

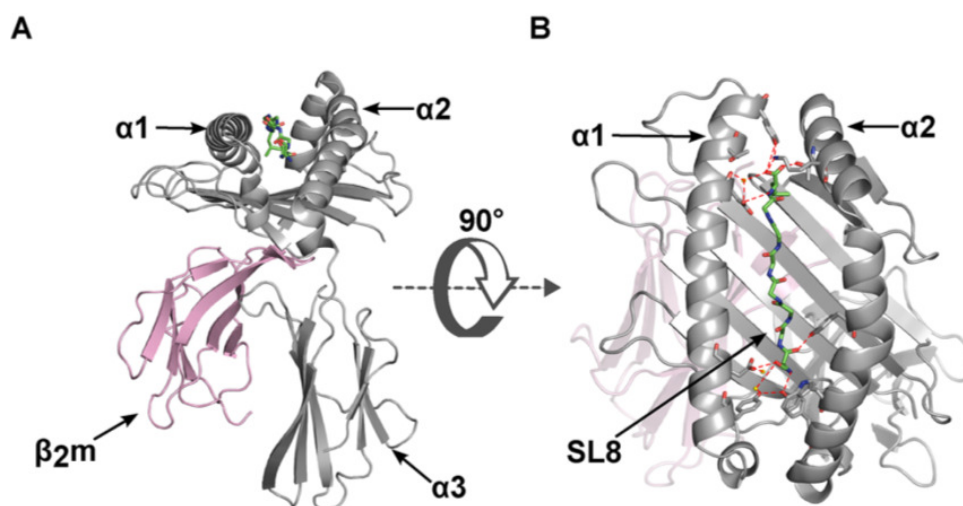


Figure 1-2. Peptide binding to the ER-luminal domain of MHC-I complex as depicted in the crystal structure (PDB ID: 1KPV)

(A) α_1 and α_2 domains (in grey) of the HC form the peptide binding groove. The α_3 domain is also shown in grey, and the light chain β_{2m} is shown in pink. (B) The peptide binding groove (top view) formed by the α_1 and α_2 helices and the beta sheet. The figure shows murine H-2K^b bound to the SIINFEKL peptide. In the cellular protein, the C terminus of the α_3 domain is followed by a transmembrane domain and a cytosolic tail. *Figures used from open access paper published by Abualrous et al. [17].*

In 1987, Bjorkman and collaborators solved the crystal structure of a human MHC-I molecule, HLA-A*02:01 (in this thesis also simply called A2) [18]. The heterotrimeric MHC-I complex consists of a non-covalently bound variable peptide, a constant 12 kDa light chain called beta-2 microglobulin (β_{2m}), and a polymorphic 44-47 kDa heavy chain (HC), which consists of three domains, α_1 , α_2 , and α_3 , the latter linked to a transmembrane helix and a cytosolic tail (**Figure 1-2 A**).

The structure of α_1 and α_2 is quite similar: both domains contain four antiparallel beta strands followed by an alpha helix on one side. These two domains are hydrogen-bonded such that the eight beta strands form a floor on top of the β_{2m} and α_3 domains. The two alpha helices sit on top of this beta sheet to form a crevice, which is the binding site for peptides of eight to ten amino acids [14,19].

1.3. How peptides bind to MHC-I molecules

From the analysis of MHC-I crystal structures, it is evident that the peptide binding groove is closed from both ends by large aromatic residues [19] such that it restricts the length of peptides (**Figure 1-3 A**). For instance, MHC-I allotypes such as H-2K^b, HLA-A*02, and HLA-B*07 frequently bind octapeptide, nonapeptide, and decapeptides, respectively [20–22]. Some peptides longer than ten residues also bind to MHC-I, albeit with lower stability [23,24]. The termini of the peptides are held by hydrogen bonds [25]. The N-terminal ammonium group binds into a region called the A pocket, and it undergoes hydrogen bonding with conserved Tyr residues at position 171, 159, 7 and 59. The C-terminal carboxylate binds, with hydrogen bonds, to the conserved residues Tyr 147, Lys 146, Tyr 84 and Thr 143 in the F pocket region. These hydrogen bonds do not form if the peptide is too long or too short, and then, the binding affinity is decreased in comparison to the peptide of correct length. This is how MHC-I molecules select for the length of the peptide [26,27].

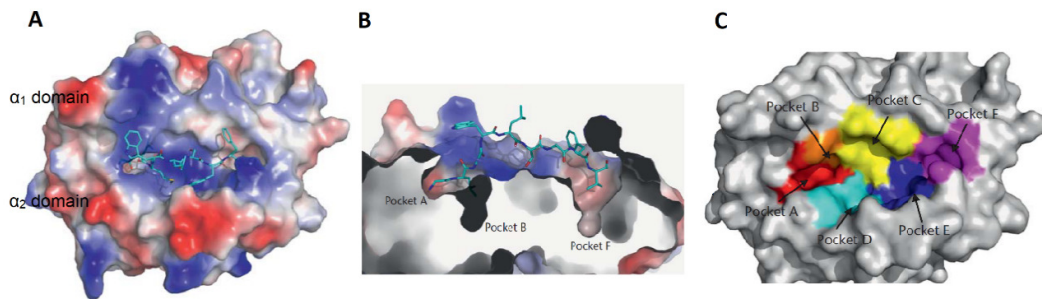


Figure 1-3. Peptide-MHC-I interaction.

(A) SARS-CoV nonamer peptide Mn2 (GLMWLSYFV) bound to A2 in the peptide binding groove (deep blue, PDB ID 3I6G). The peptide is deeply buried inside the groove, which is closed from both the ends. (B) The longitudinal cross-section of the peptide binding groove showing the anchor residues of Mn2 peptide interacting with pockets A and F at N- and C- terminal ends respectively. (C) MHC-I peptide binding groove highlighted with six pockets from A- F. *Figure above was created by combining figures 2 and figure 3 from [28] with permission.*

Some side chains of the peptide (called anchor residues) bind non-covalently into the binding ('specificity') pockets at the base of the binding groove (**Figure 1-3 B, C**). Since the variability between different MHC-I allotypes (see above) occurs mainly in the pockets, the different allotypes bind peptides of different sequence with different affinity [29]. The binding pockets are (in addition to the A pocket, where the N terminus of the peptide binds) the B, C, D, E, and F pocket [27,28,30,31]. The F pocket is special since it is used in all MHC-I molecules to bind the side chain of the C-terminal anchor residue of the peptide (P Ω or P η) [32]. That amino acid is usually hydrophobic and often bulky [19,33], but there are exceptions where positively charged amino acids are also accommodated, such as HLA-B*27:05 [32]. The key residues of the F pocket that determine the P Ω specificity are 123, 95 and 116 [34]. The conserved residue tyrosine 123 forms the entrance,

whereas residue 96 with hydrophobic side chains sits at the base of the F pocket. Residue 116 is highly polymorphic; its side chains occupy the far end [35]. There is usually one other anchor residue, commonly at the second position (P2) where it interacts with the B pocket (e.g., in HLA-A*02:01), but sometimes at the fifth/sixth position (P5/P6), interacting with the D pocket (e.g., in H-2K^b) [36,37].

1.4. MHC-I molecule polymorphism and allotype distribution

MHC-I are highly polymorphic, with more than 22,000 allotypes known [38]. Since the polymorphism is in the peptide binding groove of the molecule, it determines which peptides the class I molecule can bind.

Since there are three gene loci for human class I (HLA-A, -B, and -C), with codominant surface expression, each human cell can carry up to six different class I molecules on its surface [39]. Due to the high polymorphism and the different peptide binding characteristics of the allotypes, every individual shows unique immune responses against a given pathogen or tumor, with unique subsets of antigenic peptides. According to the divergent allele advantage hypothesis, MHC-I genotypes with divergent alleles present a wider range of antigens to the cytotoxic T cells, resulting in better immunocompetence [40]. Thus, MHC polymorphism appears to help ensure the survival of a population, since at least few individuals will develop a suitable immune response an infection by a new pathogen, or a mutated one.

The distribution of class I allotypes is not only highly heterogeneous within the population of one region of the world, but also between different populations. **Table 1-1** compares the most abundant MHC-I allotypes in Europeans and worldwide. The most studied and abundant human allotype is HLA-A*02:01. In our studies, we decided to focus on the allotypes that cover > 80% of the European population. They are as follows:

HLA-A*01:01, 02:01, 03:01, 11:01, 24:02, 68:01;
HLA-B*07:02, 08:01, 15:01, 35:01, 44:02, 44:05, 51:01;
HLA-C*02:02, 03:04, 04:01, 05:01, 07:02.

Some MHC-I molecules are statistically associated with certain diseases, which are mostly governed by unique specific mechanisms [41]. Hypersensitivity to the anti-retroviral drug Abacavir can occur in individuals that carry the HLA-B*57:01 allele [42–44]. Abacavir binds into the F pocket of the HLA-B*57:01 peptide binding groove, contacting the side chain of Ser-116. This prevents binding of the usually preferred peptide C-terminal bulky anchor residue tryptophan, which is replaced by isoleucine or leucine. This significantly changes the peptide repertoire (around 25%), triggering a strong, anti-self-polyclonal CD8⁺ T cell response.

Table 1-1. Coverage of most frequent MHC-I allotypes globally and in Europe.

Calculated based on the database available in reference [45]. The percentage is calculated from the number of people typed (sample size) for the individual allotypes in the total population with combined allele counts.

Allotypes	Most common region	% HLA coverage	
		Europe	Worldwide
HLA-A*01:01	North America, Europe, Asia	14	11
HLA-A*02:01	Global (except south Asia)	27	20
HLA-A*03:01	Europe, North America	13	9
HLA-A*11:01	Asia, Australia	6	7
HLA-A*24:02	Asia (mostly) and Global	10	10
HLA-A*68:01	North America, Europe	3	3
HLA-B*07:02	Europe, North America	11	8
HLA-B*08:01	Europe, Sub-Saharan Africa	9	7
HLA-B*15:01	North America, Europe	6	4
HLA-B*18:01	Europe, Western Asia	6	4
HLA-B*27:05	Europe, North America	4	2
HLA-B*35:01	North America, North-East Asia, Europe	6	6
HLA-B*40:01	Oceania, South-East Asia	4	4
HLA-B*44:02	Europe, North America	6	5
HLA-B*51:01	Asia, Europe	6	5
HLA-C*03:04	Europe, North America	6	7
HLA-C*04:01	Australia (mostly) and Global	13	13
HLA-C*07:02	South-East Asia (mostly) and Global	12	13

This position 116 also plays an important role in the relation of HLA-B*27 with the autoimmune inflammatory disease, ankylosing spondylitis (AS) [46]. The occurrence of HLA-B*27 in AS patients is over 85% [47]. The HLA-B*27 subtypes (most frequent is HLA-B*27:05) that are linked to AS have an aspartate at position 116, which is substituted by a different amino acid in non-disease predisposing alleles (tyrosine in B*27:06 and histidine in B*27:09) [46,48]. Generally, the F pocket of these HLA molecules is important for peptide accommodation and determines the overall molecule's flexibility as well as the surface area visible to the TCR [49].

The observation that at least three HLA-class I-related diseases, AS [50], Behçet's disease [51,52], and psoriasis [53–55], which are linked with HLA-B*27, B*51 and C*06, respectively, share a statistically significant epistatic relationship with ER aminopeptidase 1 (ERAP1) suggests the importance of antigen presentation in disease onset. Even more interesting is the fact that HLA-B*27, HLA-B*51, HLA-C*06, and HLA-B*57:01 are the alleles most protective against HIV [56,57]. Because of structural and functional restrictions in the viral proteome, some of the immunodominant peptides presented by these allotypes are less prone to mutations [58]. Perhaps this protective role

towards a virus (though not HIV, which is recent) has allowed these four alleles to be evolutionarily successful despite bringing about autoimmune diseases.

The molecular mechanisms that link these alleles to disease pathogenesis remain elusive. Since structural and functional studies are the keys to broaden our limited knowledge about these allotypes, we have also included HLA-B*27:05 and HLA-B*27:09 in our work, although their abundance in the world population is less than 4%.

1.5. Cancer Immunotherapy

Immunotherapy is a promising new field of disease treatment that works by modulating the immune system. Recent advances and promising results in cancer immunotherapy have stimulated the interest of scientists, clinicians, and pharmaceutical companies [59]. Several approaches have emerged recently [60], both MHC-dependent and -independent [61]. **Table 1-2** shows some selected immunotherapeutic examples approved by the US Food and Drug Administration (FDA).

1.5.1. Types of Cancer Immunotherapy

1.5.1.1 *Adoptive cell therapy (ACT)*

This approach mainly involves isolation, activation, (sometimes) genetical modification, and expansion of effector T cells in vitro, which are then re-infused into the same patient to detect and kill more cancer cells [62,63]. The two main types of ACTs are tumor-infiltrating lymphocyte (TIL) therapy and chimeric antigen receptor (CAR) T-cell therapy. **TIL therapies** aim to isolate tumor-reactive T cells from cancer patients, expand and activate them ex vivo, and re-infuse them to destroy the tumor and its metastases [64,65]. Such T cells can come from solid tumors (TILs), tumor-draining lymph nodes, or the blood. T cell activation can take place through gene transfection or by exposing the T cells to tumor antigens, for example with artificial antigen-presenting cells. Currently, TIL therapy treatments are only available in clinical trials [66]. Another version of ACT is **CAR T cell therapy**, which follows a similar course, but in this case, the T cells isolated from the patient blood undergo a genetic modification to express CARs at their surface. CARs are chimeras of a cell surface antigen-binding domain (such as a single-chain antibody F_{ab} fragment) linked to an intracellular T cell signaling domain [67,68]. The CAR T cells are expanded before being re-infused into the patient. Compared to unmodified T cells that rely on their TCRs for antigen recognition, CAR T cells recognize a narrower range of possible antigen targets [69]. Approved CAR-T therapeutic drugs include tisagenlecleucel (2017) to treat acute lymphoblastic leukemia [70] and axicabtagene ciloleucel (2017) for treatment of diffuse large B-cell lymphoma (DLBCL) [71].

Table 1-2. Selected list of FDA-approved immunotherapeutic drugs

Name	Class	Type of cancer	First Approval	Ref.
Amivantamab	First bispecific antibody	Lung cancer	2021	[72]
Abecma	First cell-based gene therapy	Adult multiple myeloma	2021	[73]
Pexidartinib	Small Molecule Immunomodulator	Tenosynovial giant cell tumor	2019	[74]
Tisagenlecleucel	First CAR T cell	B cell leukemia	2017	[75]
Atezolizumab	First PDL1 Inhibitor	Breast cancer	2016	[76]
Imlygic™	Oncolytic virus therapy	Metastatic Melanoma	2015	[77]
Pembrolizumab	First PD-1 inhibitor	Metastatic Melanoma	2014	[78]
Trastuzumab emtansine	Conjugated antibody	Metastatic Breast Cancer	2013	[79]
Peginterferon α -2b	Immunomodulator	Melanoma	2012	[80]
Ipilimumab	First CTLA-4 Inhibitor	Metastatic Melanoma	2011	[81]
Sipuleucel-T	First therapeutic cancer vaccine	Prostate cancer	2010	[82]
Rituximab	First monoclonal antibody	Non-Hodgkin lymphoma	1997	[83]

1.5.1.2 Immune checkpoint inhibitors

Immune checkpoint inhibitors (ICIs) have emerged as a promising option for cancer treatment [84]. They work by blocking the inhibitory interaction between PD1 and PD-L1 (PD1: programmed cell death-1, on the CTL; PD-L1: PD-ligand 1, on the antigen-presenting cell), since tumor cells utilize PD-L1 overexpression as a tumor escape mechanism to evade T cell killing [85,86]. Another type of ICIs targets cytotoxic T lymphocyte-associated antigen 4 (CTLA-4), a regulatory protein that controls peripheral tolerance in tumor cells [87,88]. The first FDA-approved anti-CTLA-4, anti-PD1, and anti-PD-L1 checkpoint inhibitors to reach the market, all antibodies, were Ipilimumab (2011), Nivolumab (2014), and Atezolizumab (2016), respectively [89–91].

1.5.1.3 Targeted antibodies

Targeted antibodies work by blocking cancer cell function and also directing the immune system towards the target to kill defective cells. They include monoclonal antibodies (mAbs), antibody-drug conjugates (ADCs), and bispecific antibodies [92–94]. Most targeted antibodies are considered passive immunotherapeutics, as they directly target tumor cells rather than stimulate an adaptive immune response in the patient. Some examples are Rituximab (anti-CD20 mAb), Gemtuzumab

ozogamicin (anti-CD33 mAb covalently attached to the cytotoxic calicheamicin), and the only FDA-approved bispecific antibody, Amivantamab [72,95,96].

1.5.1.4 Cancer vaccines

Cancer vaccines function by stimulating the immune system to help prevent or treat cancer. Attenuated cancer cells, proteins or fragments of proteins from cancer cells, or immune cells are used to make cancer vaccines [97]. The FDA has so far approved three vaccines to treat cancer: Sipuleucel-T, a dendritic cell vaccine, for advanced prostate cancer [98]; Talimogene laherparepvec (engineered herpes virus) for melanoma skin cancer; and Bacillus Calmette-Guérin (BCG vaccine) for early-stage bladder cancer. Another class of cancer vaccine in clinical trials are peptide-based vaccines also known as epitope vaccines, which are made from potent immunogenic peptides [99,100]. They promise to be safe and highly specific; they are increasingly used in personalized medicine and frequently combined with other cancer therapies [101][102].

1.5.1.5 Cytokine Therapy

Cytokines are regulatory proteins that control immune cell growth, metabolism, and activation, and thus coordinate immune responses. Cytokine immunotherapy leverages their role as immune modulators [103]. Four cytokine therapies already have FDA approval; the first was the interferon-alpha 2 (IFN- α_2) cytokine in 1986 [104]. Many cytokines are currently in clinical trials [105].

1.6. The role of MHC-I molecules in immunotherapy

1.6.1. Neoantigen identification

Since MHC-I molecules present tumor-related non-self peptides or neoantigens to elicit a cytotoxic T cell response, they are central to developing targeted vaccines and anti-cancer therapy [106]. Neoantigens are defined as novel peptide sequences that are unique to the tumor; they might arise due to point mutations, reading frame shifts, chromosomal translocations, and other mechanisms interfering with the integrity of the cellular DNA. Identification of neoantigens is of great value to therapy as they help in understanding the etiology of the disease, monitoring T cell activation, and in designing diagnostic tools. The success of immunotherapy depends on the efficient identification of immunogenic neoantigens [107]. Recent technological developments in LC-MS/MS-based immunopeptidome analysis, whole-exome sequencing (WES), gene expression studies, in silico epitope prediction, and TCR repertoire sequencing approaches have aided in identification of potential neoantigens (**Figure 1-4**) [108–111]. The experimental evaluation of immunogenicity and further optimization of neoantigen are done with ELISpot assays, MHC multimers, tandem minigenes, and other techniques [107].

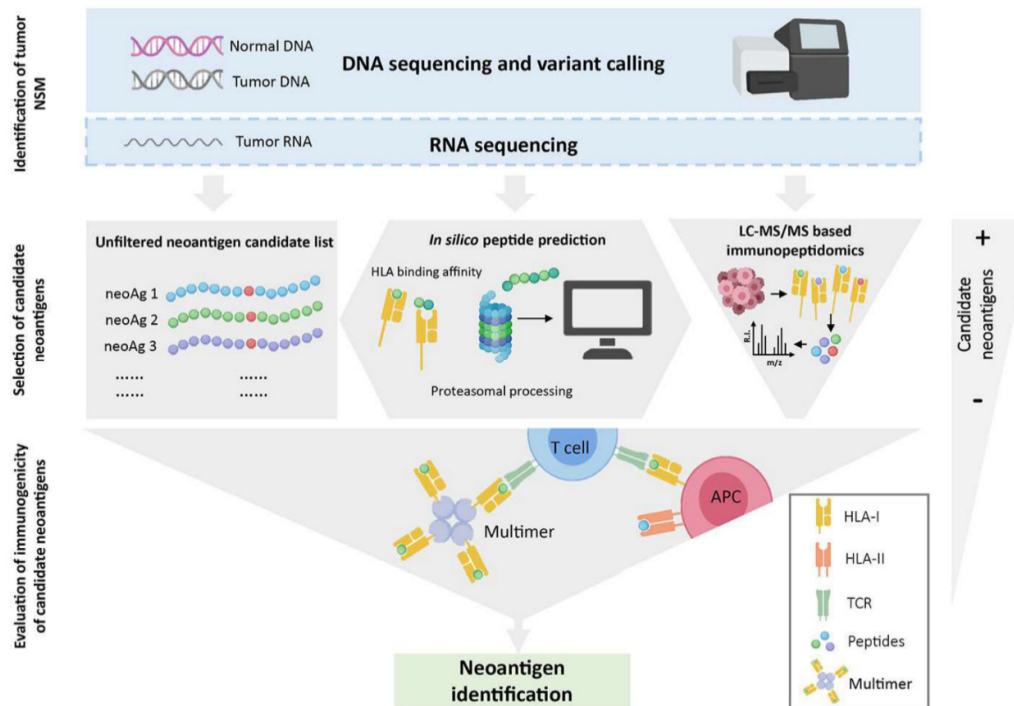


Figure 1-4. Schematics of tumor neoantigen screening process.

Whole-exome or whole-genome sequencing (WES) of tumor and normal DNA are used to identify non-synonymous mutations (NSM). Then, the expression and presentation mutations are filtered by RNA sequencing and MS-based immunopeptidomics, respectively. *In silico* peptide prediction is also applied to identify optimal neoepitopes (i.e., those most tightly binding to class I). After ranking-based sorting of peptides, a selected number of peptides are screened for immunogenicity in different functional assays using pMHC-I multimers. This figure was reused from [107].

1.6.2. pMHC multimers for immuno-monitoring

Immuno-monitoring means the precise evaluation of a patient's immune responses following an immunotherapy treatment. Most immuno-monitoring assays for an antigen-specific response of CD8⁺ T cells in a patient's blood monitor cell proliferation, cell lysis, or release of inflammatory cytokines [112,113].

The only known way to detect individual antigen-specific T cell clones in patient blood is with recombinant pMHCs that bind to their cognate TCRs and thus decorate the surface of the antigen-specific T cell for staining or sorting. Since the TCR-pMHC affinity is very low (in the micromolar range), however, individual pMHC complexes cannot be used to stain T cells as one would stain cells with antibodies. Instead, one uses pMHC multimers that bind more tightly to T cells due to their high avidity [114,115]. Such pMHC multimers can be used to detect even very rare T cell clones in patient samples. The development of vaccines is also influenced by this technology [60].

In 1996, pMHC tetramers (a type of multimers made up of four identical pMHCs held together by non-covalent interactions; see section 2.5.2) were first used to stain antigen-specific CD8⁺ T cells [116,117]. In the past two decades, scientists have expanded the multimer-based technologies towards different biotechnological and commercial applications. pMHC multimers in various manifestations [118] have been used to evaluate the frequency of CD8⁺ T cells specific for tumor-associated or viral antigens, e.g. from melanomas, influenza, or the human immunodeficiency virus (HIV) [116]. Several biotechnology companies produce and sell pMHC multimers, some of them in proprietary formats. Discussed below are the most widely used pMHC multimers.

1.6.2.1 Dimers

In pMHC dimers, immunoglobulin (antibody) HCs, which are naturally dimeric, are used to dimerize class I. For example, the DimerX I reagent from BD Bioscience, an example of commercial pMHC dimers [119], essentially consists of a dimer of recombinant MHC-I HC-immunoglobulin (Ig) fusions, each of which binds one peptide, one Ig light chain (through a disulfide bond), and one non-covalently associated human β_2m molecule [120]. In other constructs, MHC-I HCs are connected to the C_H2 and C_H3 domains of the IgG HCs only.

1.6.2.2 Tetramers

pMHC tetramers are complexes of four biotinylated pMHCs bound to streptavidin, which is labeled with a fluorescent dye [121]. They are produced following the procedure described by Altman *et al.* [116]. Briefly, the MHC-I HC and β_2m are expressed in *E. coli*, purified, and then folded *in vitro* in refolding buffer in the presence of a peptide antigen to produce a soluble monomeric pMHC. The C terminus of the HC is engineered to contain a biotinylation sequence (or AviTag), which is then biotinylated by the ligase called BirA. The purified biotinylated pMHC monomers are then tetramerized by incubating with fluorescently labeled streptavidin to generate pMHC tetramers [122]. Different companies and institutions have a wide range of pMHC tetramers [123–127].

1.6.2.3 Pentamers

Pentamers combine five pMHC monomers that are linked to a coiled-coil multimerization domain, which in turn is linked to a fluorescent dye [128]. pMHC pentamers have been used in the detection of antigen-specific CD8⁺ T cells in flow cytometry [129,130], in tissue staining, and for magnetic isolation of antigen-specific T cells [131]. They are sold by Proimmune (Oxford, UK), and they are licensed for research use only. In 2009, the only clinical use of pentamers was granted for isolating T cells for mother-daughter transfer, for life-saving treatment of EBV-associated lymphoma in the daughter [132].

1.6.2.4 Dextramers

In 2002, Immudex_(Copenhagen, Denmark) developed and trademarked dextramers [133], which consist of a dextran polymer backbone carrying pMHCs and fluorochrome molecules [134]. Dextramer reagents carry in one molecule more pMHCs and fluorophores than conventional MHC multimers, potentially increasing their avidity for the specific T cell and enhancing their staining intensity, which should improve resolution and the signal-to-noise ratio. The company claims that this allows the staining of populations with small cell numbers, which occur in many cancer samples [134,135]. The use of pMHC dextramers has expanded to various species (human, mouse, and rhesus macaque) and diseases such as cancer, viral infections, infections with mycobacterium, and graft-versus-host disease [136,137]. More recently, dextramers have been combined with DNA barcodes to create dCODE® Dextramers, allowing high-throughput screening of multiple T-cell response in a single sample [138,139]. Another dextramer variant was created by combining the easYmer® technology (which allows rapid pMHC generation by the addition of peptide to recombinant class I molecules with pre-formed disulfide bonds) from ImmunAware [140,141], resulting in so-called U-Load Dextramer® MHC reagents [142].

1.6.2.5 Streptamers

Streptamers are very similar to tetramers (see above) in that they consist of four pMHCs. The difference is that the MHC-I HCs are not biotinylated but fused to StrepTag amino acid sequences that bind tightly but non-covalently to fluorescently labeled StrepTactin protein molecules [120,143]. The StrepTag is an eight amino acid sequence with strong binding affinity for StrepTactin, which is a streptavidin derivative. Remarkably, the pMHC/StrepTag complex can be easily and physiologically removed from StrepTactin with biotin. Biotin has a much higher affinity to StrepTactin than the StrepTag, and so it can displace it from the binding site. The StrepTactin tetramer thus breaks up, and the pMHC/StrepTag monomers spontaneously dissociate from the T cells. This resolution technique is not possible with conventional MHC tetramers that use streptavidin (see **section 1.6.2.2**).

Streptamers can be used for isolation of antigen-specific CD8⁺ T cells with StrepTactin coupled to magnetic microbeads (1-3 µm in size) [144]. The StrepTag system is marketed by IBA Lifesciences, Göttingen.

1.7. Generation of pMHC multimers by peptide exchange

1.7.1. Classical generation of multimers

In the first step of multimer generation, MHC-I HC and β_2m (produced in *E.coli* as inclusion bodies and dissolved in denaturing urea or guanidinium buffer) and the peptide of interest are folded together in a suitable refolding buffer in vitro. This is followed by purification of the folded pMHC complex (usually by size-exclusion chromatography), which is then attached to a backbone depending on the type of multimer (for example, streptavidin for tetramers). These backbones usually carry a fluorophore, and hence the appropriate T cell population can be identified and sorted once they are bound to their specific multimers. Since the folding of the monomer with the antigen-specific peptide occurs early in the workflow, this method of generation of multimers takes four to six weeks (when ordered from a company) and must be performed separately for each pMHC combination.

1.7.2. Improved generation of multimers by peptide exchange

The time-consuming production of pMHC-I multimers prevents rapid experimentation or diagnosis. In addition, modern approaches such as the identification of epitopes for tumor T cell immunotherapy require many (sometimes hundreds or thousands) of multimers to be used in a single experiment. Therefore, exchange of the bound peptide for another has been explored by multiple groups to increase speed and flexibility of the pMHC multimer generation. In an exchange workflow, multimers are initially generated in the same classical fashion as described above, with one particular folding peptide that acts as a placeholder. But once the multimers are generated, the folding peptide is exchanged for another peptide of interest. This provides flexibility to the experimenter, since they can use the same stock of multimers to rapidly generate many different pMHC multimers for detecting many different populations of T cells.

There are currently three major ways to perform peptide exchange on class I molecules:

1.7.2.1 *UV-mediated peptide exchange*

The pMHC complex is initially refolded with a peptide that carries one amino acid of a special chemistry that is UV-labile. Through UV irradiation, the UV-labile peptide is then cleaved while bound. Since the obtained peptide fragments no longer meet the length requirement for high-affinity class I binding, they dissociate. When UV treatment is done in the presence of a peptide of interest, this results in an exchange of the cleaved UV-labile peptide for the incoming peptide of interest, yielding a pMHC complex with the latter [145,146].

The disadvantage of UV-mediated peptide exchange is that low UV penetration and variability in UV irradiation often led to only partial cleavage of the UV-labile peptide, with inefficient peptide

exchange. In addition, irradiation may cause damage to the protein complex, and much of the work needs to be performed in the dark.

1.7.2.2 Chemo-labile ligand-mediated peptide exchange

In this method, MHC-I folding is done with a chemically modified peptide sequence, which is labile to oxidizing (e.g., periodic acid) or reducing agents (e.g., sodium dithionite). So, the peptide bound to the complex can be chemically cleaved and exchanged with a chemically stable and high-affinity test peptide [147,148].

The disadvantage of this technique is that high concentrations of reagents (often in the millimolar range) are required to accomplish complete cleavage of the folding peptide, and extended incubation time may cause chemical modification of amino acid residues, leading to instability and denaturation of pMHC complexes. Moreover, the exchange is usually partial and inefficient, which can put the result of the subsequent analysis in question.

1.7.2.3 Dipeptide-catalyzed peptide exchange

In this method, which was invented and established by our research group, MHC-I are folded in the presence of a low-affinity peptide and subsequently purified as in the classical method. Then, peptide exchange is performed with a high-affinity peptide of interest in the presence of an allotype-specific exchange dipeptide, which acts as a catalyst and accelerates the exchange rate [149,150]. It was hypothesized that the catalytic dipeptide binds into the F pocket, displacing the C terminus of the pre-bound peptide and facilitating its dissociation [149] (**Figure 1-5**), but binding of the dipeptide to the A and/or B pockets is also possible. Crystal structures of MHC-I with dipeptides in the F pocket [151] and in the A/B pockets [152] have been published.

Dipeptide-catalyzed peptide exchange is robust and efficient, with 92-96% exchange shown for wtA2 with different full-length peptides [149]. In 2017, a company took a license from Jacobs University and launched a commercial product for tetramer generation based on this technology [153–155]. Using this method, new specific tetramers can be generated within 4 hours, with a cleverly designed subsequent test for exchange efficiency. Unlike the methods discussed above, there is no need for UV irradiation or the addition of hazardous reducing or oxidizing agents for the exchange reaction so that the class I molecules remain untouched and intact.

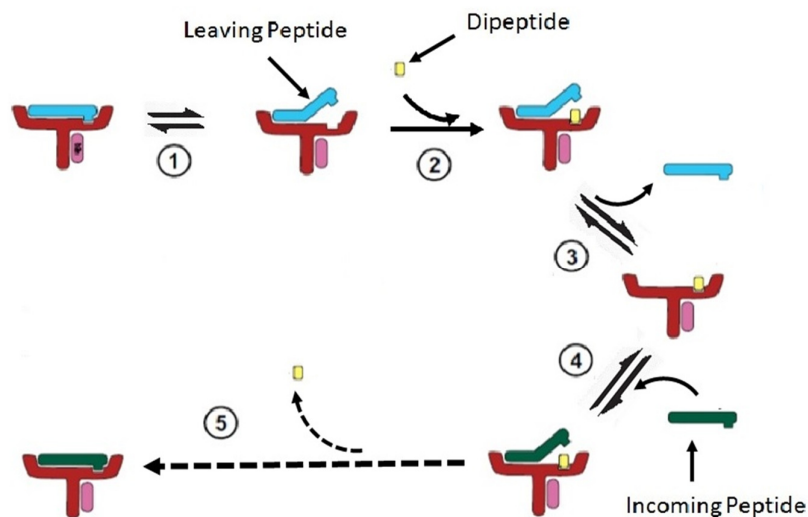


Figure 1-5. Hypothetical mechanistic model of dipeptide-catalyzed peptide exchange on MHC-I.

pMHC complexes are first prepared with low-affinity peptides. The C terminus of an MHC-I-bound peptide spontaneously dissociates and reassociates [2], just like the N terminus (not shown). Due to its high concentration, the dipeptide can bind into the F pocket and prevent the C terminus of the pre-bound peptide from re-binding. Thus, the pre-bound peptide is now only bound by its N terminus in an equilibrium reaction that is much more on the side of dissociation [4] (3). The incoming high-affinity can now bind to MHC-I [5]; the dipeptides and leaving peptides can be removed by size exclusion or with filters. *Figure modified from Saini et al. [149].*

1.7.2.4 Temperature-mediated peptide exchange

A recently described alternative method of multimer generation is temperature-mediated peptide exchange [156,157]. The concept relies on the observation that low-affinity peptides bind stably to MHC-I at a lower temperature but dissociate when the temperature increases and can then be replaced with high-affinity peptides [158,159]. So, ready-to-use conditional pMHC multimers can be generated at low temperature (such as 4 °C) and then exchanged with suitable higher-affinity peptides by increasing the temperature. The proof-of-concept studies were successfully performed for H-2K^b and HLA-A*02:01 multimers. This method has not yet been commercialized.

1.7.2.5 Chaperone-mediated peptide exchange

Tapasin is a chaperone and an essential part of the PLC. It stabilizes empty peptide-receptive MHC-I molecules and modulates the exchange of low-affinity peptides for high-affinity peptides. Peptide editing can only happen when tapasin is associated with Erp57, another component of the PLC [9,160,161]. Recently, another tapasin homolog called TAP binding protein-related (TAPBPR) was discovered and shown to catalyze peptide exchange on MHC-I [162–164]. Interestingly, TAPBPR does not engage with PLC and can function independently [165]. Boyle and co-workers have demonstrated that *in vitro* peptide exchange can be catalyzed by recombinant TAPBPR [166], and

Sgourakis and collaborators have generated a high-throughput MHC-I tetramer library by peptide exchange catalyzed by TAPBPR [167].

1.8. MHC-I disulfide mutants as empty peptide-receptive molecules

Disulfide bonds occur in more than one third of eukaryotic proteins, especially in cell surface and secreted ones, and they support protein stability and folding [168,169]. For the last few decades, researchers and biotechnologists have engineered proteins (e.g., enzymes, antibodies, etc.) in vitro by introducing additional disulfide bonds to increase their activity, stability, yield, and half-life [170–172]. These proteins have found widespread application commercially and in research. Bioinformatics prediction tools such as Disulfide by Design (DbD) [173], DISULFIND [174], Yosshi [175], DiANNA [176], etc., are currently available for designing disulfide-modified proteins. Molecular dynamics (MD) simulations are also frequently applied to predict the flexible regions of a protein that might unfold early such that they would profit from stabilization by disulfide bonds [177].

For MHC-I proteins, thermal and conformational stability depend on peptide binding affinity. In the absence of peptides, the peptide binding site of empty MHC-I molecules is conformationally unstable and flexible [178,179]. This has been so far a major limitation for the study of MHC-I, since structural information for the empty state was unavailable. Also, it was not possible to conduct classical equilibrium-based MHC-I/peptide affinity measurements, since for such measurements, stable forms of the ligand-occupied as well as the ligand-free receptor are required. Thus, true equilibrium dissociation constant (K_d) values could not be derived in biochemical experiments with isolated components. This is a problem because peptide-class I binding affinity is certainly a factor in the selection of T cells for almost any cellular immune response, including against tumours. As a result, researchers have used the kinetic dissociation rate constant to rank peptides by affinity [180]. Alternatively, they have calculated the K_d from association and dissociation rates, which is dubious, since class I molecules change their conformation upon peptide binding, such that binding kinetics do not necessarily follow the law of mass action [181]. Still, today, researchers rely mainly on in silico predictions for peptide affinity calculation, which are made by neuronal network software trained with the results of such binding assays [182]. For gold-standard measurements, empty stable MHC-I proteins are desirable.

Another field where empty stable MHC-I might be very useful is the generation of many MHC-I multimers for research and clinical use (section 1.6). This is currently still a bottleneck in their use. An easy way around the peptide exchange methods (section 1.7.) would be to generate empty stable

recombinant MHC-I multimers and use them to rapidly generate pMHC multimers for peptide-specific T cell staining.

Since 2004, the Springer group have extensively studied the structure of MHC-I molecules by MD simulation and x-ray crystallography and observed that the F pocket region of the peptide binding groove is highly conformationally flexible in the absence of peptide [17,183]. They engineered a novel disulfide linkage between the α_1 and α_2 helices by mutating positions Y84 and A139 of H-2K^b to cysteines [184]. The resulting H-2K^b(Y84C/A139C) (in the following termed dsH-2K^b, for disulfide-stabilized) demonstrated higher thermal stability in the absence of peptide than wtH2-K^b. The crystal structure of dsH-2K^b showed near-perfect superposition with wtH-2K^b. In wild-type cells, dsH-2K^b binds peptide in the ER and travels to the cell surface for presentation. However, in TAP-deficient cells, where peptide loading to MHC-I is abrogated, dsH-2K^b can still pass the cellular quality control machinery and travel to the cell surface in the empty state. At the cell surface, unlike wtH-2K^b, dsH-2K^b is stable and resistant to endocytosis even in an empty state, because of its strongly increased affinity to β_2m , which by an unknown mechanism prevents endocytic destruction [185].

1.8.1. Refolding, detection, and generation of empty MHC-I molecules

In vitro refolding of human wtA2 and mouse wtH-2K^b in the presence of dipeptides glycyl-leucine (GL) and glycyl-methionine (GM) was previously demonstrated by our group [150]. These wild type MHC-I proteins remained stable and peptide-receptive as long as the dipeptide (usually 5-10 mM) was maintained in the buffer. Likewise, we demonstrated that disulfide-stabilized A*02:01 (dsA2) could be folded with dipeptide. Due to their low binding affinities (≈ 10 mM), dipeptides are easily washed away during the purification process, and this results in stable empty peptide-receptive MHC-I molecules [150]. Anjanappa et al. have extensively discussed the peptide-empty dsA2 crystal structure [152].

1.8.2. Empty MHC-I molecules for clinical application and their benefits

From peptide-empty dsA2 monomers prepared as described above, we have recently generated empty MHC-I tetramers and later loaded them with the peptide of interest to detect antigen-specific T cells. Tetramers generated from disulfide-stabilized A*02:01, A*24:02 and H-2K^b monomers were specific and efficient in antigen-specific T cell detection. No difference in the TCR fingerprint for peptide recognition was visible between wtA2 and dsA2, which is unsurprising since the new disulfide bond is far away from the footprint of the TCR [186].

The primary benefits of empty-loadable MHC-I multimers are as follows:

- a) Rapid generation of peptide-specific multimers is achieved by simply adding the peptide of interest to the vial containing these empty-loadable MHC-I multimers.
- b) As the proteins are disulfide-stabilized, they do not require full-length peptides for folding and storage. Empty multimers can be frozen at -20 °C and still remain peptide-receptive after prolonged storage.
- c) Researchers have observed improved T cell staining (i.e., an increased staining index) with empty loadable dsA2 compared to multimers generated by UV exchange [186]; the reason for this improved quality is not yet known.
- d) Empty loadable dsA2 binds low-affinity peptides, allowing the generation of multimers with peptides that do not efficiently refold A2 in vitro, and that bind inefficiently in the exchange protocols [186]. This might be of use for detecting T cells that are specific for low-affinity sub-dominant tumor neoantigens.

In a separate study, using our dsA2 molecule, our industrial collaborators produced a diverse library of pMHCs and used them to measure the binding of bispecific TCR molecules in a high-throughput safety screen approach [187]. Other biologics targeting pMHCs, such as monoclonal antibodies or bispecifics, might benefit from this approach. These findings highlight the potential of such disulfide-stabilized MHC-I molecules in the rapidly growing field of pMHC-targeting biologics.

With the patented disulfide technology, in collaboration with Sine Hadrup and Sunil Kumar Saini from Denmark Technical University, the Springer group created a start-up company named Tetramer Shop in 2019 [188]. In 2021, Tetramer Shop was acquired by 10x Genomics [189].

1.9. Aim and scope of the thesis work

The scope of this thesis is as follows:

- a) To identify dipeptides and/or small molecules for peptide exchange and refolding of important allotypes other than wtA2 and wtH-2K^b. This was the initial aim of the project as a follow-up to the proof-of-concept study of Saini et al. [149,150]. Since exchange dipeptides are allotype-specific, they need to be discovered individually for each allotype.
- b) To study the mechanism of chaperone-independent peptide-exchange and develop an alternative universal way to exchange peptides.
- c) To develop novel methods for studying protein stability and peptide binding, such as nano differential scanning fluorimetry (nanoDSF) and microscale thermophoresis (MST).

The results from my screening studies and developed methods will allow us to use our disulfide-stabilized MHC-I molecules for commercial and clinical purposes.

1.10. Overview of the chapters of this thesis

For my PhD thesis, I have studied the kinetics and mechanism of peptide binding and exchange on several allotypes of MHC-I molecules. For the first part of my project, I focused on the dipeptide-mediated peptide exchange that was previously developed in our laboratory. Saini et al. demonstrated that allotype-specific dipeptides (such as GL and GM for A2) are required for the generation of tetramers using this peptide exchange method [149]. They also showed that these same dipeptides can assist in the refolding of MHC-I molecules. I further optimized the parameters for the fluorescence anisotropy assay and screened a panel of short peptides to identify appropriate di- or tripeptides for folding and peptide exchange on several clinically relevant MHC-I allotypes. I also developed a cELISA method to screen such short peptides. With this work, I was able to identify suitable short peptides for some of the allotypes. I have also discovered alternative methods of peptide exchange, for example using acidic pH and small molecules such as ethanol.

Next, I optimized the NanoDSF method to study the thermal and chemical stability of pMHC-I complexes. I have also developed a novel MST-based method to measure the peptide affinity *in vitro*. This was only possible with our disulfide-stabilized empty MHC-I molecules. Until recently, researchers had to rely on NetMHC prediction values, which were misleading on several occasions.

In this thesis, the results are described in six major sections (**chapters 3 to 9**). **Chapters 3 and 4** describe the developed methods and screening results which are the key to the further studies in the following sections. **Chapter 5 to 8** describe the research findings, they are published papers. Additional unpublished findings about alternative peptide exchange methods are mentioned in **chapter 9**, which is a manuscript in preparation. Whenever required, sections were divided into sub-sections for simplicity. Brief summaries of these chapters follow.

1.10.1. Summary of chapter 3

In this section, I describe the development of a cELISA assay for screening di- and tripeptides that stabilize and promote MHC-I refolding. The method is based on the competitive binding of di-/tripeptide stabilized MHC-I molecules in the folded conformation to the mAb W6/32. The refolding efficiency was calculated from the standard curve generated from the dose-response curve of a standard A2/NV9 complex. The optimization of various assay parameters is also reported in this section. The screening results are listed in section 3.5.

1.10.2. Summary of chapter 4

Chapter 4 discusses the different methods I have used to monitor the kinetics of peptide exchange and binding to MHC-I molecules. Section 4.2 introduces various kinetic parameters that we have applied throughout our studies and data analysis. The later sections applied these basic considerations in the curve fitting according to suitable kinetic models. In section 4.3, I report on the application of the fluorescence anisotropy assay for monitoring peptide exchange on MHC-I molecules. I summarize the results from screening dipeptides as modulators of peptide exchange on several MHC-I allotypes. In section 4.4, I present an MST-based MHC-I - peptide binding assay as a novel approach to monitor the affinities *in vitro*. This work is a part of ongoing project with Technical University of Denmark and the company, Nanotemper Technologies.

1.10.3. Summary of chapter 5

In this section, I demonstrate the use of nanoscale differential scanning fluorimetry (nanoDSF), a method that uses the tryptophan and tyrosine fluorescence of MHC-I molecules to measure the denaturation temperature of proteins, for thermal and chemical stability measurements of various pMHC-Is. I use this method to study the molecular mechanism of the thermal denaturation of A2. I also demonstrate how the thermal stability is influenced by various physical parameters such as buffer, solvent, heating rate, protein concentration, peptide affinity, peptide concentration, and storage conditions. This chapter contains published original data.

The full citation of the paper is:

Ankur Saikia and Sebastian Springer: Peptide-MHC-I complex stability measured by nanoscale differential scanning fluorimetry reveals molecular mechanism of thermal denaturation. *Molecular Immunology* **136** (2021), 73–81,
DOI: 10.1016/j.molimm.2021.04.028

For this and the other published papers and manuscripts, my contributions to the work are described more precisely at the beginning of the respective chapter.

1.10.4. Summary of chapter 6

This chapter consists of a published paper that presents the use of empty, functional, and peptide-receptive MHC-I tetramers as an efficient, fast method to stain peptide-specific T cells from melanoma patients. The data demonstrates that the dsA2 can be purified in the empty, loadable conformation after initial *in vitro* refolding with the dipeptide GM. We also demonstrated that these empty A2 molecules can be used to generate tetramers that remain in a peptide-receptive state, resistant to several freeze-thaw cycles, during long-term storage at -80 °C. These dsA2 tetramers provide a superior T cell staining index when compared to wtA2 tetramers. The comparison of the crystal structures of dsA2 and wtA2 bound to the NV9 peptide confirms an almost perfect overlap, suggesting that the 84-139 disulfide bond modification does not alter the conformation of the protein. The T cell fingerprint analysis also confirms that the TCR recognition pattern for dsA2 remains comparable to wtA2.

The full citation of the paper is:

Saini, S. K. et al. Empty peptide-receptive MHC class I molecules for efficient detection of antigen-specific T cells. *Sci. Immunol.* **4**, eaau9039 (2019).

DOI: 10.1126/sciimmunol.aau9039.

1.10.5. Summary of chapter 7

This chapter consists of a published paper we describe the high throughput screening (HTS) of ligands for TRC using empty dsA2 molecules. The data describes the generation of empty peptide-receptive dsA2 monomers, immobilization on biosensor surface, for performing the high-throughput affinity measurement of TCRs or TCR-like molecules using bio-layer interferometry. We also confirmed that the crystal structure of wtA2/TCR complex and dsA2/TCR 1G4 complex were identical in conformation. The disulfide bond (Y84C/A139C) significantly increases the dsA2 peptide binding groove's conformational stability but does not alter the peptide specificity and binding of soluble TCR to pMHC-I complexes. Since this method facilitates quick generation of pMHC-I libraries, a screening platform can be established to select the promising neoepitopes early during process development.

The full citation of the paper is:

Moritz, A. et al. High-throughput peptide-MHC complex generation and kinetic screenings of TCRs with peptide-receptive HLA-A*02:01 molecules. *Sci. Immunol.* **4**, eaav0860 (2019). DOI: 10.1126/sciimmunol.aav0860.

1.10.6. Summary of chapter 8

This chapter highlights the published paper about mapping the peptide binding groove of MHC-I molecules using native mass spectrometry based approach. Here, we analyse the binding of different truncated or modified version of a high affinity peptide NV9 to an empty dsA2 molecule. This novel approach allowed us to understand the binding affinity of pMHC complexes loaded with charged-reduced or truncated peptides and thereby map the favoured binding positions in the peptide. We found that both anchor residues at A pocket and F pocket of peptide binding groove can accommodate two peptides independently. Finally, we propose this method as an alternative to measure peptide affinity *in-vitro* to the widely used *in-silico* prediction tools.

The full citation of the paper is:

Kopicki et al. Mapping the peptide binding groove of MHC class I. *bioRxiv*, 2021.08.12.455998; doi: 10.1101/2021.08.12.455998

1.10.7. Summary of chapter 9

In this chapter, we tried to dissect molecular mechanism of chaperone-independent peptide exchange. We also propose an alternative method for peptide exchange triggered by acidic pH of the reaction buffer on A2 and A24 allotypes. We demonstrate that both allotype have different sensitivities towards acidification. We use this observation to dissect the individual steps of the exchange reaction. We demonstrate that acidification promotes both peptide dissociation and association, but not by destabilization of the peptide-MHC-I complex, as previously suggested. Further, we find evidence for the electrostatic attraction of the incoming peptide onto certain MHC-I allotypes, revealing that long-range interactions may influence peptide exchange. We also find that dipeptides support peptide exchange on MHC-I by two mechanisms, namely first by promoting the dissociation of the pre-bound peptide and second by stabilizing the peptide-free MHC-I intermediate.

1.11. References

- [1] Schneeweiss, C., Garstka, M., Smith, J., Hütt, M.T., Springer, S., The mechanism of action of tapasin in the peptide exchange on MHC class I molecules determined from kinetics simulation studies. *Mol. Immunol.* 2009, 46, 2054–2063.
- [2] Rammensee, H.G., Falk, K., Rötzschke, O., Peptides naturally presented by MHC class I molecules. *Annu. Rev. Immunol.* 1993, 11, 213–244.
- [3] Stevanovic, S., Schild, H., Quantitative aspects of T cell activation - peptide generation and editing by MHC class I molecules. *Semin. Immunol.* 1999, 11, 375–384.
- [4] Germain, R.N., MHC-dependent antigen processing and peptide presentation: Providing ligands for T lymphocyte activation. *Cell* 1994, 76, 287–299.
- [5] York, I.A., Rock, K.L., Antigen processing and presentation by the class I major histocompatibility complex. *Annu. Rev. Immunol.* 1996, 14, 369–396.
- [6] Momburg, F., Hämmerling, G.J., Generation and TAP-Mediated Transport of Peptides for Major Histocompatibility Complex Class I Molecules. *Adv. Immunol.* 1998, 68, 191–256.
- [7] MR, L., MF, C.-D., DY, T., DB, W., Localization of the lectin, ERp57 binding, and polypeptide binding sites of calnexin and calreticulin. *J. Biol. Chem.* 2002, 277, 29686–29697.
- [8] Michalek, M.T., Grant, E.P., Gramm, C., Goldberg, A.L., Rock, K.L., A role for the ubiquitin-dependent proteolytic pathway in MHC class I-restricted antigen presentation. *Nature* 1993, 363, 552–554.
- [9] Cresswell, P., Bangia, N., Dick, T., Diedrich, G., The nature of the MHC class I peptide loading complex. *Immunol. Rev.* 1999, 172, 21–28.
- [10] Garbi, N., Tiwari, N., Momburg, F., Hämmerling, G.J., A major role for tapasin as a stabilizer of the TAP peptide transporter and consequences for MHC class I expression. *Eur. J. Immunol.* 2003, 33, 264–273.
- [11] Koopmann, J.-O., Post, M., Neefjes, J.J., Hämmerling, G.J., Momburg, F., Translocation of long peptides by transporters associated with antigen processing (TAP). *Eur. J. Immunol.* 1996, 26, 1720–1728.
- [12] Wearsch, P.A., Cresswell, P., The quality control of MHC class I peptide loading 2008, 20.
- [13] Rock, K.L., Reits, E., Neefjes, J., Present Yourself! By MHC Class I and MHC Class II Molecules. *Trends Immunol.* 2016, 37, 724–737.
- [14] Maffei, A., Papadopoulos, K., Harris, P.E., MHC class I antigen processing pathways. *Hum. Immunol.* 1997, 54, 91–103.
- [15] Embgenbroich, M., Burgdorf, S., Current Concepts of Antigen Cross-Presentation. *Front. Immunol.* 2018, 0, 1643.
- [16] Fonteneau, J.F., Kavanagh, D.G., Lirvall, M., Sanders, C., et al., Characterization of the MHC class I cross-presentation pathway for cell-associated antigens by human dendritic cells. *Blood* 2003, 102, 4448–4455.
- [17] Abualrous, E.T., Saini, S.K., Ramnarayan, V.R., Ilca, F.T., et al., The Carboxy Terminus of the Ligand Peptide Determines the Stability of the MHC Class I Molecule H-2Kb: A Combined Molecular Dynamics and Experimental Study. *PLoS One* 2015, 10, e0135421.
- [18] Bjorkman, P.J., Saper, M.A., Samraoui, B., Bennett, W.S., et al., Structure of the human class I histocompatibility antigen, HLA-A2. *Nature* 1987, 329, 506–512.
- [19] Falk, K., Rötzschke, O., Stevanović, S., Jung, G., Rammensee, H.G., Allele-specific motifs revealed by sequencing of self-peptides eluted from MHC molecules. *Nature* 1991, 351, 290–296.
- [20] Krüger, T., Schoor, O., Lemmel, C., Kraemer, B., et al., Lessons to be learned from primary renal cell carcinomas: novel tumor antigens and HLA ligands for immunotherapy. *Cancer Immunol. Immunother.* 2004 549 2004, 54, 826–836.
- [21] Hunt, D.F., Henderson, R.A., Shabanowitz, J., Sakaguchi, K., et al., Characterization of peptides bound to the class I MHC molecule HLA-A2.1 by mass spectrometry. *Science (80-)*. 1992, 255, 1261–1263.
- [22] Bleek, G.M. Van, Nathenson, S.G., Isolation of an endogenously processed immunodominant viral peptide from the class I H-2Kb molecule. *Nat.* 1990 3486298 1990, 348, 213–216.

- [23] Hassan, C., Chabrol, E., Jahn, L., Kester, M.G.D., et al., Naturally processed non-canonical HLA-A*02:01 presented peptides. *J. Biol. Chem.* 2015, 290, 2593–2603.
- [24] Stryhn, A., Pedersen, L.Ø., Holm, A., Buus, S., Longer peptide can be accommodated in the MHC class I binding site by a protrusion mechanism.
- [25] Matsumura, M., Fremont, D.H., Peterson, P.A., Wilson, Ian A., Emerging Principles for the Recognition of Peptide Antigens by MHC Class I Molecules. *Science (80-)*. 1992, 257, 927–934.
- [26] Fahnestock, M.L., Johnson, J.L., Feldman, R.M.R., Tsomides, T.J., et al., Effects of Peptide Length and Composition on Binding to an Empty Class I MHC Heterodimer. *Biochemistry* 2002, 33, 8149–8158.
- [27] Bouvier, M., Wiley, D.C., Importance of peptide amino and carboxyl termini to the stability of MHC class I molecules. *Science (80-)*. 1994, 265, 398–402.
- [28] Liu, J., Gao, G.F., in: *eLS*, Wiley, 2011.
- [29] Stern, L.J., Wiley, D.C., Antigenic peptide binding by class I and class II histocompatibility proteins. *Structure* 1994, 2, 245–251.
- [30] Jones, E.Y., Tormo, J., Reid, S.W., Stuart, D.I., Recognition surfaces of MHC class I. *Immunol. Rev.* 1998, 163, 121–128.
- [31] Nguyen, A.T., Szeto, C., Gras, S., The pockets guide to HLA class I molecules. *Biochem. Soc. Trans.* 2021.
- [32] Johansen, T.E., Mccullough, K., Catipovic, B., Su, X.-M., et al., Peptide Binding to MHC Class I is Determined by Individual Pockets in the Binding Groove. *Scand. J. Immunol.* 1997, 46, 137–146.
- [33] Jardetzky, T.S., Lane, W.S., Robinson, R.A., Madden, D.R., Wiley, D.C., Identification of self peptides bound to purified HLA-B27. *Nat. 1991 3536342* 1991, 353, 326–329.
- [34] Zhang, C., Anderson, A., DeLisi, C., Structural principles that govern the peptide-binding motifs of class I MHC molecules. *J. Mol. Biol.* 1998, 281, 929–947.
- [35] Parker, K.C., Coligan, J.E., Biddison, W.E., Pocket Mutations of HLA-B27 Show That Anchor Residues Act Cumulatively To Stabilize Peptide Binding. *Biochemistry* 1994, 33, 7736–7743.
- [36] Fremont, D.H., Stura, E.A., Matsumura, M., Peterson, P.A., Wilson, I.A., Crystal structure of an H-2Kb-ovalbumin peptide complex reveals the interplay of primary and secondary anchor positions in the major histocompatibility complex binding groove. *Proc. Natl. Acad. Sci.* 1995, 92, 2479–2483.
- [37] Guo, H.C., Madden, D.R., Silver, M.L., Jardetzky, T.S., et al., Comparison of the P2 specificity pocket in three human histocompatibility antigens: HLA-A*6801, HLA-A*0201, and HLA-B*2705. *Proc. Natl. Acad. Sci.* 1993, 90, 8053–8057.
- [38] IPD-IMGT/HLA Database.
- [39] The Major Histocompatibility Complex (MHC) | Boundless Microbiology.
- [40] Pierini, F., Lenz, T.L., Divergent Allele Advantage at Human MHC Genes: Signatures of Past and Ongoing Selection. *Mol. Biol. Evol.* 2018, 35, 2145.
- [41] Fiorillo, M.T., Paladini, F., Tedeschi, V., Sorrentino, R., HLA Class I or Class II and Disease Association: Catch the Difference If You Can. *Front. Immunol.* 2017, 0, 1475.
- [42] Mallal, S., Nolan, D., Witt, C., Masel, G., et al., Association between presence of HLA-B*5701, HLA-DR7, and HLA-DQ3 and hypersensitivity to HIV-1 reverse-transcriptase inhibitor abacavir. *Lancet* 2002, 359, 727–732.
- [43] Hetherington, S., Hughes, A.R., Mosteller, M., Shortino, D., et al., Genetic variations in HLA-B region and hypersensitivity reactions to abacavir. *Lancet* 2002, 359, 1121–1122.
- [44] Quiros-Roldan, E., Gardini, G., Properzi, M., Ferraresi, A., et al., Abacavir adverse reactions related with HLA-B*57:01 haplotype in a large cohort of patients infected with HIV. *Pharmacogenet. Genomics* 2020, 167–174.
- [45] The Allele Frequency Net Database. <http://www.allelefrequencies.net/tools/Report.aspx>.
- [46] D'amato, M., Fiorillo, M.T., Carcassi, C., Mathieu, A., et al., Relevance of residue 116 of HLA-B27 in determining susceptibility to ankylosing spondylitis. *Eur. J. Immunol.* 1995, 25, 3199–3201.
- [47] Paladini, F., Fiorillo, M.T., Tedeschi, V., Cauli, A., et al., Ankylosing Spondylitis: A Trade Off of HLA-B27, ERAP, and Pathogen Interconnections? Focus on Sardinia. *Front. Immunol.* 2019, 0, 35.
- [48] Ziegler, A., Loll, B., Misselwitz, R., Uchanska-Ziegler, B., Implications of Structural and

- Thermodynamic Studies of HLA-B27 Subtypes Exhibiting Differential Association with Ankylosing Spondylitis. *Adv. Exp. Med. Biol.* 2009, 649, 177–195.
- [49] Fabian, H., Huser, H., Loll, B., Ziegler, A., et al., HLA-B27 heavy chains distinguished by a micropolymorphism exhibit differential flexibility. *Arthritis Rheum.* 2010, 62, 978–987.
- [50] Evans, D.M., Spencer, C.C.A., Pointon, J.J., Su, Z., et al., Interaction between ERAP1 and HLA-B27 in ankylosing spondylitis implicates peptide handling in the mechanism for HLA-B27 in disease susceptibility. *Nat. Genet.* 2011 438 2011, 43, 761–767.
- [51] McGonagle, D., Aydin, S.Z., Gül, A., Mahr, A., Direskeneli, H., 'MHC-I-opathy'- unified concept for spondyloarthritis and Behçet disease. *Nat. Rev. Rheumatol.* 2015 1112 2015, 11, 731–740.
- [52] Verity, D.H., Marr, J.E., Ohno, S., Wallace, G.R., Stanford, M.R., Behçet's disease, the Silk Road and HLA-B51: historical and geographical perspectives. *Tissue Antigens* 1999, 54, 213–220.
- [53] Chen, L., Tsai, T.-F., HLA-Cw6 and psoriasis. *Br. J. Dermatol.* 2018, 178, 854–862.
- [54] Prinz, J.C., Human Leukocyte Antigen-Class I Alleles and the Autoreactive T Cell Response in Psoriasis Pathogenesis. *Front. Immunol.* 2018, 0, 954.
- [55] Nair, R.P., Stuart, P.E., Nistor, I., Hiremagalore, R., et al., Sequence and Haplotype Analysis Supports HLA-C as the Psoriasis Susceptibility 1 Gene. *Am. J. Hum. Genet.* 2006, 78, 827–851.
- [56] Zhang, Y., Peng, Y., Yan, H., Xu, K., et al., Multilayered Defense in HLA-B51–Associated HIV Viral Control. *J. Immunol.* 2011, 187, 684–691.
- [57] Pereyra, F., Jia, X., McLaren, P.J., Telenti, A., et al., The major genetic determinants of HIV-1 control affect HLA class I peptide presentation. *Science (80-.).* 2010, 330, 1551–1557.
- [58] Schneidewind, A., Brockman, M.A., Sidney, J., Wang, Y.E., et al., Structural and Functional Constraints Limit Options for Cytotoxic T-Lymphocyte Escape in the Immunodominant HLA-B27-Restricted Epitope in Human Immunodeficiency Virus Type 1 Capsid. *J. Virol.* 2008, 82, 5594–5605.
- [59] Immunotherapy | Memorial Sloan Kettering Cancer Center.
- [60] Farkona, S., Diamandis, E.P., Blasutig, I.M., Cancer immunotherapy: the beginning of the end of cancer? *BMC Med.* 2016, 14, 73.
- [61] Stambrook, P.J., Maher, J., Farzaneh, F., Cancer Immunotherapy: Whence and Whither. *Mol. Cancer Res.* 2017, 15, 635–650.
- [62] Tey, S.-K., Bollard, C.M., Heslop, H.E., Adoptive T-cell transfer in cancer immunotherapy. *Immunol. Cell Biol.* 2006, 84, 281–289.
- [63] Wang, Z., Cao, Y.J., Adoptive Cell Therapy Targeting Neoantigens: A Frontier for Cancer Research. *Front. Immunol.* 2020, 0, 176.
- [64] Wang, S., Sun, J., Chen, K., Ma, P., et al., Perspectives of tumor-infiltrating lymphocyte treatment in solid tumors. *BMC Med.* 2021 191 2021, 19, 1–7.
- [65] Lee, S., Margolin, K., Tumor-Infiltrating Lymphocytes in Melanoma. *Curr. Oncol. Reports* 2012 145 2012, 14, 468–474.
- [66] Urbanska, K., Lynn, R.C., Stashwick, C., Thakur, A., et al., Targeted cancer immunotherapy via combination of designer bispecific antibody and novel gene-engineered T cells. *J. Transl. Med.* 2014, 12, 347.
- [67] Feins, S., Kong, W., Williams, E.F., Milone, M.C., Fraietta, J.A., An introduction to chimeric antigen receptor (CAR) T-cell immunotherapy for human cancer. *Am. J. Hematol.* 2019, 94, S3–S9.
- [68] Fischer, J.W., Bhattarai, N., CAR-T Cell Therapy: Mechanism, Management, and Mitigation of Inflammatory Toxicities. *Front. Immunol.* 2021, 0, 2423.
- [69] Adoptive Cell Therapy: CAR T, TCR, TIL, NK – Cancer Research Institute (CRI).
- [70] FDA approval brings first gene therapy to the United States | FDA.
- [71] FDA approves CAR-T cell therapy to treat adults with certain types of large B-cell lymphoma | FDA.
- [72] FDA grants accelerated approval to amivantamab-vmjw for metastatic non-small cell lung cancer | FDA.
- [73] FDA approves idecabtagene vicleucel for multiple myeloma | FDA.
- [74] Gelderblom, H., Sande, M. van de, Pexidartinib: first approved systemic therapy for patients with tenosynovial giant cell tumor. <https://doi.org/10.2217/fo-2020-0542> 2020, 16, 2345–2356.
- [75] Prasad, V., Tisagenlecleucel — the first approved CAR-T-cell therapy: implications for payers and

- policy makers. *Nat. Rev. Clin. Oncol.* 2018, 15, 11–12.
- [76] FDA approves atezolizumab for PD-L1 positive unresectable locally advanced or metastatic triple-negative breast cancer | FDA.
- [77] Bommareddy, P.K., Patel, A., Hossain, S., Kaufman, H.L., Talimogene Laherparepvec (T-VEC) and Other Oncolytic Viruses for the Treatment of Melanoma. *Am. J. Clin. Dermatology* 2016 181 2016, 18, 1–15.
- [78] Raedler, L.A., Keytruda (Pembrolizumab): First PD-1 Inhibitor Approved for Previously Treated Unresectable or Metastatic Melanoma. *Am. Heal. Drug Benefits* 2015, 8, 96.
- [79] Amiri-Kordestani, L., Blumenthal, G.M., Xu, Q.C., Zhang, L., et al., FDA Approval: Ado-Trastuzumab Emtansine for the Treatment of Patients with HER2-Positive Metastatic Breast Cancer. *Clin. Cancer Res.* 2014, 20, 4436–4441.
- [80] Herndon, T.M., Demko, S.G., Jiang, X., He, K., et al., U.S. Food and Drug Administration Approval: Peginterferon-alfa-2b for the Adjuvant Treatment of Patients with Melanoma. *Oncologist* 2012, 17, 1323–1328.
- [81] Lipson, E.J., Drake, C.G., Ipilimumab: An Anti-CTLA-4 Antibody for Metastatic Melanoma. *Clin. Cancer Res.* 2011, 17, 6958–6962.
- [82] Kantoff, P.W., Higano, C.S., Shore, N.D., Berger, E.R., et al., Sipuleucel-T Immunotherapy for Castration-Resistant Prostate Cancer. <http://dx.doi.org/10.1056/NEJMoa1001294> 2010, 363, 411–422.
- [83] Grillo-Lopez, A., White, C., Dallaire, B., Varns, C., et al., Rituximab The First Monoclonal Antibody Approved for the Treatment of Lymphoma. *Curr. Pharm. Biotechnol.* 2005, 1, 1–9.
- [84] Pardoll, D.M., The blockade of immune checkpoints in cancer immunotherapy. *Nat. Rev. Cancer* 2012 124 2012, 12, 252–264.
- [85] Okazaki, T., Honjo, T., PD-1 and PD-1 ligands: from discovery to clinical application. *Int. Immunol.* 2007, 19, 813–824.
- [86] Fife, B.T., Pauken, K.E., Eagar, T.N., Obu, T., et al., Interactions between PD-1 and PD-L1 promote tolerance by blocking the TCR-induced stop signal. *Nat. Immunol.* 2009 1011 2009, 10, 1185–1192.
- [87] Brunner-Weinzierl, M.C., Rudd, C.E., CTLA-4 and PD-1 Control of T-Cell Motility and Migration: Implications for Tumor Immunotherapy. *Front. Immunol.* 2018, 0, 2737.
- [88] Rowshanravan, B., Halliday, N., Sansom, D.M., CTLA-4: a moving target in immunotherapy. *Blood* 2018, 131, 58–67.
- [89] Poole, R.M., Pembrolizumab: First Global Approval. *Drugs* 2014 7416 2014, 74, 1973–1981.
- [90] Atezolizumab (TECENTRIQ).
- [91] Cameron, F., Whiteside, G., Perry, C., Ipilimumab. *Drugs* 2011 718 2012, 71, 1093–1104.
- [92] Zahavi, D., Weiner, L., Monoclonal Antibodies in Cancer Therapy. *Antibodies* 2020, Vol. 9, Page 34 2020, 9, 34.
- [93] Abdollahpour-Alitappeh, M., Lotfinia, M., Gharibi, T., Mardaneh, J., et al., Antibody–drug conjugates (ADCs) for cancer therapy: Strategies, challenges, and successes. *J. Cell. Physiol.* 2019, 234, 5628–5642.
- [94] Chames, P., Baty, D., Bispecific antibodies for cancer therapy. <https://doi.org/10.4161/mabs.1.6.10015> 2009, 1, 539–547.
- [95] James, D.F., Kipps, T.J., Rituximab in chronic lymphocytic leukemia. *Adv. Ther.* 2011 287 2011, 28, 534–554.
- [96] Jen, E.Y., Ko, C.-W., Lee, J.E., Valle, P.L. Del, et al., FDA Approval: Gemtuzumab Ozogamicin for the Treatment of Adults with Newly Diagnosed CD33-Positive Acute Myeloid Leukemia. *Clin. Cancer Res.* 2018, 24, 3242–3246.
- [97] Saxena, M., van der Burg, S.H., Melief, C.J.M., Bhardwaj, N., Therapeutic cancer vaccines. *Nat. Rev. Cancer* 2021 216 2021, 21, 360–378.
- [98] Di Lorenzo, G., Buonerba, C., Kantoff, P.W., Immunotherapy for the treatment of prostate cancer. *Nat. Rev. Clin. Oncol.* 2011 89 2011, 8, 551–561.
- [99] Hirayama, M., Nishimura, Y., The present status and future prospects of peptide-based cancer vaccines. *Int. Immunol.* 2016, 28, 319–328.
- [100] Skwarczynski, M., Toth, I., Peptide-based synthetic vaccines. *Chem. Sci.* 2016, 7, 842.

- [101] Stephens, A.J., Burgess-Brown, N.A., Jiang, S., Beyond Just Peptide Antigens: The Complex World of Peptide-Based Cancer Vaccines. *Front. Immunol.* 2021, 0, 2629.
- [102] Chen, X., Yang, J., Wang, L., Liu, B., Personalized neoantigen vaccination with synthetic long peptides: recent advances and future perspectives. *Theranostics* 2020, 10, 6011–6023.
- [103] C, L., T, R., X, C., Z, Z., et al., HLA-B*35:01 Allele Is a Potential Biomarker for Predicting Polygonum multiflorum-Induced Liver Injury in Humans. *Hepatology* 2019, 70, 346–357.
- [104] TAYLOR, P.C., Anti-TNF α Therapy for Rheumatoid Arthritis: an Update. *Intern. Med.* 2003, 42, 15–20.
- [105] Berraondo, P., Sanmamed, M.F., Ochoa, M.C., Etxeberria, I., et al., Cytokines in clinical cancer immunotherapy. *Br. J. Cancer* 2018 1201 2018, 120, 6–15.
- [106] Bianchi, V., Harari, A., Coukos, G., Neoantigen-Specific Adoptive Cell Therapies for Cancer: Making T-Cell Products More Personal. *Front. Immunol.* 2020, 0, 1215.
- [107] Garcia-Garijo, A., Fajardo, C.A., Gros, A., Determinants for Neoantigen Identification. *Front. Immunol.* 2019, 0, 1392.
- [108] Zhang, X., Qi, Y., Zhang, Q., Liu, W., Application of mass spectrometry-based MHC immunopeptidome profiling in neoantigen identification for tumor immunotherapy 2019, 120, 109542.
- [109] Wen, B., Li, K., Zhang, Y., Zhang, B., Cancer neoantigen prioritization through sensitive and reliable proteogenomics analysis. *Nat. Commun.* 2020 111 2020, 11, 1–14.
- [110] Faridi, P., Purcell, A.W., Croft, N.P., In Immunopeptidomics We Need a Sniper Instead of a Shotgun. *Proteomics* 2018, 18, 1700464.
- [111] Kote, S., Pirog, A., Bedran, G., Alfaro, J., Dapic, I., Mass Spectrometry-Based Identification of MHC-Associated Peptides. *Cancers (Basel)*. 2020, 12.
- [112] Romero, P., Cerottini, J.C., Waanders, G.A., Novel methods to monitor antigen-specific cytotoxic T-cell responses in cancer immunotherapy. *Mol. Med. Today* 1998, 4, 305–312.
- [113] Coulie, P.G., Karanikas, V., Colau, D., Lurquin, C., et al., A monoclonal cytolytic T-lymphocyte response observed in a melanoma patient vaccinated with a tumor-specific antigenic peptide encoded by gene MAGE-3. *Proc. Natl. Acad. Sci.* 2001, 98, 10290–10295.
- [114] Davis, M.M., Altman, J.D., Newell, E.W., Interrogating the repertoire: broadening the scope of peptide–MHC multimer analysis. *Nat. Rev. Immunol.* 2011, 11, 551–558.
- [115] Bentzen, A.K., Hadrup, S.R., Evolution of MHC-based technologies used for detection of antigen-responsive T cells. *Cancer Immunol. Immunother.* 2017, 66, 657–666.
- [116] Altman, J.D., Moss, P.A.H.H., Goulder, P.J.R.R., Barouch, D.H., et al., Phenotypic Analysis of Antigen-Specific T Lymphocytes. *Science* . 1996, 274, 94–96.
- [117] Murali-Krishna, K., Altman, J.D., Suresh, M., Sourdiv, D.J.D., et al., Counting antigen-specific CD8 T cells: A reevaluation of bystander activation during viral infection. *Immunity* 1998, 8, 177–187.
- [118] Guillaume, P., Legler, D.F., Boucheron, N., Doucey, M.A., et al., Soluble major histocompatibility complex-peptide octamers with impaired CD8 binding selectively induce Fas-dependent apoptosis. *J. Biol. Chem.* 2003, 278, 4500–4509.
- [119] DimerX I: Recombinant Soluble Dimeric Human HLA-A2:Ig Fusion Protein.
- [120] Casalegno-Garduño, R., Schmitt, A., Yao, J., Wang, X., et al., Multimer technologies for detection and adoptive transfer of antigen-specific T cells. *Cancer Immunol. Immunother.* 2010, 59, 195–202.
- [121] International, M., MHC class I tetramers 2016.
- [122] Horlock, C., Production of MHC Class I Tetramers. *Br. Soc. Immunol.*, 65.
- [123] Immunitrack, MHC Class I Monomers and Tetramers.
- [124] MBL MHC Tetramer.
- [125] MHC MONOMERS AND TETRAMERS - HLA-A, HLA-B, HLA-C, HLA-DR.
- [126] Specificities, N.T., QuickSwitch™ Custom Tetramer Kits - Technical Note.
- [127] NIH, NIH Tetramer Core Facility.
- [128] Duplan, V., Suberbielle, E., Napper, C.E., Joly, E., et al., Tracking antigen-specific CD8⁺ T cells in the rat using MHC class I multimers. *J. Immunol. Methods* 2007, 320, 30–39.
- [129] Saveanu, L., Carroll, O., Weimershaus, M., Guernonprez, P., et al., IRAP identifies an endosomal compartment required for MHC class I cross-presentation. *Science*. 2009, 325, 213–217.

- [130] Panoskaltsis-Mortari, A., Taylor, P.A., Riddle, M.J., Shlomchik, M.A., Blazar, B.R., In situ identification of allospecific B cells using pentamers. *Blood* 2008, 111, 3904–3905.
- [131] Griffioen, M., Van Egmond, H.M.E., Barnby-Porritt, H., Van Der Hoorn, M.A.W.G., et al., Genetic engineering of virus-specific T cells with T-cell receptors recognizing minor histocompatibility antigens for clinical application. *Haematologica* 2008, 93, 1535–1543.
- [132] Uhlin, M., Okas, M., Gertow, J., Uzunel, M., et al., A novel haplo-identical adoptive CTL therapy as a treatment for EBV-associated lymphoma after stem cell transplantation. *Cancer Immunol. Immunother.* 2010, 59, 473–477.
- [133] Our Technology | Immudex.
- [134] Dolton, G., Lissina, A., Skowera, A., Ladell, K., et al., Comparison of peptide-major histocompatibility complex tetramers and dextramers for the identification of antigen-specific T cells. *Clin. Exp. Immunol.* 2014, 177, 47–63.
- [135] Tungatt, K., Bianchi, V., Crowther, M.D., Powell, W.E., et al., Antibody Stabilization of Peptide–MHC Multimers Reveals Functional T Cells Bearing Extremely Low-Affinity TCRs. *J. Immunol.* 2015, 194, 463–474.
- [136] Hadrup, S.R., Strindhall, J., Kølgaard, T., Seremet, T., et al., Longitudinal Studies of Clonally Expanded CD8 T Cells Reveal a Repertoire Shrinkage Predicting Mortality and an Increased Number of Dysfunctional Cytomegalovirus-Specific T Cells in the Very Elderly. *J. Immunol.* 2006, 176, 2645–2653.
- [137] Batard, P., Peterson, D.A., Devèvre, E., Guillaume, P., et al., Dextramers: New generation of fluorescent MHC class I/peptide multimers for visualization of antigen-specific CD8⁺ T cells. *J. Immunol. Methods* 2006, 310, 136–148.
- [138] Bentzen, A.K., Marquard, A.M., Lyngaa, R., Saini, S.K., et al., Large-scale detection of antigen-specific T cells using peptide-MHC-I multimers labeled with DNA barcodes. *Nat. Biotechnol.* 2016, 34, 1037–1045.
- [139] Immudex, dCODE Dextramer® - NGS/Multi-omics | Immudex.
- [140] Oberhardt, V., Luxemburger, H., Kemming, J., Schulien, I., et al., Rapid and stable mobilization of CD8⁺ T cells by SARS-CoV-2 mRNA vaccine. *Nat.* 2021 5977875 2021, 597, 268–273.
- [141] Make custom MHC (HLA) class I monomers | Tetramers | fast and flexible.
- [142] easYmer® MHC I and U-Load MHC II Monomers | Immudex.
- [143] Neudorfer, J., Schmidt, B., Huster, K.M., Anderl, F., et al., Reversible HLA multimers (Streptamers) for the isolation of human cytotoxic T lymphocytes functionally active against tumor- and virus-derived antigens. *J. Immunol. Methods* 2007, 320, 119–131.
- [144] Laghmouchi, A., Hoogstraten, C., Falkenburg, J.H.F., Jedema, I., Long-term in vitro persistence of magnetic properties after magnetic bead-based cell separation of T cells. *Scand. J. Immunol.* 2020, 92, e12924.
- [145] Rodenko, B., Toebes, M., Hadrup, S.R., van Esch, W.J.E., et al., Generation of peptide–MHC class I complexes through UV-mediated ligand exchange. *Nat. Protoc.* 2006, 1, 1120–1132.
- [146] Celie, P.H.N., Toebes, M., Rodenko, B., Ovaa, H., et al., UV-induced ligand exchange in MHC class I protein crystals. *J. Am. Chem. Soc.* 2009, 131, 12298–12304.
- [147] Pawlak, J.B., Hos, B.J., van de Graaff, M.J., Megantari, O.A., et al., The Optimization of Bioorthogonal Epitope Ligation within MHC-I Complexes. *ACS Chem. Biol.* 2016, 11, 3172–3178.
- [148] Choo, J.A.L., Thong, S.Y., Yap, J., Van Esch, W.J.E., et al., Bioorthogonal cleavage and exchange of major histocompatibility complex ligands by employing azobenzene-containing peptides. *Angew. Chemie - Int. Ed.* 2014, 53, 13390–13394.
- [149] Saini, S.K., Schuster, H., Ramnarayan, V.R., Rammensee, H.-G., et al., Dipeptides catalyze rapid peptide exchange on MHC class I molecules. *Proc. Natl. Acad. Sci.* 2015, 112, 202–207.
- [150] Saini, S.S.K., Ostermeir, K., Ramnarayan, V.V.R., Schuster, H., et al., Dipeptides promote folding and peptide binding of MHC class I molecules. *Proc. Natl. Acad. Sci. U. S. A.* 2013, 110, 15383–15388.
- [151] Hafstrand, I., Sayitoglu, E.C., Apavaloaei, A., Josey, B.J., et al., Successive crystal structure snapshots suggest the basis for MHC class I peptide loading and editing by tapasin. *Proc. Natl. Acad. Sci. U. S. A.* 2019, 116, 5055–5060.

- [152] Anjanappa, R., Garcia-Alai, M., Kopicki, J.D., Lockhauserbäumer, J., et al., Structures of peptide-free and partially loaded MHC class I molecules reveal mechanisms of peptide selection. *Nat. Commun.* 2020, 11, 1–11.
- [153] MBL, QuickSwitch™ Quant Tetramer Kit 2017, 1–6.
- [154] Delcommenne, M.C., Hrytsenko, O., Tram, C., Weir, G., Stanford, M.M., The QuickSwitch Quant HLA-A*02:01 Tetramer Kit can be used for determining the biological activity of a cancer vaccine. *J. Immunol.* 2017, 198.
- [155] Poluektov, Y., George, M., Daftarian, P., Delcommenne, M.C., Assessment of SARS-CoV-2 specific CD4(+) and CD8 (+) T cell responses using MHC class I and II tetramers. *Vaccine* 2021, 39, 2110–2116.
- [156] Luimstra, J.J., Garstka, M.A., Roex, M.C.J., Redeker, A., et al., A flexible MHC class I multimer loading system for large-scale detection of antigen-specific T cells. *J. Exp. Med.* 2018, 215, 1493–1504.
- [157] Luimstra, J.J., Franken, K.L.M.C.M.C., Garstka, M.A., Drijfhout, J.W., et al., Production and Thermal Exchange of Conditional Peptide-MHC I Multimers. *Curr. Protoc. Immunol.* 2019, 126, e85.
- [158] De Silva, A.D., Boesteanu, A., Song, R., Nagy, N., et al., Thermolabile H-2Kb Molecules Expressed by Transporter Associated with Antigen Processing-Deficient RMA-S Cells Are Occupied by Low-Affinity Peptides. *J. Immunol.* 1999, 163, 4413 LP – 4420.
- [159] Garstka, M.A., Fish, A., Celie, P.H.N., Joosten, R.P., et al., The first step of peptide selection in antigen presentation by MHC class I molecules. *Proc. Natl. Acad. Sci.* 2015, 112, 1505–1510.
- [160] Williams, A.P., Peh, C.A., Purcell, A.W., McCluskey, J., Elliott, T., Optimization of the MHC class I peptide cargo is dependent on tapasin. *Immunity* 2002, 16, 509–520.
- [161] Garstka, M.A., Fritzsche, S., Lenart, I., Hein, Z., et al., Tapasin dependence of major histocompatibility complex class I molecules correlates with their conformational flexibility. *FASEB J.* 2011, 25, 3989–3998.
- [162] Porter, K.M., Hermann, C., Traherne, J.A., Boyle, L.H., TAPBPR isoforms exhibit altered association with MHC class I. *Immunology* 2014, 142, 289–299.
- [163] Thomas, C., Tampé, R., Structure of the TAPBPR–MHC I complex defines the mechanism of peptide loading and editing. *Science.* 2017, 358, eaao6001.
- [164] Jiang, J., Natarajan, K., Boyd, L.F., Morozov, G.I., et al., Crystal structure of a TAPBPR–MHC I complex reveals the mechanism of peptide editing in antigen presentation. *Science.* 2017, 358, 1064–1068.
- [165] Rizvi, S.M., Raghavan, M., Mechanisms of function of tapasin, a critical major histocompatibility complex class I assembly factor. *Traffic* 2010, 11, 332–347.
- [166] Hermann, C., Strittmatter, L.M., Deane, J.E., Boyle, L.H., The Binding of TAPBPR and Tapasin to MHC Class I Is Mutually Exclusive. *J. Immunol.* 2013, 191, 5743–5750.
- [167] Overall, S.A., Toor, J.S., Hao, S., Yarmarkovich, M., et al., High throughput pMHC-I tetramer library production using chaperone-mediated peptide exchange. *Nat. Commun.* 2020 111 2020, 11, 1–13.
- [168] Rajpal, G., Arvan, P., Disulfide Bond Formation. *Handb. Biol. Act. Pept.* 2013, 1721–1729.
- [169] Feige, M.J., Braakman, I., Hendershot, L.M., CHAPTER 1.1:Disulfide Bonds in Protein Folding and Stability 2018, 1–33.
- [170] Perry, L.J., Wetzel, R., Disulfide bond engineered into T4 lysozyme: stabilization of the protein toward thermal inactivation. *Science.* 1984, 226, 555 LP – 557.
- [171] Hogg, P.J., Disulfide bonds as switches for protein function. *Trends Biochem. Sci.* 2003, 28, 210–214.
- [172] Dombkowski, A.A., Sultana, K.Z., Craig, D.B., Protein disulfide engineering. *FEBS Lett.* 2014, 588, 206–212.
- [173] Dombkowski, A.A., Disulfide by Design™: A computational method for the rational design of disulfide bonds in proteins. *Bioinformatics* 2003, 19, 1852–1853.
- [174] Ceroni, A., Passerini, A., Vullo, A., Frascioni, P., DISULFIND: a disulfide bonding state and cysteine connectivity prediction server. *Nucleic Acids Res.* 2006, 34, W177–W181.
- [175] Suplatov, D., Timonina, D., Sharapova, Y., Švedas, V., Yosshi: a web-server for disulfide engineering by bioinformatic analysis of diverse protein families. *Nucleic Acids Res.* 2019, 47, W308–W314.

- [176] F, F., P, C., DiANNA: a web server for disulfide connectivity prediction. *Nucleic Acids Res.* 2005, 33.
- [177] Hollingsworth, S.A., Dror, R.O., Molecular Dynamics Simulation for All. *Neuron* 2018, 99, 1129–1143.
- [178] Fahnestock, M.L., Tamir, I., Narhi, L., Bjorkman, P.J., Thermal stability comparison of purified empty and peptide-filled forms of a class I MHC molecule. *Science (80-.).* 1992, 258, 1658–1662.
- [179] Yaneva, R., Schneeweiss, C., Zacharias, M., Springer, S., Peptide binding to MHC class I and II proteins: New avenues from new methods. *Mol. Immunol.* 2010, 47, 649–657.
- [180] Pedersen, L.E., Rasmussen, M., Harndahl, M., Nielsen, M., et al., A combined prediction strategy increases identification of peptides bound with high affinity and stability to porcine MHC class I molecules SLA-1*04:01, SLA-2*04:01, and SLA-3*04:01. *Immunogenet.* 2015 682 2015, 68, 157–165.
- [181] Springer, S., Do, K., Skipper, J.C.A., Townsend, A.R.M., et al., Fast association rates suggest a conformational change in the MHC class I molecule H-2Db upon peptide binding. *Biochemistry* 1998, 37, 3001–3012.
- [182] Nielsen, M., Lundegaard, C., Worning, P., Lauemøller, S.L., et al., Reliable prediction of T-cell epitopes using neural networks with novel sequence representations. *Protein Sci.* 2003, 12, 1007–1017.
- [183] Zacharias, M., Springer, S., Conformational flexibility of the MHC Class I $\alpha 1$ - $\alpha 2$ domain in peptide bound and free states: A molecular dynamics simulation study. *Biophys. J.* 2004, 87, 2203–2214.
- [184] Hein, Z., Uchtenhagen, H., Abualrous, E.T., Saini, S.K., et al., Peptide-independent stabilization of MHC class I molecules breaches cellular quality control. *J. Cell Sci.* 2014, 127, 2885–2897.
- [185] Montealegre, S., Venugopalan, V., Fritzsche, S., Kulicke, C., et al., Dissociation of $\beta 2$ -microglobulin determines the surface quality control of major histocompatibility complex class I molecules. *FASEB J.* 2015, 29, 2780–2788.
- [186] Saini, S.K., Tamhane, T., Anjanappa, R., Saikia, A., et al., Empty peptide-receptive MHC class I molecules for efficient detection of antigen-specific T cells. *Sci. Immunol.* 2019, 4, eaau9039.
- [187] Moritz, A., Anjanappa, R., Wagner, C., Bunk, S., et al., High-throughput peptide-MHC complex generation and kinetic screenings of TCRs with peptide-receptive HLA-A*02:01 molecules. *Sci. Immunol.* 2019, 4, eaav0860.
- [188] Tetramer Shop I MHC Tetramer I Bright and specific staining I 24h delivery.
- [189] 10x Genomics Announces New Product Lineup and Tetramer Shop Acquisition | BioSpace.

Chapter 2. Materials and Methods


2.1. Background

In this section, complete detail of all the methods is described. These methods and materials were used throughout my studies as a requirement for completing my Ph.D. project. As the shorter version of the methods described in the manuscript does not give a detailed picture, I have included the extended versions from our standard operating protocol (SOP) database. We have created these SOPs with detailed information, steps, tricks and tips. Based on our experience and observations, we have, in some cases, modified the SOPs to different versions. Here I include the current version that we follow in the laboratory.


2.2. Protein expression and inclusion body preparation

This section describes the detailed procedure for expressing MHC-I in *E. coli* bacteria in the form of inclusion bodies. The SOP has been optimized for large-scale production of MHC-I HC and light chain (LC) β_2m .

2.2.1. SOP: Large scale protein expression of MHC-I in E. coli and preparation of inclusion bodies

	Springer Group Standard Operating Procedure (SOP)
SOP No.:	SSP-SOP-BCM_001
Title:	Large scale protein expression of MHC-I in E. coli and preparation of inclusion bodies
Revision No.:	3
Revision Date:	2020-01-15

1. Information about this Standard Operating Procedure

SOP No., Title, Revision No., Revision Date: see page header			
Author of this Revision:	Raghavendra Anjanappa and Sebastian Springer		
Signature of Principal Investigator:			
Revision History:	Revision No.	Author	Date
	1	Sebastian Springer	2016-11-01
	2	Raghavendra Anjanappa, Sebastian Springer	2017-07-31
	3	Sebastian Springer	2020-01-15
	4	Franziska Köper	2020-11-17
Other SOPs, documents, or attachments required for the procedure	SSP-SOP-MOL_001: Preparation of LB Media		
Confidentiality Status	Confidential – no distribution without authorization		

2. Purpose and general description of the procedure (1-2 sentences)

Recombinant production of MHC-I related proteins (Heavy chain (HC), beta-2 microglobulin (β_2m), and alpha 3 (α_3) in *Escherichia coli* (E. coli). As the proteins will be produced as insoluble inclusion bodies, they will be purified by a series of washes and further resuspended for storage. This protocol is for a preparation from 500 ml of bacterial culture.

3. Terms and abbreviations used in this document

Term or Abbreviation	Explanation
α	alpha
β	beta
β_2m	beta-2 microglobulin
kb	Murine MHC-I molecule H-2K ^b
kDa	Kilo dalton
LB	Lysogeny Broth
dd water	double-distilled or ultra-filtered water

4. Cells or plasmids required

Transformed bacterial strains with expression plasmids.

Our h β 2m expression plasmid is called pHN1+, in E. coli Rosetta pLysS, selection antibiotic is Ampicillin and Chloramphenicol

Our HLA-A2(Y84C) in E. coli Rosetta pLysS (selection antibiotics are ampicillin and chloramphenicol). Ideally, the bacteria should be freshly transformed; in any case, they should come from a single colony on a re-streaked agar plate with the right antibiotic.

Organism	Parent strain	Parent plasmid	Insert/ Gene	Molecular weight in kDa	Antibiotic resistance
E. coli	BL21pLysS	pET3a	HLA-A*02:01	33	Ampicillin
E. coli	BL21	PHN1+	human β 2m	11.73	Ampicillin

5. Chemicals required

Chemical	Company and Catalog No.	Safety? ¹	Batch? ²
IPTG (Isopropyl β -D-1-thiogalactopyranoside)	Panreac- A1008	Warning	NA
Ampicillin	Applchem A0839	Danger	NA
Chloramphenicol	Applchem A1806	Danger	NA
Tris base	Panreac- A1379	NA	NA
Sucrose	Panreac- A3935	NA	NA
EDTA (ethylene diamine tetraacetic acid)	Panreac-131669	Warning	NA
DTT (dithiothreitol)	Applchem A11001	Warning	NA
Triton X-100	Panreac- A4975	Danger	NA
Sodium chloride	Panreac- 14884	NA	NA
Guanidinium hydrochloride	Sigma Aldrich 50950	Warning	NA
Urea	Panreac- A1361	NA	NA
PMSF (phenylmethylsulfonylfluoride)	Sigma P7626	Danger	NA
HEPES	Roth 6763	NA	NA
β -mercaptoethanol	Sigma A4338	Danger	NA

¹Insert 'Yes' if special safety considerations (GHS system) apply **and** enter safety information in table 8 (Safety).

²Insert 'Yes' if necessary to record the batch number of this chemical.

6. Safety considerations		
Chemical or Reagent	Classification according to Regulation ³	GHS Classification (Hazard)
IPTG (Isopropyl β -D-1-thiogalactopyranoside)	H319 : Eye irritation (Category 2), H351: Carcinogenicity (Category 2)	H319, H351, P281 P305 + P351 + P338
Ampicillin	H315: Skin Irritation (Category 2), H319: Eye irritation (Category 2), H334: Respiratory sensitisation (Category 1), H335: Specific target organ toxicity -single exposure, (Category 3), Respiratory system	H315, H317, H319, H334, H335, P280, P302 + P352, P305 + P351 + P338IF
Chloram-phenicol	H351: Carcinogenicity (Category 2)	H351, P201, P308 + P313
EDTA (ethylene diamine tetraacetic acid)	H332: Acute Toxicity-Inhalation (Category 4)	H332, P261, P271, P304+P340P312
DTT (dithiothreitol)	H302: Acute Toxicity-Oral (Category 4), H315: Skin Corrosion (Category 2), H319: Serious Eye Damage/Eye Irritation (Category 2A), H335: Specific Target Organ Toxicity, Single Exposure (Category 3)	H302, H315, H319, H335, P261, P302+P352, P305+P351+P338, P501
Triton X-100	H302: Acute Toxicity-Oral (Category 4), H315: Skin Corrosion (Category 2), H319: Serious Eye Damage/Eye Irritation (Category 2A), H335: Specific Target Organ Toxicity, Single Exposure (Category 3), H319: Serious Eye Damage/Eye Irritation (Category 2A)	H302, H318, H411, P264, P273, P280, P305 + P351 + P338 + P310, P391, P501
Guanidinium hydrochloride	H302: Acute toxicity, Oral (Category 4), H332: Acute toxicity, Inhalation (Category 4), H315: Skin irritation (Category 2), H319: Eye irritation (Category 2)	H302 + H332, H315, H319, P301 + P312 + P330, P302 + P352, P304 + P340 + P312, P305 + P351 + P338
PMSF (phenylmethylsulfonylfluoride)	H302: Acute toxicity, Oral (Category 4), H332: Acute toxicity, Inhalation (Category 4), H315: Skin irritation (Category 2), H319: Eye irritation (Category 2)	H318, H301, H314, P260, P280, P301 + P310 + P330, P303 + P361 + P353, P304 + P340 + P310, P305 + P351 + P338 + P310
β -mercaptoethanol	H301+ H331+ H310: Acute toxicity, Oral, Inhalation, Dermal Category 3, H315: Skin irritation Category 2, H318: Serious eye damage, Category 1, H373: Specific organ toxicity, Category 2	H301 + H331, H310, H317, H318, H373, H410, P273, P302 + P352, P304 + P340, P305 + P351 + P338, P308 + P310

³ Classification according to Regulation (EC) No. 1272/2008 [EU-GHS/CLP]

7. Stock solutions (= 'reagents')	
If using stock solutions found in the lab or made by others, make sure that they have the concentrations indicated, or else recalculate the amounts used in the protocol.	
Reagent (final conc.)	Preparation, aliquoting, storage
IPTG stock	1 M in Milli-Q water storage at -20°C
DTT stock	1 M in ddH ₂ O
PMSF stock	0.5 M in DMSO (500x)
Ampicillin stock	50 µg/ml in ddH ₂ O
Kanamycin stock	25 mg/ml in ddH ₂ O
Chloramphenicol stock	25 mg/ml in 70 % Ethanol
LB Medium	Preparation described in separate SOP: FK-01 500 ml LB medium per 2 L conical flask 500 ml for Overnight culture and OD measurements
Buffer A: 25% sucrose, 1 mM EDTA, in 50 mM Tris, pH 8.0	To make 100 mL: 5 mL 1 M Tris-Cl pH 8.0, 25 g sucrose, 200 µl 500 mM EDTA Add all the above components in sterile water, adjust the pH of the buffer to 8.0, and make up the volume to 100 mL with sterile water. Store at 4 °C for 1-2 months maximum. The following is added to Buffer A not now but before cell lysis: 10 mM (final) DTT, 1 mM (final) PMSF
Buffer B: 25% sucrose 1% Triton X 100, 5 mM EDTA, 50 mM Tris, pH 8.0	To make 200 mL: 10 mL 1 M Tris-Cl pH 8.0, 50 g sucrose, 10 mL 20% (v/v) Triton X-100, 1 mL 500 mM EDTA Adjust the pH of the buffer to 8.0, then add more dd water to the final volume. Store at 4 °C for 1-2 months maximum.
Buffer C: 2 M NaCl, 2 M Urea, 50 mM Tris, pH 8.0	To make 200 mL: 80 mL 5 M NaCl, 24 g urea, 10 mL 1 M Tris-Cl pH 8.4 Dissolve in water and adjust the pH of the buffer to 8.4, then add more dd water to the final volume.
Buffer D: 150 mM NaCl 50 mM Tris pH 7.5	To make 200 mL: 6 mL 5 M NaCl 10 mL 1 M Tris-Cl pH 7.5 Add water to 100 mL and adjust the pH of the buffer to 7.5, then add more dd water to the final volume.
Buffer E: 6 M Guanidine HCl 50 mM HEPES, pH 6.5	To make 50 mL: 27.8 g Guanidine HCl 2.5 mL 1 M HEPES pH 6.5 Dissolve in water and adjust the pH of the buffer to 6.5, then add more dd water to the final volume.

9. Procedure (numbered list)

1. Preliminary work

Start at least two days before Protein expression!

Production of LB medium including Autoclaving (500 ml LB medium per 2 L conical flask + 500 ml for Overnight culture and OD measurements)

Plate the desired competent cells on LB-agar including antibiotics incubate overnight at 37 ° C.

Starter culture preparation: Inoculate one single colony into one flask with 50 ml LB medium with selection antibiotics.

Which antibiotics are used depends on the strain and the plasmid. The concentration that is generally used in the lab is 1 µl antibiotic per ml LB.

2. Protein expression in *E. coli*:

Incubate at 37 °C, 180 rpm, overnight . After 16 hrs of growth, centrifuge at 5000 rpm (3000 x g, Avanti, JA-14 rotor) for 10 minutes at RT or 4 °C.

Resuspend the bacterial cell pellet in fresh 25 mL LB media with antibiotics. Use 10 ml to inoculate one flask with 500 ml LB containing antibiotics. In the same way, inoculate the other flask.

Grow the large cultures to an OD₆₀₀ of about 0.6, and then add IPTG to induce expression (final concentration 0.5 mM) and incubate further in the 37 °C shaker incubator for 4 hrs.

Harvest by centrifugation at 5000 x g (Avanti, JA-10 rotor) for 10 minutes at 4°C.

Resuspend each bacterial pellet (*i.e.*, from each flask individually) in 20 mL Buffer A (sucrose buffer). Transfer to an Oak Ridge tube.

The best resuspension volume depends on the volume of the cell mass. Some variation is possible.

Freeze the resuspended bacterial pellets. They can be stored at -20 °C (for a few days) or -80°C.

3. Lysis of the bacteria and isolation and purification of inclusion bodies

The volumes given in this section are for one OakRidge tube with the bacterial pellet from one 500 ml culture.

If the number of samples is large, you can also unite the two bacterial pellets of one sample into one OakRidge tube; in this case, double the volumes of buffers.

Add 10 mM DTT and 1 mM PMSF (final concentrations) to the cell suspension.

Lyse the cells by thawing in a 30 °C water bath. Swirl the tubes to make sure the thawing is fast and uniform. From now on, always keep the samples at 4 °C (on ice).

Sonicate (medium tip, pulse: 2 seconds on and 3 seconds off, amplitude 80%) until the solution is no longer viscous.

This should take no longer than 3 minutes. Oversonication is not good for the protein.

Take a 50 µl sample from the lysate and label it #1. (Keep all samples at -20 °C until they are run on SDS-PAGE.)

Spin the cell lysates in Oak Ridge tubes at 40,000 x g, 4 °C, for 15 minutes (Avanti, JA25.50 rotor). Take a sample from the supernatant and label it #2. Discard the supernatant.

Add 10 mL Buffer B (detergent buffer). Add DTT to 2 mM final concentration. Resuspend by sonication as above. Take a sample from the suspension and label it #3.

Spin as above, and discard the supernatant.

Repeat this procedure of resuspension, sonication, and centrifugation for two more washing steps in following buffers:

Buffer C (urea buffer). Add DTT to a final concentration of 2 mM before resuspension. After resuspension, take a sample from suspension and label it #4.

Buffer D (tris-buffered saline). Add PMSF to a final volume of 0.5 mM before resuspension. After resuspension, take a sample from the suspension and label it #5.

After the final centrifugation step, resuspend the pellet by sonication in 5 mL Buffer E. Add PMSF to a final concentration of 0.5 mM. Add beta-mercaptoethanol to a final concentration of 100 µM. Take sample #6.

Leave the suspension to solubilize by gentle shaking at 4 °C (rotor in the cold room).

After 48 hours, centrifuge the solubilized protein suspension at 40,000 x g, 4 °C, for 15 minutes. Spin the supernatant a second time to make sure you get rid of the insoluble pellet.

Determine the protein concentration of the final supernatant (see below).

Aliquot the supernatant (1 mL/1.5 mL tube) (take sample #7).

Label the tubes and store it at -20°C:

[name of the protein],[concentration], [date of preparation] [Lot-Number]

Lot Numbers:

[Protein abbreviation e.g. β_2m , α_3k^b], [Name abbreviated], [Production Month and Year]

Add lot number to overview table: [Lot numbers - IB preparation proteins](#)

To assess the quality of the preparation, run 1 μ l each of samples 1-7 on an 17 % SDS-PAGE gel with a size marker and some purified protein of an earlier preparation.

4. Determine the concentration of the purified protein by UV absorption

Measure extinction at 280 nm against buffer E using a UV cuvette.

Dilute if necessary, usually 1/20.

Calculate the extinction coefficient from the sequence of the protein. Some useful extinction coefficients (ϵ) and molecular weights (MW):

Protein	a.a.	ϵ (M ⁻¹ cm ⁻¹)	MW (g/mol)	E ₂₈₀ of 1 mg/mL sol.
HLA-A*02:01	25-308	82 390	32 728	2.3
h β_2m	21-119	19 300	11 731	1.65

From the extinction coefficient and your measurement, calculate the concentration and the yield of the protein. (or simply use the online calculator: [Protein Concentration Calculator](#)).

The yield from one liter culture should be in the range of 15-25 mg protein.

8. Equipment required

Type of equipment	Vendor / Specification	Special Instruction? ⁴
EpiShear™ Probe Sonicator	Active Motif, Model number: Q120AM	No
Shaker incubator	Sartorius stedim biotech, Certomat®BS-1	No
Water bath	Julabo GmbH, 19 A, 60 °C max	No
High-Speed centrifuge	Beckman Coulter, Avanti® J-E	Yes
Rotor JA-25	Beckman Coulter, For 50 ml Oak Ridge tubes	Yes
Rotor JA-14	Beckman Coulter, For 250 ml Polypropylene tubes	Yes
Rotor JA-10	Beckman Coulter, For 500 ml Polypropylene tubes	Yes
Shaker	IKA®, Rocker 2D basic	No
Scale	Sartorius, E313S	No
Autoclave	Systec, DX-200 / D-2317	Yes
Spektrometer	ThermoSpectronic, Genesys 10uv	Yes

⁴Insert 'Yes' if special instruction is necessary to operate this equipment.

10. Potential pitfalls, errors, and other issues

Issue	Known resolution
No protein expression	Confirm that the right glycerol stock was used for expression Prepare fresh plasmid and transform into expression strain Use freshly prepared LB media Confirm the IPTG concentration
Little protein obtained (yield too low)	Check the protein expression level by SDS-PAGE before purification Check proper cell lysis Check for over-sonication Use only freshly prepared buffer with exact pH

11. Instructions for the use of SOPs

General Rules:

Use the newest version of an SOP for your experiment.

Record the number of the SOP (found in the page header) in your experiment protocol.

Any changes between the SOP and your experiment must be documented in your experiment protocol.

If you believe that the SOP needs to be changed or extended, bring it up in the subgroup meeting.

Explanations of the individual points:

3. Abbreviations: Abbreviations of chemicals are explained in 5.

4. "Material" is everything specific to the particular experiment, such as plasmids, cells, lysates, etc.

5. "Chemicals" are all powders (but not stock solutions, see 6.)


2.3. Protein refolding

Protein refolding was performed on different scale depending on the requirement of the following assays. The table below summarizes the refolding format.

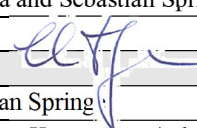
No.	Refolding Volume (mL)	Purpose	Approx. Protein Yield (mg)
1	1000	General	5 - 10
2	10 – 100	Immune assays	0.1 – 1
3	1	Refold Efficiency, FP	<0.1
4	0.25	Competitive ELISA	<0.05

The refolding protocol from 10 – 1000 mL remains the same and the quantities of the ingredients are altered proportionately. For refolding volume <1 mL, the concentration of protein and pipetting strategies varies as mentioned in the respective protocols.

2.3.1. SOP: Large scale Refolding of MHC-I - 1L

	Springer Group Standard Operating Procedure (SOP)
SOP No.:	SSP-SOP-BCM_002
Title:	MHC-I large scale refolding followed by SEC purification
Revision No.:	2
Revision Date:	2021-07-12

1. Information about this Standard Operating Procedure

SOP No., Title, Revision No., Revision Date: see page header			
Author of this Revision:	Raghavendra Anjanappa and Sebastian Springer		
Signature of Principal Investigator:			
Revision History:	Revision No.	Author	Date
	1	Sebastian Spring	2017-08-01
	2	Franzi Koeper, Ankur Saikia, Sebastian Springer	2021-07-12
Other SOPs, documents, or attachments required for the procedure	None.		
Confidentiality status	Confidential – no distribution without authorization		

2. Purpose and general description of the procedure (1-2 sentences)

MHC-I protein is trimeric complex that contains heavy chain and light chain together with peptide. This protocol describes the procedure for in vitro refolding of MHC-I protein by the dilution method, here specifically for folding HLA-A*02:01(Y84C/A139C) with the dipeptide Glycyl-leucine (GM).

3. Terms and abbreviations used in this document

Term or Abbreviation	Explanation
dd water	double-distilled or ultra-filtered water
SOP	Standard Operating Procedure
SEC	Size exclusion chromatography
CV	column volume(s)

5. Chemicals required			
Chemical	Company and Catalog No.	Safety?	Batch?
Tris base	Panreac- A1379	NA	NA
L-Arginine	Applichem –A3709	NA	NA
Sodium chloride	Panreac- 14884	NA	NA
EDTA (ethylene diamine tetra acetic acid)	Panreac-131669	NA	NA
PMSF (phenyl methyl sulfonyl fluoride)	Sigma P7626	Danger	NA
L-Glutathione reduced (MW 307.3)	Applichem A2084	NA	NA
L-Glutathione oxidized (MW 612.6)	Applichem A2243	NA	NA
Dipeptide GM	BACHEM 4001203	NA	NA

6. Safety considerations		
Chemical or Reagent	Classification according to Regulation	Safety consideration (H/P numbers)
L-Arginine	H319- Serious eye damage/ eye irritation	H319, P280, P305+P351+P338IF
EDTA	H332 - Acute Toxicity-Inhalation (Category 4)	H332, P261, P271, P304+P340, P312

7. Buffers and stock solutions (='reagents')	
Reagent	Preparation, aliquoting, storage
Refolding buffer 100 mM Tris·Cl 500 mM L-Arginine 2 mM EDTA 5 mM reduced glutathione 0.5 mM oxidized glutathione 10 mM GM or 1 µM full length peptide 100 µM PMSF	Take make 1 liter of refolding buffer 100 mL of 1 M Tris-Cl pH 8.0 500 mL of 1 M L-Arginine 4 mL of 500 mM EDTA Dissolve the above components in water and then adjust the buffer to pH 8.0. Make up the volume to 1 L using autoclaved Milli-Q water. Note: Glutathione, PMSF and the peptide are added to the chilled refolding buffer. Note: The working concentration for the protease inhibitor PMSF is 0.1-1 mM (millimolar). We recommend here 100 µM = 0.1 mM. Note: The concentration of a full-length peptide in the refold depends on the allotype, the peptide, and other considerations.
PMSF stock	1 M in DMF (dimethylformamide) or DMSO (dimethylsulfoxide). Note: PMSF decomposes quickly in water, especially at alkaline pH, and thus must be added to the refolding buffer only just before the refolding reaction starts.
SEC buffer 50 mM Tris·Cl pH 8.0 150 mM NaCl 10 mM GM (if refolding with dipeptide)	To make 1 liter: 50 mL of 1 M Tris·Cl pH 8.0 30 mL of 5 M NaCl 2061 mg of dipeptide (if refolding with dipeptide) Dissolve the above reagents in water, then make up the final volume with autoclaved Milli-Q water.

8. Equipment required

Type of equipment	Special Instruction? ⁵
Spectrophotometer	No
Magnetic stirrer and bead	No
Avanti high-speed centrifuge	Yes
Table top centrifugation	No
Autoclaved Oak Ridge tubes	No
ÄKTA FPLC instrument	Yes
Sartorius Vivaflow 200 Ultra filtration unit	Yes
Hi Load 26/600 Superdex 200 pg	Yes

8. Procedure (numbered list)

This protocol is described for a refold volume of 1 L.

The refolding reaction is performed in the cold room.

- The day before the folding reaction, prepare the refold buffer (without glutathione, PMSF, peptide) as described in table 6 in a one-litre Schott Duran bottle.
- Filter the refold buffer through a 0.45 µm disc filter.
- Put the refold buffer into the cold room to cool down overnight.
- Thaw out the frozen vials of class I heavy chain and light chain. Keep them on ice.
- The final molar concentration of heavy chain (MW ≈ 30 kDa) is 1 µM, which corresponds to 30 mg in a one-litre refolding reaction, and the concentration of the light chain (MW ≈ 11 kDa) is 2 µM, which corresponds to 22 mg in a one-litre refolding reaction.
- To the cold refold buffer, add glutathiones (as powders, 1.53 g of reduced and 0.306 g of oxidized glutathione), the peptide (from 1 mM stock or as powder), and the PMSF (from a stock, see above). Stir for 5 minutes to dissolve.
- To begin with refolding, dilute the light chain by slowly (spanning 5 minutes) injecting the protein into cold refold buffer with constant stirring, and then allow it to refold on its own for 1 hour.
- Then start injecting the class I heavy chain in to the refold buffer in 9 portions. First 6 portions will be added at every one-hour intervals and the remaining 3 portions will be added at after 15 hours. (See below table for one litre refold.) *Addition intervals may be customized depending on allotype, peptide, and other considerations.*

Protein	Injection	Amount (mg)	Time (hours)
hβ2m	1st	22	0
HLA-A2 (Y84C)	1st	3.4	1
	2nd	3.4	2
	3rd	3.4	3
	4th	3.4	4
	5th	3.4	5
	6th	3.4	6
	7th	3.4	15
	8th	3.4	16
	9th	3.4	17

⁵Insert 'Yes' if special instruction is necessary to operate this equipment.

- Then allow the refolding reaction for 4-5 days with constant stirring in the cold room. *Refolding time may vary with allotype, peptide, and other parameters.*
- *Depending on the refold volume, and on the amount of precipitation, it might be a good idea to insert here a centrifugation step with at least 20,000 x g. Discard the pellet.*
- Filter the refolding reaction by passing through a 0.45 µm filter to remove aggregates/protein precipitate.
- Then concentrate the refolding reaction to approximately 50-100 mL by using a Sartorius ultrafiltration membrane with a cut-off range (MWCO) of 30,000.
- Alternatively, VivaFlow spin filters 30 kDa (similar to Centricons) can be used to concentrate the protein further. The desired end volume depends on the FPLC column used for the subsequent purification.

Size Exclusion Chromatography: (Refer to SSP-SOP-BCM_023 for more detail)

- Prepare the SEC buffer as described in table 6.
- Note:** Always maintain the GM dipeptide throughout the purification in SEC buffer. As in case of full length peptide mediated refolding, don't add peptide to the SEC buffer
- Before purification, wash the Superdex-200 (26/600) column by passing 2 column volumes (CV) of autoclaved Milli-Q water.
 - Then equilibrate the column by passing 1 CV of SEC buffer.
 - Then filter the concentrated protein with a 0.45 µm syringe filter and then inject it into the SEC column.
 - The SEC-purified protein is analyzed on a 12% SDS-PAGE gel with standard protein markers.
 - Then pool the desired protein fractions and concentrate for further studies.

10. Potential pitfalls, errors, and other issues

Issue	Known resolution
Heavy Precipitation while refolding	Include enough protease inhibitors Use only properly washed autoclaved bottles for refolding Do not over-speed the magnetic stirrer Use the exact heavy chain: light chain ratio
Errors in FPLC purification	Make sure column is properly connected to the machine Make sure that protein is collected in fraction collector Try to maintain the optimum flow rate for the FPLC column

11. Instructions for the use of SOPs

General Rules:


Use the newest version of an SOP for your experiment.

Record the number of the SOP (found in the page header) in your experiment protocol.

Any changes between the SOP and your experiment must be documented in your experiment protocol.

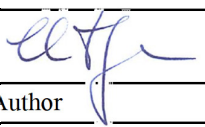
If you believe that the SOP needs to be changed or extended, bring it up in the subgroup meeting.

2.3.2. SOP: Small scale refolding - 1 mL

	Springer Group Standard Operating Procedure (SOP)
SOP No.:	SSP-SOP-BCM_003
Title:	Small-scale (1 mL) refolding of MHC-I
Revision No.:	4
Revision Date:	15-Jul-21

1. Information about this Standard Operating Procedure

SOP No., Title, Revision No., Revision Date: see page header

Author of this Revision:	Ankur Saikia		
Signature of Principal Investigator:			
Revision History:	Revision No.	Author	Date
	1	Nouria	unknown
	2	Sebastian and Nouria	2-Jul-19
	3	Franzi	12-Nov-20
	4	Ankur Saikia	15-Jul-21
Other SOPs, documents, or attachments required for the procedure	SSP-SOP-BCM_001 for Inclusion body preparation. SSP-SOP-BCM_012 for TDTF measurements. SSP-SOP-BCM_013 for nDSF measurements		

2. Purpose and general description of the procedure (1-2 sentences)

Small scale (1 mL) refolding of MHC-I molecules.

3. Terms and abbreviations used in this document

Term or Abbreviation	Explanation
β_2m	Beta-2-microglobulin
α_3	alpha 3
HC	heavy chain
Kb	Murine MHC-I molecule H-2Kb
A2	Human MHC-I molecule HLA-A*01:02
EDTA	Ethylenediaminetetraacetic Acid
SOP	Standard Operating Procedure

4. Chemicals required

Chemical	Company and Catalog No.	Safety?	Batch?
Tris base	Sigma-Aldrich	n/a	n/a
L-Arginine	Sigma-Aldrich	Warning	n/a
EDTA	Sigma-Aldrich	Warning	n/a
Oxidized glutathione	Applichem	n/a	n/a
Reduced glutathione	Applichem	n/a	n/a

6. Safety considerations

Chemical or Reagent	Classification according to Regulation	Safety consideration (H/P numbers)
L-Arginine	H319- Serious eye damage/ eye irritation	H319, P280, P305+P351+P338
EDTA	H332 - Acute Toxicity-Inhalation (Category 4)	H332, P261, P271, P304+P340, P312

7. Buffers and stock solutions (='reagents')

Reagent	Preparation, aliquoting, storage			
50 x Glutathione stock	For storage and stability prepare separate 100x stocks of reduced and oxidized Glutathione Stock.			
	Parameters	Reduced Glutathione		Oxidized Glutathione
	Final Conc. (1x)	5 mM		0.5 mM
	Stock Conc. (100x)	500 mM		50 mM
	Molecular weights	612.64 g/mol		307.33 g/mol
	Amount for 5 ml 50x	770 mg		150 mg
	Prepare sufficient amount of reduced and oxidized Glutathione stocks (5 mL would give ~ 50 aliquots) Oxidized Glutathione dissolves easily at 50 mM concentration (100x). Reduced Glutathione at 500 mM concentration (100x) requires prolonger mixing to dissolve at RT. For faster dissolving warm the sample to 37°C (<10 min) and vortex thoroughly. Aliquot in 100 µl stocks and freeze them at -20 °C.			
2 x Refolding Buffer pH 8.0	Reagent	Stock conc.	2 x	Amount/volume
	Tris-HCl, pH 8	1 M	200 mM	20 mL
	L-Arginine HCl	Powder	1 M	16.8 g
	EDTA	500 mM	4 mM	0.8 mL
	H ₂ O (Milli-Q)	Make-up the volume to 100 mL		
	This 2x stock can be kept at 4 °C for a month. Aliquot and freeze in -20 °C for longer duration.			
Buffer E	6 M Guanidine HCl, 50 mM HEPES, pH 7.5			
Peptide/Dipeptide	1 mM for full-length peptides, 100 mM for dipeptides.			
hβ ₂ m	10 mg/mL (usually)			
HC or α ₃	10 mg/mL (usually)			

8. Equipment and accessories required

Type of equipment	Special Instruction?
Ultracentrifugation	Yes.
Eppendorf centrifuge 5415R	No.
Prometheus nDSF reader	yes
1.5 mL ultracentrifuge tubes	No.
Tube rotator in 4 degrees.	No.

9. Procedure (numbered list)

Add the following components, except HC, to a 1.5 mL Eppendorf tube in the order given important:
Keep the order, always work on ice!

Component	Stock concentration	Final concentration	Amount for 1 mL refold
Water	-	-	450 μ L or 360 μ L*
2 x Refolding Buffer	2x	1x	500 μ L
Red./Ox. Glutathione mix	50x (after mixing)	1.0 x	20 μ L
Peptide or Dipeptide	1mM or 100 mM	10 μ M or 10 mM	10 μ L or 100 μ L
h β ₂ m	10 mg/mL	100 μ g	10 μ L*
HC (e.g. HLA-A*02:01)	10 mg/mL	100 μ g	10 μ L*

* If the concentration of HC or α ₃ or β ₂m inclusion bodies vary, please calculate the amount accordingly and adjust the volume of water in the first step of addition.

If HC is used, wait 30 minutes before adding. Keep the tube on ice during this time.

Through the waiting time, β ₂m or α ₃ can fold, which in turn promotes the folding of the heavy chain.

Add 100 μ g (or whatever amount desired) of the heavy chain of interest.

Fix the tube on the tube rotator in the cold room and incubate 2-4 days for murine allotypes and 4-7 days for human allotypes.

For murine β ₂m/ HC/peptide refolds, 2 days are sufficient

For β ₂m and α ₃ refolds, 30 minutes are sufficient.

Ultracentrifuge the sample at 100,000 g for 20 minutes at 4°C.

Make sure to balance the tubes before! The maximum tolerance is \pm 0.001 grams.

Collect the supernatant in fresh 1.5 mL ultracentrifuge tube and discard the palette.

These refolds can be stored at 4 °C for later use or further processed for TDTF/nDSF and peptide exchange studies.

11. Potential pitfalls, errors, and other issues (each in one table row)

Issue	Known resolution
HC Precipitation	Slowly add HC in smaller (2 -3 μ L) aliquots followed by gentle mixing by inverting the tubes. Wait 15 minutes in-between addition.

12. Instructions for the use of SOPs

General Rules:

Use the newest version of an SOP for your experiment.

Record the number of the SOP (found in the page header) in your experiment protocol.

Any changes between the SOP and your experiment must be documented in your experiment protocol.


If you believe that the SOP needs to be changed or extended, bring it up in the subgroup meeting.

Explanations of the individual points:

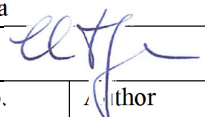
3. Abbreviations: Abbreviations of chemicals are explained in 5.

5. "Chemicals" are all powders (but not stock solutions, see 6.)

2.3.3. SOP: Micro-scale refolding: 250 μ L

	Springer Group Standard Operating Procedure (SOP)
SOP No.:	SSP-SOP-BCM_020
Title:	MHC-I refolding from inclusion bodies in 96-well formats
Revision No.:	1
Revision Date:	Oct 10, 2019

1. Information about this SOP

Author of this revision	Ankur Saikia		
Signature of principal investigator			
Revision history	Revision No.	Author	Date
	1	Ankur Saikia	10.10.2019
Other SOPs, documents, or attachments required for this procedure	SSP-SOP-BCM_019: Dipeptide plate preparation		

2. Purpose and general description of the procedure (background)

This protocol describes how to prepare 250 μ l refolds in a 96-well format. These refold are used in competitive ELISA assays to screen small molecules (e.g. dipeptides) that efficiently promote the refolding of MHC-I molecules.

3. Terms and abbreviations used in this document

Term or abbreviation	Explanation
DTT	1,4-Dithiothreitol
EDTA	Ethylenediaminetetraacetic acid
ELISA	Enzyme-linked immunosorbent assay
FB	Flat bottom
h β ₂ m	Human beta-2 microglobulin
HC	Heavy chain of the class I allotype
HCL	Hydrochloric acid
LB	Low-binding
LC	Light chain (human β ₂ m, h β ₂ m)
MQ	Ultrapure water (Milli-Q)
NB	Non-binding
PMSF	Phenylmethanesulfonyl fluoride
PS	Polystyrene
UB	U-shaped bottom

4. Chemicals required	
Chemical	Company and Catalog No.
Heavy chain of MHC class I, in -80 °C	In-house
Light chain (human β_2m), in -80 °C	In-house
Full length peptide, in -20 °C	Customized (Genecast, Genescript)
Dipeptides	Customized (Genecast, Genescript)
Trizma® base	Sigma Aldrich # T1503
L-Arginine HCl	PanReac # 1119-34-2
Reduced glutathione	Sigma Aldrich # G6529
Oxidized glutathione	Sigma Aldrich # G4626
PMSF	Sigma Aldrich # 78830-1G
EDTA	Sigma Aldrich # E6758-100G
DTT	Merck # 3483-12-3
Guanidine hydrochloride	Sigma Aldrich # G3272

6. Safety considerations		
Chemical or Reagent	Classification according to Regulation	Safety consideration (H/P numbers)
L-Arginine	H319- Serious eye damage/ eye irritation	H319, P280, P305+P351+P338IF
EDTA	H332 - Acute Toxicity-Inhalation (Category 4)	H332, P261, P271, P304+P340, P312

6. Buffers and stock solutions (= reagents)	
Reagent	Preparation, aliquotting, storage
Refolding buffer, pH 8.0 (This is a special refolding buffer used for 96-well plates only.)	200 mM Tris-HCl, pH 8.0 1.67 M L-Arginine HCl 6.67 mM EDTA Adjust pH to 8.0 with 5 M NaOH. Make up the volume by MQ water. Aliquot and store at -20 °C for longer duration.
Resolubilization Buffer	6 M Guanidine HCl, 50 mM HEPES, pH 7.5
100x stock of reduced glutathione	Dissolve 500 mM reduced glutathione in water. Aliquot and freeze at -20 °C until use. Do not freeze repeatedly. Discard the remaining solution once the aliquot is thawed.
100x stock of oxidized glutathione	Dissolve 500 mM reduced glutathione in water. Aliquot and freeze at -20 °C until use. Do not freeze repeatedly. Discard the remaining solution once the aliquot is thawed.

7. Equipment and accessories required

Type of equipment	Special instruction
96-well microplate, black, NB, FB, PS	n/a
96-well plate, clear, LB, UB, PS	n/a
Plate shaker, MS 3 digital, IKA	n/a
Multichannel pipettes	n/a
Plate sealer	n/a

8. Procedure (numbered list)

All steps on ice or at 4 °C (in the cold room) if not mentioned otherwise!

Dilute the solubilized inclusion bodies of MHC-I HC and of b2m in Resolubilization buffer to a final concentration of 5 mg/ml.

Prepare a 1 mM stock of a class I-specific reference peptide in water.

Prepare a 50x glutathione mix by mixing equal volumes of the two different 100x glutathione stocks (see section 6).

Take a Dipeptide plate (see section 13.1, step 2) already containing 100 µl of all the dipeptides of interest (see SSP-SOP-BCM_019, dipeptide stock concentration is 100 mM, final concentration in the refolding assay is 40 mM).

Prepare the Refolding mix according to the table below (except for the dipeptides that are already provided in the Dipeptide plate you use). The final volume of each well, i.e., each refolding reaction, is

Reagent	Stock concentration	Final concentration	Amount (µl)
Refolding buffer	-	-	75
MQ water	-	-	60
Glutathione mix	50x	1x	5
These three components are pooled together as a premix in a multichannel reservoir (identify the total volume of your premix according to the final number of wells you have). From there, the premix is added to the Dipeptide plate with a multichannel pipette.			
Reference peptide	1 mM	20 µM	100
To obtain a 20 µM final peptide concentration in a 100 µl volume, you have to include an additional dilution step in 100 mM Tris buffer, pH 8.0!			
Human β ₂ m	5 mg/ml	100 µg/ml	5
Class I HC	5 mg/ml	100 µg/ml	5
Both components are prepared separately in one lane of an extra 96-well plate. From there, you can transfer the reagents fast and easily with a multichannel pipette to the Dipeptide plate. Caution! The class I heavy chain is loaded last because it tends to precipitate. This step has to be carried out in the cold room where the Dipeptide plate can be shaken during pipetting of the heavy chain (of course, shaking has to be paused while actually pipetting).			
Total volume			250 µl

250 µl. The table thus indicates the volumes of each component in the mix in one single well.

The Dipeptide plate is now the Refolding plate. Seal it and leave it on a shaker rotating at 300 rpm in a cold room (4 °C) for a total of 7-10 days to allow proper refolding. Keep it dark.
 Centrifuge the plate at 4,000 rpm, 4 °C for 15 min to precipitate insoluble impurities.
 The Refolding plates can be stored at 4 °C until use. The preferred loading scheme of a Refolding plate is shown in 13.2.

For competition, gently transfer 5 µl of supernatant from the top to the Sample plate (see section 13.1, step 4, and SSP-SOP-BCM_021).

Tip: Oxidized glutathione is sensitive to light and oxygen. Therefore, always keep the Refolding plate in the dark by covering it with aluminium foil and make sure that the stirring is at a setting where it is not creating bubbles.

9. Potential pitfalls, errors, and other issues (each in one table row)

Issue	Known solution
Evaporation at the outer wells (surrounding outer wells of the plate, see section 13.2)	Avoid using the outer plates wells at all for refolding. Add buffer to the outer wells. Always use plate sealers.
Low refolding efficiency	Protect from light. Further dilute the HC and β 2m inclusion bodies solutions. Use already folded β 2m if available. Try to keep the concentration of guanidine hydrochloride as low as possible.
Variability between different assays	Precise pipetting is required for smaller volumes. Use calibrated pipettes. Pipette carefully to avoid cross-contamination. Always change tips between steps.

10. General instructions for the use of SOPs

It is important to follow these instructions thoroughly! Please ask Sebastian in case of unclarities!
 There will only be one SOP for each technique available online, which represents the newest version of that SOP. Download the respective SOP before starting your experiment (do not use a pdf or Microsoft word version of it because that one might not be up-to-date anymore).

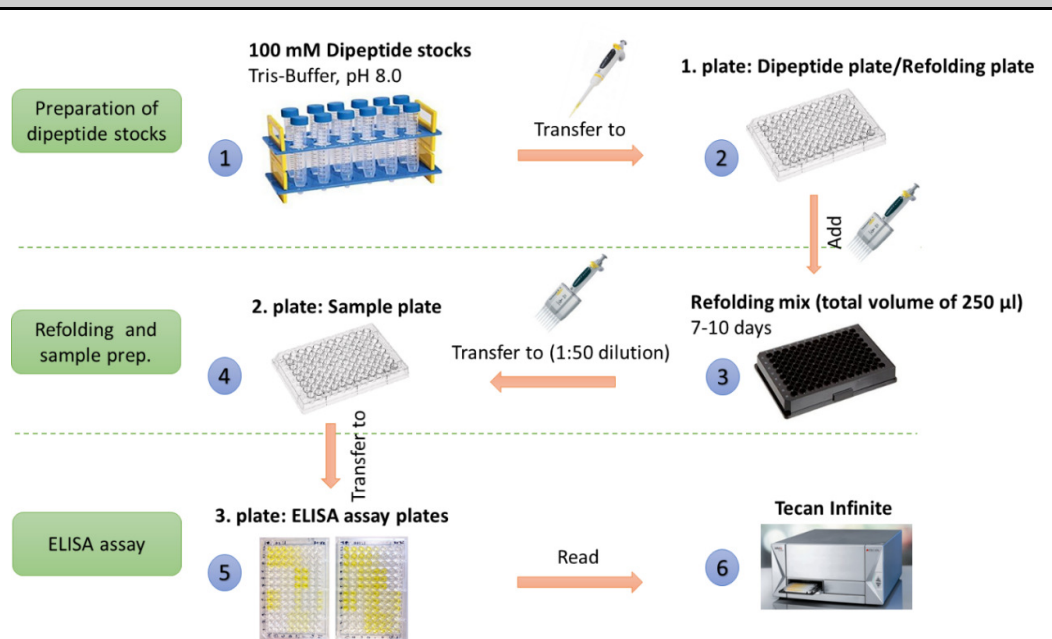
Record the number of the SOP (found in the page header) in your experiment protocol.

Any changes between the SOP and your experiment must be documented in your experiment protocol.

If you believe that the SOP needs to be changed or extended, do never try to change the online SOP but talk to Sebastian or bring up your suggestions in the subgroup meeting.

11. Appendix⁶

1. Dipeptide screening workflow



The first plate in the work flow is the Dipeptide plate, in which the different dipeptides are prepared (steps 1+2). After addition of the refolding mix, the Dipeptide plate becomes the refolding plate, where class I refolding can take place (step 3). For preparation of the ELISA assay, 5 µl of supernatant are transferred from the Dipeptide/Refolding plate to a second plate, the Sample plate, to which antibody is added for competition ELISA (step 4). To read the assay, each sample/well in the Sample plate is divided in half and transferred as duplicates to two ELISA assay plates (steps 5+6). This SOP describes step 3 of the entire procedure.

⁶ Insert everything helpful and worth mentioning such as clarifying figures, loading or pipetting schemes etc..

2. Loading scheme of the Refolding plate

	1	2	3	4	5	6	7	8	9	10	11	12
A	Buffer	Buffer	Buffer	Buffer	Buffer	Buffer	Buffer	Buffer	Buffer	Buffer	Buffer	Buffer
B	Buffer	AcF	AcG	AcI	AcK	AcL	AcM	AcR	AcV	Class I/Pep.	A2/NV9	Buffer
C	Buffer	AcW	AcY	AG	AH	AI	AK	AL	AM	Buffer	Buffer	Buffer
D	Buffer	GA	GD	GE	GF	GG	GH	GI	GK	No β_2m	No β_2m	Buffer
E	Buffer	GL	GV	GW	GM	GR	GY	GGA	GGF	Class I/Pep.	A2/NV9	Buffer
F	Buffer	GGG	GGH	GGI	GGK	GGL	GGM	GGR	GGV	Buffer	Buffer	Buffer
G	Buffer	GGY	LG	GCi	GGSL	GSFG	GSGM	GSGI	SGGL	No β_2m	No β_2m	Buffer
H	Buffer	Buffer	Buffer	Buffer	Buffer	Buffer	Buffer	Buffer	Buffer	Buffer	Buffer	Buffer

Overview of the total plate loading scheme

The light green wells are the outer wells that are kept empty (loaded with buffer only) to avoid evaporation of sample.

The light pink wells (columns 2-9) contain the various dipeptides to be screened.

Columns 10 and 11 contain the negative and positive controls (see also table below).

B10 and B11 = positive controls containing class I complexes folded with full-length reference peptides (B10 contains the class I allotype on which the dipeptides are tested, B11 contains a different allotype plus a respective high-affinity peptide).

C10 and C11 = negative controls without peptide.

D10 and D11 = negative controls without peptide and β_2m

For further information to the controls, see also table below.

Sample	Refolding buffer	HC	β_2m	peptide
Class I/peptide	✓	✓	✓	✓
Buffer	✓	✓	✓	-
No β_2m	✓	✓	-	-

Components in the control columns (10 and 11)


Column 10 contains the HC allotype of interest with a reference full-length peptide.

Column 11 is a positive control generally containing human HLA-A2 (disulfide mutant) in complex with the NV9 peptide.

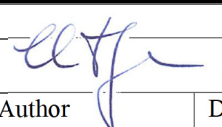
2.4. Protein Purification

This section describes the detailed procedure for purification of folded MHC-I protein using gel-filtration chromatography also known as size exclusion chromatography. The SOP has been optimized purification of MHC-I proteins after completion of refolding. Different throughput can be achieved by varying the columns size

2.4.1. SOP: MHC-I purification by size exclusion chromatography (SEC)

	Springer Group Standard Operating Procedure (SOP)
SOP No.:	SSP-SOP-BCM_023
Title:	Operating instructions for Äkta™ go and the Unicorn system
Revision No.:	2
Revision Date:	Oct 20, 2021

1. Information about this SOP

Author of this revision	Ankur Saikia		
Signature of principal investigator			
Revision history	Revision No.	Author	Date
	1	Franziska Köper	31.05.2021
	2	Ankur Saikia	20.10.2021
Other SOPs, documents, or attachments required for this procedure	If you want to evaluate your results with the classic evaluation panel, see SSP-SOP-BCM_008 “Handling and setup”		

2. Purpose and general description of the procedure (background)

ÄKTA™ go is a small and compact liquid chromatography system that is developed for the purification of biomolecules, in particular proteins. With flow rates of up to 25 mL/min and pressure of up to 5 MPa it can be used for affinity chromatography, size exclusion chromatography (SEC, also known as gel filtration), and ion exchange chromatography. This SOP gives an overview about the instrumentation, handling and maintenance of the ÄKTA™ go and the Unicorn system.

3. Terms and abbreviations used in this document

Term or abbreviation	Explanation
SOP	Standard operating procedure
MHC-I	Major histocompatibility complex class I
SEC	Size exclusion chromatography

4. Chemicals required

Chemical	Company and Catalog No.	Safety	Batch
Tris	Applichem	n/a	n/a
Sodium chloride	Applichem	n/a	n/a
Ethanol	Applichem	Danger	n/a

5. Safety considerations

Chemical or Reagent	Classification according to Regulation	GHS Classification (H/P sentences)
Ethanol	H225: flammable liquid (Section 2.6), H319: serious eye damage/eye irritation (Section 3.3)	H225, H319, P210, P233, P305+P351+P338

6. Buffers and stock solutions (= reagents)

Reagent	Preparation, aliquoting, storage
Ethanol 20 %	Dilute with ddH ₂ O, store at room temperature, Filter before use.
SEC Buffer	Prepare an appropriate buffer for running the sample. e.g. 1xPBS. Filter before use.
MQ water	Filter before use.

7. Equipment and accessories required

Type of equipment	Special instruction ⁷
Superdex™ 200 Increase 5/150 GL (3 mL bed volume)	Yes
Superdex™ 200 Increase 10/300 GL (24 mL bed volume)	Yes
Superdex™ 75 Increase 10/300 GL (24 mL bed volume)	Yes
HiLoad™ 16/600 Superdex™ 200 prep grade (120 mL bed volume)	Yes
HiLoad™ 26/600 Superdex™ 200 prep grade (320 mL bed volume)	Yes
Mono Q™ 5/50 GL	Yes
AKTA unicorn 7.5	Yes
Computer system	Yes
Fraction collector F9-R	Yes
5 mL sample loop	No
2 mL sample loop	No
1 mL sample loop	No
500 µL sample loop	No
100 µL sample loop	No
50 µL sample loop	No
Sartorius cellulose acetate filter (0.45 µm)	No

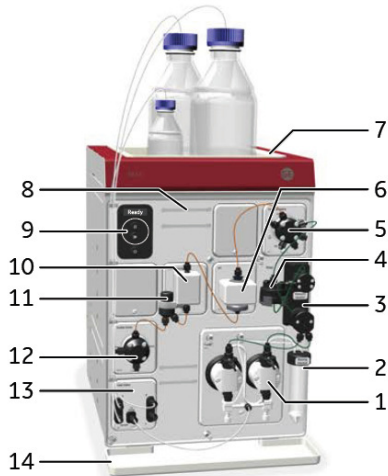
⁷ Insert “yes” if special instruction is necessary to operate this equipment.

8. Instrument General Information

8.1 General Overview of

8.1.1 the Äkta go instrument

The ÄKTA go instrument is delivered with standard modules installed. Six additional modules can be installed in the system, two inside the chassis and four connected via cables at the rear of the instrument. The following modules are installed in the instrument.



Part	Function
1	Pump
2	Pump rinsing solution tube
3	Pressure monitor
4	Mixer
5	Injection valve
6	UV monitor
7	Top tray
8	Holder rails
9	Instrument control panel
10	Conductivity monitor
11	Flow restrictor
12	Outlet valve
13	Inlet valve
14	Bottom tray

The illustration below shows the ÄKTA go instrument after installation.

To access the product page for ÄKTA go, go to www.gelifesciences.com/aktago.

8.1.2. UNICORN modules overview

UNICORN consists of four modules: Administration, Method Editor, System Control, and Evaluation. The main functions of each software module are described in the following table.

Administration	Perform user and system setup, system log, and database
Method Editor	Create and edit methods using one or a combination of: <ul style="list-style-type: none">• Predefined methods with built-in application support• Drag-and-drop function to build methods with relevant steps• Method text editing
System Control	Start, monitor, and control runs. The current flow path is illustrated in the Process Picture, which allows manual interactions with the system and provides feedback on run parameters.
Evaluation	Open results and evaluate runs. The Evaluation module includes a user interface optimized for workflows such as quick evaluation, comparing results, and working with peaks and fractions. Advanced features requires Evaluation Classic, available from GE Healthcare.

58

When working with the software modules *Administration*, *Method Editor*, *System Control*, and *Evaluation*, it is possible to access descriptions of the active window or software instruction by pressing the F1 key.

9. UNICORN software starting and operation

Modules to open are selected at log in, but can also be opened from another module when the software is already open. In the *Administration*, *Method Editor*, or *System Control* modules, to open a software module, click *Tools* and select the desired module. When in the *Evaluation* module, to open a software module, click *File:Applications* and select the desired module.

9.1. Start UNICORN and connect to system

Double click on the UNICORN icon on the desktop → Log on dialog box opens.

In the Log On box, select User Name (Default) and enter Password (default).

Tick the boxes for the UNICORN modules that you want to start.

Click “OK”.

If necessary, connect the system:

In the System Control module, click the Connect to Systems button →

Result: The “Connect to Systems” dialog box opens.

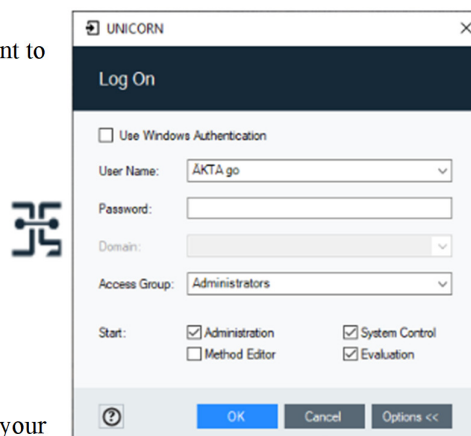
Select a system in the checkbox

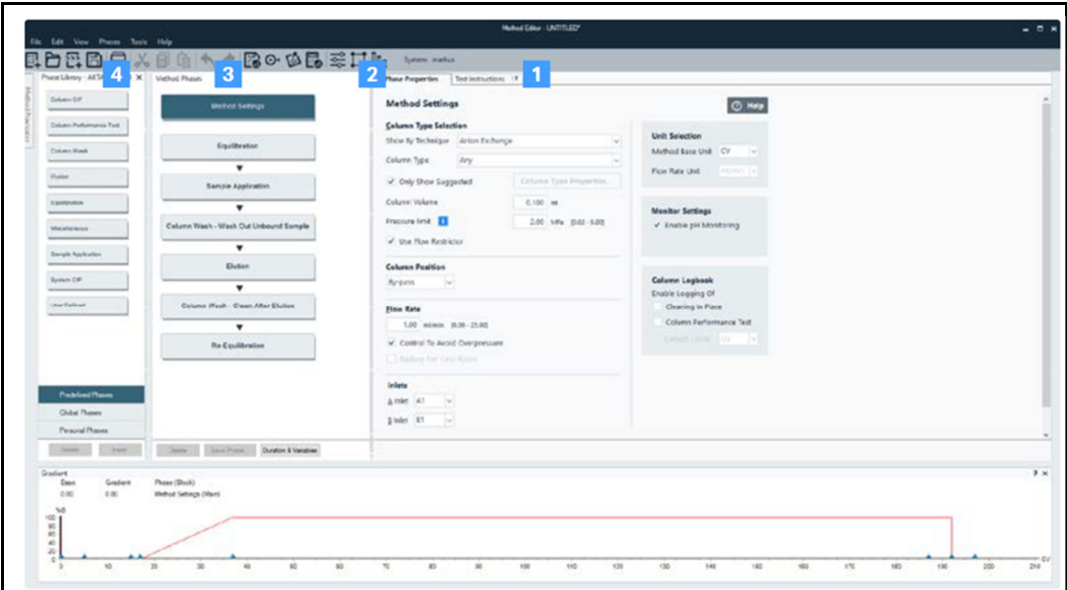
Click Control for that system

Click ok

9.2. Method Editor

Allows you to create or adjust methods to suit your application needs. A method is simply created by drag-and-drop of modules called phases. Each phase represents a step in the run - such as sample application or wash - and a chromatography run (method) is represented by several phases. Unicorn also includes a library of predefined Cytiva columns and column parameters (e.g. flow rate and pressure limits) that are automatically programmed into the method. For added flexibility, you can edit programming instructions directly in the Text instructions pane.





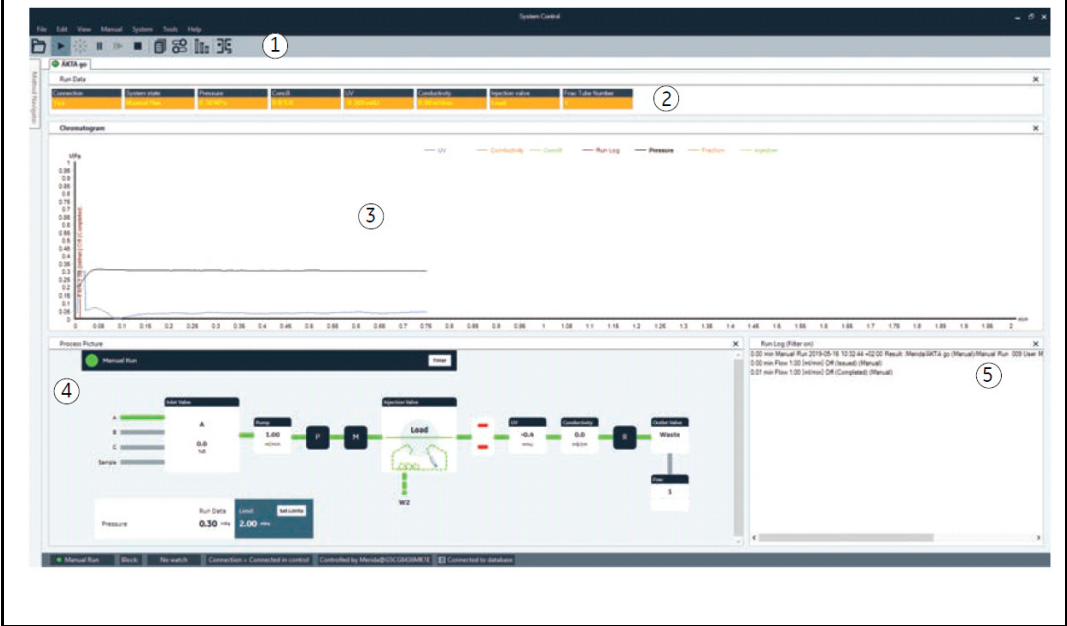
t	Description
	Tweaking of the method can be performed using Text instructions
	Set conditions to match your application in Phase properties
	Method phases shows the outline of a specific method
	Drag and drop phases (steps) from the Phase library to create methods or use preprogrammed metho

9.3. System Control

In this mode, all method run is performed either in manual mode or automatic predefined methods with the help of the interactive software interface as shown below.

9.3.1. User Interface











This module is used to start, view, and control a method run. The module consists of three panes - Chromatogram pane, Process picture, and Run log - that provide an overview of the status of the run



Part	Description
1	The toolbar buttons are used for quick access to instrument controls. For descriptions, see System Control toolbar buttons below.
2	The run data field shows the value of run data in boxes. This field is hidden by default. To make this field visible, go to View: run data.
3	The Chromatogram pane illustrates the chromatogram of the run.
4	The interactive Process Picture pane allows manual interactions with the system, illustrates the current flow path, and provides feedback on component status and run parameters.
5	The Run Log pane shows all registered events during the run.

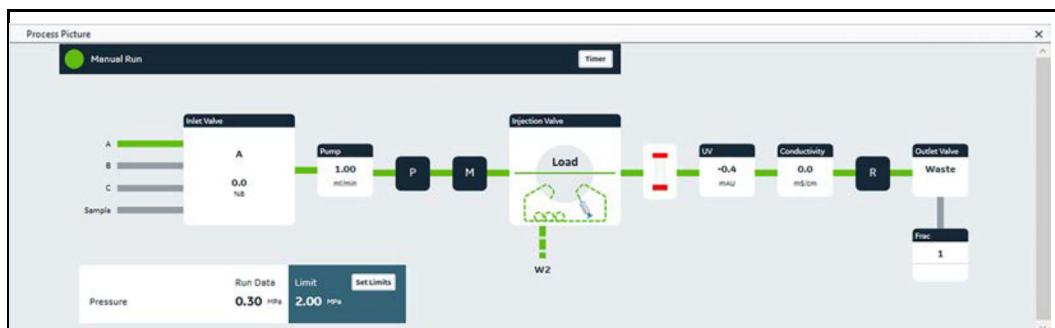
9.3.2. System Control toolbar buttons

The following table shows the System Control toolbar buttons.

Button	Function	Button	Function
	Open Method Navigator This button opens the Method Navigator where saved methods are listed.		Run This button starts a method run. The last method run will be started.
	Hold This button suspends the method run, while current flow rate and valve positions are sustained.		Pause This button suspends the method run and stops all pumps.
	Continue This button resumes a held or paused method run.		End This button permanently ends the run.
	Documentation This button opens a dialog containing information about the system and the current run.		Customize This button opens the Customize dialog box where curve settings, run data groups and run log contents can be set.
	Column Handling This button opens the Column Handling tool, which contains a column list, with parameters for GE Healthcare columns. With an additional license, a Column Logbook to keep track of user-purchased columns is also available.		Connect to Systems This button opens the Connect to Systems dialog box where systems can be connected, and currently connected users are displayed.

9.3.3. Process Picture pane

The most commonly used manual interactions can be done using the Process Picture. Click on the different parts of the Process Picture pane to interact with the system.



The interactive Process picture helps to quickly start manual runs and enables manual interaction during automated runs. It allows monitoring of the run, clearly displaying all relevant run data and system state. Among the most important attributes is the ability to monitor system pressure. The column pressure limits are easily set in the Process picture, either by importing them from the Column library or by manual settings, all to ensure the highest level of safety and integrity for the column and run. Estimated remaining time gives the user the estimated time for a method run to complete, providing the possibility to focus on other tasks, and still return to the system on time when the chromatography run ends. The timer function can be set to either volume or time, for smooth and easy equilibration or preparation of columns. In summary, the Process picture gives you intuitive access to all essential information and necessary functionality.

10. Method Editor

Creating a customized method

Follow the steps below to create a method using a predefined method template. The example given uses an Size Exclusion Chromatography method from UNICORN7.4. The Method Settings phase sets up parameters that are used throughout the method, such as unit for method base and flow rate. There are more ways to create methods in UNICORN. Refer to the UNICORN Method Manual for more information.

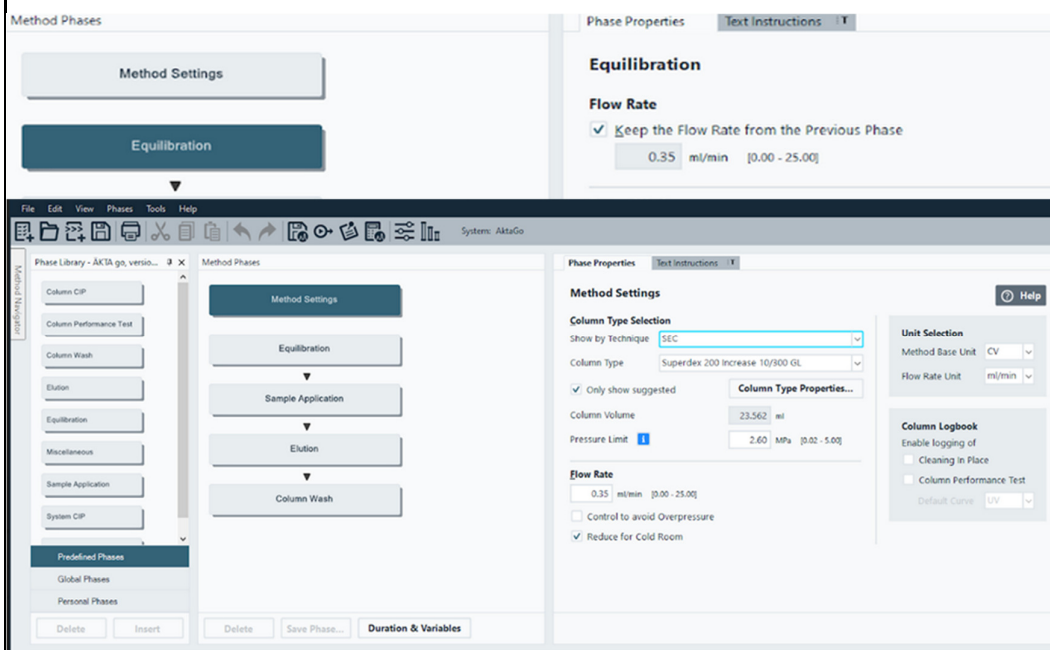
Open the Method Editor module, click the New Method button and choose the system and suitable predefined method.

Open the Phase Properties tab and confirm that all of the selections made in the phases correspond to your intended method allowing the steps below.

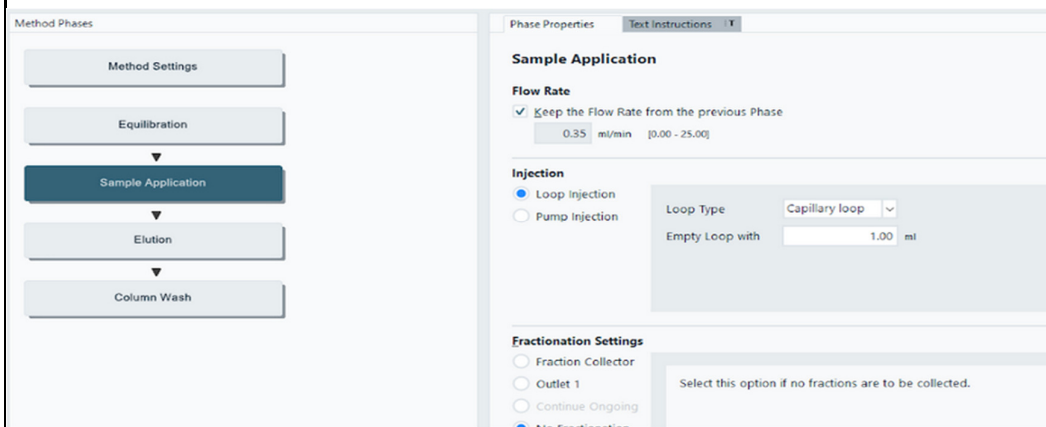
In the Method Settings phase, select column type to get suitable values, or enter correct values at Column volume, Pressure limit and Flow rate.

An optional Column wash phase is advised before Equilibration phase to make sure the column is free from 20% Ethanol (in which the column is stored). Choose a suitable volume (e.g. 1.5 CV) and 100% concentration of B solution that is water.

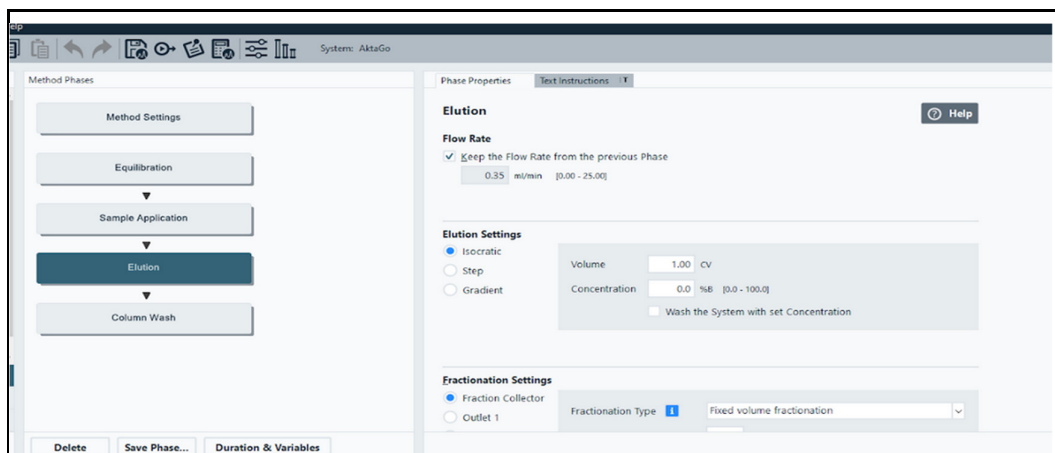
In the Equilibration phase, set a suitable volume and concentration of buffer B.



In the Sample Application phase, choose an appropriate sample application technique and volume. Flow rate = from previous, Injection = capillary loop, empty loop with 2x loop volume. Fractionation = no.



In the Elution phase, set buffer settings at isocratic (default inlet is A), how to elute the sample, the duration of the elution (1.5 CV), and volume of sample to be collected in each fraction tube. Allow initial 0.2 CV to bypass to the waste, as it do not contain any sample.



In the Column wash phase, choose a suitable volume (2 CV) and 100% concentration B (water), and bypass to waste container.

Click and save the button, choose the system, name, and location for your method and click Save.

NOTE: It is advisable to run a blank run, without a sample, before running the method with the sample. This makes sure that the column is clean and that the method and the system are set up properly.

11. Procedure for maintenance and method run

11.1. Prerequisites

Make sure that the system is correctly prepared. Confirm the following:

The sample inlet is primed and pump head is purged

The correct sample loop is loaded

The column is properly connected

The pressure alarm has an appropriate limit set.

That there is no air in the system

The buffer inlet tubing(s) is immersed in the correct buffer vessels

All waste tubing is immersed in the appropriate waste vessels that have sufficient empty volume

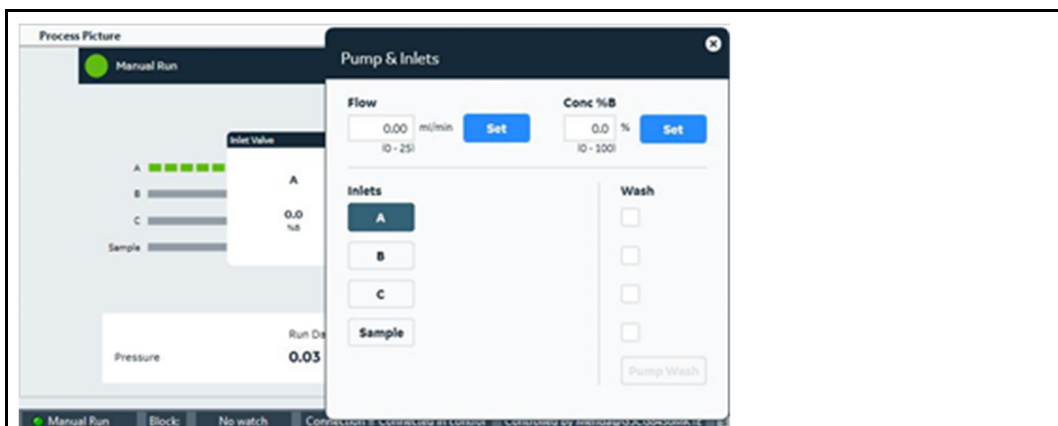
No tubing is twisted and the flow path is free from leakage

11.2. Prime inlets and purge pump heads

Make sure that all inlet tubing that is to be used during the run is placed in the correct buffer.

Open the System Control module.

In the Process Picture pane, click on Inlet Valve and select one of the inlets to be primed



Result: The inlet valve opens the selected inlet.

Connect a 25 to 30 mL syringe to the purge valve of one of the pump heads.

Open the purge valve by turning it counter-clockwise one and a half turns. Draw liquid slowly into the syringe until liquid reaches the pump and the inlet tubing is filled with liquid.

Close the purge valve by turning it clockwise. Disconnect the syringe and discard its contents.

Repeat steps 3 to 6 for each inlet that is to be used during the run.

11.3. Prime the pump rinsing system

11.3.1. Rinsing solution

The pistons and the back of the pump heads need to be washed with 20% ethanol. Reason: the seal/gasket that seals the pump head is a little bit leaky (by design) because it needs to be lubricated by the buffer (else it becomes too hot). Because of that, a little bit of the chromatography buffers leaks behind the seal. If it evaporates, then salt crystals will form and destroy the seal. So, the back of the pump head needs to be rinsed. That is what the rinsing solution is for.

The rinsing solution should be changed every 4 weeks. Use 25-35 ml of 20% ethanol in water.

11.3.2. Filling the pump rinsing system with rinsing solution

Unscrew and remove the rinsing solution tube from the holder.

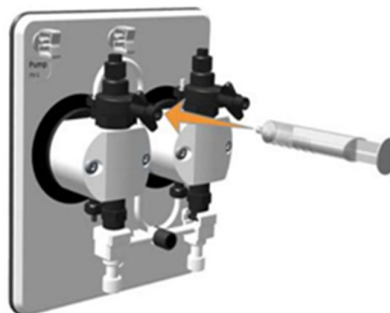
Fill the rinsing solution tube with 50 mL of 20% ethanol or aqueous buffer.

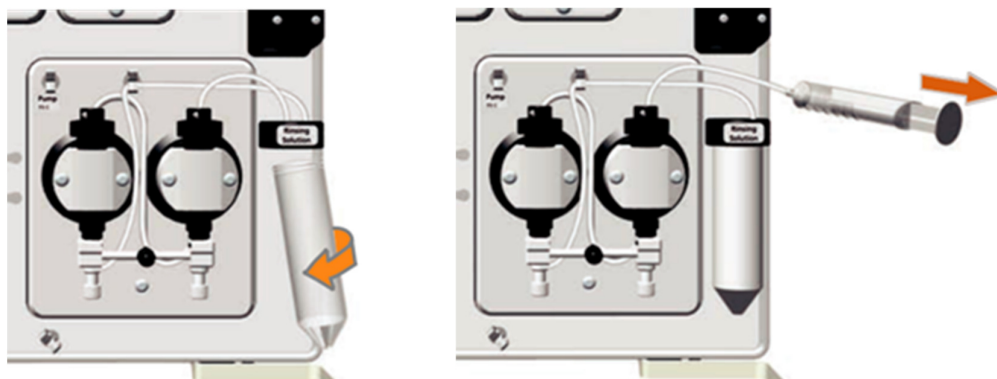
Screw the rinsing solution tube back into the holder (left panel in figure below).

Insert the inlet tubing into the solution in the rinsing solution tube.

Note: Make sure that the inlet tubing reaches close to the bottom of the rinsing liquid tube.

Connect a 25 to 30 mL syringe to the outlet tubing. Draw liquid slowly into the syringe until the rinsing system tubing is filled (right panel in figure below).





11.4. Connect a column

Before connecting the column to the ÄKTA SEC, start the system and the pump to remove all air bubbles from the system, the loops and valves.

Clean the tubings A or B (depends of which of them will be in use) with Milli-Q water.

11.4.1. Connecting a new column

Attach an appropriate column holder to the rail on the instrument

Attach the column to the holder

Cut a tubing of appropriate length to connect it between the injection valve and the top of the column.

Connect this tubing to the column port “Col” of the injection valve.

NOTE: Use red finger lights for columns with a red top and black for other columns.

In the Process Picture pane, select “Pump”, enter a low System flow (e.g. 0.2 mL/min), and click “Set”

In the Process Picture pane, select “Select limits” in the Pressure pane. Choose an appropriate column or manually enter a pressure limit suitable for your column. Click “Set”. Result: A pressure limit for your column is set.

Remove the stop plug from the top of the column

When the buffer is dripping from tubing prepared in step 3, fill the top part of the column with the buffer by letting it drip from the tube. When it is filled, connect the tubing drop-to-drop to the top of the column.

Note: Make sure that the connectors are properly tightened, but do not overtighten when connecting the columns. Overtightening might rupture the connectors or squeeze the tubing and thereby result in higher back pressure.

Cut a piece of tubing with appropriate length to connect the bottom of the column to the UV monitor. Remove the stop plug from the bottom of the column and connect this tubing in its place.

When the buffer is dripping from the tubing connected to the bottom of the column, connect this piece of tubing to the UV monitor.

11.4.2. Uninstalling the connected column

Ensure continuous flow: Choose inlet “C” in the system control panel (C inlet should be connected to 20% Ethanol or select the appropriate inlet) and set a flow rate of 0.3 – 0.5 ml/min.

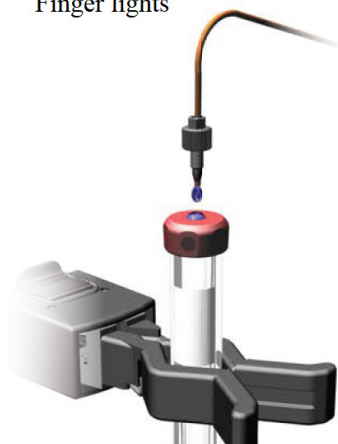
Go to the device and start with the bottom tube first. Disconnect the bottom tube connected to the UV monitor.

Add the stop plug to the bottom of the tube, and wait until the plug is partially filled (mark).

Press “pause” manually on the Äkta machine.



Finger lights



Add the spring to the stop plug to create reverse pressure on the bottom of the column.
Remove the upper tube from the old column that is connected to the “col” channel of the inlet valve and add a cap.

Leave the disconnected column in the hanger or storage for future use.

11.5. Connecting a sample loop to the system

The used loop depends on injection volume e.g. 5 mL loop for 5 mL injection.

In the Process Picture make sure the the injection valve is in position Load.

Note: Load is the default position for the valve.

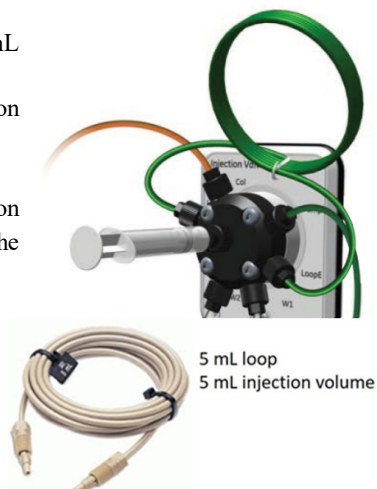
The sample loop and the super loop will be connected at the injection valve at the ports LoopF (fill) and LoopE (empty). (shown on the diagram).

At injection valve port Syr. a luer female/1/16" male union will be attached (shown below).

Then a syringe filled with water is attached to the luer union and the water is injected into the valve. Leave the syringe attached.

Note: Make sure to remove the air bubbles from the syringe before the injection.

Repeat the cleaning step 3 times until the total volume of the loop was reached.



11.6. Prepare the system for a run

Install the appropriate column according to instruction above. Before you apply your sample, you need to wash the column.

With Water , SEC Buffer

Column wash can either be added to the chosen method (see section 10) or be performed manually. Therefore, the parameters Flow rate and Pressure Alarms have to be defined individually for each column type. This can be done in the Process Picture of the System control panel.



11.7. Column wash and equilibration (Manual Method)

Note: Equilibrate the column a day before the estimated usage to save time.

Ensure that an appropriate pressure limit has been set for the specific column using the process picture of the System control panel. It can be selected automatically or entered manually if the limits are known.

First, equilibrate the column with water (2 Column Volumes (CV)). Inlet A.

Fill the tube with SEC buffer (50 mM Tris pH 8.0; 150 mM NaCl). Inlet B.

Setting values using process picture in system control panel

For washing the column, select the inlet A containing water.

Run pump wash using inlet A.

Set flow rate to depending on the column used (usually 0.3 - 0.5 ml/min). Run process starts.

Set the timer to required volume.

Repeat steps 1 to 4 for equilibrating the column with buffer of interest.

Use the Run/Pause/Stop buttons at the top for manually controlling the process.

Note: If the column is filled with 20 % ethanol, do not use a salt-containing liquid for equilibration, because salt might precipitate in 20 % ethanol. Start by washing the column with water first.

11.8. Purification Run (Using Predefined Method)

11.8.1. Prepare sample for application

After the protein refolding, the solution is filtered and then concentrated (VivaSpin, Sartorius ultra filtration device). This section describes how to prepare the sample for loading onto the column by using a sample loop.

Choose column: The needed column will be chosen by considering the volume of the refold and the

Refold volume	Concentrate to	Loop volume	Column used, bed volume
1000 mL	10 to 5 mL	5 mL	HiLoad 26/600 Superdex 200 prep grade, 320 mL
500 mL	5 to 2 mL	5 mL	HiLoad 16/600 Superdex 200 prep grade, 120 mL
100 - 250 mL	500 µL	500 µL	Superdex 200 Increase 10/300 GL, 25 mL
50 mL	250 µL-100 µL	100 or 500 µL	Superdex 200 Increase 10/300 GL, 25 mL
10 mL	50 µL	50 µL	Superdex TM 200 Increase 5/150 GL, 3 mL

volume of the concentrated refold.

Superdex-200 prepacked columns are the best choice for the purification of MHC-I molecules with a broad molecular weight separation range between 10,000 and 600,000 Da.

Sample preparation: Centrifuge the concentrated protein at high speed (15000 rpm/ 15 min) to remove unwanted particles in the protein sample.

Buffer preparation: Prepare the SEC buffer (50 mM Tris pH 8.0, 150 mM NaCl buffer)(with or without dipeptide) and filter the buffer solution through 0.45 µm or 0.22 µm filters before use.

Sample Injection:

Connect a suitable sample loop to the injection valve ports Loop F (fill) and Loop E (empty)

Prime the sample loop with 1 - 2 loop volume using a syringe.

Fill a syringe with sample. Avoid air bubbles!

Note: If all the sample must be conserved/loaded, use 50% of the sample loop size (e.g., 250 µl into a 500 µl loop)

In the Process Picture, make sure that the injection valve is in position Load

Note: Do not the load protein sample before the inject valve is in the load mode.

Connect the syringe to the injection valve port Syr.

Carefully inject the sample completely using mild pressure.

Note: Leave the syringe in the port after loading, otherwise air might get in and the sample will run into the waste (siphoning).

Run Method:

Open the System control module and click the button Open Method Navigator



Select a method to run, and click the Run button



Step through the display pages in the Start protocol, add requested input and make appropriate changes if necessary, Click Next.

Click Start on the last page of the Start Protocol.

12. Interpretation and reporting of the data

12.1 Evaluate the run

After the run is completed, the results can be evaluated using the Evaluation module. To open the results, use the following steps. For more information on evaluating results, refer to the UNICORN user documentation. If intended, you can also evaluate your results with the classical evaluation method (SSP-SOP-BCM_008 "[Handling and setup](#)")

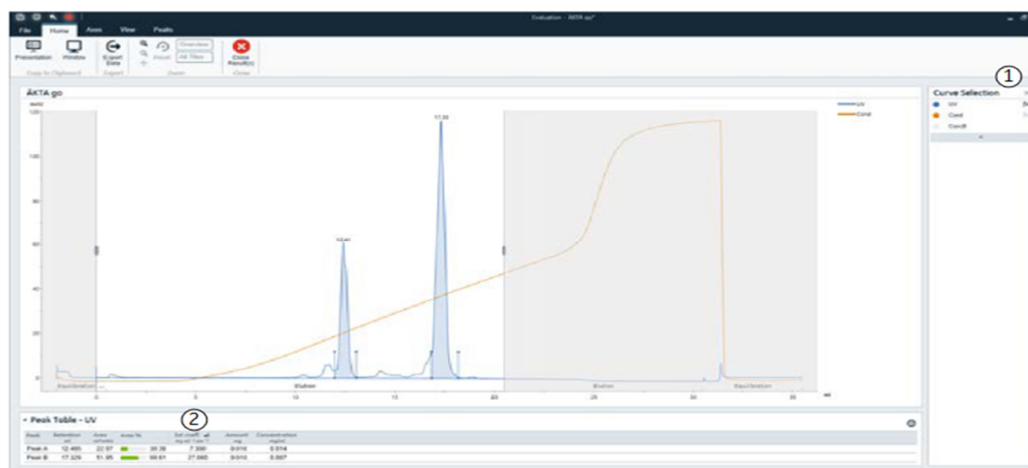
In the Evaluation module, click Result. Browse or search for your result file.

Check in the preview that you have the correct result file and click Open.

To save the evaluation file, click File:Save.

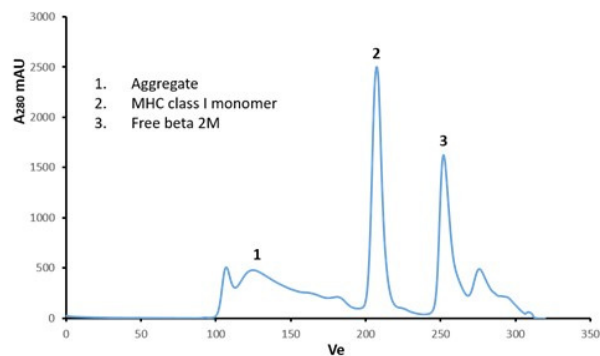
12.2. Illustration of an evaluated run

The image below shows an example of the features available in the Evaluation module UNICORN 7.4.



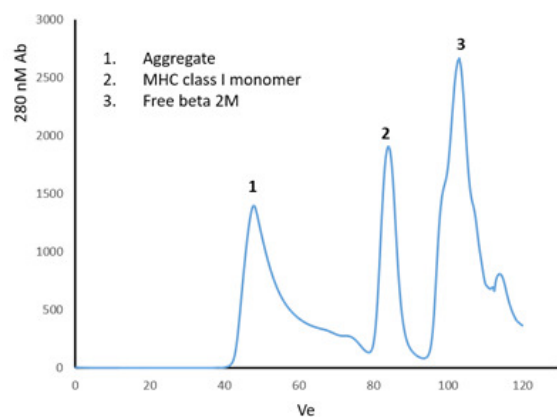
Part	Function
1	To integrate or remove integration click the fx button next to the curve name. To adjust integration parameters go to the Peak tab.
2	Data from the integration is shown in a Peak table below the chromatogram. Customize the Peak data table by clicking the settings icon on the top right of the Peak table.

12.3. Profile for the MHC-I protein in different columns



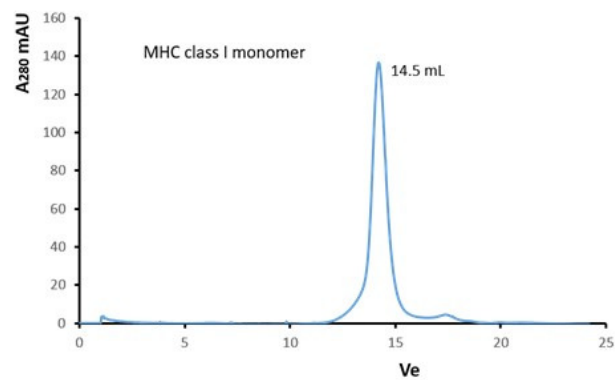
HiLoad 16/600 Superdex 200 prep grade (120 mL)

Peak elution volume (Ve) for the complex is 84 mL At 4 °C



HiLoad 26/600 Superdex 200 prep grade 320 mL Bed

Peak elution volume (Ve) for the complex is 212 mL At 4 °C



Superdex 200 Increase 10/300 GL (25 mL)

Peak elution volume (Ve) for the complex is 14.5 mL At 4 °C

13. Potential pitfalls, errors, and other issues (each in one table row)

Issue	Known resolution
Peak of interest is poorly resolved	Decrease sample volume and apply sample carefully. Clean the column and re-equilibrate. Re-equilibrate column, filter sample, and repeat.
Molecule does not elute as expected.	Prepare fresh samples. Clean the column, exchange or clean the filter, or use a new column.
Back pressure increases during a run or during successive runs.	Clean the column using recommended methods. (Refer CIP)
Air bubbles in the bed.	Degas buffers thoroughly. Repack column if needed
Gap between resin bed and adapter.	Clean the column if dirty. Adjust the adapter to the resin bed. Do not exceed maximum flow rate for resin or packed column.

14. General instructions for the use of SOPs

It is important to follow these instructions thoroughly! Please ask Sebastian in case of unclarities!
 There will only be one SOP for each technique available online, which represents the newest version of that SOP. Download the respective SOP before starting your experiment (do not use a pdf or microsoft word version of it because that one might not be up-to-date anymore).
 Record the number of the SOP (found in the page header) in your experiment protocol.
 Any changes between the SOP and your experiment must be documented in your experiment protocol.
 If you believe that the SOP needs to be changed or extended, do never try to change the online SOP but talk to Sebastian or bring up your suggestions in the subgroup meeting.

15. Appendix


For further information see:

Äkta go Operating Instructions (<https://www.cytivalifesciences.co.kr/wp-content/uploads/2020/04/29360951AC.pdf>, 02.06.21)

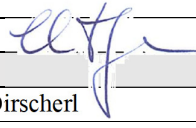
UNICORN 7.5 System Control Manual

(<https://www.cytivalifesciences.co.kr/wp-content/uploads/2020/04/UNICORN-7.5-System-Control-Manual.pdf> 02.06.21)

2.4.2. SOP: Antibody purification from hybridoma supernatant

	Springer Group Standard Operating Procedure (SOP)
SOP No.:	SSP-SOP-BCM_017
Title:	Antibody Purification from Hybridoma Supernatant
Revision No.:	3
Revision Date:	17. August 2017

1. Information about this Standard Operating Procedure

SOP No., Title, Revision No., Revision Date: see page header			
Author of this Revision:	Cindy Dirscherl		
Signature of Principal Investigator:			
Revision History:	Revision No.	Author	Date
	1	Cindy Dirscherl	(2018)
	2	Nouria Jantz	15. 8. 2019
Other SOPs, documents, or attachments required for the procedure	Production of hybridoma supernatant		

2. Purpose and general description of the procedure (1-2 sentences)

To purify antibodies from prepared hybridoma using protein A beads, elution, and dialysis.

3. Terms and abbreviations used in this document

Term or Abbreviation	Explanation
TRIS	TRIS-(hydroxymethyl)-aminomethane
PBS	phosphate buffered saline
SDS PAGE	sodium dodecyl sulfate polyacrylamide gel electrophoresis

4. Buffers and stock solutions (= 'reagents')

Reagent	Preparation, aliquotting, storage
1 M Tris base	For 1 L, dissolve 121.14 g of Tris in 1 L ddH ₂ O, store at room temperature and check before use for precipitation or other contaminations
100 mM Tris pH 8.0	For 1 L, dissolve 12.14 g of Tris in 1 L ddH ₂ O, or dilute from 1 M TRIS Stock, 1:10, store at room temperature and check before use for precipitation or other contaminations
10 mM Tris pH 8.0	For 1 L, dissolve 1.21 g of Tris in 1 L ddH ₂ O, or dilute from 1 M TRIS Stock, 1:100, store at room temperature and check before use for precipitation or other contaminations
100 mM Glycine	For 1 L, dissolve 7.51 g of Glycine in ddH ₂ O and adjust the pH to 2.5.
10 x PBS	For 1 L, dissolve 80 g of sodium chloride (NaCl), 2 g of potassium chloride (KCl), 14.4 of disodium phosphate (Na ₂ HPO ₄), and 2.4 g of monopotassium Phosphate (KH ₂ PO ₄) in 1 L ddH ₂ O, store at room temperature and check before use for precipitation or other contaminations
1x PBS	Prepare from 10 x PBS stock via a 1:10 dilution with ddH ₂ O.

8. Equipment and accessories required

Type of equipment	Special Instruction?
pH strips	No
BIO-RAD poly-prep chromatography column	No
Protein A bead slurry	No
Centrifuge tubes (15 and 50 mL)	No
5 L beaker for dialysis	No
Dialysis tubing and clamps	No
Microcentrifuge tube 1.5 mL	No
NanoDrop	No
Centrifuge	No

9. Procedure (numbered list)

1. Retrieve the desired hybridoma supernatant from the freezer.
2. Thaw the hybridoma supernatant in a water bath at 37 °C.
3. Adjust the pH of the hybridoma supernatant with 1 M Tris base to pH 8.0. Start by adding 1/20 of the volume of the hybridoma. Check pH with pH strips.
1. *Optional: Take a 10 µL sample for SDS PAGE for quality control later - store in freezer (-20°C).*
2. Add 1-1.5 mL of protein A slurry to a 15 mL centrifuge tube.
- Optional: Re-use protein A beads from previous purifications:*
 - I. *Retrieve the specific BIO-RAD column for the desired antibody with the bead slurry inside.*
 - II. *Using 1 mL of 100 mM TRIS, pH 8.0, (if the column does not already contain sufficient buffer) pipette up and down to resuspend the beads in the column.*
 - III. *Pipette the suspended beads from the column into a 15 mL centrifuge tube.*
 - IV. *Add a small amount, ~500 µL, of 100 mM TRIS, pH 8.0, to the BioRad column so that it will not dry out and return it to the refrigerator.*
 - V. *Proceed with step 6.*
1. Add 10 mL of 100 mM Tris, pH 8.0, to the slurry in the 15 mL centrifuge tube.
2. Centrifuge at 60 x g for 5 minutes at 4°C.
3. Remove supernatant (not the beads! Those should be pelleted at the bottom) and discard it.
4. *Optional: Repeat washing step*
5. Re-suspend the beads in ≈2 mL of the hybridoma supernatant.
6. Transfer the bead suspension to the centrifuge tube containing the hybridoma supernatant.
7. Pipette the hybridoma supernatant up and down with the same tip in order to ensure the complete transfer of all the beads into the hybridoma supernatant.
8. Incubate for 48 hours at 4 °C in the cold room on a turning wheel.
9. Retrieve the beads from the cold room and pipette everything onto the columns. (Washes and elution are done on a column because we realized that we lose a lot of beads which remain in the supernatant after centrifugation, and which would get discarded by discarding the supernatant.)
10. Let everything run through the column. The beads will accumulate at the bottom of the column.
11. Use up to 5 mL extra 100 mM TRIS, pH 8.0, to wash the centrifuge tube and ensure the complete transfer of all the beads to the column.

12. Wash the beads in the column by adding an additional 5 ml 100 mM Tris pH 8.0 to the column.
13. Prepare five 1.5 ml microcentrifuge tubes containing 50 μ L 1 M Tris pH 8.0.
14. Elute five fractions of the antibody from the column with 500 μ L 100 mM glycine, pH 2.5, into these five tubes.
15. Mix each fraction immediately after elution by flipping them upside down.
16. Shortly spin down the five fractions to ensure no drops are caught in the cap.
17. Measure the protein concentration of each fraction at the NanoDrop.
Blank: 500 μ L 100 mM glycine, pH 2.5 + 50 μ L 1 M TRIS, pH 8.0.
1. Pool the fractions that contain the protein (a significant concentration of the protein is usually > 0.100 mg/mL).
2. Prepare dialysis of the samples by cutting 5 – 7 cm of tubing and soaking it in 1 x PBS.
3. Close one end of the tubing with the dialysis tubing clamp.
4. Add the necessary protein fractions.
5. Close the remaining end of the tubing with another dialysis tubing clamp.
6. Label the samples in a clear manner if there is more than one.
7. Dialyze overnight against 5 L 1x PBS, pH 7.4, at 4°C (in the cold room).
8. Change the buffer the next day and dialyze again overnight against 5 L 1x PBS, pH 7.4, at 4°C (in the cold room).
9. Collect the antibody from the dialysis tube in a microcentrifuge tube.
10. Measure the concentration of the samples at the NanoDrop. (Blank: 1x PBS.)
1. *Optional: Run 11% SDS PAGE to check purification.*
2. *Alternative to steps 24-31: Desalting by buffer exchange, ask Sebastian.*

11. Potential pitfalls, errors, and other issues (each in one table row)

Issue	Known resolution
Elution of antibody from column	The antibody is usually found in the first two fractions. I have sometimes observed that the antibody comes only in fraction 3, so I recommend to always collect 5 fractions for elution.
Stock of protein A bead slurry	Common stock of protein A bead slurry is prepared: Buffer of protein A beads is exchanged for PBS+0.1% triton. Slurry is stored in aliquots at 4°C.

12. Instructions for the use of SOPs

General Rules:

Use the newest version of an SOP for your experiment.

Record the number of the SOP (found in the page header) in your experiment protocol.

Any changes between the SOP and your experiment must be documented in your experiment protocol.

If you believe that the SOP needs to be changed or extended, bring it up in the subgroup meeting.

Explanations of the individual points:


3. Abbreviations: Abbreviations of chemicals are explained in 5.

5. "Chemicals" are all powders (but not stock solutions, see 6.)

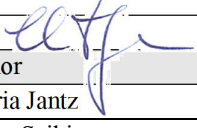
2.5. Thermal Stability Measurement

This section describes about the methods that I have utilized for thermostability measurement of MHC-I molecules. The methods that I have used are based on label-free technologies that provide rapid, sensitive and robust results. Over a period of time and repeated optimization we have included the most recent working parameters into the SOPs.

2.5.1. SOP: TDTF method for thermostability measurement

	Springer Group Standard Operating Procedure (SOP)
SOP No.:	SSP-SOP-BCM_012
Title:	TDTF measurements for determining melting temperatures of proteins
Revision No.:	2
Revision Date:	July 24, 2021

1. Information about this Standard Operating Procedure

SOP No., Title, Revision No., Revision Date: see page header			
Author of this Revision:	Ankur Saikia		
Signature of Principal Investigator:			
Revision History:	Revision No.	Author	Date
	1	Nouria Jantz	August 26, 2019
	2	Ankur Saikia	July 24, 2021
Other SOPs, documents, or attachments required for the procedure	SSP-SOP-BCM_003		

2. Purpose and general description of the procedure (1-2 sentences)

Determination of the melting temperature (T_m) of a protein of interest (mostly MHC-I). Tryptophan fluorescence (λ excitation = 290 nm, λ emission = 330 nm) of the test protein is monitored while increasing the temperature. The thermal transition is measured by plotting the first derivative of fluorescence intensity against temperature. The resulting valley in the plot corresponds to T_m of the test protein.

3. Terms and abbreviations used in this document

Term or Abbreviation	Explanation
SOP	Standard Operating Procedure
TDTF	Thermal denaturation by tryptophan fluorescence
PBS	Phosphate buffered saline
CPB	Citrate Phosphate Buffer

4. Chemicals required

Chemical	Company and Catalog No.	Safety?	Batch?
Citric acid monohydrate	Sigma, C0706-500G	Warning	n/a
Na ₂ HPO ₄ ·2H ₂ O	Applichem, PAN 142507.1211	n/a	n/a
KH ₂ PO ₄	Applichem, APP A1043,1000	n/a	n/a
KCl	Applichem, PAN 282775.1209	n/a	n/a
Hellmanex™ III	Sigma, Z805939-1EA	Danger	n/a

5. Safety considerations

Chemical or Reagent	Classification according to Regulation	Safety considerations (H/P numbers)
Hellmanex TM III	Serious eye damage (Category 1), H318, Specific target organ toxicity - single exposure (Category 3), Respiratory system, H335	H318, H335, P261, P271, P280, P304 + P340 + P312, P305 + P351 + P338, P403 + P233
Citric acid	Eye irritation (Category 2), H319	H319, P305 + P351 + P338

6. Buffers and stock solutions (= 'reagents')

Reagent	Preparation, aliquotting, storage
Phosphate-buffered saline (1xPBS)	137 mM NaCl, 2.7 mM KCl, 10 mM Na ₂ HPO ₄ , 1.8 mM KH ₂ PO ₄
Citrate Phosphate Buffer (CPB)	Prepare buffer at required pH by mixing 0.1 M Citric acid and 0.2 M Na ₂ HPO ₄ at different proportions.

7. Equipment and accessories required

Type of equipment	Special Instruction?
Agilent Cary Eclipse Fluorescence spectrophotometer	Yes
Cary Eclipse Software	Yes
Quartz cuvettes	No

8. Procedure (numbered list)

1. Crude refold samples are ultracentrifuged at 100,000 g for 20 minutes and the clear supernatants are used for TDTF analysis.
2. Switch on the Cary fluorimeter in the following order: first switch on the cooling unit underneath the bench. Then switch on the little switch on the front of the Cary machine. Lastly, switch on the Cary itself with the switch on the side of the machine.
3. Retrieve cuvettes, cuvette lids and magnetic stir bars from the cleaning box. The objects are submerged in detergent cleaning solution (0.5% HellmanexTM III) and therefore need to be rinsed with normal water, followed by a short wash with MQ water.
4. Dry the cuvettes using the soft tissues (usually Kimwipes works well). Do not use any metal (such as tweezers) or glass objects (such as glass pipettes) on the cuvettes as they might scratch.
5. Use the appropriate amount of sample as below:
For a crude refolds: 500 µL refold + 2.5 mL Buffer (1x PBS or 1x CPB).
SEC purified protein: 25 - 50 µg protein in 3 ml total volume.
Note: The fluorescence signal might go beyond instrument detection limit if too less or too high amount of protein is used for analysis. So, the concentration must be selected carefully.
6. Add magnetic stir bar and lid to all sample tubes.
7. Fill one cuvette with cold water (usually position 4, see settings below). This will serve as the temperature probe in the machine.
8. Place the cuvettes into the holders in the machine. Add the metal temperature probe (labelled with red tape as Probe 1) to the cuvette containing water.
9. Open the program 'Thermal' on the computer.

10. Open your previously created and saved TDTF method or to create a new method use the following settings:

Parameters	Settings value
Gradient	20 to 80 degrees
Ramp time	0.3 Kelvin per minute
Wavelengths	Excitation 290 nm, Emission 345 nm
Slits and power	5/20, no filter, PM voltage 600 V (medium)
Sampling rate	0.1, averaging (AVE) 1 second,
Hold at start	10 minutes, no hold at end.
Temperature monitoring	By probe or by block (not very accurate)

11. Typical sample positions for 1 mL crude refolds:

Position #	1	2	3	4
which refold	A	B	C	water
Volume of refold (ml)	0.5	0.5	0.5	0
Sample ultracentrifuged?	Y	Y	Y	-
Buffer added (ml)	2.5	2.5	2.5	3

Once all parameters have been set, click Start and wait for several minutes. A 'holding time' is set, usually to 5 or 10 minutes, for the machine to reach the indicated start temperature. Once this holding time is over, you will get to a window that asks you to assign sample names to each cuvette holder. Now the measurements will start and the file will be saved automatically.

12. Once your run is finished, switch off the instruments in the reverse order (first the Cary machine with the switch on the side, then the small metal switch in the front, and lastly the cooling unit underneath the bench).
13. Sign out, clean up and further analyse your sample.

9. Interpretation and reporting of the data:

The data will be saved as a .csv file which can be subsequently edited and processed with Excel.

10. Instructions for the use of SOPs

General Rules:

Use the newest version of an SOP for your experiment.

Record the number of the SOP (found in the page header) in your experiment protocol.

Any changes between the SOP and your experiment must be documented in your experiment protocol.


If you believe that the SOP needs to be changed or extended, bring it up in the subgroup meeting.

Explanations of the individual points:

3. Abbreviations: Abbreviations of chemicals are explained in 5.

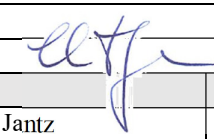
5. "Chemicals" are all powders (but not stock solutions, see 6.)

2.5.2. SOP: method for thermostability measurement

	Springer Group Standard Operating Procedure (SOP)
SOP No.:	SSP-SOP-BCM_013
Title:	NanoDSF measurements for the determination of melting temperature of MHC-I molecules.
Revision No.:	2
Revision Date:	July 24, 2021

1. Information about this Standard Operating Procedure

SOP No., Title, Revision No., Revision Date: see page header

Author of this Revision:	Ankur Saikia		
Signature of Principal Investigator:			
Revision History:	Revision No.	Author	Date
	1	Nouria Jantz	August 26, 2019
	2	Ankur Saikia	July 15, 2021
Other SOPs, documents, or attachments required for the procedure	None.		

2. Purpose and general description of the procedure (1-2 sentences)

The aim is to determine the melting temperature (T_m) of a protein of interest (usually MHC Class I). NanoDSF is a modified differential scanning fluorimetry method that monitors intrinsic tryptophan and tyrosine fluorescence as a function of temperature, time, or denaturant concentration. Significant changes in fluorescence occur when buried or packed aromatic side chains become solvent exposed upon unfolding. NanoDSF measures fluorescence emission at 330 nm and 350 nm, compares the ratio as a function of temperature or denaturant concentration. The thermal transition is measured by plotting the first derivative of fluorescence intensity ratio against temperature. The resulting peak in the plot corresponds to T_m of the test protein.

3. Terms and abbreviations used in this document

Term or Abbreviation	Explanation
NanoDSF	Nano - differential scanning fluorimetry
SEC	Size Exclusion Chromatography
SOP	Standard Operating Procedure
T_m	Melting temperature

4. Equipment and accessories required

Type of equipment	Special Instruction?
Nanotemper Prometheus Instrument	No.
PR.ThermControl for thermal stability data collection	Yes

5. Procedure

1. Retrieve your protein of interest from storage and keep on Ice.
2. Switch on the machine and connect the cable to the laptop provided.
3. Start the program 'PR.ThermControl' on the laptop and assign a file name to your measurement run.
4. Open the drawer of the machine by pressing the open drawer icon on the touchscreen.

Sample Loading:

5. Remove the magnetic cover on the sample rack and clean everything carefully with ethanol and soft tissue paper.
6. Load the protein samples into the special glass capillaries (standard or high sensitivity, depending on the measured or estimated concentration of your protein) by dipping into the samples. The volume required is 10 μ L per capillary. For reference on what concentration suits best for which capillaries, please refer to the figure below.

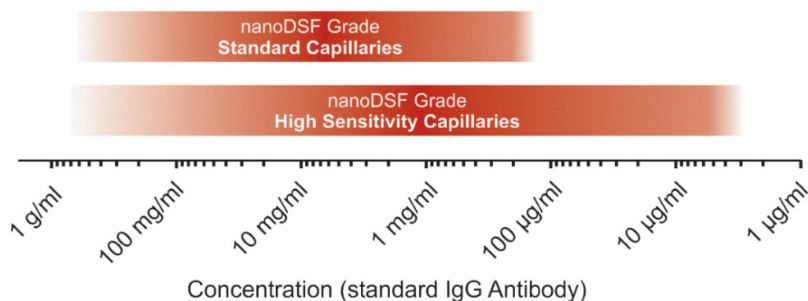
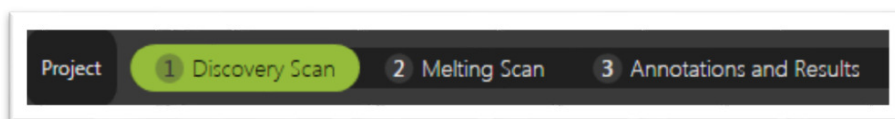


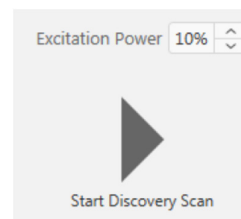
Figure 1: Capillary grade range according to standard IgG Antibody concentration

7. Place the loaded capillary onto the sample rack.
8. Repeat step 5 - 7 for loading all the samples. A maximum of 48 samples can be loaded at once.
9. Replace the magnetic lid on the sample rack and close the drawer by pressing the close drawer icon on the touch screen.

Discovery Scan:



1. After creating a new project or loading a previous project file, perform a Discovery Scan (1) to determine optimal settings for the unfolding experiment.
2. You can vary the excitation power between 1 % and 100 %. Re-scan with different excitation power settings if necessary. See figure below.
3. The discovery scan is used to detect the fluorescence intensity and position of each capillary along the entire length of the capillary tray. Each capillary will be visible as a combination of two peaks, which represent the fluorescence intensity at 330 nm and 350 nm, respectively (see figure below).



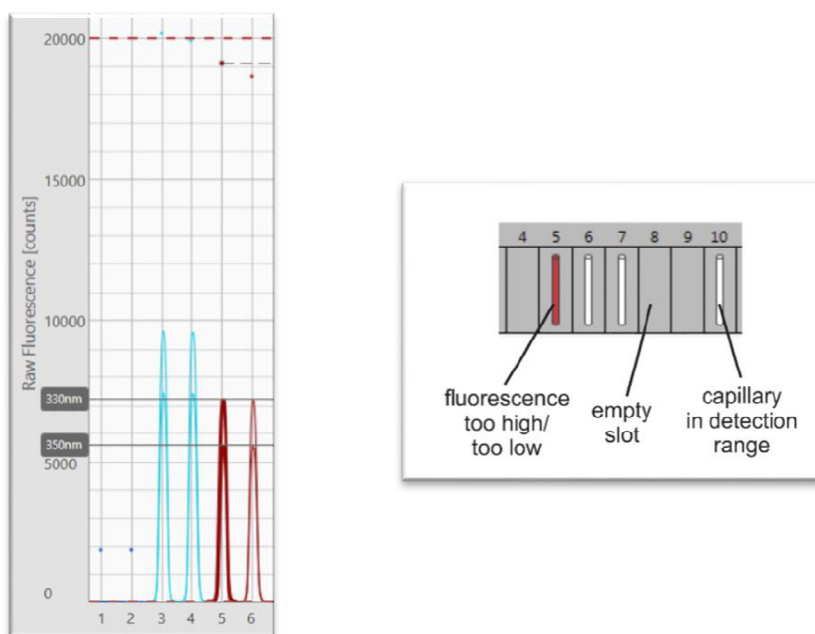
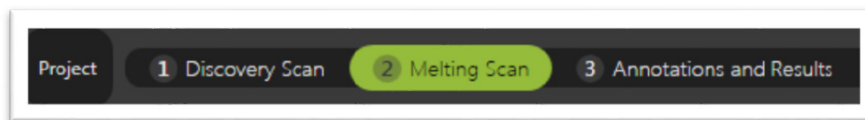


Figure 2: Optimal measurement settings and the positions of occupied capillary slots. (Left) The fluorescence intensities of the 330 nm channel and 350 nm channel are displayed as two separate, nested peaks for each capillary. Clicking on a specific peak or capillary will highlight this capillary's fluorescence at 330 nm and 350 nm, and also display its values for Peak Fluorescence and Integrated Fluorescence on the right of the screen. Both wavelength peaks should be between the upper and lower detection limits (dotted red lines). (Right) Capillaries with fluorescence intensities within the dynamic detection range are coloured white; capillaries with too high fluorescence intensities are coloured red.

4. For a standard sample like SEC purified A2/NV9 (100 µg/mL), using the standard capillary, 90 % excitation is ideal.

Note: The optimal detection range is between 2,000 and 18,000 counts. If the capillary fluorescence exceeds the upper limit, the capillary position will be indicated in red and excluded from the measurement. Capillaries with fluorescence intensities below the measurement limit may not be recognized by the software but can be manually chosen in the Melting Scan submenu (see below).

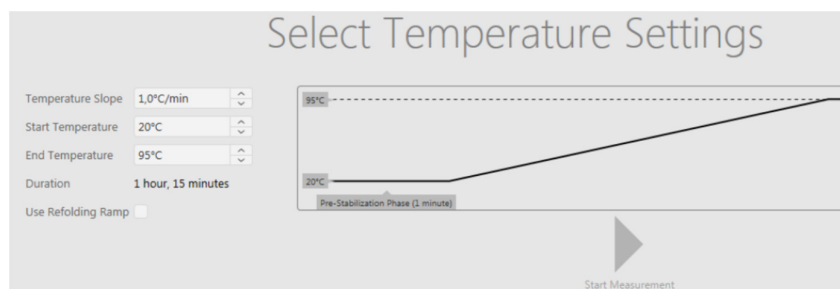
Melting Scan:



1. Once the optimal excitation power settings are determined, continue with the Melting Scan (2). The PR.ThermControl software automatically identifies the capillaries for unfolding analysis from the discovery scan. By default, only capillaries that lie in the dynamic detection range are pre-selected for the unfolding experiment. However, you can also add capillaries that fall below the detection limits.

Tips: You can multi-select capillaries using shift or ctrl + left click.

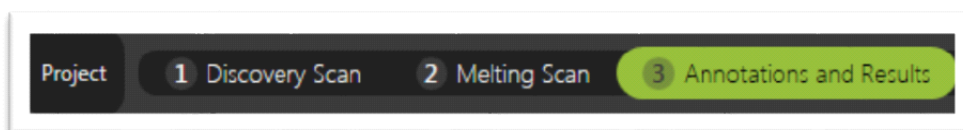
- Next, define the “Start” and “End” temperature for the thermal unfolding experiment, and set the “Temperature Ramp” to the desired heating rate.



- Start the thermal unfolding experiment by pressing “Start Measurement”.
- For visualization purposes, the fluorescence emission values at 330 nm and 350 nm and the F350/F330 ratio can be displayed either together or separately.

Tips: If desired activate the “Use Refolding Ramp” checkbox to include a refolding experiment with temperature slopes identical to the unfolding experiment.

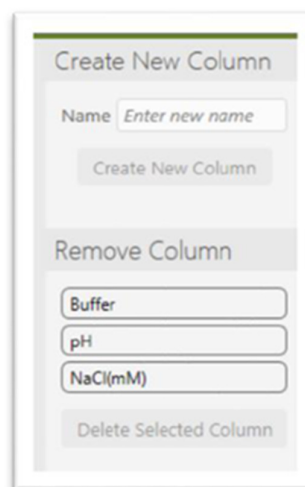
Annotations and Results:



- It is not required to enter sample annotations prior to the experiment. Annotations for each capillary can be entered at any time while the melting scan is running or after it is finished. Annotations can either be entered by simple copy-and-paste from a spreadsheet software like Excel or manually. Columns can be added or removed by using the Create New Column and Remove Column buttons on the right side of the screen:

Note: Annotation of samples before the run or along sample loading is advisable to follow the loading sequence avoid future confusion.

- Annotations can be entered into multiple fields simultaneously after multi-selection, and subsequently sorted in ascending or descending manner by left-clicking on the column header.
- Here you can also assign different colours to each sample for better visualization.
- The annotations table includes separate columns for melting onsets (ON), unfolding transition midpoints (inflection points, IP) and manually annotated points (M).
- After the run is complete, export the graph and data to your folder on the laptop
- Open the drawer, remove the sample capillaries and discard them in the Falcon tubes provided next to the machine.
- Clean the sample rack again with ethanol.
- Replace the magnetic cover on the sample rack, close the drawer and switch off the machine and the laptop.
- Sign out on the logbook and further analyse your data.



6. Interpretation and reporting of the data:

The data can be exported either in processed or raw format and can then easily be plotted using Excel.

7. Instructions for the use of SOPs

General Rules:

Use the newest version of an SOP for your experiment.

Record the number of the SOP (found in the page header) in your experiment protocol.

Any changes between the SOP and your experiment must be documented in your experiment protocol.

If you believe that the SOP needs to be changed or extended, bring it up in the subgroup meeting.

Explanations of the individual points:


3. Abbreviations: Abbreviations of chemicals are explained in 5.

5. "Chemicals" are all powders (but not stock solutions, see 6.)


2.6. Peptide binding and peptide exchange

The methods to monitor MHC-I peptide binding and exchange have been extensively described previously (Dédier et al, 2001 and Saini et al, 2013). This section will describe the methods we have optimized and adapted in our laboratory. The SOP for fluorescence anisotropy was for measuring both peptide binding and peptide exchange. We recently developed a novel peptide binding assay based on microscale thermophoresis (unpublished), and the SOP is described here.

2.6.1. SOP – Fluorescent anisotropy assay

	Springer Group Standard Operating Procedure (SOP)
SOP No.:	SSP-SOP-BCM_022
Title:	MHC-I peptide-binding monitored by fluorescent anisotropy
Revision No.:	1
Revision Date:	Oct 12, 2019

1. Information about this SOP

Author of this revision	Ankur Saikia		
Signature of principal investigator			
Revision history	Revision No.	Author	Date
	1	Ankur Saikia	12.10.2019
Other SOPs, documents, or attachments required for this procedure	n/a		

2. Purpose and general description of the procedure (background)

Fluorescent anisotropy or polarisation (FA) can be used as a measure of a fluorophore's rotational movements in space, i.e. its rotational velocity, which becomes restricted by binding to another molecule. If a fluorophore is excited with polarised light, the emitted light is usually also polarised, but the rotational velocity of the fluorophore, however, influences the polarisation intensity of the emission. Changes in FP intensity occur when the fluorescent small molecule binds to a much larger molecule affecting its rotational velocity.

Fluorescent polarisation can thus be used to measure binding constants and kinetics of reactions that cause changes in the rotational velocity of the molecules. This protocol describes an FP assay to monitor the binding of a fluorescently-labelled peptide (e.g. NV9-FITC) to a pMHC complex (e.g. A2/NA9; the bound peptide should usually have a lesser affinity than the labelled peptide). The bound peptide is replaced with the fluorescent peptide, thus changing the fluorophore's rotational velocity and FP intensity.

This assay is typically used in our lab for monitoring peptide binding to class I irrespective of whether they are in an empty form (e.g. class I disulfide mutants such as A2-Y84C) or folded pMHC's with a bound dipeptide/low affinity peptide. We also use the same protocol for dipeptide-catalyzed peptide exchange.

3. Terms and abbreviations used in this document

Term or abbreviation	Explanation
A2/NV9	pMHC of human HLA-A2 in complex with the NLVPMVATV peptide
A2-Y84C	Disulfide mutant of human HLA-A2
DMSO	Dimethyl sulfoxide
FB	Flat bottom
FITC	Fluorescein isothiocyanate
FP	Fluorescent polarisation, fluorescent anisotropy
HEPES	(4-(2-hydroxyethyl)-1-piperazineethanesulfonic acid
K _d	Dissociation constant
K _{off}	Dissociation rate [m ⁻¹]
K _{on}	Association rate [M ⁻¹ m ⁻¹]
NB	Non-binding
pMHC	MHC-I molecule in complex with a bound peptide
PS	Polystyrene
UB	U-shaped bottom

4. Chemicals required

Chemical	Company and Catalog No.	Safety	Batch
Dipeptides	Customized (e.g., from Bachem)	Warning	No
Fluorescent peptide	Customized (e.g., from Bachem)	n/a	n/a
HEPES	AppliChem # A3724,1000	n/a	n/a
Sodium chloride (NaCl)	AppliChem # A4857,5000	n/a	n/a
Trizma® base	AppliChem # A1379,1000	n/a	n/a
DMSO	AppliChem # A3672,0100	n/a	n/a

5. Buffers and stock solutions (= reagents)

Reagent	Preparation, aliquotting, storage
Assay buffer	50 mM HEPES, pH 7.5, 150 mM NaCl
Fluorescent peptides	1 mM stock in 100% DMSO Aliquot and keep at -20 °C protected from light. Dilute to 10 µM in Assay buffer before use. Use one aliquot for one experiment and toss the aliquot afterwards.
MHC-I refolds (e.g., A2-Y84C/empty) OR pMHC complex (e.g., A2/NV9)	1-5 mg/ml (MW of MHC-I complex is ~45,000 MW, thus 1 mg/ml is about ~22 µM). Aliquot and keep at -80 °C. Before use, thaw an aliquot rapidly in the hands and then place on ice. Folded class I/dipeptide or empty complexes are more unstable and should be carefully handled.
Dipeptide stock	100 mM in water Adjust the pH to 7.5 if necessary. Store at -20 °C until use.

6. Equipment and accessories required

Type of equipment	Special instruction
Plate reader, Infinite® M1000 PRO (TECAN)	Yes
96-well plate, black, NB, FB, PS, Greiner # 655900	n/a
96-well plate, clear, LB, UB, PS, Corning # 3474	n/a
Multichannel pipettes	n/a

7. Procedure (numbered list)**Experimental setup**

- In a 96-well plate, one well is one reaction (volume is 100 μ l).
Perform duplicate or triplicate reactions (see plate map in section 13.2). For one sample (= one well) with a total volume of 100 μ l, the final concentrations of the reactants are:

MHC-I refolds	1 μ M (crude refolds); 300 nM (SEC-purified refolds)
Dipeptides or Assay buffer	10 mM or Assay buffer
Fluorescent peptide (e.g. NV9-FITC)	100 nM (or an allotype optimized concentration)

- For this, prepare the working stocks in Assay buffer as follows
2x MHC class refolds, 600 nM
4x Dipeptide stocks, 40 mM
4x Fluorescent peptide, 400 nM
- Put the stocks together according to the following pipetting scheme. The pipetting sequence is from left to right, total volume is 100 μ l. Crosscheck with plate map in section 13.2:

	Dipeptides	MHC-I refo.	buffer	Fluorescent pept.
Background (green)	-	-	75 μ l	25 μ l
CTRL = pos. control (orange)	25 μ l (reference dipeptide)	50 μ l	-	25 μ l
D1, D2, ..., Dn = samples (yellow)	25 μ l	50 μ l	-	25 μ l
B1, B2, ..., Bn = neg. control (light blue)	25 μ l	-	50 μ l	25 μ l

Note: Before adding fluorescent peptide, incubate (Dipeptide + MHC-I mix) for 10 -15 minutes at room temperature for the dipeptide to equilibrate

Do not forget to follow the pipetting sequence from left to right: 25 μ l dipeptides, 50 μ l MHC-I refolds, and Assay buffer (to the respective wells), and 25 μ l fluorescent peptide to all wells.

Immediately, transfer the plate into the TECAN infinity plate reader.

Start the kinetic read.

Plate reader settings and experimental conditions

Reading format: Fluorescent anisotropy

Filters (for FITC): λ_{exc} - 470 nm, λ_{emi} - 517 nm

Reading is usually 2-3 hours with data points every 30 sec

Reading mode: Kinetic (3 hours, read per 30 sec)

Assay temperature: Room temperature

Adjusting the gain

In a well that will not be used, add the amount of fluorescent peptide and measure the fluorescence units. 100,000 units is the absolute maximum for the machine. Adjust the gain such that fluorescence is between 40,000 and 50,000. It is advisable to adjust the gain for a fluorophore only once at the beginning of the assay. For subsequent experiments, the gain adjustment should be fixed. This is necessary to monitor instrument performance and fluorophore quality over a period of time.

9. Interpretation and reporting of the data

A non-linear regression model - Association kinetics (one ligand concentration) - is used to fit the data in the Graphpad Prism Software. Association kinetics are analyzed using a single concentration of fluorophore to determine K_{on} . One must constrain Hotnm (fluorescence peptide in nM) and K_{off} (previously obtained, approximately 10^{-7} min^{-1} for MHC-I) to constant values.

Average the duplicate FP values for each background, controls, and samples.

The average background is subtracted from the raw counts.

The background-subtracted values are used for curve plotting.

The data are plotted and fit to the following equations:

$$K_d = K_{\text{off}} / K_{\text{on}}$$

$$L = \text{Hotnm} * 10^{-9}$$

$$K_{\text{ob}} = K_{\text{on}} * L + K_{\text{off}}$$

$$\text{Occupancy} = L / (L + K_d)$$

$$Y_{\text{max}} = \text{Occupancy} * B_{\text{max}}$$

$$Y = Y_{\text{max}} * (1 - \exp(-1 * k_{\text{ob}} * X))$$

Where,

X = Time in min

Y = Specific binding using convenient units

Hotnm = Fluorophore in nM. Set to constant value.

B_{max} = Maximal binding in Y units

K_{on} = Set to constant value

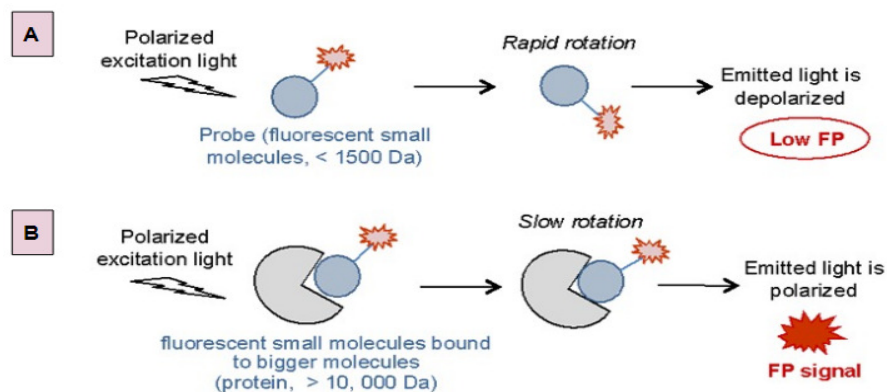
K_{off} = Set to constant based on other experiments

10. Potential pitfalls, errors, and other issues (each in one table row)	
Issue	Known solution
Assay variability	Precise pipetting is required for small volumes. Use calibrated pipettes. Ensure no bubbles are present prior to reading the plate.
Gain adjustment	Make sure the signal strength is not too high by adjusting the gain. Saturation of the detector will result in error values.
Different fluorescent peptides	Avoid using differently labelled peptides in the same plate. Each fluorophore needs to be calibrated individually.
Sample preparation	Make sure the dipeptide does not precipitate when added to the reaction. Reducing the concentration of dipeptide usually works.
Instrument settings	In case different fluorophores are used, instrument filter settings must be changed accordingly. Adjust the gain accordingly.
Low anisotropy value	Use of high concentration of fluorophore can significantly reduce anisotropy values. Please use optimized concentrations.
Low pH solution	At low pH, the overall fluorescence intensity usually decreases. Gain adjustment is advisable in such situations.

11. General instructions for the use of SOPs
<p>It is important to follow these instructions thoroughly! Please ask Sebastian in case of unclarities!</p> <p>There will only be one SOP for each technique available online, which represents the newest version of that SOP. Download the respective SOP before starting your experiment (do not use a pdf or microsoft word version of it because that one might not be up-to-date anymore).</p> <p>Record the number of the SOP (found in the page header) in your experiment protocol.</p> <p>Any changes between the SOP and your experiment must be documented in your experiment protocol.</p> <p>If you believe that the SOP needs to be changed or extended, do never try to change the online SOP but talk to Sebastian or bring up your suggestions in the subgroup meeting.</p>

12. Appendix

1. Diagram of a fluorescent anisotropy assay



A. If a rapidly rotating fluorescent small molecule, such as a peptide, is excited with polarized light, the emitted light is depolarized and the FP signal is low. This would be the case for an unbound fluorescent peptide in solution. B. The association with a larger molecule, such as class I, slows down the motion of the fluorophore, the emitted light remains highly polarized leading to an increased FP signal. Modified from <https://www.ncbi.nlm.nih.gov/books/NBK92000/figure/ppi.F2/>.

2. Plate map

	1	2	3	4	5	6	7	8	9	10	11	12
A	Back-ground	B1	B2	B3	B4	B5	B6	B7	B8	B9	B10	CTRL
C		D1	D2	D3	D4	D5	D6	D7	D8	D9	D10	
E	CTRL	B11	B12	B13	B14	B15	B16	B17	B18	B19	B20	Buffer
G		D11	D12	D13	D14	D15	D16	D17	D18	D19	D20	

Background:

75 µl Assay buffer + 25 µl fluorescent peptide

CTRL (pos. control with reference dipeptide):

25 µl reference dipeptide + 50 µl MHC-I + 25 µl fluorescent peptide


D1, D2, ..., Dn (samples):

25 µl test dipeptide + 50 µl MHC-I + 25 µl fluorescent peptide


B1, B2, ..., Bn (neg. controls without MHC-I):

25 µl dipeptides + 50 µl Assay buffer + 25 µl fluorescent peptide

2.6.2. SOP: Microscale thermophoresis assay

	Springer Group Standard Operating Procedure (SOP)
SOP No.:	SSP-SOP-BCM_024
Title:	Measurement of K_d for peptide-MHC-I interaction using Microscale Thermophoresis (MST).
Revision No.:	1
Revision Date:	August 1, 2021

1. Information about this SOP

Author of this revision	Ankur Saikia		
Signature of principal investigator			
Revision history	Revision No.	Author	Date
	1	Ankur Saikia	August 2, 2021
Other SOPs, documents, or attachments required for this procedure	n/a		

2. Purpose and general description of the procedure (background)

Microscale Thermophoresis (MST) is a method for biophysical analysis of biomolecular interactions. It detects changes in the hydration shell, charge, or size of molecules as they move along microscopic temperature gradients. MST provides a method to measure the molecular interactions by combining fluorescence detection with thermophoresis. The measurement of a temperature-induced change in fluorescence of a target as a function of the concentration of a non-fluorescent ligand is the basis of microscale thermophoresis.

This protocol describes a MST assay to monitor the binding of a fluorescently-MHC-I protein as target (e.g. A2-Red-tris-NTA) to an unlabeled peptide as ligand (e.g. NV9). The ligand is titrated while the target concentration is fixed. This protocol is designed for calculation of K_d for peptide-MHC-I interaction. exchange.

3. Terms and abbreviations used in this document

Term or abbreviation	Explanation
NT.A02	Disulfide stabilized A*02:01-Avi-His. C terminus His tag for the attachment of the Tris-NTA-Red dye.
NT.A24	dsA*24:02-His (clone 1)
NT.B07	dsB*07:02-His (clone 2)
DMSO	Dimethyl sulfoxide
HEPES	(4-(2-hydroxyethyl)-1-piperazineethanesulfonic acid
K_d	Dissociation constant
K_{off}	Dissociation rate [m^{-1}]
K_{on}	Association rate [$M^{-1} m^{-1}$]
NB	Non-binding
PS	Polystyrene
UB	U-shaped bottom

4. Chemicals required

Chemical	Company and Catalog No.	Safety	Batch
Monolith His-Tag Labeling Kit RED-tris-NTA 2nd Generation	Nanotemper # MO-L018	n/a	n/a
PBS-T	In-house	n/a	n/a
HEPES	AppliChem # A3724,1000	n/a	n/a
Sodium chloride (NaCl)	AppliChem # A4857,5000	n/a	n/a
Triton™ X-100	Sigma # T8787-100ML	Danger	n/a
DMSO	AppliChem # A3672,0100	n/a	n/a

6. Safety considerations

Chemical or Reagent	Classification according to Regulation	GHS Classification (Hazard)
Triton X-100	H302: Acute Toxicity-Oral (Category 4), H315: Skin Corrosion (Category 2), H319: Serious Eye Damage/Eye Irritation (Category 2A), H335: Specific Target Organ Toxicity, Single Exposure (Category 3), H319: Serious Eye Damage/Eye Irritation (Category 2A)	H302, H318, H411, P264, P273, P280, P305 + P351 + P338 + P310, P391, P501

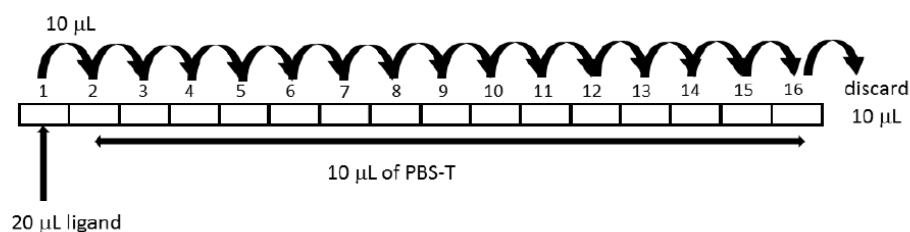
6. Buffers and stock solutions (= reagents)	
Reagent	Preparation, aliquotting, storage
HBS-T Buffer	50 mM HEPES, pH 7.5, 150 mM NaCl, 0.05 % Tween 20
Red-Tris-NTA dye (From His-Tag Labeling Kit)	Suspend the dye in 25 μ L of HBS-T to obtain 5 μ M dye solution Aliquot 5 μ L/vial and keep at -20 °C protected from light. Dilute in HBS-T buffer before use. Avoid multiple freeze thaw.
MHC-I refolds (e.g., SEC purified empty NT.A02)	1 mg/ml (usually) (MW of MHC-I complex is ~45,000 MW, thus 1 mg/ml is about ~22 μ M). Aliquot and keep at -80 °C. Before use, thaw an aliquot rapidly in the hands and then place on ice. Empty complexes are more unstable and should be carefully handled.
Peptide stock	1 mM in water (or DMSO). Store at -20 °C until use. Avoid multiple freeze thaw.

7. Equipment and accessories required	
Type of equipment	Special instruction
Monolith NT.115™ Pico Instrument	Yes
Monolith NT.115™ Premium Capillaries	No
0.2 mL PCR tubes	No
96-well plate, clear, LB, UB, PS, Corning # 3474	No
Multichannel pipettes	n/a

8. Procedure (numbered list)**Step a. Affinity of dye to target protein**

To determine the affinity of the His-labeling dye for the His-tagged MHC-I protein, follow the steps below in HBS-T Buffer:

1. Prepare 250 μL of 20 nM solution of the RED-tris-NTA 2nd Generation dye (target) in HBS-T by mixing 1 μL of dye (5 μM) and 249 μL HBS-T.
2. Prepare 30 μL of 2 μM His-tagged MHC-I (e.g. NT.A02) in HBS-T.
3. Transfer 10 μL of HBS-T into wells/PCR-tubes **2-16**.
4. Transfer 20 μL of 2 μM His-tagged MHC-I solution into the first well/PCR-tube.
5. Transfer 10 μL of the His-tagged MHC-I (ligand) from well/PCR-tube **1** to well/PCR-tube **2** with a pipette and mix by pipetting up-and-down multiple times. Transfer 10 μL to well **3** and mix. Repeat the procedure for wells **4-16**. Discard the extra 10 μL from well 16.



6. Add 10 μL of 20 nM RED-tris-NTA 2nd Generation dye solution to each well (1-16) and mix by pipetting.
7. Incubate for 30 min at room temperature.
8. Load the capillaries and measure the samples at 20 % LED/excitation power (or automatic mode) and medium MST power (40 % MST power in NT.Control).
9. The K_d can be determined in MO.Control or MO.Affinity Analysis using the K_d fit.

If the affinity of the RED-tris-NTA 2nd Generation dye to the His-tagged MHC-I of interest is stronger than 10 nM ($K_d \leq 10$ nM), please continue with Step B protein labeling section I.

If the affinity of the RED-tris-NTA 2nd Generation dye to the His-tagged protein of interest is weaker than 10 nM ($K_d > 10$ nM), please continue with Step B protein labeling section II.

Step b. Protein labeling

I) Affinity of His-labeling dye to your protein of interest equals or is stronger than 10 nM ($K_d \leq 10$ nM). The following protocol describes the labeling procedure for one experiment with 16 capillaries. Volumes can be scaled up- or down when needed.

1. Prepare a 100 nM dye solution by mixing 2 μL of dye (5 μM) and 98 μL PBS-T.
2. Adjust the protein concentration to 200 nM in a volume of 100 μL .
3. Mix 90 μL of protein (200 nM) with 90 μL of dye (100 nM).
4. Incubate for 30 minutes at room temperature.
5. Centrifuge the sample for 10 min at 4 $^{\circ}\text{C}$ and 15 000 g and transfer the supernatant to a fresh tube.
6. The protein is labeled and ready for the binding assay.

II) Affinity of RED-tris-NTA 2nd Generation dye to your protein of interest is weaker than 10 nM ($K_d > 10$ nM). The following protocol describes the labeling procedure for one experiment with 16 capillaries. Volumes can be scaled up- or down when needed.

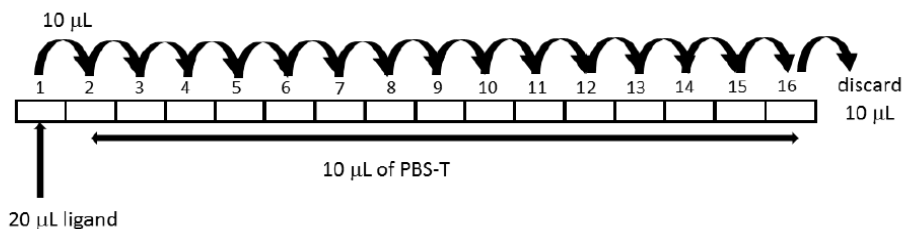
1. Add 8.0 mL ddH₂O to the vials containing 5 x HBS-T to obtain 1 x HBS-T.
2. Suspend the dye in 25 μ L of HBS-T to obtain 5 μ M dye solution
3. Prepare a 100 nM dye solution by mixing 2 μ L of dye (5 μ M) and 98 μ L HBS-T.
4. Adjust the protein concentration to 20 times of the K_d measured in Step A in a volume of 100 μ L (e.g. prepare 100 μ L of 800 nM protein for a K_d of 40 nM between dye and protein. The final protein concentration in the assay is 1/4 of this value = 200 nM)
5. Mix 90 μ L of protein with 90 μ L of dye (100 nM).
6. Incubate for 30 minutes at room temperature.
7. Centrifuge the sample for 10 min at 4 °C and 15 000 g and transfer the supernatant to a fresh tube.
8. The protein is labeled and ready for the binding assay.

Please note: For high affinity interactions the usage of a higher protein concentration can influence your K_d determination (if the protein concentration in the assay is above the K_d of your interaction you can only determine an EC_{50}). If the affinity between RED-tris-NTA 2nd Generation dye and your protein of interest is too low ($K_d > 50$ nM) we recommend adjusting your assay buffer to improve the affinity or switching to a covalent labeling strategy for lysine (Cat. # MO-L011) or cysteine (Cat. # MO-L014) residues.

Step c: binding assay

We recommend preparation of serial dilutions in PCR tubes or in 384-well multi-well plates with non-binding surface.

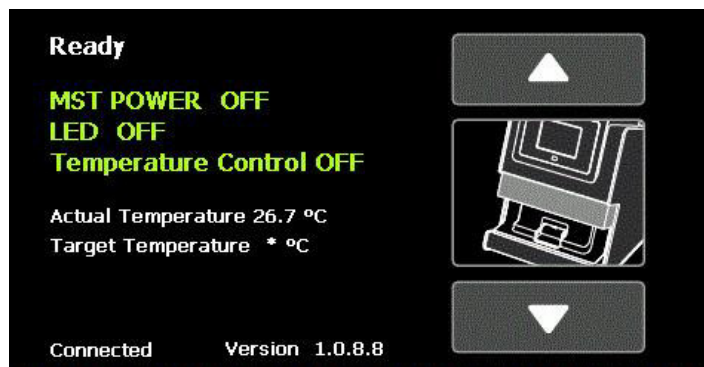
1. Prepare 25 μ L of the ligand at 2 x concentration in HBS-T or your assay buffer of choice (e.g. for a final concentration of 500 nM, prepare ligand at a concentration of 1000 nM). Make sure to avoid buffer mismatches within your titration series.
2. Add 10 μ L of HBS-T into the wells/PCR-tubes 2-16.
3. Transfer 20 μ L of the ligand into well/PCR-tube 1.
4. Transfer 10 μ L of the ligand from well/PCR-tube 1 to well/PCR-tube 2 with a pipette and mix by pipetting up-and-down multiple times. Transfer 10 μ L to well/PCR-tube 3 and mix. Repeat the procedure for well/PCR-tube 4-16. Discard the extra 10 μ L from well/PCR-tube 16.



5. Add 10 μ L of labeled protein to each well (1-16) and mix by pipetting. The final target protein concentration in the assay is 10 nM (or higher, depending on the affinity and instrument sensitivity). This concentration should be used for the calculation of the K_d value.
6. Load the capillaries and measure the samples. Recommended settings are 20 % LED/excitation power and medium MST power (40 % MST power in NT.Control).

9. Using the Monolith® NT.115 Instrument

Turn on the Monolith NT.115 instrument using the power toggle switch on the back of the instrument and start the control notebook. The display of the Monolith NT.115 instrument will show the following screen:



The words “Ready” in the first line and “Connected” in the last line indicate the successful connection between the Monolith NT.115 instrument and the control notebook.

The arrows on the right hand side (up and down) are used to open and to close the front door of the instrument in order to load/remove the sample tray.

The activities of the instrument are shown in green letters “MST POWER OFF” and “LED OFF”. When the experiment starts, these letters will turn red and indicate “MST POWER ON” and “LED ON”, respectively. The status of the LED informs you if fluorescence detection is running and the status of the MST power shows if the IR laser is working and generating temperature gradients in the samples.

In the middle of the screen you find information on the “Temperature Control”. First, you can see if the “Temperature Control” is activated (“OFF” or “ON”) – this is set with the control software. Below this, the “Actual Temperature” and the “Target Temperature” of the instrument is displayed. Please note that this is not the laser induced temperature gradient used for MST measurements.

For most measurements room temperature is appropriate, so there is no adjustment necessary.

10. Interpretation and reporting of the data

Use M.O. Affinity Analysis Software to determine binding constants. After loading the MST curves to the NT Analysis Software of a full binding study (all points of a serial dilution) the following picture will be obtained:

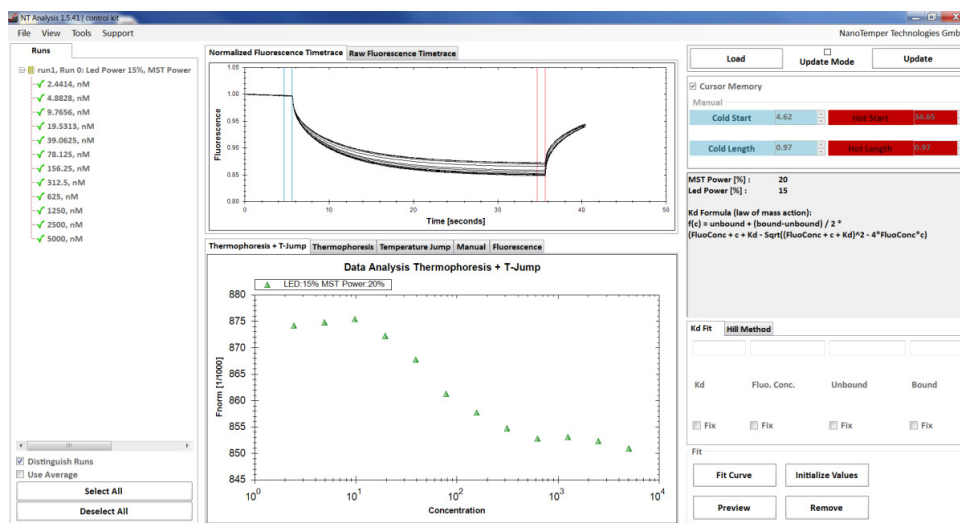


Figure 1.

After deciding for an analysis setting you can perform a curve fitting. There are two options: the first is to perform a K_d fit according to the law of mass action and the second is to perform a Hill fit according to the Hill equation.

K_d Fitting:

Type in the box “Concentr.” the concentration of the fluorescently labeled molecule and choose the option “Fix” below. Afterward press the button “Complete” and then “Fit Curve”. The calculated K_d will appear.

Hill Fitting:

For fitting your data with the Hill equation, you just have to press the button “Complete” and then “Fit Curve”. The calculated EC_{50} will appear.

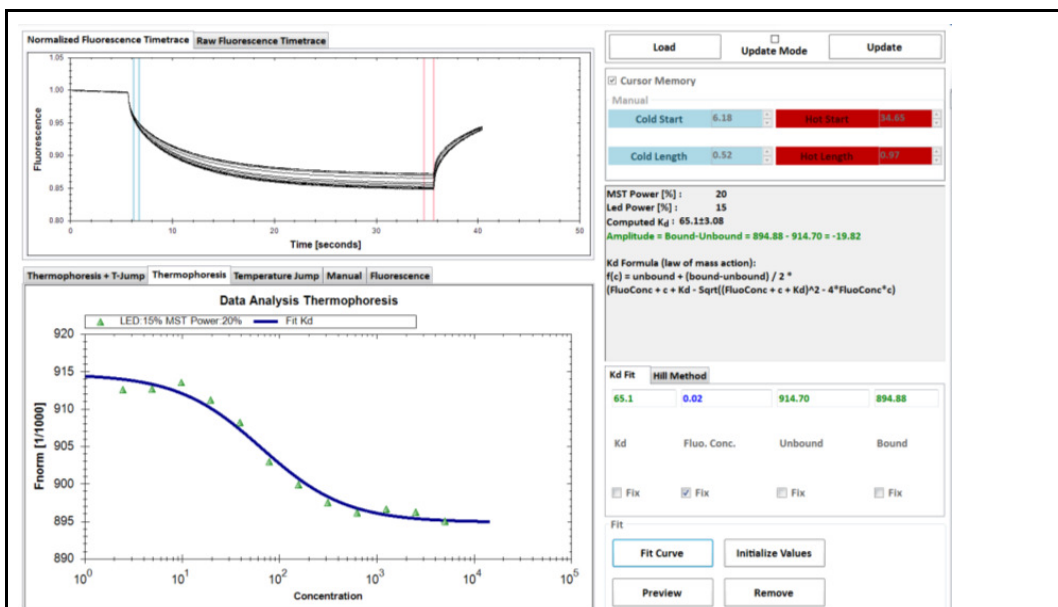
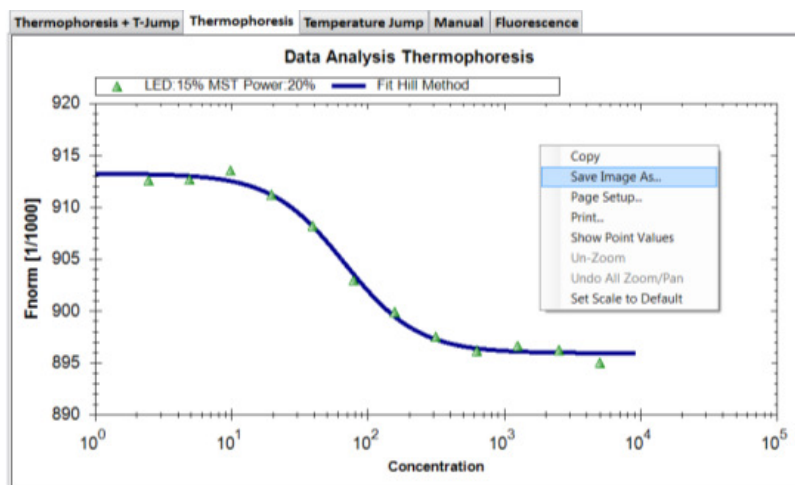


Figure 2

Save as Image File

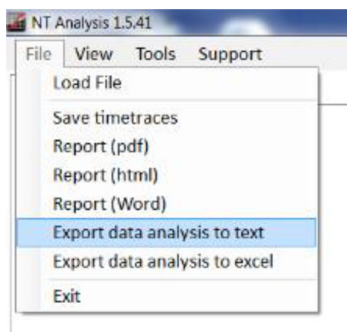
For saving figures from the NT Analysis Software make a right click onto the picture of



interest MST curves, data points or fitted curve box and choose “Save Image As...”.

Save as Text File

For exporting your data in a text file format (.txt) select the “File” function in the upper menu bar and choose the function “Export Measurements”. A new window will open in which you select storage medium and file name of your new txt-file. Verify by clicking “Save”. The txt-file can be opened with most common statistics/graphics software as Microsoft Excel, Origin, Prism and Sigma Plot.



Generation of MST Report

It is possible to generate a quick report of the obtained data and the analysis, which contains the following information: experiment name, date and time of the measurement, MST power, LED power, the fitting method and the fitted value. Furthermore there are two images showing the MST curves and the fitted binding curve. In this report you can also add comments that will be displayed in the document. For exporting your data in this way select the “File” function in the upper menu bar and choose the function “Report (html)”. A new window will open in which you can enter your comments, then click “Continue >>>”. The report will be opened in an html format that can be saved.


11. Potential pitfalls, errors, and other issues (each in one table row)	
Issue	Known solution
Assay variability	Precise pipetting is required for small volumes. Use calibrated pipettes. Ensure no bubbles are present prior to reading the plate.
Gain adjustment	Make sure the signal strength is not too high by adjusting the gain. Each fluorophore needs to be calibrated individually.
Different fluorescent peptides	Avoid using differently labelled peptides in the same plate. Differently labelled peptides with similar molar concentration might give different anisotropy values depending on their affinity and labelling efficiency.
Sample preparation	Make sure the dipeptide does not precipitate when added to the reaction. Reducing the concentration of dipeptide usually works.
Instrument settings	In case different fluorophores are used, instrument filter settings must be changed accordingly. Adjust the gain accordingly.
Low anisotropy value	Use of high concentration of fluorophore can significantly reduce anisotropy values. Please use optimized concentrations.
Low pH solution	At low pH, the overall fluorescence intensity usually decreases. Gain adjustment is advisable in such situations.

12. General instructions for the use of SOPs
<p>It is important to follow these instructions thoroughly! Please ask Sebastian in case of unclarities!</p> <p>There will <u>only be one SOP for each technique available online</u>, which represents the newest version of that SOP. Download the respective SOP before starting your experiment (do not use a pdf or microsoft word version of it because that one might not be up-to-date anymore).</p> <p>Record the number of the SOP (found in the page header) in your experiment protocol. Any changes between the SOP and your experiment must be documented in your experiment protocol. If you believe that the SOP needs to be changed or extended, <u>do never try to change the online SOP</u> but talk to Sebastian or bring up your suggestions in the subgroup meeting.</p>


2.7. Competitive ELISA

This section describes about the methods that I have developed and optimized for screening short-peptides that can assist and accelerate the refolding of MHC-I molecules. I have used this method as an alternative to the classical sandwich ELISA as MHC-I/short-peptide complexes are labile to repeated washing cycle.

2.7.1. SOP: Dipeptide Plate Preparation

	Springer Group Standard Operating Procedure (SOP)
SOP No.:	SSP-SOP-BCM_019
Title:	Preparation of Dipeptide plates
Revision No.:	1
Revision Date:	Nov 29, 2019

1. Information about this SOP

Author of this revision	Ankur Saikia		
Signature of principal investigator			
Revision history	Revision No.	Author	Date
	1	Ankur Saikia	Nov 29, 2019
Other SOPs, documents, or attachments required for this procedure	n/a		

2. Purpose and general description of the procedure (background)

This SOP describes the preparation of a Dipeptide plate to be used for MHC-I refolding in 96-well formats (see SSP-SOP-BCM_020).

3. Terms and abbreviations used in this document

Term or abbreviation	Explanation
DMSO	Dimethyl sulfoxide
FB	Flat bottom
LB	Low-binding
PS	Polystyrene
UB	U-shaped bottom

4. Chemicals required

Chemical	Company and Catalog No.	Safety	Batch
Dipeptides	Custom synthesis	Warning	n/a
Trizma base	Sigma # T1503	n/a	n/a
DMSO	AppliChem # A3672,0100	n/a	n/a

5. Buffers and stock solutions (= reagents)

Reagent	Preparation, aliquotting, storage
Tris buffer	100 mM Tris-HCl, pH 8.0
Dipeptide stocks	100 mM in Tris buffer Adjust the pH to 8.0 with either 5 M NaOH or 5 M HCl if necessary. Store frozen at -20 °C until use.

6. Equipment and accessories required

Type of equipment	Special instruction
96-well plate, clear, LB, UB, PS	n/a
Deep well plates, 1 ml capacity	n/a
Plate sealer, clear	n/a
pH meter	n/a
Singlechannel pipettes	n/a
Multichannel pipettes	n/a
Ice bucket	n/a

7. Procedure (numbered list)

All steps on ice or at 4 °C if not mentioned otherwise!

- For each dipeptide, prepare 5 ml of a 100 mM Dipeptide stock in Tris buffer, pH 8.0 (in a 15 ml Falcon tube). Adjust pH if necessary.
- Vortex thoroughly to solubilize. Some of the dipeptides might need to be warmed at 37 °C for ~10 min to solubilize completely.
- Using a singlechannel pipette, transfer 1 ml/well of the individual dipeptide to a Deep well plate (this is used as a reservoir) according to the workflow shown in section 13.1.
- Using a multichannel pipette, transfer 100 µl to 96-well Dipeptide plates. The preferred loading scheme for a dipeptide plate is shown in section 13.2. From one Deep well plate, approximately 9 Dipeptide plates can be generated (leaving some dead volume).
- Immediately, seal the Dipeptide plates using transparent plate sealers to prevent evaporation.
- Label the Dipeptide plates and freeze them at -20 °C for further use (up to year at least).
- One the day of use, the plate can be thawed at room temperature and should be mixed in a plate shaker at 1,000 rpm for 5 min to solubilize properly. If needed, spin the plate at 2,000 rpm for 5 min to settle down the solution.
- The Dipeptide plates can be used for both MHC-I refolding in 96-well formats (see SSP-SOP-BCM_020) and competition ELISA (see SSP-SOP-BCM_021).

8. Potential pitfalls, errors, and other issues (each in one table row)

Issue	Known solution
Sample precipitation	Make sure to properly vortex the dipeptide stocks.
Pipetting precision	The multichannel pipettes need calibration and servicing If the tips do not properly fit, change the o-rings or the tip source.
Low solubility of dipeptides	Increasing the pH to 9.0 may improve the solubility for some dipeptides. Reducing the dipeptide concentration of the Dipeptide stocks usually works.

9. General instructions for the use of SOPs

It is important to follow these instructions thoroughly! Please ask Sebastian in case of unclarities!

There will only be one SOP for each technique available online, which represents the newest version of that SOP. Download the respective SOP before starting your experiment (do not use a pdf or microsoft word version of it because that one might not be up-to-date anymore).

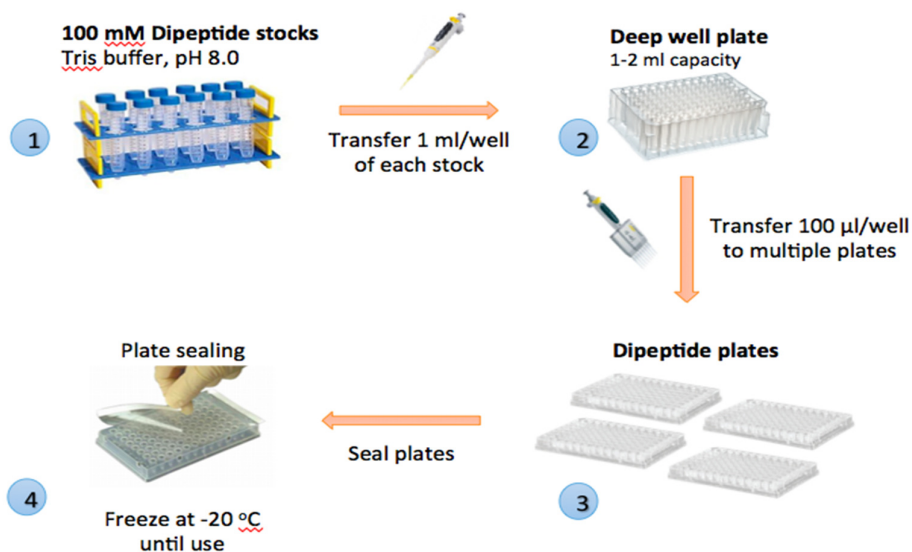
Record the number of the SOP (found in the page header) in your experiment protocol.

Any changes between the SOP and your experiment must be documented in your experiment protocol.

If you believe that the SOP needs to be changed or extended, do never try to change the online SOP but talk to Sebastian or bring up your suggestions in the subgroup meeting.

10. Appendix

1. Preparation of Dipeptide plates, workflow



in Falcon tubes (1). Of each Dipeptide stock, 1 ml is transferred with a singlechannel pipette to a Deep well plate (2). With a multichannel pipette, 100 µl/well are transferred to the final Dipeptide plates. That way, out of one Deep well plate nine Dipeptide plates can be generated (3). The Dipeptide plates are sealed and can be kept at -20 °C for several months (4).

2. Loading scheme example of a Dipeptide plate


	1	2	3	4	5	6	7	8	9	10	11	12
A	Empty	Empty	Empty	Empty	Empty	Empty	Empty	Empty	Empty	Empty	Empty	Empty
B	Empty	DP-1	DP-2	DP-3	DP-4	DP-5	DP-6	DP-7	DP-8	Buffer	Buffer	Empty
C	Empty	DP-9	DP-10	DP-11	DP-12	DP-13	DP-14	DP-15	DP-16	Buffer	Buffer	Empty
D	Empty	DP-17	DP-18	DP-19	DP-20	DP-21	DP-22	DP-23	DP-24	Buffer	Buffer	Empty
E	Empty	DP-25	DP-26	DP-27	DP-28	DP-29	DP-30	DP-31	DP-32	Buffer	Buffer	Empty
F	Empty	DP-33	DP-34	DP-35	DP-36	DP-37	DP-38	DP-39	DP-40	Buffer	Buffer	Empty
G	Empty	DP-41	DP-42	DP-43	DP-44	DP-45	DP-46	DP-47	DP-48	Buffer	Buffer	Empty
H	Empty	Empty	Empty	Empty	Empty	Empty	Empty	Empty	Empty	Empty	Empty	Empty

Empty = All outmost corner wells are left empty to avoid evaporation of sample.


Buffer = Column 10 and 11 contain 100 µl of Tris buffer (100 mM), pH 8.0, and will later incorporate the controls of the refolding reaction (see SOP...).

DP1 - DP48 = Contain 100 µl of each Dipeptide stock (#1 - #48).

2.7.2. SOP: MHC-I refolding in 96 well plate format

	Springer Group Standard Operating Procedure (SOP)
SOP No.:	SSP-SOP-BCM_020
Title:	MHC-I refolding from inclusion bodies in 96-well formats
Revision No.:	1
Revision Date:	Oct 10, 2019

1. Information about this SOP

Author of this revision	Ankur Saikia		
Signature of principal investigator			
Revision history	Revision No.	Author	Date
	1	Ankur Saikia	Oct 10, 2019
Other SOPs, documents, or attachments required for this procedure	SSP-SOP-BCM_019 : Dipeptide plate preparation		

2. Purpose and general description of the procedure (background)

This protocol describes how to prepare 250 µl refolds in a 96-well format. These refolds are used in competitive ELISA assays for the screening of small molecules (e.g. dipeptides) that efficiently promote refolding of MHC-I molecules.

3. Terms and abbreviations used in this document

Term or abbreviation	Explanation
DTT	1,4-Dithiothreitol
EDTA	Ethylenediaminetetraacetic acid
ELISA	Enzyme-linked immunosorbent assay
FB	Flat bottom
hβ2m	Human beta-2 microglobulin
HC	Heavy chain of the class I allotype
HCL	Hydrochloric acid
LB	Low-binding
LC	Light chain (human β2m, hβ2m)
MQ	Ultrapure water (Milli-Q®)
NB	Non-binding
PMSF	Phenylmethanesulfonyl fluoride
PS	Polystyrene
UB	U-shaped bottom

4. Chemicals required

Chemical	Company and Catalog No.	Safety	Batch
Heavy chain of MHC-I, in -80 °C	In-house	n/a	n/a
Light chain (human β2m), in -80 °C	In-house	n/a	n/a
Full length peptide, in -20 °C	Customized (Genecast, Genescript)	n/a	n/a
Dipeptides	Customized (Genecast, Genescript)	n/a	n/a
Trizma® base	Sigma Aldrich # T1503	n/a	n/a
L-Arginine HCl	PanReac # 1119-34-2	n/a	n/a
Reduced glutathione	Sigma Aldrich # G6529	n/a	n/a
Oxidized glutathione	Sigma Aldrich # G4626	n/a	n/a
PMSF	Sigma Aldrich # 78830-1G	Danger	n/a
EDTA	Sigma Aldrich # E6758-100G	Warning	n/a
DTT	Merck # 3483-12-3	Warning	n/a
Guanidine hydrochloride	Sigma Aldrich # G3272	Warning	n/a

6. Safety considerations		
Chemical or Reagent	Classification according to Regulation	GHS Classification (Hazard)
EDTA (ethylene diamine tetraacetic acid)	H332: Acute Toxicity-Inhalation (Category 4)	H332, P261, P271, P304+P340P312
Guanidinium hydrochloride	H302: Acute toxicity, Oral (Category 4), H332: Acute toxicity, Inhalation (Category 4), H315: Skin irritation (Category 2), H319: Eye irritation (Category 2)	H302 + H332, H315, H319, P301 + P312 + P330, P302 + P352, P304 + P340 + P312, P305 + P351 + P338
PMSF (phenylmethylsulfonylfluoride)	H302: Acute toxicity, Oral (Category 4), H332: Acute toxicity, Inhalation (Category 4), H315: Skin irritation (Category 2), H319: Eye irritation (Category 2)	H318, H301, H314, P260, P280, P301 + P310 + P330, P303 + P361 + P353, P304 + P340 + P310, P305 + P351 + P338 + P310

6. Buffers and stock solutions (= reagents)	
Reagent	Preparation, aliquotting, storage
Refolding buffer, pH 8.0 (This is a special refolding buffer used for 96-well plates only.)	200 mM Tris-HCl, pH 8.0, 1.67 M L-Arginine HCl, 6.67 mM EDTA Adjust pH to 8.0 with 5 M NaOH. Make up the volume by MQ water. Aliquot and store at -20 °C for longer duration.
Resolubilization buffer	6 M Guanidine hydrochloride, 50 mM HEPES, pH 7.5, 100 µM EDTA, 100 µM DTT The buffer can be stored at 4 °C for a few weeks.
100x stock of reduced glutathione	Dissolve 500 mM reduced glutathione in water. Aliquot and freeze at -20 °C until use. Do not freeze repeatedly. Discard the remaining solution once the aliquot is thawed.
100x stock of oxidized glutathione	Dissolve 500 mM reduced glutathione in water. Aliquot and freeze at -20 °C until use. Do not freeze repeatedly. Discard the remaining solution once the aliquot is thawed.

7. Equipment and accessories required	
Type of equipment	Special instruction ⁸
96-well microplate, black, NB, FB, PS	n/a
96-well plate, clear, LB, UB, PS	n/a
Plate shaker, MS 3 digital, IKA	n/a
Multichannel pipettes	n/a
Plate sealer	n/a

⁸ Insert “yes” if special instruction is necessary to operate this equipment.

8. Procedure (numbered list)

All steps on ice or at 4 °C (in the cold room) if not mentioned otherwise!

Dilute the solubilized inclusion bodies of MHC-I HC and of β_2m in Resolubilization buffer to a final concentration of 5 mg/ml.

Prepare a 1 mM stock of a class I-specific reference peptide in water.

Prepare a 50x glutathione mix by mixing equal volumes of the two different 100x glutathione stocks (see section 7).

Take a Dipeptide plate (see section 13.1, step 2) already containing 100 μ l of all the dipeptides of interest (see SSP-SOP-BCM_019, dipeptide stock concentration is 100 mM, final concentration in the refolding assay is 40 mM).

Prepare the Refolding mix according to the table below (except for the dipeptides that are already provided in the Dipeptide plate you use). The final volume of each well, i.e. each refolding reaction, is 250 μ l. The table thus indicates the volumes of each component in the mix in one single well.

Reagent	Stock concentration	Final concentration	Amount (μ l)
Refolding buffer	-	-	75
MQ water	-	-	60
Glutathione mix	50x	1x	5
These three components are pooled together as a premix in a multichannel reservoir (identify the total volume of your premix according to the final number of wells you have). From there, the premix is added to the Dipeptide plate with a multichannel pipette.			
Full-length reference peptide	1 mM	20 μ M	100
To obtain a 20 μ M final peptide concentration in a 100 μ l volume, you have to include an additional dilution step in 100 mM Tris buffer, pH 8.0!			
Human β_2m	5 mg/ml	100 μ g/ml	5
Class I HC	5 mg/ml	100 μ g/ml	5
Both components are prepared separately in one lane of an extra 96-well plate. From there, you can transfer the reagents fast and easily with a multichannel pipette to the Dipeptide plate. Caution! The class I heavy chain is loaded last because it tends to precipitate. This step has to be carried out in the cold room where the Dipeptide plate can be shaken during pipetting of the heavy chain (of course, shaking has to be paused while actually pipetting).			
Total volume			250 μ l

The Dipeptide plate is now the Refolding plate. Seal it and leave it on a shaker rotating at 300 rpm in a cold room (4 °C) for a total of 7-10 days to allow proper refolding. Keep it dark.

Centrifuge the plate at 4,000 rpm, 4 °C for 15 min to precipitate insoluble impurities.

The Refolding plates can be stored at 4 °C until use. The preferred loading scheme of a Refolding plate is shown in 13.2.

For competition ELISA (see SSP-SOP-BCM_021), gently transfer 5 μ l of supernatant from the top to the Sample plate (see section 13.1, step 4, and SSP-SOP-BCM_019).

Tip: Oxidized glutathione is sensitive to light and oxygen. Therefore, always keep the Refolding plate in the dark by covering it with aluminium foil and make sure that the stirring is at a setting where it is not creating bubbles.

9. Potential pitfalls, errors, and other issues (each in one table row)

Issue	Known solution
Evaporation at the outer wells (surrounding outer wells of the plate, see section 13.2)	Avoid using the outer plates wells at all for refolding. Add buffer to the outer wells. Always use plate sealers.
Low refolding efficiency	Protect from light. Further dilute the HC and β_2m inclusion bodies solutions. Use already folded β_2m if available. Try to keep the concentration of guanidine hydrochloride as low as possible.
Variability between different assays	Precise pipetting is required for smaller volumes. Use calibrated pipettes. Pipette carefully to avoid cross-contamination. Always change tips between steps.

10. General instructions for the use of SOPs

It is important to follow these instructions thoroughly! Please ask Sebastian in case of unclarities!

There will only be one SOP for each technique available online, which represents the newest version of that SOP. Download the respective SOP before starting your experiment (do not use a pdf or microsoft word version of it because that one might not be up-to-date anymore).

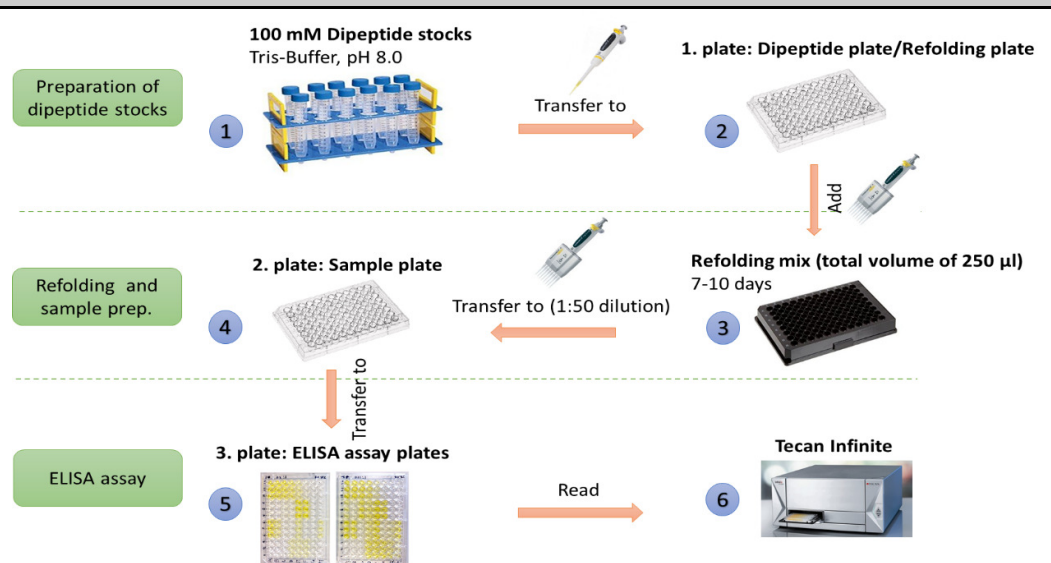
Record the number of the SOP (found in the page header) in your experiment protocol.

Any changes between the SOP and your experiment must be documented in your experiment protocol.

If you believe that the SOP needs to be changed or extended, do never try to change the online SOP but talk to Sebastian or bring up your suggestions in the subgroup meeting.

11. Appendix

1. Dipeptide screening workflow



The first plate in the work flow is the Dipeptide plate, in which the different dipeptides are prepared (steps 1+2). After addition of the refolding mix, the Dipeptide plate becomes the refolding plate, where class I refolding can take place (step 3). For preparation of the ELISA assay, 5 µl of supernatant are transferred from the Dipeptide/Refolding plate to a second plate, the Sample plate, to which antibody is added for competition ELISA (step 4). To read the assay, each sample/well in the Sample plate is divided in half and transferred as duplicates to two ELISA assay plates (steps 5+6).

This SOP describes step 3 of the entire procedure.

2. Loading scheme of the Refolding plate

	1	2	3	4	5	6	7	8	9	10	11	12
A	Buffer	Buffer	Buffer	Buffer	Buffer	Buffer	Buffer	Buffer	Buffer	Buffer	Buffer	Buffer
B	Buffer	AcF	AcG	AcI	AcK	AcL	AcM	AcB	AcV	Class I/Pep.	A2/NV9	Buffer
C	Buffer	AcW	AcY	AG	AH	AI	AK	AL	AM	Buffer	Buffer	Buffer
D	Buffer	GA	GD	GE	GF	GG	GH	GI	GK	No β_2m	No β_2m	Buffer
E	Buffer	GL	GV	GW	GM	GR	GY	GGA	GGF	Class I/Pep.	A2/NV9	Buffer
F	Buffer	GGG	GGH	GGI	GGK	GGL	GGM	GGR	GGV	Buffer	Buffer	Buffer
G	Buffer	GGY	LG	GCit	GSGL	GSFG	GSGM	GSGL	SGGL	No β_2m	No β_2m	Buffer
H	Buffer	Buffer	Buffer	Buffer	Buffer	Buffer	Buffer	Buffer	Buffer	Buffer	Buffer	Buffer

Overview of the total plate loading scheme

The light green wells are the outer wells that are kept empty (loaded with buffer only) to avoid evaporation of sample.

The light pink wells (columns 2-9) contain the various dipeptides to be screened.

Columns 10 and 11 contain the negative and positive controls (see also table below).

B10 and B11 = positive controls containing class I complexes folded with full-length reference peptides (B10 contains the class I allotype on which the dipeptides are tested, B11 contains a different allotype plus a respective high-affinity peptide).

C10 and C11 = negative controls without peptide.

D10 and D11 = negative controls without peptide and β_2m

For further information to the controls, see also table below.


Sample	Refolding buffer	HC	β_2m	peptide
Class I/peptide	✓	✓	✓	✓
Buffer	✓	✓	✓	-
No β_2m	✓	✓	-	-

Components in the control columns (10 and 11)


Column 10 contains the HC allotype of interest with a reference full-length peptide.

Column 11 is a positive control generally containing human HLA-A2 (disulfide mutant) in complex with the NV9 peptide.

2.7.3. SOP: Quantification of pMHC-I in Competitive ELISA Assay

	Springer Group Standard Operating Procedure (SOP)
SOP No.:	SSP-SOP-BCM_021
Title:	MHC-I competition ELISA
Revision No.:	1
Revision Date:	Oct 10, 2019

1. Information about this SOP

Author of this revision	Ankur Saikia		
Signature of principal investigator			
Revision history	Revision No.	Author	Date
	1	Ankur Saikia	10.10.2019
Other SOPs, documents, or attachments required for this procedure	SSP-SOP-BCM_019 Dipeptide stock plates preparation SSP-SOP-BCM_020 MHC-I refolding in 96 well formats		

2. Purpose and general description of the procedure (background)

The competition ELISA, also known as blocking ELISA, is the most complex of all ELISA techniques. It is predominantly used to measure the concentration of an antigen in a sample by detecting interference in an expected signal output. Essentially, sample pMHC (sMHC, *e.g.* from dipeptide refolding experiments (see SSP-SOP-BCM_020) competes with an immobilized reference pMHC (rMHC, *e.g.* A2/NV9) for binding to a limited amount of antibody (*e.g.* W6/32, see also section 13.1). After pre-incubation with sMHC, leftover antibody is added to the plate coated with the rMHC; both MHC-I complexes compete for antibody binding, hence the name of the technique. Detection is by addition of a HRP-conjugated secondary antibody and relevant substrate (*e.g.* 3,3',5,5'-TMB), which produces a colour that can be read out with a plate reader. Thus, a high concentration of sMHC as a result of efficient folding significantly reduces the signal output and vice versa (the lower the signal output, the more efficient the sMHC folding had been; the higher the signal output, the less efficient the sMHC folding had been).

3. Terms and abbreviations used in this document

Term or abbreviation	Explanation
A2/NV9	pMHC of human HLA-A*02:01 and the NLVPMVATV peptide
BSA	Bovine serum albumin
EIA	Enzyme immune assay
ELISA	Enzyme-linked immunosorbent assay
hβ ₂ m	Human beta-2 microglobulin
HRP	Horseradish peroxidase
LB	Low-binding
pMHC	MHC-I in complex with a peptide
PS	Polystyrene
RIA	Radioactive immune assay
rMHC	Reference pMHC (immobilized, <i>e.g.</i> A2/NV9)
SEC	Size-exclusion chromatography
sMHC	Sample pMHC (<i>e.g.</i> dipeptide refolds from SSP-SOP-BCM_020 MHC)
TMB	3,3',5,5'-Tetramethylbenzidine
UB	U-shaped bottom
W6/32	Mouse anti-HLA class I monoclonal antibody (detects fully folded HLA only)

4. Chemicals required

Chemical	Company and Catalog No.	Safety	Batch
A2/NV9 (SEC-purified)	In-house	n/a	Yes
pMHC refolds	In-house	n/a	Yes
Guanidine hydrochloride	Sigma # G3272	Warning	n/a
Sodium chloride	Sigma # S7653-5KG	n/a	n/a
Sodium carbonate	Sigma # S7795-1KG	n/a	n/a
Sodium bicarbonate	Sigma # S5761-1KG	n/a	n/a
BSA fraction V	Sigma # 126609-5GM	n/a	n/a
W6/32 hybridoma	ATCC® HB-95™	n/a	n/a
Tween-20	Sigma # P1379-100ML	n/a	n/a
Goat anti-mouse IgG-HRP	Jackson Imm. lab	n/a	n/a
Pierce™ TMB substrate kit	Thermofisher # 34021	Danger	n/a
Sulfuric acid (H ₂ SO ₄)	Sigma # 339741-500ML	Danger	n/a
Trizma® base	Sigma # T1503	n/a	n/a

5. Safety considerations				
Chemical or reagent	Toxic	Carcinogenic	All	Safety consideration (H/P numbers, S1/S2, radioactivity)
Guanidine hydrochloride	X			H302+H332, H315, H319, P261, P280, P301+P312+P330, P304+P340+312, P304+P351, P338, P337+P313
Pierce™ TMB substrate	X			H302+H312+H332, H370, P280, P260, P308+P311, P304+P340, P501
Sulfuric acid	X			H290, H314, P280, P301+P330+P331 P303+P361+P353, P305+P351+P338+P310

6. Equipment and accessories required	
Type of equipment	Special instruction
Plate reader Infinite® M1000 PRO, TECAN	Yes
ELISA plate washer, TECAN	Yes
Plate shaker, MS 3 digital, IKA	n/a
Multichannel pipettes	n/a
Corning® 96-well EIA/RIA plates	n/a
96-well plate, clear, LB, UB, PS	n/a
Plate sealer	n/a

7. Buffers and stock solutions (= reagents)	
Reagent	Preparation, aliquotting, storage
1x Sample dilution buffer	50 mM Tris-HCl, pH 8.0, 150 mM NaCl
10x Carbonate coating buffer, pH 9.6	150 mM sodium carbonate (Na_2CO_3) 350 mM sodium bicarbonate (NaHCO_3) <i>Take the respective quantities of the different components and dissolve in 180 ml MQ water. Adjust the pH to 9.6 with 5 M HCl and make up to a final volume of 200 ml with water. The buffer can be stored at 4 °C for several months. Dilute 10fold before use.</i>
20x Tris buffer, pH 8.0	1 M Trizma® base Dissolve in 800 ml MQ water and adjust the pH to 8.0 using 5 M HCl. Make up to 1 l with MQ water. Store at room temperature. For 1x buffer, dilute to 50 mM in autoclaved MQ water.
Blocking buffer	50 mM Tris-HCl, pH 8.0 1% BSA fraction V <i>The volume of buffer to be prepared depends on the number of wells. For calculation, assume 150 µl buffer/well.</i>
Wash buffer	50 mM Tris-HCl, pH 8.0 0.05% Tween-20 <i>For calculation, assume 2 l/plate (if the Plate washer is used).</i>
Antibody dilution buffer	50 mM Tris-HCl, pH 8.0 1% BSA fraction V 0.05% Tween-20 <i>For calculation, assume 100 µl/well.</i>
TMB substrate kit and Stop solutions	<i>The TMB substrate kit consists of the TMB substrate solution and peroxide solution. Immediately before use, mix equal volumes of the TMB substrate solution and the peroxide solution and add 100 µl/well (see section 9). Stop with 2 M sulfuric acid.</i>
Sample dilution	<i>Sample dilution depends on the initial concentration of the sample. The detection range of this ELISA assay is 10-200 ng/ml. Normal refold concentrations, considerably exceed this detection range. Thus, the sample have to be diluted beforehand, i.e. if screening 250 µl or 1 ml refolds, dilute 50fold in the final assay. For 1 l refolds, which are less concentrated, the dilution step can be less as well.</i>

9. Interpretation and reporting of the data

From the Plate reader data (they come in an Excel sheet), plot a Four Parameter Logistic (4PL) curve with the ELISA standards. Interpolate the sMHC's from the plot and analyze with the GraphPad software. (see [here](#)).

10. Potential pitfalls, errors, and other issues (each in one table row)	
Issue	Known solution
Assay variability	Precise pipetting is inevitable, especially for smaller volumes. Use calibrated pipettes. Ensure that no bubbles are present prior to reading the plate.
High signal	Insufficient plate washing. Not stopped the TMB reaction. Added too much TMB substrate reagent. Reduce incubation time.
No or low signal	Increase TMB substrate incubation time. Target below detection of assay. Intermediate step skipped. Insufficient protection from direct light. Expired reagents.
Out of detection range	Samples may require further dilution.
Precipitate formed in wells upon TMB substrate addition	Increase dilution factor of sample or decrease concentration of the TMB substrate.
Incorrect standard curve	Check pipetting technique and calculations. Ensure all wells are filled with Wash buffer and are being aspirated completely. Use an automated Plate washer. Increase number of washes.

11. General instructions for the use of SOPs
<p>It is important to follow these instructions thoroughly! Please ask Sebastian in case of unclarities!</p> <p>There will only be one SOP for each technique available online, which represents the newest version of that SOP. Download the respective SOP before starting your experiment (do not use a pdf or Microsoft word version of it because that one might not be up-to-date anymore).</p> <p>Record the number of the SOP (found in the page header) in your experiment protocol.</p> <p>Any changes between the SOP and your experiment must be documented in your experiment protocol.</p> <p>If you believe that the SOP needs to be changed or extended, do never try to change the online SOP but talk to Sebastian or bring up your suggestions in the subgroup meeting.</p>

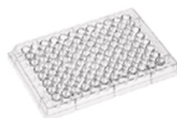
12. Appendix

1. Workflow of the assay

1 Refolding plate (final volume: 250 μ l)

Prepare 1/25 fold refolds in Tris Buffer

(total volume: 125 μ l; *i.e.* 5 μ l of refolds/samples + 120 μ l Tris buffer, pH 8.0)

2 Sample plate (final volume: 250 μ l)

+ first antibody

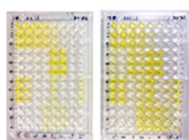
Results in 1/50 fold of the refolds in the Sample plate

(125 μ l 1/25 fold refold/sample dilution + 125 μ l first antibody (*e.g.* W6/32))



Transfer 100 μ l to each Assay plate (in duplicates)

3 ELISA Assay plates



Read out



4 Tecan Infinite



From the Refolding plate, transfer 5 μ l to the Sample plate and add to a total volume of 125 μ l with Tris buffer, pH 8.0, thus generating a 1/25 fold refold or sample solution (1). To the 125 μ l sample volume, add 125 μ l of first antibody, which results in a 1/50 fold sample dilution (*i.e.* 5 refold/sample + 120 Tris buffer + 125 antibody) (2). The antibody solution should be 2x concentrated as it becomes diluted to 1x during mixing with the sample solution (*e.g.* 30 ng/ml for W6/32 is 2x, final concentration is 15 ng/ml). The 250 μ l sample/antibody mix is sufficient for two duplicate Assay plates, to each of which 100 μ l of the sample/antibody mix is added leaving about 50 μ l of dead volume (3). After addition of secondary antibody and detection substrate (not shown), the Assay plates can be read out (4).

2. Loading schemes of Sample and Assay plates

Sample plate

Sample plate											
	1	2	3	4	5	6	7	8	9	10	11
A	Buffer	Buffer	Buffer	Buffer	Buffer	Buffer	Buffer	Buffer	Buffer	Buffer	Buffer
B	Buffer	ACT	ACG	ACT	ACK	ACL	ACM	ACR	ACV	Class I/Pept	A2/NV9
C	Buffer	ACW	ACT	AG	AH	AI	AK	AL	AM	Buffer	Buffer
D	Buffer	GA	GD	GE	GF	GG	GH	GI	GK	No β_2m	No β_2m
E	Buffer	GL	GV	GW	GSR	GR	GY	GGA	GGF	Class I/Pept	A2/NV9
F	Buffer	GGG	GGH	GGI	GGK	GGL	GGM	GGR	GGV	Buffer	Buffer
G	Buffer	GGY	GG	GGR	GGN	GGP	GGM	GGI	GGG	No β_2m	No β_2m
H	Buffer	Buffer	Buffer	Buffer	Buffer	Buffer	Buffer	Buffer	Buffer	Buffer	Buffer

Assay plate 1											
	1	2	3	4	5	6	7	8	9	10	11
A	PC	Std 1	Std 2	Std 3	Std 4	Std 5	Std 6	Std 7	Std 8	Std 9	NC
B	PC	ACT	ACG	ACT	ACK	ACL	ACM	ACR	ACV	Class I/Pept	A2/NV9
C	PC	ACW	ACT	AG	AH	AI	AK	AL	AM	Buffer	Buffer
D	PC	ACW	ACT	AG	AH	AI	AK	AL	AM	Buffer	Buffer
E	NC	GA	GD	GE	GF	GG	GH	GI	GK	No β_2m	No β_2m
F	NC	GA	GD	GE	GF	GG	GH	GI	GK	No β_2m	No β_2m
G	NC	Std 1	Std 2	Std 3	Std 4	Std 5	Std 6	Std 7	Std 8	Std 9	PC
H	NC	Std 1	Std 2	Std 3	Std 4	Std 5	Std 6	Std 7	Std 8	Std 9	PC

Assay plate 2											
	1	2	3	4	5	6	7	8	9	10	11
A	PC	Std 1	Std 2	Std 3	Std 4	Std 5	Std 6	Std 7	Std 8	Std 9	NC
B	PC	GL	GV	GW	GM	GR	GY	GGA	GGF	Class I/Pept	A2/NV9
C	PC	GGG	GGH	GGI	GGK	GGL	GGM	GGR	GGV	Buffer	Buffer
D	PC	GGG	GGH	GGI	GGK	GGL	GGM	GGR	GGV	Buffer	Buffer
E	NC	GGW	GGY	GGH	GGI	GGK	GGM	GGI	GGG	No β_2m	No β_2m
F	NC	GGW	GGY	GGH	GGI	GGK	GGM	GGI	GGG	No β_2m	No β_2m
G	NC	Std 1	Std 2	Std 3	Std 4	Std 5	Std 6	Std 7	Std 8	Std 9	PC
H	NC	Std 1	Std 2	Std 3	Std 4	Std 5	Std 6	Std 7	Std 8	Std 9	PC

The light green wells are the outer wells that are kept empty (loaded with buffer only) to avoid evaporation of sample.

The light pink and the light blue wells (columns 2-9) contain the various dipeptides to be screened.

Columns 10 and 11 contain the negative and positive controls:

B10 and B11 = positive controls containing class I complexes folded with full-length reference peptides (B10 contains the class I allotype on which the dipeptides are tested, B11 contains a different allotype plus a respective high-affinity peptide).

C10 and C11 = negative controls without peptide.

D10 and D11 = negative controls without peptide and β_2m

Assay plates

From the Sample plate, two Assay plates are generated:

We usually transfer the samples in lines B-D from the Sample plate in duplicates to Assay plate 1, the samples in lines E-G from the Sample plate in duplicates to Assay plate 2.

Std 1-10 = dilution series of the ELISA standards (A2/NV9)

Concentration of the standards [ng/ml]

Std 1 = 10.000

Std 2 = 3.333,33

Std 3 = 1.111,11

Std 4 = 370,37

Std 5 = 123,46

Std 6 = 41,15

Std 7 = 13,72

Std 8 = 4,57

Std 9 = 1,52

Std 10 = 0,17

The negative and positive controls (columns 10 and 11) are also prepared in duplicates on each Assay plate.

PC = additional positive control (20 μ g/ml A2/NV9)

NC = additional negative control (10x Tris buffer, pH 8.0)

Chapter 3. Screening for dipeptides/tripeptides that stabilize and promote MHC-I refolding in a competitive ELISA assay

3.1. Background

The cellular adaptive immune system has evolved a sophisticated strategy to monitor the internal environment of cells, in which all proteins, whether self or non-self, are broken down within antigen presenting cells, and the resulting pool of peptides is loaded onto MHC-I, presented, and inspected [1,2]. The MHC-I molecules perform the task of sampling and presenting the loaded peptides to CTLs [3,4]. Peptide binding to MHC-I is highly sequence-specific for a given allotype, and the pMHC complex is detected by antigen-specific T cells [5,6]. Self-reactive CTL are usually deleted in the thymus or otherwise anergized, and thus, the CTL population as a whole is specialized in differentiating non-self from self peptides to further determine the course of action for the immune system [7].

For the researcher, the ability to identify and evaluate peptide binding to MHC-I is of great scientific and practical importance. It serves as the foundation for creating extensive databases such as NetMHC with predictions of peptide binding to the MHC-I [8,9]. It is also critical for any comparison between predicted and actual peptide binding, which is currently far from ideal and leaves no alternative to conducting actual experiments [10,11].

The discovery of neoepitopes should thus consider screening of MHC-I binding peptide to be of primary importance. Furthermore, the recent development in immunotherapy has resulted in growing need for MHC multimers – dimers, tetramers, pentamers, streptamers, dextramers and octamers, see the Introduction to monitor T cell responses in research or diagnostics [12–14]. These T cell staining methods also highlight the need for experimental methods to identify low-affinity peptide binders that are immunogenic but not good candidates for either generating stable multimer (e.g., tetramer) complexes, or where the pMHC-TCR affinity threshold required for tetramer staining is higher than that required for efficient T cell activation [15].

Many different peptide-MHC binding assays have been suggested over the years [16–25]. The existing methods are limited to low throughput, and no generally accepted universal methods are available till date. In this respect, our group have previously developed dsMHC-I molecules for efficient T cell staining without compromising the specificity [26]. These recombinant MHC-I allotypes can be generated in an empty, stable, and peptide-receptive conformation. The peptide of

interest can be added to the complex immediately before the assay, which is a very efficient alternative to conventional peptide exchange strategies [27–29]. But these dsMHC-I molecules need very low-affinity but allotype-specific dipeptides or tripeptides at millimolar concentration in the reaction mix as chemical chaperones during the refolding process. These short peptides can be later washed off with excess of buffer during SEC purification, with a dissociation half-time thought to be in the milliseconds to seconds range [30]. Since the di-/tripeptides need to fit into the MHC-I peptide binding groove to fulfil their role, and since different MHC-I allotypes have peptide binding grooves of different shape and charge, each MHC-I allotypes requires a specific di- or tripeptide for folding. Thus, challenges still exist in finding the right di-/tripeptides to support the folding process.

Here, we have developed a competitive ELISA (cELISA) using the conformation-specific antibody W6/32, which allows us to differentially detect MHC-I molecules in the folded conformation only [31]. This is a quantitative assay capable of measuring the affinity of the peptide-MHC-I interaction. This technique is simple and sensitive, and the required reagents and standards are easily available. A Sandwich ELISA for detection of pHLA complexes already exists but is limited to the detection of MHC-I – full length peptide complexes [32]. The extensive washing steps in ELISA assays require pMHCs with relatively stable and full-length peptides to sustain the steps. Very low affinity peptides or short peptides (e.g. dipeptides) always require millimolar concentrations of free peptide continuously maintained in the refold mixture to stabilize the MHC-I complexes. This makes sandwich ELISAs unsuitable for screening such complexes. Therefore, we developed an alternative cELISA to overcome such limitations.

Use of a cELISA for MHC-I quantification has only been reported by us recently [26]. This method has several benefits over other strategies that researchers have developed for MHC-I detection. Among these, most are low-throughput, conducted in a poorly controlled environment (cell lysate or cell surface), and readouts are semiquantitative. The cELISA, on the other hand, is adaptable to a high-throughput format and can be done in the 96 or 384 well formats. The test samples containing MHC-I refolds are used just in the beginning step (see details below). The signals are detected in a high-throughput plate reader.

There are just a few quantitative biochemical peptide-MHC binding assays reported till date [18,22,33]. Most of these biochemical binding assays are tedious and are performed in specialist laboratories only (as radioactive materials have special regulatory and safety requirements). As a result, these assays have not been universally adopted by the scientific community. Hence, there is an unmet need for a high throughput quantitative peptide-MHC-binding assay that is free of radioactivity, simple to perform, robust, and easily adaptable.

3.2. Assay principle

The cELISA, also known as a blocking ELISA or inhibition ELISA, is the most complex of all ELISA techniques. This method was initially developed by Yorde et. al. in 1976 [34] and later adapted for detecting *West Nile virus* [35], *Francisella tularensis* [36], *Bluetongue Virus* [37], *Mycoplasma meleagridis* [38], and porcine reproductive and respiratory syndrome virus (PRRSV) [39], to name a few.

The cELISA approaches the final signal readout in the reverse direction compared to the other versions of ELISA assays. The microplate is first coated with a reference antigen (e.g., the folded A2/NV9 complex) at 4 °C overnight. The test samples (containing pMHC-I refolds) are then mixed with the capture antibody, i.e., the conformation-specific primary antibody (1° Ab, e.g., W6/32, which binds to only folded human MHC-I molecules) and preincubated before transferring the entire mixture to the reference antigen-coated wells. Only the remaining free 1° Ab that did not bind to the test sample can now bind to the antigen-coated plate. Thus, the more successful the refolding in the test sample has been, the less 1° Ab is now available for binding to the coated plate. The bound 1° Ab is then detected by addition of horseradish peroxidase (HRP)-conjugated 2° antibody against the 1° antibody. After washing, relevant substrate (e.g., 3,3',5,5'-Tetramethylbenzidine, TMB) is added, which produces a soluble color that can be measured with a plate reader. As stated above, the presence of folded pMHC-I in the test sample decreases the signal output proportionate with its concentration. If there is a high concentration of folded pMHC-I in the test sample, i.e., if the folding reaction was successful, then a significant reduction in the signal output will be observed. In contrast, if there is very little folded pMHC-I in the test sample, i.e., if the folding reaction was unsuccessful, then there will be very little decrease in the expected signal output. This reverse approach allows for testing of an unknown sample containing crude refolds without need for purification, but the most important feature of the cELISA is that it allows the quantification of pMHCs that are so unstable that they would not survive the washing steps, e.g., complexes of MHC-I with di- or tripeptides.

3.3. The species- and conformation-specific mAbs, W6/32 (HLA-I) and 30-5-7 (L^d)

Researchers have developed several monoclonal antibodies that bind to the folded conformation of peptide-MHC-I complexes. These antibodies are commonly referred to as conformation-specific antibodies. These antibodies are widely used for detection of folded class I molecules using different methods like flow cytometry, fluorescence microscopy, radioimmunoprecipitation and pulse-chase [40–43]. Some of these antibodies are W6/32 [31], B9.12.1 [44], BB7.2 [45], F4/326 [46], 3F10 [47], and ME1 [48], which are either pan-HLA, monomorphic peptide-HLA complex or allotype-specific.

We selected W6/32 for our assay as it can recognize HLA-A, B, C, E, F, and G allotypes [49] and is widely accepted as a conformation-specific anti-HLA monoclonal antibody.

Not all conformation-specific antibodies have known epitopes, but for W6/32, it is known that the peptide itself is not part of the epitope. So in principle, W6/32 might recognize peptide-empty folded HLA-I molecules, but this is not an impediment for the use in the cELISA, since its purpose is the detection of the result of the folding process, which does not occur without an appropriate di- or tripeptide.

3.4. cELISA assay development

The cELISA assay development involved several steps. I have divided these steps according to the logical sequence that needs to be followed throughout the screening process. They are as follows:

- i. Preparation of dipeptide stock and buffers
- ii. Refolding and sample preparation
- iii. Quantification of pHLAs in cELISA assay

The above steps are explained in detail in the standard operating procedures (SOPs, SSP-SOP-BCM_019, 020, and 021) in chapter 2. In this section, I discuss the steps that were involved in the optimization of assay conditions and the validation according to the standard quality control parameters. I also compared the cELISA method using different endpoint readings – absorbance and fluorescence – to determine what would work best for our setup.

Figure 3-1 shows the workflow for the cELISA. The most critical steps in this assay that needed optimization were the A2/NV9 concentration for coating, the concentration and specificity of primary antibody (W6/32), the temperature, and the secondary antibody dilution. The parameter optimization is necessary to ensure the following:

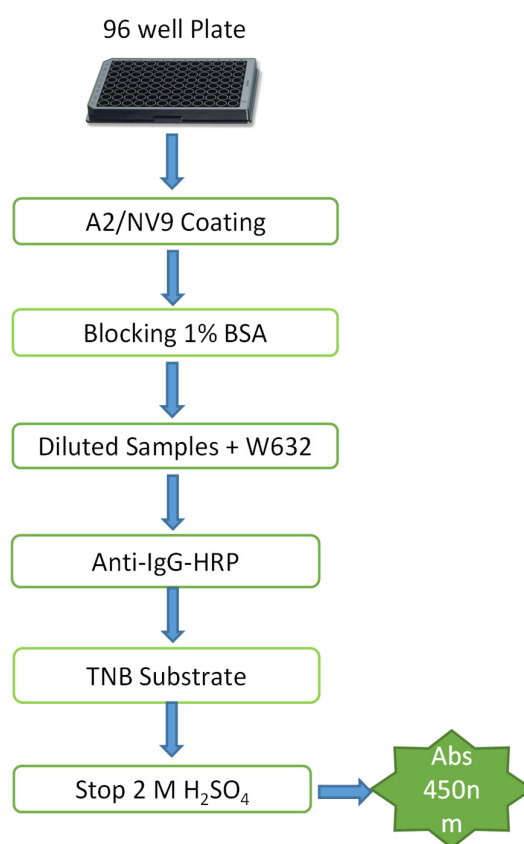


Figure 3-1. Steps involved in the cELISA

1. Reproducibility and robustness of the assay;
2. Lower background signal and appropriate signal-to-background (S:B) ratio;
3. Optimal detection range of the assay (the concentration of the diluted test samples must be within this range);
4. Selection of appropriate assay controls to monitor day-to-day variability;
5. Reagent stability;
6. Avoidance of false positive results.

While developing cELISA assays, some of the experiments were performed in an iterative manner to achieve full optimization. In addition, preliminary experiments were required to assess the system. In many instances, a multi-variable experimental design was set up to investigate the impact of several parameters simultaneously, or to determine the optimum level of a factor.

3.4.1. Assay conditions

3.4.1.1 Plate type

The type of plate that is used for ELISA assays may be influenced by the following factors:

- Counting instrument used (Tecan Infinity M1000)
- Miniaturization (96-well or 384-well)
- Binding of reagents to plastics
- Liquid dispensing equipment (single or multichannel pipettes)

Table 3-1. Different plate types used in cELISA assay

Plate Type	Plate Details	Purpose
Corning # CLS3590	96 well, Black, High binding, Flat bottom, non-sterile	For cELISA assay. Immobilization of A2/NV9 on the plate surface.
Greiner # 650901	96 well, Clear, LB, UB, PS	Preincubation of sample and w6/32.
Greiner # 780215	96 well, Deep-well, 1 mL	Used as reservoir for preparing the dipeptide plate.

3.4.1.2 Coating buffer

The coating buffer needs to be optimized for maximum binding of the pHLA protein (the reference antigen) to the plate surface. In **Figure 3-2 A**, we tested the assay signal window for two commonly used coating buffers, 1xPBS, pH 7.4 and bicarbonate buffer, pH 9.4, at different concentrations of the capture antibody W6/32. We selected multiple concentrations of W6/32, as the optimal concentration was not known at that point. The result suggested that bicarbonate buffer was better,

with a higher S:B ratio at all concentrations of W6/32. So, we decided to use bicarbonate buffer for future experiments.

3.4.1.3 *Blocking buffers*

We have used 96 well plates with high binding surface for coating with the reference antigen A2/NV9, which gets immobilized to the well surface due to adsorption and hydrophobic interactions. Although most of the plate surface is covered by the reference antigen, there will be some free binding sites left. These sites must be blocked to prevent a high background due nonspecific binding of the detection (1°) antibody alongside the antigen.

Different blocking buffers usually contain a blocking component such as serum, casein, skimmed milk, or bovine serum albumin (BSA). These blocking buffers should be selected based on the compromise between low background and minimal interference with the antibody binding. The optimal conditions such as concentration, incubation time, etc. can be tested in parallel, to discover the best blocking conditions. For our purpose, we used the most common blocking buffer with 1% BSA. As this worked well with our setup, we decided to use this buffer without further investigation.

3.4.1.4 *Sample dilution*

It is necessary to dilute the test samples – MHC-I refolds in this case - for the ELISA assay, so the choice of the dilution buffer is important. Generally, the dilution buffer should be as similar as possible to the refolding buffer. Non-ionic detergent (we used 0.05% Tween-20) is an important component of dilution buffer, since it prevents non-specific (hydrophobic) protein–protein interactions. The specific binding is usually more resistant to the detergent.

It is also necessary to check the standard curve and linearity of dilution for the experimental sample. Such experiments provide information about the precision of the assay results for different diluted samples in the chosen sample diluent. A linearity-of-dilution experiment in practice means the measurement of 2-3 dilutions in the appropriate range in the dilution buffer. The diluted test samples were measured in duplicate in conjunction with a known standard (A2/NV9) to ensure that the results fall within the linear portion of the standard curve. This ensures the accuracy of the result.

Figure 3-2 B suggests that the detection was more sensitive at 1:100-fold dilution as compared to 1:20-fold dilution. This was because at 1:20 dilution, the measured OD specially for high-affinity peptide-MHC refolds (the concentration of folded proteins was higher here) did not fall in the linear range of the A2/NV9 standard curve, thereby reducing the sensitivity. So, we decided that a dilution of 1:50 fold should suffice as a universal practice without compromising the detection sensitivity.

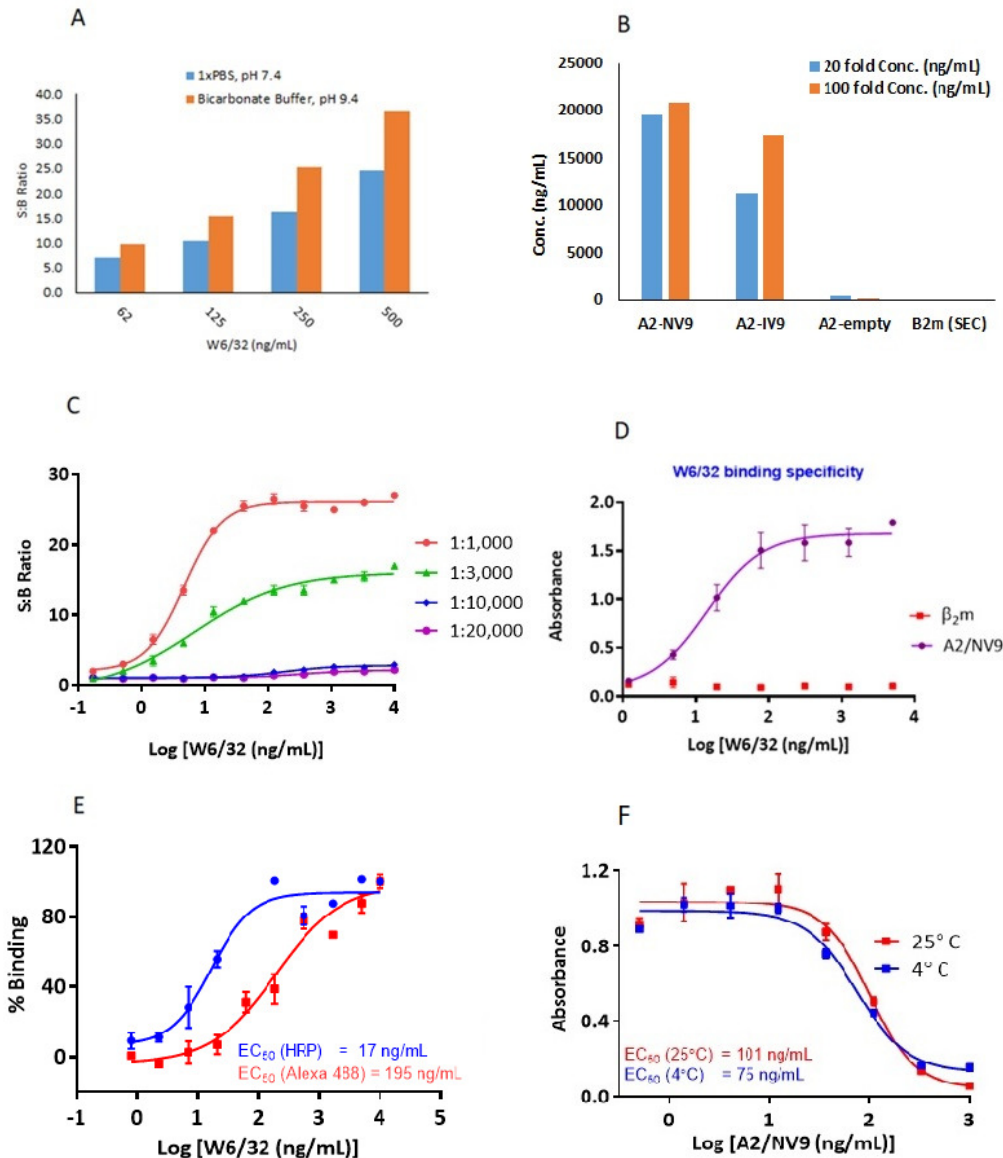


Figure 3-2. Assay parameter optimization (see text for details)

3.4.1.5 Antibody concentration – W6/32, 2° antibody-HRP

The next step was to optimize the concentration of the 1° Ab W6/32 and the dilution factor for the 2° Ab. Proper titration of antibody concentration was accomplished by serial dilutions of the 1° Ab and four dilutions of the 2° Ab in a matrix setup. The S:B values were then compared, and an optimal antibody concentration was determined based on the dynamic range of detection as well as the presence of any artifacts. The best concentrations of the antibodies were selected that provided the highest S:B ratio and the largest linear range for the assay. In **Figure 3-2 C**, we observed that the EC_{50} values for W6/32 (1° Ab) were 14, 20, 542 and 1021 ng/well, and for the 2° Ab, a dilution of

1000, 3000, 10000 and 20000-fold, respectively. This suggested that the detection sensitivity of the assay is inversely proportional to the dilution of secondary antibody. At the dilution of 1:3000 for 2° Ab, the S:B was more than 10-fold, which is sufficient for the assay robustness. At this dilution, the EC₅₀ for the 1° Ab (W6/32) was 20 ng/ml, and so we decided to use the concentration of 15-20 ng/mL of W6/32 for further experiments.

3.4.1.6 W6/32 binding specificity

One of the primary criteria for the selection of a capture antibody is the antigen specificity. Specificity means that the capture antibody W6/32 must differentiate folded human MHC-I molecules from all other refolding buffer components, especially the folded β_2m light chain that is not associated to the class I heavy chain. This 'free' β_2m is always present in excess. W6/32 was reported to recognize an epitope on residue $\beta 3$ -Arg of β_2m along with the residue $\alpha 121$ -Lys in the α_2 domain of the MHC-I heavy chain in the folded conformation [31,50].

In **Figure 3-2 D**, we planned to check the binding of folded β_2m alone to W6/32. We performed the cELISA at 10 μ g/mL concentration of β_2m and wtA2/NV9, while varying the concentration of W6/32 from 0.001-5 μ g/mL. We observed dose-dependent binding of W6/32 to folded wtA2/NV9, whereas there was no measurable binding observed against folded β_2m . This confirms that W6/32 is very specific to folded MHC-I molecules and does not bind to β_2m alone.

3.4.1.7 The choice of the detecting antibody and detection method

The performance of a cELISA depends on the choice of detection antibodies, and hence they should be carefully chosen. The choice of detection antibody depends on: a) specificity, b) affinity, and c) the detection method.

The most important quality of antibody is the specificity upon which ELISA is based, so careful selection is required. Affinity describes the strength with which an antibody binds to an antigen. High-affinity antibodies should be used in all types of immunoassays because they provide stable interactions and sensitive detection. ELISA detection sensitivity can be amplified by using additional polyclonal 2° Ab against the 1° Ab instead of direct detection with the monoclonal 1° Ab due to higher levels of polyclonal antibody binding to the target antigen. Our assay used monoclonal W6/32 as a 1° Ab followed by polyclonal anti-mouse IgG 2° Ab.

The detection methodologies in ELISA are mostly limited to colorimetry, fluorescence, or luminescence. In **Figure 3-2 E**, we tested two 2° Abs based on colorimetry or fluorometry: goat-anti-mouse-IgG-HRP and goat-anti-mouse-IgG-Alexa 488, respectively. The binding of the detection antibodies was monitored at the dilution of 1:3000 against a series of dilution for W6/32. The endpoint measurement was done separately in absorbance or fluorescence detection mode, accordingly. We observed that the EC₅₀ values for W6/32 binding were 17 ng/ml, and 195 ng/mL for

Goat-anti-mouse-IgG-HRP and Goat-anti-mouse-IgG-Alexa 488 detection antibodies, respectively. This indicated that, in our experimental setup, the colorimetric method was more sensitive. We decided to use Goat-anti-mouse-IgG-HRP for our further studies.

3.4.1.8 Temperature and incubation time

Incubation time and temperature are critical factors that affect protein immobilization and stability on surfaces. Typically, with the increase in the temperature, incubation time can be decreased, and vice versa. In most ELISA methods, the preferred initial surface coating step takes place at 4 °C overnight. This allows the stabilization of the equilibrium between bound and free antigens to the plate surface. However, for convenience and speed, it is more practical to perform the assay at room temperature for short, typically one hour, incubations. This time and temperature allow adequate surface coating to occur in a precise manner in a reasonable time frame.

In **Figure 3-2 F**, we tested the optimal incubation time and temperature. We performed the cELISA assay at 4 °C and room temperature (22 -25 °C). All the incubation durations were kept constant, except for the first coating step. Coating was done for overnight (16 – 18 hrs) or for 1 hr at 4 °C or room temperature (RT), respectively. The standard curve for the known concentration of antigen wtA2/NV9 was plotted for each condition and compared. We observed that the EC₅₀s for wtA2/NV9 were 75 ng/mL for 4 °C and 101 ng/ml for RT. Although 4 °C incubation slightly improved the assay sensitivity, the difference was not significant. So, for efficiency, we decided to continue our further experiments at room temperature.

3.5. Screening results:

The **Table 3-2** below shows the details about the optimal short peptides dipeptides/tripeptides that are specific for different MHC-I allotypes. These peptides were shown to modulate the refolding in the ELISA screening, further confirmed by peptide binding assay (anisotropy) and SEC purification.

Table 3-2. Short peptide screening in cELISA for different HLA allotypes.

Allotypes	Type	250 μ L Refold (96 well format)					Retest in 1 mL Refold		SEC Purification	Which peptide have passed through the entire pipeline?
		ELISA Assay (N)	Full length peptide	Did it fold?	Short Peptides	Conc. (mM)	ELISA assay	Peptide Exchange	20 mL refold	
HLA-A*01:01	WT	3	VTEHDTLLY, STDHIKILY	yes	AcY, GY	20	yes	yes	Tried for AcY and GY (high background)	Maybe GY
HLA-A*01:01	Y84C	3	VTEHDTLLY, STDHIKILY	yes	AcY, GY	20	yes	Not tried	Not tried	
HLA-A*02:01	WT	1	NLVPMVATV, ILKEPVHGV	yes	GM, GL	40	yes	yes	yes	GM, GL
HLA-A*02:01	Y84C	5	NLVPMVATV, ILKEPVHGV	yes	GM, GL	20	yes	yes	yes	GM, GL
HLA-A*03:01	WT	2	RIKEHMLKK, GVLGTVVHGK	yes	GK, GKG, GSFG	40, 20, 10	yes	yes	yes	GSFG
HLA-A*03:01	Y84C	4	GVLGTVVHGK	yes	AM, GKG, GSFG	20, 10, 20	yes	no	Not tried	GSFG, GKG
HLA-A*11:01	WT	2	GPISGHVLK, KIADRFLH	yes	GGM, GL	40	yes	no	Not tried	
HLA-A*11:01	Y84C	5	KIADRFLH	yes	GL	20	yes	yes	yes	GL
HLA-A*24:02	WT	4	QYDPVAALF, TYGPVFMCL	yes	GF, GGF	20, 10	yes	yes	Yes	GF
HLA-A*24:02	Y84C	7	QYDPVAALF, TYGPVFMCL	yes	GF, GGF	20	yes	yes	yes	nothing or GF, GGF
HLA-A*68:01	WT	4	TSAFVFPTK, ETSFVPSRR	Yes*	GSFG, maybe GGF	40	yes	no	Not tried	

Screening results:

Allotypes	Type	250 µL Refold (96 well format)					Retest in 1 mL Refold		SEC Purification	Which peptide have passed through the entire pipeline?
		ELISA Assay (N)	Full length peptide	Did it fold?	Short Peptides	Conc. (mM)	ELISA assay	Peptide Exchange	20 mL refold	
HLA-A*68:01	Y84C	1	ETSFVPSRR	yes	GGF, GSFG	20	yes	no	Not tried	GGF
HLA-B*07:02	WT	3	RPHERNGFTV, APGIRDHESL	yes	GM, GI, GL, AL, AM also	40	yes	no	yes	GL
HLA-B*07:02	Y84C	3	RPHERNGFTV, APGIRDHESL	yes	AL, GL, GM	40, 20	yes		yes	AL (not clear if able to bind peptide)
HLA-B*08:01	WT	8	QIKVRVDMV, DLNEKAKAL	yes	none	20	yes	Not tried	Not tried	
HLA-B*08:01	Y84C	3	DLNEKAKAL	yes*	GL, GGF, GGY	20	yes	Not tried	Not tried	GL might work
HLA-B*13:01	Y84C	1	YLLEMLWRL	no	none	20	yes	Not tried	Not tried	None
HLA-B*15:01	Y84C	3	GQRKGAGSVF	yes*	GK, GGF, GSFG	20	yes	Not tried	Not tried	None
HLA-B*27:05	WT	3	KRWIIMGLNK, RRIYDLIEL	yes	None	40	yes	Not tried	Not tried	None
HLA-B*27:05	Y84C	2	KRWIIMGLNK, RRIYDLIEL	Yes*	GL, GGY	20	yes	Not tried	Not tried	None
HLA-B*27:09	WT	3	KRWIIMGLNK, RRIYDLIEL	yes	None	40	yes	Not tried	no	None
HLA-B*35:01	WT	3	IPSINVHHY	yes	AM, GGM, GGF	40	yes	Not tried	Not tried	None
HLA-B*35:01	Y84C	4	IPSINVHHY	yes	GL, GGY	20	yes	Not tried	Not tried	GL, GGY
HLA-B*44:02	WT	2	EEYGRAFSF, SEEDLKVLV	no	None	40	yes	no	no	none

Chapter 3

Allotypes	Type	250 µL Refold (96 well format)					Retest in 1 mL Refold		SEC Purification	Which peptide have passed through the entire pipeline?
		ELISA Assay (N)	Full length peptide	Did it fold?	Short Peptides	Conc. (mM)	ELISA assay	Peptide Exchange	20 mL refold	
HLA-B*44:03	Y84C	2	EEYGRAFSF, SEEDLKVLF	yes	None	40	yes	Not tried	Not tried	
HLA-B*44:05	WT	2	EEYGRAFSF, SEEDLKVLF	yes	GF, SGGL	20	yes	Not tried	Not tried	
HLA-B*44:05	Y84C	3	EEYGRAFSF, SEEDLKVLF	yes	GL, AL, GM	20	yes	Not tried	Not tried	GF, GL
HLA-B*51:01	Y84C	1	LPYVVAKEI	yes	None	20	yes	Not tried	Not tried	none
HLA-C*02:02	Y84C	1	FLYDDNQRV	no	none	20	yes	Not tried	Not tried	
HLA-C*03:04	Y84C	2	YVDRFFKTL	yes	GGL, GGM	20	yes	Not tried	Not tried	
HLA-C*04:01	Y84C	1	QYDPVAALF	Yes*	none	20	yes	Not tried	Not tried	none
HLA-C*05:01	Y84C	1	YVDRFFKTL	yes	GGM	20	yes	Not tried	Not tried	GGM or empty
HLA-C*07:02	WT	4	CRVLCCYVL, FRKDVNMVL	yes	AK	40	yes	Not tried	Not tried	none
HLA-C*07:02	Y84C	2	FRKDVNMVL	yes	GW, GGF?	20	yes	Not tried	Not tried	

*Refolding efficiency was low

3.6. Discussion

We established the cELISA method for screening short peptides such as dipeptides and tripeptides, which can modulate the refolding of different human MHC-I allotypes. We selected the allotypes based on their abundance in human population and therapeutic relevance. The main purpose of identifying the short peptides was to use them in producing stable MHC-I refolds that can be readily available for peptide exchange with full length peptides. Since the dipeptides/tripeptides had very low affinity for MHC-I molecules ($K_d > 1$ mM) as compared to the full length peptides (pM to lower μ M), the former are easily replaced and can be washed away in subsequent SEC purification steps. This process will greatly accelerate the process of pMHC production, which is a tedious and time-consuming process in the conventional methods where every peptide-MHC-I pair needs to be folded from scratch. This will reduce the timeline for the generation of new peptide-MHC complexes from 2 – 3 weeks to just a few hours. This can be a major advantage over current techniques as this method enables rapid production of epitope-specific MHC tetramers.

The dipeptides can also be used to enhance peptide loading onto live cells for cancer immunotherapy [51]. Further applications include the large-scale generation of pMHC complexes for T cell detection platforms. There are other peptide exchange technologies developed for rapid production of tetramers which include the use of dipeptide-catalyzed peptide exchange [51], ultraviolet (UV)-mediated peptide exchange [28], and temperature-induced exchange [52]. However, exchange technologies have drawbacks that include optimizing HLA-specific leaving peptide, appropriate temperature, and inefficient peptide exchange when low-affinity incoming peptides are used.

The cELISA screening was successfully concluded with identification of dipeptides/tripeptide that can be used for refolding their cognate MHC-I allotypes. We observed that some allotypes were efficiently folded, whereas some allotypes did not refold efficiently with short-peptides, which can be linked to the intrinsic properties of these allotypes. Further investigation of alternative small molecules or modified non-natural dipeptides (such as the dipeptide found to best support folding, of H-2K^b, glycyl-cyclohexylalanine or GCha) might result in the discovery of new reagents for refolding of difficult MHC-I molecules.

These ready-to-use stable and easily exchangeable dipeptide-MHC-I complexes can be used in multimer generation, which can be efficiently utilized in T cell monitoring, diagnostics, and in therapeutic applications such as the priming and isolation antigen-specific T cells for adoptive T cell transfer in immunotherapy.

Reference

- [1] Brodsky, F.M., Guagliardi, L.E., The cell biology of antigen processing and presentation. *Annu. Rev. Immunol.* 1991, 9, 707–744.
- [2] Germain, R.N., Margulies, D.H., The biochemistry and cell biology and antigen processing and presentation. *Annu. Rev. Immunol.* 1993, 11, 403–450.
- [3] Anton, L.C., Yewdell, J.W., Bennink, J.R., et al, MHC class I-associated peptides produced from endogenous gene products with vastly different efficiencies. *J. Immunol.* 1997, 158, 2535–42.
- [4] Yewdell, J.W., Bennink, J.R., Cell Biology of Antigen Processing and Presentation to Major Histocompatibility Complex Class I Molecule-Restricted T Lymphocytes. *Adv. Immunol.* 1992, 52, 1–123.
- [5] Yewdell, J.W., Bennink, J.R., Immunodominance in major histocompatibility complex class I-restricted T lymphocyte responses. *Annu. Rev. Immunol.* 1999, 17, 51–88.
- [6] Falk, K., Rötzschke, O., Stevanović, S., Jung, G., Rammensee, H.G., Allele-specific motifs revealed by sequencing of self-peptides eluted from MHC molecules. *Nature* 1991, 351, 290–296.
- [7] Rammensee, H.G., Falk, K., Rötzschke, O., Peptides naturally presented by MHC class I molecules. *Annu. Rev. Immunol.* 1993, 11, 213–244.
- [8] Ruppert, J., Sidney, J., Celis, E., Kubo, R.T., et al., Prominent role of secondary anchor residues in peptide binding to HLA-A2.1 molecules. *Cell* 1993, 74, 929–937.
- [9] Kast, W.M., Brandt, R.M., Sidney, J., Drijfhout, J.W., et al., Role of HLA-A motifs in identification of potential CTL epitopes in human papillomavirus type 16 E6 and E7 proteins. *J. Immunol.* 1994, 152, 3904–3912.
- [10] Andersen, M.H., Tan, L., Søndergaard, I., Zeuthen, J., et al., Poor correspondence between predicted and experimental binding of peptides to class I MHC molecules. *Tissue Antigens* 2000, 55, 519–531.
- [11] Shao, X.M., Bhattacharya, R., Huang, J., Sivakumar, I.K.A., et al., High-throughput prediction of MHC Class I and II neoantigens with MHcnuggets. *Cancer Immunol. Res.* 2020, 8, 396–408.
- [12] Altman, J.D., Moss, P.A.H.H., Goulder, P.J.R.R., Barouch, D.H., et al., Phenotypic Analysis of Antigen-Specific T Lymphocytes. *Science*. 1996, 274, 94–96.
- [13] Casalegno-Garduño, R., Schmitt, A., Yao, J., Wang, X., et al., Multimer technologies for detection and adoptive transfer of antigen-specific T cells. *Cancer Immunol. Immunother.* 2010, 59, 195–202.
- [14] Bentzen, A.K., Hadrup, S.R., Evolution of MHC-based technologies used for detection of antigen-responsive T cells. *Cancer Immunol. Immunother.* 2017, 66, 657–666.
- [15] Rius, C., Attaf, M., Tungatt, K., Bianchi, V., et al., Peptide–MHC Class I Tetramers Can Fail To Detect Relevant Functional T Cell Clonotypes and Underestimate Antigen-Reactive T Cell Populations. *J. Immunol.* 2018, 200, 2263–2279.
- [16] Werdelin, O.L.E., Chemically related antigens compete for presentation by accessory cells to T cells. *J. Immunol.* 1982, 129, 1883–1889.
- [17] Buus, S., Werdelin, O., Oligopeptide antigens of the angiotensin lineage compete for presentation by paraformaldehyde-treated accessory cells to T cells. *J. Immunol.* 1986, 136, 459–465.
- [18] Babbitt, B.P., Matsueda, G., Haber, E., Unanue, E.R., Allen, P.M., Antigenic competition at the level of peptide-Ia binding. *Proc. Natl. Acad. Sci. U. S. A.* 1986, 83, 4509–4513.
- [19] Luescher, I.F., Allen, P.M., Unanue, E.R., Binding of photoreactive lysozyme peptides to murine histocompatibility class II molecules. *Proc. Natl. Acad. Sci. U. S. A.* 1988, 85, 871–874.
- [20] Townsend, A., Elliott, T., Cerundolo, V., Foster, L., et al., Assembly of MHC class I molecules analyzed in vitro. *Cell* 1990, 62, 285–295.
- [21] Olsen, A.C., Pedersen, L.Øs., Hansen, A.S., Buus, S., et al., A quantitative assay to measure the interaction between immunogenic peptides and purified class I major histocompatibility complex molecules. *Eur. J. Immunol.* 1994, 24, 385–392.
- [22] Khilko, S.N., Corr, M., Boyd, L.F., Lees, A., et al., Direct detection of major histocompatibility complex class I binding to antigenic peptides using surface plasmon resonance. Peptide immobilization and characterization of binding specificity. *J. Biol. Chem.* 1993, 268, 15425–15434.

- [23] Buus, S., Stryhn, A., Winther, K., Kirkby, N., Østergaard Pedersen, L., Receptor-ligand interactions measured by an improved spun column chromatography technique A high efficiency and high throughput size separation method. *Biochim. Biophys. Acta - Gen. Subj.* 1995, 1243, 453–460.
- [24] Regner, M., Claësson, M.H., Bregenholt, S., Röpke, M., An improved method for the detection of peptide-induced upregulation of HLA-A2 molecules on TAP-deficient T2 cells. *Exp. Clin. Immunogenet.* 1996, 13, 30–35.
- [25] Harndahl, M., Rasmussen, M., Roder, G., Buus, S., Real-time, high-throughput measurements of peptide-MHC-I dissociation using a scintillation proximity assay. *J. Immunol. Methods* 2011, 374, 5–12.
- [26] Saini, S.K., Tamhane, T., Anjanappa, R., Saikia, A., et al., Empty peptide-receptive MHC class I molecules for efficient detection of antigen-specific T cells. *Sci. Immunol.* 2019, 4, eaau9039.
- [27] Rodenko, B., Toebe, M., Celie, P.H.N., Perrakis, A., et al., Class I Major Histocompatibility Complexes Loaded by a Periodate Trigger. *J. Am. Chem. Soc.* 2009, 131, 12305–12313.
- [28] Rodenko, B., Toebe, M., Hadrup, S.R., van Esch, W.J.E., et al., Generation of peptide–MHC class I complexes through UV-mediated ligand exchange. *Nat. Protoc.* 2006, 1, 1120–1132.
- [29] Luimstra, J.J., Franken, K.L.M.C.M.C., Garstka, M.A., Drijfhout, J.W., et al., Production and Thermal Exchange of Conditional Peptide-MHC I Multimers. *Curr. Protoc. Immunol.* 2019, 126, e85.
- [30] Anjanappa, R., Garcia-Alai, M., Kopicki, J.D., Lockhauserbäumer, J., et al., Structures of peptide-free and partially loaded MHC class I molecules reveal mechanisms of peptide selection. *Nat. Commun.* 2020, 11, 1–11.
- [31] Barnstable, C.J., Bodmer, W.F., Brown, G., Galfre, G., et al., Production of monoclonal antibodies to group A erythrocytes, HLA and other human cell surface antigens-new tools for genetic analysis. *Cell* 1978, 14, 9–20.
- [32] Sylvester-Hvid, C., Kristensen, N., Blicher, T., Ferré, H., et al., Establishment of a quantitative ELISA capable of determining peptide - MHC class I interaction. *Tissue Antigens* 2002, 59, 251–258.
- [33] Buus, S., Sette, A., Colon, S.M., Jenis, D.M., Grey, H.M., Isolation and characterization of antigen-la complexes involved in T cell recognition. *Cell* 1986, 47, 1071–1077.
- [34] Yorde, D.E., Sasse, E.A., Wang, T.Y., Hussa, R.O., Garancis, J.C., Competitive enzyme-linked immunoassay with use of soluble enzyme/antibody immune complexes for labeling. I. Measurement of human choriogonadotropin. *Clin. Chem.* 1976, 22, 1372–1377.
- [35] Hirota, J., Shimizu, S., A new competitive ELISA detects West Nile virus infection using monoclonal antibodies against the precursor-membrane protein of West Nile virus. *J. Virol. Methods* 2013, 188, 132–138.
- [36] Sharma, N., Hotta, A., Yamamoto, Y., Fujita, O., et al., Detection of Francisella tularensis-specific antibodies in patients with tularemia by a novel competitive enzyme-linked immunosorbent assay. *Clin. Vaccine Immunol.* 2013, 20, 9–16.
- [37] Reddington, J.J., Reddington, G.M., Maclachlan, N.J., A competitive ELISA for detection of antibodies to the group antigen of bluetongue virus. *J. Vet. Diagnostic Investig.* 1991, 3, 144–147.
- [38] Dufour-Gesbert, F., Kempf, I., Kobisch, M., Development of a blocking enzyme-linked immunosorbent assay for detection of turkey antibodies to Mycoplasma meleagridis. *Vet. Microbiol.* 2001, 78, 275–284.
- [39] Ferrin, N.H., Fang, Y., Johnson, C.R., Murtaugh, M.P., et al., Validation of a blocking enzyme-linked immunosorbent assay for detection of antibodies against porcine reproductive and respiratory syndrome virus. *Clin. Diagn. Lab. Immunol.* 2004, 11, 503–514.
- [40] Garstka, M.A., Fritzsche, S., Lenart, I., Hein, Z., et al., Tapasin dependence of major histocompatibility complex class I molecules correlates with their conformational flexibility. *FASEB J.* 2011, 25, 3989–3998.
- [41] Martayan, A., Sibilio, L., Tremante, E., Monaco, E. Lo, et al., Class I HLA Folding and Antigen Presentation in β 2 -Microglobulin-Defective Daudi Cells. *J. Immunol.* 2009, 182, 3609–3617.
- [42] Brodsky, F.M., Parham, P., Barnstable, C.J., Crumpton, M.J., Bodmer, W.F., Monoclonal Antibodies for Analysis of the HLA System. *Immunol. Rev.* 1979, 47, 3–61.

- [43] Montealegre, S., Venugopalan, V., Fritzsche, S., Kulicke, C., et al., Dissociation of β 2-microglobulin determines the surface quality control of major histocompatibility complex class I molecules. *FASEB J.* 2015, 29, 2780–2788.
- [44] Malissen, B., Rebai, N., Liabeuf, A., Mawas, C., Human cytotoxic T cell structures associated with expression of cytolysis. I. Analysis at the clonal cell level of the cytolysis-inhibiting effect of 7 monoclonal antibodies. *Eur. J. Immunol.* 1982, 12, 739–747.
- [45] Parham, P., Brodsky, F.M., Partial purification and some properties of BB7.2 a cytotoxic monoclonal antibody with specificity for HLA-A2 and a variant of HLA-A28. *Hum. Immunol.* 1981, 3, 277–299.
- [46] Martayan, A., Sibilio, L., Setini, A., Lo Monaco, E. Lo, et al., N-linked glycosylation selectively regulates the generic folding of HLA-Cw. *J. Biol. Chem.* 2008, 283, 16469–16476.
- [47] Eisenbarth, G.S., Haynes, B.F., Schroer, J.A., Fauci, A.S., Production of monoclonal antibodies reacting with peripheral blood mononuclear cell surface differentiation antigens. *J. Immunol.* 1980, 124.
- [48] Malik, P., Baba, E., Strominger, J.L., Biotinylation of class I MHC molecules abrogates recognition by W6/32 antibody. *Tissue Antigens* 1999, 53, 576–579.
- [49] Uchanska-Ziegler, B., Ziegler, A., On the reactivity of monoclonal antibodies specific for different forms of HLA class I molecules [3]. *Rheumatology* 2007, 46, 555–556.
- [50] Ladasky, J.J., Shum, B.P., Canavez, F., Seuánez, H.N., Parham, P., Residue 3 of β 2-microglobulin affects binding of class I MHC molecules by the W6/32 antibody. *Immunogenetics* 1999, 49, 312–320.
- [51] Saini, S.K., Schuster, H., Ramnarayan, V.R., Rammensee, H.-G., et al., Dipeptides catalyze rapid peptide exchange on MHC class I molecules. *Proc. Natl. Acad. Sci.* 2015, 112, 202–207.
- [52] Luimstra, J.J., Garstka, M.A., Roex, M.C.J., Redeker, A., et al., A flexible MHC class I multimer loading system for large-scale detection of antigen-specific T cells. *J. Exp. Med.* 2018, 215, 1493–1504.

Chapter 4. Methods to monitor MHC-I peptide exchange and binding

4.1. Introduction

Peptide binding to MHC-I molecules is the most selective step in the pathway of presenting cytosolic peptides [1–3]. Therefore, measuring the information about the interaction of MHC-I and their peptide epitopes acts as a basis for neoepitope discovery, vaccine design, diagnostics, and immune-based therapies [4–6]. Several methods were developed in the last two decades to monitor peptide binding to MHC-I molecules on the cell surface (such as radio-labelled peptide binding assays) or as in-vitro biochemical assays using soluble recombinant proteins (such as surface plasmon resonance) (see **Table 4-1**). So far, these assays could not measure direct peptide association, as empty, functional MHC-I molecules were highly unstable.

Table 4-1: Assays developed so far to monitor peptide-MHC-I interactions.

Assay Types	Reference
Cell surface stabilization assay (radioactive)	[7–9]
Cell surface binding after acid stripping (Flow cytometry)	[10,11][12]
Cell surface Fluorescence Polarization	[13]
cell surface biotinylated-peptide Binding (Flow cytometric)	[14]
Gel Filtration Assay (SEC)	[15]
Monoclonal Antibody Capture	[15]
Spin column filtration assay	[16]
Competitive peptide binding assay (radioactive)	[17–19]
Surface plasmon resonance	[20,21]
Ultra-dense peptide array	[22]
Scintillation Proximity Assay (radioactive)	[23,24]
AlphaScreen™ Assay	[24]
NeoScreen® assay (Urea denaturation)	[25]
Fluorescence Anisotropy Assay	[26–28]
NanoDSF Isothermal analysis (label-free)	[29]

Recently, our group has successfully generated stable, peptide-receptive, empty, disulfide-stabilized MHC-I molecules [30,31]. We can now monitor the binding of peptides directly to the peptide-binding groove of these empty functional MHC-I molecules in vitro. So, we will use the term *direct peptide binding* in reference to peptide binding to the empty disulfide-stabilized MHC-I molecules.

Our lab has used fluorescence anisotropy (FA) assay to monitor peptide exchange and direct peptide binding studies. In this chapter, I would like to elaborate on this FA assay.

We are currently developing a novel MHC-I-peptide binding assay based on the Microscale Thermophoresis platform from NanoTemper Technologies GmbH. Our pilot studies successfully measured the peptide binding affinity (K_d) for a few clinically significant MHC-I allotypes, which I intend to discuss in this chapter.

4.2. Kinetic parameters of receptor-ligand binding

4.2.1. The law of mass action: binding equilibrium

For the binding of a **ligand (L)** to a **target protein (P)**, most descriptions successfully use a simple model called the law of mass action:



The equilibrium constant of dissociation, K_d , is defined as follows for the concentrations of $L \cdot P$, L , and P at equilibrium:

$$\frac{[L]_{eq} \times [P]_{eq}}{[L \cdot P]_{eq}} = K_d \quad \text{Equation 4-2}$$

The K_d , expressed in units of moles per litre (M), is the concentration of ligand at which half of the available ligand-binding sites on the protein are occupied. So, a lower value of K_d corresponds to a higher affinity of the ligand for the protein.

Where the free concentrations of each partner are not known, the total concentrations at the beginning, $[L_0]$ and $[P_0]$, are used according to the following formula (with LP as an alternative symbol to $L \cdot P$):

$$K_d = \frac{([L_0] - [LP]_{eq})([P_0] - [LP]_{eq})}{[LP]_{eq}} \quad \text{Equation 4-3}$$

The **equation 4-3** will be helpful while deriving the K_d model for curve fitting in **section 4.4.5.1**.

4.2.2. Binding kinetics

For the same reaction, k_{on} is usually called the association (forward) rate constant, and k_{off} the dissociation (reverse) rate constant. Then, the following points apply:

- The rate of the forward reaction equals $[L] \times [P] \times k_{on}$. Here, the reaction involves two molecules, $L + P \rightarrow L \cdot P$, and is therefore called a second-order reaction, and k_{on} has the unit of $M^{-1} \text{ min}^{-1}$.

- b) The rate of the reverse reaction equals $[LP] \times k_{off}$. Here, the reaction involves one molecule, $L \cdot P \rightarrow L + P$, is thus called a first-order reaction, and k_{off} has the unit of min^{-1} .

At equilibrium, it is considered that the rate of association equals the rate of dissociation:

$$[L]_{eq} \times [P]_{eq} \times k_{on} = [L \cdot P]_{eq} \times k_{off} \quad \text{Equation 4-4}$$

Rearranging for K_d gives

$$\frac{[L]_{eq} \times [P]_{eq}}{[L \cdot P]_{eq}} = \frac{k_{off}}{k_{on}} = K_d \quad \text{Equation 4-5}$$

4.2.3. Occupancy fraction

Following the law of mass action, the occupancy fraction $f_{occupancy}$ is a function of ligand concentration at equilibrium.

$$f_{occupancy} = \frac{[L \cdot P]_{eq}}{P_{total}} = \frac{[L \cdot P]_{eq}}{[P]_{eq} + [L \cdot P]_{eq}} \quad \text{Equation 4-6}$$

Combining Equation 4.5 and Equation 4.6 gives

$$f_{occupancy} = \frac{[L]_{eq}}{[L]_{eq} + K_d} \quad \text{Equation 4-7}$$

Equation 4.7 is useful to understand the $f_{occupancy}$ at different ligand concentrations. The progression to the saturation with the increase of $[L]$ is not as fast as we might imagine. For example, when there is zero $[L]$, the $f_{occupancy}$ is at zero. When $[L]$ is significantly high ($\gg K_d$), the $f_{occupancy}$ approaches 1.00. When $[L] = K_d$, $f_{occupancy}$ is 0.5. When the $[L] = 4 \times K_d$, $f_{occupancy}$ equals 80% of the receptors at equilibrium. When the $[L] = 99 \times K_d$, $f_{occupancy}$ equals 99% of the receptor at equilibrium (**Figure 4-1**). B_{max} is the total density (concentration) of receptors in a sample. This refers to the concentration of available (free) receptors in the reaction mix. The specific binding at equilibrium for a particular $[L]$ is $f_{occupancy}$ times the number of the total receptor (B_{max}) [32]:

$$\text{Specific Binding} = f_{occupancy} \times B_{max} = \frac{B_{max} \times [L]_{eq}}{K_d + [L]_{eq}} \quad \text{Equation 4-8}$$

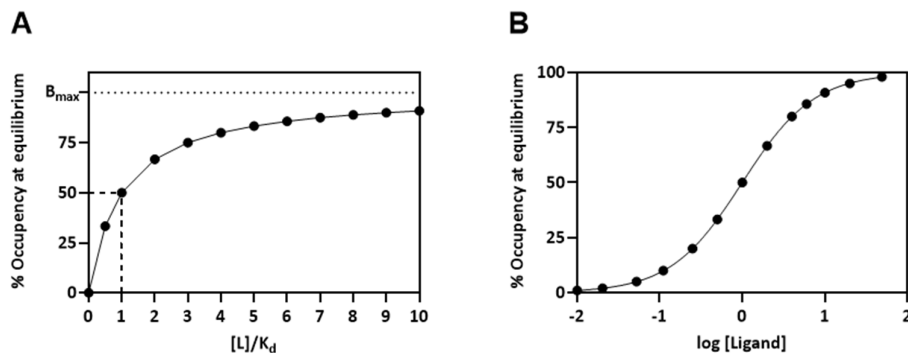


Figure 4-1. Occupancy at equilibrium.

The % occupancy at equilibrium depends on the concentration of the ligand compared to its K_d .

4.2.4. Half-life ($t_{1/2}$)

Kinetic processes such as peptide binding to MHC-I follow the exponential path like in **Figure 4-2**. The exponential curve is characterized by a constant half-life ($t_{1/2}$), which means that the duration of the reaction time between 0% to 50% is the same as 50% to 75% completion and so on. An exponential process is about 90% complete after three half-lives ($3t_{1/2} = 87.5\%$), close enough to equilibration for most applications. A more standard practice of running the reaction to $5 \times t_{1/2}$ or 96.6% is usually practiced for binding experiments.

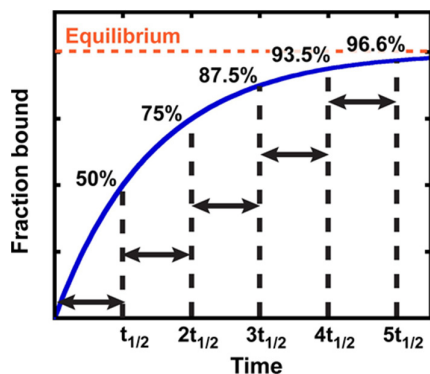


Figure 4-2. Schematic of binding equilibrium shown by exponential kinetics.

The reaction half-life $t_{1/2}$ is indicated by arrows. This figure was adapted from [33]

4.3. Fluorescence anisotropy

4.3.1. Principle

Fluorescence anisotropy (FA) or fluorescence polarization (FP) is a robust technique for studying molecular interactions by monitoring changes in the apparent movement of a small fluorophore, often referred to as the tracer or ligand [34–36]. First described in 1926 by Perrin [37], this method measures the changing speed of rotation (tumbling) of a molecule in solution by comparing the fluorescence intensity between emission and excitation. If a fluorophore is excited with plane-polarized light, some of the polarization will be retained depending on how quickly the tracer tumbles. The faster the molecular rotation, the more depolarized the emission, and the slower the rotation, the more polarized the emission. When the tracer binds a much larger molecule, it will rotate more slowly, and most of the light emitted will remain polarized (**Figure 4-3**).

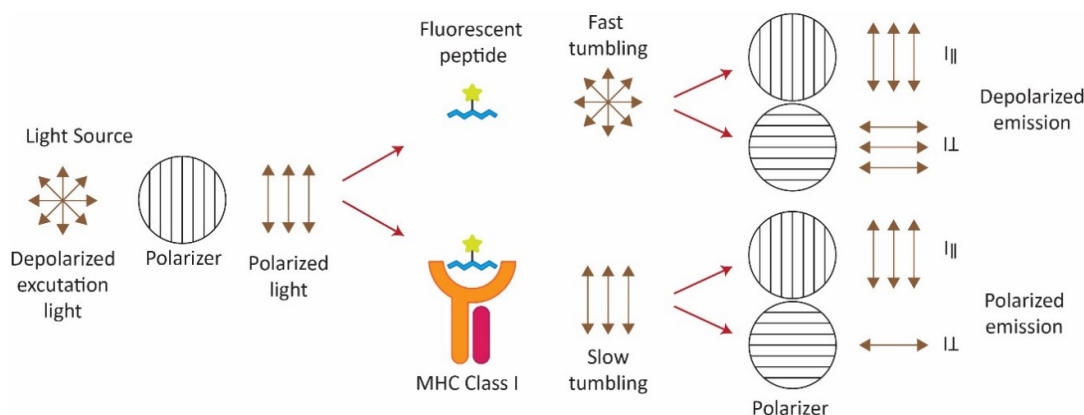


Figure 4-3. Principle of fluorescence anisotropy assay to measure peptide-MHC-I interaction.

Free fluorescent peptide (tracer) excited with a linear-polarized light rotate quickly and emit light in a depolarized manner. When the fluorescent peptide is bound to larger class I protein, it tumbles slowly and results in emission of polarized light. The degree of peptide binding can be calculated by measuring the amount of polarized emission.

FA can be used to measure any binding event in which the ligand and the receptor differ in size by factor 10 or greater. The application of FA was demonstrated for receptor-ligand [38], DNA-protein [35,39], and peptide-protein interactions [40]. The mathematical calculations were previously described in detail [34,41,42] and later corrected [43] and discussed in detail in the book by Lakowicz [44].

The anisotropy is calculated as shown in equation 4.9 below and is a measure of the extent of molecular rotation between the time frame of excitation and emission [44]:

$$r = \frac{I_{\parallel} - I_{\perp}}{I_{\parallel} + 2I_{\perp}}, \quad \text{Equation 4-9}$$

where r is the anisotropy factor, and I_{\parallel} and I_{\perp} are the intensities of the observed parallel and perpendicular components. The anisotropy value is independent of fluorescence intensity, as it is a dimensionless quantity. This is because the difference ($I_{\parallel} - I_{\perp}$) is normalized by the total intensity, which is $I_T = I_{\parallel} + 2I_{\perp}$. The anisotropy is a ratiometric measurement.

An alternative to anisotropy measurement is polarization. Both the methods share the same content of information. Polarization (P) is calculated by the **equation 4.10** below:

$$P = \frac{I_{\parallel} - I_{\perp}}{I_{\parallel} + I_{\perp}} \quad \text{Equation 4-10}$$

The polarization and anisotropy values can be interchanged using equation 4.11:

$$r = \frac{2P}{3 - P} \quad \text{Equation 4-11}$$

FA for monitoring peptide-class I interaction was first described by Buchli et al. [26,27] and later widely adopted by researchers as an alternative to the cell- and radioisotope-based peptide binding assays [9,28,45]. Here, fluorescent peptide is used as the tracer. Since class I is much larger, the binding of the peptide can be easily quantified using FA (Figure 4-3). The increase in the FA value upon peptide binding can be monitored in real time. An additional advantage of this method includes eliminating washing steps (i.e., it is homogeneous).

4.3.2. Scope of the assay

In our laboratory, we use FA to study peptide binding to MHC-I molecules. We use it to monitor **a)** peptide exchange of pMHC-I complexes with fluorescent peptide and **b)** direct peptide binding to empty recombinant class I complexes.

Peptide exchange on MHC-I has many clinical and commercial applications, as discussed in the introduction **Section 1.7, chapter 1**. For the past few years, we have used this method to screen dipeptide-mediated peptide exchange on different MHC-I allotypes as previously reported [40]; more recently, we have also used FA to screen peptide exchange assisted by small molecules (e.g., Ethanol, DMSO, etc.).

Studying peptide association was not possible until recently because of the instability of MHC-I molecules in the absence of bound peptides, with a few exceptions such as H-2K^b and HLA-E ([28] and unpublished data). This is no longer a limitation with the availability of our disulfide-stabilized MHC-I molecules.

This chapter reports my MHC-I peptide exchange results and the kinetic evaluation of a few standard peptides upon direct binding to MHC-I molecules.

4.3.3. Procedure

The detailed method of FA is described in SSP-SOP-BCM_022 in **section 2.6.1**.

4.3.4. Results

Figure 4.4 shows the peptide exchange catalyzed by dipeptides on two MHC-I allotypes A2 and A24. Here, we screened the degree of peptide exchange on these allotypes catalyzed by the dipeptides GM, GL, and GF compared to the control without dipeptides, i.e., buffer-only control. The preference for dipeptides is generally specific to allotypes. This is perhaps because of different anchor residues across MHC-I allotypes [31]. In panel A, exchange on A2 was preferentially catalyzed by GM and followed by GL, whereas GF was ineffective. On the contrary, exchange on A24 was preferentially catalyzed by GF and, to some extent, by GM and GL. This demonstrates that the MHC-I allotypes need to be individually screened for their optimal dipeptide/tripeptide to achieve optimal peptide exchange.

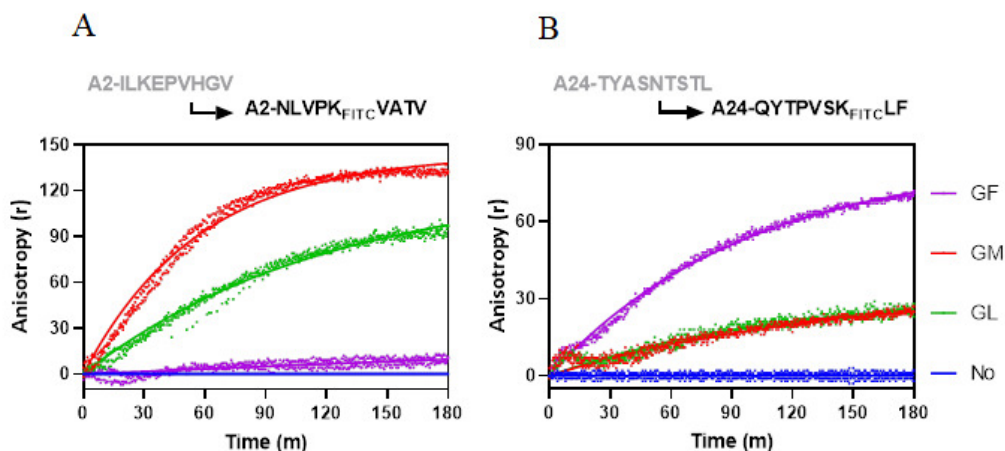


Figure 4-4. Representative dipeptide-mediated peptide exchange assay.

The exchange assay was performed in buffer containing 50 mM HEPES, 150 mM NaCl, pH 7.5. Protein A2 and A24 were folded with medium affinity peptides and SEC purified. 30 nM of A2-ILKEPVHGV and A24-TYASNTSTL protein complexes were pre-incubated with or without 10 mM of dipeptides GM, GL, and GF. Fluorescent labelled (FITC) allotype specific high affinity peptides (NLVPKFITCVATV for A2, QYTPVSKFITCLF for A24) were added and the followed by immediate monitoring of the anisotropy values. The detail methods are described in **section 2.5.1**.

In the **Table 4-2**, I have summarized the screening results of the dipeptides that were effective against various clinically significant MHC-I allotypes.

Table 4-2. Dipeptides modulating peptide exchange⁹

Non-standard amino acids: GCha, Glycyl-cyclohexylalanine; GCit, Glycyl-citrulline

Allotype	Bound Peptide	Fluorescent Peptide	Exchange Dipeptide	Exchange Efficiency
A*01:01	XXDXXXXXXY	LTDITK[FITC]GVQY	GY, GD, GCha	+++ , +, ++
A*02:01	IGKEPVHGV	NLVPK[FITC]VATV	GL, GM	+++ , ++++
A*03:01	XVXXXXXXXXK	KLKK[FITC]TETQEK	GL	+
A*11:01	XVXXXXXXXXK	ASFDK[FITC]AKLK	GL, GCit	+, +
A*24:02	XYXXXXXXL	QYTPVSK[FITC]LF	GL, GF	++, ++++
A*68:01	XTXXXXXXR	EVPNK[FITC]IINR	GL, GCha	+, +
B*07:02	XPXXXXXXL	RPSGPSK[FITC]AL	GL	+++
B*08:01	XXKXXXXXL	DLERK[FITC]VKSL	None	-
B*15:01	XMXXXXXXY	GQRK[FITC]GAGSVF	GL	+
B*27:05	XRXXXXXXA	IRAAPPK[FITC]F	GL, GCha	+, ++
B*27:09	XRXXXXXXA	IRAAPPK[FITC]F	GCha	+
B*44:05	XEXXXXXXXY	AEKLITK(FITC)TF	GCha	++
B*51:01	XAXXXXXXV	DPAK[FITC]FKSI	GL, GCha	+, +

4.3.5. Data analysis: curve fitting

The detailed data analysis is discussed in the method **section 2.6.1**.

⁹ Original peptide sequences were replaced with letter X for the proprietary peptides. Only anchor residues are shown.

4.4. Microscale thermophoresis

4.4.1. Principle

Microscale Thermophoresis (MST) is a method for the biophysical analysis of biomolecular interactions. MST detects changes in the hydration shell, charge, or size of molecules as they move along microscopic temperature gradients. MST provides a method to measure the molecular interactions by combining fluorescence detection with thermophoresis. The measurement of a temperature-induced change in fluorescence of a target as a function of the concentration of a non-fluorescent ligand is the basis of MST (Figure 4-5).

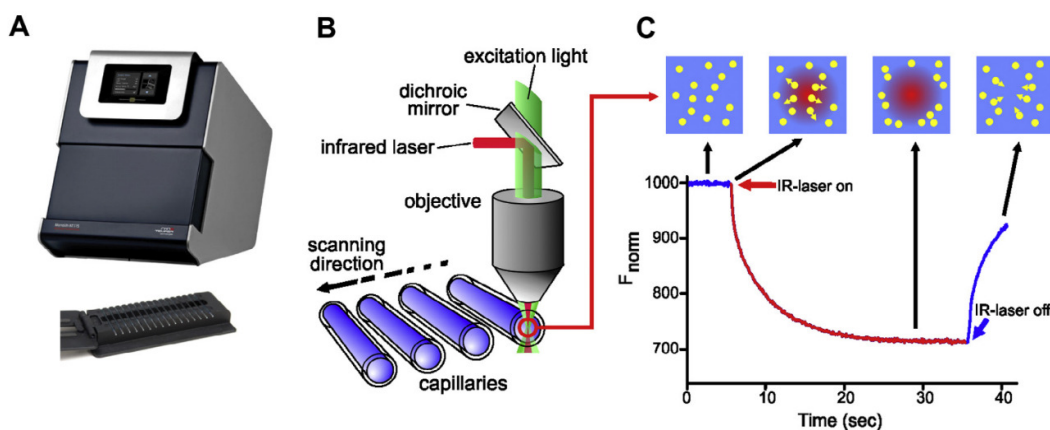


Figure 4-5. Thermophoresis assay.

Figure adapted from [46]. (A) The Monolith NT.115 from NanoTemper Technologies GmbH. Up to 16 capillaries (sample volume $\sim 10 \mu\text{L}$) can be loaded to the capillary tray shown below. (B) Schematic representation of MST optics. The fluorescence within the capillary is excited and detected through the same objective. A focused IR-Laser is used to locally heat a defined sample volume. Thermophoresis of fluorescent molecules through the temperature gradient is detected (C) Typical signal of a MST experiment. Initially, the molecules are homogeneously distributed and a constant “initial fluorescence” is detected. Within the first second after activation of the IR laser, the “T-Jump” is observed, which corresponds to a rapid change in fluorophore properties due to the fast temperature change. Subsequently, thermophoretic movement of the fluorescently labeled molecules out of the heated sample volume can be detected. Typically, the fluorescence change is measured for 30 s. After deactivation of the IR-Laser, an inverse T-Jump occurs, followed by the “back-diffusion” of molecules, which is solely driven by mass diffusion. MST, Microscale Thermophoresis; IR, infrared; T-Jump, temperature jump. Figure and legend were adapted from open access article [46].

The biophysical parameters of thermophoresis are elaborated in earlier publications [47,48]. The contributing factors are size, hydration shell, and charge, quantified by the *Soret coefficient* S_T in equation 4.12 [49].

$$S_T = \frac{A}{\kappa T} (-\Delta S_{hyd}(T)) + \frac{\beta \sigma_{eff}^2}{4\epsilon\epsilon_0 T} \times \lambda_{DH} \quad \text{Equation 4-12}$$

where A is the molecular surface area, κ is the Boltzmann constant, T is the temperature of system, σ_{eff} is the effective charge, ΔS_{hyd} is the hydration shell effect, λ_{DH} is the Debye-Hückel screening length, ϵ and ϵ_0 are permittivity of water and free space, respectively, and β is temperature derivative of ϵ .

The change in overall fluorescence signal with temperature followed by IR-laser activation can be expressed as follows [50]:

$$\frac{\partial}{\partial T}(cF) = F \frac{\partial c}{\partial T} + c \frac{\partial F}{\partial T} \quad \text{Equation 4-13}$$

where, $c \frac{\partial F}{\partial T}$ is change in fluorescence with temperature (TRIC). The change in concentration with temperature (thermophoresis) is described by $F \frac{\partial c}{\partial T} = -S_T c$. The Soret coefficient, S_T , is the percentage of change in the concentration per Kelvin [48] (equation 4.12).

MST is based on the observed change in fluorescence from two distinct effects as shown in equation 4.8. First, a temperature related intensity change (TRIC) of the fluorescent probe that can be affected by binding events. Second is thermophoresis, which is the directed movement of particles in a microscopic temperature gradient. When a temperature gradient is applied, any change in the chemical micro-environment of the fluorescent probe and changes in the hydration shell of biomolecules results in a relative change in the fluorescence measured, which can be utilized to evaluate binding affinities. The ability to work under near-native conditions is the most important feature of MST, as it is performed immobilization-free and in any buffer, serum, or cell lysate. Low sample consumption (<10 μ L) at nanomolar concentrations and a wide dynamic range of dissociation constants (sub-nM to mM) are further important advantages.

4.4.2. Scope of the assay

This MST method was used to measure the peptide affinity to empty MHC-I molecules. This method can be helpful to identify the MHC-I-binding peptides and rank them based on their affinity. Here, the MST measurements were done to determine the peptide-MHC-I binding affinity under the condition of a fixed target concentration (5 -10 nM his-tagged MHC-I, fluorescently labeled labeled with Red-Tris-NTA) and varying concentrations of ligands (titrate peptides). Detailed experimental parameters are described in section 2.5.2.

4.4.3. Procedure

The MST procedure used in this work is described in detail in the SOP, SSP-SOP-BCM_024, in chapter 2. Briefly, the MST measurements were performed using the Monolith.NT.115^{pico} instrument (Nanotemper technologies). The samples are loaded into capillaries (<10 μ l per capillary), with premium-grade capillaries used here. The instrument uses a dichroic mirror to focus an infrared laser beam and light (for fluorescence excitation and emission) on the sample, which heats a small region of the sample and forms a temperature gradient when it is turned on. The fluorescence intensity of the focused heated region of the capillary is measured continuously over time, but for the evaluation, only narrow time slots are taken into consideration, under two conditions: a) IR laser off (F_{cold}) and b) IR laser on (F_{hot}).

The settings for the experiment described here were: LED power = 10-20%, λ_{ex} = 625 nm, λ_{em} = 680 nm, MST laser power = medium (40%), fluorescence before = 5 s, MST on = 30 s, fluorescence after = 3 s. The MST measurements were performed at room temperature (22-25 °C).

4.4.4. Results

In **Figure 4.6**, we demonstrate the successful evaluation of the MST-based assay for measuring the affinity of peptide binding to MHC-I. We have optimized the assay parameters that include buffer, detergents, incubation time, temperature, and type of dyes (data not shown). The final results from the initial validation screen are shown in **Table 4.3**.

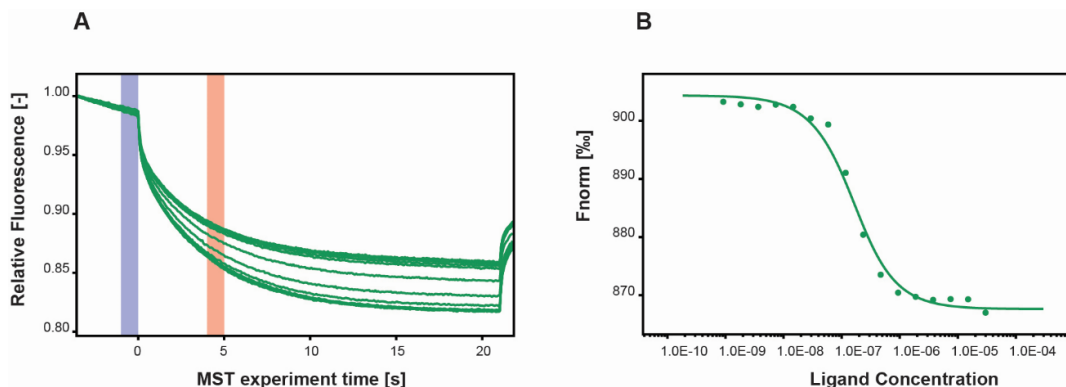


Figure 4-6. Representative graph for typical MHC-I peptide binding measured by MST assay

MST binding assay was performed in assay buffer (50 mM Hepes pH 7.5, 150 mM NaCl, 0.5% Tween 20) by incubating 100 nM of VMAPK(FITC)TVLL peptide with serial dilution of HLA-E*01:03 ranging from 30 μ M to 915 pM concentration. Before the MST measurement, the reaction mix was pre-incubated at room temperature for 30 minutes. **(A)** Relative fluorescence between the initial cold state (blue bar, F_0) and the hot state of the sample (red bar, F_1), in this case, 5 s, after the infrared laser was switched on from 0 to 20 s at medium MST power. **(B)** The K_d value was calculated using standard data analysis with MO.Affinity Analysis Software.

Table 4-3. MST Screening Data

Allotype	Peptide ID	Peptide	Repeats	Avg K_d (nM) \pm SEM	K_d NetMHC
Red-A*02:01(Y84C)	NV9	NLVPMVATV	3	4.8 \pm 0.1	25.9
Red-A*02:01(Y84C)	IV9	ILKEPVHGV	3	136.6 \pm 19.7	100
Red-A*02:01(Y84C)	NA9	NLVPMVATA	2	62.55 \pm 20.2	188.8
Red-A*02:01(Y84C)	GV9	GLGGGGGGV	3	942.6 \pm 133.2	2738.8
Red-A*02:01(Y84C)	Ac-NV9	Ac- NLVPMVATV	3	33288 \pm 3039	NA
Red-A*24:02(Y84C)	QF9	QYTPVSQFLF	3	10.30 \pm 3.9	19.5
Red-A*24:02(Y84C)	QA9	QYTPVSQALA	1	10603	3714.5
Red-A*24:02(Y84C)	TL9	TYASNTSTL	1	3.51	45.1
Red-A*24:02(Y84C)	TA9	TYASNTSTA	1	50989	1065.6
Red-A*24:02(Y84C)	RI10	TYASNTSTA	1	12.2	1065.6
Red-B*07:02(Y84C)	RL9	RPSGPSRAL	1	3.275	3.49
Red-B*07:02(Y84C)	RL9G2	RGSGPSRAL	1	979.8	242.86
A*02:01(Y84C)	NV9-FITC	NLVPK[FITC]VATV	2	7.89 \pm 3.7	25.9
A*24:02(Y84C)	QF9-FITC	QYTPVSK[FITC]LF	2	65.19 \pm 1.9	104.98
E*01:03	VL9-FITC	VMAPK(FITC)TVLL	3	272.3 \pm 89.2	211.58
E*01:03	IL9-FITC	IMYNK(FITC)PAML	3	288 \pm 15.1	6804
E*01:03	RL9-FITC	RMYSPTK(FITC)IL	2	5991 \pm 565	4216.34
E*01:03	EK9-FITC	EKQK(FITC)ESREK	1	13650	43149.87
E*01:03/VL9-FITC	VL9	VMAPTTVLL	2	130 \pm 69.1	211.58
E*01:03/RL9-FITC	RL9	RMYSPTSIL	1	3439	4216.34

4.4.5. Data analysis

The normalized fluorescence (F_{norm}) measures primarily the ratio of total fluorescence at F_{hot} to F_{cold} and dye's temperature dependence. In the linear approximation, we expect [51]:

$$F_{\text{norm}} = \frac{F_{\text{hot}}}{F_{\text{cold}}} = 1 - \left(S_T - \frac{\partial F}{\partial T} \right) \Delta T \quad \text{Equation 4-14}$$

F_{norm} varies during the titration experiment based on:

$$F_{\text{norm}} = (1 - x)F(A)_{\text{norm}} + xF(AT)_{\text{norm}} \quad \text{Equation 4-15}$$

Where, $F(A)_{\text{norm}}$ and $F(AT)_{\text{norm}}$ are the contributing factors of unbound and bound complex of the fluorescent molecule A, respectively. T is interacting titrant and x is fraction of labelled target molecule forming the complex.

The fraction of complexes increases as the concentration of the non-labelled titrant (e.g. unlabelled peptide) is increased and mixed with a constant concentration of fluorescent labelled target molecule

(e.g. labelled MHC-I) until all fluorescent molecules form complexes with the titrant. As a result, the observed change in normalized fluorescence F_{norm} can be used to calculate the fraction of bound molecules x .

The MO.Affinity Analysis software allows straightforward analysis and evaluation of MST data. It allows quantification of binding parameters by two models, the dissociation constant (K_d) model or the EC_{50} from Hill's equation [49].

4.4.5.1 The K_d model

The K_d model is derived from the law of mass action. By rearranging equation 4.3, the fraction bound (FB) can be correlated with K_d parameter as follows [49,50]:

$$FB = \frac{[LP]}{[P_0]} = \frac{[L_0] + [P_0] + K_d - \sqrt{([L_0] + [P_0] + K_d)^2 - 4 \cdot [L_0] \cdot [P_0]}}{2[P_0]} \quad \text{Equation 4-16}$$

Here, linearity with normalized fluorescence from MST measurements is represented by FB. The binding curve is created by plotting F_{norm} on the y-axis against the total concentration of the titrated ligand (L), and the dissociation constant K_d can be calculated easily. If the binding ratio is 1:1 stoichiometry, this model fits the collected data.

4.4.5.2 The Hill model

If the K_d is much smaller than the target concentration and cannot be determined due to detector limitation (i.e., insufficient sensitivity of the detector), then the alternative approach of Hill's equation is used to calculate an EC_{50} . The EC_{50} is defined as the half-maximal concentration of the titrated ligand, a relative value (not a physical constant) that provides information about the binding cooperativity in the multivalent interactions. EC_{50} is represented as:



Where, h is Hill coefficient and FB can be calculated as follows:

$$FB = \frac{[LP]}{[P_0]} = \frac{1}{1 + (EC_{50}/[L])^h} \quad \text{Equation 4-18}$$

with L = concentration of titrated ligand.

4.5. Discussion

We have shown that peptide exchange on different allotypes of MHC-I molecules is achievable with careful selection of short peptides or small molecules using our screening procedure. We have screened the dipeptides using a fluorescence anisotropy based assay that was described previously [52]. The findings can act as the starting point for optimizing the peptide exchange assay. Another important factor for efficient exchange is the selection of optimal low or medium affinity leaving peptide. Once the methods are optimized for each of the allotypes, we can use it for rapid generation of multimers. Such a method for generating tetramer was already commercialized for A2 [53].

As summarized in **Table 4.3**, here, we have demonstrated that the direct peptide binding assay based on MST technology is validated for measuring the affinity peptide binding to MHC-I molecules *in vitro*, which was not possible before. This method has the potential to change the screening approach of neoantigen discovery. We believe that the affinity data generated with this method will be more reliable than the *in silico* prediction.

4.6. Reference

- [1] Wearsch, P.A., Cresswell, P., The quality control of MHC class I peptide loading 2008, 20.
- [2] Yewdell, J.W., Nicchitta, C. V., The DRiP hypothesis decennial: support, controversy, refinement and extension. *Trends Immunol.* 2006, 27, 368–373.
- [3] Saunders, P.M., Endert, P. van, Running the gauntlet: from peptide generation to antigen presentation by MHC class I. *Tissue Antigens* 2011, 78, 161–170.
- [4] Kast, W.M., Brandt, R.M., Sidney, J., Drijfhout, J.W., et al., Role of HLA-A motifs in identification of potential CTL epitopes in human papillomavirus type 16 E6 and E7 proteins. *J. Immunol.* 1994, 152, 3904–3912.
- [5] Farkona, S., Diamandis, E.P., Blasutig, I.M., Cancer immunotherapy: the beginning of the end of cancer? *BMC Med.* 2016, 14, 73.
- [6] Comber, J.D., Philip, R., MHC class I antigen presentation and implications for developing a new generation of therapeutic vaccines. *Ther. Adv. Vaccines* 2014, 2, 77.
- [7] Schumacher, T.N.M., Heemels, M.T., Neefjes, J.J., Kast, W.M., et al., Direct binding of peptide to empty MHC class I molecules on intact cells and in vitro. *Cell* 1990, 62, 563–567.
- [8] Hosken, N., Bevan, M., Defective presentation of endogenous antigen by a cell line expressing class I molecules. *Science (80-.)*. 1990, 248, 367–370.
- [9] Kessler, J.H., Mommaas, B., Mutis, T., Huijbers, I., et al., Competition-based cellular peptide binding assays for 13 prevalent HLA class I alleles using fluorescein-labeled synthetic peptides. *Hum. Immunol.* 2003, 64, 245–255.
- [10] Storkus, W.J., Zeh, H.J. 3rd, Salter, R.D., Lotze, M.T., Identification of T-cell epitopes: rapid isolation of class I-presented peptides from viable cells by mild acid elution. *J. Immunother. with Emphas. tumor Immunol. Off. J. Soc. Biol. Ther.* 1993, 14, 94–103.
- [11] van der Burg, S.H., Visseren, M.J., Brandt, R.M., Kast, W.M., Melief, C.J., Immunogenicity of peptides bound to MHC class I molecules depends on the MHC-peptide complex stability. *J. Immunol.* 1996, 156, 3308–14.
- [12] Shunji Sugawara, Toru Abo, Katsuo Kumagai, A simple method to eliminate the antigenicity of surface class I MHC molecules from the membrane of viable cells by acid treatment at pH 3. *J. Immunol. Methods* 1987, 100, 83–90.
- [13] Rocheleau, J. V., Edidin, M., Piston, D.W., Intrasequence GFP in Class I MHC Molecules, a Rigid Probe for Fluorescence Anisotropy Measurements of the Membrane Environment. *Biophys. J.* 2003, 84, 4078–4086.
- [14] Schweitzer, S., Schneiders, A.M., Langhans, B., Kraas, W., et al., Flow Cytometric Analysis of Peptide Binding to Major Histocompatibility Complex Class I for Hepatitis C Virus Core T-Cell Epitopes 2000.
- [15] Sidney, J., Southwood, S., Oseroff, C., Guercio, M.-F. del, et al., Measurement of MHC/Peptide Interactions by Gel Filtration. *Curr. Protoc. Immunol.* 1999, 31, 18.3.1-18.3.19.
- [16] Buus, S., Lauemøller, S.L., Stryhn, A., Pedersen, L.Ø., Measurement of Peptide-MHC Interactions in Solution Using the Spin Column Filtration Assay. *Curr. Protoc. Immunol.* 1999, 31, 18.4.1-18.4.12.
- [17] Buus, S., Sette, A., Colon, S.M., Jenis, D.M., Grey, H.M., Isolation and characterization of antigen-la complexes involved in T cell recognition. *Cell* 1986, 47, 1071–1077.
- [18] Sette, A., Sidney, J., del Guercio, M.F., Southwood, S., et al., Peptide binding to the most frequent HLA-A class I alleles measured by quantitative molecular binding assays. *Mol. Immunol.* 1994, 31, 813–822.
- [19] Springer, S., Do, K., Skipper, J.C.A., Townsend, A.R.M., et al., Fast association rates suggest a conformational change in the MHC class I molecule H-2Db upon peptide binding. *Biochemistry* 1998, 37, 3001–3012.
- [20] Khilko, S.N., Corr, M., Boyd, L.F., Lees, A., et al., Direct detection of major histocompatibility complex class I binding to antigenic peptides using surface plasmon resonance. Peptide immobilization and characterization of binding specificity. *J. Biol. Chem.* 1993, 268, 15425–15434.

- [21] Khilko, S.N., Jelonek, M.T., Corr, M., Boyd, L.F., et al., Measuring interactions of MHC class I molecules using surface plasmon resonance. *J. Immunol. Methods* 1995, 183, 77–94.
- [22] Haj, A.K., Breitbach, M.E., Baker, D.A., Mohns, M.S., et al., High-Throughput Identification of MHC Class I Binding Peptides Using an Ultradense Peptide Array. *J. Immunol.* 2020, 204, 1689–1696.
- [23] Harndahl, M., Rasmussen, M., Roder, G., Buus, S., Real-time, high-throughput measurements of peptide-MHC-I dissociation using a scintillation proximity assay. *J. Immunol. Methods* 2011, 374, 5–12.
- [24] Harndahl, M., Justesen, S., Lamberth, K., Røder, G., et al., Peptide binding to HLA class I molecules: Homogenous, high-throughput screening, and affinity assays. *J. Biomol. Screen.* 2009, 14, 173–180.
- [25] Prachar, M., Justesen, S., Steen-Jensen, D.B., Thorgrimsen, S., et al., Identification and validation of 174 COVID-19 vaccine candidate epitopes reveals low performance of common epitope prediction tools. *Sci. Reports* 2020 101 2020, 10, 1–8.
- [26] Rico Buchli, *, ‡, §, Rodney S. VanGundy, ‡, Heather D. Hickman-Miller, §, Christopher F. Giberson, ‡, et al., Real-Time Measurement of in Vitro Peptide Binding to Soluble HLA-A*0201 by Fluorescence Polarization. *Biochemistry* 2004, 43, 14852–14863.
- [27] Rico Buchli, *, ‡, §, Rodney S. VanGundy, ‡, Heather D. Hickman-Miller, §, Christopher F. Giberson, ‡, et al., Development and Validation of a Fluorescence Polarization-Based Competitive Peptide-Binding Assay for HLA-A*0201A New Tool for Epitope Discovery. *Biochemistry* 2005, 44, 12491–12507.
- [28] Saini, S.K., Abualrous, E.T., Tigan, A.S., Covella, K., et al., Not all empty MHC class I molecules are molten globules: Tryptophan fluorescence reveals a two-step mechanism of thermal denaturation. *Mol. Immunol.* 2013, 54, 386–396.
- [29] Niebling, S., Burastero, O., Bürgi, J., Günther, C., et al., FoldAffinity: binding affinities from nDSF experiments. *Sci. Reports* 2021 111 2021, 11, 1–17.
- [30] Saini, S.K., Tamhane, T., Anjanappa, R., Saikia, A., et al., Empty peptide-receptive MHC class I molecules for efficient detection of antigen-specific T cells. *Sci. Immunol.* 2019, 4, eaau9039.
- [31] Anjanappa, R., Garcia-Alai, M., Kopicki, J.D., Lockhauserbäumer, J., et al., Structures of peptide-free and partially loaded MHC class I molecules reveal mechanisms of peptide selection. *Nat. Commun.* 2020, 11, 1–11.
- [32] The GraphPad Guide to Analyzing Radioligand Binding Data.
- [33] Jarmoskaite, I., Alsadhan, I., Vaidyanathan, P.P., Herschlag, D., et al., How to measure and evaluate binding affinities. *Elife* 2020, 9, 1–34.
- [34] Checovich, W.J., Bolger, R.E., Burke, T., Fluorescence polarization — a new tool for cell and molecular biology. *Nat.* 1995 3756528 1995, 375, 254–256.
- [35] T, H., Y, M., H, T., RH, E., Fluorescence anisotropy: rapid, quantitative assay for protein-DNA and protein-protein interaction. *Methods Enzymol.* 1996, 274, 492–503.
- [36] Pope, A.J., Haupts, U.M., Moore, K.J., Homogeneous fluorescence readouts for miniaturized high-throughput screening: theory and practice. *Drug Discov. Today* 1999, 4, 350–362.
- [37] Perrin, F., Polarisation de la lumière de fluorescence. Vie moyenne des molécules dans l'état excité. *J. Phys. le Radium* 1926, 7, 390–401.
- [38] Bolger, R., Wiese, T.E., Ervin, K., Nestich, S., Checovich, W., Rapid screening of environmental chemicals for estrogen receptor binding capacity. *Environ. Health Perspect.* 1998, 106, 551.
- [39] Ozers, M.S., Hill, J.J., Ervin, K., Wood, J.R., et al., Equilibrium Binding of Estrogen Receptor with DNA Using Fluorescence Anisotropy. *J. Biol. Chem.* 1997, 272, 30405–30411.
- [40] Wu, P., Bresseur, M., Schindler, U., A High-Throughput STAT Binding Assay Using Fluorescence Polarization. *Anal. Biochem.* 1997, 249, 29–36.
- [41] Weber, G., Polarization of the fluorescence of macromolecules. 1. Theory and experimental method. *Biochem. J.* 1952, 51, 145–155.
- [42] Weber, G., Rotational Brownian Motion and Polarization of the Fluorescence of Solutions. *Adv. Protein Chem.* 1953, 8, 415–459.
- [43] Owicki, J.C., Fluorescence Polarization and Anisotropy in High Throughput Screening: Perspectives

- and Primer: <http://dx.doi.org/10.1177/108705710000500501> 2016, 5, 297–306.
- [44] Lakowicz, J.R., Principles of fluorescence spectroscopy. *Princ. Fluoresc. Spectrosc.* 2006, 1–954.
 - [45] Hawse, W.F., Gloor, B.E., Ayres, C.M., Kho, K., et al., Peptide Modulation of Class I Major Histocompatibility Complex Protein Molecular Flexibility and the Implications for Immune Recognition *. *J. Biol. Chem.* 2013, 288, 24372–24381.
 - [46] Jerabek-Willemsen, M., André, T., Wanner, R., Roth, H.M., et al., MicroScale Thermophoresis: Interaction analysis and beyond. *J. Mol. Struct.* 2014, 1077, 101–113.
 - [47] Duhr, S., Braun, D., Thermophoretic Depletion Follows Boltzmann Distribution. *Phys. Rev. Lett.* 2006, 96, 168301.
 - [48] Duhr, S., Braun, D., Why molecules move along a temperature gradient. *Proc. Natl. Acad. Sci.* 2006, 103, 19678–19682.
 - [49] Asmari, M., Ratih, R., Alhazmi, H.A., El Deeb, S., Thermophoresis for characterizing biomolecular interaction. *Methods* 2018, 146, 107–119.
 - [50] Wienken, C.J., Baaske, P., Rothbauer, U., Braun, D., Duhr, S., Protein-binding assays in biological liquids using microscale thermophoresis. *Nat. Commun.* 2010 11 2010, 1, 1–7.
 - [51] Nanotemper Technologies, User Manual Monolith NT.115 2018, 1–24.
 - [52] Saini, S.K., Schuster, H., Ramnarayan, V.R., Rammensee, H.-G., et al., Dipeptides catalyze rapid peptide exchange on MHC class I molecules. *Proc. Natl. Acad. Sci.* 2015, 112, 202–207.
 - [53] Delcommenne, M.C., Hrytsenko, O., Tram, C., Weir, G., Stanford, M.M., The QuickSwitch Quant HLA-A*02:01 Tetramer Kit can be used for determining the biological activity of a cancer vaccine. *J. Immunol.* 2017, 198.

Chapter 5. Peptide MHC-I complex stability measured by nanoscale differential scanning fluorimetry reveals the molecular mechanism of thermal denaturation

Chapter 5 contains published original data. All the experiments in this paper were performed by me. In this section, I demonstrate the use of the NanoDSF method for the study of the thermal and chemical stability of recombinant MHC-I molecules by monitoring the intrinsic fluorescence of tryptophan and tyrosine residues. I report how this method can be utilized to understand the molecular mechanism of MHC-I thermal denaturation.

The manuscript was written by Ankur Saikia and Sebastian Springer.

The full citation of the paper is:

Ankur Saikia and Sebastian Springer; “Peptide-MHC class I complex stability measured by nanoscale differential scanning fluorimetry reveals molecular mechanism of thermal denaturation”.

Molecular Immunology, Volume 136, August 2021, Pages 73-81

The paper is online at

<https://doi.org/10.1016/j.molimm.2021.04.028>

The figure numbers were changed to match the format of this thesis.

5.1. Abstract

Recombinant major histocompatibility complex class I molecules are used in diagnostic and therapeutic approaches in cancer immunotherapy, with many studies exploring their binding to antigenic peptides. Current techniques for kinetic peptide binding studies are hampered by high sample consumption, low throughput, interference with protein stability, and/or high background signal. Here, we validate nanoscale differential scanning fluorimetry (nanoDSF), a method using the tryptophan fluorescence of class I molecules, for class I/peptide binding, and we use it to determine the molecular mechanism of the thermal denaturation of HLA-A*02:01.

5.2. Introduction

Major histocompatibility complex class I (MHC-I) molecules are the central agents of adaptive immunity against intracellular pathogens and cancer. They present intracellular peptides – derived from cellular proteins – on the cell surface to cytotoxic T lymphocytes (CTL), which kill cells that present non-self peptides. To detect, isolate, and stimulate CTL in research and therapy, recombinant MHC-I molecules are used in diagnostics and vaccination as soluble multimers, artificial antigen-presenting cells (aAPCs), and bifunctional MHC-I-antibody fusion proteins [1- 4]

MHC-I genes are extremely polymorphic, and a patient's MHC-I genotype is a critical determinant of their immune response for cancer immunotherapy [5]. In any tumor or pathogen-infected cell, each MHC-I allotype binds only a subset of the many potential neoantigen peptides, according to its binding motif. Thus, affinity to the patient's MHC-I molecules is the critical parameter for neoantigen identification in personalized vaccines [6, 7] to generate a strong immune response [8]. Peptide-MHC-I binding affinity is very difficult to measure directly though, since the peptide-free form denatures rapidly [7], [9], such that equilibrium approaches are out of question [10]. Researchers have attempted to derive peptide affinities from dissociation rates [11, 12] with unreliable results due to nonspecific binding and bleaching of fluorophores [13] and measurement instabilities due to long dissociation times.

Measuring the thermostability of a particular recombinant peptide/MHC-I complex (rpMHC-I) is potentially superior as a predictor of vaccine potential as well as a measure of denaturation resistance and ease of handling of that rpMHC-I [9], [14–16]. The midpoint temperature of thermal unfolding (T_m) is determined both by the intrinsic denaturation resistance of the MHC-I allotype and by the binding affinity of the peptide [7], [17], [18]. So far, T_m measurement has been hampered by the impracticability of existing methods (**Table 5-1**, and Error! Reference source not found.). In this work, we validate nanoscale differential scanning fluorimetry (nanoDSF) as a novel means of measuring the T_m of rpMHC-Is with high accuracy and low sample consumption, and we use it to measure their folding energy and to determine the mechanism of their thermal unfolding.

Table 5-1. Features of the prominent methods for pMHC thermal stability measurements

Method	UV-CD	μ DSC	ThermoFluor	TDTF	nanoDSF
<i>Monitors</i>	Secondary structure	Heat of denaturation	Hydrophobic dye binding	Tryptophan fluorescence	Tryptophan fluorescence
<i>Application</i>	Protein stability, Structure, Kinetics	Thermal and chemical stability	Thermal stability	Thermal Stability	Thermal and chemical stability, Aggregation
<i>Measurement spectra</i>	Adjustable wavelength	N/A	Adjustable wavelength	Adjustable wavelength	Fixed wavelength
<i>Sample loading format</i>	Cuvette or capillaries	Cuvette or capillaries	Microplate	Cuvette	Capillaries
<i>Throughput</i>	1- 6 samples per run	1- 4 samples per run	96 or 384 well plate	1- 3 samples per run	1- 48 samples per run
<i>Sample amount required</i>	> 100 μ g	> 100 μ g	10 μ g	100 μ g	100 ng
<i>Sample purity required</i>	High	High	High	Low	Medium
<i>Method Complexity</i>	Complex	Complex	Simple	Simple	Simple
<i>Buffer Compatibility</i>	Selective	Wide range	Selective	Wide range	Wide range
<i>Label free</i>	Yes	Yes	No	Yes	Yes
<i>Liquid formulation Studies</i>	No	Yes	No	Yes	Yes
<i>Instrument cleaning</i>	Yes	Yes	No	Yes	No

5.3. Results

5.3.1.1 NanoDSF-derived T_m of rpMHC-I are comparable to established measurements

NanoDSF (**Figure 5-1 A**) measures the shift of the fluorescence emission peak of tryptophan (Trp) and tyrosine (Tyr) side chains in the protein interior upon exposure to water that occurs during protein unfolding (**Figure 5-1 B, C**) [19–21]. The change in the ratio of emissions at 350 and 330 nm (F350/F330) quantifies the red shift, and the T_m is read as the peak of its first derivative (d[F350/F330]/dT) plotted against temperature (**Figure 5-1 D, E**). For our measurements, we selected the frequent human MHC-I allotype, HLA-A*02:01 (abbreviated as A2), consisting of the A2 heavy chain (HC) and the invariant light chain, beta-2 microglobulin (β_2m). The two chains were folded *in vitro* with the high-affinity peptide NLVPMVATV (single-letter code; abbreviated NV9), or with the very low-affinity dipeptide GM, and purified by size exclusion (**Figure S5-1**).

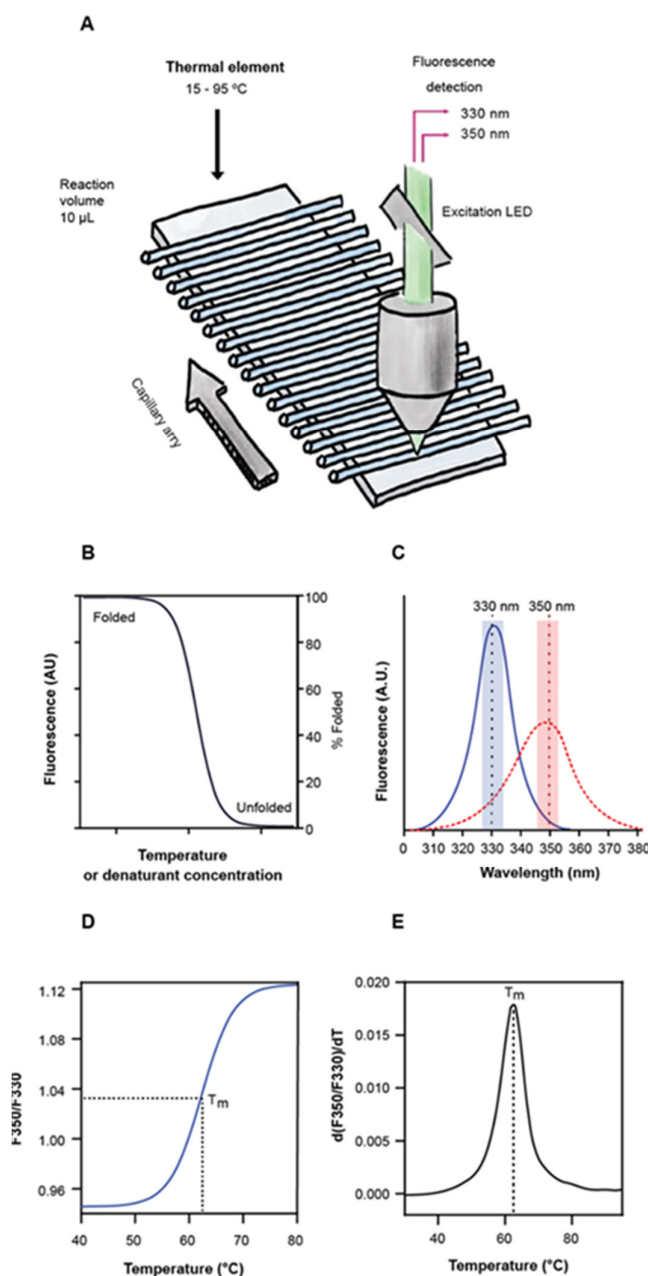


Figure 5-1: Measuring protein unfolding with nanoDSF.

(A) Schematic of the nanoDSF instrument. Up to 48 protein samples are heated in 10 μ L capillaries from 15 to 95 °C. Tryptophan fluorescence is excited at 280 nm, and emission is measured at 330 and 350 nm. (B) Monitoring temperature- or denaturant-mediated rpMHC unfolding by tryptophan fluorescence. Curves at 350 and 330 nm emission have the same shape, but fluorescence might increase with denaturation in some cases. (C) Theoretical fluorescence emission curves of a folded (blue) and an unfolded (red) protein, with red shift and fluorescence decrease upon unfolding. (D) The T_m as the inflection point of F_{350}/F_{330} plotted against the temperature. (E) First derivative of D.

The nanoDSF measurements (with 10 μ L of 100 μ g/mL (2 μ M) protein) showed two distinct peaks for the A2/GM complex (**Figure 5-2 A**), one of which ($T_m = 64.3$ °C) represents free β_2m , as shown by comparison with a pure β_2m sample ($T_m = 65.3 \pm 0.09$ °C; **Figure 5-2 B**). The other peak ($T_m = 36.9 \pm 0.06$ °C) thus represents the denaturation of the low-affinity A2/GM complex, in agreement with published results [16], [22]. For the A2/NV9 complex, only one peak was visible

($T_m = 62.3 \pm 0.11$ °C; **Figure 5-2 C**), suggesting that either thermal unfolding occurred cooperatively for HC and β_2m [15, 16], or that the single peak is an addition of two closely spaced peaks of independent melting transitions. The T_m values were very close to those obtained by monitoring tryptophan fluorescence emission at 345 nm (TDTF, see the discussion; **Figure 5.2 D-G**). We also compared the T_m s obtained by nanoDSF with previously reported values using CD and ThermoFluor methods [15] for 16 peptides (**Figure 5-2 HI** and **Table S5-1**) This demonstrates that nanoDSF is a valid method for label- and dye-free T_m measurement of rpMHC-I.

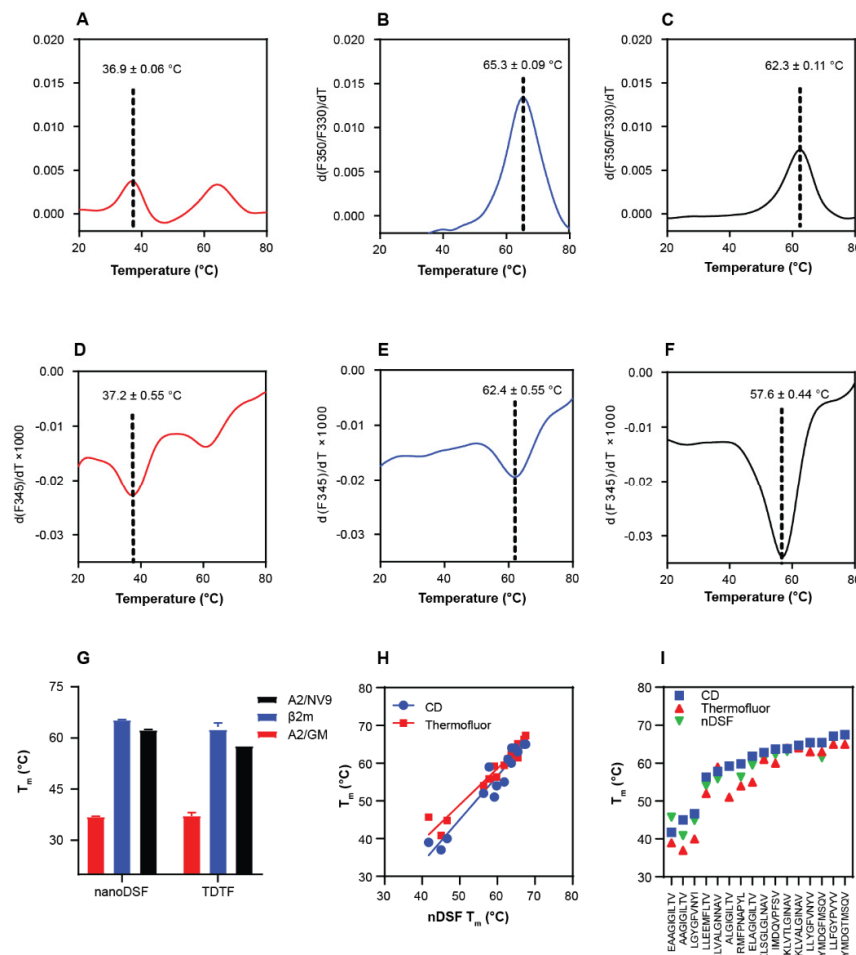


Figure 5-2. Comparing nanoDSF with other methods.

NanoDSF (A, B, C) and TDTF measurements (D, E, F). Red = A2/GM; blue = β_2m ; black = A2/NV9. First-derivative plots were used to determine the T_m . (G) Comparison of T_m values between nanoDSF and TDTF; mean \pm SEM (n=3). (H, I) Comparison of T_m values between nanoDSF, CD, and ThermoFluor; mean \pm SEM (n=2).

5.3.1.2 The T_m of rpMHC-I depends on the rate of heating and protein concentration

We next investigated the extent of rate-dependent hysteresis in nanoDSF, *i.e.*, the dependence of the T_m on the heating rate [23, 24], using the A2/NV9 complex and heating rates from 0.1 to 4.0 °C/min. The T_m increased with the heating rate (**Figure 5-3 AB**), demonstrating kinetic control of unfolding [23]. A reverse scan (80 to 20 °C) after unfolding showed no refolding transition, *i.e.*, the A2/NV9 thermal denaturation was irreversible (**Figure S5-2 A**). The T_m of A2/peptide complexes increased moderately with the protein concentration over almost three orders of magnitude (2 to 1000 µg/ml) with only small changes resulting from a two-fold change in concentration (**Figure 5-3 C**).

We conclude that to compare nanoDSF measurements, heating rate and complex concentration need to be kept constant. We used 1 °C/min and 100 µg/ml in the following.

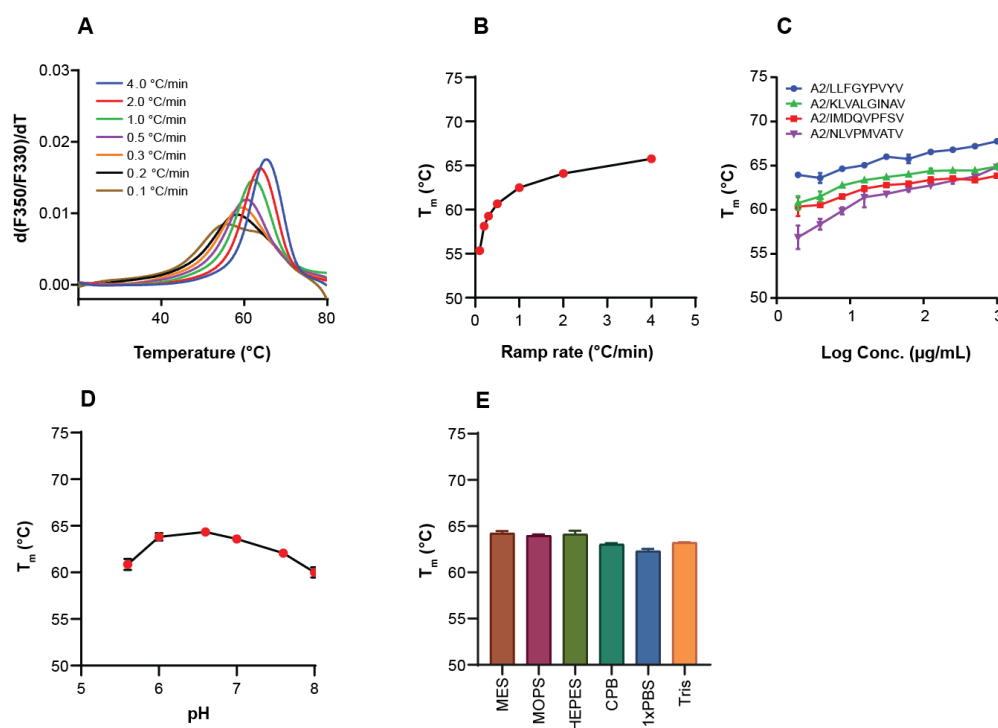


Figure 5-3. Biophysical parameters influencing rpMHC thermal denaturation.

(A, B) Rate-dependent hysteresis of A2/NV9. T_m values were measured at ramp rates of 0.1 - 4 °C/min. (A) representative experiment; (B) means \pm SEM. Error bars not visible as variability between runs was low. (C) Concentration-dependent stabilization of four different rpMHC complexes. (D) Influence of pH and (E) of different buffers (see **Table S5-1**) upon the T_m of A2/NV9. All experiments in the figure were performed at least twice.

5.3.1.3 High-affinity rpMHC-I are pH-stable, but buffer substances influence T_m

We next performed nanoDSF analysis of A2/NV9 at pH values between 5.5 and 8.0 in citrate-phosphate buffer [25, 26]. While the optimum of thermal stability was at pH 6.6, the T_m variation over this range was ≤ 4 °C (**Figure 5-3 D**). This suggests that complex destabilization and peptide exchange in the cell at acidic pH are unlikely to occur with high-affinity A2 complexes [27, 28]. The pH and salt dependence of peptide-MHC-I binding stability and antigen presentation was described previously [29–32]. Different buffer substances also gave different T_m s (**Figure 5-3 E**); especially, values in MES and MOPS were >1 °C higher than in PBS, even though the pH (7.4) at 20 °C was the same. For MES, but not for MOPS, this difference was due to a negative temperature coefficient [33] (**Table S5-2**). We conclude that not just the pH but also the specific buffer substance influences the stability of pMHC complexes, and that a standardized buffer system should be used in nanoDSF.

5.3.1.4 NanoDSF allows quality control of rpMHCs

We next used nanoDSF to test the stability of rpMHCs in different buffer formulations and storage conditions. First, we compared samples of A2/NV9 stored at -80 and +4 °C for 60 days (**Table S5-3, Figure S5-2 B**). While the T_m values were the same, Boltzmann sigmoidal curve fitting of F350/F330 vs. T showed that compared to the -80 °C sample, about 23% of A2/NV9 had denatured during storage at 4 °C (**Figure 5-4 A**). A similar experiment showed that during storage at -80 °C, glycerol is slightly cryo-protective (**Figure 5-4 B, Figure S5-2 C**). The solvents ethanol and DMSO dramatically lowered the T_m of A2/NV9 (**Figure 5-4 C**).

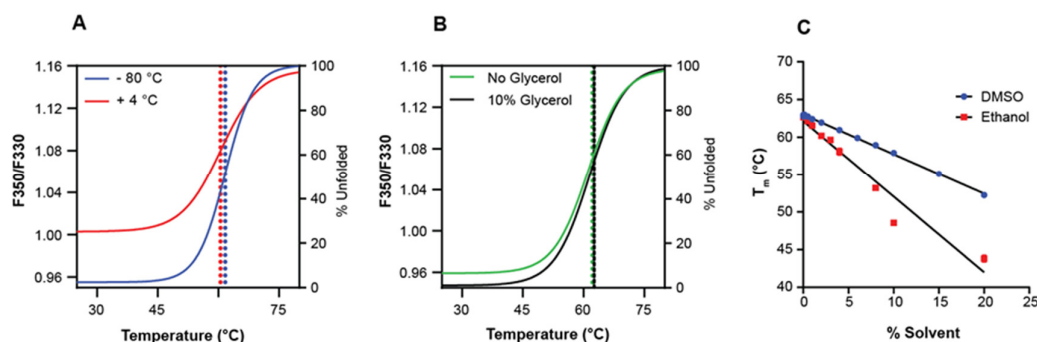


Figure 5-4. NanoDSF studies for the quality control of rpMHCs.

(A, B) The F350/F330 was plotted against temperature using Boltzmann's sigmoidal model. Values at 25 °C and 80 °C were considered completely folded and unfolded, respectively. (A) Storage of A2/NV9 at 4 °C for 2 months (red curve) resulted in loss of folded conformation compared to -80 °C (blue curve). (B) Freezing and storage of A2/NV9 at -80 °C for 24 hours in PBS resulted in 5.5% denaturation compared to addition of 10% glycerol. See Figure S3B, Table S2. (C) Influence of ethanol and DMSO on the T_m of A2/NV9. All experiments in the figure were performed at least twice.

5.3.1.5 Determination of *rpMHC-I* folding energies

We next used nanoDSF to determine the reaction free energy of chemical denaturation (ΔG^0_D) [34], [35] of β_2m and A2/NV9 in an isothermal experiment. This is done without heating, but instead by adding different amounts of guanidinium chloride (**Figure 5-5 A**). The critical denaturant concentrations (C_m), at which 50% of the proteins were unfolded, were 2.2 ± 0.01 M (β_2m) and 1.6 ± 0.02 M (A2/NV9), supporting the thermal stability results that β_2m alone is more stable than the A2/NV9 complex. By extrapolation [34], [36], we found ΔG^0_D values of 22.0 ± 0.42 (β_2m) and 10.65 ± 0.39 kJmol⁻¹ (A2/NV9) (**Figure 5-5 B**).

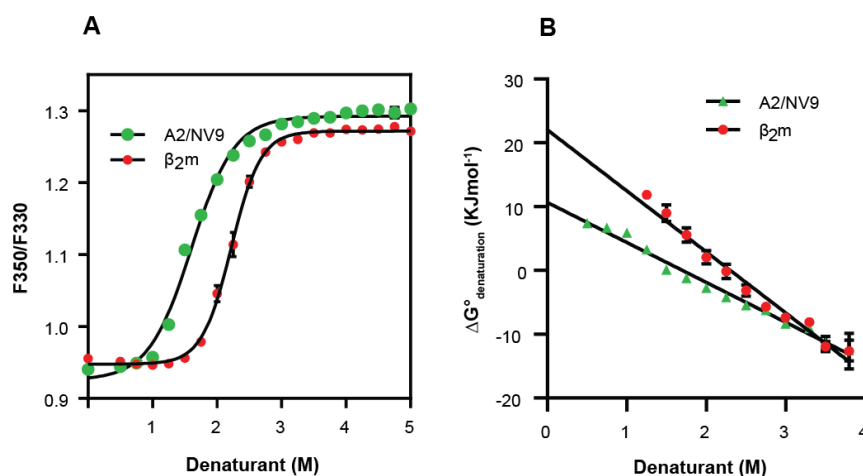


Figure 5-5. Isothermal analysis of folding energies.

A2/NV9 and β_2m were incubated in 100 mM HEPES pH 7.5 at 0.2 mg/mL with guanidinium chloride (GuaHCl) at final concentrations of 0–6 M for 30 minutes at RT ($\approx 25^\circ\text{C}$). Mean \pm SEM ($n=3$). **(A)** Boltzmann sigmoidal fit (black lines) of F350/F330 vs. [GuaHCl]. **(B)** Deriving the folding energies of A2/NV9 and β_2m : the plots of ΔG^0_D vs. [GuaHCl] extrapolated to zero denaturant yield the $\Delta G^0_D(\text{H}_2\text{O})$ (see the Methods).

5.3.1.6 Screening mutant peptides with nanoDSF

Neopeptides, which stem from DNA mutations in tumor cells, are often highly immunogenic and are considered ideal targets for cancer vaccines and personalized adoptive T cell therapy [37][38]. While exome sequencing enables rapid prediction of neopeptides, a major challenge is to confirm specific binding of the peptide to the patient's MHC molecules. We therefore investigated nanoDSF as a method to measure the binding affinity of a set of wild-type and mutant peptides to their cognate MHC allotype. While the four peptides NV9, ILKEPVHGV, GLAGGVSAV, and ELAGIGILTV, which fulfill the anchor residue criteria for high-affinity binding (leucine in position two, and valine in the last position), showed T_m values around 60°C , the T_m s of five mutant peptides (derived from the high-affinity peptides by altering anchor residues to glycines or alanines, [39]) were significantly

lower (**Figure 5-6 A**). The T_m also correlated with the dissociation rate of the peptides measured by fluorescent peptide exchange [39] (**Figures 5-6 B and Figure S5-3, Table S5-4**). Thus, nanoDSF is suitable for estimating the binding affinity of peptides to MHC-I.

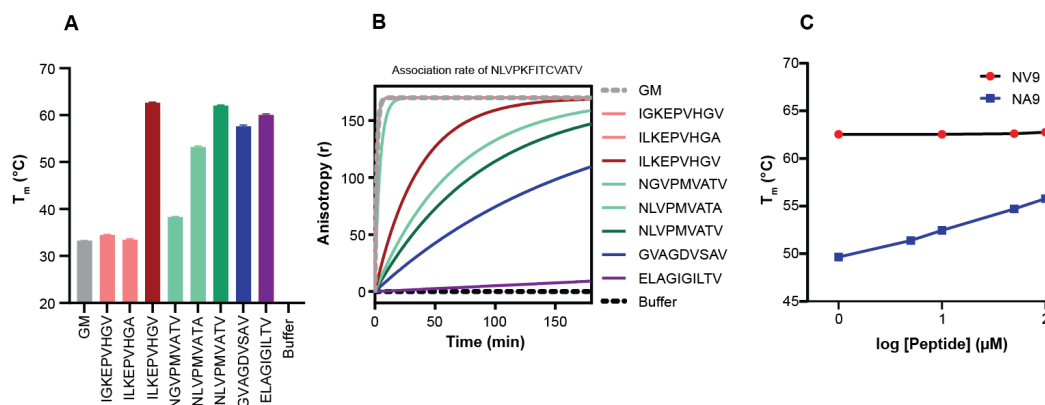
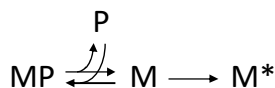


Figure 5-6. Affinity screening of mutant peptides and sequence-specific influence of free peptide concentration on rpMHC thermostability.

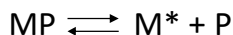
(A) T_m of A2 with four high-affinity peptides (saturated colors) and low-affinity peptides derived from them (pastel colors), and the dipeptide GM. No free peptide was present except for GM (2.5 μM). (B) The fluorescently labelled high-affinity peptide NLVPK_{FITC}VATV (*i.e.*, NV9 with a lysine substitution and a FITC fluorophore attached to its side chain) was added to the solution containing each A2/peptide complex, and its binding (k_{on}) to A2 was measured in real time by fluorescence anisotropy, thus monitoring peptide exchange. (C) Influence of free NLVPMVATV (NV9) and NLVPMVATA (NA9) peptides from 1 to 100 μM. All experiments in the figure were performed at least twice.

5.3.1.7 Sequence-specific influence of free peptide on rpMHC thermostability shows a two-step mechanism of thermal denaturation

Free peptide in the solution containing murine rpMHC may influence its T_m [40]. For A2, we found that free low-affinity peptide NLVPMVATA (NA9) dramatically increased the T_m , whereas high-affinity NV9 did not (**Figure 5-6 C**). The simplest mechanistic explanation of this difference is as follows. The A2/NA9 complex denatures in two steps, first the heat-induced dissociation of the peptide, and then the unfolding of the empty molecule:



with MP = rpMHC-I, M = MHC, M* = denatured MHC, and P = peptide (NA9). Clearly, the first step can be reversed by a high concentration of free peptide, protecting the pMHC from denaturation. In contrast, the high-affinity peptide NV9 is bound so tightly that other regions of the protein unfold before the peptide dissociates:



Thus, thermal denaturation of A2/NA9 likely occurs via a peptide-free intermediate, whereas the T_m of A2/NV9 represents the denaturation of the peptide-bound MHC-I.

5.3.2. Discussion

Besides differential scanning calorimetry (DSC), which measures the decrease in the heat capacity of a protein upon thermal denaturation [41], three methods are established to measure the T_m of rpMHC-Is [42]–[44]. They report on different events in the unfolding of a protein: circular dichroism (CD) monitors protein secondary structure [9], [18]; thermofluor detects the fluorescence increase of a dye (SYPRO Orange) as it binds to the hydrophobic regions of the unfolded protein [15], [45]–[47]; and TDTF (thermal denaturation monitored by tryptophan fluorescence) measures the quenching of the fluorescence of tryptophan side chains as they are exposed to the solvent upon protein denaturation [14], [16].

The established methods have shortfalls (**Table 5-1**): DSC and CD require large amounts of pure protein (>100 μ g) and are thus impractical for high-throughput neoantigen discovery [48]–[50]. CD is incompatible with many buffers (phosphate, sulfate, carbonate, acetate, Good's) above 10 mM [51]–[53]. Thermofluor shows high background with samples that contain unfolded proteins [54] and common assay components such as EDTA [55]. TDTF can measure impure samples with good results [16] but is hampered by low sample throughput and high sample requirement.

We show here that nanoDSF, which has been used for protein quality control [56]–[58] and for screening enzyme stabilities in crude extracts in high-throughput format [59], is a fast and reproducible method for measuring the T_m of pMHCs, with several advantages. NanoDSF, like TDTF, uses tryptophan fluorescence and thus requires no fluorescent label that might give rise to artefacts. It is not disturbed by unfolded proteins, yielding robust and sensitive measurements folded rpMHCs even with crude refolds of 20-30% purity (**Supplementary Figure S5-2 D**). It functions in most buffers [59] and at a wide range of protein concentrations (0.01 to 250 mg/ml) [60]. Since A2/NV9 has 13 Trp and 19 Tyr residues, nanoDSF was highly sensitive in our hands (**Figure 5-3 C**), with a lowest practical protein concentration of 2 μ g/ml, which translates to a minimum sample requirement of 20 ng in the 10 μ l capillary cuvettes. Finally, data acquisition with nanoDSF is parallel and fast, with 20 readings per minute for each of 48 capillaries, which allows a heating rate of 1 $^{\circ}$ C/min, making nanoDSF suitable for high-throughput approaches.

Our measurements allow us to decipher, for the first time, the molecular mechanism of the thermal denaturation of any human MHC class I allotype. When we measured the folding energy of A2/NV9

and compared it with that of β_2m in a chemical denaturation experiment (**Figure 5-5**), we found that the higher ΔG_D^0 of β_2m correlates with its higher T_m , suggesting that in the future it will be possible to derive ΔG_D^0 values, and peptide binding affinities, from T_m values [34], [35]. Importantly, we also found that the T_m is limited, plateauing at about 62.5 °C even for peptides of very high affinity and slow dissociation rate (**Figures 5-6 AB, Supplementary Figure S5-3**). This becomes understandable through the results of the experiments with free peptide (**Figure 5-6 C**): in complexes with low-affinity peptide, the peptide-bound binding groove is first to lose peptide and then denatures; whereas in complexes with high-affinity peptide, the peptide binding site is stabilized by the peptide up to high temperatures, and another region of the protein (perhaps the α_3 domain) denatures first, resulting in a uniform denaturation temperature of 62.5 °C, the T_m of that region.

Because the T_m s of all high-affinity peptides are quite similar, T_m measurements of rpMHCs in principle cannot distinguish between very high-affinity peptides, but they can clearly distinguish strongly from weakly (or non-binding) peptides. This is important because in the future, given the genetic diversity of humanity, many more allotypes will have to be used in immunotherapy, and the measurement of their biochemical properties will become more important than it is today.

5.3.3. Materials and Methods

5.3.3.1 Peptides, buffers and reagents

All peptides (NLVPMVATV, NGVPMVATV, NLVPMVATA, ILKEPVHGV, IGKEPVHGV, ILKEPVHGA, GLAGGVSAV, ELAGIGILTV, and GM) were synthesized with >90% purity by either Genecust (Ellange, Luxembourg) or Bachem (Rhein, Germany). Other reagents were from AppliChem (Darmstadt, Germany) or Sigma Aldrich (Darmstadt, Germany).

The buffers used in the experiments were MES (50 mM 4-Morpholineethanesulfonic acid, 150 mM NaCl, pH 6.5), MOPS (50 mM 3-(N-morpholino)-propanesulfonic acid, 150 mM NaCl, pH 7.4), HEPES (50 mM 4-(2-hydroxyethyl)-1-piperazineethane-sulfonic acid, 150 mM NaCl, pH 7.4), CPB (citrate-phosphate buffer, pH 6.0 - 8.0), PBS (phosphate-buffered saline -137 mM NaCl, 2.7 mM KCl, 10 mM Na_2HPO_4 , and 1.8 mM KH_2PO_4 , pH 7.4) and Tris (50 mM tris(hydroxymethyl)aminomethane, pH 8.0). CPB with different pH (5 – 8) values was prepared as described [25].

5.3.3.2 MHC-I purification and refolding

MHC-I HCs and β_2m were produced in *E. coli* and purified as described [40]. A2 HC (1 μ M) and β_2m (2 μ M) were diluted in a refolding buffer with 0.1 M Tris pH 8.0, 500 mM L-arginine-HCl, 2 mM EDTA, 0.5 mM oxidized glutathione and 5 mM reduced glutathione with 10-20 μ M peptide or with 10 mM of dipeptide (GM). The refolding mix was kept at 4 °C for 1 week under gentle

stirring. Proteins were purified by size exclusion chromatography (SEC) using an ÄKTA system with a HiLoad 16/600 Superdex 200pg gel filtration column (GE Healthcare).

5.3.3.3 *nanoDSF*

The thermal denaturation was measured using nanoDSF by diluting rpMHC-Is or human β_2m in PBS buffer, pH 7.4, at 100 $\mu\text{g/mL}$ (2 μM). Measurements were performed with the Prometheus NT.48 (NanoTemper Technologies, Munich, Germany) using 10 μl sample per capillary and up to 48 capillaries per run (**Figure 1A**) [60]. Samples were heated at 1.0 $^{\circ}\text{C}/\text{min}$, and fluorescence ($\lambda_{\text{ex}} = 280$ nm, $\lambda_{\text{em}} = 330$ nm and 350 nm) was measured. A2/GM was measured in the presence of 10 mM dipeptide GM. Other purified pMHC complexes were measured without any additional peptide in the solution.

For Figure 2 HI, to compare T_m s from ThermoFluor and CD methods, rpMHC-Is for each peptides were purified by SEC and analyzed at 5 μM concentration using nanoDSF.

For isothermal experiments of chemical unfolding, GlnHCl dilutions were prepared with concentrations from 0-6 M in 50 mM HEPES buffer, pH 7.5. 1 mg/mL of β_2m was used. Measurements were performed at 25 $^{\circ}\text{C}$.

5.3.3.4 *TDTF*

TDTF measurements and T_m determinations were performed as described [14], [16]. Briefly, 3 mL (100 $\mu\text{g/mL}$) of folded rpMHC-I or human β_2m were measured in 1x PBS pH 7.4 in a 1x1 cm cuvette in a Cary Eclipse fluorimeter (Agilent, Germany). The samples were heated at the rate of 1.0 $^{\circ}\text{C}/\text{min}$, and fluorescence values ($\lambda_{\text{ex}} = 290$ nm, $\lambda_{\text{em}} = 345$ nm) were measured at intervals of 0.06 $^{\circ}\text{C}$.

5.3.3.5 *Peptide exchange*

Peptide exchange was performed using fluorescence anisotropy as previously described [39]. Briefly, 100 nM NLVPK_{FITC}VATV was added to 300 nM A2/peptide complex in PBS, and kinetic measurements were performed at RT with a Tecan Infinite M1000 PRO (Tecan, Crailsheim, Germany) plate reader using the anisotropy module (FITC $\lambda_{\text{ex}} = 494$ nm, $\lambda_{\text{em}} = 517$ nm) and calculated with Prism.

5.3.4. Data analysis

5.3.4.1 nanoDSF and TDTF

Data from nanoDSF were exported from PR.ThermControl and PR.ChemControl and plotted and evaluated in Prism. For the chemical denaturation analysis, the critical denaturant concentration (C_m) was calculated using a nonlinear four-parameter logistic curve.

TDTF analysis was performed as described earlier [16]. Briefly, the first derivative of the fluorescence intensity was plotted vs. the temperature in a LOWESS fit curve in Prism.

5.3.4.2 Thermal stability

Melting curve fitting: A Boltzmann sigmoidal function was used to fit the protein thermal denaturation curve (**Figure 5-1 D**). The F350/F330 was plotted as a sigmoidal function against the temperature.

$$Y = Y_{min} + \frac{Y_{max} - Y_{min}}{1 + \exp\left(\frac{T_m - x}{Slope}\right)}$$

where Y = F350/F330; X = temperature; Y_{min} = baseline Y at low temperature; Y_{max} = maximal Y at plateau of the curve.

The T_m was calculated as the temperature at which the fluorescence ratio reaches 50% of its maximum value [61].

First derivative curve: In the second approach, the melting temperature was determined by plotting the first derivative of F350/F330 as a function of temperature (**Figure 1E**). The curve was smoothed by a LOWESS fit. Here, T_m is temperature that corresponds to the top of the peak. The first derivative (FD) of each data point is calculated as follows:

$$FD(R_n) = \frac{R(n+1) - R(n-1)}{2 * \Delta t}$$

with R = F350/F330; $R(n)$, the moving average of several neighboring points around the n^{th} value of R ; Δt , the temperature interval between two neighboring data points.

5.3.4.3 Chemical denaturation

The simplest assumption is that pMHC complexes unfold according to a two-state equilibrium [16]. The reaction free energy (a.k.a. Gibbs energy, ΔG) has been linearly linked to denaturant concentration as follows [35], [36]:

$$\Delta G_D = \Delta G_D(H_2O) - m [\text{denaturant}],$$

where $\Delta G_D(\text{H}_2\text{O})$, the y axis intercept, is the Gibbs energy of structural stability of protein at zero denaturant concentration, and the m value (slope) represents the amount of nonpolar surface area exposed to solvent upon unfolding [35].

To obtain the plot in **Figure 5-5**, the fractional degree of protein denaturation (F_D) at each concentration of denaturant is calculated as follows:

$$F_D = \frac{Y_0 - Y_N}{Y_D - Y_N},$$

where Y_0 is the measured signal and Y_N and Y_D are the characteristic signals of the native and denatured states.

From the F_D values, the apparent equilibrium constants, K_{eq} , are then calculated:

$$K_{eq} = \frac{[D]}{[N]} = \frac{F_D}{1 - F_D},$$

And from K_{eq} the free energy change for denaturation (ΔG_D) at each denaturant concentration:

$$\Delta G_D = -RT(\ln K_{eq}) \quad .$$

The plot of ΔG_D versus denaturant concentration (**Figure 5-5 B**) is a straight line with $\Delta G_D(\text{H}_2\text{O})$ as the y-axis intercept.

5.3.5. Author contributions

Ankur Saikia: Conceptualization, Investigation, Validation, Formal analysis, Writing - Original Draft. **Sebastian Springer**: Supervision, Writing- Reviewing and Editing.

5.3.6. Funding

This study was funded by Deutsche Forschungsgemeinschaft SP583/12-1 (to S.Sp.) and the Tönjes Vagt Foundation of Bremen (XXIX to S.Sp.)

5.3.7. Conflict of interest

The authors declare no conflict of interest and approve it for publication.

5.3.8. Acknowledgements

We thank Christian Kleusch (Nanotemper Technologies) for training and providing instrument consumables to support this study; Cindy Dirscherl and Raghavendra Anjanappa for preparative work; Cindy Dirscherl for a drawing; and Uschi Wellbrock for excellent technical assistance.

5.4. References

- [1] P. Klenerman, V. Cerundolo, and P. R. Dunbar, “Tracking T cells with tetramers: New tales from new tools,” *Nat. Rev. Immunol.*, vol. 2, no. 4, pp. 263–272, 2002, doi: 10.1038/nri777.
- [2] A. K. Bentzen and S. R. Hadrup, “Evolution of MHC-based technologies used for detection of antigen-responsive T cells,” *Cancer Immunol. Immunother.*, vol. 66, no. 5, pp. 657–666, 2017, doi: 10.1007/s00262-017-1971-5.
- [3] L. J. Eggermont, L. E. Paulis, J. Tel, and C. G. Figdor, “Towards efficient cancer immunotherapy: Advances in developing artificial antigen-presenting cells,” *Trends Biotechnol.*, vol. 32, no. 9, pp. 456–465, 2014, doi: 10.1016/j.tibtech.2014.06.007.
- [4] M. Schmittnaegel et al., “A new class of bifunctional major histocompatibility class I antibody fusion molecules to redirect CD8 T cells,” *Mol. Cancer Ther.*, vol. 15, no. 9, pp. 2130–2142, 2016, doi: 10.1158/1535-7163.MCT-16-0207.
- [5] D. Chowell et al., “Patient HLA class I genotype influences cancer response to checkpoint blockade immunotherapy,” *Science*, vol. 359, no. 6375, pp. 582 LP – 587, Feb. 2018, doi: 10.1126/science.aao4572.
- [6] P. A. Ott et al., “An immunogenic personal neoantigen vaccine for patients with melanoma,” *Nature*, vol. 547, no. 7662, pp. 217–221, 2017, doi: 10.1038/nature22991.
- [7] M. Bouvier and D. C. Wiley, “Importance of peptide amino and carboxyl termini to the stability of MHC class I molecules,” *Science*, vol. 265, no. 5170, pp. 398–402, 1994, doi: 10.1126/science.8023162.
- [8] S. H. van der Burg, M. J. Visseren, R. M. Brandt, W. M. Kast, and C. J. Melief, “Immunogenicity of peptides bound to MHC class I molecules depends on the MHC-peptide complex stability,” *J. Immunol.*, vol. 156, no. 9, pp. 3308–14, 1996. <http://www.ncbi.nlm.nih.gov/pubmed/8617954>.
- [9] M. L. Fahnstock, I. Tamir, L. Narhi, and P. J. Bjorkman, “Thermal stability comparison of purified empty and peptide-filled forms of a class I MHC molecule,” *Science*, vol. 258, no. 5088, pp. 1658–1662, 1992, doi: 10.1126/science.1360705.
- [10] R. Yaneva, C. Schneeweiss, M. Zacharias, and S. Springer, “Peptide binding to MHC class I and II proteins: New avenues from new methods,” *Mol. Immunol.*, vol. 47, no. 4, pp. 649–657, 2010, doi: 10.1016/j.molimm.2009.10.008.
- [11] M. Harndahl et al., “Peptide-MHC class I stability is a better predictor than peptide affinity of CTL immunogenicity,” *Eur. J. Immunol.*, vol. 42, no. 6, pp. 1405–1416, 2012, doi: 10.1002/eji.201141774.
- [12] D. H. Margulies, M. Corr, L. F. Boyd, and S. N. Khilko, “MHC Class I / Peptide Interactions : Binding Specificity and Kinetics,” vol. 6, pp. 59–69, 1993.
- [13] L. Song, E. J. Hennink, I. T. Young, and H. J. Tanke, “Photobleaching kinetics of fluorescein in quantitative fluorescence microscopy,” *Biophys. J.*, vol. 68, no. 6, pp. 2588–2600, 1995, doi: 10.1016/S0006-3495(95)80442-X.
- [14] S. Springer, K. Döring, J. C. A. Skipper, A. R. M. Townsend, and V. Cerundolo, “Fast association rates suggest a conformational change in the MHC class I molecule H-2Db upon peptide binding,” *Biochemistry*, vol. 37, no. 9, pp. 3001–3012, 1998, doi: 10.1021/bi9717441.
- [15] L. M. Hellman et al., “Differential scanning fluorimetry based assessments of the thermal and kinetic stability of peptide-MHC complexes,” *J. Immunol. Methods*, vol. 432, pp. 95–101, 2016, doi: 10.1016/j.jim.2016.02.016.
- [16] S. K. Saini, E. T. Abualrous, A. S. Tigan, K. Covella, U. Wellbrock, and S. Springer, “Not all empty MHC class I molecules are molten globules: Tryptophan fluorescence reveals a two-step mechanism of thermal denaturation,” *Mol. Immunol.*, vol. 54, no. 3–4, pp. 386–396, 2013, doi: 10.1016/j.molimm.2013.01.004.
- [17] S. M. Rizvi et al., “Distinct Assembly Profiles of HLA-B Molecules,” *J. Immunol.*, vol. 192, no. 11, pp. 4967 LP – 4976, Jun. 2014, doi: 10.4049/jimmunol.1301670.
- [18] C. S. Morgan, J. M. Holton, B. D. Olafson, P. J. Bjorkman, and S. L. Mayo, “Circular dichroism determination of class I MHC-peptide equilibrium dissociation constants,” *Protein Sci.*, vol. 6, no. 8,

- pp. 1771–1773, Aug. 1997, doi: 10.1002/pro.5560060819.
- [19] D. E. Schlamadinger and J. E. Kim, “Thermodynamics of membrane protein folding measured by fluorescence spectroscopy,” *J. Vis. Exp.*, no. 50, pp. 2–5, 2011, doi: 10.3791/2669.
 - [20] C. P. Moon and K. G. Fleming, “Chapter six - Using Tryptophan Fluorescence to Measure the Stability of Membrane Proteins Folded in Liposomes,” in *Biothermodynamics, Part D*, vol. 492, M. L. Johnson, J. M. Holt, and G. K. B. T.-M. in E. Ackers, Eds. Academic Press, 2011, pp. 189–211.
 - [21] J. T. Vivian and P. R. Callis, “Mechanisms of tryptophan fluorescence shifts in proteins,” *Biophys. J.*, vol. 80, no. 5, pp. 2093–2109, 2001, doi: 10.1016/S0006-3495(01)76183-8.
 - [22] R. Anjanappa et al., “Structures of peptide-free and partially loaded MHC class I molecules reveal mechanisms of peptide selection,” *Nat. Commun.*, vol. 11, no. 1, pp. 1–11, 2020, doi: 10.1038/s41467-020-14862-4.
 - [23] M. L. Galisteo, P. L. Mateo, and J. M. Sanchez-Ruiz, “Kinetic study on the irreversible thermal denaturation of yeast phosphoglycerate kinase,” *Biochemistry*, vol. 30, no. 8, pp. 2061–2066, Feb. 1991, doi: 10.1021/bi00222a009.
 - [24] A. Tischer, M. A. Cruz, and M. Auton, “The linker between the D3 and A1 domains of vWF suppresses A1-GPIIb catch bonds by site-specific binding to the A1 domain,” *Protein Sci.*, vol. 22, no. 8, pp. 1049–1059, 2013, doi: 10.1002/pro.2294.
 - [25] T. C. McIlvaine, “A buffer solution for colorimetric comparison,” *J. Biol. Chem.*, vol. 49, pp. 183–186, 1921.
 - [26] P. Link, “Biological Buffers,” Applichem, pp. 1–20, 2008. www.aplichem.com.
 - [27] P. J. Chefalo and C. V. Harding, “Processing of Exogenous Antigens for Presentation by Class I MHC Molecules Involves Post-Golgi Peptide Exchange Influenced by Peptide-MHC Complex Stability and Acidic pH,” *J. Immunol.*, vol. 167, no. 3, pp. 1274–1282, 2001, doi: 10.4049/jimmunol.167.3.1274.
 - [28] A. Stryhn et al., “pH dependence of MHC class I-restricted peptide presentation,” *J. Immunol.*, vol. 156, no. 11, pp. 4191–7, 1996. <http://www.ncbi.nlm.nih.gov/pubmed/8666787>.
 - [29] D. M. Ojcius, L. Gapin, and P. Kourilsky, “Dissociation of the peptide/MHC class I complex: Ph dependence and effect of endogenous peptides on the activation energy,” *Biochem. Biophys. Res. Commun.*, vol. 197, no. 3, pp. 1216–1222, Dec. 1993, doi: 10.1006/bbrc.1993.2606.
 - [30] Z. Reich et al., “Stability of empty and peptide-loaded class II major histocompatibility complex molecules at neutral and endosomal pH: Comparison to class I proteins,” *Proc. Natl. Acad. Sci. U. S. A.*, vol. 94, no. 6, pp. 2495–2500, 1997, doi: 10.1073/pnas.94.6.2495.
 - [31] M. Grommé et al., “Recycling MHC class I molecules and endosomal peptide loading,” *Proc. Natl. Acad. Sci. U. S. A.*, vol. 96, no. 18, pp. 10326–10331, 1999, doi: 10.1073/pnas.96.18.10326.
 - [32] M. A. Batalia et al., “Class I MHC is stabilized against thermal denaturation by physiological concentrations of NaCl,” *Biochemistry*, vol. 39, no. 30, pp. 9030–9038, 2000, doi: 10.1021/bi000442n.
 - [33] N. E. Good, G. D. Winget, W. Winter, T. N. Connolly, S. Izawa, and R. M. M. Singh, “Hydrogen Ion Buffers for Biological Research*,” *Biochemistry*, vol. 5, no. 2, pp. 467–477, Feb. 1966, doi: 10.1021/bi00866a011.
 - [34] E. Freire, A. Schön, B. M. Hutchins, and R. K. Brown, “Chemical denaturation as a tool in the formulation optimization of biologics,” *Drug Discov. Today*, vol. 18, no. 19–20, pp. 1007–1013, 2013, doi: 10.1016/j.drudis.2013.06.005.
 - [35] J. K. Myers, C. Nick Pace, and J. Martin Scholtz, “Denaturant m values and heat capacity changes: Relation to changes in accessible surface areas of protein unfolding,” *Protein Sci.*, vol. 4, no. 10, pp. 2138–2148, 1995, doi: 10.1002/pro.5560041020.
 - [36] D. W. Bolen and M. M. Santoro, “Unfolding Free Energy Changes Determined By The Linear Extrapolation Method. 2. Incorporation of ΔG°_u Values In A Thermodynamic Cycle,” *Biochemistry*, vol. 27, no. 21, pp. 8069–8074, 1988, doi: 10.1021/bi00421a015.
 - [37] R. Bareli and C. J. Cohen, “MHC-multimer guided isolation of neoepitopes specific T cells as a potent-personalized cancer treatment strategy,” *Oncoimmunology*, vol. 5, no. 7, pp. 1–3, 2016, doi: 10.1080/2162402X.2016.1159370.
 - [38] V. Alcazer, P. Bonaventura, L. Tonon, S. Wittmann, C. Caux, and S. Depil, “Neoepitopes-based

- vaccines: challenges and perspectives,” *Eur. J. Cancer*, vol. 108, pp. 55–60, Feb. 2019, doi: 10.1016/j.ejca.2018.12.011.
- [39] S. K. Saini, H. Schuster, V. R. Ramnarayan, H. G. Rammensee, S. Stevanović, and S. Springer, “Dipeptides catalyze rapid peptide exchange on MHC class I molecules,” *Proc. Natl. Acad. Sci. U. S. A.*, vol. 112, no. 1, pp. 202–207, 2015, doi: 10.1073/pnas.1418690112.
- [40] S. S. K. Saini, K. Ostermeir, V. V. R. Ramnarayan, H. Schuster, M. Zacharias, and S. Springer, “Dipeptides promote folding and peptide binding of MHC class I molecules,” *Proc. Natl. Acad. Sci. U. S. A.*, vol. 110, no. 38, pp. 15383–15388, 2013, doi: 10.1073/pnas.1308672110.
- [41] M. Hülsmeier et al., “Thermodynamic and structural equivalence of two HLA-B27 subtypes complexed with a self-peptide,” *J. Mol. Biol.*, vol. 346, no. 5, pp. 1367–1379, 2005, doi: 10.1016/j.jmb.2004.12.047.
- [42] M. J. O’Neill, “The Analysis of a Temperature-Controlled Scanning Calorimeter,” *Anal. Chem.*, vol. 36, no. 7, pp. 1238–1245, 1964, doi: 10.1021/ac60213a020.
- [43] W. M. Jackson and J. F. Brandts, “Thermodynamics of Protein Denaturation. A Calorimetric Study of the Reversible Denaturation of Chymotrypsinogen and Conclusions Regarding the Accuracy of the Two-State Approximation,” *Biochemistry*, vol. 9, no. 11, pp. 2294–2301, 1970, doi: 10.1021/bi00813a011.
- [44] B. Mitchell, “Differential Thermal Analysis,” *Analyst*, no. 1035, 1962, doi: 10.1021/ac60197a799.
- [45] M. C. Lo et al., “Evaluation of fluorescence-based thermal shift assays for hit identification in drug discovery,” *Anal. Biochem.*, vol. 332, no. 1, pp. 153–159, 2004, doi: 10.1016/j.ab.2004.04.031.
- [46] D. T. Blaha et al., “High-throughput stability screening of neoantigen/HLA complexes improves immunogenicity predictions,” *Cancer Immunol. Res.*, vol. 7, no. 1, pp. 50–61, Jan. 2019, doi: 10.1158/2326-6066.CIR-18-0395.
- [47] K. Malik, P. Matejtschuk, C. Thelwell, and C. J. Burns, “Differential scanning fluorimetry: Rapid screening of formulations that promote the stability of reference preparations,” *J. Pharm. Biomed. Anal.*, vol. 77, pp. 163–166, 2013, doi: 10.1016/j.jpba.2013.01.006.
- [48] K. Bowers and N. Markova, “Value of DSC in Characterization and Optimization of Protein Stability,” in *Microcalorimetry of Biological Molecules: Methods and Protocols*, E. Ennifar, Ed. New York, NY: Springer New York, 2019, pp. 33–44.
- [49] L. Zhou et al., “PULSE SPR: A High Throughput Method to Evaluate the Domain Stability of Antibodies,” *Anal. Chem.*, vol. 90, no. 20, pp. 12221–12229, 2018, doi: 10.1021/acs.analchem.8b03452.
- [50] S. Fiedler, L. Cole, and S. Keller, “Automated circular dichroism spectroscopy for medium-throughput analysis of protein conformation,” *Anal. Chem.*, vol. 85, no. 3, pp. 1868–1872, 2013, doi: 10.1021/ac303244g.
- [51] S. R. Martin and P. M. Bayley, “Absorption and circular dichroism spectroscopy,” in *Methods in molecular biology* (Clifton, N.J.), vol. 173, H. J. Vogel, Ed. Totowa, NJ: Springer New York, 2002, pp. 43–55.
- [52] S. Kelly and N. Price, “The Use of Circular Dichroism in the Investigation of Protein Structure and Function,” *Curr. Protein Pept. Sci.*, vol. 1, no. 4, pp. 349–384, 2005, doi: 10.2174/1389203003381315.
- [53] N. J. Greenfield, “Using circular dichroism spectra to estimate protein secondary structure,” *Nat. Protoc.*, vol. 1, no. 6, pp. 2876–2890, 2007, doi: 10.1038/nprot.2006.202.
- [54] S. Boivin, S. Kozak, and R. Meijers, “Optimization of protein purification and characterization using Thermofluor screens,” *Protein Expr. Purif.*, vol. 91, no. 2, pp. 192–206, 2013, doi: 10.1016/j.pep.2013.08.002.
- [55] T. Kroeger et al., “EDTA aggregates induce SYPRO Orange-Based fluorescence in thermal shift assay,” *PLoS One*, vol. 12, no. 5, pp. 1–21, 2017, doi: 10.1371/journal.pone.0177024.
- [56] S. K. Saini et al., “Empty peptide-receptive MHC class I molecules for efficient detection of antigen-specific T cells,” *Sci. Immunol.*, vol. 4, no. 37, p. eaau9039, 2019, doi: 10.1126/sciimmunol.aau9039.
- [57] C. Zhang et al., “Recombinant expression, purification and bioactivity characterization of extracellular domain of human tumor necrosis factor receptor 1,” *Protein Expr. Purif.*, vol. 155, no. November 2018,

- pp. 21–26, 2019, doi: 10.1016/j.pep.2018.11.002.
- [58] D. B. Temel, P. Landsman, and M. L. Brader, “Chapter Fourteen - Orthogonal Methods for Characterizing the Unfolding of Therapeutic Monoclonal Antibodies: Differential Scanning Calorimetry, Isothermal Chemical Denaturation, and Intrinsic Fluorescence with Concomitant Static Light Scattering,” in *Calorimetry*, vol. 567, A. L. B. T.-M. in E. Feig, Ed. Academic Press, 2016, pp. 359–389.
- [59] S. Wedde, C. Kleusch, D. Bakonyi, and H. Gröger, “High-Throughput Feasible Screening Tool for Determining Enzyme Stabilities against Organic Solvents Directly from Crude Extracts,” *ChemBioChem*, vol. 18, no. 24, pp. 2399–2403, 2017, doi: 10.1002/cbic.201700526.
- [60] D. Breitsprecher et al., “Automated nanoDSF for High-Throughput Thermal, Colloidal and Chemical stability screenings,” Prometh. NT.Plex Prod. information, NanoTemper Technol. GmbH, no. April, 2016, doi: 10.13140/RG.2.1.4488.6647.
- [61] F. H. Niesen, H. Berglund, and M. Vedadi, “The use of differential scanning fluorimetry to detect ligand interactions that promote protein stability,” *Nat. Protoc.*, vol. 2, no. 9, pp. 2212–2221, 2007, doi: 10.1038/nprot.2007.321.

5.5. Supplementary Materials

5.5.1. Supplementary Tables:

Table S5-1. Comparison of peptide-wtA2 T_m (°C) values determined by nanoDSF with Thermofluor and circular dichroism (CD) methods.

T_m values for CD and Thermofluor methods were taken from Journal of Immunological Methods, 432 (2016) 95–101, L.M. Hellman et al.

Gene/Peptide name	Sequence	T_m by CD	T_m by Thermofluor	T_m by nDSF
MART-127–35	AAGIGILTV	37	40.8 (± 0.1)	45.0 (± 0.16)
MART-127(2L)–35	ALGIGILTV	51	59.2 (± 0.2)	59.2 (± 0.03)
MART-126–35	EAAGIGILTV	39	45.7 (± 0.3)	41.7 (± 0.10)
MART-126(2L)–35	ELAGIGILTV	55	59.4 (± 0.3)	61.8 (± 0.10)
Tax9-A2	LLFGYPVYV	65	66.3 (± 0.1)	67.1 (± 0.08)
LLE	LLEEMFLTV	52	54.0 (± 0.6)	56.4 (± 0.08)
gp100209(2M)–217	IMDQVPFSV	60	62.2 (± 0.5)	63.7 (± 0.06)
HUD	LGYGFVNYI	40	44.8 (± 0.3)	46.6 (± 0.04)
HUD87(2L,9V)–95	LLYGFVNYV	63	65.1 (± 0.5)	65.4 (± 0.04)
NS31406–1415	KLVALGINAV	64	64.0 (± 0.6)	64.7 (± 0.18)
NS31406(4T)–1415	KLVTLGINAV	64	63.0 (± 0.1)	63.8 (± 0.06)
NS31406(7N)–1415	KLVALGNNAV	59	55.8 (± 0.2)	57.8 (± 0.16)
NS31406(3S,4G,7L)–1415	KLSGLGLNAV	61	61.1 (± 0.1)	62.8 (± 0.05)
WT1	RMFPNAPYL	54	56.3 (± 0.3)	59.8 (± 0.11)
TYR	YMDGTMSQV	65	67.3 (± 0.1)	67.5 (± 0.07)
TYR (T5F)	YMDGFMSQV	63	61.4 (± 0.3)	65.4 (± 0.06)

Table S5-2. QC studies with different buffer conditions.

Buffers	T _m (°C)	pK _a /20 °C	ΔpK _a /10 °C	pH at 20 °C	pH at T _m	T _m in CPB*
MES	64.25 ± 0.21	6.15	-0.11	6.50	6.01	64.2
MOPS	63.99 ± 0.16	7.20	-0.013	7.40	7.34	62.8
HEPES	64.14 ± 0.55	7.55	-0.14	7.40	6.78	64.0
CPB	63.05 ± 0.11	–	0	7.00	7.00	63.6
PBS	62.32 ± 0.32	7.2	-0.003	7.40	7.39	62.5
Tris	63.23 ± 0.11	8.30	-0.31	8.00	6.66	64.4

* At the pH in column 5. Estimated from **Figure 3D**. The difference between the values in column 1 and 6 gives the net effect of the buffer substance, without the influence of the pH value.

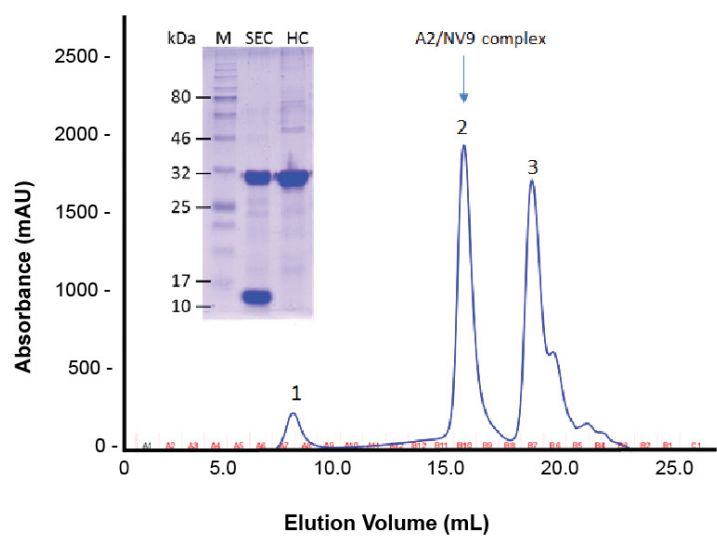
Table S5-3. QC studies with different storage conditions.

Sample	T _m (°C)
+4 °C, 60 days	61.67 ± 0.01
-80 °C, 60 days	62.44 ± 0.04
10% Glycerol, 1 day	63.70 ± 0.02
No Glycerol, 1 day	62.27 ± 0.26

Table S5-4. Correlation between T_m and peptide affinity.

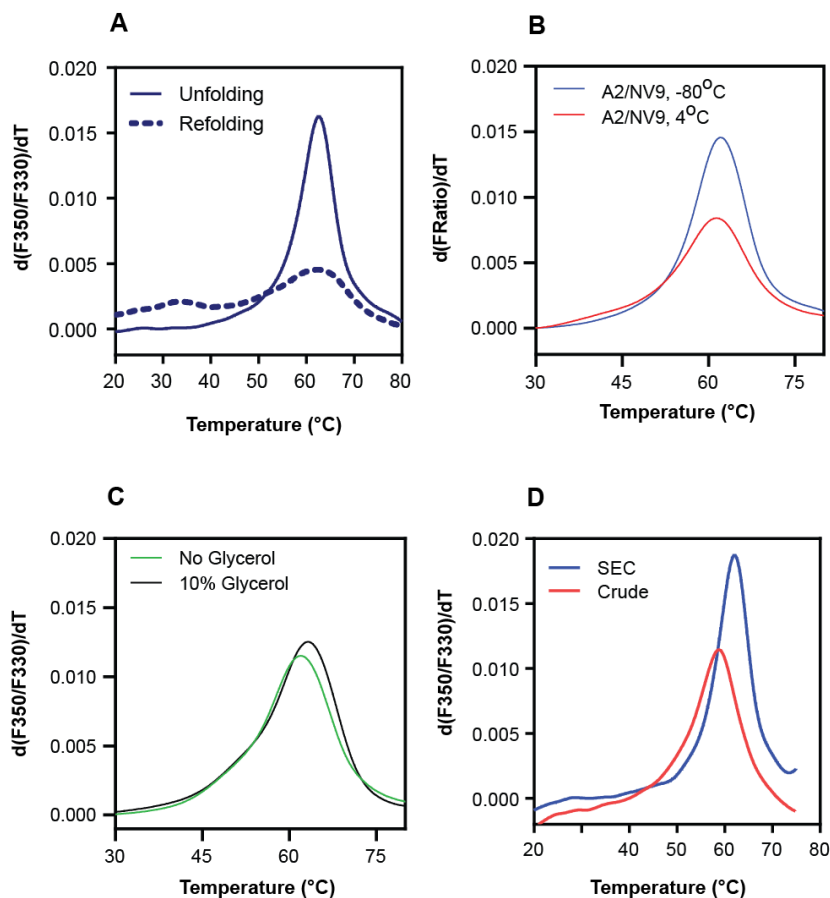
Peptides	Conc. (mM)	T_m (°C)*	k_{on} ($M^{-1}min^{-1}$)**	NetMHC affinity (nM)***
GM	5	33.25 ± 0.06	$6,624,651 \pm 277,616$	NA
IGKEPVHGV	0.01	34.48 ± 0.10	$6,388,026 \pm 236,056$	21792
ILKEPVHGA	0.01	33.43 ± 0.24	$6,780,662 \pm 258,759$	1095
ILKEPVHGV	0.01	62.63 ± 0.13	$273,976 \pm 4,152$	100
NGVPMVATV	0.01	38.33 ± 0.05	$2,419,700 \pm 61,797$	10881
NLVPMVATA	0.01	53.18 ± 0.24	$151,289 \pm 2,195$	189
NLVPMVATV	0.01	62.03 ± 0.13	$111,339 \pm 238$	26
GLAGDVSAV	0.01	57.60 ± 0.29	$57,430 \pm 53$	612
ELAGIGILTV	0.01	60.05 ± 0.21	$3,065 \pm 29$	254

* See Figure 6A. ** See Figure 6B. *** From NetMHC, <http://www.cbs.dtu.dk/services/NetMHC/>.



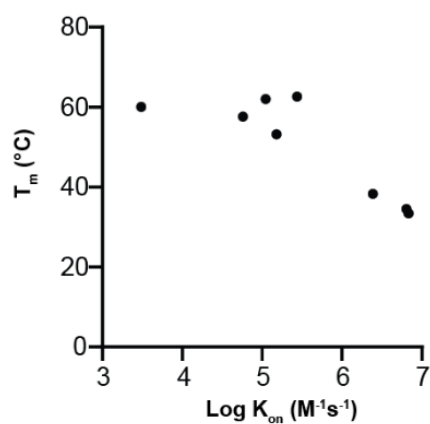
Supplementary Figure S5-1.

Superdex 200 size exclusion chromatography (SEC) elution profile of the refolded HLA-A*02:01/NV9 complex. Peak 1 contains soluble aggregated heavy chain, peak 2 contains the correctly refolded complex (44 kDa), and peak 3 contains the excess folded β_2m . The inset shows a reducing SDS-PAGE gel of the SEC-purified protein (SEC) and denatured heavy chain inclusion bodies (HC). Lane M contains molecular-weight markers (labelled in kDa).



Supplementary Figure S5-2.

pMHC unfolding measured based on fluorescence ratio F_{350}/F_{330} values. The LOWESS fit of the first derivative of the fluorescence ratios was plotted against temperature. **(A)** NanoDSF shows that A2/peptide denaturation is irreversible. The blue solid curve shows the nanoDSF scan of 100 $\mu\text{g/mL}$ purified A2/NV9 in PBS. The observed T_m for this complex is 62.45 ± 0.17 °C ($n=2$). After the unfolding scan, a reverse scan was performed with the same sample (blue dashes, 80 to 20 °C at 1 °C/min). **(B)** A2/NV9 stability measured after storing at +4 °C and -80 °C for 2 months. Red curve, storage at +4 °C; blue curve, storage at -80 °C. **(C)** Stability measured after freezing A2/NV9 with or without 10% glycerol at -80 °C for 24 hours. $n = 2$. **(D)** Comparison of crude and purified refolds. The blue line shows the curve for 100 $\mu\text{g/mL}$ of SEC purified A2/NV9 sample in PBS with $T_m 62.52 \pm 0.38$ °C ($n=3$). The red line shows the curve for 100 $\mu\text{g/mL}$ of crude A2/NV9 refold directly taken from a 7-day old refolding reaction, in the presence of 1 M arginine (which decreases the T_m), containing an estimated $\leq 30\%$ folded protein. The T_m value was 58.82 ± 0.20 °C, lower than the other curve due to the presence of arginine.



Supplementary Figure S5-3

Scatter plot showing the correlation between melting temperature (T_m) of different A2/peptide complexes vs association constant (k_{on}) of incoming peptide NLVPK_{FITC}VATV in a peptide exchange experiment. The k_{on} values for the incoming peptide in peptide exchange assay were measured using fluorescence anisotropy. The results demonstrate that lower affinities (as measured by the T_m) correlate with faster dissociation (measured as the on-rate of the incoming labeled peptide).

Chapter 6. Empty MHC class I molecules for improved detection of antigen-specific T cells

In this published manuscript, we provide a rapid and effective method for detecting antigen-specific T cells in tumour samples using dsA2 molecules.

Sunil Kumar Saini, our collaborators at the Technical University of Denmark, was responsible for the majority of the experimental data (DTU). For this manuscript, I have performed the in vitro peptide binding assay (Figure 6-1 C) to compare k_{on} values between wtA2 and dsA2 and cELISA assay for comparing folding efficiency of dipeptides for dsA2 and dsA24 allotypes (Figure S6-2). Rob Meijers and Maria Garcia-Alai, our EMBL Hamburg collaborators, analyzed the crystal data and generated the figure 6.1 E, F, and G. The manuscript was written by Sunil Kumar Saini, Sine Reker Hadrup and Sebastian Springer.

The full citation of the paper is:

Sunil Kumar Saini, Tripti Tamhane, Raghavendra Anjanappa, **Ankur Saikia**, Sofie Ramskov, Marco Donia, Inge Marie Svane, Søren Nyboe Jakobsen, Maria Garcia-Alai, Martin Zacharias, Rob Meijers, Sebastian Springer, and Sine Reker Hadrup; “**Empty peptide-receptive MHC class I molecules for efficient detection of antigen-specific T cells**”.

Science Immunology 19 Jul 2019, Vol. 4, Issue 37, DOI: 10.1126/sciimmunol. aau9039

The paper is online at <https://immunology.sciencemag.org/content/4/37/eaau9039>

The figure numbers were changed to match the format of this thesis.

6.1. Abstract

The peptide-dependent stability of MHC-I molecules poses a substantial challenge for their use for peptide-MHC multimer-based approaches to comprehensively analyze T cell immunity. To overcome this challenge, we demonstrate the use of functionally empty MHC-I molecules stabilized by a disulfide bond to link the α_1 and α_2 helices close to the pocket. Peptide-loaded disulfide-stabilized HLA-A*02:01 shows complete structural overlap with wild-type HLA-A*02:01. Peptide-MHC multimers prepared using disulfide-stabilized HLA-A*02:01, HLA-A*24:02, and H-2K^b can be used to identify antigen-specific T cells, and they provide a better staining index for antigen-specific T cell detection compared to multimers prepared with wild-type MHC-I molecules. Disulfide-stabilized MHC-I molecules can be loaded with peptide in the multimerized form without affecting the T cell staining capacity. We demonstrate the value of empty-loadable tetramers that are converted to antigen-specific tetramers by a single-step peptide addition, for the identification of T cells specific to several neo- and cancer-associated antigens in melanoma.

6.2. Introduction

Major histocompatibility complex class I (MHC-I) proteins display the cellular proteome, as small peptide fragments, at the cell surface to mediate T cell immune surveillance, which is essential for countering cellular abnormalities such as viral infections and cancer. The identification and characterization of antigen-specific T cells are of substantial importance for therapeutic development and mechanistic insights into immune-affected diseases. In 1996, Altman and colleagues introduced the concept of fluorochrome-labelled MHC multimers to identify antigen-specific T cells [1]. Since then, MHC multimer-based T cell detection approaches have evolved from the detection of few antigen-specific T cell populations per sample to the identification of more than 1000 specificities in parallel [2–6]

A major constraint that limits the flexibility, rapidity, and quality assurance of these state-of-the-art T cell detection platforms is the generation of large libraries of different peptide-MHC complexes (pMHC), which are often 100-1000 different pMHC. To overcome this challenge, peptide exchange technologies have been developed to facilitate the generation of multiple pMHC from a single stock of conditional ligand MHC-I for a given HLA or H-2 molecule. These strategies include the use of dipeptides as catalysts for peptide exchange [7], the widely used UV-mediated peptide exchange technology [8,9], and a more recently developed temperature-induced exchange technology [10]. Alternatively, individual small-scale parallel refolding reactions can be utilized [11]; however, apart from requiring an additional peptide exchange process step, exchange technologies have disadvantages, including HLA-specific design and optimization, inefficient peptide exchange of low-affinity incoming peptides, the ability to multimerize only after peptide exchange, and time-constraints related to duration of the exchange reaction.

We previously demonstrated that a disulfide-stabilized variant of the murine MHC-I, H-2K^b, exhibits peptide-independent stability in the cellular context [12]. A disulfide bond was introduced to link the α_1 and α_2 helices close to the F pocket of the peptide binding groove to provide stability to the MHC-I complex. We further examined this molecule with the hypothesis that such disulfide-stabilized MHC-I molecules might be stable even in the absence of peptide and hence instantly peptide-receptive. Such stable empty MHC-I have the potential to become the ideal solution for a rapid and flexible MHC multimer preparation. To achieve this, we introduced the same disulfide bond close to the F pocket of HLA-A*02:01 molecules. We show that these disulfide-stabilized HLA-A*02:01 molecules can be purified peptide-receptive and functionally empty after in vitro folding assisted by dipeptides [13]. MHC-I multimers prepared with peptide-loaded disulfide-stabilized HLA-A*02:01, HLA-A*24:02 and H-2K^b molecules efficiently detect antigen-specific T cells. We further demonstrate the application of empty disulfide-stabilized MHC-I to make peptide-loadable MHC-I

tetramers that are advantageous for generating flexible reagents for T cell detection in highly antigen-variable situations.

6.3. Results

6.3.1. Disulfide-stabilized empty MHC-I monomers

We designed a disulfide mutant variant of the human MHC-I protein HLA-A*02:01 (A2) by introducing two cysteines at positions 84 and 139 (replacing tyrosine and alanine, respectively), based on molecular dynamics (MD) simulations. MD simulations of this disulfide variant suggested that it had restricted conformational flexibility and a consequently increased stability of the peptide-free state compared to wild-type A2 (wt-A2), as measured by free energy profiles associated with the width of the peptide binding cleft. Introducing the disulfide bond between the α_1 and α_2 helices at positions 84 and 139 eliminated the tendency of the empty binding groove to collapse, suggesting that the disulfide variant would be stable even in the peptide-empty state, while still holding the capacity to bind exogenous peptide (**Figure 6-1 A, Figure S6-1**). We then expressed the disulfide variant of A2 (hereafter called dsA2) in *Escherichia coli*, isolated the denatured protein from inclusion bodies, and folded it *in vitro* with human beta-2 microglobulin (β_2m). The folding reaction of dsA2 was assisted by adding a small molecule with low affinity for MHC-I, such as a dipeptide, which promotes the folding of MHC-I [13]. Such dipeptides can be identified by a simple ELISA-based screen for MHC-I folding efficiency (**Figure S6-2**). Folded dsA2 molecules were purified by the standard size exclusion chromatography procedure, during which the small molecules dissociate from the MHC-I, leaving a purified, functionally empty and peptide-receptive molecule available for further use (**Figure 6-1 B**).

Functional evaluation of purified dsA2 molecules demonstrated that the dsA2 molecules were instantly peptide-receptive, and hence functionally empty, with a higher peptide on-rate (K_{on}) than a dipeptide-loaded dsA2 molecule, as shown by the binding of the fluorophore-labelled A2-restricted high-affinity peptide NLVPMVATV (CMV pp65) to purified dsA2 (**Figure 6-1 C**). We demonstrated, by thermal stability analysis, that the stability of empty dsA2 molecules was greater than that of wt-A2 and that it further increased upon binding to a high-affinity peptide, suggesting the formation of a stable peptide-MHC complex (**Figure 6-1 D**). Wt-A2 molecules that were folded in a similar process, using the dipeptide GM, were likewise peptide-receptive after folding with an on-rate (K_{on}) compared to the dipeptide-loaded dsA2 molecule, and display similar thermal stability profile in the peptide-loaded state (**Figure S6-3, A and B**). The wtA2 molecules fold only with low yield and are unstable in the purification process, whereas the dsA2 can be efficiently purified without dipeptide addition during the purification process) at high yield (**Figure S6-3, C and D**).

Thus, although we show no formal proof, all data are consistent with the assumption that the dsA2 molecule is stable in an empty form, with no or minimal retention of the dipeptide in the binding groove. The stability and peptide-receptive profile of dsA2 is accomplished by the disulfide bond close to the F pocket.

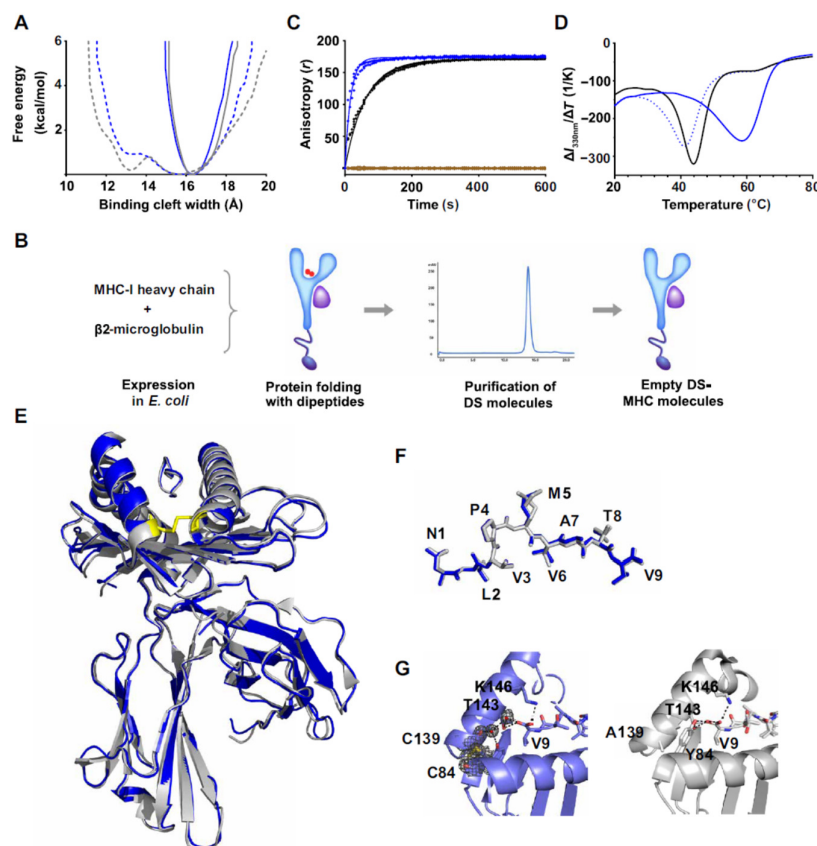


Figure 6-1: dsA2 molecules are peptide-receptive and form stable complexes with associated peptides.

(A) Calculated free energy profiles vs. width of the peptide binding cleft extracted from MD simulations for wt-A2 (gray) and dsA2 (blue) in the presence (solid line) and in the absence (dotted line) of bound peptide. (B) Process of generating empty MHC-I molecules. (C) Binding of 100 nM NLVPKFITCVATV Peptide, measured by fluorescence anisotropy, to purified empty dsA2 molecules alone (blue) or in the presence of 10 mM dipeptide GM (black). Brown dots represent anisotropy values of nonspecific binding. Data are plotted in duplicates, with solid line indicating association rate kinetics. Association rates (K_{on}) = $5.9 \pm 0.11 \times 10^5$ (dsA2), and $1.6 \pm 0.02 \times 10^5$ (dsA2 plus GM). (D) Thermal stability of purified dsA2 without peptide (blue dotted line), with 10 mM dipeptide GM (black line), and with 10 μ M NLVPMVATV (blue line). The minimum of each curve represents the T_m value (dsA2, 40 °C; dsA2 + 10 mM GM, 42 °C; dsA2 + 10 μ M NLVPMVATV, 60 °C). Each sample was analyzed in duplicate or triplicate; representative curves are shown. (E) Crystal structure overlay of dsA2 (blue) and wtA2 (gray) associated with NLVPMVATV peptide. The C84-C139 disulfide bond is highlighted in yellow. (F) Overlay of NLVPMVATV peptide in the binding groove of dsA2 (blue) and wt-A2 (gray). (G) Binding of the C-terminus of the NLVPMVATV peptide in the F pocket of the peptide binding groove of dsA2 (blue) and wtA2 (gray). A 2mF_o-D_fc electron density map is shown at contour level 1 σ for the engineered disulfide bond and two water molecules that fill the area that is occupied in the wt-A2 by the side chain of tyrosine-84.

For further validation of the structural and functional properties of dsA2, we generated a crystal structure with the NLVPMVATV peptide, which confirmed the formation of the disulfide bond between the α_1 and α_2 helices in the F pocket region of the peptide-binding groove (**Figure 6-1 E**). The additional disulfide bond did not alter conformation of the bound peptide or the A2 protein itself, as complete structural overlap was observed with the wild-type structure (**Figure 6-1 E and F**). In dsA2, the C-terminus of the peptide formed a novel hydrogen bond with a water molecule since the hydroxyl group of tyrosine-84 was no longer available (**Figure 6-1 G**).

6.3.2. T cell detection using peptide-loaded empty MHC-I molecules

Since empty dsMHC-I molecules are peptide-receptive and can instantly be loaded with MHC-I peptide ligands, we next investigated whether pMHC-specific multimers prepared with this process can be used to detect antigen-specific CD8⁺ T cells (**Figure 6-2 A**). We loaded NLVPMVATV peptide onto empty dsA2 molecules by direct incubation at room temperature for 15 minutes. The resulting pMHC monomers were multimerized on allophycocyanin (APC) or phycoerythrin (PE)-coupled streptavidin and used to stain A2-NLVPMVATV-specific CD8⁺ T cells from donor PBMCs. We compared the dsA2 multimers with wt-A2 pMHC monomers prepared by UV-mediated peptide exchange [8]. dsA2 NLVPMVATV tetramers efficiently detected A2-NLVPMVATV-specific CD8⁺ T cells across different donors with a comparable frequency to the wt tetramers (**Figure 6-2 B**). Surprisingly, dsA2 tetramers showed a higher fluorescence intensity and better separation from the tetramer-negative CD8⁺ T cell population than tetramers made from wtA2, resulting in a better staining (**Figure 6-2 C**). We further validate and confirm the T cell detection efficiency and improved staining by DS molecules compared to wt molecules using another human MHC-I molecule HLA-A*24:02 (A24), (**Figure 6-2, B and C**).

We controlled that all ds and wtA2 molecules were equally biotinylated (**Figure S6-4**). The folding efficiency of the DS molecules was clearly superior to the wt (folded with UV-ligand), but throughout all experiments the molecular concentration of both molecules were identical (**Table S6-2**). Further, in all cases, tetramer generation was conducted with an excess of pMHC monomer to ensure complete tetramerization and avoid biases from minor (non-measurable) variations in MHC monomer concentration.

Next, we tested the antigen-specific CD8⁺ T cell detection efficiency of dsA2 tetramers with several known A2-restricted viral epitopes (EBV BRLF1 [YVLDHLIVV]; CMV IE1 [VLEETSVML]; HIV POL [ILKEPVHGV]) in comparison with wt-A2 tetramers. The frequencies of all antigen-specific CD8⁺ T cells detected by dsA2 tetramers were comparable to those detected by wtA2 tetramers but with a consistently better staining index, even for very low-frequency antigen-specific CD8⁺ T cells, suggesting that dsA2 provides improved T cell staining irrespective of antigen specificity and the

frequency of T cells (**Figure 6-2, C and D**). No unspecific T cell binding was observed when dsA2 tetramers were associated with a non-binding peptide or a negative-control A2-binding peptide (ILKEPVHGV from HIV pol) (**Figure 6-2 D**).

To further investigate the potency of the dsA2 in T cell detection, we compared dsA2 and wtA2, both classically folded with a panel of virus-derived peptides, or both folded with a UV-sensitive peptide followed by UV-activated ligand exchange [9]. The resulting T cell staining displayed superior or equal properties for T cell staining using dsA2 compared to wtA2 for all folding comparisons (**Figure 6-2 E**). Especially the dsA2 outperformed the UV exchange wtA2 in all combinations, whereas for the classically folded molecules, no difference was observed (**Figure 6-2 F**).

To ascertain that the introduction of the disulfide bond does not alter the T cell receptor (TCR) recognition pattern of the pMHC complex, we determined the fingerprint of the TCR recognition using two T cell clones that both recognize a Merkel Cell Polyomavirus-derived epitope, A2-KLLEIAPNY, but carry different TCR sequences [14]. We recently showed the use of DNA barcode-labeled MHC multimers for the in-depth characterization of the patterns that govern peptide-MHC recognition [5,15]. This strategy provides a TCR fingerprint that identifies the requirement for the TCR-pMHC interaction. The TCR fingerprint was determined using 192 pMHC combinations derived from the original peptide KLLEIAPNY by the sequential replacement of each amino acid position with the 20 naturally occurring amino acids. Each of these peptide variants was either loaded onto dsA2 empty monomers or exchanged for a UV-cleavable ligand in wt-A2. Then, MHC multimers were generated and tagged with DNA barcodes. A mixture of all pMHC multimer combinations was used to stain the T cell clones, allowing for a measure of the affinity-based TCR-pMHC interaction and consequently providing the TCR's recognition preferences. Comparative analysis using both dsA2 and wtA2 molecules was applied to reveal potential differences in the TCR fingerprint. Based on the TCR fingerprints, no differences can be observed between the peptide recognition in the wtA2 and dsA2 variants (**Figure 6-2 G**).

Together, these data demonstrate that empty ds-MHC-I molecules can be used as an efficient tool for antigen-specific T cell detection. They eliminate the requirement for a peptide exchange process, and pMHC tetramers prepared using ds-MHC-I improve the detection of antigen-specific CD8⁺ T cells across various viral antigenic specificities and frequencies compared to the UV exchange procedure.

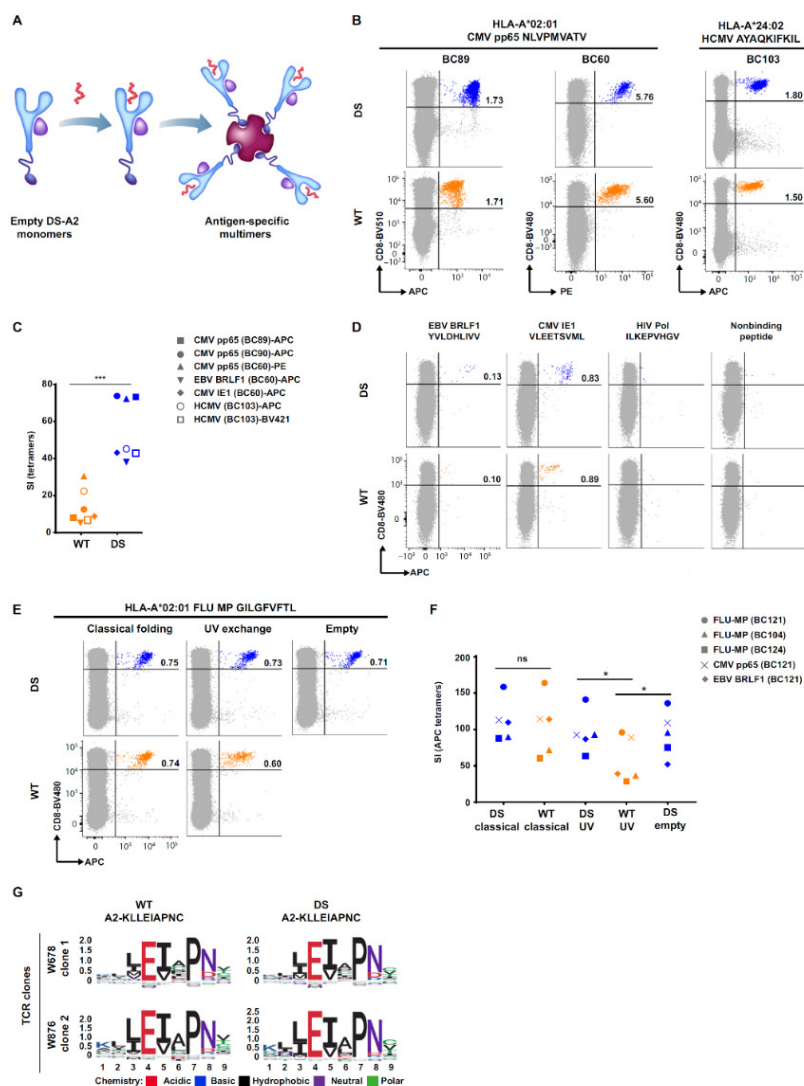


Figure 6-2. Improved and efficient antigen-specific T cell detection using dsA2 molecules.

(A) Schematic illustration of pMHC multimer preparation using dsA2. dsA2 molecules were first incubated with the desired peptide for 15 minutes and then multimerized on fluorochrome-labeled streptavidin. (B) Dot plots of flow cytometry analysis for antigen-specific T cell detection across different donor samples. PBMCs were stained with dsA2 and dsA24 tetramers (DS) prepared after direct loading of peptides on dsmonomers, or with wtA2 and wtA24 tetramers (WT) prepared after UV-mediated peptide exchange on wt monomers. (C) Staining index (SI) of DS (blue) and WT (orange) tetramers for plots in panel B (and one additional donor) and D. The staining index was calculated as (Median of Positive - Median of Negative) / (SD of Negative * 2). (D) Dot plots of T cells stained by dsA2 (DS) and wtA2 (WT) tetramers for several virus-

associated antigens in one donor's PBMCs. As controls, an HIV-derived A2 epitope and a non-binding peptide were used. (E) Representative dot plots of FLU MP (GILGFVFTL) specific T cell detections in donor PBMCs comparing dsA2 and wtA2 tetramers assembled from pMHC monomers produced by classical folding, UV-mediated peptide exchange or using empty dsA2. (F) Staining index comparison for tetramers prepared using ds- and wtA2 molecules across several viral specificities and donor PBMCs. Paired t-test was used for statistical analysis; p = 0.015 (ds-UV vs wt-UV), p = 0.013 (wt-UV vs empty ds). (G) TCR recognition profile of dsA2 and wtA2 molecules. Shannon logos display the amino acid requirements for pMHC-TCR interaction at each position of the peptide. TCR recognition profiles were generated using a DNA barcode-labeled library of 192 peptide-A2 multimers with amino acid substitutions of the original KILLEIAPNY peptide. TCR recognition for each of these peptide variations was measured with pMHC dextramers prepared from dsA2 molecules or from wtA2 molecules for two T cell clones that recognized the Merkel Cell Polyomavirus-derived epitope A2-KILLEIAPNY. Numbers on dot plots represent the percentage of pMHC multimer-positive cells out of total CD8⁺ T cells.

6.3.3. Application of empty MHC molecules in T cell detection strategies

Next, we evaluated the use of empty dsMHC-I molecules in pMHC multimer-based T cell detection strategies using combinatorial labeling of MHC-I multimers [3,4]. The pMHC specificities of eight well-characterized A2-restricted viral antigens were determined using empty dsA2 monomers by direct incubation with peptide, and, for comparison, with wt-A2 monomers loaded by UV-mediated peptide exchange. pMHC monomers were then tetramerized using streptavidin labeled with two different, predefined fluorochromes, forming a unique dual-color code for each individual pMHC. We analyzed healthy donor PBMCs by pooling all eight dual-color-coded pMHC tetramer specificities in a single staining. pMHC tetramers made from dsA2 allowed the detection of several antigen-specific CD8⁺ T cell populations based on the dual color code. We identified T cell populations specific to four out of the eight tested viral antigens, and identical T cell populations, both in terms of specificity and frequency, were detected in parallel using wtA2 pMHC tetramers (**Figure 6-3 A**). Again, an increased staining index was observed using dsA2 pMHC tetramers (**Figure 6-3 B**), validating our observations from the single-color dsA2 tetramers (**Figure 6-2 B-F**). We further verified the antigen-specific T cell detection efficiency using dsA2 pMHC tetramers in two additional donors (**Figure S6-5**).

We then extended the use of empty dsA2 molecules to discover cancer-associated antigen-specific T cells in melanoma samples. Tumor-infiltrating lymphocytes from melanoma lesions were expanded and analyzed for CD8⁺ T cell recognition against a library of 21 melanoma-associated antigens. In a single staining, using the combinatorial labelling approach, we discovered T cells specific to three cancer-associated antigens (gp100 ITDQVPFSV, gp100 AMLGTHTMEV, Mart-1 EAAGIGILTV; **Figure 6-3 C**). Again, both the specificity and the frequency of antigen-specific CD8⁺ T cells were comparable with the wt-pMHC tetramers, but an increased staining index was observed when using the dsA2 (**Figure 6-3 D**). The Mart-1 EAAGIGILTV cancer antigen is a known low-affinity A2 peptide, and detection of Mart-1-specific T cells using dsA2 further establishes that the disulfide-stabilized molecule can be loaded even with a very low affinity peptide to obtain a functional interaction with T cells. Across all samples, including detection of both virus-derived and cancer-associated antigen-specific T cells, we demonstrate a tight correlation in the observed T cell frequency, using either wt- or dsA2 for the T cells (**Figure 6-3 E**).

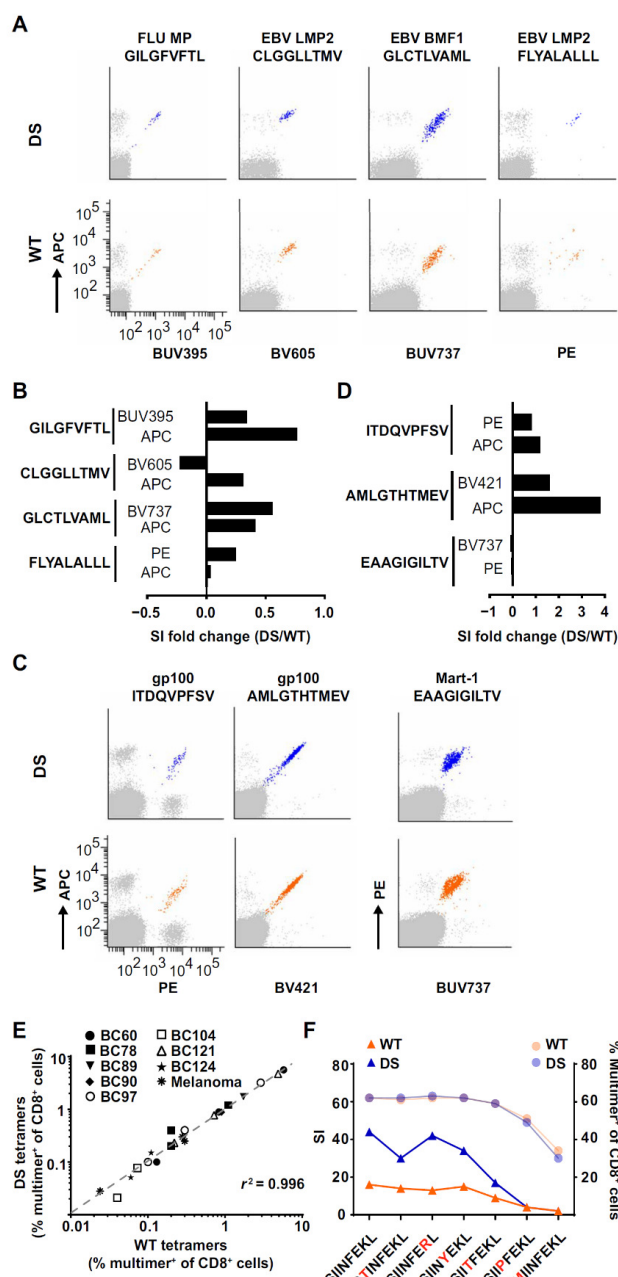


Figure 6-3. dsA2 molecules used in combinatorial color-encoding effectively detects virus- and melanoma-associated antigen-specific T cells.

(A) Flow cytometry plot of antigen-specific CD8⁺ T cells detected using combinatorial color-encoding. Dot plots represent detected antigen-specific CD8⁺ T cells, grey dots represent pMHC multimer-negative or single color-positive cells, and colored dots represent dual-color multimer-positive cells. Staining was conducted using dsA2 (DS) and wt-A2 (WT) in parallel (wt-A2 tetramers were generated after UV-mediated peptide exchange). (B) Fold change of staining index, comparing dsA2 over wt-A2 tetramers for each color label used for the given T cell population detected in panel A. (C) Melanoma-associated antigen-specific T cells detected using dsA2 and wt-A2 (UV exchange) tetramers from expanded TILs of a melanoma patient. A library of 21 melanoma-associated antigenic peptides was screened using the combinatorial color encoding strategy. Dot plots of three identified T cell populations. (D) Fold change in staining index, similar to panel B, for melanoma-associated antigen-specific T cells shown in panel C. (E) Correlation of antigen-specific T cell frequencies identified using dsA2 tetramers and wt-A2 tetramers from donor PBMCs and in melanoma patient (combined from Figure 6.2B, 6.2D, 6.2E, 6.3A, and 6.3C, and Figure S6.5). (F) Comparative staining index and frequency of OT1 splenocytes detected by DS and wt tetramers of murine MHC H-2K^b. SIINFEKL peptide and six variants hereof, highlighted in red, with different affinities to the OT1-TCR (plotted high to low on the X-axis) were used to compare the detection efficiency of DS to wt-H-2K^b tetramers. Dot plots are shown in Figure S6-6.

To further validate the capacity for T cell detection in a situation when T cells are expected to have low TCR-pMHC avidity, we made use of OT-1 and OT-3 T cells, measuring the T cell detection capacity of several previously described peptide variants that compromise the TCR-pMHC interaction. All selected peptides binds strongly to H-2K^b (7 nM - 38 nM, predicted NetMHC), but each provides decreasing TCR-binding capacity to the resulting peptide H-2K^b complex [15]. We

demonstrated T cell detection using dsH-2K^b compared to wt-H-2K^b for all peptides, and again observed a superior staining index for the antigen-specific T cell population with most peptide variants (**Figure 6-3 F, S6-6**). dsH-2K^b can be applied also to detect very low-affinity T cell interaction at same potency as wt-H-2K^b.

In summary, we demonstrate that dsMHC-I molecules can be used in T cell detection strategies for both viral and cancer-associated antigen-specific T cells over a broad range of both T cell and peptide-MHC affinities as an efficient tool to make pMHC multimers without the need for any peptide exchange process.

6.3.4. Empty loadable tetramers for neoantigen discovery

To further ease the pMHC tetramer production, we explored the use of empty pre-labeled MHC tetramers for post-assembly loading with the peptide of interest as a simple and flexible approach to MHC multimer-based T cell detection. Empty-loadable tetramers can be converted to pMHC-specific tetramers by direct incubation with the desired peptide (**Figure 6-4 A**). pMHC tetramers are generated instantly after addition of peptide (1 min), but increased peptide-loading time can be used for low-to-medium affinity peptides (**Figure 6-4 B**). We prepared ds-empty loadable tetramers (dsELT) for A2, A24, and H-2K^b. All three MHC-I allotypes formed dsELTs that were suitable for T cell detection (**Figure 6-4 C**).

We further evaluated the functional stability of dsELTs both before and after peptide loading. First, we kept dsELT at either 4 °C, 20 °C, or 37 °C for 0 to 168 hours prior to peptide loading, to determine their stability in the empty form. Both at 4 °C and 20 °C, the dsELT retained their full staining capacity after 7 days (**Figure 6-4 D, S6-7**). Second, we compared the stability of dsA2 tetramers to wt-A2 tetramers after peptide loading of GILGFVFTL. The tetramers were filtered to remove excess peptide and incubated at the indicated temperature (4°C, 20°C, and 37°C) for 0 to 168 hours. The results again showed an increased MFI of the GILGFVFTL dsA2 tetramer-stained T cell population over that of wt-A2 (**Figure 6-4 E**). Moreover, for the wt-A2 tetramer, we observed a substantial loss of staining intensity starting from 12 h incubation at 37 °C, whereas complete staining intensity was still retained up to 48 h for the dsA2 variant, indicating a prolonged stability of the dsA2 complex (**Figure 6-4 E, S6-8**).

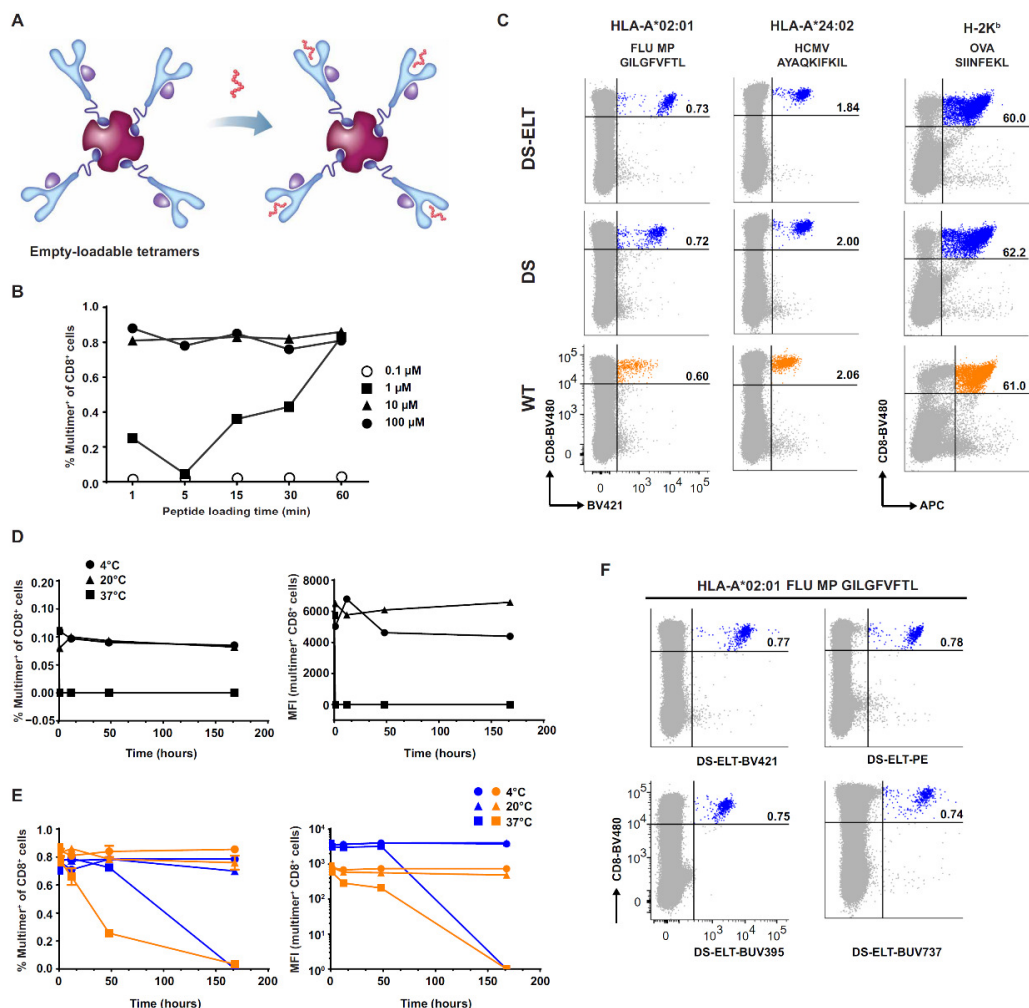


Figure 6-4. Empty-loadable MHC-I multimers for efficient detection of antigen-specific T cells.

(A) Schematic illustration of empty-loadable MHC-I multimers assembled using dsMHC-I molecules. Empty-loadable dsA2 multimers were stored at -20°C and loaded with peptide on demand. (B) Conditions for peptide loading to empty-loadable multimers. Detection of GILGFVFTL-specific T cells after addition of FLU MP GILGFVFTL peptide is shown as the frequency of multimer-positive CD8^{+} T cells at varying peptide concentration and time. (C) Detection of antigen-specific CD8^{+} T cells using empty-loadable tetramers (dsELT) for A2, A24, and H-2Kb MHC alleles compared with wt and DS tetramers. Wt tetramers were prepared after UV-mediated peptide exchange. (D) Stability of empty-loadable multimers. dsA2 ELT conjugated with APC were stored for up to one week at 4°C , 20°C , and 37°C and then loaded with CMV pp65 (NLVPMVATV) specific peptide to detect T cells from donor PBMCs. The frequency (left) and MFI (right) of detected antigen-specific T cells is shown for varying conditions. Dot plots are shown in Figure S7. (E) Peptide dissociation rate measured as FLU MP GILGFVFTL-specific T cell detection efficiency by wt-A2 (orange) or empty-loadable dsA2 multimers (blue). pMHC multimers (without excess peptide) were incubated at 4°C , 20°C , and 37°C up to one week and used for T cell detection from donor PBMCs. The frequency (left) and MFI (right) of detected antigen-specific T cells is shown for varying conditions. Dot plots are shown in Figure S8. (F) Dot plots showing T cell detection efficiency of dsA2 ELT stored for six months. dsA2 ELT conjugated with different fluorophores stored at -20°C for six months were incubated with FLU MP peptide and used for T cell detection. Compare with freshly prepared dsA2 ELT in panel C.

We assembled empty-loadable tetramers using dsA2 molecules on a fluorochrome-labeled streptavidin core and stored them at -20°C without adding any HLA-specific peptide or dipeptide.

After 6 months, the functionality and stability of these empty-loadable dsA2 tetramers was evaluated by detecting viral antigen-specific CD8⁺ T cells from healthy donor PBMCs. Empty tetramers incubated with FLU MP GILGFVFTL for 15 minutes were able to stain GILGFVFTL-specific T cells indistinguishably from the wt-pMHC tetramers, validating the long-term use of the empty-loadable tetramers for T cell detection (**Figure 6-4 F**).

6.3.5. Detection of T cell recognition to cancer-neoantigens

In cancer immunotherapy, there is a great interest in understanding T cell recognition of mutation-derived neoepitopes and the potential to explore these for therapeutic strategies. In most cases, large pMHC library screening is necessary for a comprehensive evaluation of neoepitope recognition [16,17]. The ability to apply post-loadable MHC multimers of dsA2 may ease the process of generating such large pMHC libraries.

To prove the value of dsA2 for the detection of neoantigen-responsive T cells in cancer patients, we analyzed tumor-infiltrating lymphocytes (TILs) from a melanoma patient for the recognition of mutation-derived neoepitopes. Based on tumor DNA whole exome and RNA sequencing, 276 mutations were identified. From these mutations, 43 A2-restricted neoepitopes were predicted using MuPeXI [18] with an A2 binding rank score of < 2 for the mutant peptide variant (using netMHCpan v2.8). We used empty-loadable tetramers to detect neoantigen-specific T cells in the TIL sample. A library of 54 peptides, including 48 cancer-derived peptides (43 from neoantigens and 5 from melanoma-associated antigens) and 6 virus-derived epitopes were analyzed for T cell recognition using empty dsA2 tetramers post-loaded with peptide. Using combinatorial fluorescence labelling, we identified CD8⁺ T cells specific to eight of the predicted neoantigens; several of these neoantigens shared overlapping peptide sequences (**Figure 6-5 A and B**). We also identified T cells for three melanoma-associated antigens (gp100 AMLGTHTMEV, Mart-1 EAAGIGILTV, and gp100 ITDQVPFSV), which were previously detected in a different TIL preparation from this patient [19], and for two viral antigens (EBV BRLF1, YVLDHLIVV; and FLU MP, GILGFVFTL) (**Figure 6-5 A and B**). Taken together, we demonstrate here the successful application of empty-loadable tetramers in the discovery of cancer-associated antigens, including mutation-derived neoepitopes.

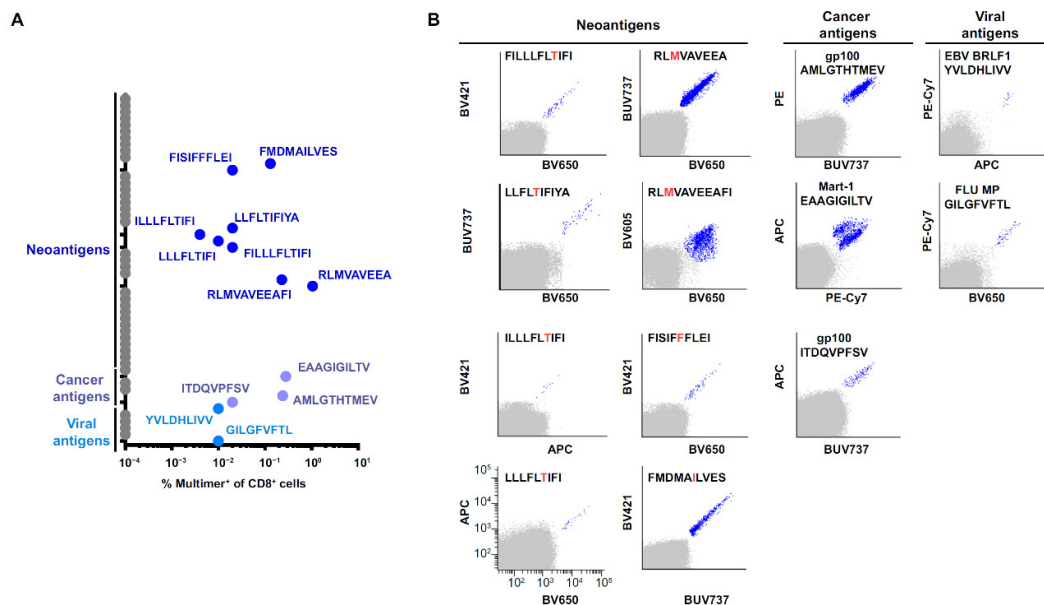


Figure 6-5. Detection of neoantigen specific T cell recognition in cancer.

(A) Antigen-specific T cells in melanoma TILs identified by the combinatorial color-encoding strategy using empty-loadable dsA2 multimers. pMHC multimers for 54 A2-restricted peptides (43 neoantigens, 5 melanoma-associated cancer antigens, and 6 virus-derived antigens) were generated, each in a two-color combination. Frequency of pMHC multimer-positive cells out of total CD8⁺ T cells is shown as colored dots across three categories. Multimer-negative cells are plotted in grey for each pMHC combination (Zero values are converted to 0.0001 to plot on log scale). (B) Dot plots of the antigen-specific T cell populations from panel A, each is shown with indicated fluorochromes and peptide sequences. The mutated amino acid position of the neoantigens is highlighted in red.

6.4. Discussion

We here introduce empty-loadable MHC-I multimers. We demonstrate their potential in the identification of T cells specific to cancer-associated antigens, including mutation-derived neoantigens (Figure 6-5). These stable, ready-to-use MHC-I multimers, which can be converted to antigen-specific pMHC multimers in a single-step peptide addition, perfectly align with the state-of-the-art antigen-specific T cell detection platforms that require the rapid generation of large arrays of MHC multimers [6,20]. We have shown the feasibility of using dsA2 in both combinatorial color encoding strategies and DNA barcoding-based methods of T cell detection (Figure 6-2, 6-3, 6-5). Empty-loadable MHC-I multimers will be of great advantage for the fast and effective evaluation of T cell recognition for personalized immunotherapy [21].

The disulfide bond-stabilized MHC-I molecules do not require MHC-restricted high-affinity peptide neither for their *in-vitro* folding nor for stability after folding (as required for wt-MHC-I), and they remain peptide-receptive even after long-term storage at -20 °C. Thus, they provide a flexible and convenient peptide loading system that does not require the use of peptide exchange technologies. Furthermore, antigen-specific A2 tetramers prepared with empty dsA2 provide better T cell staining

(as measured by the staining index) than wt-A2 multimers of the same antigen specificities prepared via UV-mediated peptide exchange technology (**Figure 6-2 to 6-4**) [8,9]. A possible explanation for the increased staining index using dsMHC relates to the potentially incomplete removal of photocleavable peptide or the retention of partly unfolded empty wt-A2 molecules after peptide exchange [8] that may result in fewer functional molecules per tetramer, potentially reducing the functional tetrameric form to a trimeric form. This is supported by the minimal differences observed between conventionally folded pMHC-I complexes of either wt or DS form (**Figure 6-2**). Another explanation is the enhanced stability of peptide-loaded dsA2 molecules, compared to wt-A2 molecules, which may impact the staining capacity (**Figure 6-4**).

The specific locations for the insertion of the two cysteines forming the disulphide bond (Y84C and Y139A) is conserved across MHC-I molecules. Hence we expect this strategy to be applicable across all MHC-I allotypes. For each allotype a small molecules (di or tripeptide) should be identified to facilitate the folding reaction. Here we demonstrate the use of ds A2, A24 and H-2Kb, as three examples of MHC-I molecules frequently applied for immunological investigation.

Empty-loadable MHC multimers provide a fast and convenient option to generate antigen-specific MHC multimers, which appear superior over other methods. The UV-exchange strategy requires a longer peptide exchange period and is inefficient for peptide exchange in pre-tetramerized reagents [9]. An alternative technology using peptide exchange on MHC multimers was recently pursued based on temperature-mediated peptide exchange that uses a HLA-specific, low-affinity peptide to exchange for the incoming peptide directly on MHC multimers at an elevated temperature [10]; however, in the temperature exchange system, an incoming peptide competes with a low-affinity, temperature-sensitive ligand, which may compromise the exchange for low-affinity incoming peptides, and A2 multimers require significantly more time for peptide exchange to be completed (three hours). Similarly, all peptide exchange technologies require the design of HLA-specific ligands (photocleavable peptides or peptides suitable for temperature exchange) for optimal peptide exchange processes, whereas the generation of empty dsMHC monomers is free of such requirements. dsMHC molecules require the assistance of small molecules, such as dipeptides, for their folding, but these are relatively cheap and easy to identify (**Figure S6-2**) [13].

An important concern relates to the induction of potential changes in peptide recognition when peptide is presented in the dsA2 versus wt-A2. As empty-dsMHC-I molecules are a non-natural variant, due to the insertion of the additional disulfide bond. Even though it is formed outside the peptide binding area, it might have functional implications either on peptide binding or on T cell recognition. To address this, we obtained the crystal structure of the CMV pp65 NLVPMVATV/dsA2 complex and determined the TCR fingerprint of two T cell clones, using either the dsA2 or the wt-A2. The crystal structure demonstrates identical peptide binding properties of wt

versus dsA2 (**Figure 6-1**). The TCR fingerprint likewise shows identical recognition of the dspMHC-I complex compared to the wt (**Figure 6-2**). dsA2 empty-MHC-multimers are functional after long-term storage and pMHC-specific conversion of them is independent of any exchange technology that may alter their quality. Hence, they provide an efficient tool to produce quality-assured reagents for immune monitoring, for diagnostics, and in therapeutic applications such as the isolation or specific stimulation of antigen-specific T cells for adaptive T cell transfer in immunotherapy approaches [21,22].

6.5. Materials and Methods

6.5.1. Study design

This study was designed to investigate the use of empty-dsMHC-I molecules as an advanced tool for the detection of human CD8⁺ T cells using antigen-specific pMHC multimers, and to explore the advantages of dsMHC-I for identification of cancer associated antigens, including neo-antigens, over the existing methods. We used established technologies for T cell detection to demonstrate the applicability of dsMHC-I molecules. The dsMHC-I molecules were designed based on MD simulation analysis and previously available literature. Standard biochemical assays and crystal structure analysis were performed to validate the peptide-receptive empty MHC-I. We show the use of dsMHC multimers across two human (A2, and A24) and one murine (H-2K^b) MHC alleles. For identification of antigen-specific T cells, PBMCs from healthy volunteers, splenocytes from OT1 and OT3 transgenic mice, and TILs from a melanoma patient was used.

6.5.2. Production of MHC-I heavy chains and beta-2 microglobulin

MHC-I HCs, and β_2m were produced in *E.coli* as described previously [23,24]. Briefly, proteins were expressed in *E.coli* strain BL21(DE3)pLysS using pET series plasmids. Inclusion bodies containing expressed proteins were harvested using sonication in lysis buffer followed by washing in detergent buffer and wash buffer and solubilizing the protein in 8 M urea buffer (8 M Urea, 50 mM K⁺-HEPES pH 6.5, and 100 μ M β -mercaptoethanol). Proteins were stored at -80 °C until used for in vitro folding.

6.5.3. *In vitro* folding and purification of MHC-I molecules

MHC-I HC (1 μ M) and β_2m (2 μ M) were diluted in a folding buffer (0.1 M Tris pH 8.0, 500 mM L-Arginine-HCl, 2 mM EDTA, 0.5 mM oxidized glutathione and 5 mM reduced glutathione) with 60 μ M high-affinity peptide (NLVMPVATV or GILGFVFTL or YVLDHLIVV), or photocleavable peptide (KILGFVF-J-V;DS and wt-A2, VYG-J-VRACL; wt-A24, FAPGNY-J-AL; wt-H-2K^b), or with 10 mM of dipeptide GM (DS and wt-A2), or GL (dsH-2K^b) [13], or GF (dsA24), and incubated at 4 °C for 3-5 days, followed by concentrating folded proteins with 30 kDa cut-off membrane filters

(Vivaflow-200; Sartorius). Proteins were then biotinylated with the BirA biotin-protein ligase standard reaction kit (Avidity, LLC-Aurora, Colorado). Biotinylated MHC-I monomers were purified by size exclusion chromatography using HPLC (Waters Corporation, USA) or an ÄKTA HiLoad 26/600 Superdex-200 gel filtration column (bed volume 120 or 320 mL) or Superdex 200 10/300 GL (bed volume 24 ml) (GE Healthcare Life Sciences). All MHC-I folded monomers were quality controlled for their concentration, biotinylation efficiency, and UV degradation (wherever applicable), and stored at -80 °C until further use. For dsA2 folded with dipeptide GM, two different batches of purified protein used for data shown in **Figure 6-2** and **Figure 6-4**.

6.5.4. Electrophoretic mobility shift assay

Post biotinylation, purified MHC-I monomers were tested for biotinylation efficiency. 2 µg of purified monomers were incubated with 4 µg of Streptavidin PLUS (ProZyme SA10) for 30 minutes at 4 °C. After incubation, proteins were separated on 4–20% Mini-PROTEAN® TGX™ Gel (Bio-Rad, 4561095) along with a PAGE ruler pre-stained protein ladder (Bio-Rad, 1610374) and stained with Coomassie (Bio-Rad, 161-0786).

6.5.5. *In vitro* Folding of MHC-I molecules for dipeptide screening

In vitro folding of MHC-I molecules was performed in black, non-binding, 96 well plates in 250 µL volume. HC and β₂m were used at the concentration of 3 µM (100 µg/ml) and 8 µM (100 µg/mL) respectively in folding buffer (0.1 M Tris pH 8.0, 500 mM L-Arginine-HCl, 2 mM EDTA, 0.5 mM oxidized glutathione and 5 mM reduced glutathione). 20 mM of dipeptide was maintained throughout the sample wells whereas 10 µM of high-affinity HLA specific peptides (dsA2; NLVPMVATV, dsA24; QYDPVAALF) were used for positive control wells. The folding reactions were then incubated at 4°C, 300 rpm (plate-shaker) for 7 days. After folding, the plates were centrifuged at 3000 x g for 15 minutes and samples were diluted 50 fold for competitive ELISA assay.

6.5.6. Competitive ELISA assay

For competitive ELISA assay, clear, high binding, 96-Well Microplates (Corning, 3590) were coated overnight with 100 µL/well of 10 µg/mL A2-NLVPMVATV prepared in carbonate coating buffer (15 mM Na₂CO₃, 35 mM NaHCO₃, pH 9.5). Plates were washed (2 x 300 µL) in wash buffer (Tween-20, 50 mM Tris-HCl, pH 8.0) and blocked with 150 µL blocking buffer (1% BSA, 50 mM Tris-HCl, pH 8.0) at 4 °C for 2 hours. Samples or standards (folded MHC-I e.g. A2-NLVPMVATV complex) were diluted in dilution buffer (1% BSA, 0.05 % Tween-20, 50 mM Tris-HCl, pH 8.0). Diluted samples were pre-incubated in a clear, U-bottom, non-binding 96 well plate (Greiner 650901) with 15 ng/mL of W6/32 antibody in dilution buffer for 1 hour, following which 100 µL of this mixture

was transferred to the blocked assay plate after 2 washes in wash buffer and incubated at 4 °C for 2 hour. Post incubation, wells were washed 2 times with wash buffer and 100 μ L of HRP-conjugated goat-anti-mouse IgG (Jackson ImmunoResearch Europe Ltd 115-035-003) were added (1/2000 dilution in dilution buffer) and incubated for 1 hour at room temperature. After another 5 washes, 100 μ L of substrate (Pierce™ TMB Substrate, Thermofisher 34021) were added to each well and incubated at room temperature for 10 min. Reaction was immediately stopped by adding equal volume of 2 M H₂SO₄ solution. Fluorescence intensity was measured at 450 nm absorbance in TECAN Infinite® M1000 PRO (Tecan Group Ltd., Switzerland) plate reader. Standard curve was plotted using Graphpad Prism software and concentrations for folded MHC-I molecules in the unknown samples were interpolated. Folding efficiencies were calculated relative to the folding with the high-affinity full-length peptide.

6.5.7. Peptide binding measured by fluorescence anisotropy

To assess peptide binding by fluorescence anisotropy, 100 nM of the fluorochrome-labeled peptide NLVPK_{FITC}VATV (from GeneCust Biotechnology) was added to 300 nM of purified folded dsA2 MHC-I complexes \pm GM, and kinetic measurements were performed with a Tecan Infinite M1000 PRO (Tecan, Crailsheim, Germany) multimode plate reader by measuring anisotropy (FITC λ_{ex} = 494 nm, λ_{em} = 517 nm). For Peptide binding study wt-A2 molecules folded with dipeptide were purified with the SEC buffer containing 10 mM GM. All peptide binding measurements were performed at room temperature (22–24 °C) in 50 mM HEPES buffer, pH 7.5 with a total reaction volume of 100 μ L. Data were plotted using GraphPad Prism software.

6.5.8. Thermal stability measurements

Thermal stability was measured using differential scanning fluorimetry by dissolving MHC-I in 50 mM HEPES buffer, pH 7.5, at 200 μ g/mL. Experiments were carried out using the Prometheus NT.48 (NanoTemper Technologies, Germany). Each of the capillaries was loaded with 10 μ L of test samples in either duplicates or triplicates. The temperature gradient was set to an increase of 1 °C/minute in a range from 20 °C to 80 °C. Protein unfolding was measured by detecting the temperature-dependent change in tryptophan fluorescence at emission wavelengths of 330 and 350 nm. Thermal stability of purified empty dsA2 molecules was measured alone or in the presence of 10 mM dipeptide GM or after incubating with 10 μ M NLVPMVATV peptide. Melting curve and T_m values were generated by the PR.ThermControl v2.1 software from the first derivative of the fluorescence at 350 nm and plotted using GraphPad prism software.

6.5.9. Molecular Dynamics Simulations

For all simulations, the Amber16 Molecular Dynamics Package in combination with the parm14SB force field for proteins was used [25]. The pdb3GSO structure of A2 in complex with the peptide NLVPMVATV served as start structure for the wt-A2. For the dsA2, the reported structure served as the start structure. The same start structures without coordinates for the bound peptide served as start structures for simulations in the absence of bound peptide. The structures were solvated in octahedral TIP3P water [26] boxes and keeping a 10 Å minimum distance between the structures and the box boundaries. Sodium and chloride ions were added to achieve neutrality and a salt concentration of 0.15 M. After extensive energy minimization (2500 steps), the systems were heated to 300 K (within 50 ps) keeping the solute (heavy atoms) restraint to the starting positions (force constant: 25 kcal·mol⁻¹Å⁻²) followed by gradual removal of the positional restraints over a period of 0.5 ns. After equilibration the unrestraint data gathering MD simulations were extended up to 1 μs and coordinates were saved every 2 ps. The hydrogen-mass repartitioning scheme was employed allowing a 4fs time step [27]. Analysis of trajectories was performed using the cpptraj module of Amber16. The distance between the center-of-mass of residues 66-84 in the α₁ helix and residues 139-159 in the α₂ helix of MHC-I molecules were used to monitor the width of the peptide binding cleft. Free energy profiles were calculated based on the center-of-mass distance probability distribution observed during the unrestraint MD production simulations. Relative free energies were obtained from the distance probability distribution p(d) using the equation dG=-RTln(p(d)), with R indicating the gas constant and T the temperature (300 K).

6.5.10. Crystal structure determination

The dsA2 mutant in complex with the NLVPMVATV peptide was concentrated to 10 mg/mL, and crystals were obtained using a mother liquor containing 5 mM cobalt chloride, 5 mM cadmium chloride, 5 mM magnesium chloride, 5 mM nickel chloride, 0.1 M HEPES pH 7.5, and 12 % PEG 3350. A single crystal was transferred to a cryo-protectant solution containing 5 mM cobalt chloride, 0.1 M Hepes buffer pH 7.5, 15 % PEG 3350 and 10 % glycerol. The crystal was mounted and cryo-cooled to 100 K on the EMBL P13 beamline at DESY (Deutsches Elektronen-Synchrotron, Hamburg, Germany) containing an EIGER 16M detector. An X-ray data set was collected to a resolution of 1.5 Å (**Supplementary table 6-1**). The data were processed with XDS [28] and scaled with AIMLESS [29]. Molecular replacement was performed using MOLREP [30] with the coordinates of an A2 molecule (PDB id 3GSO), and the structure was refined with REFMAC5 [31]. The engineered disulfide bond was manually built with Coot [32]. The structure was refined to an R factor of 17.5% (R_{free} 20.0%). Molprobability [33] was used to validate the geometry, and indicated that

98.7% of the residues were in the allowed regions of the Ramachandran plot (with no residues in the disallowed regions).

6.5.11. Preparation of MHC multimers

To prepare pMHC multimers using wt-A2, dsA2, wt-A24, and wt-H-2K^b monomers, pMHC complexes with desired peptide were generated by UV-mediated peptide exchange technology [8]. Briefly, 100 µg/mL purified UV light-sensitive pMHC complex (A2- KILGFVF-J-V; A24- VYG-J-VRACL; H-2K^b-FAPGNY-J-AL; J represents UV cleavable moiety) were incubated with 200 µM of peptide in PBS for 1 hour under UV light (366 nm). pMHC complexes of dsA2, dsA24, and dsH-2K^b were prepared by incubating 100 µg/mL purified dsMHC monomers with 100 µM peptide for 15 minutes in PBS. Classically folded A2 pMHC monomer were directly used for multimer preparation. pMHC complexes were centrifuged for 5 minutes at 10,000 x g, and supernatants were used to make MHC multimers. For each 100 µL of pMHC monomers, 9.02 µL (0.2 mg/mL stock, SA-PE (Biolegend 405204), SA-PE-Cy7 (Streptavidin - Phycoerythrin/Cy7; Biolegend 405206), SA-APC (Biolegend 405207)) or 18.04 µL (0.1 mg/mL stock, SA-BUV395 (Brilliant Ultraviolet 395; BD 564176), SA-BV421 (Brilliant Violet 421; BD 563259), SA-BV605 (Brilliant Violet 605; BD 563260), SA-BV650 (Brilliant Violet 650; BD 563855), and SA-BUV737 (Brilliant Ultraviolet 737; BD 564293)) of streptavidin conjugates were added and incubated for 30 minutes at 4 °C, followed by addition of D-biotin (Sigma) at 25 µM final concentration to block any free binding site. Empty-loadable MHC multimers were prepared from dsA2 monomers by incubating 100 µL of monomers with 9.02 µL (0.2 mg/mL stock) or 18.04 µL (0.1 mg/mL stock) streptavidin conjugates for 30 minutes 4 °C and stored at -20 °C with 5% glycerol and 0.5% BSA. Empty-loadable MHC multimers were converted to pMHC multimers by incubating 100 µM peptide (unless stated otherwise) for 15 minutes at 4 °C. For combinatorial encoding strategy [34], pMHC multimers of each peptide specificity were prepared in two colors following any of the above process and mixed in a 1:1 ratio before staining the cells.

6.5.12. T cell staining and analysis

For human T cell staining, pooled pMHC multimers (in combinatorial encoding) or pMHC multimers of individual specificity were incubated with 1×10^6 to 2×10^6 PBMCs or expanded TILs from a melanoma lesion [thawed and washed twice in RPMI 1640 +10% fetal calf serum (FCS) and washed once in fluorescence-activated cell sorting (FACS) buffer; PBS + 2% FCS] for 15 min at 37°C in 80 µl total volume. Cells were then mixed with 20 µl of antibody staining solution CD8-BV480 (BD B566121) or CD8-BV510 (BD 563919) (final dilution, 1:50), dump channel antibodies CD4-FITC (final dilution, 1:80; BD 345768), CD14-FITC (final dilution, 1:32; BD 345784), CD19-FITC (final dilution, 1:16; BD 345776), CD40-FITC (final dilution, 1:40; Serotec, MCA1590F), and CD16-FITC

(final dilution, 1:64; BD 335035), and a dead cell marker (final dilution, 1:1000; LIVE/DEAD Fixable Near-IR; Invitrogen, L10119) and incubated for 30 min at 4°C. Cells were then washed twice in FACS buffer (PBS + 2% FCS) and acquired on a flow cytometer (LSRFortessa, Becton Dickinson). Lymphocytes were gated on the basis of forward and side scatter, and multimer-positive CD8 T cells were identified from singlets and live lymphocytes according to the above detailed cell surface markers (**Figure S6-4**) [3,35]. For a detailed comparison between wt- and dsMHC multimers, we have chosen to illustrate MHC multimer-positive CD8 T cells on singlets and live lymphocytes to elucidate any dspMHC multimer-specific binding to CD8+ population (**Figure 2** and **Figure S6-4**). However, for routine T cell identification, a more stringent gating strategy is recommended to exclude any non-CD8 T cell-associated multimer binding. Data were analysed and plotted using FACSDiva (Becton Dickinson) or FlowJo analysis software. For staining for mouse splenocytes, OT1 and OT3 T cells, the following antibodies were used: CD8a-BV480 (BD 566096), CD3-FITC (BioLegend, 100206), and dead cell marker (LIVE/DEAD Fixable Near-IR; Invitrogen, L10119). MHC multimer-positive cells were identified using the gating strategy illustrated in **Figure S6-4 B**.

6.5.13. TCR fingerprinting analysis

For the TCR fingerprinting analysis, DNA barcode-labelled pMHC multimers were generated as described previously [5] using PE-labelled streptavidin-conjugated dextran obtained from FINA Biosolutions (Rockville, US). PE-labelled dextramers were incubated with pMHC monomers (192 pMHC combinations derived from the original peptide KLLLEIAPNY by sequential replacement of each amino acid position by the 20 naturally occurring amino acids, prepared either using wt-A2 or dsA2) for 30 minutes. Resulting pMHC dextramers were used to stain A2-KLLLEIAPNY specific T cell clones (2×10^6 cells). After staining, cells were acquired on FACS Aria (AriaFusion, Becton Dickinson). PE-positive CD8⁺ T cells from each sample were sorted and subjected to PCR amplification of their associated DNA barcodes. PCR-amplified DNA barcodes were purified with the QIAquick PCR Purification kit (Qiagen, 28104) and sequenced at Sequetech (USA) or GeneDx (USA) using Ion Torrent PGM 314 or 316 chip (Life Technologies). Sequenced barcodes were then analyzed using Barracoda (<http://www.cbs.dtu.dk/services/barracoda>) to identify the log₂ fold change of the barcode signal related to the sorted cell population versus the signal of the barcode in the total MHC multimer library prior to T cell staining. The TCR fingerprints were created based on the log₂ fold changes calculated by Barracoda. The amino acid substitution setup that we applied allowed us to assign a single log₂ fold change value to each amino acid residue at each position in the peptide sequence. The log₂ fold change of the original peptide was assigned to each of the respective amino acid residues at each position. This way, a position-specific scoring matrix (PSSM) for each clone was calculated with the number of rows corresponding to the number of positions in

the peptide and number of columns corresponding to the number of naturally occurring amino acids. We then normalized each row of the PSSMs to sum to 1, and the resulting position-specific frequency matrices were then converted into Shannon logos.

6.5.14. Ethical approval

All healthy donor material was collected under approval by the local Scientific Ethics Committee, and written informed consent was obtained according to the Declaration of Helsinki. Healthy donor PBMC was obtained from the central blood bank, Rigshospitalet, Copenhagen in an anonymized form. TILs from melanoma patients were obtained based on collaboration with Herlev Hospital, Dept. of Oncology and Center for Cancer Immune therapy, approved by the local ethics committee. Splenocytes from OT1 and OT3 transgenic mice were collected from collaborators, under regular approval from the national committee of animal health (approval no. M165-15, University of Lund, Sweden).

6.5.15. Lymphocyte preparations

Peripheral blood mononuclear cells (PBMCs) from healthy donors were isolated from buffy coat blood products by density centrifugation on Lymphoprep (Axis-Shield PoC) and cryopreserved at -150°C in FCS (FCS; Gibco) + 10% DMSO. TILs from melanoma patients were obtained from resected tumor lesions from individuals with stage IV melanoma (American Joint Committee on Cancer, AJCC). Tumor lesions were resected following surgical removal. Tumor fragments from were cultured individually in complete medium (RPMI with 10% human serum, 100 U/mL penicillin, 100 $\mu\text{g/mL}$ streptomycin, 1.25 $\mu\text{g/mL}$ fungizone (Bristol-Myers Squibb) and 6,000 U/mL IL-2) at 37°C and 5% CO_2 , allowing TILs to migrate into the medium. TILs were expanded to reach $>50 \times 10^6$ total cells originated from ~ 48 individual fragments, which had expanded to confluent growth in 2 mL wells and eliminated adherent tumor cells (average of $\sim 2 \times 10^6$ cells per well from each tumor fragment). TIL cultures were further expanded using a standard rapid expansion protocol (REP) as previously described (35). Briefly, TILs were stimulated with 30 ng/mL anti-CD3 antibody (OKT-3; Ortho Biotech) and 6,000 U/mL IL-2 in the presence of irradiated (40 Gy) allogenic feeder cells (healthy donor PBMCs) at a feeder/TIL ratio of 200:1. Initially, TILs were rapidly expanded in a 1:1 mix of complete medium and REP medium (AIM-V (Invitrogen) + 10% human serum, 1.25 $\mu\text{g/mL}$ fungizone and 6,000 U/mL IL-2), but after 7 days, complete medium and serum were removed stepwise from the culture by adding REP medium without serum to maintain cell densities around $1 - 2 \times 10^6$ cells/mL. TIL cultures were cryopreserved at -150°C in human serum + 10% DMSO. Mouse spleen suspensions were obtained by mashing the full spleen through a 70 μm cell strainer (Fischer

Scientific). Red blood cells were lysed with RBC Lysis buffer (BioLegend) and used directly or cryopreserved at -150°C in FCS (FCS; Gibco) + 10% DMSO.

6.5.16. Mutation analysis and neoantigen prediction

DNA and RNA was extracted and purified from tumor fragments and PBMCs (germline DNA reference) using the AllPrep DNA/RNA Mini kit (Qiagen, 80204), with the addition of DNase during RNA purification (Qiagen, 79254). Hereafter DNA/RNA concentrations were analyzed by NanoDrop (ThermoFischer Technologies) and RNA RIN values were analyzed by 2100 Bioanalyzer (Agilent Technologies). DNA whole exome and RNA sequencing was performed at the DTU Multi Assay Core (DMAC). 276 identified missense mutations from tumor fragments of melanoma patient MM909.37, were used to predict 9-11 amino-acid-long HLA restricted peptides, and sorted according to Mut_MHCrank up to the score of 2 using MuPeXI and netMHCpan-2.8 [18]. A total of 43 A2 restricted neoepitopes were predicted.

6.5.17. Peptides

Sequences of peptides are denoted in single letter amino acid code. All peptide were custom synthesized either by Pepscan (Presto BV, Lelystad, The Netherlands) or by GeneCust (Ellange, Luxembourg). Dipeptide GM was procured from Sigma-Aldrich. UV sensitive peptide ligands for MHC-I folding were custom synthesized by the Peptide Synthesis facility at the Leiden University Medical Center (LUMC), Leiden, The Netherlands, as described previously [8,9,36]. Peptide stocks were prepared in 100% DMSO and stored at -20°C .

6.5.18. Statistical analysis

All the statistical analysis were done using GraphPad Prism 7 data analysis software. Paired t-test was performed to compare staining indexes shown in **Figure 6-2 C** and **6-2 F**.

6.6. Acknowledgments

We thank Natalie J. Miller, Candice D. Church, and Paul Nghiem, Department of Medicine, Divisions of Dermatology, University of Washington, Seattle, WA, for sharing T cell clones. We thank Leon E. Jessen, Andrea M. Marquard and Anne-Mette Bjerregaard for bioinformatics assistance related to the generation of Shannon logo plots and predictions of neoepitopes. We thank Amalie Kai Bentzen for sharing her expertise related to the TCR fingerprinting and Bente Rotbøl for excellent technical assistance related to flow cytometry. This research was funded in part through the European Research Council (ERC), StG 677268 NextDART, The Lundbeck Foundation Fellowship R190-2014-4178 (to SRH) and R181-2014-3828 (to SKS), The Danish Research Council, Sapere

Aude, DFF – 4004-00422 (to SRH), Deutsche Forschungs-gemeinschaft (SP583/12-1 to S.Sp.) and iNEXT (grant number 653706, funded by the Horizon 2020 programme of the European Commission, to S.Sp.).

6.7. Author contributions

SKS designed research, performed experiments, analyzed data, prepared figures, and wrote the manuscript. TT designed research, performed experiments, analyzed data and prepared figures. RA, and AS designed research, performed experiments, and analyzed data. SR, performed experiments on melanoma patient materials related to neoantigen prediction, and revised the manuscript. MD, and IM, sampled and provided patient material. SNJ, designed experiments, revised manuscript. MGA and RM designed research, analyzed data for crystal structure. MZ, designed research, analyzed data, and prepared figures for MD simulation studies. SS and SRH conceived the concept, supervised the study, designed experiments, and wrote the manuscript.

6.8. Competing interests

SS, and MZ are listed as inventors for a patent granted to produce empty MHC-I molecules (Patent # US9494588B2). SKS, SRH and SNJ are inventors of a patent application related to T cell detection using dsMHC-I. Other authors have no competing interests.

6.9. Data and materials availability

The crystal structure data shown in this study for CMV pp65-NLVPMVATV/dsA2 has been deposited in the PDB with an ID number 6Q3K.

6.10. References

- [1] Altman, J.D., Moss, P.A.H.H., Goulder, P.J.R.R., Barouch, D.H., et al., Phenotypic Analysis of Antigen-Specific T Lymphocytes. *Science* (80-.). 1996, 274, 94–96.
- [2] Chattopadhyay, P.K., Price, D.A., Harper, T.F., Betts, M.R., et al., Quantum dot semiconductor nanocrystals for immunophenotyping by polychromatic flow cytometry. *Nat. Med.* 2006, 12, 972–977.
- [3] Hadrup, S.R.S.R., Bakker, A.H.A.H., Shu, C.J.C.J., Andersen, R.S.R.S., et al., Parallel detection of antigen-specific T-cell responses by multidimensional encoding of MHC multimers. *Nat. Methods* 2009, 6, 520–526.
- [4] Newell, E.W., Klein, L.O., Yu, W., Davis, M.M., Simultaneous detection of many T-cell specificities using combinatorial tetramer staining. *Nat. Methods* 2009 67 2009, 6, 497–499.
- [5] Bentzen, A.K., Marquard, A.M., Lyngaa, R., Saini, S.K., et al., Large-scale detection of antigen-specific T cells using peptide-MHC-I multimers labeled with DNA barcodes. *Nat. Biotechnol.* 2016 3410 2016, 34, 1037–1045.
- [6] Bentzen, A.K., Hadrup, S.R., Evolution of MHC-based technologies used for detection of antigen-responsive T cells. *Cancer Immunol. Immunother.* 2017, 66, 657–666.
- [7] Saini, S.K., Schuster, H., Ramnarayan, V.R., Rammensee, H.-G., et al., Dipeptides catalyze rapid peptide exchange on MHC class I molecules. *Proc. Natl. Acad. Sci.* 2015, 112, 202–207.
- [8] Toebe, M., Coccoris, M., Bins, A., Rodenko, B., et al., Design and use of conditional MHC class I ligands. *Nat. Med.* 2006, 12, 246–251.
- [9] Bakker, A.H., Hoppes, R., Linnemann, C., Toebe, M., et al., Conditional MHC class I ligands and peptide exchange technology for the human MHC gene products HLA-A1, -A3, -A11, and -B7. *Proc. Natl. Acad. Sci.* 2008, 105, 3825–3830.
- [10] Luimstra, J.J., Garstka, M.A., Roex, M.C.J., Redeker, A., et al., A flexible MHC class I multimer loading system for large-scale detection of antigen-specific T cells. *J. Exp. Med.* 2018, 215, 1493–1504.
- [11] Leisner, C., Loeth, N., Lamberth, K., Justesen, S., et al., One-Pot, Mix-and-Read Peptide-MHC Tetramers. *PLoS One* 2008, 3, e1678.
- [12] Hein, Z., Uchtenhagen, H., Abualrous, E.T., Saini, S.K., et al., Peptide-independent stabilization of MHC class I molecules breaches cellular quality control. *J. Cell Sci.* 2014, 127, 2885–2897.
- [13] Saini, S., Ostermeir, K., Ramnarayan, V., Schuster, H., et al., Dipeptides promote folding and peptide binding of MHC class I molecules. *Proc. Natl. Acad. Sci. U. S. A.* 2013, 110, 15383–8.
- [14] Miller, N.J., Church, C.D., Dong, L., Crispin, D., et al., Tumor-Infiltrating Merkel Cell Polyomavirus-Specific T Cells Are Diverse and Associated with Improved Patient Survival. *Cancer Immunol. Res.* 2017, 5, 137–147.
- [15] Bentzen, A.K., Such, L., Jensen, K.K., Marquard, A.M., et al., T cell receptor fingerprinting enables in-depth characterization of the interactions governing recognition of peptide–MHC complexes. *Nat. Biotechnol.* 2018 3612 2018, 36, 1191–1196.
- [16] Bjerregaard, A.M., Nielsen, M., Jurtz, V., Barra, C.M., et al., An analysis of natural T cell responses to predicted tumor neoepitopes. *Front. Immunol.* 2017, 8, 1566.
- [17] McGranahan, N., Furness, A.J.S., Rosenthal, R., Ramskov, S., et al., Clonal neoantigens elicit T cell immunoreactivity and sensitivity to immune checkpoint blockade. *Science* (80-.). 2016, 351, 1463–1469.
- [18] Nielsen, M., Lundegaard, C., Blicher, T., Lamberth, K., et al., NetMHCpan, a Method for Quantitative Predictions of Peptide Binding to Any HLA-A and -B Locus Protein of Known Sequence. *PLoS One* 2007, 2, e796.
- [19] Andersen, R.S., Thru, C.A., Junker, N., Lyngaa, R., et al., Dissection of T-cell antigen specificity in human melanoma. *Cancer Res.* 2012, 72, 1642–1650.
- [20] Hadrup, S.R., Newell, E.W., Determining T-cell specificity to understand and treat disease. *Nat. Biomed. Eng.* 2017 110 2017, 1, 784–795.

- [21] Saini, S.K., Rekers, N., Hadrup, S.R., Novel tools to assist neoepitope targeting in personalized cancer immunotherapy. *Ann. Oncol.* 2017, 28, xii3–xii10.
- [22] Zacharakis, N., Chinnasamy, H., Black, M., Xu, H., et al., Immune recognition of somatic mutations leading to complete durable regression in metastatic breast cancer. *Nat. Med.* 2018, 24, 724–730.
- [23] Garboczi, D.N., Hung, D.T., Wiley, D.C., HLA-A2-peptide complexes: refolding and crystallization of molecules expressed in *Escherichia coli* and complexed with single antigenic peptides. *Proc. Natl. Acad. Sci. U. S. A.* 1992, 89, 3429–33.
- [24] Saini, S.K., Abualrous, E.T., Tigan, A.S., Covella, K., et al., Not all empty MHC class I molecules are molten globules: Tryptophan fluorescence reveals a two-step mechanism of thermal denaturation. *Mol. Immunol.* 2013, 54, 386–396.
- [25] D.A. Case, I.Y. Ben-Shalom, S.R. Brozell, D.S. Cerutti, T.E. Cheatham, III, V.W.D. Cruzeiro, T.A. Darden, R.E. Duke, D. Ghoreishi, M.K. Gilson, H. Gohlke, A.W. Goetz, D. Greene, R Harris, N. Homeyer, S. Izadi, A. Kovalenko, T. Kurtzman, T.S. Lee, S. LeGra, D.M.Y. and P.A.K., No Title 2016, AMBER 16.
- [26] Jorgensen, W.L., Chandrasekhar, J., Madura, J.D., Impey, R.W., Klein, M.L., Comparison of simple potential functions for simulating liquid water. *J. Chem. Phys.* 1983, 79, 926–935.
- [27] Hopkins, C.W., Le Grand, S., Walker, R.C., Roitberg, A.E., Long-Time-Step Molecular Dynamics through Hydrogen Mass Repartitioning. *J. Chem. Theory Comput.* 2015, 11, 1864–1874.
- [28] Kabsch, W., XDS. *Acta Crystallogr. D. Biol. Crystallogr.* 2010, 66, 125–32.
- [29] Evans, P., Scaling and assessment of data quality. *Acta Crystallogr. Sect. D Biol. Crystallogr.* 2006, 62, 72–82.
- [30] Vagin, A., Teplyakov, A., Molecular replacement with MOLREP. *Acta Crystallogr. Sect. D Biol. Crystallogr.* 2010, 66, 22–25.
- [31] Kovalevskiy, O., Nicholls, R.A., Long, F., Carlon, A., Murshudov, G.N., Overview of refinement procedures within REFMAC5: utilizing data from different sources. *Acta Crystallogr. Sect. D, Struct. Biol.* 2018, 74, 215–227.
- [32] Emsley, P., Lohkamp, B., Scott, W.G., Cowtan, K., Features and development of Coot. *Acta Crystallogr. Sect. D Biol. Crystallogr.* 2010, 66, 486–501.
- [33] Chen, V.B., Arendall, W.B., Headd, J.J., Keedy, D.A., et al., MolProbity: All-atom structure validation for macromolecular crystallography. *Acta Crystallogr. Sect. D Biol. Crystallogr.* 2010, 66, 12–21.
- [34] Sick Andersen, R., Kvistborg, P., Frich, Pedersen, N.W., et al., Parallel detection of antigen-specific T cell responses by combinatorial encoding of MHC multimers. *Nat. Protoc.* 2012, 7.
- [35] Van Oijen, M., Bins, A., Elias, S., Sein, J., et al., On the Role of Melanoma-Specific CD8⁺ T-Cell Immunity in Disease Progression of Advanced-Stage Melanoma Patients. *Clin. Cancer Res.* 2004, 10, 4754–4760.
- [36] Rodenko, B., Toebe, M., Hadrup, S.R., van Esch, W.J.E., et al., Generation of peptide–MHC class I complexes through UV-mediated ligand exchange. *Nat. Protoc.* 2006, 1, 1120–1132.

6.11. Supplementary information

6.11.1. Supplementary tables

Table S6-1. Crystal structure data collection and refinement statistics.

Data collection	
Space group	P2 ₁ 2 ₁ 2 ₁
Cell dimensions	
<i>a</i> , <i>b</i> , <i>c</i> (Å)	60.16 80.57 109.69
α , β , γ (°)	90.0 90.0 90.0
Resolution (Å)	1.50 (1.53 – 1.50) *
<i>R</i> _{pim}	0.055 (0.53)
<i>I</i> / σ <i>I</i>	7.3 (1.4)
CC (1/2)	100.0 (0.56)
Completeness (%)	99.9 (100.0)
Redundancy	5.4 (5.3)
Refinement	
Resolution (Å)	65 – 1.50
No. reflections	81571
<i>R</i> _{work} / <i>R</i> _{free}	0.175 (0.20)
No. atoms	
Protein	3180
Ligand/ion	19
Water	589
<i>B</i> -factors	
Protein	22.1
Ligand/ion	28.2
Water	37.4
R.m.s. deviations	
Bond lengths (Å)	0.013
Bond angles (°)	1.51

*Number of crystals for each structure should be noted in footnote. *Values in parentheses are for highest-resolution shell.

[AU: Equations defining various R-values are standard and hence are no longer defined in the footnotes.]

[AU: Ramachandran statistics should be in Methods section at the end of Refinement subsection.]

[AU: Wavelength of data collection, temperature and beamline should all be in Methods section.]

Table S6-2. Protein yield after in vitro folding and purification of WT and dsA2 molecules.

S.No.	Folding volume	wtA2 with KILGFVF-J-V		dsA2 with GM	
		Before biotinylation	After biotinylation	Before biotinylation	After biotinylation
1	1000 mL	4 mg	N/A	12.0 mg	N/A
2	1000 mL	3,5 mg	N/A	10.0 mg	N/A
3	200 mL	2.5 mg	1.5 mg	5.6 mg	4.0 mg

6.11.2. Supplementary Figures

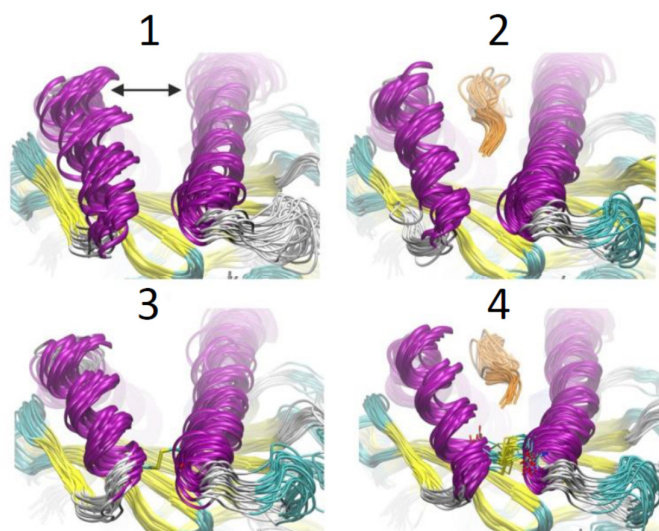


Figure. S6-1. MD simulation of dsA2.

Snapshot of MD simulations. (1) Superposition of snapshots obtained from the simulation of wt-A2 in the absence of bound peptide (cartoon representation, color-coded according to secondary structure; the view is from the F pocket along the binding cleft). The binding cleft width is indicated as a double arrow. (2) Snapshots obtained from the wt-A2 simulation with peptide (peptide backbone in orange). (3) Same as (1) for the dsA2 without peptide and with bound peptide illustrated in (4).

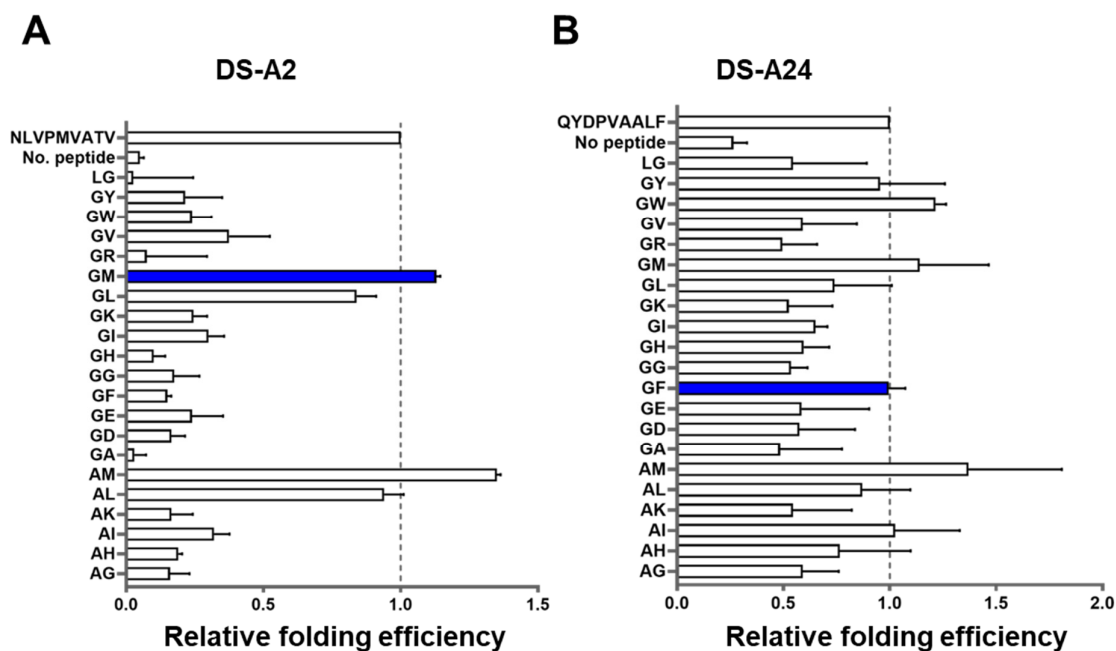


Figure. S6-2. Dipeptide mediated folding efficiency of dsMHC molecules.

Dipeptide mediated folding efficiency of (A) dsA2 and (B) dsA24 was assessed using a competitive ELISA assay after in-vitro folding in a 96 well assay format. Dipeptides are listed in single letter amino acid codes. Folding efficiency is represented as relative to folding in the presence of full-length HLA specific high-affinity peptide. Blue highlighted bar represents the dipeptides used for large-scale production of respective DS molecules.

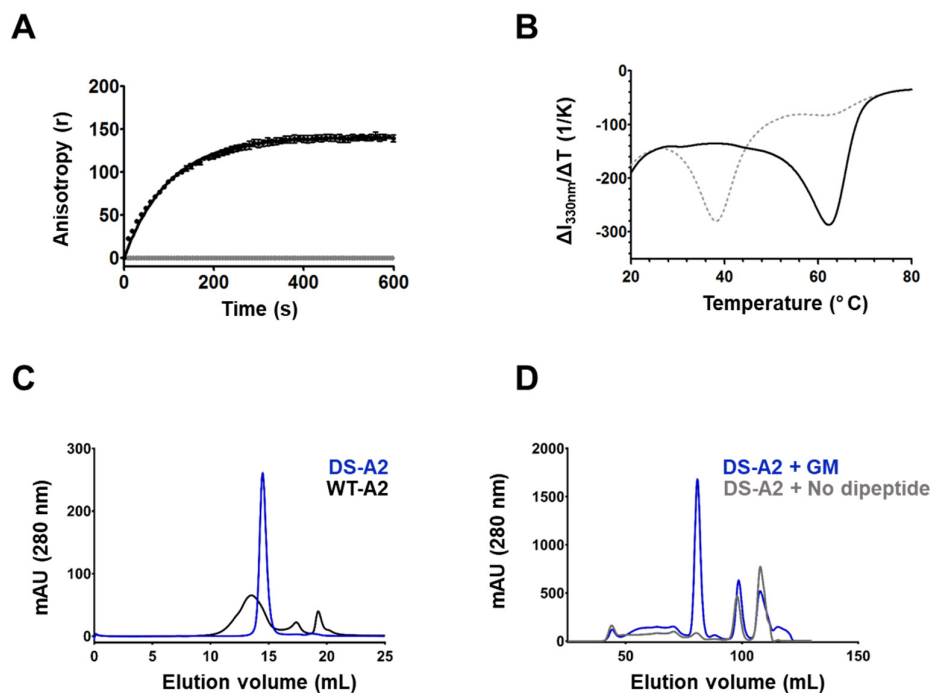


Figure. S6-3. Peptide binding measurements and comparative purification profiles.

(A) Peptide binding to wt-A2 molecules folded with the dipeptide GM measured by fluorescence anisotropy. 100 nM NLVPK_{FITC}VATV was added to wt-A2 molecules (folded with GM, but not purified), and binding kinetics were measured (black). Gray dots represent the anisotropy values of nonspecific binding. (B) Thermal stability of wt-A2 molecules folded with 10 mM GM (gray dotted line, T_m 39 $^{\circ}$ C), and 10 μ M NLVPMVATV (black line, T_m 62 $^{\circ}$ C). The minimum of each curve represents the T_m . Each sample was analyzed in duplicate. (C) Size exclusion chromatography (SEC) profiles of dsA2 and wtA2 folded with dipeptide GM. (D) SEC profiles of dsA2 folded with and without dipeptide GM.

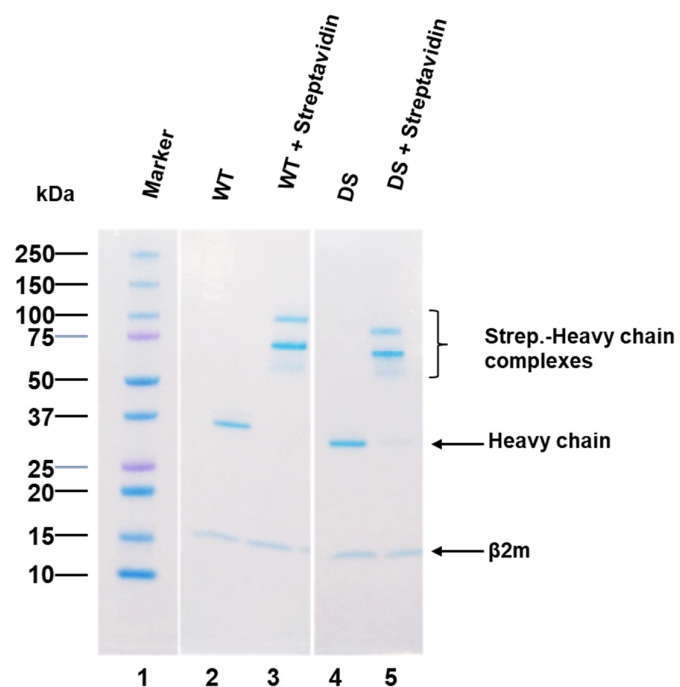


Figure. S6-4. Purity and biotinylation efficiency.

Electrophoretic mobility shift assay comparing biotinylation and purity of WT and dsA2 molecules. wtA2 molecules were folded with a UV-ligand and dsA2 molecules were folded with dipeptide GM. After purification, 2 μ g of each protein incubated with and without 4 μ g of streptavidin for 30 minutes, followed by SDS-PAGE analysis.

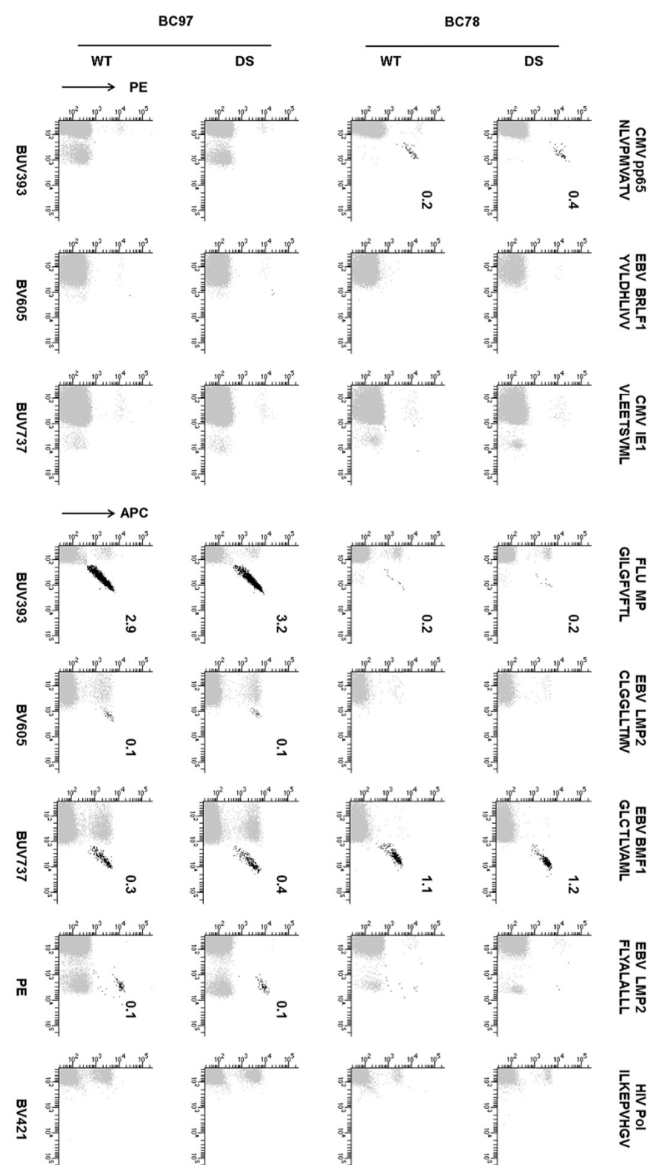


Figure. S6-5. Detection of virus-derived antigen-specific T-cells from donor PBMCs in a combinatorial encoding strategy.

pMHC multimers generated from pMHC monomers prepared from empty dsA2 molecules and wt-A2 molecules (UV-mediated peptide exchange process). Numbers on dot plots represent frequency of identified multimer-positive T-cells (percentage of total CD8⁺ T-cells).

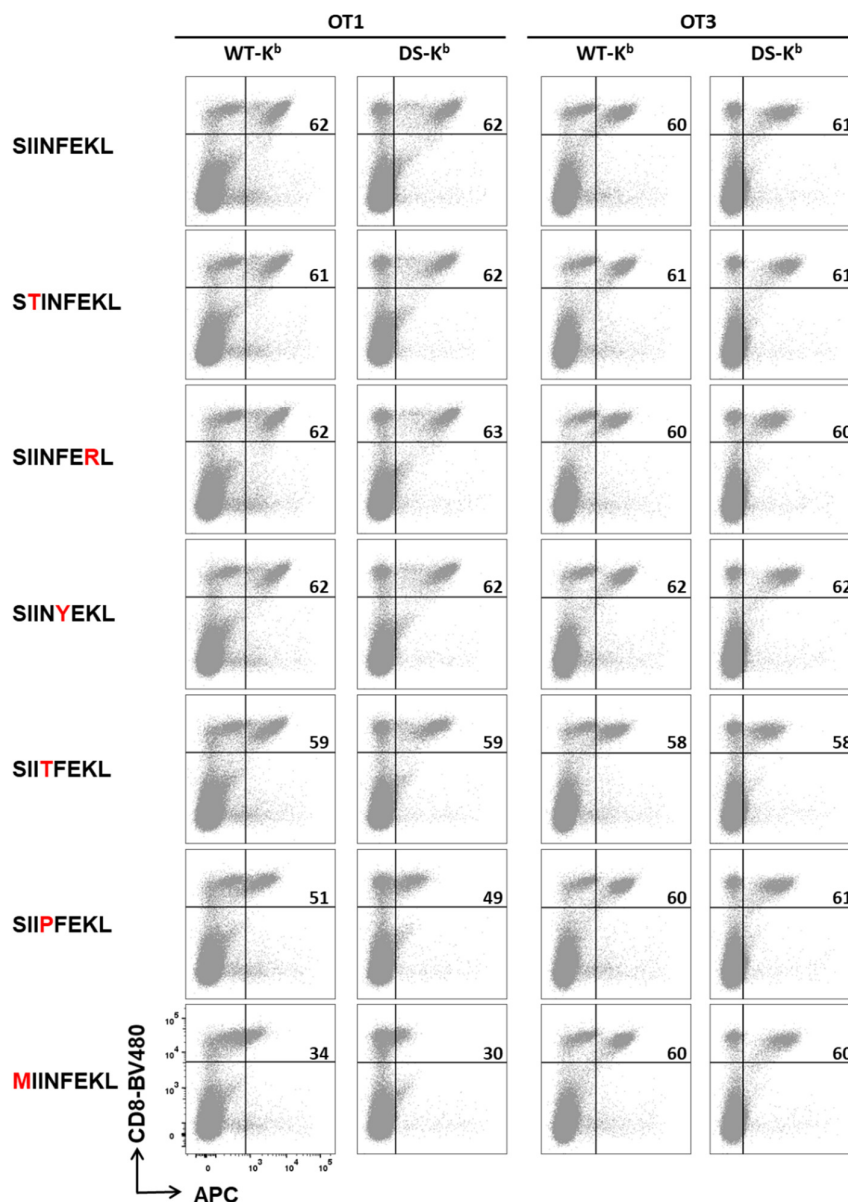


Figure. S6-6. Detection of low-avidity pMHC-TCR interactions using dSK^b multimers.

Dot plots showing comparative T-cell detection efficiency (OT1 and OT3 cells) of WT and dSH2-K^b tetramers. Seven different peptides, modified with single-residue change (highlighted in red) from SIINFEKL (OVA) peptide, shown to have high to low pMHC-TCR avidity were used to generate pMHC multimers using WT (using UV exchange) or DS-H2-K^b. Numbers on dot plots represent frequency of identified multimer-positive T-cells (percentage of total CD8⁺ T-cells).

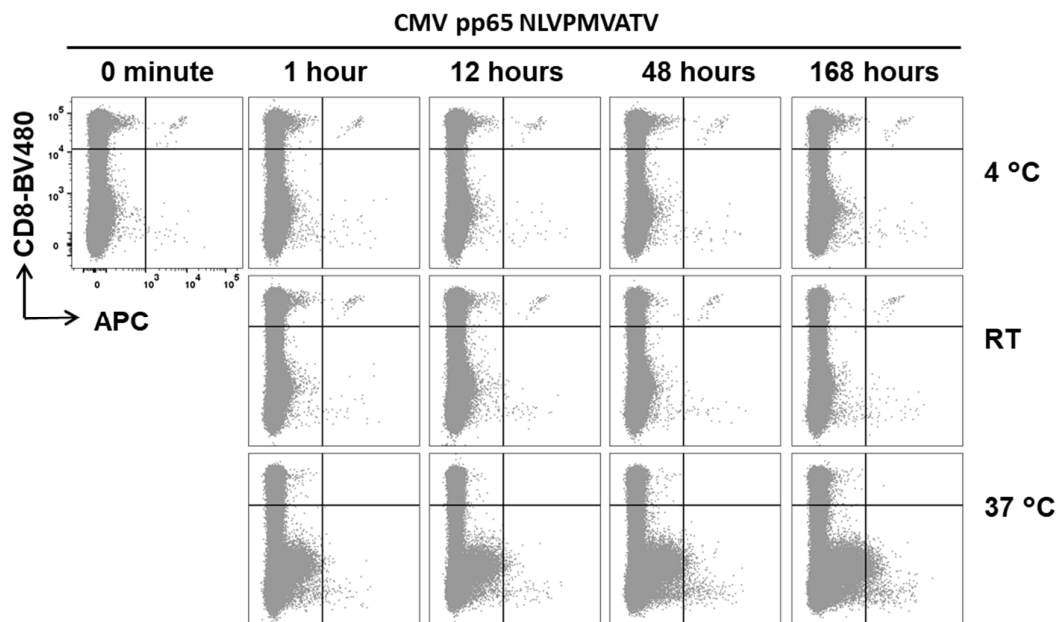


Figure. S6-7. T-cell detection plots for the stability analysis of dsA2 empty-loadable tetramers.

Dot plots of CMV pp65 NLVPMVATV-specific T-cells detected by pMHC multimers prepared after dsA2 empty-loadable tetramers were incubated at different time points and temperatures.

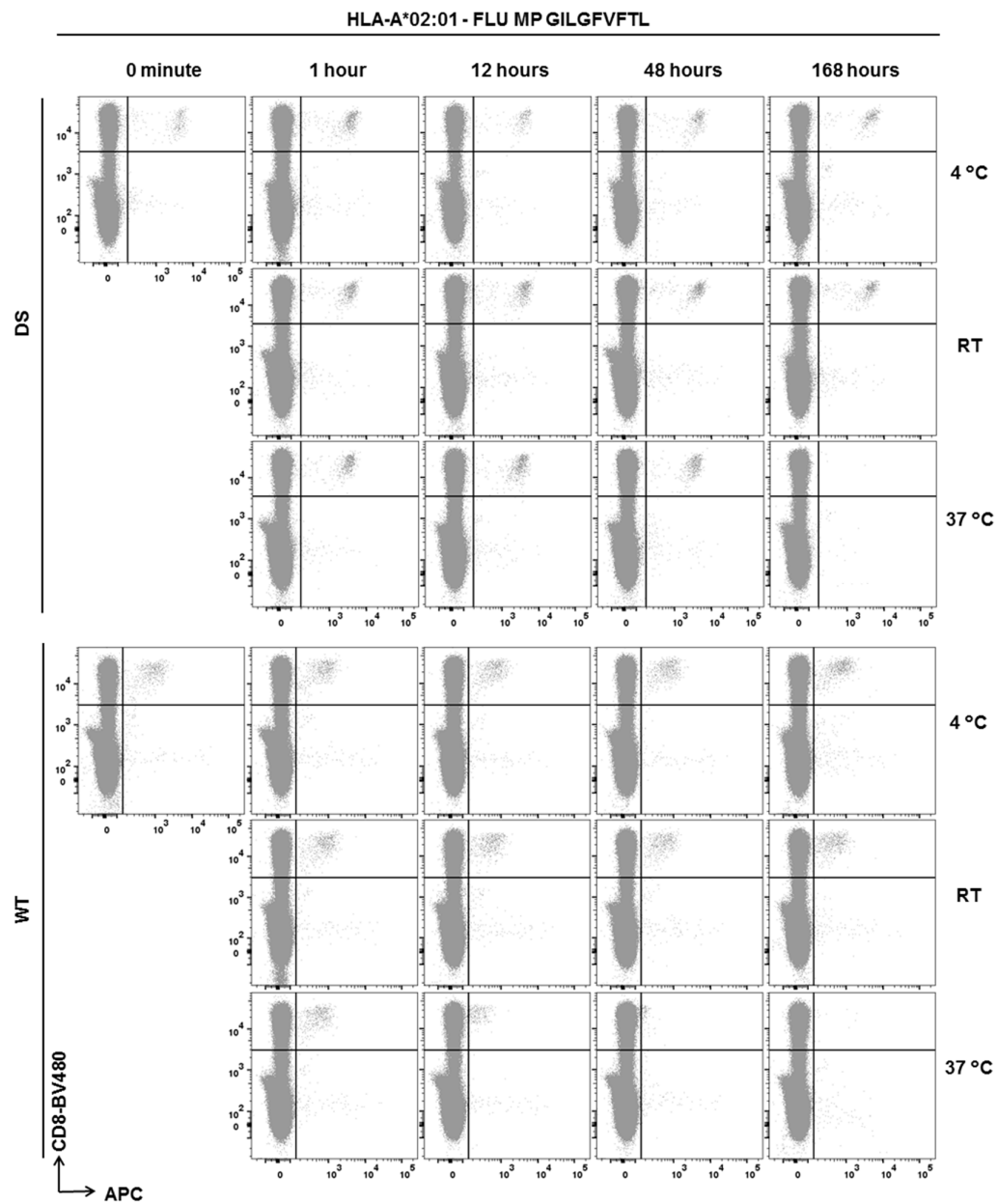


Figure. S6-8. T-cell detection plots of peptide dissociation analysis.

Dot plots of FLU MP GILGFVFTL-specific T-cells detected by pMHC multimers prepared by wt-A2 or dsA2 at different time points and temperatures after removing excess peptide.

Chapter 7. Use of empty disulfide-stabilized A2 molecule for the high-throughput screening of TCR ligands.

In this published manuscript, we provide a high throughput method for screening TCR ligands using empty dsA2 molecules.

Andreas Moritz, our collaborator at Immatix biotechnologies GmbH, was responsible for the majority of the experimental data. For this manuscript, I have performed the *in vitro* peptide binding assay by fluorescence anisotropy (Figure S7.2) to analyze the peptide receptiveness of dsA2 molecules when stored for different duration at -80°C. Rob Meijers and Maria Garcia-Alai, our EMBL Hamburg collaborators, analyzed the crystal data and generated the figure 7.3. The manuscript was written by Andreas Moritz, Dominik Maurer, and Sebastian Springer.

The full citation of the paper is:

Moritz A, Anjanappa R, Wagner C, Bunk S, Hofmann M, Pszolla G, Saikia A, Garcia-Alai M, Meijers R, Rammensee HG, Springer S, Maurer D. **“High-throughput peptide-MHC complex generation and kinetic screenings of TCRs with peptide-receptive HLA-A*02:01 molecules”**

(2019) *Science Immunology*, Jul 19; vol. 4(37)

Online link: <https://doi.org/10.1126/sciimmunol.aav0860>

The figure numbers were changed to match the format of this thesis.

7.1. Abstract

Major histocompatibility complex (MHC) class I molecules present short peptide ligands on the cell surface for interrogation by cytotoxic CD8⁺ T cells. MHC-I complexes presenting tumor-associated peptides like neoantigens represent key targets of cancer immunotherapy approaches currently in development, making them important for efficacy as well as safety screenings. Without peptide ligand, MHC-I complexes are unstable and decay quickly, making the production of soluble monomers for analytical purposes labor intensive. We have developed a disulfide-stabilized HLA-A*02:01 molecule that is stable without peptide but can form peptide-MHC complexes (pMHC) with ligands of choice in a one-step loading procedure. We illustrate the similarity between the engineered mutant and the wild type variant with respect to affinity of wild type or matured high-affinity TCRs and present a crystal structure corroborating the binding kinetic measurements. In addition, we demonstrate a high-throughput binding kinetics measurement platform to analyze the binding characteristics of bispecific TCR molecules (bsTCR) against diverse pMHC libraries produced with the disulfide-stabilized HLA-A*02:01 molecule. We show that bsTCR affinities for pMHCs are indicative of *in vitro* function and generate a bsTCR binding motif to identify potential off-target interactions in the human proteome. These findings showcase the potential of the platform and the engineered HLA-A*02:01 molecule in the emerging field of pMHC-targeting biologics.

7.2. Introduction

Presentation of peptides on cell surface MHC molecules plays a fundamental role for the immune response against viral infection or cancer [1]. MHC-I molecules are trimeric complexes that consist of a polymorphic HC, the light chain beta-2 microglobulin (β_2m) and a peptide ligand, typically between 8 and 10 amino acids long and derived from cellular proteins by degradation. T cells can recognize specific peptide-MHC complexes with their T cell receptor (TCR) and initiate an immune response.

Soluble pMHCs were first generated using protein expression and refolding techniques in 1992 and have since found use for many immunological research applications, e.g. identification of antigen-specific T cells through flow cytometry or affinity measurements of pMHC-TCR interactions [2–5]. The binding affinity of TCRs for their cognate pMHC has a substantial impact on the functionality of T cells [6]. Thus, efforts have been made to increase the affinity of TCRs for clinical applications [7]. Extensive maturation experiments have produced TCRs with picomolar affinities, a range typically found only in antibodies. They bind specific pMHCs with a long interaction half-life and have attracted attention as tumor cell engaging component in bi-specific T cell engager formats [8,9].

A potential downside of TCR binding affinity enhancement is the introduction of off-target toxicities. These can occur by unintentionally increasing the affinity towards other pMHCs in parallel to the target, due to the inherent cross-reactivity of TCRs [10]. Multiple cases of cross-reactivity have been reported in clinical studies [11–13]. Comprehensive screening is therefore necessary to not only ensure efficacy but also specificity and safety of therapeutic candidates [14]. This is a task of high complexity given the currently established size of the immunopeptidome, with at least 150,000 MHC-I ligand peptides identified by mass spectrometry [15].

We here present a disulfide-stabilized and peptide-receptive HLA-A*02:01 molecule (dsA*02:01) that can be produced as a functionally-empty molecule and form pMHC complexes in a simple one-step peptide loading procedure, allowing high-throughput pMHC generation. We show that pMHCs generated using this modified MHC molecule are representative of the wild type with respect to their interactions with TCRs. We also present a high-throughput pMHC-bsTCR binding kinetics measurement platform that uses dsA*02:01 to generate large libraries of pMHC complexes for screening against affinity-enhanced bsTCRs. We generate a comprehensive pMHC-bsTCR binding motif with this platform and use it to identify potential off-target pMHC interactions.

7.3. Results

7.3.1. Design and production of disulfide-stabilized HLA-A*02:01 molecules

Molecular dynamics simulations of empty and peptide loaded MHC-I molecules have indicated an increased mobility in the F pocket, the region that typically accommodates the C terminus of peptide ligands, in absence of bound peptide [16]. In previous studies with the mouse MHC-I molecule H-2K^b, introduction of a disulfide bond between opposing residues in the F pocket, by mutating a tyrosine at position 84 and an alanine at position 139 to cysteines, resulted in the stabilization of the complex. The mutant could be refolded as empty MHC molecule and was capable of binding peptide ligands [17,18].

We hypothesized that the same concept could be applied to the human MHC-I molecule HLA-A*02:01. The modifications were introduced into an HLA-A*02:01 HC expression plasmid, produced as inclusion bodies in *E. coli*, and incubated with similarly produced β_2m , and the dipeptide GM (**Figure 7-1 A**). This dipeptide has a very low affinity for the MHC-I complex and assists the refolding [19]. During size exclusion chromatography (SEC) it dissociates quickly from the binding pocket by buffer exchange against the running buffer, yielding purified and presumably empty disulfide-stabilized HLA-A*02:01 (dsA*02:01).

While the absence of the dipeptide in the final product couldn't be confirmed directly due to its small size, indirect evidence supports the assumption that the peptide-binding pocket of the disulfide-stabilized molecule is indeed empty. Thermal stability analysis of the dsA*02:01 molecule with and without dipeptide removal through buffer exchange revealed a lower melting temperature of the former, supporting the hypothesis that the complex stabilizing dipeptide had dissociated (Saini et al., in submission at Science Immunology). Wild type A*02:01 complexes (wtA*02:01) can also be produced with the dipeptide but denature when attempting to remove the dipeptide by buffer exchange. Taken together, we demonstrate that dsA*02:01 can be produced in a stable and presumably-empty state through introduction of the disulfide bond.

7.3.2. Analyzing binding kinetics using soluble TCRs and wild type or disulfide-stabilized MHC complexes

Next, we investigated whether the presumably-empty HLA molecule could also be regarded as functionally-empty, specifically whether the molecule was capable of peptide-MHC complex formation and TCR ligand binding. Binding kinetics measurements were performed by bio-layer interferometry (BLI) on an Octet RED384 using the refolded TCR 1G4 as soluble analyte. This TCR recognizes the HLA-A*02:01 specific peptide SLLMWITQC (ESO 9C) derived from the cancer

testis antigen NY-ESO-1 or its synthetic variant SLLMWITQV (ESO 9V) [20,21]. Biotinylated dsA*02:01 was immobilized on streptavidin-coated biosensors, either directly in its empty state or after 5 minutes of incubation with the peptide ESO 9V (**Figure 7-1 B**). Kinetics were measured across multiple 1G4 concentrations and wild type HLA-A*02:01 directly refolded with ESO 9V served as control.

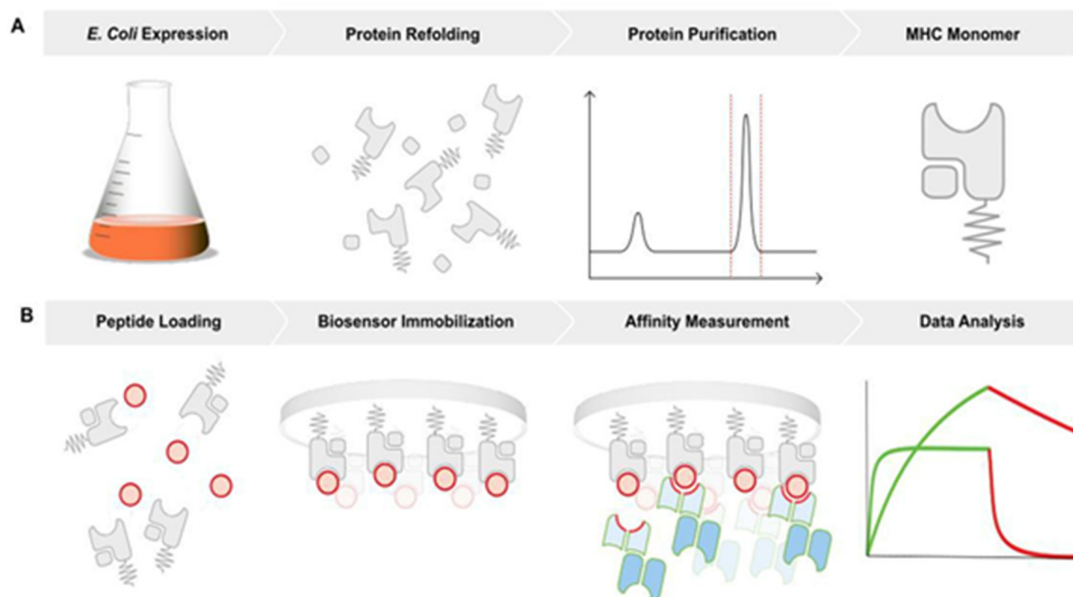


Figure 7-1. Overview of disulfide-stabilized HLA-A*02:01 production and usage for affinity measurements.

(A) Expression plasmids of HC and β_2m are transfected into *E. coli* and proteins of interest expressed in inclusion bodies. HLA monomers are purified using size exclusion. (B) Functionally-empty dsA*02:01 molecules can be loaded with peptide ligands by incubation at room temperature. For affinity measurements they can be immobilized on functionalized biosensors, e.g. by biotin streptavidin interaction, and used to record association and dissociation of TCRs or TCR-like molecules.

1G4 TCR binding to either dsA*02:01 9V or wtA*02:01 ESO 9V was very similar with respect to sensorgrams and dissociation constants (K_D) identified by curve fittings, indicating successful peptide loading as well as no interference of the disulfide bridge with TCR binding (**Figure 7-2, A, B**). A weak binding signal (but no dissociation) could be detected for the functionally-empty immobilized dsA*02:01 monomer at high concentrations of 1G4 (**Figure 7-2 C**) which was not observed when loaded with peptide not recognized by 1G4, such as SLYNTVATL (**Figure 7-2 D**). The weak signal obtained with functionally-empty dsA*02:01 might be explained by unspecific interactions of the TCR at high concentrations with the empty binding pocket, a state that is typically not encountered by TCRs *in vivo*. Other A*02:01 restricted soluble TCRs with varying specificities behaved similarly, showing no binding to irrelevantly loaded dsA*02:01 pMHCs but association to

functionally-empty molecules, albeit but with a relatively lower response (**Figure S7-1**). dsA*02:01 can be stored for a least a year at -80°C and no degradation or impaired peptide receptiveness could be detected compared to fresh preparations (**Figure S7-2**).

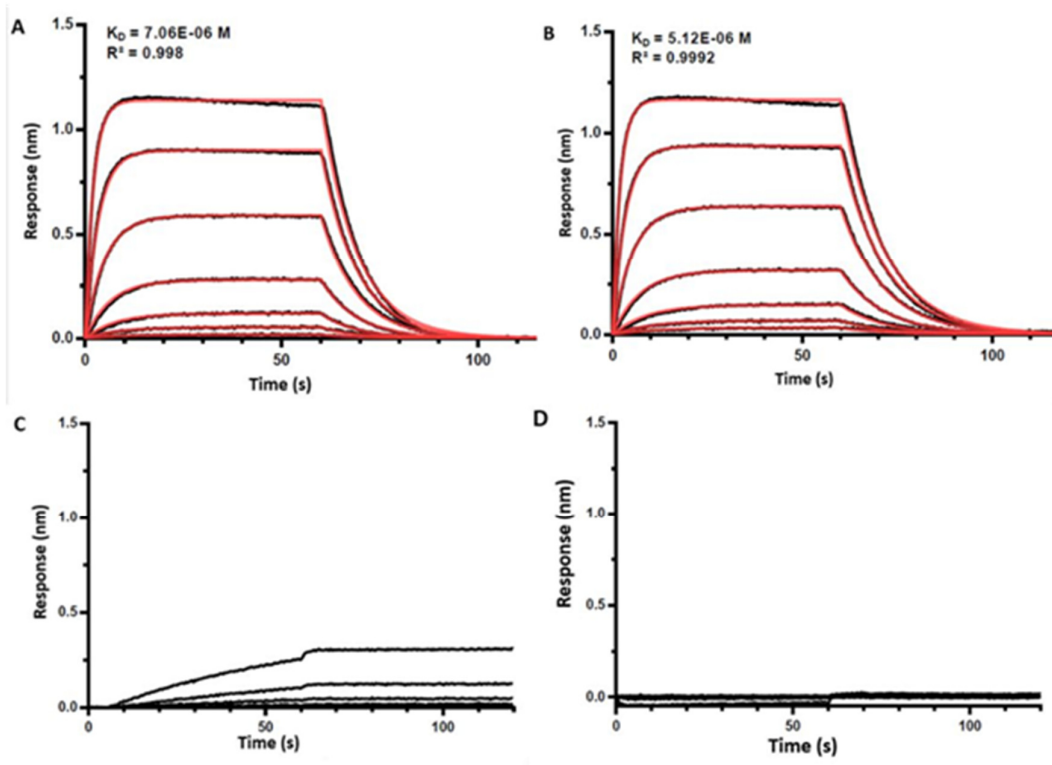


Figure 7-2. Association and dissociation behavior of 1G4 TCR with different pMHC complexes.

Raw data is displayed in black, curve fittings in red. All measurements performed as 1:2 analyte dilution series starting at 24 μ M. (A) Binding curve of the 1G4 TCR against immobilized ESO 9V dsA*02:01 pMHC. (B) Binding curve of the 1G4 TCR against immobilized ESO 9V wtA*02:01 pMHC. (C) Binding curve of the 1G4 TCR against immobilized empty dsA*02:01. (D) Binding curve of the 1G4 TCR against immobilized SL9 dsA*02:01 pMHC.

7.3.3. Crystal structure of the 1G4 dsA*02:01 ESO 9V TCR-pMHC complex

To further confirm that the 1G4 TCR recognizes ESO 9V dsA*02:01 indistinguishably from ESO 9V wtA*02:01, TCR and disulfide-stabilized MHC refolded with ESO 9V were co-crystallized as reported previously for the wild type ESO 9V HLA-A*02:01 molecule and analyzed by X-ray crystallography (**Table S7-1**) [21]. Comparison of the crystal structures revealed a high degree of structural overlap between both complexes. The backbone of both HLA-A*02:01 molecules aligned almost perfectly with a rmsd value of 1.14 Å calculated over C_{α} (**Figure 7-3A**). The same was true for both bound peptides

including their side chains with a rmsd value of 1.27 Å calculated over all atoms, even when in close vicinity to the disulfide bond (**Figure 7-3B**).

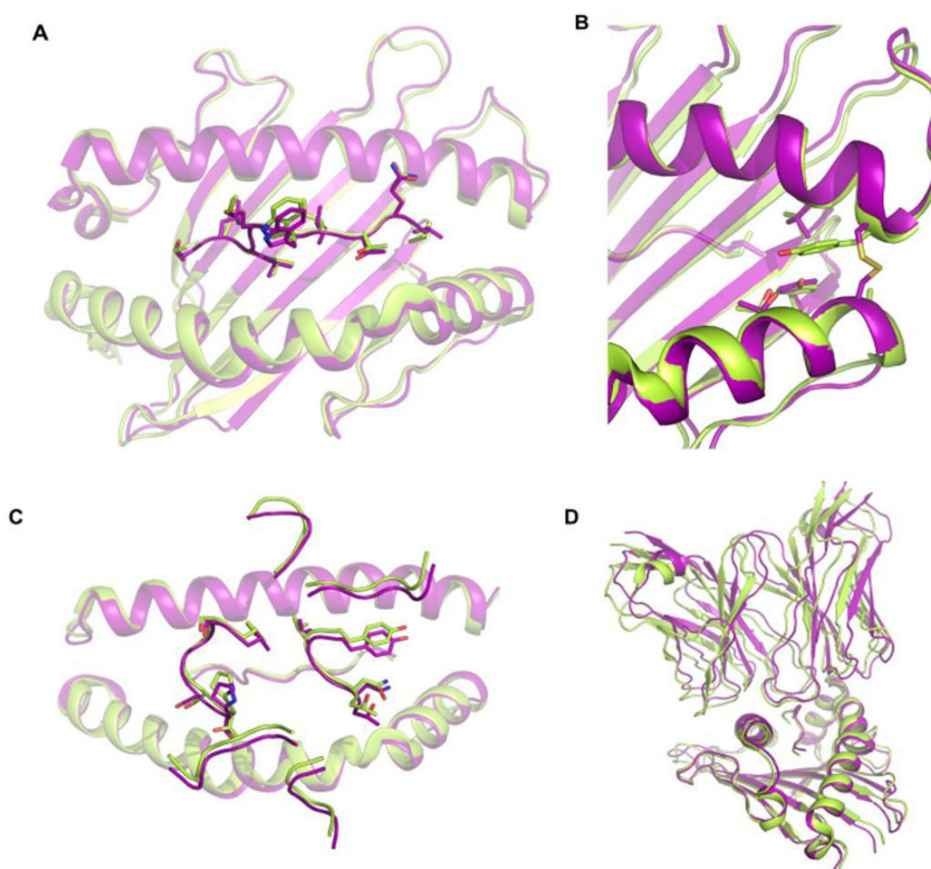


Figure 7-3. Crystal structure of ESO 9V dsA*02:01 and ESO9V wtA*02:01 in complex with 1G4.

(A) Overlay of WT and dsA*02:01 structure with focus on peptide and amino acid side chain orientation. (B) Close-up of the F-pocket and the introduced disulfide bond between α_1 and α_2 . (C) Overlay of the 1G4 CDR loops interacting with the peptide and the MHC backbone. (D) Overlay of both crystal structures from a lateral perspective.

Similar conclusions could be made for the interaction with the 1G4 TCR. The CDR loop regions interacting with the peptide and the MHC backbone did show slight deviations of the interface and a small change in the docking angle of 4.13° , when comparing wtA*02:01-1G4 with the dsA*02:01-1G4 crystal structure. This shift was still within the range of expected deviations for the same complex when crystallized repeatedly (**Figure 7-3 C, D**).

Taken together, determined binding affinities and crystal structure showcase peptide-receptiveness and similar properties of the dsA*02:01 pMHCs compared to wild type complexes with respect to TCR binding.

7.3.4. TCR binding affinities to peptide libraries displayed using wild type or disulfide-stabilized MHC complexes

Having established the application of the dsA*02:01 molecule as ligand equivalent to wtA*02:01 for unmodified TCRs, we wanted to expand this analysis towards mutated high-affinity TCRs and a larger number of peptide ligands. To this end, we employed the bsTCR bs-868Z11-CD3 as a second analyte. This molecule is comprised of the single chain TCR (scTv) 868Z11, an affinity matured TCR recognizing the HIV p17 Gag (77-85) derived and HLA-A*02:01 presented peptide SLYNTVATL (SL9) with antibody-like affinity, linked to a humanized anti-CD3 antibody functioning as T cell engaging domain (**Figure S7-3** [8,22,23])

First, binding kinetics measurements were performed to measure binding of bs-868Z11-CD3 to the SL9 pMHC complex. Empty or SL9 peptide-loaded dsA*02:01 molecules were immobilized on streptavidin biosensors and kinetics measured with soluble bs-868Z11-CD3. Binding affinity for SL9 dsA*02:01 pMHC was similar to the SL9 wtA*02:01 pMHC with 2.35 nM and 3.24 nM, respectively (**Figure 7-4, A and B**). Weak binding was measurable to functionally-empty MHC molecules but not for irrelevantly loaded dsA*02:01 complexes at a high molar concentration of 13.3 μ M (**Figure S7-1**). Next, we analyzed bs-868Z11-CD3 binding affinities towards a positional scanning library based on the SL9 peptide sequence. This library was created by exchanging an amino acid at one position of the wild type SL9 peptide against the 18 remaining proteinogenic amino acids while maintaining all other positions, resulting in 162 distinct peptides when performed at all positions of the nonamer (cysteine was excluded because of its propensity to dimerize) [24]. pMHC complexes were generated either by addition of peptide to empty dsA*02:01 molecules, or by performing an UV light-mediated peptide ligand exchange, a construct also capable of pMHC generation after initial refolding [25]. Respective pMHC complexes were immobilized on streptavidin biosensors, and kinetics were measured at two different bs-868Z11-CD3 concentrations. As expected, using alternated peptide ligands resulted in a wide range of different pMHC-bsTCR binding affinities, ranging from undetectable within the sensitivity range to equally strong compared to the interaction with the SL9 pMHC.

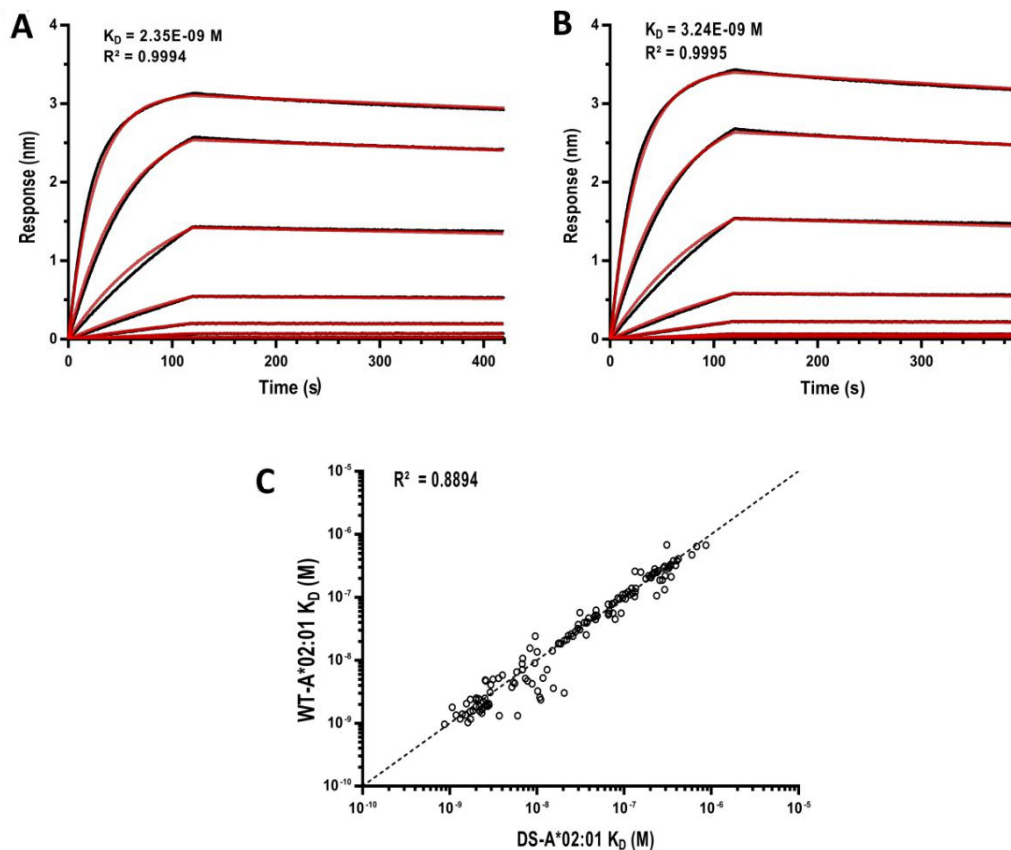


Figure 7-4. Affinities of the SV9 specific bs-868Z11-CD3 bsTCR with different MHC monomers and peptide ligands.

(A) Binding curve of bs-868Z11-CD3 against immobilized SL9 dsA*02:01 pMHC. Raw data is displayed in black, curve fittings in red. Measured using 1:2 analyte dilution series starting at 500 nM. (B) Binding curve of bs-868Z11-CD3 against immobilized SL9 wtA*02:01 pMHC. Raw data is displayed in black, curve fittings in red. Measured using 1:2 analyte dilution series starting at 500 nM. (C) Correlation between affinities measured using dsA*02:01 pMHCs or wtA*02:01 pMHC complexes generated using UV-exchange. KDs were plotted for 140 different peptide ligands generated using both methods and measured during successive experiments. KDs were fitted using 500 nM and 158 nM analyte concentrations. Peptides were included if peak signal levels reached at least 0.05 nM for both concentrations and individual fits had a R^2 above 0.9. The in-picture R^2 is the calculated correlation coefficient, dashed line represents optimal 1:1 ratio.

For direct comparison, all measured pMHC complexes were selected that had evaluable curves at both analyte concentrations and curve fitting results accompanied by R^2 values of at least 0.9. K_D values for the resulting 140 peptide ligands correlated well across the whole range (Figure 7-4 C). Discrepancies

were within 2-fold range for over 90 % of the pMHC pairs and 6.82-fold differences at most. Within the group with higher than 2-fold changes, a trend towards a larger dissociation constant for measurements with the dsA*02:01 molecule was observed. The amount of functional pMHC

immobilized on each biosensor expressed by the reported R_{max} value was equally comparable for both wild type and disulfide-stabilized pMHCs (**Figure S7-4**).

7.3.5. High-throughput pMHC-bsTCR kinetics screenings for binding motif generation

Quick and flexible generation of pMHC complexes is a key requirement to facilitate the collection of large binding affinity datasets against many different pMHCs. One example of such datasets is screening of the presented positional scanning library to generate a pMHC-bsTCR binding motif, which can serve as one component in a bsTCR safety screening approach. To perform such measurements, the pMHC should ideally be used as a soluble analyte as this offers multiple advantages: First, immobilizing the same ligand with known activity repeatedly, for example a bsTCR, allows better interpretation of the fitting results, especially the reported R_{max} value. Secondly, it enables quicker and much more cost effective high-throughput screenings, as a broad variety of regenerable biosensors capable of repeatedly immobilizing bsTCRs exists. Thirdly, immobilizing the bsTCR is the only orientation available for measuring monovalent affinity when a bsTCR or antibody has of multiple pMHC binding moieties, as only avidity could be measured with immobilized pMHCs.

While the UV-mediated peptide ligand exchange offers similar throughput, its exchange efficiency is dependent on rapid complex stabilization by the new peptide during the UV exposure. Especially lower affinity peptides can fail to do so, resulting in a decreased functional pMHC concentration after the exchange which can be detected using an anti-b2m ELISA assay (**Figure S7-5a**). This makes it a less reliable tool to produce pMHCs as soluble analytes for binding kinetics, since precise knowledge of the concentration is necessary to obtain correct curve fitting results. Because the functionally-empty dsA*02:01 molecule is stable without peptide, it offers less restrictions in this specific context: When added and kept in appropriate peptide concentration to saturate the MHC complexes, the effective concentration of pMHC can be expected to be equal to that of dsA*02:01 initially supplied. Direct comparison of selected peptides from the positional scanning library prepared as soluble analytes, either through dsA*02:01 peptide loading or UV-exchange, did show decreased binding signals with UV exchange preparations for lower affinity peptides, indicative of a reduced functional pMHC content (**Figure S7-5a**). This would have resulted in improper curve fittings and incorrect affinity constants (**Figure S7-5b**). Accurately measuring bsTCR affinities for such peptides can be important in the context of binding motif generation, as these substitutions may result in relevant MHC binders when combined with substitutions at other positions. Tolerance of these amino acids by the bsTCR should thus be reflected correctly in a comprehensive binding motif.

By immobilizing the bs-868Z11-CD3 bsTCR on a regenerable Anti-F(ab) sensor, we were able to analyze the positional scanning library at 4 different soluble pMHC concentrations for each peptide ligand, ranging from 500 to 15.8 nM, within 4 hours of unattended measurement time and with 20-fold reduced cost compared to a matching pMHC immobilization setup. This measurement resulted in an informative pMHC-bsTCR binding motif (Figure 7-5A, Table S7-2). Soluble dsA*02:01 pMHC preparations can be stored for at least 2 weeks at 4°C without loss of quality and used for multiple analysis (Figure S7-6).

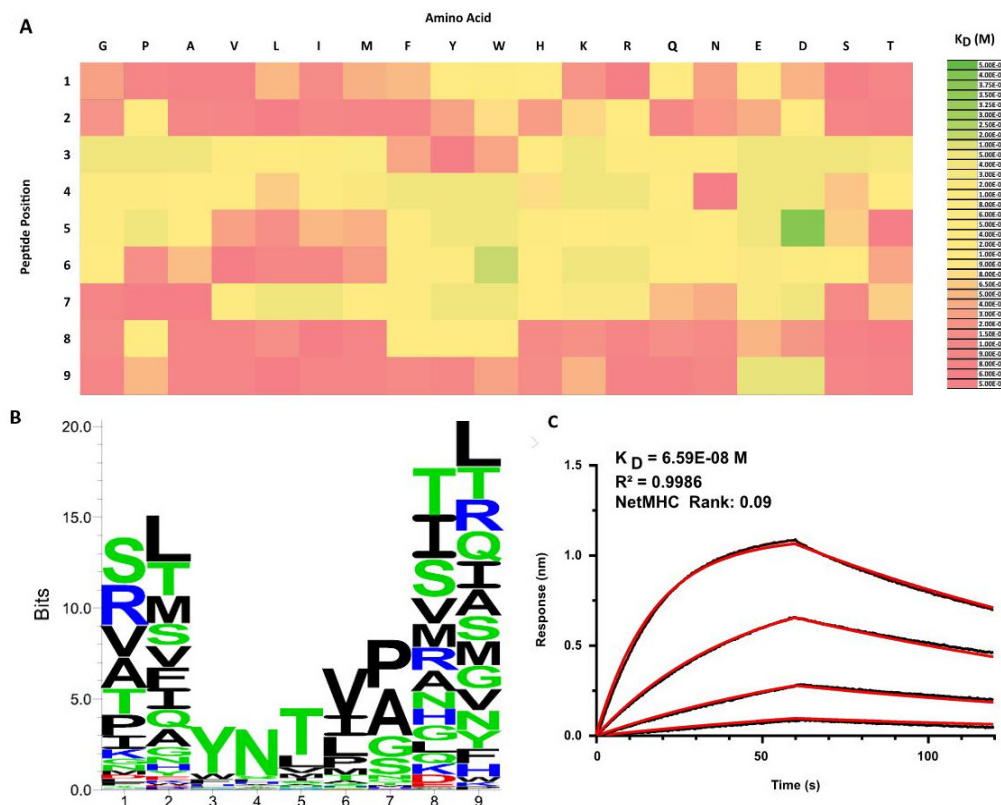


Figure 7-5. Binding motif of bs-868Z11-CD3 generated using dsA*02:01 generated positional scanning library as soluble analyte and immobilized bsTCR.

Measurements were performed using four soluble analyte concentrations. Interactions without fitable curves were assigned a KD of 5 μ M. Soluble analyte concentration range produced by 1/ analyte dilution series starting at 500 nM. (A) Heat map depicting bs-868Z11-CD3 affinities for the respective SLYNTVATL mutants from the positional scanning library. (B) Visualization of the binding motif as seq2logo graph. Size of individual letters inversely represents measured affinity for the respective amino acid at this position, calculated using the inverse KD value divided by 108 and the PSSM-Logo algorithm. (C) Binding curve of bs-868Z11-CD3 bsTCR against ALYNVLAKV dsA*02:01 pMHC. Measured using 1/ analyte dilution series starting at 500 nM. Raw data is displayed in black, curve fittings in red.

The 868Z11 bsTCR displayed an expected pattern of recognition for a T cell receptor: changes of amino acids between positions 3 and 7 of SLYNTVATL, the region that directly interacts with the CDR3 loops of the scTv, had the biggest influence on bsTCR binding affinity. Replacements at these positions retaining strong binding were only possible with the few amino acids sharing the physiochemical characteristics of the parental amino acid. This behavior can also be graphically illustrated when visualizing the binding motif as Seq2Logo graph (**Figure 7-5 B**) [26].

These results demonstrate that pMHC complexes can be generated quickly with the peptide-receptive dsA*02:01 MHC molecule and are suitable as soluble analytes for high-throughput pMHC-bsTCR binding kinetics screenings.

7.3.6. Identification of peptide ligands cross-reactive with bs-868Z11-CD3

We further wanted to demonstrate that we could use the generated binding motif to identify cross-reactive peptide ligands from the human proteome. We created a peptide ligand search motif from the binding affinity dataset by introducing an exemplary K_D threshold of 50 nM: all single amino acid substitutions increasing the bs-868Z11-CD3 K_D above that threshold were excluded from the motif (**Table S7-3**). Based on this motif, we performed a search in the NCBI human non-redundant protein sequence database for nonamer sequences matching combinations allowed by the motif. The search identified over 400 hits within the proteome, with sequence identity to the wild type sequence SLYNTVAL ranging from 1 to 6 identical positions. 140 peptides were selected, sampled to be representative of the sequence identity distribution in the larger group, synthesized and used for binding kinetics measurements (**Table S7-4**). We were able to detect affinities of single digit μ M K_D s or larger for 91 of those peptides.

One of them, ALYNVLAKV, was worth of special notice as it is presented on the cell surface of multiple human tissue samples according to the XPRESIDENTTM immunopeptidomics database. This database combines quantitative HLA peptidomics based on LC-MS analysis and quantitative transcriptomics provided by RNAseq from healthy tissues and tumor tissues to identify peptides presented exclusively or predominately on tumor tissue [27,28]. ALYNVLAKV, an antigen from intermediate filament family orphan 1 or 2 (IFFO1/2), was detected on multiple healthy tissue and tumor tissue samples, ranging from head and neck, spleen, or kidney to non-small cell lung carcinoma or renal cell carcinoma. The K_D of the interaction was 65.9 nM (**Figure 7-5 C**). We were also able to identify a second LC-MS detected peptide, KTFNLIPAV, with a lower K_D of 413 nM which was previously detected on 3 tumor tissue samples.

Taken together, we show that pMHC-bsTCR binding motifs, generated with the high-throughput pMHC-bsTCR binding kinetics screening platform, can be used to identify cross-reactive peptide ligands which occur in the human proteome and have the potential be presented as pMHC complexes.

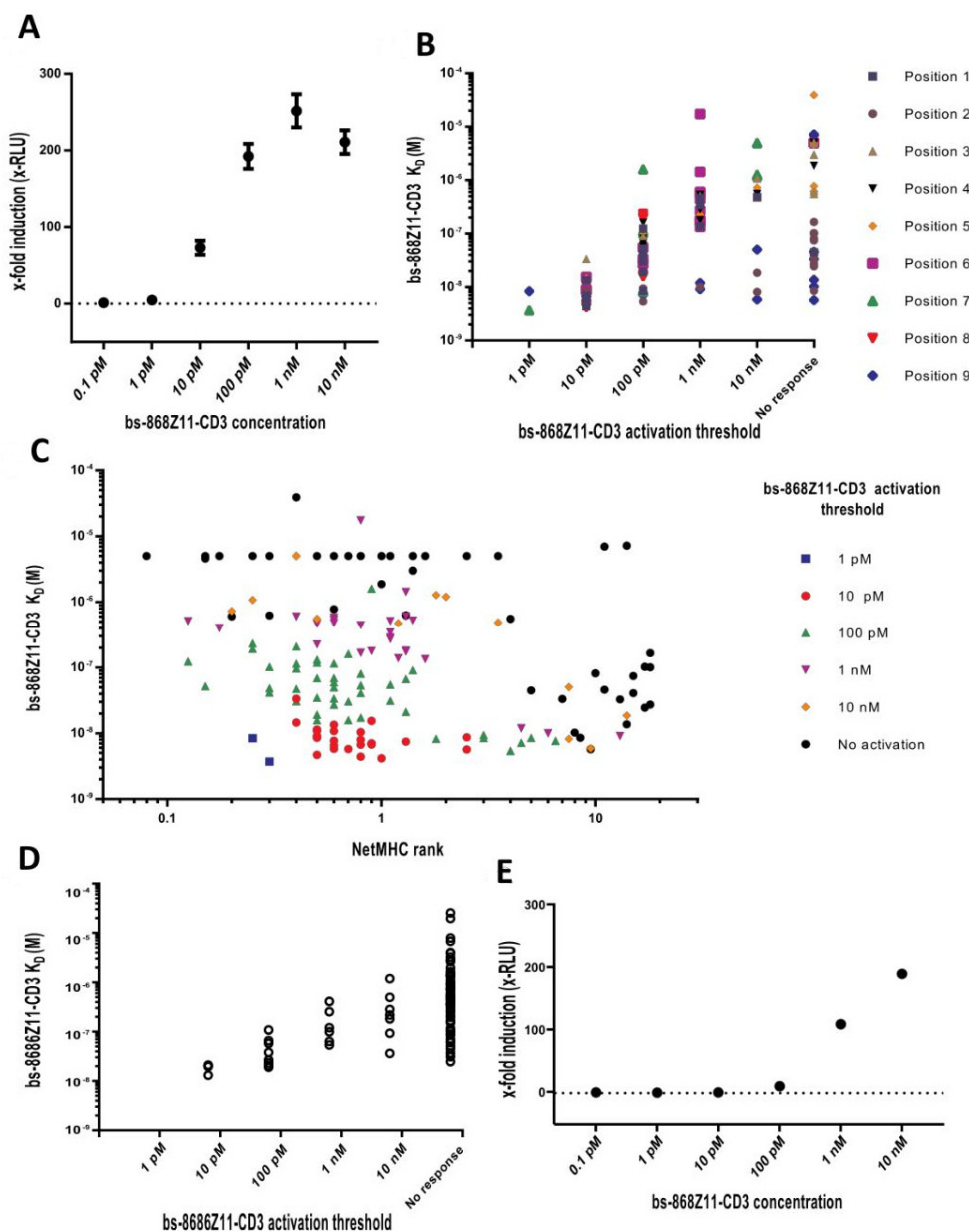


Figure 7-6. Result of coincubation assays with peptide-loaded target cells, Jurkat effector cells, and bs-868Z11-CD3 at six different concentrations.

(A) Measured fold-induction above background for Jurkat effector cells activated at different concentrations of bs-868Z11-CD3 against SL9 peptide-loaded T2 target cells. Error bars represent biological triplicates. (B) Measured binding affinities for peptide ligands from the positional scanning library and their respective bsTCR activation threshold, the lowest bsTCR concentration necessary to induce Jurkat effector cell activation 3-fold over background based on bioluminescence. Peptides are grouped based on the location of the exchange in the wild type sequence. (C) Measured binding affinities for peptide ligands from the positional scanning library and their respective NetMHC predicted binding rank. Peptides are grouped based on the bsTCR activation threshold. (D) Measured binding affinities for the cross-reactive peptide ligand candidates and their respective bsTCR activation threshold. (E) Measured fold-induction above background for Jurkat effector cells stimulated at different concentrations of bs-868Z11-CD3 against ALYNVLAKV peptide-loaded T2 target cells. Error bars represent biological triplicates.

7.3.7. Correlation of pMHC-bsTCR binding affinity with bsTCR-mediated T cell activation

While pMHC-bsTCR binding affinity can be measured quickly using this high-throughput screening platform, it should correlate with the *in vitro* activity of the functional T cell engaging bsTCR to be even more useful. Commonly, *in vitro* coin incubations of target and effector cells coupled with an appropriate readout are used to characterize these constructs. T2 cells, a TAP-deficient A*02:01 cell line with restorable pMHC presentation through exogenous peptide loading, were loaded separately with all peptides of the positional scanning library and the 140 selected peptides to serve as target cells. These were then incubated together with GloResponse™ NFAT-luc2 Jurkat effector cells, a cell line that expresses a luciferase reporter gene driven by a NFAT-response element, and different concentrations of bs-868Z11-CD3 [29,30]. Jurkat effector cell activation was detected after 18 hours by measuring bioluminescence.

We encountered a broad spectrum of activation levels against the positional scanning library, ranging from no detectable T cell activation with any bsTCR concentration to strong bioluminescence signals starting at low bsTCR concentrations, e.g. for the wild type peptide (**Figure 7-6 A**). Since EC50 values could not be determined for every interaction with the selected bsTCR concentration range, we categorized the individual peptides by their bsTCR activation threshold, defined as the lowest bsTCR concentration that was able to induce a 3-fold increased bioluminescence signal compared to the background. These values were plotted for each peptide against the previously identified K_D values (**Figure 7-6 B**).

Overall, we detected a robust connection between the binding affinities and Jurkat effector cell activation. We also identified one group of outliers with strong pMHC-bsTCR binding affinities but higher activation thresholds than expected when compared to the overall trend. For the peptides of this group, the activation threshold seemed increase in conjunction with decreasing peptide binding affinities for the MHC, based on predictions using the NetMHC 4.0 algorithm (**Figure 7-6 C**) [31].

This offered a potential explanation as different peptide binding affinities could result in different presentation levels of the respective pMHC complexes on the target cells after exogenous loading. These levels might in turn influence pMHC-bsTCR complex numbers and ultimately Jurkat effector cell activation. To corroborate the hypothesis, we performed a flow cytometric T2 peptide binding assay using an anti-HLA-A2 antibody and could indeed detect less elevated HLA-A2 surface levels after peptide loading for peptides with lower binding affinities, especially NetMHC ranks of 2 and above, supporting the initial hypothesis (**Figure S7**). Of the 140 peptide ligands selected by binding motif search, 24 were capable of inducing a 3-fold T cell activation over background with at least one of the supplied bsTCR concentrations (**Figure 7-6 D**). We found a similar connection between

binding affinities and T cell activation compared to the results obtained with the positional scanning library. The previously highlighted IFFO1 peptide ALYNVLAKV was also reactive in the reporter assay (**Figure 7-6 E**).

In conclusion, we show that pMHC-bsTCR binding affinity is a good indicator for the *in vitro* function of the 868Z11 scTv coupled with the used anti-CD3 T cell engager. This highlights the value of the pMHC-bsTCR binding kinetics screening platform as it allows quick but adequate characterization of bsTCR early in the development of such molecules.

7.4. Discussion

Here we present a disulfide-stabilized and functionally-empty HLA-A*02:01 molecule which can be refolded and purified without the use of typically required high affinity peptides. The resulting monomers can form peptide-MHC complexes after addition of peptides in a one-step loading procedure. Even though the disulfide bridge enhances the stability of the MHC molecule, introduction does not inhibit or significantly alter binding of TCRs to dsA*02:01 pMHC complexes compared to the wild type.

This represents a great tool to quickly produce large pMHC libraries that are suitable for affinity measurements. Combining dsA*02:01 produced pMHC libraries with BLI-based analysis results in a platform capable of high throughput pMHC-bsTCR binding kinetics screenings. This setup could also be useful for the analysis of other biologics targeting pMHCs, like monoclonal antibodies or bispecifics (e.g. BITEs).

In one application of this platform, we were able to quickly collect a pMHC-bsTCR binding affinity dataset for the HIV restricted bsTCR bs-868Z11-CD3. bsTCR binding affinities for respective pMHCs were indicative of *in vitro* activity when coupled with the presented T cell engager and tested in a cellular reporter assay, making these datasets valuable for bsTCR characterization. Analysis of the relationship between binding affinity and mediated cellular activation over a wide range of pMHC-bsTCR affinities has been difficult thus far as a result of the limited tools available to feasibly collect such datasets.

The collected binding motif revealed similarities to the binding motif of the wild type TCR 868: Analysis of an 868-SV9 crystal structure as well as an accompanying alanine scan by Cole et al. revealed prominent interactions between the CDR3 α region and the amino acids 4N and 5T of SLYNTVATL (32). Interestingly, this behavior seems to be conserved even though a significant part of the CDR3 α is mutated in the 868Z11 construct. Using the binding motif and a model search strategy, we were able to identify multiple peptides from the human proteome which demonstrated

high affinity interactions with the bsTCR and the potential to induce bsTCR mediated Jurkat effector activation when presented on target cells.

It should be noted that TCR binding motifs derived from single amino acids substitution libraries may still not reflect all possible peptides a specific TCR can recognize, as the exchange of multiple amino acids at the same time might have different effects than the isolated exchanges. Alternative approaches include screening of more complex libraries, for example through target cell loading with high diversity peptide pools, each randomized at all but one position of the peptide, or screenings against randomized peptide libraries presented as pMHC molecules on yeast surfaces (10, 33, 34). Further research directly comparing these approaches will be necessary to gain a deeper understanding of the respective strengths and weaknesses. Ultimately, safety screenings of clinical candidates should always be comprised of multiple approaches, for example by combining binding motif guided analysis together with cellular screenings of large panels of healthy tissue derived cell lines, to minimize risks.

Nevertheless, our results highlight the capability of this approach to identify potentially relevant off-target interactions in combination with the pMHC-bsTCR binding kinetics screening platform. Because it offers quick analysis of complex pMHC libraries, it can be used early in the development process to select promising candidates and thus complements established methods.

This platform can also facilitate larger and more comprehensive screenings of late stage candidates, potentially against mass spectrometry data-driven tissue-specific pMHC libraries covering the known immunopeptidome. Due to its stability and low-effort peptide loading procedure, the dsA*02:01 molecule could potentially enable even higher throughput platforms. Thanks to these properties, it could be perfectly suited for the creation of high complexity pMHC microarrays with thousands of different pMHCs, for example by combining large scale coating of dsA*02:01 and modern high-throughput peptide microarray inkjet printers.

7.5. Materials and method

7.5.1. Study design

The goal of this study was to test and characterize a newly developed disulfide-stabilized empty HLA-A*02:01 molecule as tool to generate large libraries of high-quality pMHC complexes and to demonstrate the its use case in a high-throughput kinetic screening platform for the screening of bispecific T cell engagers. Individual experiments were designed in accordance with current best practices to ensure validity and are discussed in context with the respective method.

7.5.2. Peptide synthesis

All peptides were generated in house using standard Fmoc chemistry with a Syro II peptide synthesizer. Peptides were subsequently analyzed using HPLC and had an average purity of 74 %. UV-light sensitive peptides contained a light-sensitive building block with a 2-nitrophenylamino acid residue. The dipeptide GM was procured from Bachem. Before use, peptides were dissolved in DMSO (Sigma, Cat. Nr. 41640), 0.5% TFA (Sigma, Cat. Nr. T6508) at concentrations ranging from 2 mg ml⁻¹ to 10 mg ml⁻¹ depending on the desired use case.

7.5.3. Generation of MHC complexes by refolding and purification

Recombinant HLA-A*02:01 wild type (wtA*02:01) or the HLA-A*02:01 disulfide mutant (dsA*02:01) HC with C-terminal BirA signal sequences and human β_2m light chain were produced in *Escherichia coli* as inclusion bodies and purified as previously described [2]. HLA-A*02:01 complex refolding reactions were performed as previously described with minor modifications [18]. In brief, wtA*02:01 or dsA*02:01 HC, β_2m light chain, and peptide were diluted in refolding buffer (100 mM Tris-Cl pH 8, 0.5 M arginine, 2 mM EDTA, 0.5 mM oxidized glutathione, 5 mM reduced glutathione) and incubated for 2 to 8 days at 4°C while stirring before concentration. The concentrated protein was purified by size exclusion chromatography (SEC) in 20 mM Tris-HCl, pH 8/150 mM NaCl on an ÄKTA prime system (GE Healthcare) using a HiLoad 26/600 200 μ g column (GE Healthcare). Peak fraction was either concentrated directly to 2000 μ g ml⁻¹, aliquoted and frozen at -80 °C or biotinylated by BirA biotin-protein ligase (Avidity) overnight at 4 °C according to the manufacturer's instructions and subjected to a second gel-filtration before final concentration to 2000 μ g ml⁻¹, aliquotiation and storage at -80 °C.

To produce wild type HLA-A*02:01 peptide-MHC complexes, full-length peptides or UV light-sensitive full-length peptides were added to the refolding buffer at a concentration of 30 μ M. To produce dsA*02:01 complexes, the dipeptide GM was added to the refolding buffer at a concentration of 10 mM.

7.5.4. Generation of peptide exchanged HLA-A*02:01 pMHC complexes using UV-mediated peptide ligand exchange or empty dsA*02:01 complexes

Peptide exchange reactions with UV light-cleavable peptides were performed as previously described. In short, desired nonamer peptides were mixed with biotinylated UV light-sensitive pMHC complexes at 100 to 1 molar ratio and subjected to at least 30 minutes of 366 nm UV light (Camag). Peptide loading reactions with empty dsA*02:01 MHC complexes were performed by

addition and mixing of desired peptides of at least a 100 to 1 molar ratio to the monomer solution and 5-minute incubation at room temperature.

7.5.5. Soluble TCR production

Soluble TCRs were produced as previously described [20]. In short, TCR alpha and TCR beta chain constructs were expressed separately in *Escherichia coli* as inclusion bodies and purified. TCR alpha chains are mutated at position 48 by replacing a threonine with a cysteine and TCR beta chains at position 57 by replacing a serine with a cysteine to form an inter-chain disulfide bond.

7.5.6. bsTCR design and production

The bs-868Z11-CD3 molecule was generated by linking the scTv 868Z11 to the C terminus of the F(ab')-domain of a humanised anti-CD3 antibody [22,23]. To this end, the V_{β} domain of the scTv was directly fused to the upper CH2 region derived from human IgG₂ (APPVAG). Cysteine-knock-outs C₂₂₆S and C₂₂₉S within the hinge prevent the formation of F(ab)₂ molecules. HCMV-driven expression vectors coding either for the construct described above or the light chain of the humanised anti-CD3 antibody were transiently co-transfected in ExpiCHO cells (Thermo). After 12 days, the supernatant was processed by tandem chromatography (protein L followed by preparative size exclusion, GE Biosciences), and highly pure monomeric bsTCR was formulated in PBS.

7.5.7. Crystallization and imaging

The dsA*02:01/SLLMWITQV complex and the 1G4 TCR were concentrated and mixed in a 1:1 ratio to achieve a concentration of 7 mg ml⁻¹ for crystallization. A sitting drop vapor diffusion experiment resulted in crystals in the presence of a mother liquor containing 0.1 M ammonium acetate, 0.1 M bis-tris pH 5.5, 17% PEG 10.000. A single crystal was transferred to a cryo-protectant solution containing 0.1 M ammonium acetate 0.1 M bis-tris pH 5.5, 20% (w/v) PEG 10.000, and 10% glycerol. The crystal was mounted and cryo-cooled to 100 K on the EMBL P14 beamline at DESY containing an EIGER 16M detector. An X-ray data set was collected to a resolution of 2.5 Ångström (**Table S1**). The data were processed with XDS and scaled with AIMLESS [32,33]. Molecular replacement was performed using MOLREP with the coordinates of the TCR portion of the native complex first, followed by the peptide/MHC complex (PDB id 2BNR), and the structure was refined with REFMAC5 [34,35]. The engineered disulphide bond was manually built with Coot [36]. The structure was refined to an R factor of 22.9% (Rfree 27.3%). Molprobit was used to validate the geometry and indicated 93.9% of the residues were in the allowed regions of the Ramachandran plot (with one glycine residue (Gly 143) in the disallowed regions) [37]

7.5.8. Octet RED384 based bio-layer interferometry binding kinetics measurements

The affinity of sTCR or bsTCR molecules for different pMHC complexes was measured on an Octet RED384 system (Pall Fortébio) using kinetic or steady state binding analysis. All analytes or ligands were diluted to their final concentration in kinetics buffer (PBS, 0.1% BSA, 0.05% Tween-20) if not specified otherwise. All biosensors were hydrated for at least 10 minutes in kinetics buffer before use. Loadings and measurements were performed in 384 tilted well plates (Pall Fortébio) with at least 40 μ l at a 3 mm sensor offset. Plate temperature was set at 25 °C and shaker speed at 1000 rpm. To allow inter-step correction, baselines before association phases and the following dissociation phase were performed in the same well. Kinetics buffer was used as dissociation buffer with DMSO at an appropriate concentration added if necessary, to match the analyte composition. In the case of pMHC immobilization, dip and read streptavidin (SA; Pall Fortébio Cat. Nr. 18-5021) biosensors were used to immobilize biotinylated pMHC monomers at a presumed concentration of 25 μ g ml⁻¹ for 60 seconds followed by a 60 seconds baseline and association and dissociation phases of 60 seconds each if not specified otherwise. In the case of bsTCR immobilization, dip and read anti-human Fab-CH1 2nd generation (FAB2G; Pall Fortébio Cat. Nr. 18-5127) biosensors were used to immobilize bsTCR molecules at a concentration of 100 μ g ml⁻¹ for 60 seconds followed by a 15 seconds baseline and association and dissociation phases of 60 seconds each if not specified otherwise. FAB2G biosensors were regenerated up to 4 times by incubating the loaded biosensor for 5 seconds each in 10 mM Glycine pH1.5 and kinetics buffer consecutively for three times. FAB2G were also pre-conditioned that way before their first ligand immobilization.

All sensorgrams were analyzed using the Octet RED384 system software “Data Analysis HT” version 10.0.3.7 (Pall Fortébio). Raw sensor data was aligned at the Y axis by aligning the data to the end of the baseline step, and inter-step correction was used to align the start of the dissociation to the end of the association phase. No Savitzky-Golay filtering was applied. Resulting sensorgrams were then fitted using a 1:1 Langmuir kinetics binding model.

7.5.9. Cell lines

The TAP-deficient HLA-A*02:01-expressing cell line T2 was procured from ATCC (CRL-1992) and cultured in RPMI Medium 1640 GlutaMAXTM (Thermo Fisher, Cat. Nr. 61870010) supplemented with 10% heat inactivated FCS (Life Technologies, Cat. Nr. 10270106) and the antibiotics penicillin and streptomycin (Biozym, Cat. Nr. 882082, 100 μ g ml⁻¹ each) up until passage number 16 if necessary.

The GloResponseTM NFAT-luc2 Jurkat cell line was procured from Promega (Cat. Nr. CS1764) at passage number 6 and cultured in RPMI Medium 1640 GlutaMAXTM (Thermo Fisher, Cat. Nr. 61870010) supplemented with 10% heat inactivated FCS (Life Technologies, Cat. Nr. 10270106), 1% Sodium Pyruvate (C.C.Pro, Cat. Nr. Z-20M) and the antibiotics hygromycin B (Merck Millipore, Cat. Nr. 400052, 200 µg ml⁻¹), penicillin and streptomycin (Biozym, Cat. Nr. 882082, 100 µg ml⁻¹ each) up until passage number 14 if necessary.

7.5.10. T cell activation assay

T cell activation assays using GloResponseTM NFAT-luc2 Jurkat cells and peptide loaded T2 target cells were performed according to manufacturer instructions. In short, T2 cells were harvested from continuous cell culture, washed and resuspended in T2 culture medium at a concentration of 3.3×10^6 cells ml⁻¹ and transferred to 96 well round bottom plates (Corning costar®, Cat. Nr. 3799). Peptide in DMSO, 0.5% TFA was added to a final concentration of 100 nM and the suspension incubated for 2 to 3 hours at 37°C, 5% CO₂. bsTCR formulated in PBS was diluted in T2 culture medium to desired concentration and 25 µl of the respective dilution was distributed to white 96 well flat bottom plates (Brand, Cat. Nr. 781965). GloResponseTM NFAT-luc2 Jurkat cells were harvested from continuous cell culture, washed and resuspended in T2 culture medium at a concentration of 3.0×10^6 cells ml⁻¹ and 25 µl of the cell suspension was distributed to the white 96 well flat bottom plates with bsTCR dilutions. After peptide loading, T2 cells were resuspended and 25 µl distributed to the white 96 well flat bottom plates with bsTCR dilutions and GloResponseTM NFAT-luc2 Jurkat cells for a final effector to target ratio of 1:1 (75.000 cells each). Fully assembled plates were mixed for 5 minutes at 300 rpm on a plate shaker and the incubated for 18 to 20 hours at 37 °C, 5% CO₂. After the incubation period, 75 µl of Bio-GloTM luciferase reagent was added to each well and the plates incubated for minutes at 300 rpm on a plate shaker in the dark before reading luminescence at a 0.5 second integration time with a Synergy2 plate reader (Biotek). Luminescence as measured in relative light units (RLU) was converted to fold induction for each well by dividing measured RLU through those of control wells.

7.5.11. Motif-based identification of potentially cross-reactive peptide ligands

Searches for nonamer peptide ligands matching one of the potential combinations allowed by the search motif were performed using the NCBI human protein database. This database covers all non-redundant GenBank CDS translations, as well as records from PDB, SwissProt, PIR and PRF but excluding environmental samples from the WGS projects. The database was directly acquired from the NCBI servers.

7.5.12. Seq2Logo generation

Seq2Logos visualizing the binding motif were created by taking the inverse value of measured K_{DS} for the respective interaction and dividing them by 10^8 . These values were assembled in form of a position-specific scoring matrix file and processed using the PSSM-Logo type at the Seq2Logo online resource of the DTU Bioinformatics department [26].

7.5.13. Statistical analysis

All data was plotted using the GraphPad Prism software version 7. Correlation between x and y data sets were calculated by computing the Pearson correlation coefficient and are reported as r squared using the GraphPad Prism software version 7. R^2 and X^2 values for curve fittings of BLI binding kinetics measurements were calculated using the Octet RED384 system software “Data Analysis HT version” 10.0.3.7.

7.6. Acknowledgments

We thank Sonja Dorner and Christian Flohr for peptide synthesis and HPLC analysis. We thank Martin Priemer, Heike Hoffmann, Antje Arthur and Heiko Schuster for mass spectrometry analysis and data evaluation. We thank Jens Fritsche and Toni Weinschenk for bioinformatics support with respect to motif-based peptide search and alignment with the XPRESIDENT database. We also thank the SPC facility at EMBL Hamburg for the technical support.

We acknowledge funding from the Deutsche Forschungsgemeinschaft (SP583/12-1 to S.Sp.) and from iNEXT (grant number 653706, funded by the Horizon 2020 programme of the European Commission, to S.Sp.).

7.7. Authors contributions

S.Sp., R.A. and A.S. designed the disulfide bond, devised the pMHC refolding protocol and fluorescence anisotropy. R.A., R.M. and M.A. performed performed crystallization and X-ray crystallography. G.P. crystal structure analysis. M.H. designed and produced bsTCR constructs. A.M. performed protein refoldings, affinity measurements, cellular assays and wrote the manuscript. HG.R., C.W., S.B. and S.Sp. revised manuscript. D.M. revised the manuscript and supervised the study.

7.8. Data and materials availability

The crystal structure of the 1G4-dsA*02:01-ESO-9V complex has been deposited in the Protein Data Bank under the accession number 6Q3S.

7.9. References

- [1] Rammensee, H.G., Falk, K., Rötzschke, O., Peptides naturally presented by MHC class I molecules. *Annu. Rev. Immunol.* 1993, 11, 213–244.
- [2] Garboczi, D.N., Hung, D.T., Wiley, D.C., HLA-A2-peptide complexes: refolding and crystallization of molecules expressed in *Escherichia coli* and complexed with single antigenic peptides. *Proc. Natl. Acad. Sci. U. S. A.* 1992, 89, 3429–33.
- [3] Altman, J.D., Moss, P.A.H.H., Goulder, P.J.R.R., Barouch, D.H., et al., Phenotypic Analysis of Antigen-Specific T Lymphocytes. *Science* (80-.). 1996, 274, 94–96.
- [4] Hadrup, S.R., Toebes, M., Rodenko, B., Bakker, A.H., et al., High-throughput T-cell epitope discovery through MHC peptide exchange. *Methods Mol. Biol.* 2009, 524, 383–405.
- [5] Garcia, K.C., Tallquist, M.D., Pease, L.R., Brunmark, A., et al., Alphabeta T cell receptor interactions with syngeneic and allogeneic ligands: affinity measurements and crystallization. *Proc. Natl. Acad. Sci. U. S. A.* 1997, 94, 13838–43.
- [6] Stone, J.D., Kranz, D.M., Role of T Cell Receptor Affinity in the Efficacy and Specificity of Adoptive T Cell Therapies. *Front. Immunol.* 2013, 4, 1–16.
- [7] Robbins, P.F., Li, Y.F., El-Gamil, M., Zhao, Y., et al., Single and dual amino acid substitutions in TCR CDRs can enhance antigen-specific T cell functions. *J. Immunol.* 2008, 180, 6116–6131.
- [8] Varela-Rohena, A., Molloy, P.E., Dunn, S.M., Li, Y., et al., Control of HIV-1 immune escape by CD8 T cells expressing enhanced T-cell receptor. *Nat. Med.* 2008, 14, 1390–1395.
- [9] Oates, J., Hassan, N.J., Jakobsen, B.K., ImmTACs for targeted cancer therapy: Why, what, how, and which. *Mol. Immunol.* 2015, 67, 67–74.
- [10] Wooldridge, L., Ekeruche-Makinde, J., Van Den Berg, H.A., Skowera, A., et al., A single autoimmune T cell receptor recognizes more than a million different peptides. *J. Biol. Chem.* 2012, 287, 1168–1177.
- [11] Cameron, B.J., Gerry, A.B., Dukes, J., Harper, J. V, et al., Identification of a Titin-derived HLA-A1-presented peptide as a cross-reactive target for engineered MAGE A3-directed T cells. *Sci. Transl. Med.* 2013, 5, 197ra103.
- [12] Linette, G.P., Stadtmayer, E.A., Maus, M. V., Rapoport, A.P., et al., Cardiovascular toxicity and titin cross-reactivity of affinity-enhanced T cells in myeloma and melanoma. *Blood* 2013, 122, 863–871.
- [13] Raman, M.C.C., Rizkallah, P.J., Simmons, R., Donnellan, Z., et al., Direct molecular mimicry enables off-target cardiovascular toxicity by an enhanced affinity TCR designed for cancer immunotherapy. *Sci. Rep.* 2016, 6, 18851.
- [14] Bijen, H.M., van der Steen, D.M., Hagedoorn, R.S., Wouters, A.K., et al., Preclinical Strategies to Identify Off-Target Toxicity of High-Affinity TCRs. *Mol. Ther.* 2018.
- [15] Shao, W., Pedrioli, P.G.A., Wolski, W., Scurtescu, C., et al., The SysteMHC Atlas project. *Nucleic Acids Res.* 2018, 46, D1237–D1247.
- [16] Zacharias, M., Springer, S., Conformational flexibility of the MHC Class I $\alpha 1$ - $\alpha 2$ domain in peptide bound and free states: A molecular dynamics simulation study. *Biophys. J.* 2004, 87, 2203–2214.
- [17] Hein, Z., Uchtenhagen, H., Abualrous, E.T., Saini, S.K., et al., Peptide-independent stabilization of MHC class I molecules breaches cellular quality control. *J. Cell Sci.* 2014, 127, 2885–2897.
- [18] Saini, S.K., Abualrous, E.T., Tigan, A.S., Covella, K., et al., Not all empty MHC class I molecules are molten globules: Tryptophan fluorescence reveals a two-step mechanism of thermal denaturation. *Mol. Immunol.* 2013, 54, 386–396.
- [19] Saini, S.S.K., Ostermeir, K., Ramnarayan, V.V.R., Schuster, H., et al., Dipeptides promote folding and peptide binding of MHC class I molecules. *Proc. Natl. Acad. Sci. U. S. A.* 2013, 110, 15383–15388.
- [20] Boulter, J.M., Glick, M., Todorov, P.T., Baston, E., et al., Stable, soluble T-cell receptor molecules for crystallization and therapeutics. *Protein Eng.* 2003, 16, 707–711.
- [21] Chen, J.-L., Stewart-Jones, G., Bossi, G., Lissin, N.M., et al., Structural and kinetic basis for heightened immunogenicity of T cell vaccines. *J. Exp. Med.* 2005, 201, 1243–55.
- [22] Aggen, D.H., Chervin, A.S., Insaioo, F.K., Piepenbrink, K.H., et al., Identification and engineering

- of human variable regions that allow expression of stable single-chain T cell receptors. *Protein Eng. Des. Sel.* 2011, 24, 361–372.
- [23] Zhu, Z., Carter, P., Identification of heavy chain residues in a humanized anti-CD3 antibody important for efficient antigen binding and T cell activation. *J. Immunol.* 1995, 155, 1903–10.
 - [24] Burrows, S.R., Rodda, S.J., Suhrbier, A., Geysen, H.M., Moss, D.J., The specificity of recognition of a cytotoxic T lymphocyte epitope. *Eur. J. Immunol.* 1992, 22, 191–195.
 - [25] Rodenko, B., Toebe, M., Hadrup, S.R., van Esch, W.J.E., et al., Generation of peptide-MHC class I complexes through UV-mediated ligand exchange. *Nat. Protoc.* 2006, 1, 1120–1132.
 - [26] Thomsen, M.C.F., Nielsen, M., Seq2Logo: a method for construction and visualization of amino acid binding motifs and sequence profiles including sequence weighting, pseudo counts and two-sided representation of amino acid enrichment and depletion. *Nucleic Acids Res.* 2012, 40, W281–7.
 - [27] Weinschenk, T., Gouttefangeas, C., Schirle, M., Obermayr, F., et al., Integrated functional genomics approach for the design of patient-individual antitumor vaccines. *Cancer Res.* 2002, 62, 5818–5827.
 - [28] Fritsche, J., Rakitsch, B., Hoffgaard, F., Römer, M., et al., Translating Immuno-peptidomics to Immunotherapy-Decision-Making for Patient and Personalized Target Selection. *Proteomics* 2018, 18, 1700284.
 - [29] Elliott, T., Willis, A., Cerundolo, V., Townsend, A., Processing of major histocompatibility class I-restricted antigens in the endoplasmic reticulum. *J. Exp. Med.* 1995, 181, 1481–1491.
 - [30] Bossi, G., Gerry, A.B., Paston, S.J., Sutton, D.H., et al., Examining the presentation of tumor-associated antigens on peptide-pulsed T2 cells. *Oncoimmunology* 2013, 2, e26840.
 - [31] Andreatta, M., Nielsen, M., Gapped sequence alignment using artificial neural networks: application to the MHC class I system. *Bioinformatics* 2016, 32, 511–517.
 - [32] Kabsch, W., XDS. *Acta Crystallogr. D. Biol. Crystallogr.* 2010, 66, 125–32.
 - [33] Evans, P., Scaling and assessment of data quality. *Acta Crystallogr. Sect. D Biol. Crystallogr.* 2006, 62, 72–82.
 - [34] Vagin, A., Teplyakov, A., Molecular replacement with MOLREP. *Acta Crystallogr. Sect. D Biol. Crystallogr.* 2010, 66, 22–25.
 - [35] Kovalevskiy, O., Nicholls, R.A., Long, F., Carlon, A., Murshudov, G.N., Overview of refinement procedures within REFMAC5: utilizing data from different sources. *Acta Crystallogr. Sect. D, Struct. Biol.* 2018, 74, 215–227.
 - [36] Emsley, P., Lohkamp, B., Scott, W.G., Cowtan, K., Features and development of Coot. *Acta Crystallogr. Sect. D Biol. Crystallogr.* 2010, 66, 486–501.
 - [37] Chen, V.B., Arendall, W.B., Headd, J.J., Keedy, D.A., et al., MolProbity: All-atom structure validation for macromolecular crystallography. *Acta Crystallogr. Sect. D Biol. Crystallogr.* 2010, 66, 12–21.

7.10. Supplementary information

7.10.1. Supplementary figures

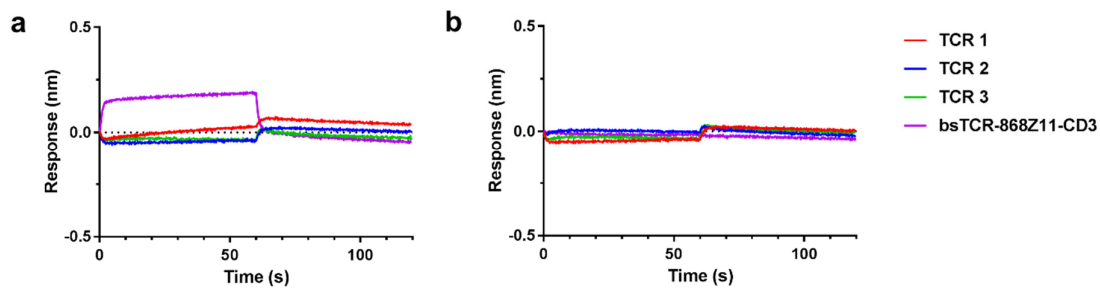


Figure S7-1. Binding of multiple different soluble TCRs and bsTCR bs-868Z11-CD3 to non-loaded dsA*02:01 or dsA*02:01 loaded with an irrelevant peptide.

(a) Binding of three different HLA-A*02:01 restricted soluble TCRs as well as bs-868Z11-CD3 to functionally-empty dsA*02:01. dsA*02:01 was immobilized onto a streptavidin sensor, each TCR supplied at 1 mg/ml (20 μ M for soluble TCRs, 13.3 μ M for bsTCR). **(b)** Binding of the same TCRs to dsA*02:01 loaded with an irrelevant peptide.

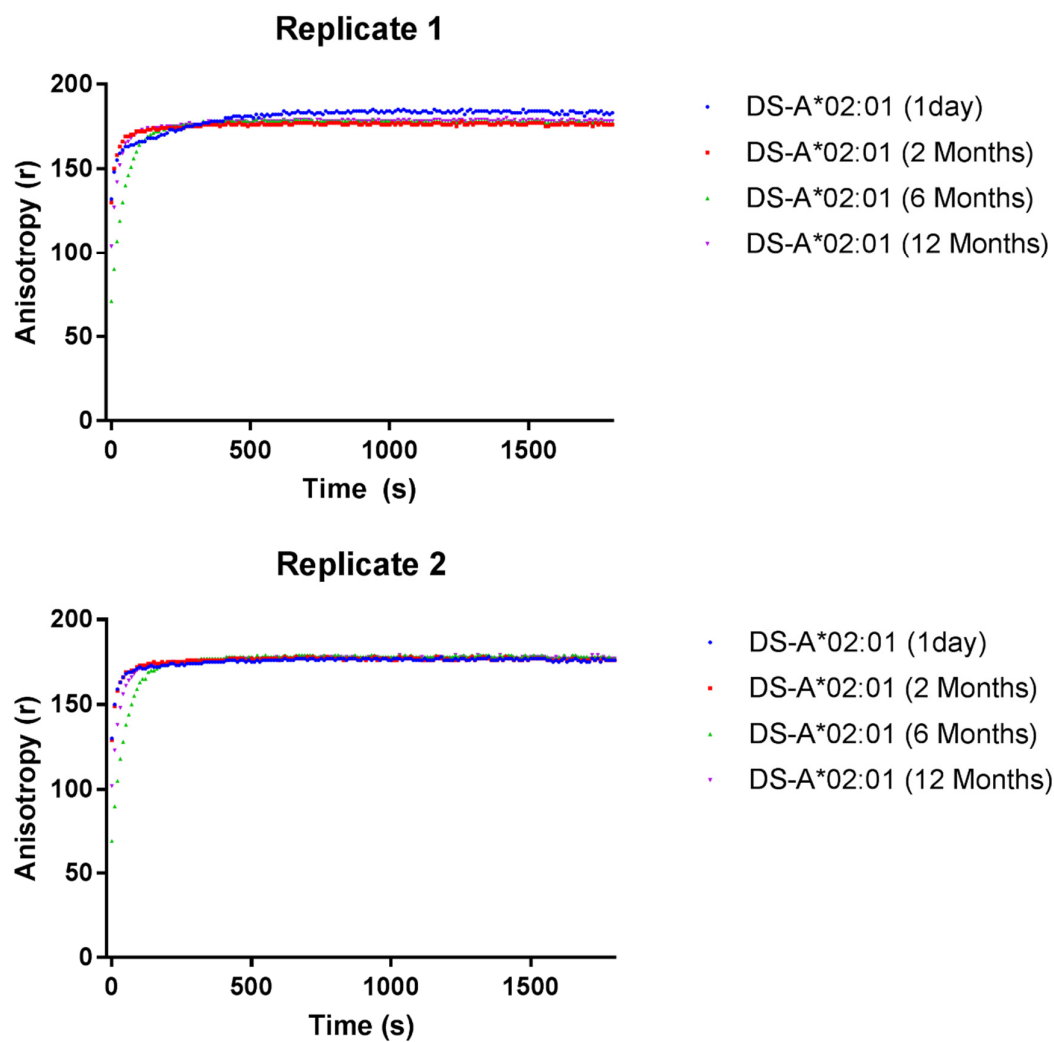


Figure S2. Analysis of dsA*02:01 peptide receptiveness after different storage durations at -80°C measured by fluorescence anisotropy.

Binding of 100 nM NVLPK_{FITC}VATV to 300 nM dsA*02:01 diluted based on determined concentration before storage. Binding was measured in duplicates and is plotted individually.

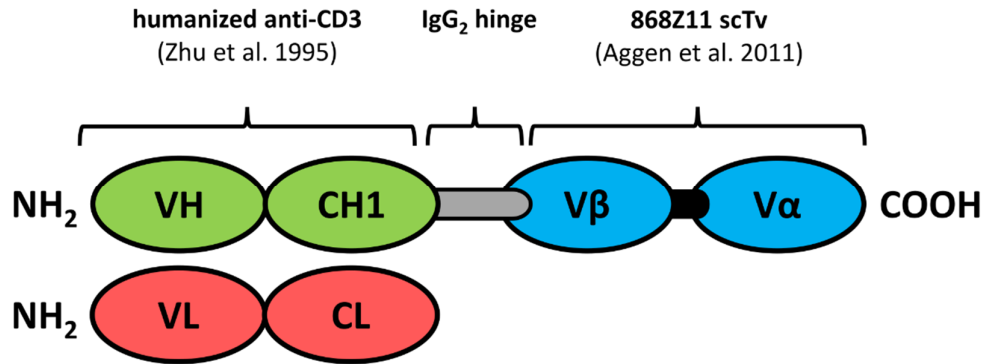


Figure S3. Illustration of bsTCR bs-868Z11-CD3 construct.

The 868Z11 domain is based on the SLYNTVATL-reactive TCR 868 and incorporates affinity enhancing mutations in the CDR2 β (YYEEEEE to YVRGEE) and CDR3 α region (CAVRTNSGYALN to CAVRGAHDYALN) identified by Varela-Rohena et al. [8]. The V β and V α domains of the affinity enhanced TCR were linked through a single chain linker (GSADDAKKDAAKKDGKS) and further modified with a surface stability conferring mutation in the V α 2 region (F49S) to allow for soluble expression by Aggen et al. [22]. To create the bs-868Z11-CD3 molecule, this 868Z11 scTv domain was fused to the F(ab') heavy chain portion of a humanized anti-CD3 antibody through an IgG2 derived CH2 hinge domain (APPVAG) with two cysteine-knock-outs (C₂₂₆S and C₂₂₉S), incorporated to prevent the formation of F(ab)₂ homodimers on expression.

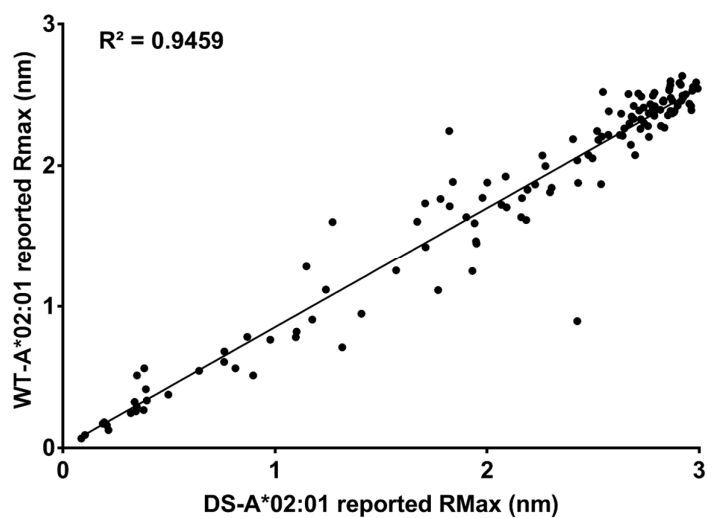


Figure S4. R_{max} values reported for immobilized dsA*02:01 and UV exchange generated wtA*02:01 pMHCs.

R_{max} is plotted for 140 different peptide ligands from the positional scanning library analyzed with soluble bs-868Z11-CD3. R_{max} reported after fitting using 500 nM and 158 nM analyte concentrations. The in-picture R² is the calculated correlation coefficient.

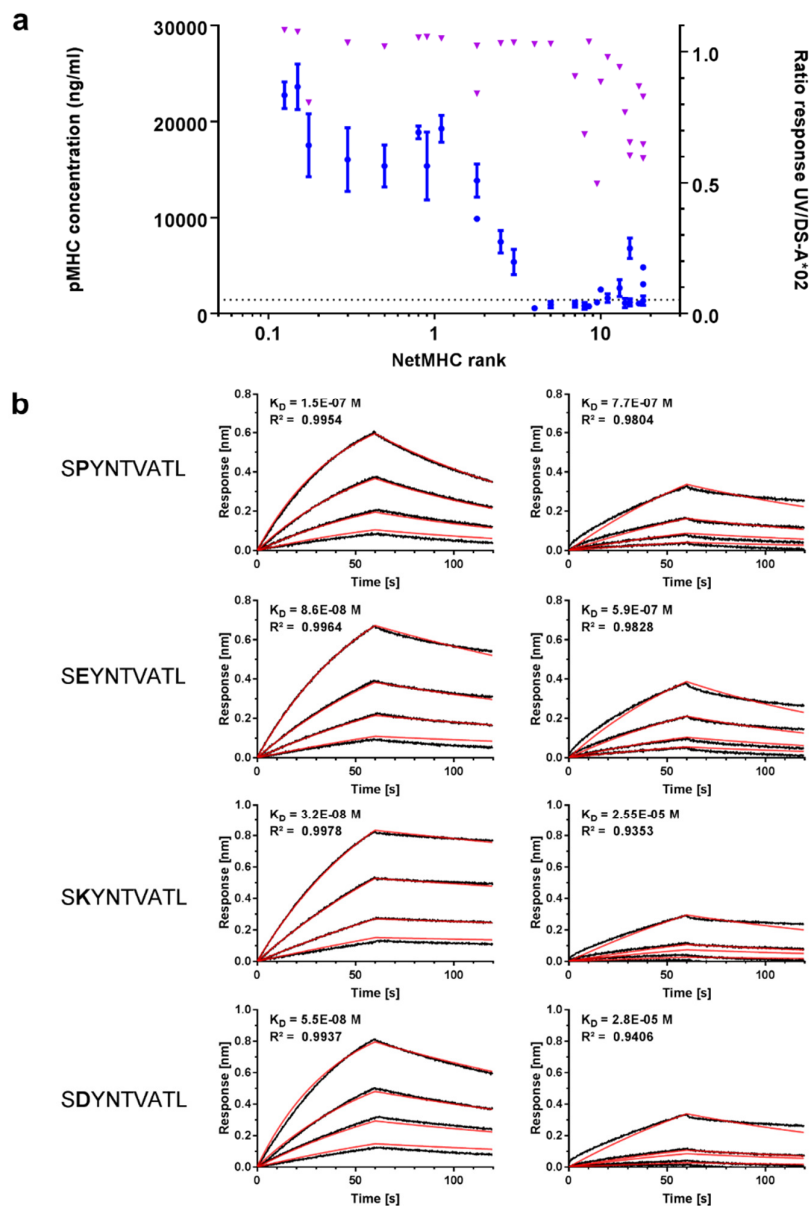


Figure S5. Analysis of UV exchange efficiency and Octet measurement results for 28 different peptides selected from SLYNTVATL based positional scanning library.

(a) Left axis: pMHC concentration after UV exchange with 25000 ng/ml of UV-sensitive pMHC monomer determined using an anti- β 2m ELISA. Dotted line represents ELISA/UV exchange background signal based on an UV exchange without peptide. Error bars represent technical triplicates. Right axis: Ratio of binding responses of soluble pMHC analytes to immobilized bs-868Z11-CD3 on Octet RED384 system. pMHCs were either prepared using UV exchange or by dsA*02:01 peptide loading. Ratios calculated by dividing UV-A*02:01 response by the dsA*02:01 response after 60s of association with similarly loaded anti-F(ab) biosensors. (b) Detailed curve fittings for four peptides with NetMHC ranks 15 and larger. dsA*02:01 complexes left, wtA*02:01 complexes right. All measurements were performed using 1:2 analyte dilution series starting at 500 nM. Raw data is displayed in black, curve fittings in red.

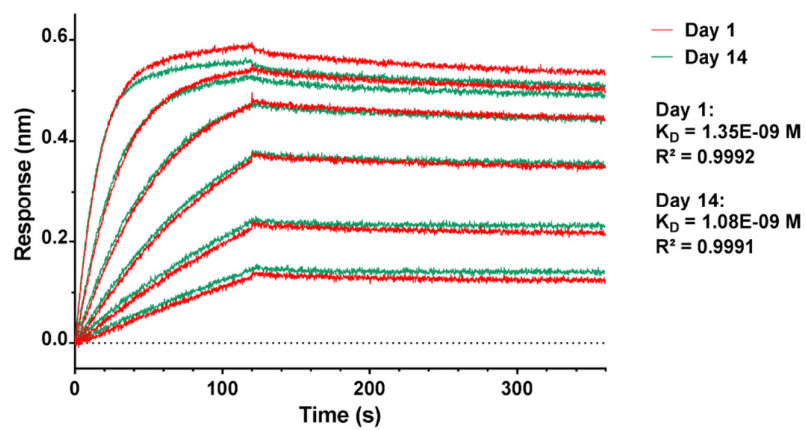


Figure S6.

Octet affinity measurements for dsA*02:01 SLYNTVATL pMHC with immobilized bs-868Z11-CD3 directly after exchange and after 2 weeks of storage at 4°C. Both measurements were performed using 1:2 analyte dilution series starting at 277.8 nM.

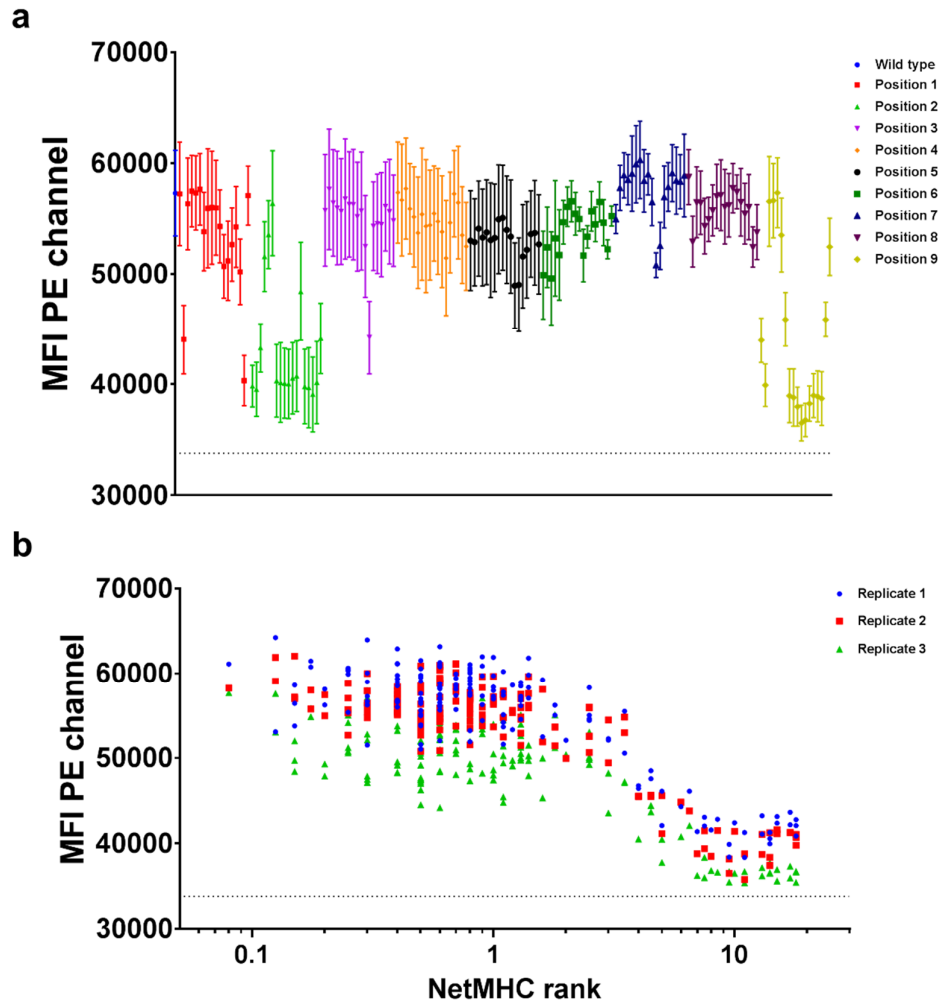


Figure S7. Flow cytometric peptide binding assay with an anti-human HLA-A2 antibody staining of T2 cells after exogenous peptide loading.

(a) PE channel MFI of T2 cells loaded individually with one specific peptide from the SLYNTVATL positional scanning library for 2 hours and stained afterwards using a PE labelled anti-human HLA-A2 antibody. Results are colored based on the position of the substitution compared to the wild type sequence. Error bars represent technical triplicates. (b) Correlation between PE channel MFI measured after peptide loading and staining and NetMHC predicted peptide affinity for the MHC.

7.10.2. Supplementary tables

Table S1: Data collection and refinement statistics 1G4/dsA*02/SLLMWITQV

*Values in parentheses are for highest-resolution shell.

1G4/dsA*02/SLLMWITQV	
Data collection	
Space group	P2 ₁
Cell dimensions	
<i>a</i> , <i>b</i> , <i>c</i> (Å)	75.44, 53.67, 121.74
α , β , γ (°)	90.0 98.0 90.0
Resolution (Å)	2.50 (2.60 – 2.50) *
<i>R</i> _{pim}	0.037 (0.69)
<i>I</i> / σ <i>I</i>	9.6 (1.1)
CC (1/2)	100.0 (0.68)
Completeness (%)	99.3 (99.1)
Redundancy	4.8 (5.0)
Refinement	
Resolution (Å)	30 – 2.50
No. reflections	33552
<i>R</i> _{work} / <i>R</i> _{free}	0.229 (0.273)
No. atoms	
Protein	3180
Ligand/ion	19
Water	589
<i>B</i> -factors	
Protein	98.1
Ligand/ion	97.8
Water	66.2
R.m.s. deviations	
Bond lengths (Å)	0.002
Bond angles (°)	0.47

Table S2: bs-868Z11-CD3 binding affinity for SV9 peptide SLYNTVATL and peptides from positional scanning library.

Table includes K_D , k_{on} and k_{off} values determined by curve fittings following a 1:1 Langmuir binding model using the Fortébio Data Analysis HT 10.0.3.7 software. Respective errors are reported as well as accuracy of the fit according to the model. Peptides reported as “No fit” had no evaluable curves reaching at least a peak signal of 0.05 nm at any concentration.

Peptide	K_D (M)	K_D Error	k_{on} ($M^{-1}s^{-1}$)	k_{on} Error	k_{off} (s^{-1})	k_{off} Error	Full X^2	Full R^2
SLYNTVATL	3.81E-09	1.49E-10	1.03E+05	1.45E+02	3.91E-04	1.53E-05	0.262	0.9993
GLYNTVATL	3.05E-08	3.55E-10	1.04E+05	3.42E+02	3.19E-03	3.56E-05	1.0915	0.9966
PLYNTVATL	8.54E-09	3.46E-10	9.65E+04	3.03E+02	8.24E-04	3.33E-05	1.2363	0.9969
ALYNTVATL	5.82E-09	3.18E-10	1.04E+05	3.14E+02	6.04E-04	3.29E-05	1.2791	0.9969
VLYNTVATL	5.74E-09	2.24E-10	1.05E+05	2.27E+02	6.04E-04	2.35E-05	0.6719	0.9984
LLYNTVATL	4.99E-08	2.99E-10	1.04E+05	2.67E+02	5.17E-03	2.80E-05	0.5623	0.9981
ILYNTVATL	1.35E-08	2.35E-10	1.06E+05	2.40E+02	1.43E-03	2.47E-05	0.6748	0.9982
MLYNTVATL	4.19E-08	2.95E-10	1.09E+05	2.93E+02	4.56E-03	2.96E-05	0.6922	0.9978
FLYNTVATL	5.22E-08	3.07E-10	1.15E+05	3.20E+02	6.02E-03	3.13E-05	0.6452	0.9976
YLYNTVATL	1.24E-07	5.65E-10	1.15E+05	4.01E+02	1.43E-02	4.21E-05	0.4931	0.9972
WLYNTVATL	4.62E-07	4.57E-09	1.66E+05	1.48E+03	7.66E-02	3.27E-04	0.1216	0.9955
HLYNTVATL	3.43E-07	2.50E-09	1.34E+05	8.87E+02	4.60E-02	1.43E-04	0.1908	0.9961
KLYNTVATL	1.91E-08	2.14E-10	9.03E+04	1.67E+02	1.73E-03	1.91E-05	0.3239	0.999
RLYNTVATL	4.42E-09	5.15E-10	8.86E+04	3.93E+02	3.92E-04	4.56E-05	2.0699	0.9944
QLYNTVATL	1.38E-07	5.55E-10	9.85E+04	3.05E+02	1.36E-02	3.50E-05	0.3534	0.9981
NLYNTVATL	3.13E-08	3.42E-10	9.84E+04	2.98E+02	3.08E-03	3.23E-05	0.9466	0.9973
ELYNTVATL	4.85E-07	4.84E-09	9.29E+04	8.66E+02	4.50E-02	1.63E-04	0.4525	0.9948
DLYNTVATL	4.49E-08	3.46E-10	9.55E+04	2.77E+02	4.28E-03	3.06E-05	0.7816	0.9977
TLYNTVATL	6.94E-09	2.07E-10	1.02E+05	1.98E+02	7.07E-04	2.10E-05	0.544	0.9988
SGYNTVATL	1.86E-08	4.56E-10	8.40E+04	3.18E+02	1.56E-03	3.79E-05	1.3876	0.9964
SPYNTVATL	1.65E-07	2.27E-09	6.80E+04	7.29E+02	1.12E-02	9.66E-05	2.2025	0.9852
SAYNTVATL	1.00E-08	1.28E-10	1.02E+05	1.23E+02	1.02E-03	1.30E-05	0.2052	0.9995
SVYNTVATL	8.47E-09	1.64E-10	1.01E+05	1.55E+02	8.57E-04	1.65E-05	0.3327	0.9992
SIYNTVATL	8.68E-09	9.77E-11	1.02E+05	9.42E+01	8.89E-04	9.97E-06	0.1192	0.9997
SMYNTVATL	6.55E-09	2.07E-10	1.01E+05	1.95E+02	6.61E-04	2.08E-05	0.4808	0.9987
SFYNTVATL	8.52E-09	3.97E-10	9.54E+04	3.41E+02	8.13E-04	3.77E-05	1.5251	0.996
SYNTVATL	3.26E-08	3.90E-10	5.83E+04	1.62E+02	1.90E-03	2.21E-05	0.23	0.9989
SWYNTVATL	8.16E-08	1.74E-09	4.46E+04	4.66E+02	3.64E-03	6.77E-05	0.9827	0.991
SHYNTVATL	2.73E-08	8.86E-10	6.92E+04	4.66E+02	1.89E-03	5.99E-05	2.1947	0.9915
SKYNTVATL	7.43E-08	1.57E-09	5.08E+04	5.00E+02	3.77E-03	7.06E-05	2.0162	0.9899
SRYNTVATL	1.02E-07	2.33E-09	4.84E+04	6.42E+02	4.95E-03	9.17E-05	0.6946	0.9837
SQYNTVATL	9.41E-09	2.19E-10	1.09E+05	2.35E+02	1.03E-03	2.37E-05	0.6976	0.9984
SNYNTVATL	2.45E-08	6.68E-10	6.85E+04	3.45E+02	1.68E-03	4.50E-05	1.7367	0.9953
SEYNTVATL	4.09E-08	1.77E-09	5.16E+04	6.23E+02	2.11E-03	8.78E-05	4.5691	0.9843
SDYNTVATL	1.01E-07	1.68E-09	6.51E+04	6.61E+02	6.56E-03	8.69E-05	3.2507	0.9854
SSYNTVATL	8.17E-09	1.97E-10	9.64E+04	1.72E+02	7.88E-04	1.89E-05	0.4063	0.999
STYNTVATL	5.41E-09	1.49E-10	9.87E+04	1.35E+02	5.34E-04	1.47E-05	0.2427	0.9994

Peptide	KD (M)	KD Error	k_{on} ($M^{-1}s^{-1}$)	k_{on} Error	k_{off} (s^{-1})	k_{off} Error	Full X ²	Full R ²
SLGNTVATL	No fit							
SLPNTVATL	No fit							
SLANTVATL	No fit							
SLVNTVATL	5.11E-07	5.80E-09	1.95E+05	2.01E+03	9.96E-02	4.80E-04	0.0769	0.9966
SLLNTVATL	1.32E-07	8.45E-10	1.21E+05	6.09E+02	1.60E-02	6.33E-05	1.038	0.9944
SLINTVATL	4.77E-07	5.50E-09	1.40E+05	1.48E+03	6.69E-02	3.15E-04	0.325	0.9939
SLMNTVATL	1.07E-06	5.52E-08	2.35E+05	1.12E+04	2.50E-01	5.13E-03	0.1244	0.979
SLFNTVATL	3.47E-08	1.92E-10	9.54E+04	1.59E+02	3.31E-03	1.75E-05	0.2445	0.9992
SLWNTVATL	3.36E-08	1.91E-10	9.34E+04	1.53E+02	3.14E-03	1.71E-05	0.2479	0.9992
SLHNTVATL	9.09E-08	3.31E-10	1.16E+05	2.84E+02	1.06E-02	2.85E-05	0.3676	0.9984
SLKNTVATL	No fit							
SLRNTVATL	5.55E-07	5.54E-09	9.64E+04	9.00E+02	5.35E-02	1.88E-04	0.1675	0.9957
SLQNTVATL	6.29E-07	9.45E-09	2.62E+05	3.51E+03	1.65E-01	1.11E-03	0.0384	0.9961
SLNNTVATL	4.74E-07	5.90E-09	1.81E+05	2.05E+03	8.59E-02	4.48E-04	0.1049	0.9953
SLENTVATL	No fit							
SLDNTVATL	No fit							
SLSNTVATL	No fit							
SLTNTVATL	3.01E-06	3.45E-06	1.88E+05	2.15E+05	5.66E-01	6.50E-02	0.1123	0.9199
SLYGTVATL	5.33E-07	1.20E-08	2.07E+05	4.15E+03	1.11E-01	1.12E-03	0.5678	0.9842
SLYPTVATL	5.54E-07	1.44E-08	3.62E+05	8.18E+03	2.00E-01	2.58E-03	0.0884	0.9892
SLYATVATL	1.15E-07	6.46E-10	1.40E+05	6.09E+02	1.60E-02	5.72E-05	0.9354	0.9952
SLYVTVATL	1.80E-07	9.65E-10	1.31E+05	5.98E+02	2.35E-02	6.64E-05	0.4669	0.9962
SLYLTVATL	6.70E-08	3.12E-10	1.11E+05	2.85E+02	7.44E-03	2.89E-05	0.5152	0.9981
SLYITVATL	5.25E-07	5.68E-09	1.18E+05	1.18E+03	6.19E-02	2.55E-04	0.2208	0.9949
SLYMTVATL	1.88E-06	2.10E-06	3.58E+05	3.96E+05	6.72E-01	1.11E-01	0.09	0.876
SLYFTVATL	No fit							
SLYYTVATL	No fit							
SLYWTVATL	No fit							
SLYHTVATL	8.11E-08	6.16E-10	1.38E+05	7.03E+02	1.12E-02	6.26E-05	1.8422	0.9923
SLYKTVATL	No fit							
SLYRTVATL	No fit							
SLYQTVATL	2.84E-07	3.23E-09	1.71E+05	1.73E+03	4.86E-02	2.53E-04	0.6721	0.9898
SLYETVATL	No fit							
SLYDTVATL	No fit							
SLYSTVATL	5.95E-08	2.69E-10	1.27E+05	3.13E+02	7.57E-03	2.87E-05	0.5404	0.9981
SLYTTVATL	1.61E-07	7.59E-10	1.35E+05	5.34E+02	2.18E-02	5.63E-05	0.3965	0.9968
SLYNGVATL	6.03E-07	1.50E-07	5.42E+05	1.29E+05	3.27E-01	2.34E-02	0.0452	0.9399
SLYNPVATL	No fit							
SLYNAVATL	9.66E-08	5.82E-10	1.27E+05	5.41E+02	1.22E-02	5.20E-05	0.9944	0.995
SLYNVVATL	3.07E-08	4.63E-10	9.09E+04	3.58E+02	2.79E-03	4.06E-05	1.3333	0.9958
SLYNLVATL	1.46E-08	3.05E-10	9.80E+04	2.73E+02	1.43E-03	2.97E-05	0.917	0.9976
SLYNIVATL	4.85E-08	3.37E-10	8.41E+04	2.21E+02	4.08E-03	2.62E-05	0.4314	0.9984
SLYNMVATL	4.26E-08	3.52E-10	1.20E+05	4.09E+02	5.12E-03	3.86E-05	1.2415	0.9962
SLYNFVATL	7.26E-07	3.75E-08	2.97E+05	1.36E+04	2.16E-01	5.09E-03	0.3346	0.9697

Peptide	KD (M)	KD Error	$k_{on} (M^{-1}s^{-1})$	k_{on} Error	$k_{off} (s^{-1})$	k_{off} Error	Full X ²	Full R ²
SLYNYVATL	4.60E-06	9.88E-06	1.37E+05	2.94E+05	6.31E-01	9.34E-02	0.1113	0.8904
SLYNWVATL	No fit							
SLYNHVATL	6.23E-07	4.07E-08	4.00E+05	2.26E+04	2.49E-01	8.17E-03	0.2106	0.9526
SLYNKVATL	2.24E-07	1.05E-09	1.35E+05	5.55E+02	3.02E-02	6.82E-05	0.2572	0.9973
SLYNRVATL	7.78E-07	7.24E-08	3.54E+05	3.19E+04	2.76E-01	6.54E-03	0.02	0.9899
SLYNQVATL	4.72E-07	7.25E-09	2.10E+05	2.90E+03	9.91E-02	6.64E-04	0.131	0.9936
SLYNNVATL	1.19E-07	5.68E-10	1.32E+05	4.88E+02	1.58E-02	4.76E-05	0.5956	0.9966
SLYNEVATL	No fit							
SLYNDVATL	3.91E-05	5.33E-04	1.23E+04	1.67E+05	4.79E-01	5.67E-02	0.1685	0.904
SLYNSVATL	6.91E-08	3.75E-10	1.21E+05	3.86E+02	8.39E-03	3.68E-05	0.7181	0.997
SLYNTGATL	1.34E-07	6.48E-10	1.37E+05	5.33E+02	1.84E-02	5.26E-05	0.5267	0.9965
SLYNTPATL	1.54E-08	1.56E-10	1.19E+05	1.93E+02	1.83E-03	1.82E-05	0.3561	0.999
SLYNTAATL	5.48E-08	3.74E-10	1.10E+05	3.59E+02	6.05E-03	3.62E-05	0.8843	0.9967
SLYNTLATL	9.08E-09	1.01E-10	1.12E+05	1.15E+02	1.02E-03	1.13E-05	0.15	0.9996
SLYNTIATL	8.74E-09	1.86E-10	9.97E+04	1.72E+02	8.71E-04	1.85E-05	0.3788	0.999
SLYNTMATL	2.72E-08	3.66E-10	9.75E+04	3.17E+02	2.65E-03	3.46E-05	0.9551	0.9966
SLYNTFATL	5.79E-07	6.47E-09	7.96E+04	8.39E+02	4.61E-02	1.69E-04	0.1416	0.9946
SLYNTYATL	4.43E-07	8.76E-09	4.61E+04	8.61E+02	2.04E-02	1.33E-04	0.1286	0.9831
SLYNTWATL	1.74E-05	1.28E-05	1.91E+03	1.41E+03	3.33E-02	2.40E-04	0.0063	0.9878
SLYNTHATL	1.75E-07	1.46E-09	7.39E+04	4.94E+02	1.30E-02	6.42E-05	0.3653	0.9929
SLYNTKATL	No fit							
SLYNTRATL	No fit							
SLYNTQATL	2.71E-07	1.50E-09	1.19E+05	5.86E+02	3.22E-02	7.94E-05	0.1392	0.9969
SLYNTNATL	1.79E-07	7.80E-10	1.20E+05	4.42E+02	2.15E-02	5.03E-05	0.2983	0.9974
SLYNTAATL	1.43E-06	5.11E-08	5.54E+04	1.93E+03	7.94E-02	5.83E-04	0.0772	0.99
SLYNTDATL	6.04E-07	7.08E-09	1.12E+05	1.22E+03	6.77E-02	2.89E-04	0.1139	0.995
SLYNTSATL	1.66E-07	6.43E-10	1.43E+05	4.69E+02	2.38E-02	4.93E-05	0.2673	0.9979
SLYNTTATL	3.37E-08	4.58E-10	1.07E+05	4.51E+02	3.59E-03	4.64E-05	1.7673	0.9938
SLYNTVGTL	8.29E-09	4.59E-10	8.24E+04	3.12E+02	6.83E-04	3.77E-05	1.2283	0.996
SLYNTVPTL	3.71E-09	4.42E-10	1.22E+05	5.76E+02	4.51E-04	5.36E-05	4.052	0.9904
SLYNTVVTL	5.99E-07	1.07E-08	1.44E+05	2.37E+03	8.64E-02	6.15E-04	0.1883	0.9892
SLYNTVLTL	No fit							
SLYNTVITL	No fit							
SLYNTVMTL	1.02E-07	4.28E-10	6.90E+04	1.80E+02	7.04E-03	2.31E-05	0.1333	0.9988
SLYNTVFTL	5.14E-07	1.01E-08	1.72E+05	3.07E+03	8.85E-02	7.06E-04	0.1274	0.9897
SLYNTVYTL	No fit							
SLYNTVWTL	No fit							
SLYNTVHTL	1.14E-07	2.51E-10	8.42E+04	1.27E+02	9.63E-03	1.53E-05	0.0763	0.9995
SLYNTVKTL	1.20E-06	5.58E-08	5.35E+04	2.43E+03	6.42E-02	6.41E-04	0.0792	0.9775
SLYNTVRTL	1.28E-06	2.41E-08	2.49E+04	4.61E+02	3.20E-02	9.10E-05	0.0547	0.9967
SLYNTVQTL	5.38E-08	7.00E-10	6.84E+04	3.40E+02	3.68E-03	4.43E-05	0.9296	0.9952
SLYNTVNIL	4.11E-08	8.02E-10	7.22E+04	4.32E+02	2.97E-03	5.51E-05	1.5878	0.9921
SLYNTVETL	1.61E-06	2.46E-07	5.74E+03	8.80E+02	9.22E-03	1.00E-04	0.007	0.989
SLYNTVDIL	No fit							

Peptide	KD (M)	KD Error	k_{on} ($M^{-1}s^{-1}$)	k_{on} Error	k_{off} (s^{-1})	k_{off} Error	Full X ²	Full R ²
SLYNTVSTL	1.04E-08	4.47E-10	9.80E+04	4.00E+02	1.02E-03	4.36E-05	1.9634	0.9944
SLYNTVTTL	6.90E-08	2.99E-10	9.23E+04	2.09E+02	6.37E-03	2.36E-05	0.2893	0.9987
SLYNTVAGL	1.14E-08	1.42E-10	1.14E+05	1.65E+02	1.30E-03	1.61E-05	0.302	0.9992
SLYNTVAPL	2.34E-07	1.20E-09	1.35E+05	6.11E+02	3.16E-02	7.71E-05	0.3155	0.9969
SLYNTVAAL	8.50E-09	1.51E-10	1.14E+05	1.75E+02	9.69E-04	1.72E-05	0.3504	0.9991
SLYNTVAVL	6.98E-09	1.19E-10	1.05E+05	1.20E+02	7.31E-04	1.25E-05	0.1881	0.9995
SLYNTVALL	1.58E-08	1.20E-10	9.58E+04	1.03E+02	1.51E-03	1.14E-05	0.1259	0.9996
SLYNTVAIL	4.16E-09	7.48E-10	9.74E+04	6.62E+02	4.05E-04	7.28E-05	5.8607	0.9834
SLYNTVAML	7.69E-09	5.22E-10	9.75E+04	4.63E+02	7.50E-04	5.08E-05	2.7181	0.9922
SLYNTVAFL	1.93E-07	1.68E-09	9.29E+04	6.77E+02	1.80E-02	8.45E-05	0.9456	0.9906
SLYNTVAYL	4.00E-07	3.75E-09	9.61E+04	8.32E+02	3.85E-02	1.39E-04	0.2451	0.994
SLYNTVAWL	2.09E-07	1.94E-09	9.65E+04	7.69E+02	2.01E-02	9.70E-05	1.0358	0.9893
SLYNTVAHL	1.09E-08	5.55E-10	9.19E+04	4.47E+02	1.00E-03	5.07E-05	2.6388	0.9925
SLYNTVAKL	1.73E-08	2.87E-10	1.02E+05	2.76E+02	1.77E-03	2.90E-05	0.9054	0.9975
SLYNTVARL	7.93E-09	3.98E-10	1.06E+05	4.06E+02	8.37E-04	4.19E-05	2.1201	0.9946
SLYNTVAQL	1.59E-08	6.14E-10	1.01E+05	5.74E+02	1.61E-03	6.13E-05	4.0059	0.9888
SLYNTVANL	1.08E-08	6.43E-10	1.01E+05	6.03E+02	1.09E-03	6.46E-05	4.5943	0.9874
SLYNTVAEL	4.73E-08	2.37E-10	9.22E+04	1.79E+02	4.36E-03	2.02E-05	0.291	0.999
SLYNTVADL	2.12E-08	3.17E-10	8.90E+04	2.40E+02	1.88E-03	2.77E-05	0.6889	0.9979
SLYNTVASL	4.68E-09	2.55E-10	1.09E+05	2.71E+02	5.08E-04	2.76E-05	0.918	0.9977
SLYNTVATG	7.71E-09	4.30E-10	1.01E+05	4.05E+02	7.79E-04	4.34E-05	2.1199	0.9943
SLYNTVATP	5.03E-08	1.57E-09	3.41E+04	3.34E+02	1.72E-03	5.08E-05	0.6961	0.9945
SLYNTVATA	6.74E-09	4.88E-10	1.13E+05	5.56E+02	7.61E-04	5.49E-05	3.6905	0.9904
SLYNTVATV	8.41E-09	6.00E-10	1.04E+05	5.95E+02	8.76E-04	6.23E-05	4.752	0.988
SLYNTVATI	6.70E-09	2.87E-10	1.13E+05	3.25E+02	7.53E-04	3.22E-05	1.2712	0.9968
SLYNTVATM	7.45E-09	2.48E-10	9.88E+04	2.26E+02	7.36E-04	2.44E-05	0.6922	0.9982
SLYNTVATF	1.19E-08	2.46E-10	7.18E+04	1.37E+02	8.51E-04	1.76E-05	0.2228	0.9992
SLYNTVATY	1.02E-08	3.37E-10	7.11E+04	1.85E+02	7.24E-04	2.39E-05	0.4625	0.9985
SLYNTVATW	3.32E-08	5.59E-10	3.70E+04	1.34E+02	1.23E-03	2.02E-05	0.0824	0.9991
SLYNTVATH	1.37E-08	3.64E-10	4.75E+04	1.19E+02	6.51E-04	1.72E-05	0.089	0.9993
SLYNTVATK	4.57E-08	1.20E-09	2.70E+04	2.00E+02	1.23E-03	3.11E-05	0.0929	0.9982
SLYNTVATR	5.71E-09	2.30E-10	9.59E+04	1.99E+02	5.48E-04	2.20E-05	0.5532	0.9986
SLYNTVATQ	5.88E-09	3.12E-10	8.96E+04	2.41E+02	5.27E-04	2.79E-05	0.7397	0.9978
SLYNTVATN	9.10E-09	3.77E-10	9.76E+04	3.36E+02	8.88E-04	3.67E-05	1.5971	0.9961
SLYNTVATE	6.96E-06	9.43E-06	3.79E+02	5.13E+02	2.64E-03	8.02E-05	0.1997	0.9908
SLYNTVATD	7.18E-06	8.48E-06	3.95E+02	4.67E+02	2.83E-03	7.30E-05	0.1137	0.9924
SLYNTVATS	7.19E-09	2.13E-10	1.16E+05	2.54E+02	8.33E-04	2.46E-05	0.7637	0.9981
SLYNTVATT	5.66E-09	1.27E-10	1.12E+05	1.42E+02	6.32E-04	1.41E-05	0.2627	0.9994

Table S3. Cross-reactive peptide ligand search motif for bs-868Z11-CD3 based on the affinities measured using the positional scanning library.

All amino acids of the 19 proteinogenic amino acids investigated at each position that increased the respective affinity of the bsTCR above 50 nM were removed to reach the search motif.

Peptide Position	Permitted Amino Acids
1	GPAVLIMKRNDST
2	GAVLIMFYHQNEST
3	FYW
4	N
5	VLIMT
6	PVLIMT
7	GPANS
8	GAVLIMHKRQNEDST
9	GAVLIMFYWHKRQNST

Table S4.

bs-868Z11-CD3 binding affinity for selected peptide ligands identified based on the bs-868Z11-CD3 binding motif. Peptide sequences and associated genes according to the NCBI data base are reported and peptides are sorted by decreasing KDs. Table includes KD, kon and koff values determined by curve fittings following a 1:1 Langmuir binding model using the Fortébio Data Analysis HT 10.0.3.7 software. Respective errors are reported as well as accuracy of the fit according to the model. Peptides reported as “No fit” had no evaluable curves reaching at least a peak signal of 0.05 nm at any concentration.

Peptide	Associated Gene	KD (M)	KD Error	kon (M ⁻¹ s ⁻¹)	kon Error	koff (s ⁻¹)	koff Error	Full X ²	Full R ²
RVYNTVPLV	HIPK3	1.32E-08	1.76E-10	9.50E+04	1.69E+02	1.26E-03	1.66E-05	0.2908	0.9993
RMYNLVSRI	CUL1	1.91E-08	2.52E-10	9.25E+04	2.28E+02	1.76E-03	2.29E-05	0.5429	0.9986
SLYNMVPPI	OVOS	1.97E-08	1.71E-10	1.31E+05	2.89E+02	2.57E-03	2.16E-05	0.586	0.9987
TVYNMVPPI	OVOS	2.07E-08	1.54E-10	1.28E+05	2.50E+02	2.66E-03	1.91E-05	0.4228	0.999
ALYNVIAMA	SECISBP2L	2.11E-08	1.51E-10	9.28E+04	2.25E+02	1.96E-03	1.32E-05	0.114	0.9997
AIYNLLPDI	NCAPD2	2.33E-08	1.82E-10	1.01E+05	1.90E+02	2.36E-03	1.79E-05	0.3299	0.9992
STYNLVSTS	KIAA2018	2.47E-08	2.16E-10	7.07E+04	1.28E+02	1.75E-03	1.49E-05	0.1772	0.9995
SVYNMVPPI	OVOS2	2.68E-08	1.96E-10	1.32E+05	3.26E+02	3.53E-03	2.43E-05	0.6471	0.9984
RTYNVLAIL	ATP8B1	3.11E-08	1.55E-10	7.54E+04	9.93E+01	2.34E-03	1.12E-05	0.0937	0.9997
SVYNLVSIA	KPTN	3.65E-08	2.01E-10	7.97E+04	2.13E+02	2.91E-03	1.40E-05	0.0926	0.9997
RAYNLIGTV	LOC100128501	3.72E-08	1.71E-10	8.94E+04	1.40E+02	3.33E-03	1.43E-05	0.1721	0.9995
ALFNLPVVG	FGF12	3.83E-08	3.22E-10	6.64E+04	1.71E+02	2.54E-03	2.04E-05	0.266	0.999
RIYNVIGTL	FOLH1,FOLH1B	4.53E-08	3.00E-10	5.75E+04	1.28E+02	2.61E-03	1.62E-05	0.1095	0.9994
RIYNVVGTI	NAALAD2	5.15E-08	4.13E-10	5.94E+04	1.81E+02	3.06E-03	2.27E-05	0.2723	0.9989
TLFNLPVNS	CLASP2	5.40E-08	3.31E-10	9.76E+04	2.90E+02	5.28E-03	2.82E-05	0.4822	0.9981
SLFNVISIL	KCNK12,KCNK13	5.83E-08	3.11E-10	6.94E+04	1.64E+02	4.05E-03	1.94E-05	0.2068	0.9992
STFNLVAIS	CCKAR	6.06E-08	2.91E-10	4.96E+04	9.98E+01	3.01E-03	1.31E-05	0.0436	0.9996
TLFNLPVVG	FGF12,FGF13,FGF14	6.32E-08	3.97E-10	6.72E+04	1.98E+02	4.25E-03	2.36E-05	0.3044	0.9988
TIFNLIPNS	CLASP1	6.41E-08	2.67E-10	8.97E+04	1.99E+02	5.75E-03	2.03E-05	0.2655	0.999
ALYNVLAKV	IFFO1,IFFO2	6.59E-08	2.96E-10	1.02E+05	2.63E+02	6.75E-03	2.49E-05	0.3602	0.9986
AVFNLLPHT	SMYD4	7.11E-08	2.72E-10	8.53E+04	1.82E+02	6.07E-03	1.93E-05	0.2344	0.9991
RMYNLLGHM	ZNF710	8.71E-08	7.55E-10	5.30E+04	2.55E+02	4.62E-03	3.33E-05	0.2278	0.9977
STWNTPPNM	KIAA0922	8.98E-08	3.45E-10	9.05E+04	2.28E+02	8.13E-03	2.36E-05	0.2591	0.9989
NIYNLIAII	BICD2	9.32E-08	3.91E-10	1.06E+05	3.10E+02	9.84E-03	2.95E-05	0.3894	0.9983
RIYNLPPEL	WRAP53	9.95E-08	3.78E-10	9.47E+04	2.51E+02	9.42E-03	2.56E-05	0.3026	0.9988
TTFNLPSAA	WDR17	1.02E-07	6.71E-10	7.87E+04	3.47E+02	8.04E-03	3.91E-05	0.579	0.997
MFFNVIAIV	UGGT2	1.06E-07	1.29E-09	5.21E+04	3.95E+02	5.52E-03	5.23E-05	0.0772	0.9934
SLWNTVSGI	HHLA1	1.08E-07	5.04E-10	8.88E+04	2.94E+02	9.60E-03	3.14E-05	0.3873	0.9982
MLWNLLALR	COX7A2	1.17E-07	1.03E-08	1.26E+06	1.05E+05	1.47E-01	4.25E-03	0.0448	0.9675
VFWNLLPTV	C12orf74	1.20E-07	7.20E-10	1.24E+05	5.97E+02	1.49E-02	5.29E-05	0.9116	0.9955
STFNTTSNG	QSER1	1.52E-07	6.60E-09	1.76E+05	7.05E+03	2.67E-02	4.39E-04	0.0311	0.9225
GFFNLLSHV	PCP2	1.59E-07	9.88E-09	6.24E+05	3.64E+04	9.94E-02	2.08E-03	0.0321	0.9717
LLYNVPAVA	APP	1.67E-07	1.27E-08	7.41E+05	5.29E+04	1.24E-01	3.21E-03	0.0164	0.9712
ALFNTISQG	VTG1	1.83E-07	8.26E-10	7.15E+04	2.68E+02	1.31E-02	3.28E-05	0.2214	0.9984
TTFNTLAGS	MUC16	1.97E-07	8.70E-10	9.03E+04	3.44E+02	1.78E-02	3.98E-05	0.1556	0.9981
SLWNLLGNA	LMAN2L	2.14E-07	3.02E-08	1.02E+06	1.35E+05	2.19E-01	1.07E-02	0.0324	0.952

Chapter 7

Peptide	Associated Gene	KD (M)	KD Error	k_{on} ($M^{-1}s^{-1}$)	k_{on} Error	k_{off} (s^{-1})	k_{off} Error	Full X ²	Full R ²
SLYNLLNLT	SLC4A5	2.19E-07	8.40E-10	6.75E+04	2.24E+02	1.48E-02	2.85E-05	0.094	0.9988
GVWNLLSIV	ZSWIM8	2.52E-07	4.59E-08	1.09E+06	1.86E+05	2.74E-01	1.73E-02	0.0545	0.9403
ALFNVVNSI	SLC38A11	2.55E-07	2.10E-09	6.83E+04	4.99E+02	1.74E-02	6.59E-05	0.2897	0.9956
VIYNLLGLA	SH3TC2	2.64E-07	1.88E-09	1.07E+05	7.25E+02	2.83E-02	5.92E-05	0.2115	0.9983
SIFNIVAIA	GPR50	2.84E-07	1.60E-09	4.44E+04	2.37E+02	1.26E-02	2.25E-05	0.0369	0.9995
TVYNTVSEG	SLC39A6	3.04E-07	2.50E-09	4.71E+04	3.50E+02	1.43E-02	4.99E-05	0.2538	0.997
DLWNTLSSL	EFCAB13,ITGB3	3.39E-07	2.60E-08	4.15E+05	3.02E+04	1.41E-01	3.55E-03	0.0238	0.9752
IFFNLLAVL	POMT1	3.50E-07	4.75E-08	8.47E+05	1.08E+05	2.97E-01	1.35E-02	0.023	0.9688
DLFNLLPDV	PSMD7	3.60E-07	1.08E-08	7.69E+04	2.15E+03	2.77E-02	3.14E-04	0.0881	0.9367
LSWNVVPNA	SPCS3	3.67E-07	2.91E-08	4.13E+05	3.09E+04	1.52E-01	3.89E-03	0.0234	0.9734
MLWNLLALH	COX7A2P2	3.67E-07	2.04E-08	1.07E+06	4.75E+04	3.94E-01	1.33E-02	0.1159	0.9595
TIFNTVNTS	TIMMDC1	3.87E-07	2.77E-09	4.20E+04	2.80E+02	1.63E-02	4.19E-05	0.0304	0.9978
KTFNLIPAV	MRPL4	4.13E-07	2.59E-09	1.12E+05	6.52E+02	4.62E-02	1.07E-04	0.1185	0.9979
NLFNVTPLI	ZNF66P	4.28E-07	1.38E-07	1.05E+06	3.19E+05	4.49E-01	4.68E-02	0.0447	0.9139
SYWNIISTV	OR2D3	4.39E-07	4.84E-09	4.56E+04	4.74E+02	2.00E-02	7.23E-05	0.1373	0.9952
GVFNLI AVL	AC002365.5,	4.59E-07	4.94E-09	7.59E+04	7.70E+02	3.48E-02	1.26E-04	0.3268	0.9946
	LOC100288814								
RLFNITSSA	IFITM10	4.74E-07	4.12E-08	2.51E+05	2.08E+04	1.19E-01	3.08E-03	0.0167	0.9706
NLWNLVAVI	WDR17	4.97E-07	1.16E-08	2.07E+05	4.34E+03	1.03E-01	1.04E-03	0.256	0.9836
RIFNLIGMM	HCN1,HCN3	4.98E-07	1.26E-08	2.29E+04	5.51E+02	1.14E-02	8.55E-05	0.0712	0.9889
RLFNVVSRG	TRPV2	5.02E-07	6.55E-09	6.50E+04	8.05E+02	3.26E-02	1.34E-04	0.1875	0.9931
LVFNVIPTL	ABCB6	5.35E-07	3.99E-09	1.33E+05	9.21E+02	7.13E-02	2.00E-04	0.0445	0.9982
TTWNILSSA	COX1	5.36E-07	4.08E-08	2.26E+05	1.65E+04	1.21E-01	2.63E-03	0.0214	0.9794
KLFNVLSTL	NUP210P2	5.76E-07	3.35E-08	2.97E+05	1.65E+04	1.71E-01	2.83E-03	0.0131	0.9912
RVYNLTAKS	VWA3B	5.95E-07	4.57E-09	4.53E+04	3.35E+02	2.69E-02	5.65E-05	0.0219	0.9981
LTFNTISLS	ENTHD1	7.09E-07	2.12E-07	4.78E+05	1.37E+05	3.39E-01	2.72E-02	0.0387	0.929
AQFNLLSST	TP73	7.13E-07	9.97E-09	8.59E+04	1.15E+03	6.12E-02	2.58E-04	0.1658	0.9947
VVYNVLSEL	SP100,SP140L	7.35E-07	6.29E-08	1.84E+05	1.52E+04	1.35E-01	2.89E-03	0.0255	0.9785
KVYNTPTS	AEBP2	7.51E-07	1.39E-08	1.71E+05	2.91E+03	1.28E-01	9.13E-04	0.0718	0.9945
GIFNIIPST	CAPN7	7.90E-07	8.67E-09	1.32E+05	1.36E+03	1.04E-01	4.00E-04	0.0364	0.9979
NIYNTLSGL	UBR4	8.73E-07	1.71E-08	1.59E+05	2.89E+03	1.38E-01	9.89E-04	0.0564	0.9947
RLFNLTSTF	FLJ44715,FUT11	9.32E-07	2.82E-08	1.72E+05	4.83E+03	1.60E-01	1.79E-03	0.0525	0.9894
TVWNTLSSL	DNAH9	9.39E-07	1.22E-08	4.52E+04	5.73E+02	4.25E-02	1.20E-04	0.0344	0.9971
RLFNMLSAV	CFAP221,PCDP1	9.71E-07	3.06E-08	1.73E+05	5.09E+03	1.68E-01	1.94E-03	0.0714	0.9892
SIWNVTAIA	HTR5A	1.10E-06	5.12E-07	3.21E+05	1.45E+05	3.54E-01	3.47E-02	0.0576	0.9051
ALFNLMSCI	EGR4	1.19E-06	3.21E-08	9.57E+04	2.48E+03	1.14E-01	8.53E-04	0.0645	0.9931
IVYNLLSAM	SLC39A10	1.30E-06	1.62E-07	1.61E+05	1.98E+04	2.10E-01	4.82E-03	0.0245	0.987
ISFNMLPSI	GPR98	1.37E-06	4.65E-08	1.24E+05	4.04E+03	1.70E-01	1.70E-03	0.0581	0.991
NTYNILPGS	C9orf173	1.38E-06	1.17E-07	1.14E+05	9.57E+03	1.57E-01	2.30E-03	0.025	0.9925
RLWNMVNVT	IL12RB2	1.39E-06	2.57E-07	1.52E+05	2.77E+04	2.11E-01	6.87E-03	0.049	0.9763
SAFNITSLI	WAC	1.41E-06	3.21E-07	1.65E+05	3.70E+04	2.32E-01	9.29E-03	0.0314	0.9682
NIFNLPNIV	OMD	1.48E-06	6.62E-07	4.19E+05	1.85E+05	6.20E-01	4.90E-02	0.0905	0.9596
GVYNLP GAS	GPX2	1.58E-06	3.07E-07	1.17E+05	2.23E+04	1.84E-01	5.65E-03	0.0488	0.9756
GTYNVISLV	TRPC4,TRPC5	1.64E-06	4.18E-07	1.23E+05	3.10E+04	2.02E-01	8.00E-03	0.0666	0.965
SIFNTLSDI	SGSM3	1.97E-06	5.86E-08	4.07E+04	1.20E+03	8.01E-02	3.78E-04	0.0856	0.9957

Peptide	Associated Gene	KD (M)	KD Error	k_{on} ($M^{-1}s^{-1}$)	k_{on} Error	k_{off} (s^{-1})	k_{off} Error	Full X ²	Full R ²
TIFNILSGI	ABCA3	2.66E-06	2.37E-07	4.68E+04	4.13E+03	1.24E-01	1.66E-03	0.1728	0.9807
LLFNLISSS	MON1A	2.79E-06	2.57E-06	1.51E+05	1.38E+05	4.20E-01	4.10E-02	0.0599	0.9183
RTFNLTAGS	PDXDC1	2.85E-06	5.89E-07	4.63E+04	9.54E+03	1.32E-01	2.56E-03	0.0356	0.9845
TVFNILPGG	PAFAH2	3.23E-06	1.06E-06	3.69E+04	1.21E+04	1.19E-01	3.22E-03	0.025	0.968
GLFNIPPAS	CYP2S1	3.91E-06	4.13E-06	8.52E+04	8.97E+04	3.33E-01	2.74E-02	0.0395	0.9216
RMFNIISDS	RASA1	3.99E-06	4.08E-07	1.51E+04	1.54E+03	6.02E-02	4.39E-04	0.0509	0.9862
TTFNIVGTT	GABRA3	6.79E-06	3.10E-06	8.68E+03	3.96E+03	5.89E-02	8.72E-04	0.0351	0.9743
ALFNLMGVS	EGR4	7.87E-06	1.14E-05	3.17E+04	4.60E+04	2.50E-01	1.45E-02	0.1115	0.9454
SVFNITAIA	MTNR1B	1.96E-05	2.39E-04	2.58E+04	3.15E+05	5.06E-01	1.06E-01	0.2805	0.7869
KIYNTPSAS	NCAM1	2.56E-05	2.88E-05	8.86E+03	9.95E+03	2.27E-01	5.62E-03	0.2474	0.9662
LLYNLLGSS	ABCC9	1.41E-04	6.82E-03	3.21E+03	1.55E+05	4.54E-01	5.27E-02	0.1153	0.9007
SLYNMMGEA	TMTC2	No fit							
SLWNLMGNA	LMAN2L	No fit							
GLYNIVGNA	SUMF1	No fit							
LTWNLTPKA	DLEC1	No fit							
LIFNVTGLA	ZDHHC23	No fit							
SIFNITGIA	MTNR1A	No fit							
LTFNLVSDA	CASP8AP2	No fit							
MQWNILAQA	CCRN4L	No fit							
LSWNLVPEA	COL7A1	No fit							
DLWNTLSEA	TRHDE	No fit							
GLFNIPPAF	CYP2S1	No fit							
LIWNILASF	TTC29	No fit							
LLFNMLPGG	EXT2	No fit							
LVYNIMSSG	FAM120B	No fit							
IIYNVPGTG	RNF133	No fit							
VIYNVTSDG	TTN	No fit							
GTFNLPSDG	BAG6	No fit							
KLWNTLNLI	ENPP5	No fit							
LMWNIISII	VTGN1	No fit							
GLFNNTSNI	SEMA3E	No fit							
LIFNTLSLI	PDCD6IP	No fit							
SVFNLMNAI	SLC38A6	No fit							
LTFNILGQI	DOCK11	No fit							
GLFNMVSSL	RRN3	No fit							
KIFNIINSL	FER1L5	No fit							
AVWNVLGNL	BAG5	No fit							
KVFNIIVSDL	FSIP2	No fit							
DLWNVVSHL	DDX60L	No fit							
LQFNTVSKL	JAM2	No fit							
MSFNTVSEL	ZNF33A,ZNF33B	No fit							
ASWNIVNLL	TRPA1	No fit							
ISFNIISAL	MS4A18	No fit							
AFFNILNEL	FBNP1L	No fit							
LVFNLLPIM	ABCB7	No fit							

Chapter 7

Peptide	Associated Gene	KD (M)	KD Error	k_{on} ($M^{-1}s^{-1}$)	k_{on} Error	k_{off} (s^{-1})	k_{off} Error	Full X ²	Full R ²
KIFNTVPDM	ARHGAP26	No fit							
MLFNLIGLS	OR10J1	No fit							
LLFNLPPGS	VGLL1	No fit							
MTFNLIGES	CR1,CR1L	No fit							
KVYNIPGIS	KLHL10	No fit							
GIYNIPGDS	TNS1	No fit							
GLYNLMNIT	INSR	No fit							
LTWNMINTT	LRIT3	No fit							
IVFNVLSDT	HCN3	No fit							
IVFNVVSDT	HCN2,HCN4	No fit							
LIFNITASV	SVEP1	No fit							
IVFNLTNNV	MNAT1	No fit							
KSFNVLSSV	ZNF557	No fit							
LAFNILGMV	SLC46A1	No fit							
VSWNITGTV	SEH1L	No fit							

7.10.3. Supplementary Methods

7.10.3.1 Peptide binding measured by fluorescence anisotropy

Peptide binding was evaluated in fluorescence anisotropy assay with 300 nM of purified refolded dsA*02:01. 100 nM of the fluorescently labeled high-affinity peptide NLVPK_{FITC}VATV (Genecast) was added to the folded dsA*02:01 and kinetic measurements were performed with Tecan Infinite M1000 PRO (Tecan, Crailsheim, Germany) multimode plate reader measuring anisotropy (FITC λ_{ex} = 494 nm, λ_{em} = 517 nm). dsA*02:01 were either used directly after refolding or preserved at -80°C in storage buffer (10% Glycerol, 50 mM Tris-HCL, pH 8.0) for the indicated amount of time before measurement. The kinetic measurements were performed at room temperature (22-24°C) in 50 mM HEPES buffer, pH 7.5. Data was plotted using GraphPad Prism v7.

7.10.3.2 Anti-beta-2 microglobulin ELISA

Streptavidin (Molecular Probes, Cat. Nr. S888) at a final concentration of 2 µg/ml in PBS was added to Nunc MAXIsorp plates (Thermo Fisher, Cat. Nr. 439454) and sealed plates incubated over night at room temperature in a damp environment. The following day plates were washed 4 times with washing buffer (PBS, 0.05% TWEEN-20) using a ELx405 plate washer (Biotek). 300 µl blocking buffer (PBS with 2% BSA) was added to each well and sealed plates incubated at 37°C for 1 hour. Blocking buffer was discarded before adding 100 µl of a 1:100 dilution in blocking buffer of the respective UV exchange pMHC preparation. A standard series ranging from 500 ng/ml to 15.6 ng/ml based on a conventionally refolded pMHC monomer was included on each plate. Edge wells were filled with 300 µl blocking buffer to reduce edge effects and sealed plates were incubated at 37°C for 1 hour. Plates were again washed 4 times before adding 100 µl anti-beta 2 microglobulin HRP conjugated secondary antibody (Acris, Cat. Nr. R1065HRP) at a final concentration of 1 µg/ml to each well. Sealed plates were incubated at 37°C for 1 hour. Plates were washed again 4 times with washing buffer before adding 100 µl of room temperature TMB substrate (Sigma, Cat. Nr. T0440) to each well. Plates were incubated for 5 minutes at room temperature before stopping by adding 50 µl 1N H₂SO₄ to each well. Plates were immediately analyzed by reading absorbance at 450 nm for 5 seconds using a Synergy2 plate reader. pMHC concentration was calculated based on standard curve fitting ($\text{Log}(Y)=A*\text{Log}(X)+B$) using the Synergy2 software. Data was plotted using GraphPad Prism v7.

7.10.3.3 Flow cytometric T2 peptide binding assay

The TAP-deficient HLA-A*02:01-expressing cell line T2 was procured from ATCC (CRL-1992) and cultured in RPMI Medium 1640 GlutaMAX™ (Thermo Fisher, Cat. Nr. 61870010) supplemented with 10% heat inactivated FCS (Life Technologies, Cat. Nr. 10270106) and the antibiotics penicillin and streptomycin (Biozym, Cat. Nr. 882082, 100 µg ml⁻¹ each) up until passage number 16 if necessary. T2 cells were harvested from continuous cell culture, washed and resuspended in T2 culture medium at a concentration of 3.3 x 10⁶ cells ml⁻¹ and transferred to 96 well round bottom plates (Corning costar®, Cat. Nr. 3799). Peptide in DMSO, 0.5% TFA was added to a final concentration of 10 µM and the suspension incubated for 2 hours 37°C, 5% CO₂. Plates were washed twice with PFEA (PBS, 2% FCS, 2 mM EDTA, 0.01% sodium azide) before addition of 50 µl PE labelled anti-human HLA-A2 (Biolegend, Cat. Nr. 343305) per well diluted 1:250 with PFEA to a final concentration of 0.8 µg/ml. Plates were incubated at 4°C for 30 minutes before being washed twice with PFEA. Finally, cells were resuspended in fixation solution (PFEA, 1% formaldehyde) and kept at 4°C before analysis using an iQue Screener (Intellicyt). T2 cells were gated based on the FSC-A/SSC-A signal and doublets removed using an FSC-H/FSC-A doublet exclusion. The PE channel positive gate coordinates were based on an unstained control. Data was plotted using GraphPad Prism v7.

Chapter 8. Mapping the peptide binding groove of MHC class I

This chapter highlights the published manuscript about mapping the peptide binding groove of MHC-I molecules using native mass spectrometry based approach.

Janine-Denise Kopicki, our collaborator at Heinrich Pette Institute, Leibniz Institute for Experimental Virology (HPI), was responsible for the majority of the experimental data. For this manuscript, I have expressed the recombinant protein and performed the *in vitro* refolding and purification to generate the empty dsA2 molecule for the studies. I have also performed the thermal stability studies using nanoDSF method to generate the data for figure 8-4 B, 8-7 B, S8.3 and table S8-4.

The manuscript was written by Janine-Denise Kopicki, Sebastian Springer and Charlotte Uetrecht.

The full citation of the paper is:

Janine-Denise Kopicki, Ankur Saikia, Stephan Niebling, Christian Günther, Maria Garcia-Alai, Sebastian Springer, Charlotte Uetrecht. **“Mapping the peptide binding groove of MHC class I”**.

bioRxiv, 2021.08.12.455998;

Online link: <https://doi.org/10.1101/2021.08.12.455998>

The figure numbers were changed to match the format of this thesis.

8.1. Abstract

An essential element of adaptive immunity is the selective binding of peptide antigens by major histocompatibility complex (MHC) class I proteins and their presentation to cytotoxic T lymphocytes on the cell surface. Using native mass spectrometry, we here analyze the binding of peptides to an empty disulfide-stabilized HLA-A*02:01 molecule. This novel approach allows us to examine the binding properties of diverse peptides. The unique stability of our MHC-I even enables us to determine the binding affinity of complexes, which are suboptimally loaded with truncated or charge-reduced peptides. Notably, a unique erucamide adduct decouples affinity analysis from peptide identity alleviating issues usually attributed to clustering. We discovered that two anchor positions at the binding surface between MHC and peptide can be stabilized independently and further analyze the contribution of other peptidic amino acids on the binding. We propose this as an alternative, likely universally applicable method to artificial prediction tools to estimate the binding strength of peptides to MHC-I complexes quickly and efficiently. This newly described MHC-I-peptide binding affinity quantitation represents a much needed orthogonal, confirmatory approach to existing computational affinity predictions and has the potential to eliminate binding affinity biases and thus accelerate drug discovery in infectious diseases autoimmunity, vaccine design, and cancer immunotherapy.

8.2. Teaser

Native mass spectrometry determines both specific binding properties and affinities of different peptides to an empty disulfide-stabilized HLA-A*02:01 molecule in an unbiased fashion.

8.3. Introduction

Major histocompatibility complex (MHC) class I molecules are central to the cellular adaptive immune response, presenting the intracellular peptidome to cytotoxic T lymphocytes, which detect non-self-peptide/MHC-I (pMHC) combinations and induce apoptosis in the presenting cell. Novel immunotherapy approaches, in which antiviral or antitumor T cells are identified, stimulated, and reintroduced into the patient, require the identification of high-affinity virus- or tumor-specific epitopes. The identification of high-affinity peptides is also key to developing efficacious peptide vaccines that have been prioritized by the WHO several years ago [1]. This is currently done either by isolating pMHCs from patient samples, eluting the peptides, and sequencing them by mass spectrometry (MS) [2]; or by sequencing the virus or the exome of a tumor and predicting the binding peptides [3].

Such prediction is informed by the well-understood structural basis of MHC-peptide binding [4], with > 1500 human and > 400 murine crystal structures in the protein data bank (PDB [5]) at this time. The peptide binds into a groove that consists of a β sheet topped by two parallel α helices with its amino terminus contacting the A pocket at one end of the groove [6] and the C-terminal carboxylate held by a network of hydrogen bonds at the other end. These interactions limit the length of a high-affinity peptide to 8-10 amino acids [7]. In addition, side chains of the peptide (usually two) bind into other pockets at the bottom of the groove; one of them is always the F pocket (which usually binds the hydrophobic side chain of the C-terminal amino acid). Together, these interactions define the peptide binding motif of a particular class I allotype (such as xLxxxxxxV for HLA-A*02:01). About 16,000 class I allotypes have been described to date, with nine of them found in > 75 % of the Caucasian and Asian population [8].

This structural knowledge, together with extensive databases of eluted peptides, has been used to train computational methods for the prediction of peptide epitopes from tumors [9]. However, this approach suffers from the uncertainty created by matching the eluted peptide to one of the six present MHC class I allotypes in a human being. Hence, to accelerate biological testing, it is desirable to rank candidate peptides by their binding affinity using a direct approach. Yet, to date, simple peptide binding assays that are amenable to high-throughput screening have not been available because they require empty peptide-receptive class I molecules, which are conformationally unstable [7, 10].

Recently, empty disulfide-stabilized class I molecules (dsMHC) have become available [11-13] that have the same peptide- and T cell receptor-binding specificities and affinities as the wildtype. Due to their stability in the empty state and their rapid binding, these dsMHC lend themselves to high-throughput approaches. We have previously employed native mass spectrometry (MS) to analyze peptide-bound

MHC-I complexes. Furthermore, we recently have shown using native MS that the dsMHC variant of the HLA-A*02:01 (dsA2) can indeed be freed from the dipeptide used to facilitate refolding. Moreover, the empty binding groove can bind an exogenous peptide with the resulting pMHC appearing as an additional signal in the mass spectrum [14]. Native MS simultaneously detects all different mass species present in solution while quaternary structures and non-covalent bonds can be preserved [15]. Even though in the gas phase, there is no longer an equilibrium of protein-ligand binding, previous studies demonstrated that native MS is an effective tool to determine dissociation constants, as the method captures and reflects the equilibrium state of the solution allowing the determination of absolute ligand binding affinities [16-22].

In this work, the use of native MS to assess the binding affinity of peptides to dsMHC is demonstrated and verified by nanoscale differential scanning fluorimetry (nDSF). Our native MS method is used to show the effects of truncations and modifications on the binding affinity of peptides, the binding of two truncated peptides to the same class I molecule, and to investigate the cooperativity between the A and F pockets in peptide binding. Finally, yet importantly, this approach can be utilized to systematically investigate MHC-I peptide binding as the method is perfectly suitable for high-throughput applications.

8.4. Results

8.4.1. Peak intensity in native mass spectra reflects peptide-MHC binding affinity

Empty dsA2 consists of the disulfide-stabilized HC (HLA-A*02:01(Y84C/A139C)) and the light chain, beta-2 microglobulin (β_2m). Bacterially expressed dsA2 hc and β_2m is folded *in vitro* into the dsA2 complex with dipeptides (GM or GL) and purified by size-exclusion chromatography (SEC) as described [10, 14]. During SEC, the dipeptide is removed and becomes undetectable by native MS, resulting in an empty binding groove (**Figure 8-1, A and B**). At a low acceleration voltage of 25 V, raw and deconvoluted spectra (**Figure 8-1, C and D**) demonstrate a stable complex of HC and β_2m in the absence of any peptide. Some minor in-source dissociation (ISD, < 5 %) occurs upon activation in the mass spectrometer, with hc and β_2m detected individually. The remaining fraction of dsA2 carries a small molecule adduct (337 Da by tandem MS analysis), which is easily released at ≥ 50 V by collision-induced dissociation (CID). Since protein production and sample preparation use no substance of this mass, the 337 Da molecule hypothetically originates from laboratory plastic ware as reported [23-25]. Indeed, small molecule MS reveals several common contaminants found in plastic-stored solutions, with

erucamide ((*Z*)-docos-13-enamide) strongly enhanced in dsA2 samples and thus identified as the adduct (**Figure S8-1**).

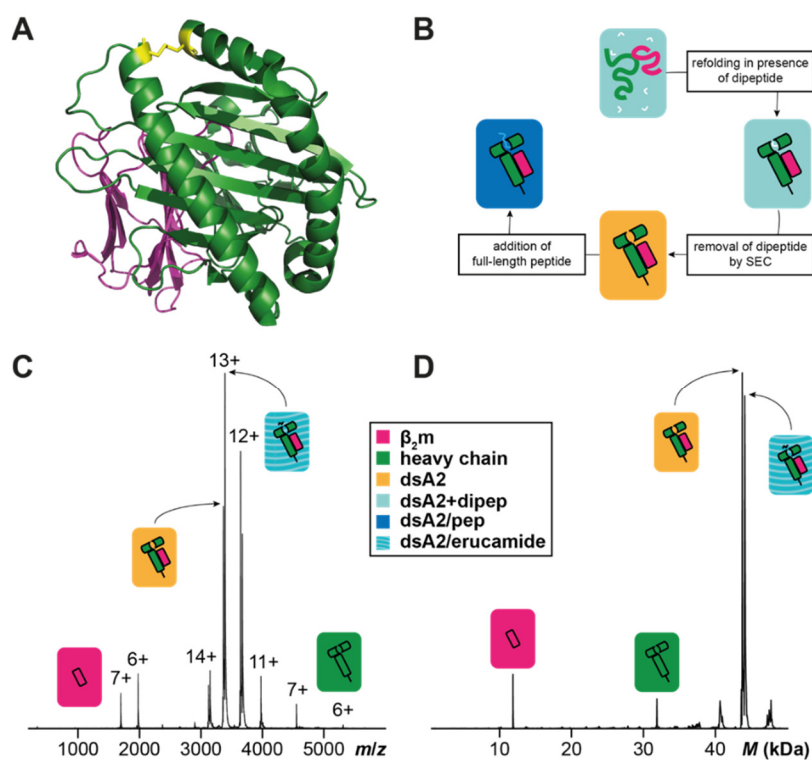
In the following, it is examined whether native MS can differentiate the binding of high-affinity and low-affinity peptides by comparing the A2 epitope NV9 from human cytomegalovirus pp65 (sequence NLVPMVATV; theoretical dissociation constant, $K_{d,th} = 26$ nM predicted by NetMHC [9]) with the irrelevant YF9 (YPNVNIHNF; $K_{d,th} = 27$ μ M) and with GV9 (GLGGGGGGV; $K_{d,th} = 2.7$ μ M), a simplified NV9 derivative that retains the anchor residues, L and V. 10 μ M dsA2 is incubated with 50 μ M peptide for ten minutes prior to native MS, where the acceleration voltage across the collision cell is increased incrementally (10, 25, 50, 75, and 100 V) to observe the dissociation behavior. At 75 and 100 V, β_2m heavily dissociates from the hc (data not shown), and so in the following, only results for 10 V, 25 V and 50 V are shown. The signal is quantified by determining the area under the curve (AUC) over the entire spectrum for each mass species (**Figure 8-2**; raw spectrum in **Figure S8-2**). While at 10 V and 25 V the distribution of the different mass species is very similar, the ratios change significantly at 50 V. This is a frequent observation with the electrospray ionization (ESI) process, where non-covalent hydrophilic bonds such as those between dsA2 and high affinity peptides are retained [16, 27-29], but hydrophobic interactions are weakened. By increasing the acceleration voltage, the dissociation of a protein-ligand complex usually does not occur gradually but spontaneously beyond a certain threshold, at which an energetic state is encountered that denatures the complex, in our case between 25 and 50 V. Therefore, the measurements at 10 V are used to calculate the dissociation constants.

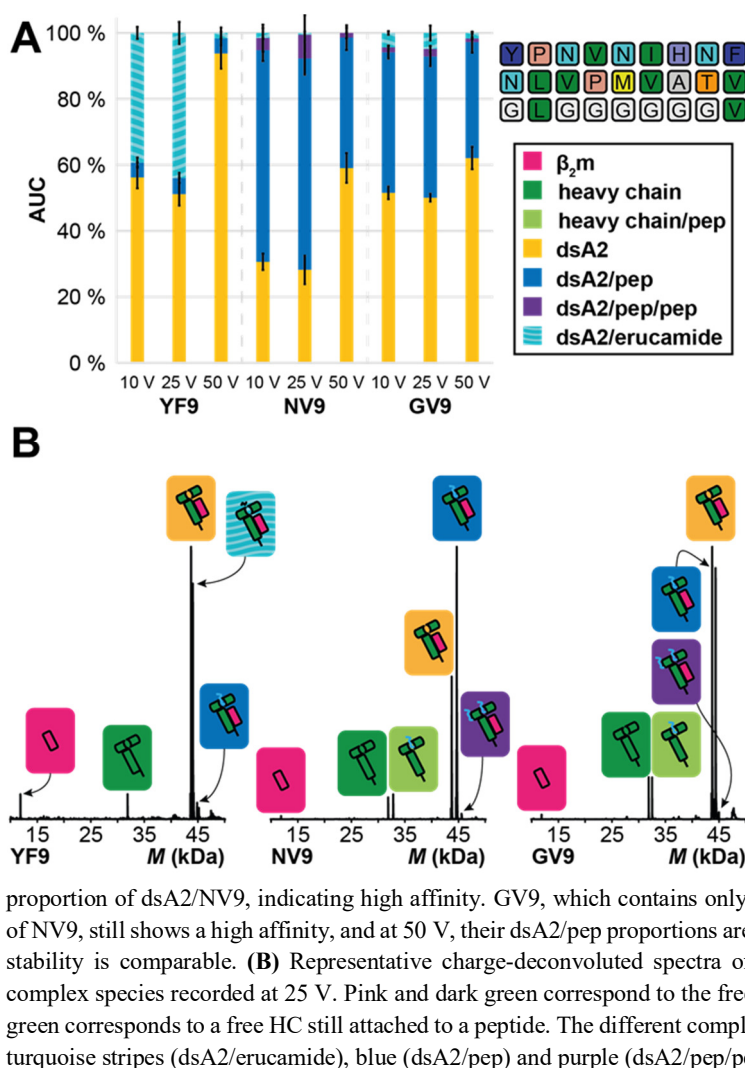
In the presence of low-affinity YF9, the empty dsA2 molecule ($43,733 \pm 4$ Da) generates the highest signal (56 ± 3 % at 10 V; **Figure 8-2 A**). Most of the remainder of dsA2 carries only the erucamide adduct ($44,071 \pm 5$ Da; 39 ± 2 %). There is very little dsA2/YF9 complex (4 ± 2 %), and because of the very low binding affinity of YF9, it can be assumed that this signal does not correspond to real binding events but rather to an artifact of the electrospray process known as non-specific clustering [17, 30-33].

Assuming that the other tested peptides cluster to the same extent, all native MS data is therefore corrected for the clustering determined with YF9. Since the data measured for the peptides of interest are therefore netted with YF9, no affinities are calculated for this control peptide. Corresponding raw data for the negative control are listed in the supplement (**Table S8-2**).

For NV9, in contrast, very efficient binding is observed, with 64 ± 3 % for dsA2/NV9 at 10 V and 40 ± 4 % at 50 V. Here, the dsA2/erucamide complex is completely absent, which suggests that erucamide is displaced by NV9. Erucamide either binds into the peptide groove, or it binds elsewhere

and is displaced by a conformational change caused by peptide binding. A small amount of another mass species ($45,624 \pm 4$ Da) that corresponds to dsA2 with two molecules of NV9 (dsA2/NV9/NV9) with an abundance of $4 \pm 4\%$ (10 V) and $1 \pm 2\%$ at 50 V is observed. The latter is likely the result of unspecific clustering as the abundance correlates with the intensity of the first binding event and is similar to the intensity of YF9 binding. Within NV9, the leucine in the second position and the C-terminal valine bind into the B and F pocket of the binding groove, respectively [12, 34, 35]. The proportion of dsA2 occupied with GV9 at 10 V ($43 \pm 2\%$, and $1.5 \pm 0.4\%$ for dsA2/GV9/GV9) is significantly lower than the proportion of dsA2/NV9. This clearly shows that the minimal binding motif cannot support the same affinity as NV9, suggesting that other amino acids contribute significantly to the binding. At 50 V, however, the abundance of the dsA2/pep complex is the same for GV9 and NV9. This indicates that the strong B and F pocket side chain interactions together with the binding of the termini determine pMHC gas phase stability.





Despite very efficient binding, the obtained K_d for NV9 is only $8 \pm 2 \mu\text{M}$, while NV9 has nM affinity [36]. Hence, a fully occupied peptide binding pocket (predicted $> 99 \%$) is expected in our measurements (Figure 8-2 A). Protein denaturation due to storage or other physicochemical stress (data not shown) is excluded, and thus ISD, which occurs in the source region of the mass spectrometer and results in reduction of the dsA2/NV9 complex, is considered next. Here, lower cone voltages can increase the proportion of the occupied complex [37, 38]. Indeed, the occupancy of the peptide binding groove with both the peptide and erucamide is higher at lower cone voltages. This linear relationship is most evident with dsA2 alone, to which erucamide is the only binding partner (Figure 8-3 A). The data suggest that at a cone voltage of $\leq 36 \text{ V}$, which is unfeasible experimentally, dsA2 is 100 % occupied with erucamide. This observation allows us to use erucamide as a reference species for peptide binding measurements,

assuming that in solution, all free dsA2 protein is initially bound to erucamide as suggested by the zero cone voltage extrapolation, and that the peptide replaces it in the binding region. From the erucamide-bound fraction measured at a cone voltage of 150 V in native MS, the fraction of dsA2/erucamide corresponding to the fraction of dsA2 not bound to peptide at the end of the binding reaction can be recalculated using the correction factor of 2.2 originating from the linear function's slope. From this, the fraction of dsA2/peptide is inferred, resulting in an apparent K_d that reflects the in-solution environment (see the Materials and Methods). This is highly advantageous, since for individual pMHCs, the ISD is naturally influenced by peptide size and sequence, precluding compensation, while the ISD of the MHC-erucamide complex is invariant, and peptide independent. Therefore, for each peptide both a dissociation constant for the high cone voltage (150 V) based on clustering-corrected MHC-peptide signal ($K_{d,high}$) and another for the theoretical low cone voltage of 36 V based on the MHC-erucamide signal ($K_{d,low}$) is described (**Figure 8-3 A**). While the experimentally determined $K_{d,high}$ is overestimated due to ISD, the $K_{d,low}$ is a more reliable approximation.

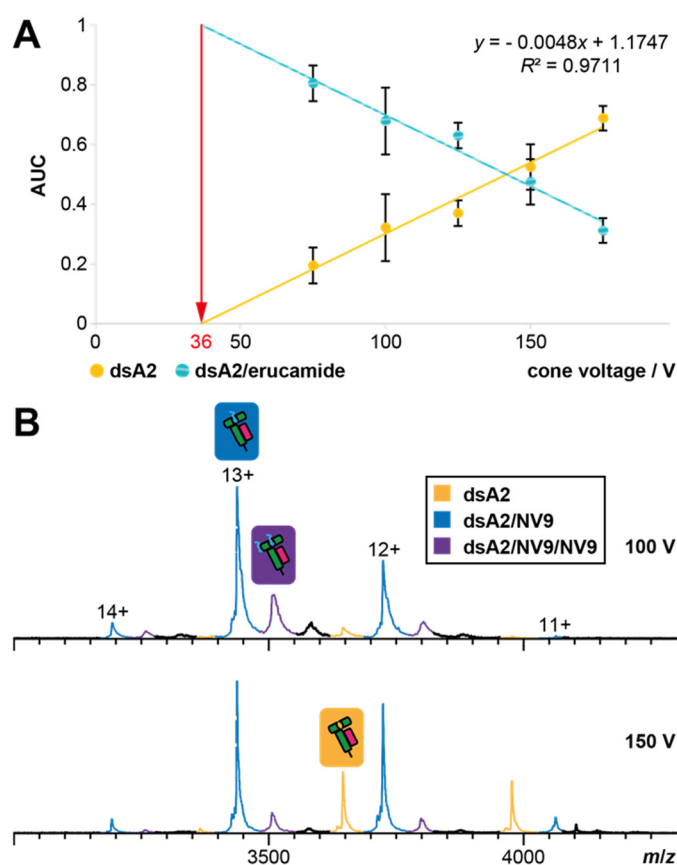


Figure 8-3. Ion-source decay causes linear dependence of the ligand-bound dsA2 fraction on cone voltage.

(A) Native MS fractions of dsA2 and dsA2/erucamide are likewise dependent on the activation energy of the cone voltage. As the cone voltage is raised, the percentage of empty dsA2 increases because the adduct binding cannot withstand the energy in the ion source and therefore dissociates. The proportionality is linear, and therefore a theoretical cone voltage of 36 V can be calculated, at which a full occupancy with ligand would be reached. In reality, this voltage is too low to obtain stable electrospray and a resolved spectrum. **(B)** Peptide binding is equally subjected to in-source dissociation. NV9-bound dsA2 (blue and purple annotated peaks) become less prominent with increasing cone voltage, while empty dsA2 (yellow) increases at the same time.

To see whether the affinities thus obtained match those measured by a previously validated method, a series of sixteen peptides, most of them variations or truncations of the sequence of NV9, are compared in native MS and in isothermal analysis of nanoscale differential scanning fluorimetry (iDSF) [39]. K_d values from native MS and iDSF correlate very well over a wide range (**Table S8-3, Figure 8-4 A**). It has to be noted though that affinities below 200 nM have to be treated with caution as the peptide concentration is very low and hence the fraction of dsA2/pep. This is also evident from the thermal stabilization discussed in the following. For NV9, the binding groove is so well stabilized that other domains unfold first [40, 41]. Nevertheless, the peptide binding affinity measured by native MS correlates very well with the thermal stabilization of dsA2 by peptide binding (protein-peptide ratio: 1:10, **Figure 8-4 B**). Conformational stabilization corresponds to an increase in the midpoint of thermal denaturation (T_m) above that of the empty dsA2, which is measured by tryptophan nanoscale differential scanning fluorimetry (nDSF [40, 42]) to be 35.7 ± 0.6 °C. While the negative control YF9 clearly shows no ($\Delta T_m = 1 \pm 1$ K), the positive control NV9 shows a high degree of stabilization ($\Delta T_m = 23.4 \pm 0.6$ K) in agreement with published data [12]. The other peptides show excellent correlation between affinity and stabilization ability. All peptides identified as strong binders by their apparent dissociation constant exhibit a ΔT_m of at least 6.4 ± 0.6 K (GV9), while the ΔT_m for the low-affinity peptides ranges between ≈ 0 K and ≈ 3 K (**Figure 8-4 B**, red area). Closer evaluation of the data shows that peptides with a $K_{d,low} < 1$ μ M also have an increased gas phase stability of the complex at 50 V (dsA2/pep + dsA2/pep/pep > 35 %) and present only negligible amounts of dsA2/erucamide at any voltage. Therefore, we define all peptides that fall within this range as strong binders for dsA2 (**Figure 8-4 B**, white area). These results demonstrate that by simply comparing the intensities in the native mass spectrum, it is possible to estimate, which properties define peptides to act as high-affinity epitopes for HLA-A*02:01.

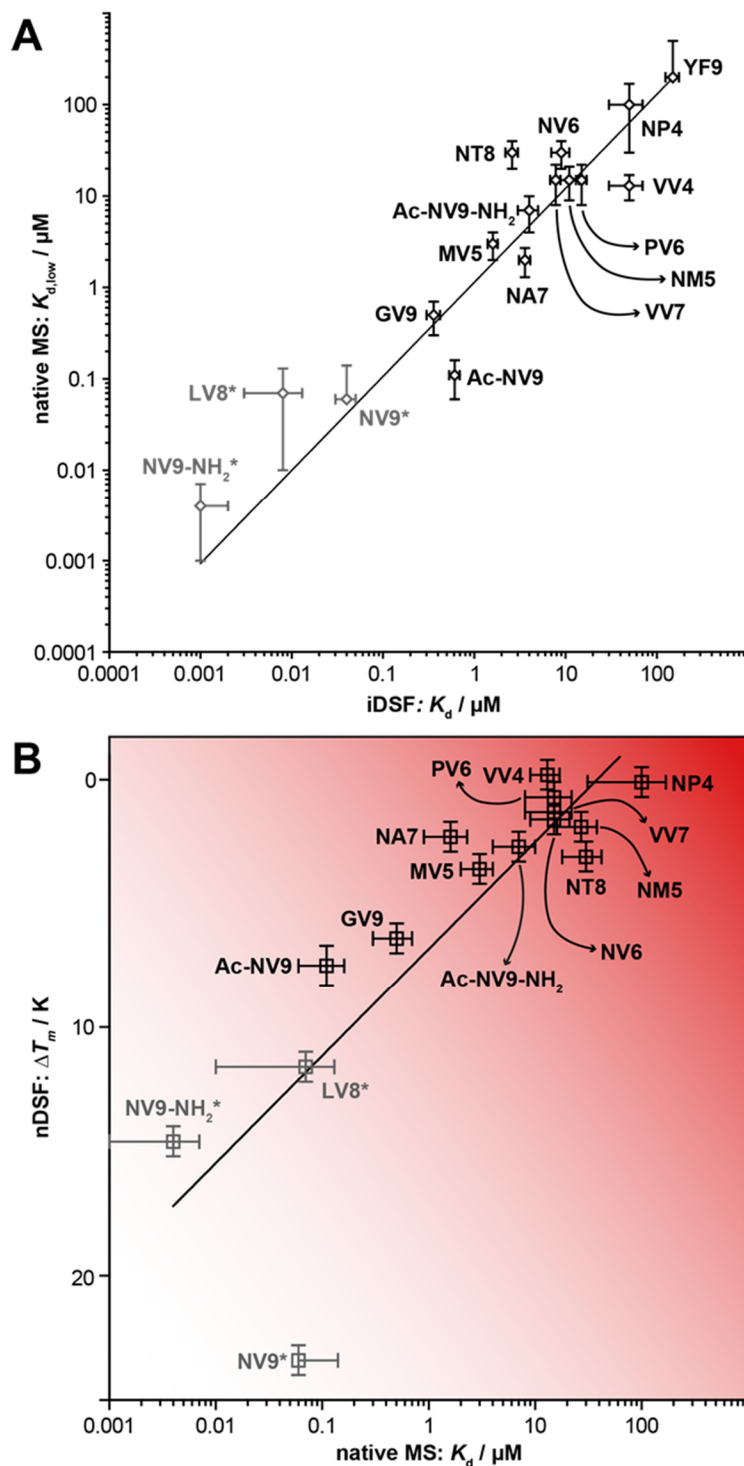


Figure 8-4. Relation of thermal stability and affinity for dsA2/peptide complexes.

(A) Affinities determined via iDSF and native MS correlate. Displayed data points represent the relationship of both apparent K_d for all different dsA2/peptide systems analyzed. Both axes are scaled logarithmically. (B) Thermal denaturation measurements availing intrinsic tryptophans' change in fluorescence are used to define protein complex stabilization upon peptide binding, whereas an apparent K_d for the various peptides is determined using native MS (10 V acceleration voltage, 150 V cone voltage). The dsA2 complex and peptide are deployed in a ratio of 1:10 (ΔT_m) or 1:5 (K_d) depending on the experiment. Peptides showing a small $K_{d,low}$ for binding dsA2 and being concomitantly able to stabilize the protein complex are defined as strong binders (white area). The remaining peptides (red area) are lacking crucial features, making them unable to form strong bonds to dsA2 indicated by low binding affinities and melting temperatures. Standard deviation for both methods is displayed by error bars. The x-coordinate is displayed logarithmically. *iDSF reaches its limits at affinities below 200 nM, hence the values of grayed-out peptides are not reliable.

8.4.2. Neutralizing the terminal charges of the peptide reduces binding efficiency

Next, the influence of the charged termini of the peptide upon the binding affinity is analyzed. For this purpose, three variants of NV9 are designed: Ac-NV9-NH₂ has an acetylated *N*-terminus and an amidated *C*-terminus, whereas Ac-NV9 and NV9-NH₂ each carry only one of these modifications. For the dsA2/pep fraction at 10 V, Ac-NV9 and NV9-NH₂ show only a small difference to the unmodified NV9, resulting in comparable apparent K_d values ($K_{d,low} = 0.11 \pm 0.05 \mu\text{M}$ and $0.004 \pm 0.003 \mu\text{M}$). Further, no increase of dsA2/erucamide is observed (**Figure 8-5 A**). For both peptides, the protein-ligand complex is still stable at 50 V (**Figure S8-5**). For Ac-NV9, the proportion of the occupancy is even higher than for NV9 itself ($57 \pm 2 \%$ and $8 \pm 1 \%$ vs. $40 \pm 4 \%$ and $1 \pm 2 \%$, **Table S8-2**). Remarkably, all modified peptides have an increased double occupancy. For the previously discussed peptides, dsA2/pep/pep is significantly lower with the result that correction for non-specific clustering reduces it to a value below threshold. For Ac-NV9, this effect is significant, since even at 50 V the proportion of dsA2/pep/pep (purple bars) is still $8 \pm 1 \%$. However, the stabilization effect on dsA2 in a 1:10 thermal denaturation approach is rather moderate for Ac-NV9 ($\Delta T_m = 7.5 \pm 0.8 \text{ K}$), while it is very strong for NV9-NH₂ ($\Delta T_m = 14.6 \pm 0.6 \text{ K}$), indicating that the *N*-terminus has more relevance for tight peptide binding than the *C*-terminus.

The correction for unspecific binding is based on the negative control YF9, with both termini unmodified. By neutralizing the positive charge at the amino group, Ac-NV9 could be more susceptible to nonspecific electrostatic interactions at the protein surface, which are then preserved in the gas phase. However, this should not be the case for the erucamide-based K_d . The variant Ac-NV9-NH₂ shows significant changes both in its affinity to dsA2 and in complex stabilization. At the same time, there is no significant increase in the formation of double binding events. The affinity decreases significantly ($K_{d,low} = 7 \pm 3 \mu\text{M}$) due to the dual modification, a high amount of erucamide is not replaced, and at an acceleration voltage of 50 V, the complex is no longer stable. The nDSF measurements likewise show that the stabilization effect with $\Delta T_m = 2.7 \pm 0.6 \text{ K}$ is rather weak. Although NV9-NH₂ is far better rated within our scheme (**Figure 8-4 A**) in terms of affinity and stabilizing effect, Ac-NV9 still falls into the category of a strong binder. For the dual-modified variant, which no longer carries terminal charges, a clear loss of binding efficiency can be observed indicating that ionic interactions are indispensable in the formation of the MHC-peptide complex and, without them, efficient binding cannot be established.

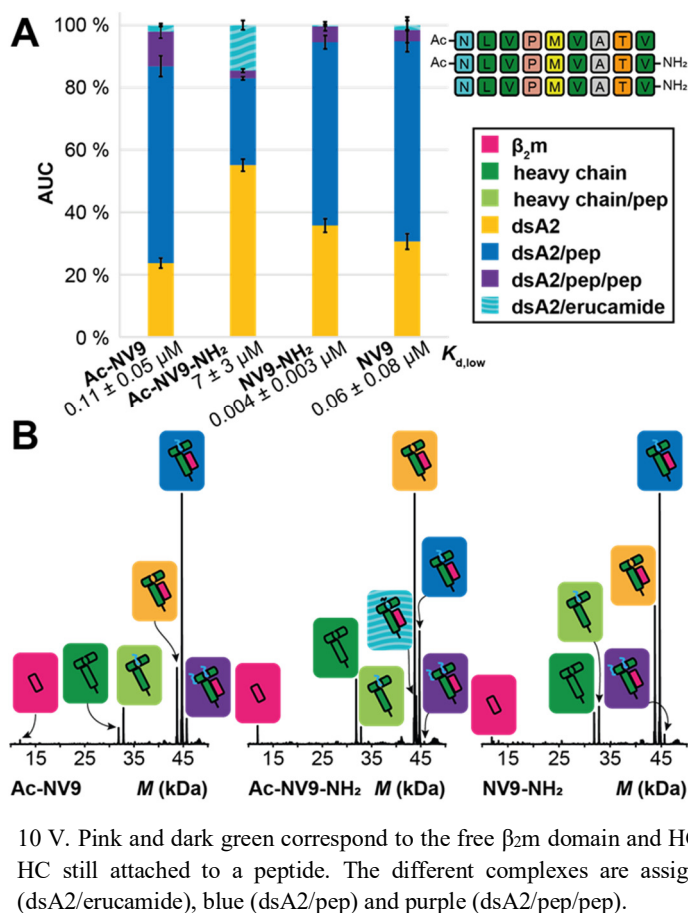


Figure 8-5. Charge-reduced NV9 variants analyzed at 10 V.

(A) The AUC is determined over the entire spectrum for the respective mass species at an acceleration voltage of 10 V. The mean value of the AUC in absence or presence of the different peptides (protein-peptide ratio 1:5) from at least three independent measurements is depicted along with error bars that represent the corresponding standard deviation. “dsA2” (yellow bars) corresponds to the empty complex, “dsA2/pep” (blue bars) to dsA2 bound to one peptide, “dsA2/pep/pep” to dsA2 bound to two molecules of this certain peptide (purple bars) and “dsA2/erucamide” to dsA2 bound to erucamide (turquoise-striped bars) respectively. By modifying only one terminus (Ac-NV9 and NV9-NH₂), the affinity of the peptide to dsA2 changes only marginally, but if the charges on both termini are neutralized (Ac-NV9-NH₂), the peptide binding is greatly reduced. The corresponding $K_{d,low}$ is shown for respective peptides. (B) Representative charge deconvoluted spectra of the distinct protein and protein-peptide complex species recorded at

8.4.3. Truncated NV9 discloses preferred binding positions in the peptide

In the following, it is analyzed how stepwise truncation of NV9 from either terminus affects binding to identify the binding contributions of individual residues by MS. Building on the knowledge from the dsA2/NV9 crystal structure [12, 14], the peptide binding groove can thus be mapped and further understood. *In vivo*, MHC-I predominantly binds peptides with a length of eight to ten amino acids [7, 43, 44]. It is therefore not surprising that octa- and nonapeptides show the highest affinity (**Figure 8-6, Table S8-3**). Looking at the effect of the loss of only one of the two terminal amino acids, asparagine and valine, the difference is striking. Despite the absence of asparagine (corresponding to LV8), the affinity ($K_{d,low} = 0.07 \pm 0.06 \mu\text{M}$) is still comparable to NV9 with a considerable stabilizing effect during thermal denaturation of dsA2 (1:10, $\Delta T_m = 11.6 \pm 0.6 \text{ K}$). At 50 V, dsA2/LV8 even appears to be more stable than dsA2/NV9. In contrast, loss of the C-terminal valine results in a strong decrease in affinity

($K_{d,low} = 30 \pm 10 \mu\text{M}$). The erucamide is no longer fully displaced by NT8, only a small fraction of the protein-peptide complex is resistant to the higher acceleration voltage and no significant stabilization effect ($\Delta T_m = 3.1 \pm 0.6 \text{ K}$) is measured. These observations suggest that the binding between the C-terminus of the peptide and the F pocket of the MHC molecule is essential, whereas the binding of the N-terminus located within the A pocket is less important for the overall binding efficiency. However, when the second amino acid in the N-terminal direction, leucine, is eliminated as well (VV7), affinity and stabilizing effects are likewise diminished. Along with our findings on GV9, it is evident that the anchor residues of the nonapeptide are in second and last position. Efficient binding between peptide and HLA-A*02:01 only occurs if both positions are covered by suitable amino acids. Nevertheless, the difference between GV9 and LV8 points towards an additional contribution of the other amino acids that is in sum larger than the N-terminal contribution.

Therefore, none of the examined tetra- to heptapeptides are strong binders. In direct comparison, VV7, which still contains the C-terminal anchor residue Val-9, performs worse than NA7, which in contrast carries Leu-2. NA7 displaces more of the erucamide, and at 50 V, significantly more NA7 than VV7 is observed (**Figure S8-5**). Thus, Leu-2 appears to possess more binding strength than Val-9. Curiously enough, the N-terminally truncated pentapeptide MV5 performs significantly better than the corresponding hexa- (PV6) and heptapeptides (VV7). The increased proportion of dsA2/MV5, which is even more evident at 50 V (**Figure S8-5**) and the simultaneous occurrence of dsA2/MV5/MV5 (purple bars, **Figure 8-6**) strongly suggest that this peptide occupies an additional binding site within the peptide groove. Since this effect is not apparent for the smaller and therefore less spatially restricted VV4, the terminal methionine seems to be the decisive factor here. Since no increased dual occupancy is observed for NM5 and since binding at 50 V is weaker in direct comparison to MV5, it seems that the terminal methionine as such is not determinant on its own, but much more the relative position within the peptide. Considering the tetrapeptides, again the N-terminally truncated peptide, VV4, performs better than the C-terminally truncated NP4 at all acceleration voltages, which points to the positioning of the erucamide within the peptide pocket. While NP4 carries only the anchor peptide Leu-2, it seems that VV4 has a higher chance to bind to the dsA2 peptide groove due to its two terminal valines.

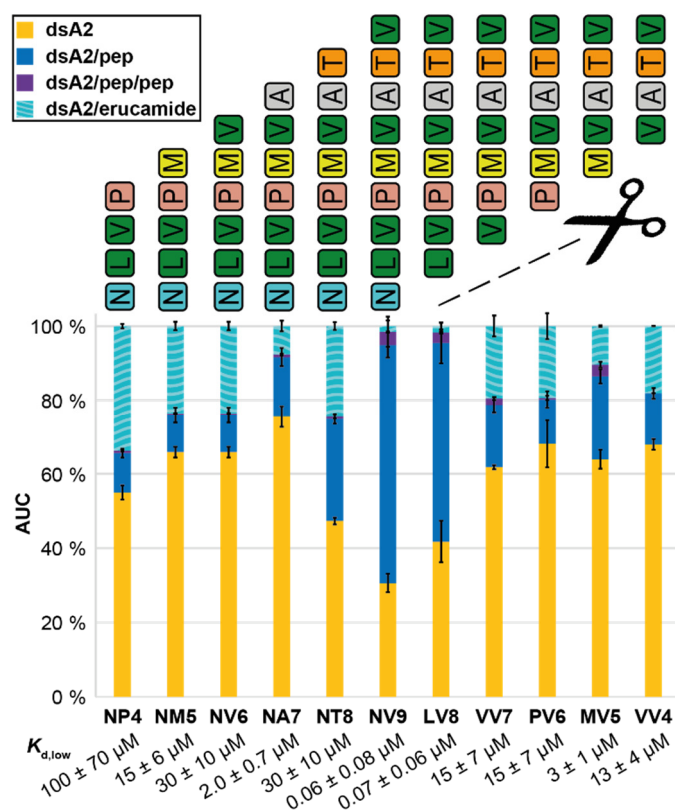


Figure 8-6. Truncated NV9 variants analyzed at 10 V.

The AUC is determined over the entire spectrum for the respective mass species at 10 V. The mean value of the AUC in absence or presence of the different peptides (protein-peptide ratio 1:5) from at least three independent measurements is depicted along with error bars that represent the corresponding standard deviation. “dsA2” (yellow bars) corresponds to the empty complex, “dsA2/pep” (blue bars) to dsA2 bound to one peptide, “dsA2/pep/pep” to dsA2 bound to two molecules of this certain peptide (purple bars) and “dsA2/erucamide” to dsA2 bound to the erucamide (turquoise-striped bars) respectively. Octa- and nonapeptides have the highest binding efficiency in accordance with their biological function. Without the anchor residues Leu-2 and Val-9 in a truncated NV9 variant, the affinity decreases drastically. A terminal methionine appears to enhance the affinity of the peptide to dsA2. The corresponding $K_{d,low}$ is shown for respective peptides.

8.4.4. The A and F pocket may be occupied simultaneously by two peptides

Encouraged by MV5 double binding, the simultaneous presence of two peptides in the binding pocket is further investigated [45]. Since binding of either peptide can be measured independently of the presence of the other in a single experiment – which, so far, no other method can provide – this allows us to assess whether the binding to the two ends of the peptide binding groove of MHC-I is cooperative. Our experiments are done with the partial peptides of NV9 that are combined with their corresponding counterparts from the opposite terminus. There are two ways in which two short peptides that bind to different sites in the binding groove could synergize in binding. They may stabilize the conformation of the molecule independently of each other, without any communication between the binding sites. In addition, it is possible that they bind in a cooperative manner. Hereby, the two binding sites communicate by a conformational or dynamic change in the protein and one peptide stabilizes (or destabilizes) the binding site for the other, such that the binding affinity for the second peptide is higher (or lower) in presence of the first.

In **Figure 8-7 A**, single and double occupancy for the first and second peptide as well as the double occupancy of both peptides are depicted. The results of the native MS measurements reveal that the previously presented affinities of the two individual peptides are also reflected well in this combined setup. This also implies that the overall proportion of dsA2/pep1/pep2 remains very low in absence of positive cooperativity. Presumably, due to spatial restriction, no double-occupied complex can be detected in the pairing of the pentapeptide NM5 and the hexapeptide PV6. In the other combinations, it is possible to detect dsA2/pep1/pep2. Yet only when MV5 is involved in the binding, the complex is able to withstand higher acceleration voltages. It is assumed, however, that this is not due to a cooperative binding between NP4 and MV5, NM5 and MV5 or NV6 and MV5, but can rather be explained by the higher affinity of MV5, which again emerges in this experiment. With the dual approach, it is visible that VV4 is more dominant than NP4. The indirect comparison between NP4+PV6 and NV6+VV4 highlights this in particular. The shorter VV4 achieves a significantly higher occupancy fraction in competition with the corresponding hexapeptide, which is not the case for NP4. This once again suggests that VATV appears to have more binding options due to its two terminal valines.

While in the native MS measurements the occupancy of two peptides can be observed simultaneously, in nDSF we can use higher peptide excess and evaluate whether two peptides are able to synergistically stabilize the complex. The melting temperature of dsA2 exposed to only one of the truncated NV9 variants (**Figure S8-3**) is compared to the resulting T_m when two peptides are utilized. The ratio between protein and total peptide concentration is kept constant at 1:1000. Assuming no synergistic effect occurs, the resulting melting temperature is expected to be just between those for the individual competing peptides according to their affinity to dsA2. The majority of the peptide pairs show a competitive behavior and do not demonstrate better stabilization by both peptides combined. Whereas for NP4 and VV4 and to a lesser extent for NP4 and PV6 as well, a higher T_m is measured for both peptides together than for each of them separately revealing that dsA2 can be stabilized by two shorter peptides in a synergistic fashion while the respective affinities are not mutually influenced (**Figures 8-7 B**). Once again, MV5 stands out particularly in this experiment. Two parts of MV5 provide significantly more thermal stability to dsA2 than one part of MV5 together with one part of one of either of the corresponding *N*-terminal peptides. These observations suggest that unfolding of MHC-I or at least of the disulfide mutant can begin at either end of the peptide binding groove. Consequently, this also means that the opposite ends of the binding groove cannot communicate conformationally, which was already described for the corresponding wildtype [11].

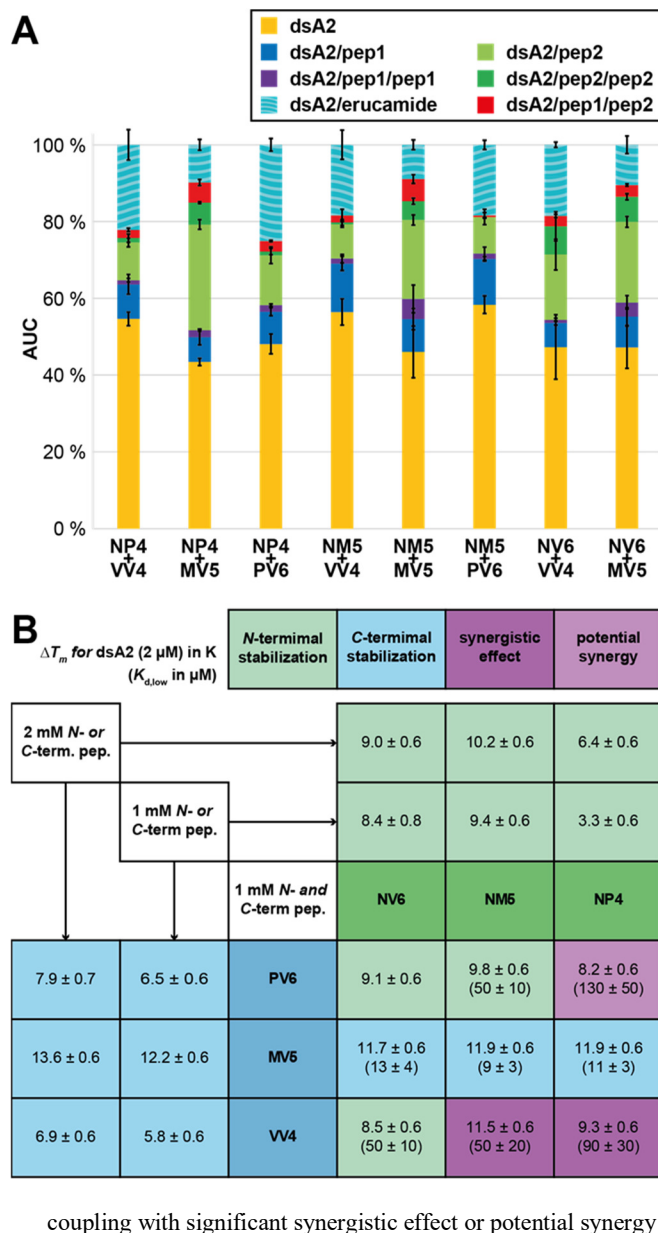


Figure 8-7. Detected dsA2 mass species in presence of two corresponding truncated NV9 variants.

(A) The native MS data suggest that the truncated peptides do not bind cooperatively as the amount of dsA2/pep1/pep2 remains small in all measurements. Rather, it can be seen that the affinity of the individual peptides is independent from each other. The AUC is determined over the entire spectrum for the respective mass species at 10 V. The mean value of the AUC in absence or presence of the different peptides (protein-peptide ratio 1:10:10) from at least three independent measurements is depicted along with error bars that represent the corresponding standard deviation. “dsA2” (yellow bars) corresponds to the empty HLA-A*02:01(Y84C) disulfide mutant complex, “dsA2/pep” (blue bars) to dsA2 bound to one peptide, “dsA2/pep/pep” to dsA2 bound to two molecules of this certain peptide (purple bars), “dsA2/pep2” to dsA2 bound to another peptide when two different peptides were present (light green), “dsA2/pep2/pep2” to dsA2 bound to two molecules of the second peptide (dark green), “dsA2/pep1/pep2” to dsA2 bound to one molecule of each of both peptides (red bars) and “dsA2/erucamide” to dsA2 bound to the erucamide (turquoise-striped bars) respectively. The corresponding $K_{d,low}$ is shown for respective peptide pairs. (B) The matrix visualizes the changes of T_m in case half of the peptide amount is either exchanged for the corresponding N- (green) or C-terminal peptide respectively or alternatively omitted. Light green marks the occurrence of major N-terminal stabilization whereas for the light blue cells, the complex is primarily stabilized by the C-terminal peptide. Purple cells show peptide

8.5. Discussion

While only wildtype pMHC were studied by native MS so far [46], we have recently demonstrated that peptides added to empty disulfide-stabilized class I molecules can be detected as well [14]. This study shows that this method, which is fast and amenable to high-throughput approaches, can be used to measure MHC-I peptide binding affinities, and it is used to map the contributions of parts of the peptide to high-affinity binding.

Our data affirms the key interactions between dsA2 and its high-affinity ligand NV9 that were described previously [47-49]. It is therefore scarcely surprising that Leu-2 and the C-terminal Val-9 contribute the major portion of the total binding. Leucine binds in the B pocket and valine in the F pocket of the binding groove, respectively. The centrally located Val-6 appears to play a minor role in binding, as long as full-length NV9 is considered. However, when situated in second position due to truncation, valine can act as an anchor residue as well. For the F pocket, it is well established that Val or Leu are the strongest anchor residues, but our data suggest that MVATV can also stabilize the B pocket via its first valine similarly and possibly even simultaneously. The extraordinary thermal stabilization observed for dsA2/MV5, especially in comparison with potentially synergistic peptide pairs, gives rise to the assumption that even more than two binding modes are available for MV5. As reported before [50], along with leucine and methionine, valine is indeed one of the amino acid residues preferred by the A*02:01 and moreover by the entire A2 supertype as an anchor residue in second position. Since proline in the N-terminal position was found to be a deleterious factor for binding, this could explain the poor performance of PV6 in our experiments despite the preferred methionine in the second position. Surprisingly, NV6 scores low in all our tests despite having leucine in the second position and a C-terminal valine. Given the two different binding modes, at least a higher proportion of singly bound species would be expected here – similar to MV5 – for statistical reasons. A potential explanation may be that the peptide competes with itself for the two separate binding sites. Based on their sheer size, two NV6 molecules sterically hinder each other as opposed to the pentapeptide MV5. As previously demonstrated [14], the F pocket can be occupied by GM with methionine as anchor residue. Methionine in the C-terminal position is not preferred but only tolerated by HLA-A*02:01, as reported before [50]. Compared to MV5, which can bind with either valines, the second pentapeptide, NM5, therefore shows the same strong binding behavior in our experiments. For larger peptides like NV9, which were found to be double bound to dsA2, it is more likely that the signal originates from nonspecific clustering of NV9 with the abundant dsA2/NV9 complex rather than from the actual binding of two peptides to the dsA2 peptide binding groove due to spatial reasons.

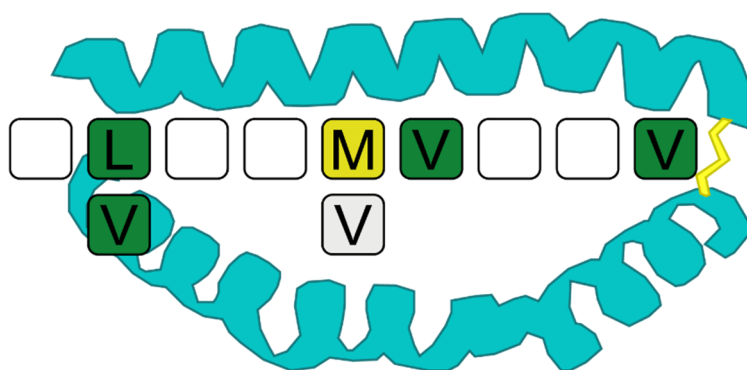


Figure 8-8. Favored amino acid positions within the HLA-A*02:01 peptide binding pocket.

Native MS confirms Leu-2 in the B pocket and Val-9 in the F pocket respectively as the main anchor positions of the pMHC. The analysis of truncated NV9 variants reveals that Val-2 is also a favored binding site. Moreover, Met-5 or Val-5 as well as Val-6 also contribute significantly to binding under certain

circumstances.

Parker *et al.* [48] claimed that GLGGGGGV, carrying the minimal binding motif, is not sufficient for stabilization of HLA-A*02:01. However, GV9 is a strong binding ligand in our native MS experiment, and GV9 binding also increases thermal stability. Nevertheless, there are significant differences compared to the high-affinity control NV9. Hence, it is clear that other amino acids contribute substantially to overall binding. We hereby propose that the disulfide-stabilized MHC-I molecule has at least two positions that can be stabilized independently upon peptide binding as seen for the shorter peptides. **Figures 8-8** presents the binding possibilities within the HLA-A*02:01 peptide pocket identified in this study.

Our findings regarding the modification of the peptide termini support the observations of Bouvier *et al.* [7] that the single-modified nonapeptides can indeed stabilize MHC-I, albeit significantly worse than the non-modified one. However, while no stabilization by the double-modified peptide could be measured there, since no complex was established at all, we succeed in scoring the fully charge-reduced peptide among the other candidates in terms of thermal stabilization and binding strength. Certainly, the comparison of exclusively methylated termini with the acetylation and amidation used in our work is not completely congruent in terms of elimination of hydrogen bonds and occurrence of steric clash. However, acetylation, an intracellular protein degradation signal [51, 52], and amidation, providing the same functional group as an additional amino acid, provide more realistic and biologically relevant modifications. Since *N*-terminal acetylation is one of the most prevalent modifications in pro- and eukaryotes [51, 53], the observed occupancy for Ac-NV9 in the native MS experiment, which is even higher than for the non-modified NV9 might even be a real effect. Nevertheless, this work confirms that one of the termini needs to be intact to form strong binding to either of the outer pockets. In turn, *N*-terminal peptides from acetylated proteins will likely not bind as decapeptides with a *C*-terminal

overhang. Moreover, this explains why undecapeptides with putative overhang on both sides have reduced affinity, as neither of the termini is intact. According to our data, the short, truncated peptides, which are unable to bind using both termini due to spatial limitations, can also stabilize their respective binding pocket individually, which once again supports our thesis concerning the independent stabilization of A and F pocket.

Binding of lipophilic small molecules into the class I binding groove has been shown several times, sometimes quite tightly and (because of alteration of the bound peptidome) with medical consequences [54]. In our MHC-I samples, erucamide is identified as the most prevalent contaminant, most likely from plastic tubes or tips [25]. It appears to bind specifically to the peptide binding groove, since it is displaced by peptides. An alternative explanation would be displacement by a peptide-induced conformational change but is considered less likely, since the empty and the peptide-bound dsA2 are structurally very similar [14]. Thus, erucamide is used as a reference species to estimate the K_d of the peptides: an increase of dsA2/pep with a simultaneous decrease of dsA2/erucamide demonstrates that the corresponding peptide actually occupies the space in the peptide pocket due to its affinity to dsA2 instead of just clustering non-specifically on the protein. Interestingly, other lipids have been shown to bind class I [55, 56], and since erucamide and related compounds are present in nutritional plants [57] and produced by *E.coli* [58], its binding to class I putatively have biological relevance worth investigating.

HLA-A*02:01 is one of the most prevalent A2 allotypes among Caucasians and Asians, and it has been shown that high binding affinity to A*02:01 correlates with binding affinity to the entire A2 supertype, making it a suitable candidate for comprehensive peptide screening [50]. Epitope-based peptide vaccines offer various advantages with regard to production, stability and mutation risk. However, since HLA is characterized by a strong polymorphism, the search for relevant, allele-spanning peptides has so far been very challenging [50]. Using native MS, we have wide latitude in our approach to identify and analyze potential epitopes. Based on measurements at low acceleration voltages, it is feasible to provide good estimates for the peptides' binding affinities. Prediction tools such as NetMHC do not provide an option to predict the K_d for shorter or modified peptides. Furthermore, inconsistencies exist between our data and the affinities predicted using NetMHC. Of course, this is reasonable in terms of absolute values. A smaller share of the observed discrepancy between predicted and approximated dissociation constants can be attributed to an incorrect folding of the protein construct or slight vulnerability against the ammonium acetate solution. Yet, our work shows that the accuracy of K_d predictions by artificial neural networks needs to be debated. Furthermore, the relative affinities for our fairly large number of peptides are also incongruent with the predictions. Moreover, the affinities determined by native MS and iDSF

are in the same order of magnitude and correlate, clearly highlighting issues with the current prediction tool.

Crucially, our measurements at higher energies allow particularly simple evaluation whether a peptide binds strongly or not. The results suggest that pMHC gas-phase stability is mainly determined by side chain interactions within the B and F pockets as well as by binding of the peptide's termini. At an acceleration voltage of 50 V, only strongly bound ligands, i.e. of true biological relevance, are retained. This value hence serves as a cut-off value in our native MS approach that could easily be employed in a native MS based screening. Apart from some attempts [59-61], to date there is no pervasive high-throughput method for the identification of MHC-I binding peptides with immunogenic potential, which is elaborated and reliable. However, such high-throughput screenings are the ultimate key to the development of synthetic peptide vaccines, which in turn offer decisive advantages over conventional vaccines, as there is lesser risk of unwanted host responses, no possibility of reversion to pathogenic phenotypes and no limitation for target diseases [1, 62, 63]. Vaccine production is rather easy and detached from the natural source itself, which may be challenging to culture [1, 63]. Their greatest advantage lies in the stability of the peptide vaccines. Especially in the context of the SARS-CoV-2 pandemic, mRNA vaccines have become very popular. However, especially these and other conventional vaccines are highly dependent on a continuous cold chain, whereas peptides show long-term thermal stability [1, 62, 64]. This feature is of particular importance, as the need for vaccination is often especially high in tropical and hot climates with a limited medical infrastructure. Nevertheless, mRNA vaccines could also be designed to encode a multitude of MHC-specific peptides. Our work not only provides a valid, sensitive and rapid method to determine the K_d of the MHC-I peptide complex but also the basis to develop a novel high-throughput peptide screening method for predicting MHC-I epitopes. Since our technique is based on mass spectrometry, it allows working with very low sample consumption and it also offers the possibility of simultaneous multi-species analysis.

8.6. Materials and Methods

8.6.1. Production of dsA2 molecules

Production followed Anjanappa, Garcia-Alai *et al.* [14]. HLA-A*02:01(Y84C) disulfide mutant (dsA2) HC and human β_2m light chain were expressed in *Escherichia coli* using a pET3a plasmid. The proteins were extracted from inclusion bodies. The dsA2 complex was refolded in presence of 10 mM GM (*Bachem*), concentrated and purified by size-exclusion chromatography on an ÄKTA system (*GE healthcare*) using a HiLoad 26/600 Superdex 200 pg column (*GE healthcare*).

8.6.2. Native mass spectrometry

Prior to native MS measurements, *Micro Bio-Spin 6 Columns* (molecular weight cutoff 6 kDa; *Bio-Rad*) were used at $1,000 \times g$ and $4^\circ C$ to exchange purified protein samples to 250 mM ammonium acetate (99.99 % purity; *Sigma-Aldrich*), pH 8.0 as buffer surrogate. For native MS experiments, the final concentration of the dsA2 protein was 10 μM . Total peptide concentration (*Genecust*) ranged between 50 μM and 200 μM . No peptidic contaminants either in the bound state or in the free form in the low m/z region were detected. Native MS analysis was implemented on a *Q-ToF II* mass spectrometer (*Waters/Micromass*) in positive ESI mode. The instrument was modified to enable high mass experiments (*MS Vision*) [65]. Sample ions were introduced into the vacuum using homemade capillaries via a nano-electrospray ionization source (source pressure: 10 mbar). Borosilicate glass tubes (inner diameter: 0.68 mm, outer diameter: 1.2 mm; *World Precision Instruments*) were pulled into closed capillaries in a two-step program using a squared box filament (2.5 mm \times 2.5 mm) within a micropipette puller (*P-1000*, *Sutter Instruments*). The capillaries were then gold-coated using a sputter coater (5.0×10^{-2} mbar, 30.0 mA, 100 s, 3 runs to vacuum limit 3.0×10^{-2} mbar argon, distance of plate holder: 5 cm; *CCU-010*, *safematic*). Capillaries were opened directly on the sample cone of the mass spectrometer. In regular MS mode, spectra were recorded at a capillary voltage of 1.45 kV and a cone voltage of 150 V. Protein species with quaternary structure were assigned by MS/MS analysis. These experiments were carried out using argon as collision gas (1.2×10^{-2} mbar). The acceleration voltage ranged from 10 V to 100 V. Comparability of results was ensured as MS quadrupole profiles and pusher settings were kept constant in all measurements. The instrument settings of the mass spectrometer were optimized for non-denaturing conditions. A spectrum of cesium iodide (25 g/L) was recorded on the same day of the particular measurement to calibrate the data.

All spectra were evaluated regarding experimental mass (*MassLynx V4.1, Waters*), full width at half maximum (FWHM; *mMass*, Martin Strohaln [66]) and area under the curve (AUC; *UniDec*, Michael T. Marty [67]) of the detected mass species. The values of the shown averaged masses, FWHM (**Table S8.1**) and AUC (**Table S8-2**) of the different species as well as the corresponding standard deviation result from at least three independent measurements. Narrow peak widths indicate rather homogeneous samples. In order to eliminate non-specific ESI clustering within the results, the raw data were corrected using the dsA2/pep fraction of the negative control YF9. Affinity $K_{d,high}$ was calculated directly from AUC measured at 150 V cone voltage and 10 V acceleration voltage, whereas $K_{d,low}$ was indirectly derived from the AUC of the dsA2/erucamide fraction. Since the cone voltage is linearly proportional to the ISD, the distribution of peptide-bound and peptide-unbound dsA2 at non-dissociating conditions can be estimated. According to the equation ($occupancy = -0.0048 \times cone\ voltage + 1.1747$) derived from the linear relationship of cone voltage and occupancy, the binding groove is fully occupied at 36 V and thus reflects the in-solution conditions of the superstoichiometric mixture. The peptide-free (erucamide-bound) fraction of the protein measured at cone voltage of 150 V can be corrected using the linear equation. Subsequently, if this fraction is subtracted from the possible 100 % occupancy, the fraction that binds the peptide is obtained.

8.6.3. Differential scanning fluorimetry

Thermal stability and binding affinity were determined using nanoscale differential scanning fluorimetry on a *Prometheus NT.48 (NanoTemper Technologies)*. Capillaries were filled with 10 μ L of respective samples in duplicates and loaded into the reading chamber. The scan rate was 1 $^{\circ}$ C/min ranging from 20 $^{\circ}$ C to 80 $^{\circ}$ C for thermal stability and 95 $^{\circ}$ C for binding affinity measurements. Protein unfolding was measured by detecting the temperature-dependent change in intrinsic tryptophan fluorescence at emission wavelengths of 330 nm and 350 nm.

8.6.3.1 Thermal stability (*nDSF*)

2 μ M of empty dsA2 were dissolved in citrate phosphate buffer, pH 7.6 [68] and incubated with peptidic ligands (0.2 μ M to 2 mM) on ice for 30 min. Melting curves and T_m values were generated by *PR.ThermControl V2.1* software (*NanoTemper Technologies*) using the first derivative of the fluorescence at 330 nm.

8.6.3.2 Binding affinity (*iDSF*)

Empty dsA2 dissolved in 20 mM Tris pH 8, 150 mM NaCl was incubated with peptidic ligands at different concentrations depending on their predicted or assumed K_d range. For each peptide, a two-fold

serial dilution series (11 concentrations) was prepared, while protein concentration was kept constant at 2.2 μ M. A pure protein was analyzed as well. *PR.ThermControl V2.1.2* software (*NanoTemper Technologies*) was used to control the device. Data processing and evaluation was executed via the *FoldAffinity* web server (*EMBL Hamburg [39]*).

8.7. Acknowledgments

The Leibniz Institute for Experimental Virology (HPI) is supported by the Freie und Hansestadt Hamburg and the Bundesministerium für Gesundheit (BMG). JDK and CU acknowledge support by the Leibniz ScienceCampus InterACt. We thank Raghavendra Anjanappa for the initial protein production and Thomas Dülcks for identifying the erucamide in our samples. We acknowledge technical support by the SPC facility at EMBL Hamburg.

8.8. Funding

Leibniz Association grant SAW-2014-HPI-4 (CU)

Deutsche Forschungsgemeinschaft grant SP583/12-1 (SS)

8.9. Author contributions

Conceptualization: CU, JDK, SS; Methodology: CU, JDK, SS; Software: SN; Formal analysis: JDK, SN; Investigation: AS, CG, JDK, TD; Writing – original draft: JDK; Writing – review & editing: JDK, CU, SS; Visualization: JDK; Supervision: CU; Funding acquisition: CU, SS, MG-A

8.10. Competing interests

Authors declare that they have no competing interests.

Data and materials availability: The mass spectrometry proteomics data have been deposited to the ProteomeXchange Consortium via the PRIDE [69] partner repository with the dataset identifier xxxxxxxxxx. (The identifier was not available at the time of the printing of the thesis, A.S.)

8.11. References

- [1] Corran, P., Griffith, E., *Technical Report Series*, World Health Organization, Geneva, Switzerland 1999, Adopted 1997, pp. 24-43.
- [2] Bassani-Sternberg, M., Coukos, G., Mass spectrometry-based antigen discovery for cancer immunotherapy. *Curr Opin Immunol* 2016, 41, 9-17.
- [3] Attermann, A. S., Bjerregaard, A. M., Saini, S. K., Grønbæk, K., Hadrup, S. R., *Ann Oncol*, England 2018, pp. 2183-2191.
- [4] Madden, D. R., The three-dimensional structure of peptide-MHC complexes. *Annu Rev Immunol* 1995, 13, 587-622.
- [5] Berman, H. M., Westbrook, J., Feng, Z., Gilliland, G., et al., The Protein Data Bank. *Nucleic Acids Research* 2000, 28, 235-242.
- [6] Garrett, T. P. J., Saper, M. A., Bjorkman, P. J., Strominger, J. L., Wiley, D. C., Specificity pockets for the side chains of peptide antigens in HLA-Aw68. *Nature* 1989, 342, 692-696.
- [7] Bouvier, M., Wiley, D. C., Importance of peptide amino and carboxyl termini to the stability of MHC class I molecules. *Science* 1994, 265, 398-402.
- [8] Effenberger, M., Stengl, A., Schober, K., Gerget, M., et al., FLEXamers: A Double Tag for Universal Generation of Versatile Peptide-MHC Multimers. *J Immunol* 2019, 202, 2164-2171.
- [9] Jurtz, V., Paul, S., Andreatta, M., Marcatili, P., et al., NetMHCpan-4.0: Improved Peptide-MHC Class I Interaction Predictions Integrating Eluted Ligand and Peptide Binding Affinity Data. *J Immunol* 2017, 199, 3360-3368.
- [10] Saini, S. K., Ostermeir, K., Ramnarayan, V. R., Schuster, H., et al., Dipeptides promote folding and peptide binding of MHC class I molecules. *Proc Natl Acad Sci U S A* 2013, 110, 15383-15388.
- [11] Hein, Z., Uchtenhagen, H., Abualrous, E. T., Saini, S. K., et al., Peptide-independent stabilization of MHC class I molecules breaches cellular quality control. *J Cell Sci* 2014, 127, 2885-2897.
- [12] Saini, S. K., Tamhane, T., Anjanappa, R., Saikia, A., et al., Empty peptide-receptive MHC class I molecules for efficient detection of antigen-specific T cells. *Sci Immunol* 2019, 4.
- [13] Moritz, A., Anjanappa, R., Wagner, C., Bunk, S., et al., High-throughput peptide-MHC complex generation and kinetic screenings of TCRs with peptide-receptive HLA-A*02:01 molecules. *Sci Immunol* 2019, 4.
- [14] Anjanappa, R., Garcia-Alai, M., Kopicki, J. D., Lockhauserbaumer, J., et al., Structures of peptide-free and partially loaded MHC class I molecules reveal mechanisms of peptide selection. *Nat Commun* 2020, 11, 1314.
- [15] Dülfer, J., Kadek, A., Kopicki, J.-D., Krichel, B., Uetrecht, C., in: Rey, F. A. (Ed.), *Advances in Virus Research*, Academic Press 2019, pp. 189-238.
- [16] Zhang, S., Van Pelt, C. K., Wilson, D. B., Quantitative determination of noncovalent binding interactions using automated nanoelectrospray mass spectrometry. *Anal Chem* 2003, 75, 3010-3018.
- [17] Sun, J., Kitova, E. N., Wang, W., Klassen, J. S., Method for distinguishing specific from nonspecific protein-ligand complexes in nanoelectrospray ionization mass spectrometry. *Anal Chem* 2006, 78, 3010-3018.
- [18] Daniel, J. M., Friess, S. D., Rajagopalan, S., Wendt, S., Zenobi, R., Quantitative determination of noncovalent binding interactions using soft ionization mass spectrometry. *Int J Mass Spectrom* 2002, 216, 1-27.
- [19] Liu, L., Bagal, D., Kitova, E. N., Schnier, P. D., Klassen, J. S., Hydrophobic protein-ligand interactions preserved in the gas phase. *J Am Chem Soc* 2009, 131, 15980-15981.
- [20] Clark, S. M., Konermann, L., Determination of ligand-protein dissociation constants by electrospray mass spectrometry-based diffusion measurements. *Anal Chem* 2004, 76, 7077-7083.
- [21] Jecklin, M. C., Touboul, D., Bovet, C., Wortmann, A., Zenobi, R., Which electrospray-based ionization method best reflects protein-ligand interactions found in solution? a comparison of ESI, nanoESI, and ESSI for the determination of dissociation constants with mass spectrometry. *J Am Soc Mass Spectrom* 2008, 19, 332-343.

- [22] Allison, T. M., Barran, P., Benesch, J. L. P., Cianferani, S., et al., Software Requirements for the Analysis and Interpretation of Native Ion Mobility Mass Spectrometry Data. *Anal Chem* 2020, 92, 10881-10890.
- [23] Keller, B. O., Sui, J., Young, A. B., Whittall, R. M., Interferences and contaminants encountered in modern mass spectrometry. *Anal Chim Acta* 2008, 627, 71-81.
- [24] McDonald, G. R., Hudson, A. L., Dunn, S. M., You, H., et al., Bioactive contaminants leach from disposable laboratory plasticware. *Science* 2008, 322, 917.
- [25] Watson, J., Greenough, E. B., Leet, J. E., Ford, M. J., et al., Extraction, identification, and functional characterization of a bioactive substance from automated compound-handling plastic tips. *J Biomol Screen* 2009, 14, 566-572.
- [26] Schrodinger, LLC, 2015.
- [27] Mehmood, S., Allison, T. M., Robinson, C. V., Mass spectrometry of protein complexes: from origins to applications. *Annu Rev Phys Chem* 2015, 66, 453-474.
- [28] Huang, E. C., Pramanik, B. N., Tsarbopoulos, A., Reichert, P., et al., Application of electrospray mass spectrometry in probing protein-protein and protein-ligand noncovalent interactions. *J Am Soc Mass Spectrom* 1993, 4, 624-630.
- [29] Yin, S., Xie, Y., Loo, J. A., Mass spectrometry of protein-ligand complexes: enhanced gas-phase stability of ribonuclease-nucleotide complexes. *J Am Soc Mass Spectrom* 2008, 19, 1199-1208.
- [30] Wang, W., Kitova, E. N., Klassen, J. S., Nonspecific protein-carbohydrate complexes produced by nanoelectrospray ionization. Factors influencing their formation and stability. *Anal Chem* 2005, 77, 3060-3071.
- [31] Daubenfeld, T., Bouin, A. P., van der Rest, G., A deconvolution method for the separation of specific versus nonspecific interactions in noncovalent protein-ligand complexes analyzed by ESI-FT-ICR mass spectrometry. *J Am Soc Mass Spectrom* 2006, 17, 1239-1248.
- [32] Ozdemir, A., Gulfen, M., Lin, J.-L., Chen, C.-H., A Comparative Study for Sonic Spray and Electrospray Ionization Methods to Determine Noncovalent Protein-Ligand Interactions. *Analytical Letters* 2019, 52, 2620-2633.
- [33] Yan, H., Lockhauserbäumer, J., Szekeres, G. P., Mallagaray, A., et al., Protein Secondary Structure Affects Glycan Clustering in Native Mass Spectrometry. *Life* 2021, 11.
- [34] Stern, L. J., Wiley, D. C., Antigenic peptide binding by class I and class II histocompatibility proteins. *Structure (London, England : 1993)* 1994, 2, 245-251.
- [35] Gras, S., Saulquin, X., Reiser, J. B., Debeaupuis, E., et al., Structural bases for the affinity-driven selection of a public TCR against a dominant human cytomegalovirus epitope. *J Immunol* 2009, 183, 430-437.
- [36] Vita, R., Mahajan, S., Overton, J. A., Dhanda, S. K., et al., The Immune Epitope Database (IEDB): 2018 update. *Nucleic Acids Research* 2019, 47, D339-D343.
- [37] Williams, J. D., Flanagan, M., Lopez, L., Fischer, S., Miller, L. A., Using accurate mass electrospray ionization-time-of-flight mass spectrometry with in-source collision-induced dissociation to sequence peptide mixtures. *J Chromatogr A* 2003, 1020, 11-26.
- [38] Liu, J., Konermann, L., Protein-protein binding affinities in solution determined by electrospray mass spectrometry. *J Am Soc Mass Spectrom* 2011, 22, 408-417.
- [39] Niebling, S., Burastero, O., Burgi, J., Gunther, C., et al., FoldAffinity: binding affinities from nDSF experiments. *Sci Rep* 2021, 11, 9572.
- [40] Saini, S. K., Abualrous, E. T., Tigan, A. S., Covella, K., et al., Not all empty MHC class I molecules are molten globules: tryptophan fluorescence reveals a two-step mechanism of thermal denaturation. *Mol Immunol* 2013, 54, 386-396.
- [41] Saikia, A., Springer, S., Peptide-MHC I complex stability measured by nanoscale differential scanning fluorimetry reveals molecular mechanism of thermal denaturation. *Mol Immunol* 2021, 136, 73-81.
- [42] Saikia, A., Springer, S., Peptide-MHC I complex stability measured by nanoscale differential scanning

- fluorimetry reveals molecular mechanism of thermal denaturation. *Molecular Immunology* 2021, 136, 73-81.
- [43] Matsumura, M., Fremont, D. H., Peterson, P. A., Wilson, I. A., Emerging principles for the recognition of peptide antigens by MHC class I molecules. *Science* 1992, 257, 927-934.
- [44] Zacharias, M., Springer, S., Conformational flexibility of the MHC class I alpha1-alpha2 domain in peptide bound and free states: a molecular dynamics simulation study. *Biophys J* 2004, 87, 2203-2214.
- [45] Gillanders, W. E., Hanson, H. L., Rubocki, R. J., Hansen, T. H., Connolly, J. M., Class I-restricted cytotoxic T cell recognition of split peptide ligands. *International Immunology* 1997, 9, 81-89.
- [46] Knapman, T. W., Morton, V. L., Stonehouse, N. J., Stockley, P. G., Ashcroft, A. E., Determining the topology of virus assembly intermediates using ion mobility spectrometry-mass spectrometry. *Rapid Communications in Mass Spectrometry* 2010, 24, 3033-3042.
- [47] Falk, K., Rötzschke, O., Stevanović, S., Jung, G., Rammensee, H.-G., Allele-specific motifs revealed by sequencing of self-peptides eluted from MHC molecules. *Nature* 1991, 351, 290-296.
- [48] Parker, K. C., Bednarek, M. A., Hull, L. K., Utz, U., et al., Sequence motifs important for peptide binding to the human MHC class I molecule, HLA-A2. *The Journal of Immunology* 1992, 149, 3580.
- [49] Parker, K. C., Bednarek, M. A., Coligan, J. E., Scheme for ranking potential HLA-A2 binding peptides based on independent binding of individual peptide side-chains. *The Journal of Immunology* 1994, 152, 163.
- [50] Sidney, J., Southwood, S., Mann, D. L., Fernandez-Vina, M. A., et al., Majority of peptides binding HLA-A*0201 with high affinity crossreact with other A2-supertype molecules. *Hum Immunol* 2001, 62, 1200-1216.
- [51] Ree, R., Varland, S., Arnesen, T., Spotlight on protein N-terminal acetylation. *Experimental & Molecular Medicine* 2018, 50, 1-13.
- [52] Nguyen, K. T., Mun, S.-H., Lee, C.-S., Hwang, C.-S., Control of protein degradation by N-terminal acetylation and the N-end rule pathway. *Experimental & Molecular Medicine* 2018, 50, 1-8.
- [53] Linster, E., Wirtz, M., N-terminal acetylation: an essential protein modification emerges as an important regulator of stress responses. *Journal of Experimental Botany* 2018, 69, 4555-4568.
- [54] Illing, P. T., Purcell, A. W., McCluskey, J., The role of HLA genes in pharmacogenomics: unravelling HLA associated adverse drug reactions. *Immunogenetics* 2017, 69, 617-630.
- [55] Shima, Y., Morita, D., Mizutani, T., Mori, N., et al., Crystal structures of lysophospholipid-bound MHC class I molecules. *J Biol Chem* 2020.
- [56] Morita, D., Yamamoto, Y., Mizutani, T., Ishikawa, T., et al., Crystal structure of the N-myristoylated lipopeptide-bound MHC class I complex. *Nature Communications* 2016, 7, 10356.
- [57] Kim, C. R., Kim, H. S., Choi, S. J., Kim, J. K., et al., Erucamide from Radish Leaves Has an Inhibitory Effect Against Acetylcholinesterase and Prevents Memory Deficit Induced by Trimethyltin. *Journal of medicinal food* 2018, 21, 769-776.
- [58] Tamilmani, E., Radhakrishnan, R., Sankaran, K., 13-Docosamide release by bacteria in response to glucose during growth-fluorescein quenching and clinical application. *Applied microbiology and biotechnology* 2018, 102, 6673-6685.
- [59] Chaparro, R. J., Burton, A. R., Serreze, D. V., Vignali, D. A. A., DiLorenzo, T. P., Rapid identification of MHC class I-restricted antigens relevant to autoimmune diabetes using retrogenic T cells. *Journal of immunological methods* 2008, 335, 106-115.
- [60] Haj, A. K., Breitbach, M. E., Baker, D. A., Mohns, M. S., et al., High-Throughput Identification of MHC Class I Binding Peptides Using an Ultradense Peptide Array. *Journal of immunology (Baltimore, Md. : 1950)* 2020, 204, 1689-1696.
- [61] Harndahl, M., Rasmussen, M., Roder, G., Buus, S., Real-time, high-throughput measurements of peptide-MHC-I dissociation using a scintillation proximity assay. *Journal of Immunological Methods* 2011, 374, 5-12.
- [62] Yang, H., Kim, D. S., in: Donev, R. (Ed.), *Advances in Protein Chemistry and Structural Biology*, Academic

- Press 2015, pp. 1-14.
- [63] Purcell, A. W., McCluskey, J., Rossjohn, J., More than one reason to rethink the use of peptides in vaccine design. *Nature Reviews Drug Discovery* 2007, 6, 404-414.
 - [64] Sun, T., Han, H., Hudalla, G. A., Wen, Y., et al., Thermal stability of self-assembled peptide vaccine materials. *Acta biomaterialia* 2016, 30, 62-71.
 - [65] van den Heuvel, R. H. H., van Duijn, E., Mazon, H., Synowsky, S. A., et al., Improving the performance of a quadrupole time-of-flight instrument for macromolecular mass spectrometry. *Analytical Chemistry* 2006, 78, 7473-7483.
 - [66] Strohalm, M., Hassman, M., Kosata, B., Kodicek, M., mMass data miner: an open source alternative for mass spectrometric data analysis. *Rapid Commun Mass Spectrom* 2008, 22, 905-908.
 - [67] Marty, M. T., Baldwin, A. J., Marklund, E. G., Hochberg, G. K., et al., Bayesian deconvolution of mass and ion mobility spectra: from binary interactions to polydisperse ensembles. *Anal Chem* 2015, 87, 4370-4376.
 - [68] McIlvaine, T. C., A BUFFER SOLUTION FOR COLORIMETRIC COMPARISON. *Journal of Biological Chemistry* 1921, 49, 183-186.
 - [69] Perez-Riverol, Y., Csordas, A., Bai, J., Bernal-Llinares, M., et al., The PRIDE database and related tools and resources in 2019: improving support for quantification data. *Nucleic Acids Research* 2019, 47, D442-D450.

8.12. Supplementary Information

8.12.1. Supplementary Figures

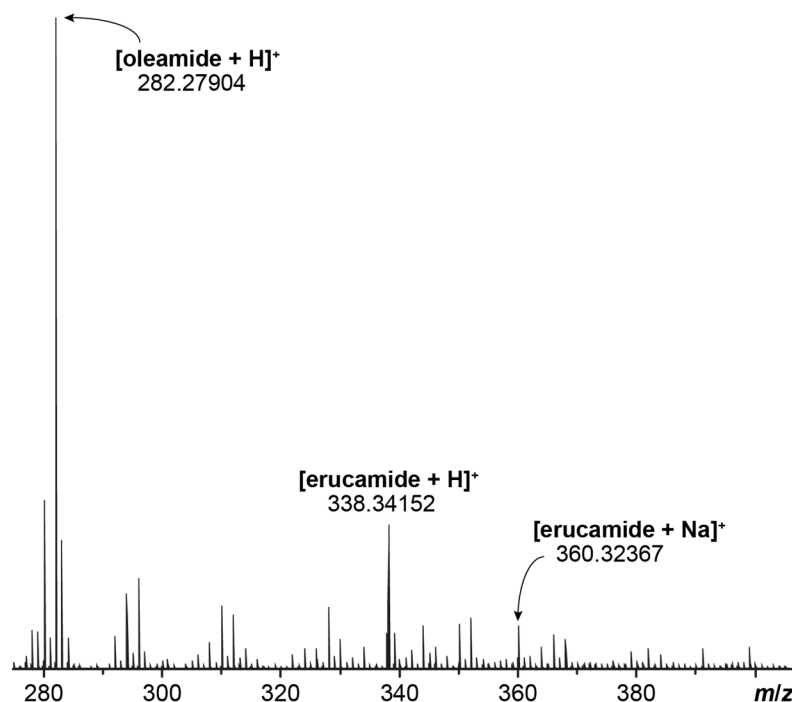


Figure S8-1. Small molecule tandem MS analysis verifies that erucamide accounts for a large proportion of the contaminants found in dsA2 samples.

Displayed is a subtraction spectrum resulting from the spectrum of plastic ware contaminants (empty vial) and one of the dsA2 sample itself. Erucamide (337 Da) is hereby identified as the contaminant adducted to dsA2. Although oleamide is also found in the sample, there was no evidence of binding to the protein in the native MS analysis, unlike for erucamide.

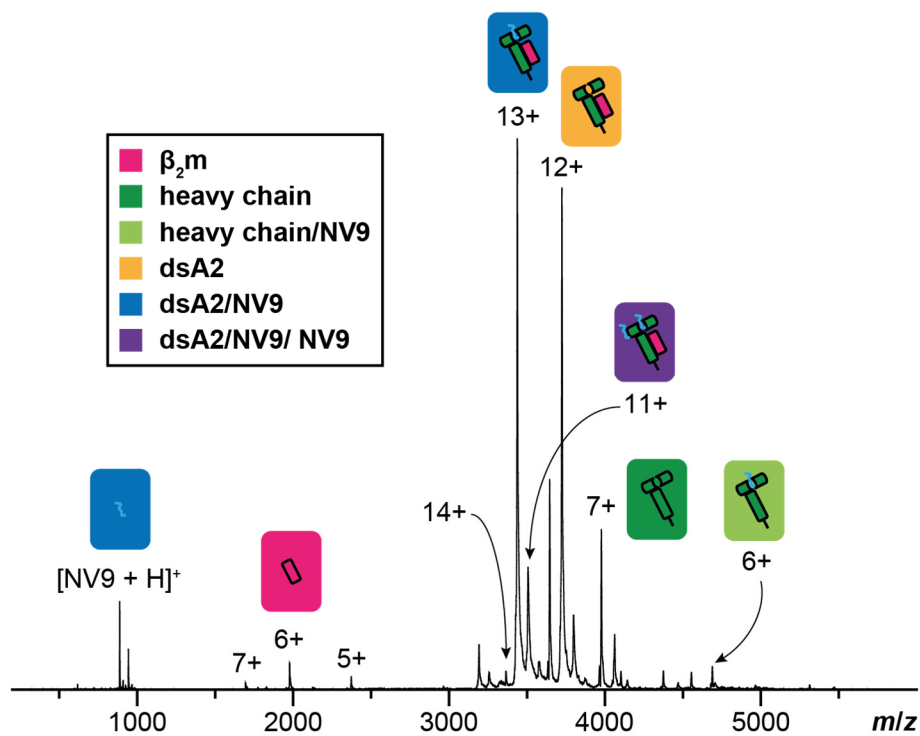


Figure S8-2. Raw spectrum of dsA2/NV9.

A native mass spectrum dsA2 in presence of NV9 (protein-peptide ratio 1:5) recorded at an acceleration voltage of 25 V is shown. The dsA2/NV9 is the predominant species (blue). In addition, peptide-free dsA2 (yellow), dissociated β_2m (pink) and HC (green) as well as free NV9 can be seen.

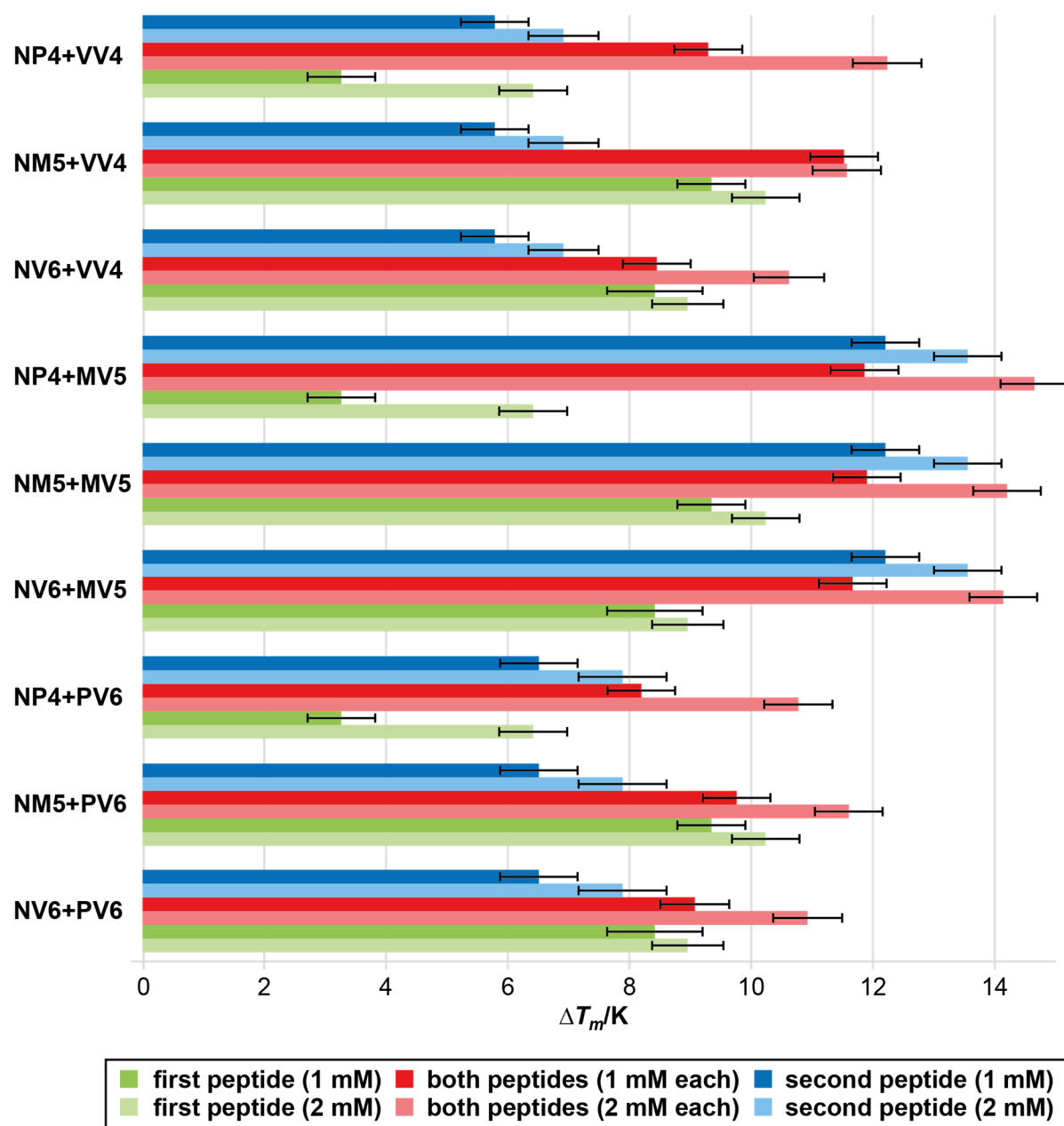


Figure S8-3. Melting temperature (T_m) of dsA2 in presence of two corresponding truncated NV9 variants.

Nanoscale differential scanning fluorimetry is employed to study thermal denaturation of dsA2 in presence of two peptides at once. 2 μ M dsA2 are combined with either exclusively the *N*- (green) or *C*-terminal peptide (blue) or both peptides together (red) at different concentrations. Results for ΔT_m along with respective standard deviations are displayed.

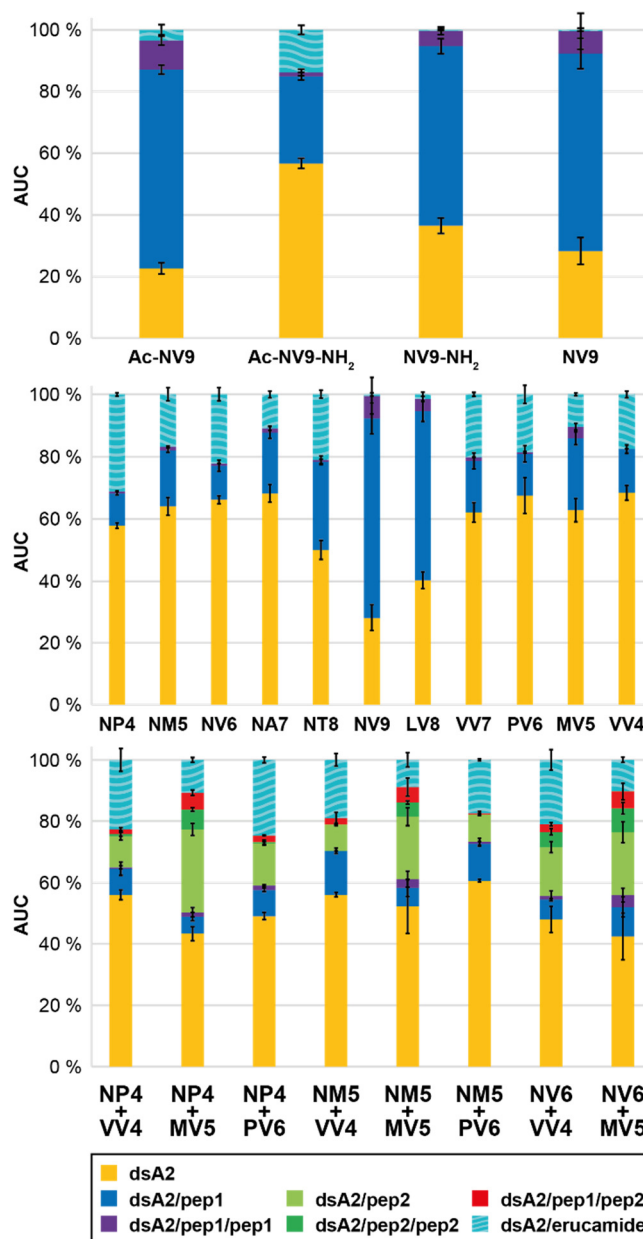


Figure S8-4. Overall area under the curve (AUC) for the detected dsA2 mass species at 25 V acceleration voltage.

The AUC is determined over the entire spectrum for the respective mass species at 25 V. The mean value of the AUC in absence or presence of the different peptides (protein-peptide ratio 1:5, 1:10:10 in dual peptide approach) from at least three independent measurements is depicted along with error bars that represent the corresponding standard deviation. “dsA2” (yellow bars) corresponds to the empty HLA-A*02:01(Y84C) disulfide mutant complex, “dsA2/pep” (blue bars) to dsA2 bound to one peptide, “dsA2/pep/pep” to dsA2 bound to two molecules of this certain peptide (purple bars), “dsA2/pep2” to dsA2 bound to another peptide when two different peptides were present (light green), “dsA2/pep2/pep2” to dsA2 bound to two molecules of the second peptide (dark green), “dsA2/pep1/pep2” to dsA2 bound to one molecule of each of both peptides (red bars) and “dsA2/erucamide” to dsA2 bound to the erucamide (turquoise-striped bars) respectively.

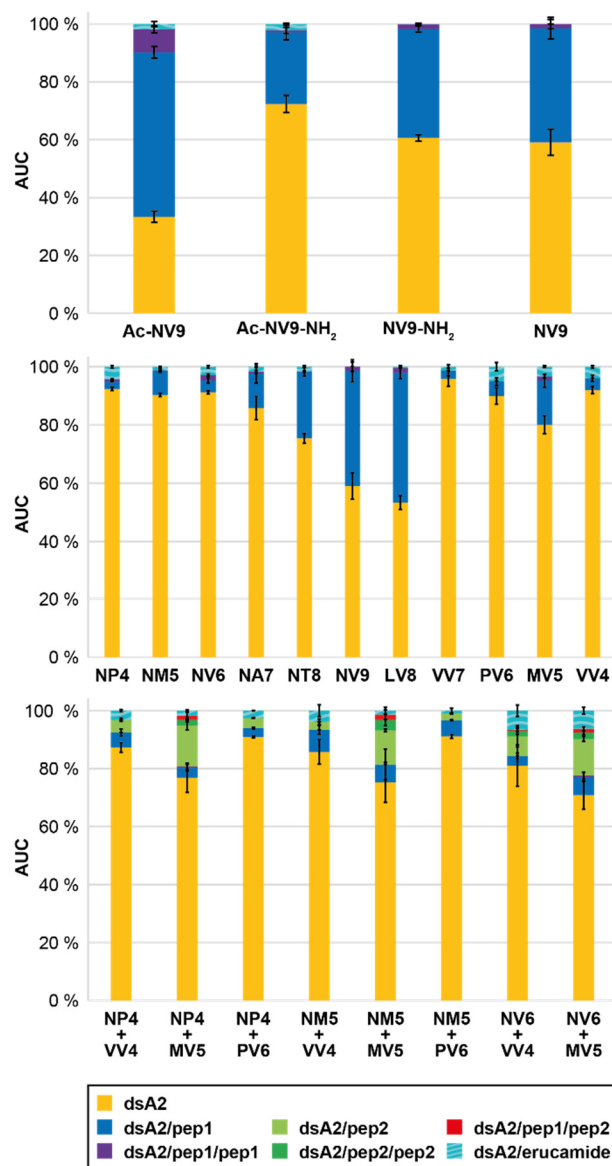


Figure S8-5. Overall area under the curve (AUC) for the detected dsA2 mass species at 50 V acceleration voltage.

The AUC is determined over the entire spectrum for the respective mass species 50 V. The mean value of the AUC in absence or presence of the different peptides (protein-peptide ratio 1:5, 1:10:10 in dual peptide approach) from at least three independent measurements is depicted along with error bars that represent the corresponding standard deviation. “dsA2” (yellow bars) corresponds to the empty HLA-A*02:01(Y84C) disulfide mutant complex, “dsA2/pep” (blue bars) to dsA2 bound to one peptide, “dsA2/pep/pep” to dsA2 bound to two molecules of this certain peptide (purple bars), “dsA2/pep2” to dsA2 bound to another peptide when two different peptides were present (light green), “dsA2/pep2/pep2” to dsA2 bound to two molecules of the second peptide (dark green), “dsA2/pep1/pep2” to dsA2 bound to one molecule of each of both peptides (red bars) and “dsA2/erucamide” to dsA2 bound to the erucamide (turquoise-striped bars) respectively.

8.12.2. Supplementary Tables

Table S8-1. Experimental masses and FWHM for dsA2 and different peptides obtained by native mass spectrometry.

Experimental masses (m_{exp}) of the different protein species of disulfide stabilized HLA-A*02:01(Y84C) disulfide mutant (dsA2) in absence or presence of the different peptides (protein-peptide ratio 1:5, 1:10:10 in dual peptide approach) are determined from at least three independent mass spectrometry measurements. They are listed together with the respective values for standard deviation s and average full width of the peak at half maximum (FWHM) along with the theoretically calculated molecular weight (M). FWHM values are given for the whole peak area where individual species are not fully resolved. ¹NV9 – high affinity control, ²YF9 – low affinity control, ³GV9 – minimal binding motif, ⁴Ac-NV9 – modified *N*-terminus, ⁵Ac-NV9 NH₂ – modified *N*- and *C*-terminus, ⁶NV9-NH₂ – modified *C*-terminus.

mass species	M/Da	m_{exp}/Da	$s(m_{\text{exp}})/\text{Da}$	FWHM/Da	$s(m_{\text{exp}})/\text{Da}$
dsA2 - M1	43,608	43,603	4	20	20
dsA2	43,739	43,733	4	3	2
heavy chain (hc)	31,877	31,873	2	2.1	0.3
$\beta_2\text{m}$ chain - M1	11,731	11,729	2	1.1	0.4
$\beta_2\text{m}$ chain	11,862	11,860	1	1.4	0.2
dsA2/NV9 ¹	44,682	44,678	1	3	2
dsA2/2×NV9	45,625	45,624	4	12	6
hc/NV9	32,820	32,816.90	0.8	2.2	0.3
dsA2/YF9 ²	44,856	44,849	1	7	3
dsA2/GV9 ³	44,369	44,363.80	0.7	2	1
dsA2/2×GV9	44,999	44,995	2	3	2
hc/GV9	32,507	32,503.00	0.5	2.08	0.09
dsA2/Ac-NV9 ⁴	44,724	44,718.30	0.5	1.6	0.3
dsA2/2×Ac-NV9	45,709	45,704	2	3	2
hc/Ac-NV9	32,862	32,857.30	0.5	1.9	0.1
dsA2/Ac-NV9-NH ₂ ⁵	44,723	44,717.40	1	1.4	0.1
dsA2/2×Ac-NV9-NH ₂	45,707	45,701.00	1	1.8	0.6
hc/Ac-NV9-NH ₂	32,861	32,857.00	0.9	1.7	0.2
dsA2/NV9-NH ₂ ⁶	44,681	44,676.40	0.5	1.38	0.06
dsA2/2×NV9-NH ₂	45,623	45,619.60	0.9	1.6	0.6
hc/NV9-NH ₂	32,819	32,815.10	0.9	1.72	0.1
dsA2/NP4	44,181	44,176	3	10	10
dsA2/2×NP4	44,623	44,619	4	30	40
hc/NP4	32,319	32,317	2	20	40
dsA2/NM5	44,312	44,309	2	6	3
dsA2/2×NM5	44,885	44,883	2	60	50

Chapter 8

mass species	M/Da	m_{exp}/Da	$s(m_{\text{exp}})/\text{Da}$	FWHM/Da	$s(m_{\text{exp}})/\text{Da}$
hc/NM5	32,450	32,449	1	2.5	0.6
dsA2/NV6	44,411	44411	1	7	2
dsA2/2×NV6	45,083	45,082	3	145	6
hc/NV6	32,549	32,547	3	6	7
dsA2/NA7	44,481	44,476.40	0.5	5	3
dsA2/2×NA7	45,223	45,225	4	30	60
hc/NA7	32,619	32,615	2	2.4	0.5
dsA2/NT8	44,583	44,579.33	1	3	2
dsA2/2×NT8	45,427	45,425	2	7	5
hc/NT8	32,721	32,718.10	0.3	2.4	0.7
dsA2/LV8	44,568	44,565.80	0.7	2.6	0.7
dsA2/2×LV8	45,397	45,396.10	0.3	3.4	1
hc/LV8	32,706	32,704.80	0.4	2.18	0.04
dsA2/VV7	44,455	44,447.80	0.8	7	3
dsA2/2×VV7	45,171	45,166	3	3	1
hc/VV7	32,593	32,586	3	3	2
dsA2/PV6	44,356	44,350	3	5	3
dsA2/2×PV6	44,973	44969	4	100	50
hc/PV6	32,194	32,487	3	2.3	0.4
dsA2/MV5	44,259	44,254	3	8	12
dsA2/2×MV5	44,779	44,774	4	20	30
hc/MV5	32,397	32,388.40	1	2.1	0.2
dsA2/VV4	44,127	44,125	5	10	10
dsA2/2×VV4	44,515	44,512	8	20	30
hc/VV4	32,265	32,255	1	10	3
dsA2/erucamide	44,077	44,071	5	10	20
dsA2/NP4/VV4	44,569	44,565	2	30	40
dsA2/NP4/MV5	44,701	44,697	2	4	5
dsA2/NP4/PV6	44,798	44,792	3	7	6
dsA2/NM5/VV4	44,700	44,699	2	30	40
dsA2/NM5/MV5	44,832	44,827	2	12	3
dsA2/NM5/PV6	44,929	44,927	2	100	40
dsA2/NV6/VV4	44,799	44,797	4	30	40
dsA2/NV6/MV5	45,451	44927	5	100	60

Table S8-2. Overall area under the curve (AUC) for the detected dsA2 mass species at different acceleration voltages.

The AUC is determined over the entire spectrum for the respective mass species at 10 V, 25 V and 50 V. The mean value of the AUC in absence or presence of the different peptides (protein-peptide ratio 1:5, 1:10:10 in dual peptide approach) from at least three independent measurements is listed together with their corresponding standard deviation *s*. “dsA2” corresponds to the empty HLA-A*02:01(Y84C) disulfide mutant complex, “dsA2/pep” to dsA2 bound to one peptide, “dsA2/pep/pep” to dsA2 bound to two molecules of this certain peptide, “dsA2/pep2” to dsA2 bound to another peptide when two different peptides were present, “dsA2/pep2/pep2” to dsA2 bound to two molecules of the second peptide, “dsA2/pep1/pep2” to dsA2 bound to one molecule of each of both peptides and “dsA2/erucamide” to dsA2 bound to the erucamide respectively. ¹NV9 – high affinity control, ²YF9 – low affinity control, ³GV9 – minimal binding motif, ⁴Ac-NV9 – modified *N*-terminus, ⁵Ac-NV9 NH₂ – modified *N*- and *C*-terminus, ⁶NV9-NH₂ – modified *C*-terminus.

peptide	acc. volt.	dsA2		dsA2/pep		dsA2/pep/pep		dsA2/pep2		dsA2/pep2/pep2		dsA2/pep1/pep2		dsA2/erucamide	
		AUC	s	AUC	s	AUC	s	AUC	s	AUC	s	AUC	s	AUC	s
NV9 ¹	10 V	31.0%	2.0%	64.0%	3.0%	4.0%	4.0%							2.0%	2.0%
	25 V	28.0%	4.0%	64.0%	5.0%	7.0%	6.0%							0.5%	0.5%
	50 V	59.0%	5.0%	40.0%	4.0%	1.0%	2.0%							0.0%	0.0%
YF9 ²	10 V	56.0%	3.0%	4.0%	2.0%	0.0%	0.0%							39.0%	2.0%
	25 V	51.0%	4.0%	5.0%	2.0%	0.0%	0.0%							44.0%	3.0%
	50 V	95.0%	5.0%	5.0%	2.0%	0.0%	0.0%							2.0%	2.0%
GV9 ³	10 V	52.0%	2.0%	43.0%	2.0%	1.5%	0.4%							4.3%	0.6%
	25 V	50.0%	1.0%	43.0%	3.0%	2.2%	0.9%							5.0%	2.0%
	50 V	62.0%	3.0%	35.0%	3.0%	1.1%	0.3%							1.7%	0.2%

peptide	acc. volt.	dsA2		dsA2/pep		dsA2/pep/pep		dsA2/pep2		dsA2/pep2/pep2		dsA2/pep1/pep2		dsA2/erucamide	
		AUC	s	AUC	s	AUC	s	AUC	s	AUC	s	AUC	s	AUC	s
Ac-NV9 ⁴	10 V	24.0%	2.0%	63.0%	3.0%	11.0%	2.0%							2.1%	0.5%
	25 V	23.0%	2.0%	64.0%	1.0%	9.0%	1.0%							3.0%	2.0%
	50 V	33.0%	2.0%	57.0%	2.0%	8.0%	1.0%							1.7%	0.9%
Ac-NV9-NH ₂ ⁵	10 V	55.0%	2.0%	27.9%	0.5%	2.4%	0.6%							15.0%	1.0%
	25 V	57.0%	2.0%	28.0%	1.0%	1.0%	1.0%							14.0%	1.0%
	50 V	72.0%	3.0%	25.0%	3.0%	1.0%	1.0%							2.2%	0.4%
NV9-NH ₂ ⁶	10 V	36.0%	2.0%	59.0%	2.0%	5.0%	1.0%							0.4%	0.2%
	25 V	36.0%	2.0%	58.0%	2.0%	5.0%	1.0%							0.3%	0.3%
	50 V	61.0%	1.0%	38.0%	1.0%	1.6%	0.3%							0.1%	0.2%
NP4	10 V	55.0%	2.0%	11.0%	1.0%	0.6%	0.2%							33.8%	0.6%
	25 V	57.8%	0.9%	10.4%	0.5%	0.7%	0.1%							31.1%	0.5%
	50 V	92.4%	0.5%	2.6%	0.1%	0.8%	0.1%							4.3%	0.3%
NM5	10 V	62.0%	2.0%	17.9%	0.6%	1.0%	0.2%							19.0%	1.0%
	25 V	64.0%	3.0%	18.0%	0.7%	1.2%	0.2%							17.0%	2.0%
	50 V	90.3%	0.6%	8.1%	0.3%	0.3%	0.6%							1.3%	0.1%
NV6	10 V	66.0%	1.0%	10.0%	2.0%	0.5%	0.1%							24.0%	1.0%
	25 V	66.0%	1.0%	11.0%	2.0%	0.7%	0.1%							22.0%	2.0%
	50 V	91.2%	0,5%	4.1%	0.8%	1.9%	0.3%							2.9%	0.4%

peptide	acc. volt.	dsA2		dsA2/pep		dsA2/pep/pep		dsA2/pep2		dsA2/pep2/pep2		dsA2/pep1/pep2		dsA2/erucamide	
		AUC	s	AUC	s	AUC	s	AUC	s	AUC	s	AUC	s	AUC	s
NA7	10 V	75.0%	3.0%	16.0%	2.0%	0.8%	0.3%							8.0%	1.0%
	25 V	68.0%	3.0%	19.0%	2.0%	1.4%	0.7%							11.0%	1.0%
	50 V	86.0%	4.0%	12.0%	3.0%	0.5%	0.5%							1.8%	0.2%
NT8	10 V	47.3%	0.9%	28.0%	1.0%	0.6%	0.5%							24.0%	1.0%
	25 V	50.0%	3.0%	28.2%	0.9%	1.0%	1.0%							21.0%	1.0%
	50 V	75.0%	2.0%	23.0%	1.0%	0.2%	0.3%							1.6%	0.3%
LV8	10 V	42.0%	6.0%	54.0%	5.0%	2.8%	0.3%							1.7%	0.9%
	25 V	40.0%	3.0%	54.0%	3.0%	3.9%	0.8%							1.5%	0.7%
	50 V	53.0%	2.0%	45.0%	2.0%	1.6%	0.2%							0.4%	0.4%
VV7	10 V	61.8%	0.5%	17.0%	2.0%	1.7%	0.3%							19.0%	3.0%
	25 V	62.0%	3.0%	17.0%	3.0%	1.2%	0.1%							20.2%	0.7%
	50 V	96.0%	3.0%	3.0%	2.0%	0.0%	0.0%							1.3%	0.6%
PV6	10 V	68.0%	6.0%	12.0%	2.0%	0.5%	0.6%							19.0%	3.0%
	25 V	68.0%	6.0%	13.0%	3.0%	0.5%	0.2%							19.0%	3.0%
	50 V	90.0%	3.0%	5.0%	1.0%	0.1%	0.1%							5.0%	1.0%
MV5	10 V	64.0%	3.0%	23.0%	2.0%	3.2%	0.7%							10.4%	0.2%
	25 V	63.0%	4.0%	23.0%	2.0%	3.7%	1.0%							10.4%	0.4%
	50 V	80.0%	3.0%	15.0%	2.0%	1.5%	0.6%							3.3%	0.3%

peptide	acc. volt.	dsA2		dsA2/pep		dsA2/pep/pep		dsA2/pep2		dsA2/pep2/pep2		dsA2/pep1/pep2		dsA2/erucamide	
		AUC	s	AUC	s	AUC	s	AUC	s	AUC	s	AUC	s	AUC	s
VV4	10 V	68.0%	1.0%	14.0%	1.0%	0.0%	0.0%							18.1%	0.0%
	25 V	68.0%	2.0%	14.0%	1.0%	0.0%	0.0%							17.6%	1.0%
	50 V	92.0%	1.0%	4.1%	1.0%	0.0%	0.0%							4.0%	0.4%
NP4 + VV4	10 V	54.0%	2.0%	9.0%	3.0%	1.1%	0.5%	10.0%	1.0%	1.2%	1.0%	2.1%	0.5%	22.0%	4.0%
	25 V	56.0%	2.0%	8.0%	2.0%	0.5%	0.5%	10.0%	1.0%	0.7%	0.7%	1.6%	0.5%	22.0%	4.0%
	50 V	87.0%	2.0%	5.0%	1.0%	0.0%	0.0%	4.4%	0.6%	0.0%	0.0%	0.0%	0.0%	3.1%	0.4%
NP4 + MV5	10 V	42.9%	0.9%	6.0%	2.0%	1.8%	0.3%	27.0%	1.0%	5.6%	0.3%	5.2%	0.8%	10.0%	1.0%
	25 V	43.0%	2.0%	5.0%	1.0%	1.0%	2.0%	27.0%	2.0%	6.4%	0.6%	5.3%	0.9%	10.5%	0.8%
	50 V	76.0%	5.0%	3.0%	1.0%	0.5%	0.9%	14.0%	2.0%	1.9%	0.8%	1.0%	1.0%	1.8%	0.3%
NP4 + PV6	10 V	48.0%	3.0%	8.0%	1.0%	1.7%	0.3%	13.0%	2.0%	0.9%	0.8%	2.8%	0.2%	25.0%	2.0%
	25 V	49.0%	1.0%	8.5%	0.6%	1.4%	0.2%	13.6%	0.5%	0.4%	0.7%	2.1%	0.1%	24.5%	0.9%
	50 V	90.8%	0.3%	3.0%	0.3%	0.0%	0.0%	3.5%	0.1%	0.0%	0.0%	0.0%	0.0%	2.5%	0.1%
NM5 + VV4	10 V	56.0%	3.0%	13.0%	2.0%	1.0%	1.0%	8.9%	0.8%	0.5%	0.8%	1.8%	1.6%	18.0%	4.0%
	25 V	55.7%	0.7%	14.2%	0.9%	0.0%	0.0%	8.6%	0.4%	0.0%	0.0%	2.0%	1.9%	19.0%	2.0%
	50 V	86.0%	4.0%	8.0%	1.0%	0.0%	0.0%	2.8%	1.0%	0.0%	0.0%	0.0%	0.0%	4.0%	2.0%
NM5 + MV5	10 V	46.0%	7.0%	8.0%	3.0%	5.0%	4.0%	20.0%	1.0%	4.9%	0.8%	6.0%	1.0%	9.0%	1.0%
	25 V	51.0%	9.0%	6.0%	3.0%	3.0%	3.0%	20.0%	3.0%	4.5%	0.5%	5.0%	3.0%	9.0%	2.0%
	50 V	75.0%	7.0%	6.0%	5.0%	0.0%	0.0%	11.7%	0.4%	4.0%	2.0%	2.0%	2.0%	1.0%	1.0%

peptide	acc. volt.	dsA2		dsA2/pep		dsA2/pep/pep		dsA2/pep2		dsA2/pep2/pep2		dsA2/pep1/pep2		dsA2/erucamide	
		AUC	s	AUC	s	AUC	s	AUC	s	AUC	s	AUC	s	AUC	s
NM5 + PV6	10 V	58.0%	2.0%	11.9%	0.6%	1.0%	2.0%	9.0%	2.0%	0.0%	0.0%	0.4%	0.7%	18.0%	1.0%
	25 V	60.3%	0.5%	12.0%	0.8%	1.0%	1.0%	8.9%	0.4%	0.0%	0.0%	0.4%	0.7%	17.3%	0.4%
	50 V	91.1%	0.7%	5.6%	0.2%	0.0%	0.0%	2.4%	0.2%	0.0%	0.0%	0.0%	0.0%	0.9%	0.8%
NV6 + VV4	10 V	47.0%	8.0%	6.0%	1.0%	1.0%	0.0%	17.0%	4.0%	7.0%	4.0%	3.0%	0.0%	18.0%	1.0%
	25 V	48.0%	4.0%	6.0%	0.0%	1.0%	2.0%	16.0%	2.0%	5.0%	1.0%	2.0%	1.0%	21.0%	3.0%
	50 V	81.0%	7.0%	3.0%	1.0%	0.0%	0.0%	7.0%	4.0%	2.0%	1.0%	0.0%	0.0%	7.0%	2.0%
NV6 + MV5	10 V	47.0%	5.0%	8.0%	2.0%	4.0%	2.0%	21.0%	1.0%	6.5%	0.8%	3.0%	0.3%	10.0%	2.0%
	25 V	42.0%	8.0%	9.0%	3.0%	4.0%	2.0%	20.0%	3.0%	8.0%	2.0%	5.0%	3.0%	10.2%	0.8%
	50 V	71.0%	5.0%	6.0%	2.0%	1.0%	1.0%	12.5%	0.9%	2.1%	0.7%	1.4%	0.6%	6.0%	1.0%

Table S8-3. Apparent dissociation constants (K_d) for dsA2 and different peptides obtained by native MS and iDSF.

The K_d is calculated from the respective area under the curve values at 10 V acceleration voltage (protein-peptide ratio 1:5). $K_{d,high}$ is an affinity determined on the basis of a real experiment at a cone voltage of 150 V, while a theoretical cone voltage of 36 V is assumed for $K_{d,low}$ to correct for ion-source decay. $K_{d,iDSF}$ is derived by two independent measurements. Protein concentration is 2.2 μM . For each ligand, a two-fold serial dilution series is prepared using 11 concentrations depending on their predicted or assumed K_d range. The listed standard deviation s for K_d is determined using common equations, which estimate the propagation of uncertainty. ¹NV9 – high affinity control, ²GV9 – minimal binding motif, ³Ac-NV9 – modified *N*-terminus, ⁴Ac-NV9 NH₂ – modified *N*- and *C*-terminus, ⁵NV9-NH₂ – modified *C*-terminus; *iDSF reaches its limits at affinities below 200 nm, hence the values of grayed-out peptides are not reliable.

Peptide	Sequence	$K_{d,high}$		$K_{d,low}$		$K_{d,iDSF}$	
		$K_d/\mu\text{M}$	$s/\mu\text{M}$	$K_d/\mu\text{M}$	$s/\mu\text{M}$	$K_d/\mu\text{M}$	$s/\mu\text{M}$
NV9 ¹	NLVPMVATV	8	2	0.06	0.08	0.04*	0.01
GV9 ²	GLGGGGGGV	35	2	0.5	0.2	0.36	0.06
Ac-NV9 ³		4.5	1	0.11	0.05	0.61	0.08
Ac-NV9-NH ₂ ⁴		80	7	7	3	4	1
NV9-NH ₂ ⁵		10	1	0.004	0.003	0.001*	0.001
NP4	NLVP	350	60	100	70	50	20
NM5	NLVPM	180	30	15	6	11	3
NV6	NLVPMV	380	70	30	10	9	2
NA7	NLVPMVA	210	40	2	0.7	3.6	0.5
NT8	NLVPMVAT	92	5	30	10	2.6	0.4
LV8	LVPMVATV	17	3	0.07	0.06	0.008*	0.005
VV7	VPMVATV	180	30	15	7	7.8	1
PV6	PMVATV	300	200	15	7	15	2
MV5	MVATV	110	10	3	1	1.6	0.2
VV4	VATV	270	30	13	4	50	20
NP4+VV4				90	30		
NP4+MV5				11	3		
NP4+PV6				130	50		
NM5+VV4				50	20		
NM5+MV5				9	3		
NM5+PV6				50	10		
NV6+VV4				50	10		
NV6+MV5				13	4		

Table S8-4. Melting temperatures (T_m) for dsA2 and different peptides obtained by nDSF.

The T_m as well as the resulting s for dsA2 in absence or presence of the different peptides is defined by at least two independent measurements. Protein concentration is 2 μM . ¹NV9 – high affinity control, ²YF9 – low affinity control, ³GV9 – minimal binding motif, ⁴Ac-NV9 – modified *N*-terminus, ⁵Ac-NV9 NH₂ – modified *N*- and *C*-terminus, ⁶NV9-NH₂ – modified *C*-terminus.

peptide	0.2 μM		2 μM		20 μM		1 mM		2 mM	
	$T_m/^\circ\text{C}$	$s/^\circ\text{C}$	$T_m/^\circ\text{C}$	$s/^\circ\text{C}$	$T_m/^\circ\text{C}$	$s/^\circ\text{C}$	$T_m/^\circ\text{C}$	$s/^\circ\text{C}$	$T_m/^\circ\text{C}$	$s/^\circ\text{C}$
empty	35.7	0.6								
NV9 ¹	35.8	0.8	59.0	0.1	59.1	0.1	60.7	0.0		
YF9 ²	36.1	0.8	36.1	0.8	36.2	0.8				
GV9 ³	36.4	0.6	38.8	0.4	42.1	0.2	47.6	0.1		
Ac-NV9 ⁴	36.6	0.7	39.6	0.6	43.2	0.6	48.4	0.0		
Ac-NV9-NH ₂ ⁵	36.0	0.8	36.6	0.4	38.4	0.3				
NV9-NH ₂ ⁶	36.0	0.9	46.9	0.2	50.3	0.3	55.5	0.0		
NP4	35.6	0.4	35.7	0.5	35.8	0.4	39.0	0.0	42.1	0.1
NM5	35.6	0.5	35.9	0.4	37.3	0.3	45.0	0.1	45.9	0.0
NV6	35.5	0.1	35.9	0.2	37.6	0.1	44.1	0.6	44.6	0.2
NA7	35.5	0.1	35.9	0.1	38.0	0.1	45.4	0.0		
NT8	35.5	0.1	36.0	0.1	38.8	0.0	46.9	0.0		
LV8	35.4	0.1	43.5	0.1	47.3	0.0	53.3	0.0		
VV7	35.5	0.1	35.7	0.2	37.0	0.1	42.3	0.0		
PV6	35.5	0.2	35.6	0.1	36.4	0.0	42.2	0.3	43.6	0.5
MV5	35.6	0.1	36.5	0.1	39.3	0.1	47.9	0.0	49.3	0.0
VV4	35.5	0.0	35.1	0.6	35.5	0.2	41.5	0.0	42.6	0.1
NP4+VV4							45.0	0.1	47.9	0.1
NP4+MV5							47.6	0.1	50.4	0.1
NP4+PV6							43.9	0.1	46.5	0.1
NM5+VV4							47.2	0.1	47.3	0.1
NM5+MV5							47.6	0.0	49.9	0.0
NM5+PV6							45.5	0.0	47.3	0.0
NV6+VV4							44.1	0.1	46.3	0.2
NV6+MV5							47.4	0.0	49.8	0.0
NV6+PV6							44.8	0.1	46.6	0.1

Chapter 9. Molecular Mechanisms of chaperone-independent peptide exchange reveal allotype specific long-range peptide-MHC-I interactions

Chapter 9 contains unpublished original data. I performed all the experiments in this paper. In this study, we propose an alternative method for peptide exchange triggered by acidic pH on A2 and A24 allotypes. We demonstrate that both allotypes have different sensitivities towards acidification. We use this observation to dissect the individual steps of the exchange reaction. Further, we find evidence for the electrostatic attraction of the incoming peptide onto certain MHC-I allotypes, revealing that long-range interactions may influence peptide exchange.

9.1. Abstract

The cell biology and biochemistry of peptide exchange on MHC-I proteins are of great interest in the study of immunodominance and cross-presentation of pathogen and tumour antigens. Immunodominance requires the exchange of low-affinity peptides for those of higher affinity, while cross-presentation involves the exchange of endogenous for exogenous peptide antigens. Although several methods have been developed to artificially catalyse peptide exchange on recombinant MHC-I proteins, the cellular conditions and mechanisms allowing for peptide exchange *in vivo* remain unclear. Here, we demonstrate that acidification also triggers peptide exchange, and we use this observation to dissect the individual steps of the exchange reaction. We find that dipeptides support peptide exchange on MHC-I through two mechanisms also used by the exchange chaperones tapasin and TAPBPR: first, by promoting the (rate-limiting) dissociation of the pre-bound peptide, and second, by stabilizing the peptide-free MHC-I intermediate - a role which resembles that of disulfide-mediated stabilization described earlier. We demonstrate that acidification promotes both peptide dissociation and association, but not destabilization of the peptide-MHC-I complex, as previously suggested. Further examining the association reaction, we find evidence for the electrostatic-attraction of the incoming peptide onto certain MHC-I allotypes, revealing that long-range interactions may influence peptide exchange.

9.2. Introduction

Major Histocompatibility Complex Class I molecules (MHC-I) bind intracellular peptides in the Endoplasmic Reticulum (ER) and present them on the cell surface, allowing for immune surveillance by CD8⁺ T cells [1]. Peptide loading onto MHC-I in the ER involves iterative optimization, with low-affinity peptides exchanged for those with higher affinity, usually aided by the chaperones tapasin or TAPBPR [2]. Peptide exchange is also thought to be central to cross-presentation, a process by which peptides previously-loaded onto MHC-I may be replaced by exogenous peptides in the endocytic pathway [3]. The molecular mechanisms and cellular conditions mediating peptide exchange, especially in the absence of exchange chaperones, with tapasin-independent allotypes, and during cross-presentation, are not well understood. Of key interest is the role of pH, as it is thought to destabilize the peptide-MHC-I complex and may enhance peptide exchange during cross-presentation through the low pH of endocytic compartments [4,5].

Peptide exchange on recombinant MHC-I is also of great technological interest, since they are used in the study of antigen-specific CD8 T-cell populations [6]. Catalysing efficient peptide exchange would allow for peptides of interest to be loaded onto MHC-I, allowing for the means of generating large numbers of peptide-MHC-I complexes for the analysis of antitumor and antiviral immune responses [7–9].

We and others have identified several techniques for accelerating peptide exchange [7,9-12]. Here, we show that acidic pH can accelerate peptide exchange on MHC-I in an allotype-specific manner, and we demonstrate that a long-range electrostatic interaction between peptide and MHC-I co-determines the rate of peptide exchange.

9.3. Results

9.3.1. A shift to low pH accelerates peptide exchange on HLA-A*02:01 and HLA-A*24:02.

It was previously proposed that low pH, corresponding to conditions in endolysosomal compartments, enhances peptide exchange on MHC-I, and there is evidence of acid-dependent release of low-affinity peptides from MHC-I [5,13]. These data suggest a general decrease in peptide binding affinity at low pH. In contrast, we hypothesized that an increase in the peptide dissociation rate might lead to faster peptide exchange. To test our hypothesis, we expressed the human MHC-I allotypes HLA-A*02:01 (in the following termed A2) and HLA-A*24:02 (A24) in *Escherichia coli* and folded them *in vitro* with the low-affinity peptides NLVPMVATA (termed NA9) and QYTPVSQLA (termed QA9), respectively. Exchange for fluorescently labelled

peptides (with FITC at a position that does not interfere with binding) was then measured by fluorescence anisotropy (**Figure 9-1 A**), an assay we have previously used to show that exchange depends on the type of dipeptide used [9].

We next investigated the pH dependence of the exchange reaction. Strikingly, lowering the pH from 8 to 6 triggered an increase in the rate of peptide exchange for both allotypes, with up to 200-fold acceleration (**Figure 9-1, B and C, Table S9-1**). Decreasing the pH any further was not feasible, since at pH 5.5, β_2m dissociates from the HC [14].

9.3.2. Lower pH accelerates peptide association to A2 but not to A24.

To understand the mechanistic details of this acidic acceleration of peptide exchange, we next investigated separately the two steps of peptide exchange, i.e., the dissociation of the pre-bound ('leaving') peptide, and the association of the incoming peptide. Since the binding site of empty MHC-I is natively unfolded and binds peptide only slowly (if at all) [15], we made use of empty, disulfide-stabilized MHC-I (dsMHC-I) to measure the association rates. These dsMHC-I have a disulfide bond linking the α_1 and α_2 helices close to the F pocket of the peptide-binding groove, conformationally stabilizing them in the absence of peptide in a structure that is close to the peptide-bound state [4],[8]. Disulfide-stabilized (ds) A2 and dsA24 bind peptides significantly faster than wild type (wt) A2 or wtA24 and show a similar acidic acceleration of exchange (**Figure S9-1; Table S9-2**). In contrast, disulfide stabilization did not significantly alter the affinity of A2 towards peptides and dipeptides (**Figure S2**).

We then measured the association rates (k_{on}) of the fluorescently labelled peptides to the empty disulfide-stabilized A2 and A24 molecules. Surprisingly, decreasing the pH had only a small effect on the rate of peptide association onto dsA24 (**Figure 9-2A; Table S9-3**), despite the strong acceleration of overall peptide exchange on dsA24 (**Figure 9-1, B and C**). For dsA2, we observed an increase in the association rate between pH 8 and pH 7 that mirrored the increase in the exchange rate seen in **Figure 9-1, B and C**; but when lowering the pH further to 6, the k_{on} decreased again. These results suggest that peptide association is not uniformly accelerated by lowering the pH. The fact that the rate of peptide association onto dsA24 remains unchanged while the overall exchange rate increases suggests that peptide dissociation is the step of the reaction that undergoes acceleration.

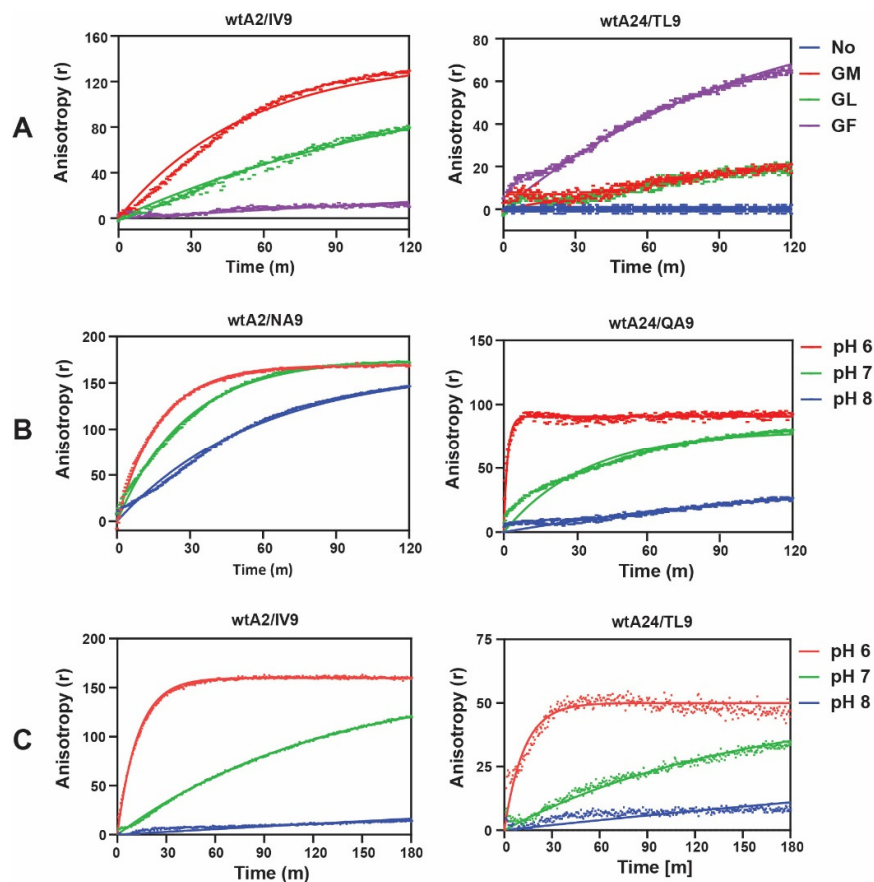


Figure 9-1. Dipeptides and acidification promote peptide exchange on wtA2 and wtA24.

(A) The high-affinity peptide-MHC-I complexes wtA2-ILKEPVHGV and wtA24-TYASNTSTL were incubated with or without 10 mM dipeptides, and the association rate of 10 nM NLVPK(FITC)VATV or QYTPVSK(FITC)LF, respectively, was measured using fluorescence anisotropy in 50 mM HEPES buffer and 100 mM NaCl at pH 7.5. (B) An analogous experiment measuring association of the same FITC peptides onto the low-affinity peptide-MHC-I complexes wtA2-NLVPVATA and wtA24-QYTPVSQLA in citrate-phosphate buffer at pH 6, 7 and 8. Association rate constants of exchange reactions are shown in Supplementary Table 2.

9.3.3. Lower pH influences dissociation but not equilibrium peptide binding affinity.

We next sought to determine whether low pH destabilizes the leaving peptide-MHC complex, promoting peptide dissociation. We measured the equilibrium dissociation constants (k_D) by peptide titration with steady-state anisotropy and found that the pH did not significantly affect the peptide binding affinity of the complexes, as indicated by the relatively stable k_D (**Figure 9-2 B**). Likewise, we measured the thermal stability of the peptide-MHC complexes by nanoscale

differential scanning tryptophan fluorimetry (nanoDSF) [16,17], which measures protein unfolding through the temperature-dependent change in fluorescence of the tryptophan residues and generates a thermal denaturation curve, the midpoint of which corresponds to the melting temperature (T_m). We found that peptide-empty dsMHC-I were significantly stabilized by lowering the pH, but there was very little – if any – influence of the pH on the T_m of peptide complexes with wtA2 or wtA24 for both low-affinity and high-affinity peptides (**Figure 9-2 C**). Finally, we directly measured the dissociation of a fluorescently labelled leaving peptide from dsA2 at different pH values and found an increased k_{off} at pH 6, compared to pH 8 and 7 (**Figure 9-2 D**).

Taken together, our data suggest that the acidic acceleration of peptide exchange might be caused by contributions of both peptide dissociation and association. For A2, peptide association is significantly accelerated from pH 8 to pH 7 (but then no further to pH 6), and dissociation is especially accelerated from pH 7 to pH 6. For A24, the strong acidic acceleration of exchange for A24 (**Figure 9-1, B and C**) is most likely fuelled by an increase in the dissociation rate at lower pH values, though we do not see this mirrored in the thermostabilities.

9.3.4. Electrostatic interactions between peptide and MHC-I accelerate peptide binding

We have seen that peptide association to dsA2 is dramatically accelerated when the pH is lowered from 8 to 7 (**Figure 9-2A**), which is not observed in the A24 allotype. We therefore aimed to understand the mechanism of the acidic acceleration of the on-rate in the A2 allotype. We reasoned that decreasing the pH may influence either MHC-I conformation, leading indirectly to a faster binding of peptide, or inter-molecular electrostatic interactions (such as attraction [18] or repulsion of the peptide), and that either of these phenomena may produce the observed faster binding. We further reasoned that a high salt concentration might help us distinguish between these two phenomena, since it disrupts the long-range electrostatic interactions more than conformational changes of the protein [19][20].

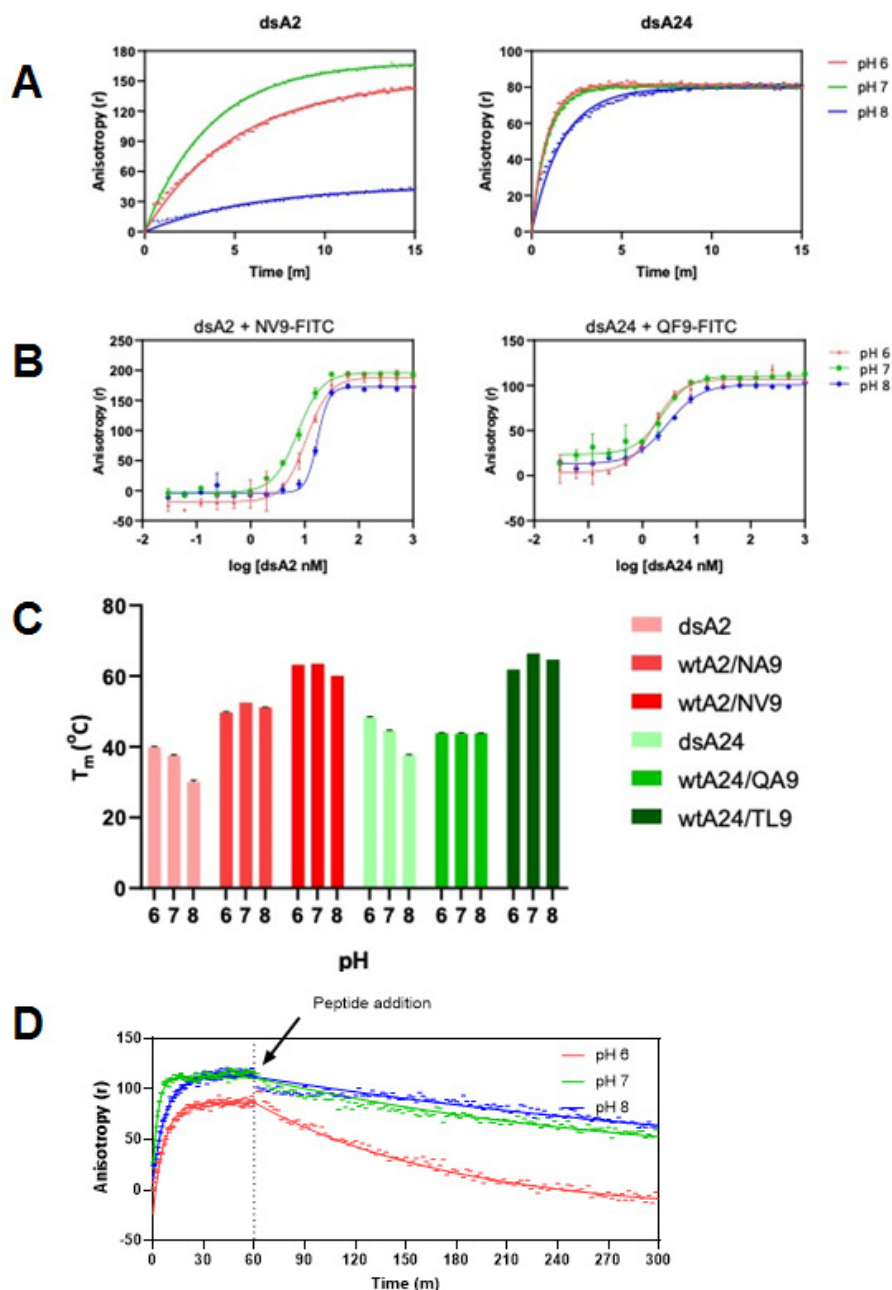


Figure 9-2. Acidification affects peptide association and dissociation on dsA2, but not peptide-dsMHC-I complex stability.

(A) Association of FITC peptides onto 30 nM empty dsA2 and dsA24 in citrate-phosphate buffer at pH 6, 7 and 8. Association rate constants from association reactions are shown in Supplementary Table 3. (B) Equilibrium binding affinity of empty dsA2 and dsA24 measured by steady-state anisotropy with 2 nM FITC peptides (fixed concentration) titrated with 1 μ M - 0.03 nM of the respective empty dsMHC-I, in citrate-phosphate buffer at pH 6, 7 and 8. (C) Thermostability of 100 μ g/mL (approx. 2.2 μ M) wtA2- and wtA24-peptide complexes, and empty dsA2 and dsA24 in PBS measured by NanoDSF. (D) Fluorescence anisotropy was used to track association of 10 nM NA9-TAM onto 30 nM empty dsA2, followed by dissociation after the addition of 10 μ M NV9 after 1 hour. Dissociation was measured for 6 hours. Full peptide sequences are shown in Supplementary Table 5.

We thus performed peptide exchange, binding affinity and association experiments in the presence of 500 mM NaCl, and we found that peptide exchange rates for dsA2 were strongly diminished by salt, whereas, in dsA24, they were even slightly increased (**Figure 9-3 A**); the same was true for the equilibrium binding affinity (**Figure 9-3 B**). High salt conditions decreased the association rates of peptide to dsA2 by a small extent, whereas for dsA24, the k_{on} was not significantly affected (**Figure 9-3 C**). We conclude that for peptide exchange, equilibrium affinity, and association, a long-range electrostatic attraction between MHC-I and peptide plays a more important role for A2 than for A24.

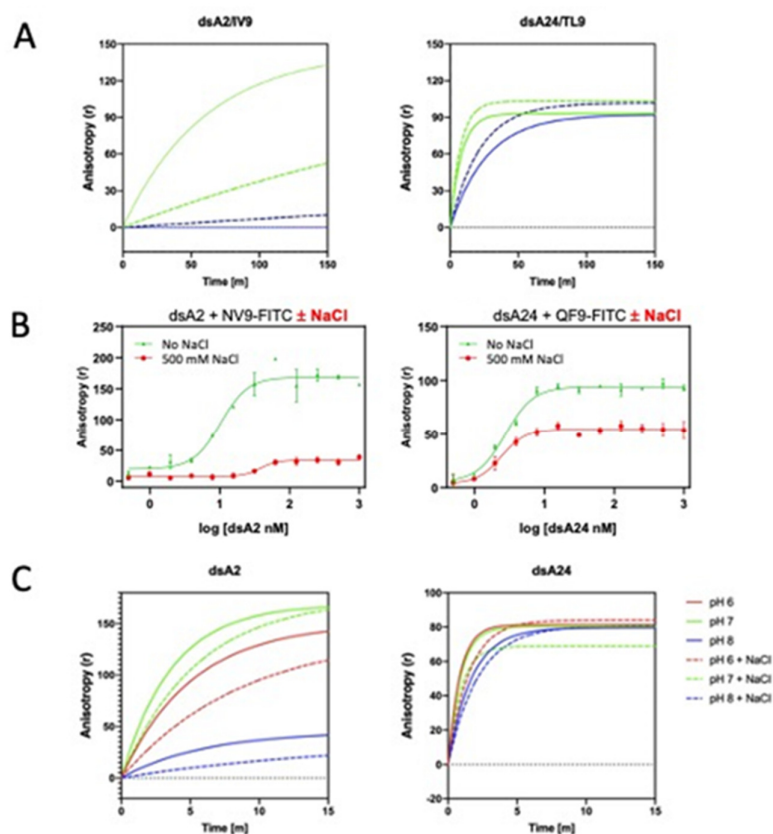


Figure 9-3. NaCl attenuates peptide exchange, equilibrium binding affinity and association on dsA2, but not dsA24.

(A) Exchange reaction with 30 nM of the high affinity peptide-MHC-I complexes dsA2-ILKEPVHGV and dsA24-TYASNTSTL with 10 nM incoming FITC peptides in citrate-phosphate buffer at pH 7 and 8, with or without 500 mM NaCl. Association rate constants of exchange reactions are shown in Supplementary Table 2. (B) Equilibrium binding affinity of empty dsA2 and dsA24 measured by steady-state anisotropy with 2 nM FITC peptides (fixed concentration) titrated with 1 μ M - 0.5 nM of the respective empty dsMHC-I, with or without 500 mM NaCl. (C) Association of 10 nM FITC peptides onto 30 nM empty dsA2 and dsA24 in citrate-phosphate buffer at pH 6, 7 and 8, with or without 500 mM NaCl. Association rate constants from association reactions are shown in Supplementary Table 3.

9.3.5. Acidic Acceleration is synergistic with dipeptide-mediated peptide exchange

To further test the hypothesis that low pH may enhance peptide association to A2, by promoting electrostatic interactions rather than by merely decreasing peptide binding affinity, we utilized dipeptide-mediated peptide exchange as a tool to distinguish between the phenomena. Dipeptides of appropriate sequence may accelerate peptide exchange by enhancing both leaving peptide dissociation and incoming peptide association. By occupying the c-terminal binding site of the partially-bound leaving peptide, dipeptides may accelerate its dissociation [9] while they may enhance association of the incoming peptide by maintaining the conformation of the binding groove in the interval of the reaction where no peptide is bound [21]. In fact, we demonstrate that dipeptides affect both association and dissociation as they further accelerate peptide exchange on dsMHC-I, in which optimal stabilization already produces a faster association (**Figure S9-1, A and B, S9-2, A and B**).

We then reasoned that if pH does enhance peptide association, equilibrium affinity, and exchange through electrostatic attraction between the MHC-I and the peptide, then acidic acceleration should have an additive effect on the dipeptide-mediated peptide exchange rate.

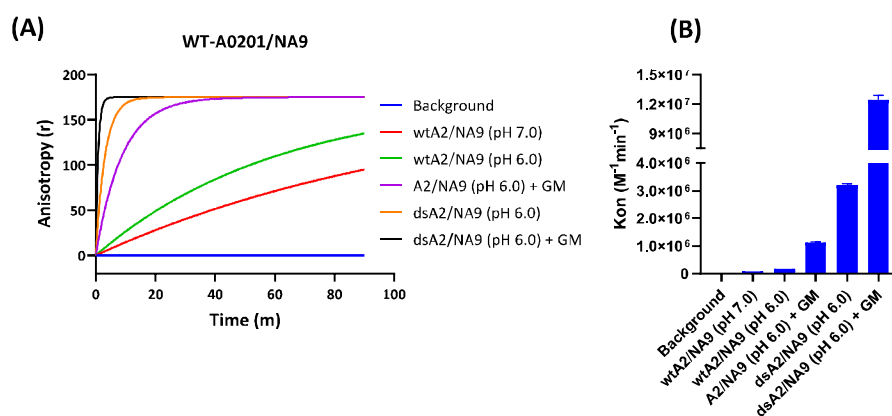


Figure 9-4. Acidification, dipeptides and disulfide stabilisation synergize in accelerating peptide exchange.

(A) Exchange reaction with 300 nM of the low affinity peptide-MHC-I complexes wtA2- and dsA2-NLVPMTATA with 100 nM incoming FITC peptide in citrate-phosphate buffer at pH 6 and 7, with or without 10 mM GM and **(B)** respective association rate constant (k_{on}) values. Association rate constants of exchange reactions are also shown in Supplementary Table 2.

Indeed, when comparing the effect of pH and dipeptide on peptide exchange for wtA2, we found that they synergized in accelerating peptide exchange (**Figure 9-4**), which is consistent with the idea that low pH increases peptide association mostly through a change in electrostatic interaction.

In contrast, dipeptides may increase dissociation of the leaving peptide and maintain the conformation of the binding groove in the interval of the reaction where no peptide is bound.

9.4. Discussion

Several methods to efficiently exchange peptides on MHC-I have been studied for biotechnological use [7,9–12]. However, they have revealed little about their mechanism, which may have important implications for MHC-I biochemistry and the cell biology of peptide optimization and cross-presentation. By studying the influence of changes to the protein itself, such as disulfide stabilization, and changes to the chemical parameters of the exchange reaction, such as pH, we hope to dissect the mechanisms of peptide exchange as they occur in vivo, for example, in cross-presentation of tumour antigens [3,22].

Disulfide stabilization. Previous work has shown that the conformational change to MHC-I upon peptide dissociation [23,24] - likely involving partial unfolding of the peptide binding site [15,25,26]- is largely inhibited in dsMHC-I by disulfide stabilization, such that the conformation of peptide-empty dsMHC-I closely resembles the peptide-bound state [6,27,28]. As the peptide-binding affinities of dsMHC-I resemble those of the wild type [27,28], dsMHC-I are ideal tools to investigate peptide association and dissociation without the accompanying MHC-I conformational change. Here, we show that peptide association is faster into dsMHC-I (**Figure S9-1 C**) than onto the wild-type (**Figure 9-1, B and C**).

We believe that this stabilization effect is also the reason for the significant acceleration of peptide exchange in the dsMHC-I compared to the wild type proteins (see k_{on} in **Table S9-3**). A typical association rate of 10 nM peptide to dsA2 is $2 \cdot 10^7 \text{ M}^{-1} \text{ min}^{-1}$ (**Figure S9-2A**), giving a collision frequency of 0.2 min⁻¹ and a half-time of 3.5 minutes for the productive binding of exogenous peptide to empty A2. Thus, during an exchange reaction, the binding site may remain empty for several minutes until an incoming peptide molecule binds productively, giving it ample time to partially unfold. Such denaturation is most likely prevented by the 84-139 disulfide bond.

Dipeptide-mediated exchange. Conformational stabilization of the peptide binding groove can also be reached with dipeptides (and maybe other small molecules), increasing the association rate of peptides to (otherwise) empty A2, as we have shown [21]. In addition, we had previously proposed a model for dipeptide-mediated peptide exchange where dipeptides bind into the F pocket and interfere with the rebinding of the C-terminus of the partially-dissociated leaving peptide [9]. Such blocking of peptide re-binding could occur in either the F or the A pocket, since the crystal structure have shown that the dipeptide GM can also bind to the A pocket region of A2 [28]. This model predicts that dipeptides still accelerate peptide exchange on dsMHC-I, whose

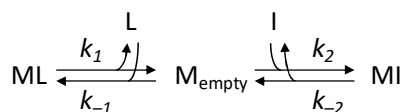
binding groove is already conformationally stabilized. We show here that this is indeed the case (**Figure S9-1 A and B, S9-2 A and B**). Remarkably, dsA2 and wtA2 bind the catalytic GM dipeptide with the same affinity (**Figure S9-2, C and D**). We conclude that dipeptides indeed support peptide exchange through two separable mechanisms, by accelerating dissociation of the leaving peptide as well as by stabilization of the peptide-empty intermediate of the exchange reaction.

This has mechanistic implications for our understanding of the role of tapasin and TAPBPR, the chaperones that aid in the peptide-editing process [29] by accelerating peptide exchange [30] through two demonstrated functions: accelerating the dissociation of the leaving peptide [31–33], and stabilizing empty MHC-I [34,35]. Our results show that dipeptides operate much like exchange chaperones, supporting both of these functions.

Low pH and rate limitation of peptide exchange. Previous studies have suggested that low pH may facilitate peptide exchange by destabilizing MHC-I [36], though little was known about the reaction mechanism. We show that low pH accelerates peptide exchange on MHC-I (**Figure 9-1 B C**) but does not decrease the stability of the peptide-MHC-I complex (**Figure 9-2, B and C**). Rather, acidification thermodynamically stabilized empty dsA2 and dsA24 (**Figure 9-2 C**), a stabilization that likely does not concern the F-pocket region, which is fixed on dsMHC-I [28]. This suggests that acidification may also stabilize the corresponding regions on empty wtA2 and wtA24, contributing to the observed acceleration in exchange.

We also show that decreasing the pH accelerated peptide association onto dsA2, but not dsA24 (**Figure 9-2 A**). This allotype-specific acceleration of association and the overall peptide exchange rate were diminished by salt (**Figure 9-3, A, C**), suggesting the involvement of electrostatic interactions (see below).

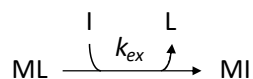
To identify the rate-limiting step of the exchange reaction, we compared the rate of the overall exchange reaction with the rate of peptide association. We assumed the simplest form of an exchange reaction



(with M = MHC-I, L = leaving peptide, I = incoming peptide), which simplifies at very short times to



In the anisotropy association experiment to empty MHC-I (Figure 2), k_2 is measured, whereas in the exchange experiment, we measure an overall exchange constant



We found that for dsA2, k_{ex} (Figure S9-1 C) was about 30-fold slower than k_2 at both pH7 and 8 (Figure 9-2 A; Table S 9-4). Therefore, the rate-limiting step of the reaction is the dissociation of the leaving peptide. Indeed, our kinetic data demonstrates - as suggested by previous studies [5,13] - that low pH promotes dissociation on A2 (Figure 9-2 D). Consequently, on A2, low pH might accelerate exchange by three mechanisms: accelerating dissociation, stabilizing the intermediate, and attracting the incoming peptide.

The big differences in the exchange and especially the association rate between A2 and A24 suggests different abilities of MHC-I allotypes to exchange peptides in an acidic environment. This is especially important for cross-presentation, where - at least in some situations - peptides from proteins endocytosed from the cell environment are loaded onto MHC-I in the acidic environment of endosomes [22]. It will be interesting to delineate the residues that determine pH dependence of peptide exchange, and perhaps to generate mutants for the investigation of cross-presentation efficiency in cells.

Long-range forces. It has been previously appreciated that the arrangement of charges in the peptide binding groove determines the biochemical properties of a particular class I allotype. Local frustration at the F-pocket - caused by energetically suboptimal contacts made by F-pocket residues - has been shown to produce electrostatic repulsion and hydration in the empty peptide binding site, which are only resolved upon peptide binding [35,37]. Peptide binding to several allotypes including HLA-B*44:02 and HLA-A*02:01 involves the rearrangement of hydrogen bonds and/or salt bridges [28,38]. This is especially true for micropolymorphisms that determine the striking differences between closely related allotypes (for example B*44:02 and B*44:05, or B*27:05 and B*27:09) in terms of tapasin dependence and peptide binding in cells [15]. We now also show that long-range electrostatic forces accelerate peptide binding to A2 (Figure 3C) at the three pH values tested. Since our peptides have no significant charges in their side chains between pH 6 and 8, the long-range electrostatic interactions might involve a terminus of the peptide and acidic or basic side chains of the protein. The influence of electrostatics is much more dramatic

on the exchange reaction, suggesting that the rate-limiting step, dissociation of the leaving peptide (see above), is also accelerated by an electrostatic effect, at least at pH 7 (Figure 3A).

Taken together, our data show that MHC-I – peptide exchange kinetics is governed by a complex interplay of protein conformation and protein-ligand attraction at long and short distances that is additionally modulated by the pH of the environment. In this way, particular allotypes might be biochemically tuned to optimally exchange peptides in an acidic environment inside the cell. It will be interesting to connect these findings with cell biological studies of cross-presentation.

9.5. Methods

9.5.1. Production of MHC-I heavy chains and β_2m

MHC-I HCs and β_2m were produced in *E.coli*, as described previously [39,40]. Briefly, proteins were expressed in BL21(DE3)pLysS using pET series plasmids. Inclusion bodies containing expressed proteins were harvested using sonication in lysis buffer followed by washing in detergent buffer, and wash buffer and solubilizing the protein in 8 M urea buffer (8 M urea, 50 mM K-HEPES pH 6.5 and 100 μ M β -mercaptoethanol). Proteins were stored at -80 °C until used for in vitro folding.

9.5.2. In-vitro folding and purification of MHC-I

All MHC-I proteins were folded and purified as previously described [6]. Briefly, wtA2, dsA2, wtA24 and dsA24 molecules, HCs (1 μ M) and β_2m (2 μ M) diluted in a folding buffer composed of 0.1 M Tris pH 8.0, 500 mM L-Arginine-HCl, 2 mM EDTA, 0.5 mM oxidized glutathione and 5 mM reduced glutathione with 10 μ M low-affinity peptides or with 10 mM of dipeptide (GM for A2, GF for A24). The folding reaction was then incubated at 4°C for 1 week, followed by concentrating folded proteins with a 30 kDa cutoff membrane filters (Vivaflow-200; Sartorius). Folded MHC-I monomers were purified with size exclusion chromatography using ÄKTA Go HiLoad 26/600 Superdex-200 pg gel filtration column (GE Healthcare Life Sciences). All MHC-I folded monomers were stored at -80 °C until further use.

9.5.3. Thermal stability measurements

Thermal stability was measured using nanoDSF by dissolving MHC-I complexes in Citrate Phosphate buffer, pH 7.6 [41] at the concentration of 100 μ g/ml. Each capillary was loaded with 10 μ L of test samples either in duplicates or triplicates. Experiments were carried out using the Prometheus NT.48 (Nano Temper Technologies, Germany). The temperature gradient was set to an increase of 1 °C/minute in a range from 20 °C to 80 °C. T_m values were calculated by

the PR.ThermControl v2.1 software from the first derivative of the fluorescence at F330 and plotted using GraphPad prism.

9.5.4. Peptide binding, exchange and dissociation

Peptide binding and exchange was performed using fluorescence anisotropy as previously described [6,9,21]. To assess peptide binding by fluorescence anisotropy, 10 nM fluorochrome-labeled peptide NLVPK(FITC)VATV or QYTPVSK(FITC)LF (GeneCust) and 30 nM of purified folded empty dsA2 or dsA24 were used unless otherwise mentioned. Peptide binding to MHC-I molecules was measured at room temperature (22–24 °C) in Citrate-Phosphate Buffer pH 6, pH 7, and pH 8, with a total reaction volume of 100 µL.

For peptide exchange studies, 10 nM of NLVPK(FITCV)ATV or QYTPVSK(FITC)LF (GeneCust) was added to 30 nM of purified MHC-I – peptide complexes of wt/dsA2 or wt/dsA24, respectively.

For peptide dissociation studies, 10 nM of NLVPK[TAMRA]VATA was added to 30 nM of purified empty dsA2, followed by the addition of 10 µM NLVPMVATV after 1 hour. Association was tracked for the first hour, followed by dissociation for 6 hours following addition of NLVPMVATV.

All kinetic measurements were performed with Tecan Infinite M1000 PRO (Tecan, Crailsheim, Germany) multimode plate reader by measuring anisotropy (FITC λ_{ex} = 494 nm, λ_{em} = 517 nm). Data were plotted using GraphPad Prism.

9.6. References

- [1] Paul, W.E., *Fundamental immunology*, Wolters Kluwer Health/Lippincott Williams & Wilkins, Philadelphia 2013.
- [2] Elliott, T., Williams, A., The optimization of peptide cargo bound to MHC class I molecules by the peptide-loading complex. *Immunol. Rev.* 2005, 207, 89–99.
- [3] Ackerman, A.L., Cresswell, P., Cellular mechanisms governing cross-presentation of exogenous antigens. *Nat. Immunol.* 2004, 5, 678–684.
- [4] Chefalo, P.J., Harding, C. V., Processing of Exogenous Antigens for Presentation by Class I MHC Molecules Involves Post-Golgi Peptide Exchange Influenced by Peptide-MHC Complex Stability and Acidic pH. *J. Immunol.* 2001, 167, 1274–1282.
- [5] Stryhn, A., Pedersen, L.O., Romme, T., Olsen, A.C., et al., pH dependence of MHC class I-restricted peptide presentation. *J. Immunol.* 1996, 156, 4191–7.
- [6] Saini, S.K., Tamhane, T., Anjanappa, R., Saikia, A., et al., Empty peptide-receptive MHC class I molecules for efficient detection of antigen-specific T cells. *Sci. Immunol.* 2019, 4, eaau9039.
- [7] Luimstra, J.J., Garstka, M.A., Roex, M.C.J., Redeker, A., et al., A flexible MHC class I multimer loading system for large-scale detection of antigen-specific T cells. *J. Exp. Med.* 2018, 215, 1493–1504.
- [8] Luimstra, J.J., Franken, K.L.M.C.M.C., Garstka, M.A., Drijfhout, J.W., et al., Production and Thermal Exchange of Conditional Peptide-MHC I Multimers. *Curr. Protoc. Immunol.* 2019, 126, e85.
- [9] Saini, S.K., Schuster, H., Ramnarayan, V.R., Rammensee, H.-G., et al., Dipeptides catalyze rapid peptide exchange on MHC class I molecules. *Proc. Natl. Acad. Sci.* 2015, 112, 202–207.
- [10] Rodenko, B., Toebes, M., Hadrup, S.R., van Esch, W.J.E., et al., Generation of peptide-MHC class I complexes through UV-mediated ligand exchange. *Nat. Protoc.* 2006, 1, 1120–1132.
- [11] Rodenko, B., Toebes, M., Celie, P., Perrakis, A., Schumacher, T.N.M., “ MHC class I complexes loaded by a periodate trigger ” by. *Water* 2013, 131, 1–10.
- [12] Overall, S.A., Toor, J.S., Hao, S., Yarmarkovich, M., et al., High throughput pMHC-I tetramer library production using chaperone-mediated peptide exchange. *Nat. Commun.* 2020, 11, 1909.
- [13] Grommé, M., Uytdehaag, F.G.C.M., Janssen, H., Calafat, J., et al., Recycling MHC class I molecules and endosomal peptide loading. *Proc. Natl. Acad. Sci. U. S. A.* 1999, 96, 10326–10331.
- [14] Hochman, J.H., Jiang, H., Matyus, L., Edidin, M., Pernis, B., Endocytosis and dissociation of class I MHC molecules labeled with fluorescent beta-2 microglobulin. *J. Immunol.* 1991, 146.
- [15] Jantz-Naeem, Springer, S., In Press. *Curr. Opin.* 2021.
- [16] Baljinnyam, B., Ronzetti, M., Yasgar, A., Simeonov, A., in: Labrou NE (Ed.), Springer US, New York, NY 2020, pp. 47–68.
- [17] Saikia, A., Springer, S., In Revision 2021.
- [18] Leckband, D.E., Israelachvili, J.N., Schmitt, F.-J., Knoll, W., AMERICAN ASSOCIATION FOR THE ADVANCEMENT OF SCIENCE. *Science (80-)*. 1881, os-2, 341–342.
- [19] Tsumoto, K., Ejima, D., Senczuk, A.M., Kita, Y., Arakawa, T., Effects of salts on protein–surface interactions: applications for column chromatography. *J. Pharm. Sci.* 2007, 96, 1677–1690.
- [20] Darling, R.J., Kuchibhotla, U., Glaesner, W., Micanovic, R., et al., Glycosylation of erythropoietin affects receptor binding kinetics: Role of electrostatic interactions. *Biochemistry* 2002, 41, 14524–14531.
- [21] Saini, S.S.K., Ostermeir, K., Ramnarayan, V.V.R., Schuster, H., et al., Dipeptides promote folding and peptide binding of MHC class I molecules. *Proc. Natl. Acad. Sci. U. S. A.* 2013, 110, 15383–15388.
- [22] Montealegre, S., Van Endert, P.M., Endocytic recycling of MHC class I molecules in non-professional antigen presenting and dendritic cells. *Front. Immunol.* 2019, 10, 1–11.
- [23] Springer, S., Do, K., Skipper, J.C.A., Townsend, A.R.M., et al., Fast association rates suggest a conformational change in the MHC class I molecule H-2Db upon peptide binding. *Biochemistry*

- 1998, 37, 3001–3012.
- [24] Wieczorek, M., Abualrous, E.T., Sticht, J., Álvaro-Benito, M., et al., Major histocompatibility complex (MHC) class I and MHC class II proteins: Conformational plasticity in antigen presentation. *Front. Immunol.* 2017, 8, 1–16.
 - [25] Bouvier, M., Wiley, D.C., Structural characterization of a soluble and partially folded class I major histocompatibility heavy chain/ β 2m heterodimer. *Nat. Struct. Biol.* 1998, 5, 377–384.
 - [26] Kurimoto, E., Kuroki, K., Yamaguchi, Y., Yagi-Utsumi, M., et al., Structural and functional mosaic nature of MHC class I molecules in their peptide-free form. *Mol. Immunol.* 2013, 55, 393–399.
 - [27] Hein, Z., Uchtenhagen, H., Abualrous, E.T., Saini, S.K., et al., Peptide-independent stabilization of MHC class I molecules breaches cellular quality control. *J. Cell Sci.* 2014, 127, 2885–2897.
 - [28] Anjanappa, R., Garcia-Alai, M., Kopicki, J.D., Lockhauserbäumer, J., et al., Structures of peptide-free and partially loaded MHC class I molecules reveal mechanisms of peptide selection. *Nat. Commun.* 2020, 11, 1–11.
 - [29] McShan, A.C., Devlin, C.A., Morozov, G.I., Overall, S.A., et al., TAPBPR promotes antigen loading on MHC-I molecules using a peptide trap. *Nat. Commun.* 2021 121 2021, 12, 1–18.
 - [30] Hermann, C., van Hateren, A., Trautwein, N., Neerinx, A., et al., TAPBPR alters MHC class I peptide presentation by functioning as a peptide exchange catalyst. *Elife* 2015, 4.
 - [31] Jiang, J., Natarajan, K., Boyd, L.F., Morozov, G.I., et al., Crystal structure of a TAPBPR–MHC I complex reveals the mechanism of peptide editing in antigen presentation. *Science (80-.).* 2017, 358, 1064–1068.
 - [32] Ilca, F.T., Neerinx, A., Hermann, C., Marcu, A., et al., TAPBPR mediates peptide dissociation from MHC class I using a leucine lever 2018, 7, 1–24.
 - [33] Praveen, P.V.K., Yaneva, R., Kalbacher, H., Springer, S., Tapasin edits peptides on MHC class I molecules by accelerating peptide exchange. *Eur. J. Immunol.* 2010, 40, 214–224.
 - [34] Thomas, C., Tampé, R., Structure of the TAPBPR–MHC I complex defines the mechanism of peptide loading and editing. *Science (80-.).* 2017, 358, eaa06001.
 - [35] Garstka, M.A., Fritzsche, S., Lenart, I., Hein, Z., et al., Tapasin dependence of major histocompatibility complex class I molecules correlates with their conformational flexibility. *FASEB J.* 2011, 25, 3989–3998.
 - [36] Chefalo, P.J., Grandea, A.G., Van Kaer, L., Harding, C. V., Tapasin $-/-$ and TAP1 $-/-$ Macrophages Are Deficient in Vacuolar Alternate Class I MHC (MHC-I) Processing due to Decreased MHC-I Stability at Phagolysosomal pH. *J. Immunol.* 2003, 170, 5825–5833.
 - [37] Serçinoğlu, O., Ozbek, P., Sequence-structure-function relationships in class I MHC: A local frustration perspective. *PLoS One* 2020, 15, e0232849.
 - [38] Ostermeir, K., Springer, S., Zacharias, M., Coupling between side chain interactions and binding pocket flexibility in HLA-B*44:02 molecules investigated by molecular dynamics simulations. *Mol. Immunol.* 2015, 63, 312–319.
 - [39] Garboczi, D.N., Hung, D.T., Wiley, D.O.N.C., PNAS-1992-Garboczi-3429-33 1992, 89, 3429–3433.
 - [40] Saini, S.K., Abualrous, E.T., Tigan, A.S., Covella, K., et al., Not all empty MHC class I molecules are molten globules: Tryptophan fluorescence reveals a two-step mechanism of thermal denaturation. *Mol. Immunol.* 2013, 54, 386–396.
 - [41] McIlvaine, T.C., A buffer solution for colorimetric comparison. *J. Biol. Chem.* 1921, 49, 183–186.

9.7. Supplementary Information

9.7.1. Supplementary figures

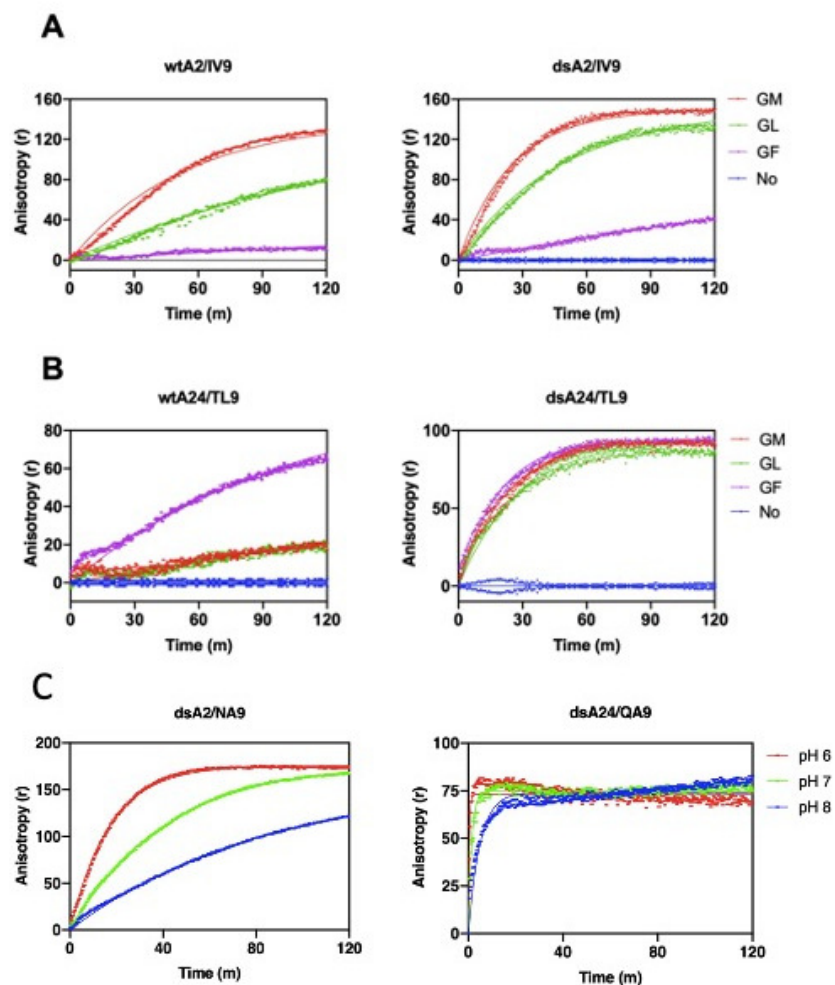


Figure S1. dsMHC-I bind peptide faster than wtMHC-I but show a similar acidic acceleration of exchange. Exchange reactions with high-affinity peptide-MHC-I complexes (A) wtA2- and dsA2-ILKEPVHGV and (B) wtA24- and dsA24-TYASNTSTL with 10 nM incoming FITC-peptide in HEPES buffer at pH 7.5, with or without 10 mM dipeptides. (C) Exchange reaction with the low-affinity peptide-MHC-I complexes dsA2-NLVPMVATA and wtA24-QYTPVSQLA with 10 nM incoming FITC peptides in citrate-phosphate buffer at pH 6, 7 and 8. Analogous to experiment with wtMHC-I complexes in Figure 1B. Association rate constants of exchange reactions are shown in Supplementary Table 2.

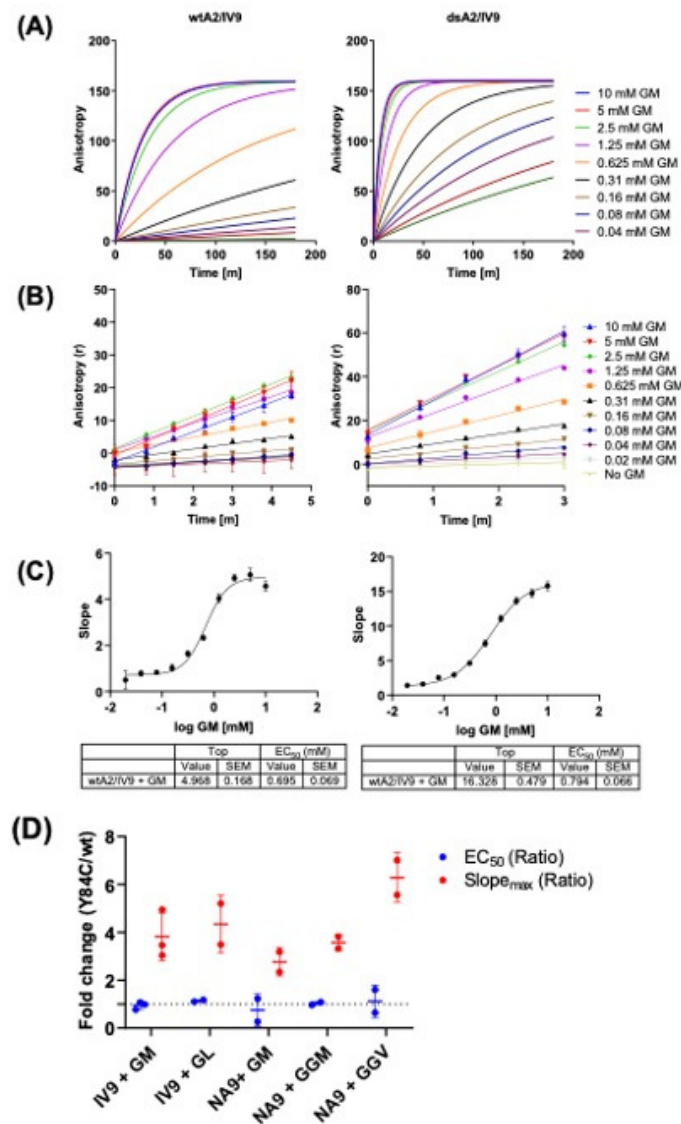


Figure S2. Disulfide stabilization accelerates dipeptide-catalyzed peptide exchange, but does not alter affinity to dipeptides measured as the concentration of half-maximal acceleration (EC₅₀). (A) Exchange reactions with 300 nM of the high affinity peptide-MHC-I complexes wtA2- and dsA2-ILKEPVHGV with 100 nM incoming FITC-peptide in HEPES buffer at pH 7.5, with 0.04 - 10 mM GM (representative figure) with (B) linear fit of initial kinetics used to calculate the slopes plotted in (C) to determine the EC₅₀. (D) EC₅₀ ratio of dsA2/wtA2 plotted with ratio of slopes of dsA2/wtA2. Association rate constants of exchange reactions are shown in Supplementary Table 2.

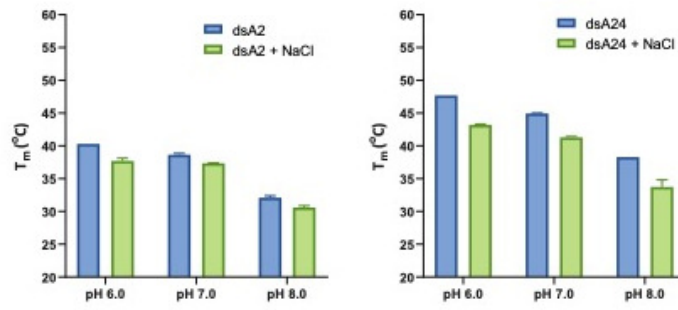


Figure S3. Acidification stabilizes empty dsMHC-I with moderate salt-sensitivity. Thermostability of 100 $\mu\text{g/mL}$ (approx. 2.2 μM) empty dsA2 (left) and dsA24 (right) in PBS, with or without 500 mM NaCl, measured by nanoDSF.

9.7.2. Supplementary tables

Table S9-1

Acceleration of peptide exchange upon acidification

	k_{on} ($M^{-1}min^{-1}$)		Fold Acceleration over pH 8	
	A2/NA9 Fig. 1B (left)	dsA2/NA9 Fig. S1C (left)	A2/NA9	dsA2/NA9
pH 6	292927 (± 2516)	23617610 (± 11025863)	11.6	5.2
pH 7	157938 (± 1226)	10590406 (± 2738543)	6.3	2.3
pH 8	25234 (± 612)	4508376 (± 376347)	1.0	1.0
	k_{on} ($M^{-1}min^{-1}$)		Fold Acceleration over pH 8	
	A24/QA9 Fig. 1B (right)	dsA24/QA9 Fig. S1C (right)	A24/QA9	dsA24/QA9
pH 6	756862223 (± 1716531)	141725490 (± 23914529)	248.1	22.2
pH 7	2117642 (± 16144)	31931941 (± 2201441)	6.9	5.2
pH 8	305057 (± 3313)	6313935 (± 183558)	1.0	1.0

Table S9-2. Summary Table of Peptide Exchange Rates

Figure	MHC-I-leaving peptide complex	Incoming peptide	k_{on} ($M^{-1}min^{-1}$)			
			No dipeptide	GL	GF	GM
1A	wtA2/IV9	NV9-FITC	2.25E-13 ($\pm 3.46E+02$)	5.35E+05 ($\pm 3.05E+03$)	9.04E+03 ($\pm 1.05E+03$)	1.50E+06 ($\pm 9.37E+03$)
	wtA24/TL9	QF9-FITC	5.78E-13 ($\pm 5.56E+02$)	9.10E+04 ($\pm 2.22E+03$)	9.54E+05 ($\pm 3.31E+03$)	1.03E+05 ($\pm 1.80E+03$)
S1A	wtA2/IV9	NV9-FITC	2.25E-13 ($\pm 3.46E+02$)	5.35E+05 ($\pm 3.05E+03$)	9.04E+03 ($\pm 1.05E+03$)	1.50E+06 ($\pm 9.37E+03$)
	dsA2/IV9	NV9-FITC	3.45E-13 ($\pm 2.97E+02$)	1.83E+06 ($\pm 1.55E+04$)	2.03E+05 ($\pm 1.36E+03$)	3.76E+06 ($\pm 2.72E+04$)
S1B	wtA24/TL9	QF9-FITC	5.78E-13 ($\pm 5.56E+02$)	9.10E+04 ($\pm 2.22E+03$)	9.54E+05 ($\pm 3.31E+03$)	1.03E+05 ($\pm 1.80E+03$)
	dsA24/TL9	QF9-FITC	2.12E-13 ($\pm 7.90E+02$)	2.38E+06 ($\pm 3.43E+04$)	3.86E+06 ($\pm 3.90E+04$)	3.19E+06 ($\pm 3.50E+04$)
Figure	MHC-I-leaving peptide complex	Incoming peptide	pH 8	pH 7	pH 6	—
1B	wtA2/NA9	NV9-FITC	7.08E+04 ($\pm 1.47E+03$)	2.29E+05 ($\pm 2.59E+03$)	4.85E+05 ($\pm 5.51E+03$)	—
	wtA24/QA9	QF9-FITC	7.39E+05 ($\pm 9.27E+04$)	2.88E+06 ($\pm 4.83E+04$)	6.22E+07 ($\pm 1.20E+06$)	—
S1C	dsA2/NA9	NV9-FITC	4.82E+05 ($\pm 8.25E+03$)	9.67E+05 ($\pm 3.02E+03$)	2.36E+06 ($\pm 8.20E+03$)	—
	dsA24/QA9	QF9-FITC	2.03E+07 ($\pm 4.73E+05$)	6.84E+07 ($\pm 1.40E+06$)	2.46E+08 ($\pm 1.52E+07$)	—
Figure	MHC-I-leaving peptide complex	Incoming peptide	pH 8	pH 8 + NaCl	pH 7	pH 7 + NaCl
3A	dsA2/IV9	NV9-FITC	1.37E+02 ($\pm 8.41E+02$)	4.94E+04 ($\pm 5.92E+02$)	1.66E+06 ($\pm 8.89E+03$)	3.01E+05 ($\pm 1.98E+03$)
	dsA24/TL9	QF9-FITC	3.69E+06 ($\pm 3.08E+04$)	4.57E+06 ($\pm 5.94E+04$)	1.22E+07 ($\pm 1.44E+05$)	4.57E+06 ($\pm 5.94E+04$)
Figure	MHC-I-leaving peptide complex	Incoming peptide	pH 7	pH 6	pH 6 + GM	—
4AB	wtA2/NA9	NV9-FITC	8.69E+04 ($\pm 4.72E+02$)	1.64E+05 ($\pm 1.22E+03$)	1.13E+01 ($\pm 7.33E+03$)	—
	dsA2/NA9	NV9-FITC	—	3.20E+06 ($\pm 5.72E+04$)	1.0E+007 ($\pm 4.72E+05$)	—

Supplementary Table S9-3. Summary Table of Peptide Association Rates

Figure	MHC-I	Incoming peptide	k_{on} ($M^{-1}min^{-1}$)					
			pH 8	pH 8 + NaCl	pH 7	pH 7 + NaCl	pH 6	pH 6 + NaCl
2A	dsA2 (empty)	NV9-FITC	1.66E+007 ($\pm 7.63E+05$)	—	2.73E+07 ($\pm 2.91E+05$)	—	1.95E+07 ($\pm 4.17E+05$)	—
	dsA24 (empty)	QF9-FITC	5.90E+007 ($\pm 8.33E+05$)	—	1.13E+08 ($\pm 1.08E+06$)	—	1.19E+08 ($\pm 2.41E+06$)	—
3A	dsA2 (empty)	NV9-FITC	1.66E+07 ($\pm 7.63E+05$)	6.38E+06 ($\pm 5.02E+05$)	2.73E+07 ($\pm 2.91E+05$)	1.84E+07 ($\pm 1.02E+05$)	1.95E+07 ($\pm 4.17E+05$)	1.14E+07 ($\pm 4.40E+05$)
	dsA24 (empty)	QF9-FITC	5.90E+07 ($\pm 8.33E+05$)	4.62E+07 ($\pm 9.30E+05$)	1.13E+08 ($\pm 1.08E+06$)	1.09E+08 ($\pm 1.38E+06$)	1.19E+08 ($\pm 2.41E+06$)	6.64E+07 ($\pm 8.33E+05$)

Supplementary Table S9-4. Comparison of Peptide Exchange and Association Rates on dsA2

pH	dsA2 k_{on} ($M^{-1}min^{-1}$)		Fold Difference
	Association	Exchange	Association/Exchange
	Figure 2A (left)	Figure S1C (left)	
pH 7	2.731e+007	9.67e+005	28.242 (± 0.3128)
pH 8	1.663e+007	4.82e+005	34.502 (± 1.690)

Supplementary Table S9-5. Peptide sequences, modifications and affinity to MHC-I allotypes

Allotype	ID	Peptides	Type
HLA-A*02:01	IV9	ILKEPVHGV	High Affinity, Leaving Peptide
	NV9	NLVPMTATV	High Affinity
	NA9	NLVPMTAT <u>A</u>	Modified low affinity peptide, Leaving Peptide
	NV9-FITC	NLVPK[FITC]VATV	High Affinity FITC labelled, Incoming Peptide
	NA9-TAM	NLVPK[TAMRA]VATA	Low Affinity TAMRA labelled, Leaving
HLA-A*24:02	QF9	QYTPVSQLF	High Affinity
	QA9	QYTPVSQLA	Modified low affinity peptide, Leaving Peptide
	QF9-FITC	QYTPVSK(FITC)LF	High Affinity FITC labelled, Incoming Peptide

Chapter 10. Discussion (Outlook)

There has been substantial progress in the understanding of the function of MHC-I in antigen presentation since it was discovered over three decades ago [1]. Much of this progress was enabled by new methods in biochemistry, cell biology, computational biology, biophysics, and crystallography. Especially, molecular modeling in combination with cryo-electron microscopy has revealed PLC structures with deep insights into peptide loading, editing, and the mechanism of peptide exchange by peptide editors (tapasin and TAPBPR) [2–5]. Molecular dynamics simulations and nuclear magnetic resonance studies have allowed detailed investigation of the conformational states and movements of MHC-I proteins and their chaperones [6–8]. At the same time, the effort of applied immunologists has become directed towards using recombinant MHC-I molecules in the development of tools for immunotherapeutics such as peptide vaccines, T cell activation reagents, and monitoring methodologies. These approaches are supported by novel MHC-I-oriented technologies.

Saini *et al.* have previously demonstrated peptide exchange on HLA-A*02:01 and H-2K^b with dipeptides [9]. They also showed that dipeptides support folding of these allotypes without any full-length peptides [10]. However, since folding and exchange require allotype-specific dipeptides, the dipeptides that support folding and peptide exchange in other allotypes remained to be investigated. So, in this project, my primary goal was to screen for dipeptides and other small molecules as modulators of peptide exchange and refolding for the most common, or relevant, MHC-I allotypes. I was able to generate a comprehensive list for MHC-I allotypes that cover more than 80% of the world population. I have also shown for the first time dipeptide-mediated MHC-I refolding in a microscale (250 μ L) volume in a high-throughput 96-well microplate cELISA screening assay (see section 3). Although my preliminary screening results are promising, further optimization might be necessary for reagent development.

10.1. How might a universal peptide exchange method revolutionize the field?

MHC-I multimers are extensively used in research and clinic for the monitoring of immune responses, and for cancer immunotherapy. The most efficient, non-classical way for the generation of many different multimers at once is by peptide exchange (see section 1.6). The most widely used exchange method is UV-mediated exchange. This method can only be performed at the monomer stage, since the fluorophores linked to the multimer backbones (*i.e.*, streptavidin, dextran, etc.) are UV-sensitive. Likewise, UV-mediated peptide cleavage produces nitroso

compounds that can damage the incoming peptide or the MHC-I protein [11–13]. Other exchange methods in the literature, such as chemical-, dipeptide- and heat-dependent peptide exchange, have specific issues that limit their universal use [9,14].

One of the aims of this thesis was to investigate a method for a quick generation of many different pMHC complexes that does not depend on allotype-specific reagents. A universal approach using either buffer conditions (such as the pH) or a small molecule exchanger (e.g., ethanol) might be the answer. Such a method will be easy to operate and economical. We have generated proof of concept data for A*02:01 and A*24:02 (see section 9). If achieved, such a method might also lead to basic science advances, e.g., better understanding of the molecular mechanism of peptide editing in cells. However, the scope of such a method might be limited by peptide affinity if only high-affinity peptides work well as incoming peptides. In that case, it would not be possible to make pMHCs with low-affinity peptides. For such tasks, dipeptide-bound or disulfide-stabilized empty MHC-I molecules may still be necessary.

10.2. Screening dipeptides for refolding different human allotypes for quick peptide exchange

In the work described in this thesis, we have screened a library of 50 short peptides – mostly dipeptides and a few tri- and tetrapeptides – for their ability to assist in the refolding of 18 MHC-I allotypes using a novel high-throughput micro-refolding set-up followed by competitive ELISA. The results are summarized in Table 3.1 (see section 3). The allotypes which we refolded with significant efficiency and yield were A*01:01, A*02:01, A*03:01, A*11:01, A*24:02, B*07:02, B*08:01, B*35:01, and C*05:01. Some other allotypes that we tested did not show significant folding efficiency. A few allotypes, namely B*13:01, B*27:05, B*44:02, and C*02:02, did not fold even in the presence of the full-length positive control peptides. Perhaps these allotypes are intrinsically very unstable, and the refolding conditions were not sufficiently optimized in our assay [15]. Data from previous studies suggest that chaperones such as tapasin stabilize unstable MHC-I molecules inside cells [12,13] and that dipeptides and tapasin, which binds to the F pocket of the peptide-binding groove, may employ similar mechanisms for MHC-I stabilization [16–19].

The short peptides we screened might not be optimal for those allotypes that did not fold, and more extensive libraries might need to be screened, including dipeptides containing non-natural amino acids such as cyclohexylalanine or homoleucine. We have observed in few cases that even the C84-C139 disulfide bond was not sufficient for stabilization. Likewise, our group has demonstrated for the first time that there are several structural and conformational changes in the amino acid side chains that line the peptide binding groove between dipeptide-bound, peptide-

bound, and empty MHC-I molecules [16]. It is evident from these observations that MHC-I stabilization is incompletely understood, and that there is scope for further improvement.

Those allotypes that can be folded with dipeptides remain in the peptide-receptive conformation and can be frozen for a longer period under appropriate conditions. These MHC-I molecules can be prepared as precursor monomers or multimers. The dipeptide has a very low affinity for MHC-I so that it can be readily replaced with different test peptides. Size exclusion chromatography or even dilution can remove the dipeptides. With this method, pMHC complexes with low-affinity peptides can be generated for research and clinical applications (see sections 1.6 and 1.8).

10.3. Development of a robust peptide screening platform using nanoDSF and MST

Another part of my work was dedicated to developing novel methods to measure MHC-I peptide binding affinity and stability. On the one hand, for the measurement of the denaturation temperature (T_m) of pMHC-I complexes, we developed the tryptophan fluorescence measurements (also called TDTF, thermal denaturation measured by tryptophan fluorescence [20,21]) into a microliter-format assay called nanoscale differential scanning fluorimetry (nanoDSF) [22]. This technique is robust, user-friendly, and consumes a minimal amount of protein (see section 5).

On the other hand, with the empty peptide-receptive MHC-I molecules, direct measurements of the peptide binding affinity at equilibrium have become possible for the first time. As described above (see section 1.7 and section 4.4), the possibility of a high-throughput experimental method to measure true peptide-MHC-I affinities will establish a much-awaited quantitative screening platform. We have performed the first steps in the process of developing a peptide binding assay based on microscale thermophoresis (MST) [23], and the initial results are encouraging.

Together, nanoDSF and MST (together with another technology, iDSF, which allows the derivation of binding constants for low-affinity peptides from tryptophan fluorescence; [24]), will be powerful tools for understanding peptide-MHC-I interactions and may help develop other methods and reagents for immunotherapeutic applications.

10.4. Understanding peptide binding in practical application

The interaction between peptides and MHC-I has been well studied in the last two decades, as is evident from the hundreds of available crystal structures [25–29]. Every MHC-I allotype has its unique preference for the anchor residues that can interact with the peptide-binding groove (see section 1.3). Several bioinformatics tools (such as NetMHC) were developed based on these

structural analyses to study peptide binding affinity [30–33]. However, there are several principal issues with affinity prediction [34–36]; one of them is that the software is trained with peptides that were eluted from tissue samples, and that must be assigned to one particular MHC-I allotype (out of 3-6 occurring in a biological sample) using the same algorithm that is supposed to be trained. Thus, to confirm that the predicted affinity values are accurate, experimental methods are necessary [37]. Disulfide-stabilized empty MHC-I molecules have made direct peptide equilibrium binding assays possible (see above and section 4), and MST, performed in multiwell plates, is high-throughput amenable since the MHC-I protein is fluorescently labeled, not the peptides, and thus, the affinity of any number of peptides can be measured economically.

Another limitation of the available computational tools such as NetMHC is that they cannot predict the binding affinity for short peptides, lipopeptides, and peptides modified with non-proteinogenic amino acids such as cyclohexylalanine, homoleucine, etc.. The methods developed in this thesis will allow us to understand the effect of such non-natural peptide modifications.

Altered peptide ligands (APLs) are peptides modified from immunodominant epitopes to improve their binding to MHC-I [38,39]. APLs are used in cancer vaccination and for shortening the activation time of T cells in adoptive cell therapy [40–42]. They are also modified to inhibit T cell responses for therapy in autoimmune diseases [43,44]. At this time, the screening of newly designed APLs to measure the actual binding affinity to MHC-I is only possible experimentally. Our MST binding assay is an ideal method for such studies. It can provide a rapid and reliable platform for in-vitro affinity assessment and help the development of epitope discovery platforms and peptide vaccines.

10.5. Future perspectives

From my studies, I have listed the dipeptide - MHC-I pairs for which the refolding experiments worked. But we still do not have the complete list. Further screening should be performed possibly after optimizing refolding conditions, more short-peptide libraries and perhaps additional mutation of unstable MHC-I allotypes. We should develop similar cELISA assays to screening the short-peptides in mouse allotypes, using the conformation-specific antibodies such as Y3 available for them.

Dipeptides catalyze peptide exchange on MHC-I molecules, possibly by accelerating the dissociation of the bound peptide [9]. From the available crystal structures, it is known that dipeptide binds to the F pocket of MHC-I and initiates the exchange, which is quite similar to intra-cellular peptide editing by tapasin [16,45]. It can be debated that inside the cell, especially in the ER, endogenous small molecules, for example dipeptides, might bind to MHC-I and play

an essential role such as support in folding (chemical chaperones) [46], peptide exchange, and peptide editing. The exact mechanism of peptide editing in the ER and the factors that influence it are still disputed. Several studies and crystal structures in the last five years have proposed the models of the mechanism of peptide editing, but the generalization is debatable [2,3,47]. Perhaps this work can be enriched with nuclear magnetic resonance studies that might yield a hint of where the dipeptides are interacting with the empty dsMHC-I molecules. The study of the effect of dipeptides inside the cellular environment might add to our understanding of peptide editing. Similarly, dipeptide-like substances might be developed to influence MHC-I antigen presentation in the experiment and maybe even in therapy, perhaps in an allotype-specific manner.

At the cell surface, empty or suboptimally loaded MHC-I molecules are short-lived and rapidly endocytosed [48]. The surface expression of such molecules can be stabilized by the external addition of high-affinity peptides. The rate of endocytosis inversely depends on the peptide affinity [49]. The Springer group have shown that dipeptides stabilize cell surface MHC-I similar to full-length peptide, probably by preventing the structural change and loss of β_2m that triggers the endocytic destruction [10]. Hence, further experimental evaluation of MHC-I endocytosis with dipeptides may provide valuable insight.

10.6. References

- [1] Gotch, F., Rothbard, J., Howland, K., Townsend, A., McMichael, A., Cytotoxic T lymphocytes recognize a fragment of influenza virus matrix protein in association with HLA-A2. *Nat.* 1987 326, 881–882.
- [2] Jiang, J., Natarajan, K., Boyd, L.F., Morozov, G.I., et al., Crystal structure of a TAPBPR–MHC I complex reveals the mechanism of peptide editing in antigen presentation. *Science*. 2017, 358, 1064–1068.
- [3] Thomas, C., Tampé, R., Structure of the TAPBPR–MHC I complex defines the mechanism of peptide loading and editing. *Science*. 2017, 358, eaao6001.
- [4] Ilca, F.T., Neerincx, A., Hermann, C., Marcu, A., et al., TAPBPR mediates peptide dissociation from MHC class I using a leucine lever 2018, 7, 1–24.
- [5] Hermann, C., van Hateren, A., Trautwein, N., Neerincx, A., et al., TAPBPR alters MHC class I peptide presentation by functioning as a peptide exchange catalyst. *Elife* 2015, 4.
- [6] Zacharias, M., Springer, S., Conformational flexibility of the MHC Class I α 1- α 2 domain in peptide bound and free states: A molecular dynamics simulation study. *Biophys. J.* 2004, 87, 2203–2214.
- [7] McShan, A.C., Devlin, C.A., Overall, S.A., Park, J., et al., Molecular determinants of chaperone interactions on MHC-I for folding and antigen repertoire selection. *Proc. Natl. Acad. Sci. U. S. A.* 2019, 116, 25602–25613.
- [8] Lan, H., Abualrous, E.T., Sticht, J., Fernandez, L.M.A., et al., Exchange catalysis by tapasin exploits conserved and allele-specific features of MHC-I molecules. *Nat. Commun.* 2021 121 2021, 12, 1–13.
- [9] Saini, S.K., Schuster, H., Ramnarayan, V.R., Rammensee, H.-G., et al., Dipeptides catalyze rapid peptide exchange on MHC class I molecules. *Proc. Natl. Acad. Sci.* 2015, 112, 202–207.
- [10] Saini, S.S.K., Ostermeir, K., Ramnarayan, V.V.R., Schuster, H., et al., Dipeptides promote folding and peptide binding of MHC class I molecules. *Proc. Natl. Acad. Sci. U. S. A.* 2013, 110, 15383–15388.
- [11] I. Pattison, D., Suryo Rahmanto, A., J. Davies, M., Photo- oxidation of proteins. *Photochem. Photobiol. Sci.* 2011, 11, 38–53.
- [12] Saini, S.K., Tamhane, T., Anjanappa, R., Saikia, A., et al., Empty peptide-receptive MHC class I molecules for efficient detection of antigen-specific T cells. *Sci. Immunol.* 2019, 4, eaau9039.
- [13] Rodenko, B., Toebe, M., Celie, P.H.N., Perrakis, A., et al., Class I Major Histocompatibility Complexes Loaded by a Periodate Trigger. *J. Am. Chem. Soc.* 2009, 131, 12305–12313.
- [14] Luimstra, J.J., Garstka, M.A., Roex, M.C.J., Redeker, A., et al., A flexible MHC class I multimer loading system for large-scale detection of antigen-specific T cells. *J. Exp. Med.* 2018, 215, 1493–1504.
- [15] Hateren, A. van, Anderson, M., Bailey, A., Werner, J.M., et al., Direct evidence for conformational dynamics in major histocompatibility complex class I molecules. *J. Biol. Chem.* 2017, 292, 20255–20269.
- [16] Anjanappa, R., Garcia-Alai, M., Kopicki, J.D., Lockhauserbäumer, J., et al., Structures of peptide-free and partially loaded MHC class I molecules reveal mechanisms of peptide selection. *Nat. Commun.* 2020, 11, 1–11.
- [17] Abualrous, E.T., Fritzsche, S., Hein, Z., Al-Balushi, M.S., et al., F pocket flexibility influences the tapasin dependence of two differentially disease-associated MHC Class I proteins. *Eur. J. Immunol.* 2015, 45, 1248–1257.
- [18] Fisette, O., Wingbermühle, S., Tampé, R., Schäfer, L. V., Molecular mechanism of peptide editing in the tapasin-MHC I complex. *Sci. Rep.* 2016, 6, 1–13.
- [19] Hafstrand, I., Sayitoglu, E.C., Apavaloaei, A., Josey, B.J., et al., Successive crystal structure snapshots suggest the basis for MHC class I peptide loading and editing by tapasin. *Proc. Natl. Acad. Sci. U. S. A.* 2019, 116, 5055–5060.
- [20] Springer, S., Do, K., Skipper, J.C.A., Townsend, A.R.M., et al., Fast association rates suggest a

- conformational change in the MHC class I molecule H-2D^b upon peptide binding. *Biochemistry* 1998, 37, 3001–3012.
- [21] Saini, S.K., Abualrous, E.T., Tigan, A.S., Covella, K., et al., Not all empty MHC class I molecules are molten globules: Tryptophan fluorescence reveals a two-step mechanism of thermal denaturation. *Mol. Immunol.* 2013, 54, 386–396.
- [22] Saikia, A., Springer, S., Peptide-MHC I complex stability measured by nanoscale differential scanning fluorimetry reveals molecular mechanism of thermal denaturation. *Mol. Immunol.* 2021, 136, 73–81.
- [23] Sparks, R.P., Fratti, R., Use of Microscale Thermophoresis (MST) to Measure Binding Affinities of Components of the Fusion Machinery. *Methods Mol. Biol.* 2019, 1860, 191–198.
- [24] Niebling, S., Burastero, O., Bürgi, J., Günther, C., et al., FoldAffinity: binding affinities from nDSF experiments. *Sci. Reports* 2021 111 2021, 11, 1–17.
- [25] Feng, L., Sun, M., Dong, S., Gao, F.-S., Progress in crystallization of major histocompatibility complex class I in vertebrates. *Chinese Sci. Bull.* 2014 5912 2014, 59, 1308–1316.
- [26] Achour, A., Persson, K., Harris, R.A., Sundbäck, J., et al., The Crystal Structure of H-2Dd MHC Class I Complexed with the HIV-1-Derived Peptide P18-I10 at 2.4 Å Resolution: Implications for T Cell and NK Cell Recognition. *Immunity* 1998, 9, 199–208.
- [27] Madden, D.R., The Three-Dimensional Structure of Peptide-MHC Complexes. <http://dx.doi.org/10.1146/annurev.iy.13.040195.003103> 2003, 13, 587–622.
- [28] Glithero, A., Tormo, J., Doering, K., Kojima, M., et al., The crystal structure of H-2Db complexed with a partial peptide epitope suggests a major histocompatibility complex class I assembly intermediate. *J. Biol. Chem.* 2006, 281, 12699–12704.
- [29] Zhang, C., Anderson, A., DeLisi, C., Structural principles that govern the peptide-binding motifs of class I MHC molecules. *J. Mol. Biol.* 1998, 281, 929–947.
- [30] Andreatta, M., Nielsen, M., Gapped sequence alignment using artificial neural networks: application to the MHC class I system. *Bioinformatics* 2016, 32, 511–517.
- [31] Phloyphisut, P., Pornputtapong, N., Sriswasdi, S., Chuangsuwanich, E., MHCSeqNet: a deep neural network model for universal MHC binding prediction. *BMC Bioinforma.* 2019 201 2019, 20, 1–10.
- [32] Venkatesh, G., Grover, A., Srinivasaraghavan, G., Rao, S., MHCAttnNet: predicting MHC-peptide bindings for MHC alleles classes I and II using an attention-based deep neural model. *Bioinformatics* 2020, 36, i399–i406.
- [33] O'Donnell, T.J., Rubinsteyn, A., Bonsack, M., Riemer, A.B., et al., MHCflurry: Open-Source Class I MHC Binding Affinity Prediction. *Cell Syst.* 2018, 7, 129–132.e4.
- [34] Yu, K., Petrovsky, N., Schönbach, C., Koh, J.L.Y., Brusica, V., Methods for Prediction of Peptide Binding to MHC Molecules: A Comparative Study. *Mol. Med.* 2002 83 2002, 8, 137–148.
- [35] Lin, H.H., Ray, S., Tongchusak, S., Reinherz, E.L., Brusica, V., Evaluation of MHC class I peptide binding prediction servers: Applications for vaccine research. *BMC Immunol.* 2008 91 2008, 9, 1–13.
- [36] Zhao, W., Sher, X., Systematically benchmarking peptide-MHC binding predictors: From synthetic to naturally processed epitopes. *PLOS Comput. Biol.* 2018, 14, e1006457.
- [37] Bonsack, M., Hoppe, S., Winter, J., Tichy, D., et al., Performance Evaluation of MHC Class-I Binding Prediction Tools Based on an Experimentally Validated MHC–Peptide Binding Data Set. *Cancer Immunol. Res.* 2019, 7, 719–736.
- [38] Schaft, N., Coccoris, miriam, Drexhage, J., Knoop, C., et al., An Altered gp100 Peptide Ligand with Decreased Binding by TCR and CD8 α Dissects T Cell Cytotoxicity from Production of Cytokines and Activation of NFAT. *Front. Immunol.* 2013, 0, 270.
- [39] Candia, M., Kratzer, B., Pickl, W.F., On Peptides and Altered Peptide Ligands: From Origin, Mode of Action and Design to Clinical Application (Immunotherapy). *Int. Arch. Allergy Immunol.* 2016, 170, 211–233.
- [40] Galloway, S.A.E., Dolton, G., Attaf, M., Wall, A., et al., Peptide Super-Agonist Enhances T-Cell

- Responses to Melanoma. *Front. Immunol.* 2019, 0, 319.
- [41] Wieckowski, S., Baumgaertner, P., Corthesy, P., Voelter, V., et al., Fine Structural Variations of $\alpha\beta$ TCRs Selected by Vaccination with Natural versus Altered Self-Antigen in Melanoma Patients. *J. Immunol.* 2009, 183, 5397–5406.
- [42] Slansky, J.E., Rattis, F.M., Boyd, L.F., Fahmy, T., et al., Enhanced Antigen-Specific Antitumor Immunity with Altered Peptide Ligands that Stabilize the MHC-Peptide-TCR Complex. *Immunity* 2000, 13, 529–538.
- [43] Minigo, G., Plebanski, M., Apostolopoulos, V., Altered Peptide Ligand Antagonism: From Immune Evasion to Immunotherapy. *Drug Des. Rev. - Online* 2005, 1, 145–151.
- [44] Iwanami, K., Matsumoto, I., Yoshiga, Y., Inoue, A., et al., Altered peptide ligands inhibit arthritis induced by glucose-6-phosphate isomerase peptide. *Arthritis Res. Ther.* 2009 116 2009, 11, 1–14.
- [45] Blees, A., Janulien, D., Hofmann, T., Koller, N., et al., Structure of the human MHC-I peptide-loading complex. *Nature* 2017, 551, 525–528.
- [46] Papp, E., Csermely, P., Chemical Chaperones: Mechanisms of Action and Potential Use. *Handb. Exp. Pharmacol.* 2006, 172, 405–416.
- [47] McShan, A.C., Devlin, C.A., Morozov, G.I., Overall, S.A., et al., TAPBPR promotes antigen loading on MHC-I molecules using a peptide trap. *Nat. Commun.* 2021 121 2021, 12, 1–18.
- [48] Ljunggren, H.-G., Stam, N.J., Öhlén, C., Neefjes, J.J., et al., Empty MHC class I molecules come out in the cold. *Nat.* 1990 3466283 1990, 346, 476–480.
- [49] Howarth, M., Williams, A., Tolstrup, A.B., Elliott, T., Tapasin enhances MHC class I peptide presentation according to peptide half-life. *Proc. Natl. Acad. Sci.* 2004, 101, 11737–11742.